Ontario Geological Survey
Miscellaneous Paper 121

Geoscience Research Grant Program

Summary of Research 1983 - 1984

edited by
V.G. Milne

1984

Ontario

Ministry of Natural Resources

Hon. Alan W. Pope
Minister

John R. Sloan
Deputy Minister

©1984 Government of Ontario
Printed in Ontario, Canada

ISSN 0704-2752 (Series)
ISSN 0225-5316 (Sub-series)

Publications of the Ontario Ministry of Natural Resources are available from the following sources. Orders for publications should be accompanied by cheque or money order payable to the *Treasurer of Ontario*.

Reports, maps, and price lists (personal shopping or mail order):

Public Service Centre, Ministry of Natural Resources
Room 1640, Whitney Block, Queen's Park
Toronto, Ontario M7A 1W3

Reports and accompanying maps only (personal shopping):

Ontario Government Bookstore
Main Floor, 880 Bay Street
Toronto, Ontario

Reports and accompanying maps (mail order or telephone orders):

Publications Services Section, Ministry of Government Services
5th Floor, 880 Bay Street
Toronto, Ontario M7A 1N8
Telephone (local calls), 965-6015
Toll-free long distance, 1-800-268-7540
Toll-free from area code 807, 0-ZENITH-67200

Every possible effort is made to ensure the accuracy of the information contained in this report, but the Ministry of Natural Resources does not assume any liability for errors that may occur. Source references are included in the report and users may wish to verify critical information.

Parts of this publication may be quoted if credit is given. It is recommended that reference to this report be made in the following form:

Redman, J.D., Strangway, D.W., and Ilkisik, O.M.
1984: Surface Electromagnetic Mapping in Selected Positions of Northern Ontario; Grant 118, p.47-58 *in* Geoscience Research Grant Program, Summary of Research 1983-1984, edited by V.G. Milne, Ontario Geological Survey, Miscellaneous Paper 121, 252p.

700-84-CSG

Contents

Introductory Remarks, *V.G. Milne* 2

Grant 100 Petrology, Geochemistry and Economic Potential of the Nipissing Gabbro, *W.F. Rowell & A.D. Edgar* 5

Grant 106 Platinum-Group Elements in Layered Intrusions, *A.A. Borthwick & A.J. Naldrett* 13

Grant 107 Platinum Group Elements in the Eastern Gabbro, Coldwell Complex, Northwestern Ontario, *D.H. Watkinson et al.* 36

Grant 114 Source, Correlation, and Thermal Maturation History of Hydrocarbon Deposits of Southern Ontario, *J.F. Barker et al.* 42

Grant 118 Surface Electromagnetic Mapping in Selected Positions of Northern Ontario, *J.D. Redman et al.* 47

Grant 128 Subsurface Quaternary Stratigraphy using Borehole Geophysics, *R.N. Farvolden et al.* 59

Grant 131 Source Rock Geochemistry of Pleistocene Tills of Southern Ontario, *U. Brand & J. Terasmae* 65

Grant 132 Geological and Geochemical Studies of the Boston and Temagami Iron Formations and Their Contiguous Volcanosedimentary Piles, *J.H. Crocket et al.* 72

Grant 134 Stratigraphy and Geochemistry of Northern Ontario Carbonaceous Deposits: Onakawana Lignites, *F. Murray et al.* 84

Grant 138 Mineralogy and Geochemistry of the Chrysotile Asbestos Deposits of Ontario: Munro Mine and Garrison Deposit, *F.J. Wicks et al.* 99

Grant 140 Direct Trace Elemental Analysis of Solid Samples by Techniques of Atomic Spectrometry, *J.C. Van Loon et al.* 111

Grant 145 Ontario Field Tests and Instrumentation of Cross-Hole Magnetometric Resistivity, *B.B.H. Lo et al.* 117

Grant 146 Crustal Contamination in the Sublayer, Sudbury Igneous Complex: A Combined Trace Element and Strontium Isotope Study, *B.V. Rao et al.* 128

Grant 148 Geochemical Study of the Salina Formation of Southern Ontario - Isotopes, Major and Minor Elements, *M.C. Miles et al.* 147

Grant 149 Structural Signature and Tectonic History of Deformed Gold-Bearing Rocks in Northwestern Ontario, *H. Hugon & W.M. Schwerdtner* 164

Grant 167 Resedimentation Associated with the Gold-Bearing Banded Iron Formation in the Geraldton-Beardmore Area, *T.J. Barrett & P.W. Fralick* 177

Grant 168 Petrogenesis of Mineralized Horizons in Uchi Lake Metavolcanics, *S.R. Noble et al.* 188

Grant 172 Strength Testing of Reservoir Strata in the Grimsby Formation (Lower Silurian) of Southwestern Ontario, *P.E. Holm* 196

Grant 173 Sedimentary Rocks and Stratabound Mineralization in the Cobalt Region, *J.A. Donaldson et al.* 198

Grant 175 Structural Geology of Northern Dome and Southern McDonough Townships, Red Lake Area, Ontario, *P.M Berger & J.M. Summers* 211

Grant 179 Petrogenesis and Metallogenesis of the Atikwa-Lawrence Volcanic-Plutonic Terrane, *G.R. Edwards & D.W. Davis* 222

Grant 187 Sedimentology of the Cambro-Ordovician Sandstones of Eastern Ontario, *R.R. Wolf & R.W. Dalrymple* 240

CONVERSION FACTORS FOR MEASUREMENTS IN ONTARIO GEOLOGICAL SURVEY PUBLICATIONS.

CONVERSION FROM SI TO IMPERIAL			CONVERSION FROM IMPERIAL TO SI		
SI Unit	*Multiplied by*	*Gives*	*Imperial Unit*	*Multiplied by*	*Gives*
			LENGTH		
1 mm	0.039 37	inches	1 inch	**25.4**	mm
1 cm	0.393 70	inches	1 inch	**2.54**	cm
1 m	3.280 84	feet	1 foot	**0.304 8**	m
1 m	0.049 709 7	chains	1 chain	20.116 8	m
1 km	0.621 371	miles (statute)	1 mile (statute)	**1.609 344**	km
			AREA		
1 cm^2	0.155 0	square inches	1 square inch	**6.451 6**	cm^2
1 m^2	10.763 9	square feet	1 square foot	**0.092 903 04**	m^2
1 km^2	0.386 10	square miles	1 square mile	2.589 988	km^2
1 ha	2.471 054	acres	1 acre	0.404 685 6	ha
			VOLUME		
1 cm^3	0.061 02	cubic inches	1 cubic inch	**16.387 064**	cm^3
1 m^3	35.314 7	cubic feet	1 cubic foot	0.028 316 85	m^3
1 m^3	1.308 0	cubic yards	1 cubic yard	0.764 555	m^3
			CAPACITY		
1 l	1.759 755	pints	1 pint	0.568 261	L
1 L	0.879 877	quarts	1 quart	1.136 522	L
1 L	0.219 969	gallons	1 gallon	**4.546 090**	L
			MASS		
1 g	0.035 273 96	ounces (avdp)	1 ounce (avdp)	28.349 523	g
1 g	0.032 150 75	ounces (troy)	1 ounce (troy)	**31.103 476 8**	g
1 kg	2.204 62	pounds (avdp)	1 pound (avdp)	**0.453 592 37**	kg
1 kg	0.001 102 3	tons (short)	1 ton (short)	**907.184 74**	kg
1 t	1.102 311	tons (short)	1 ton (short)	**0.907 184 74**	t
1 kg	0.000 984 21	tons (long)	1 ton (long)	**1016.046 908 8**	kg
1 t	0.984 206 5	tons (long)	1 ton (long)	**1.016 046 908 8**	t
			CONCENTRATION		
1 g/t	0.029 166 6	ounce (troy)/ton (short)	1 ounce (troy)/ton (short)	34.285 714 2	g/t
1 g/t	0.583 333 33	pennyweights/ton (short)	1 pennyweights/ton (short)	1.714 285 7	g/t

OTHER USEFUL CONVERSION FACTORS

1 ounce (troy) per ton (short)	20.0	pennyweights per ton (short)
1 pennyweight per ton (short)	0.05	ounces (troy) per ton (short)

Note. Conversion factors which are in bold type are exact. The conversion factors have been taken from or have been derived from factors given in the Metric Practice Guide for the Canadian Mining and Metallurgical Industries, published by the Mining Association of Canada in cooperation with the Coal Association of Canada.

Geoscience Research Grant Program

Summary of Research 1983-1984

edited by
V.G. Milne

Director, Ontario Geological Survey.

Introductory Remarks

The Ontario Geoscience Research Grants Program was initiated in 1978 to encourage geoscience research at Ontario universities. By supporting mission-oriented geologically related projects, a program of research was established which would complement the work of the Ontario Geological Survey through its mandate:

"To stimulate exploration for, and facilitate sound planning in all matters related to mineral and other earth resources by providing an inventory and analysis of the geology and mineral deposits of Ontario".

The program supports applied studies of up to three years duration towards: mineral deposit characterization involving studies of specific occurrences or groups of occurrences within Ontario; petrology, rock geochemistry, structural geology, stratigraphy and geochronology studies; field and laboratory studies leading to the development of new geophysical or geochemical concepts and techniques; engineering and environmental geology studies, and methods for improving automated or mineral processing and facilitating the interpretation of geoscience data.

In order to receive funding, applications should be forwarded to the Ontario Geological Survey prior to November 15. Project proposals are subject to review by a committee which reports to the Director of the Ontario Geological Survey. This committee consists of 3 representatives of the mineral industry, 3 representatives of the university community, 4 representatives of the Survey and a chairperson. Members review proposals based on scientific merit and relevance of the research to Ontario Geological Survey activities, concentrating on those projects which will stimulate and benefit exploration in the Province. Members of the 1983-84 committee included:

S.N. Charteris, Chairman	Corporation Falconbridge Copper Ltd.
Dr. A.C. Colvine	Ontario Geological Survey
Dr. J.A. Coope	Newmont Explorations of Canada Ltd.
Dr. J.H. Crocket	McMaster University
Dr. J.A.C. Fortesque	Ontario Geological Survey
Dr. R. Hodder	University of Toronto
Dr. J. Misener	Paterson, Grant & Watson Ltd.
Dr. B. Rust	University of Ottawa
Dr. H. Seigel	Scintrex Ltd.
Dr. P.G. Telford	Ontario Geological Survey
Dr. P.C. Thurston	Ontario Geological Survey

Successful grant recipients are expected to submit reports for publication in the annual Summary of Research and in addition participate in an annual OGS Geoscience Research Seminar held annually in December.

Publication in other scientific journals is encouraged and a final report summarizing the project objective is required to be submitted to the Ontario Geological Survey within 6 months of termination of funding.

The following research projects partially or wholly funded by this program during 1983-84 will be published as Ontario Geological Survey, Open File Reports by May 1985:

Grant 100:	The Petrology, Geochemistry and Economic Potential of the Nipissing Gabbro; A.D. Edgar, University of Western Ontario.
Grant 106:	Platinum Group Elements in Layered Intrusions; A.J. Naldrett, University of Toronto.
Grant 107:	Platinum Group Element Potential in Alkaline Rocks of Northwestern Ontario; D.H. Watkinson, Carleton University.
Grant 114:	Organic Geochemistry of Ontario's possible Oil Shales; J.F. Barker, University of Waterloo.
Grant 118:	Surface Electromagnetic Mapping in Selected Positions of Northern Ontario; D.W. Strangway, University of Toronto.
Grant 131:	Source Rock Geochemistry of Pleistocene Tills of Southern Ontario; U. Brand, Brock University.
Grant 140:	Direct Trace Elemental Analysis of Solid Samples by Techniques of Atomic Spectrometry; J.C. Van Loon, University of Toronto.
Grant 145:	Cross-Hole Magnetometric Resistivity; R.N. Edwards, University of Toronto.
Grant 152:	Seismic Reflection Investigation of the Paleozoic - Precambrian Unconformity in Eastern Ontario; D.V. Woods, Queen's University.
Grant 167:	Resedimentation Associated with Gold-Bearing Banded Iron Formation; T.J. Barrett, University of Toronto.
Grant 172:	Strength Testing of Reservoir Strata in the Grimsby Formation (Lower Silurian) of Southwestern Ontario; P.E. Holm, University of Windsor.
Grant 175:	Deformation Studies in Dome and McDonough Townships, Red Lake; J.M. Summers, Queen's University.

During 1983-84, 48 project proposals were received by the Ontario Geological Survey for funding consideration. Of these, 23 were approved for funding, 13 of which were renewal projects:

University	Approved		Rejected	
Brock	$ 9,800	1	-	0
Carleton	32,400	2	$ 26,500	1
Guelph	-	0	103,600	3
Lakehead	-	0	15,200	1
Laurentian	*	(1)	117,375	4
McMaster	34,265	1	-	0
Ottawa	**	(1)	10,000	1
Queen's	65,645	3	14,758	1
Toronto	218,120	9	105,780	5
Waterloo	59,580	3	103,465	4
Western	50,915	2	77,325	2
Windsor	7,040	1	44,552	2
York	22,235	1	33,993	1
TOTAL	$500,000	23	$652,548	25

*A grant of $45,035 was shared by the University of Western Ontario and Laurentian University.

**A grant of $27,400 was shared by Carleton University and the University of Ottawa.

The undersigned would like to thank Mr. S.N. Charteris, who acted as Committee Chairman, and the rest of the Review Committee Members who gave freely of their time. The efforts of the researchers are acknowledged and as well, Ms. W.L. Paquette who served as Grants Administrator and Secretary to the Committee deserves thanks.

V.G. Milne
Director
Ontario Geological Survey

Grant 100 Petrology, Geochemistry and Economic Potential of the Nipissing Gabbro

W.F. Rowell and A.D. Edgar

Department of Geology, University of Western Ontario

ABSTRACT

Platinum group elements and gold are concentrated in a small Cu-Ni sulphide deposit hosted in a Nipissing-type intrusion in the Lake Wanapitei - Portage Bay area of Ontario. Sulphide samples from the deposit average 9% Cu, 0.5% Ni, 9736 ppb Pt, 20,829 ppb Pd and 3053 ppb Au. Pd resides in merenskyite and to a lesser extent kotulskite, while Pt is concentrated in sperrylite. Most platinum group mineral grains are situated in the gangue rather than being associated with the principal sulphides chalcopyrite and pyrite. In contrast to most other sulphide deposits that are enriched in platinum group elements, the Rathbun Lake deposit appears to be hydrothermal in origin. The mineralogy of the host gabbronorite has been highly altered by fluids, and primary silicates have been replaced by sulphides and alteration silicates such as chlorite, quartz, sericite and biotite. Oxygen isotope analyses suggest that the fluid was at least partially meteoric in origin and was 300° to 400°C in temperature.

INTRODUCTION

The petrology and geochemistry of a Nipissing-type intrusion located in the Lake Wanapitei - Portage Bay area of Ontario (Figure 1) have been examined in two previous annual reports. Finn *et al.* (1982) described cycles of reverse differentiation within the intrusion and attributed them to successive injections of a mantle-derived magma undergoing differentiation in one or more underlying auxillary magma chambers. This hypothesis has been reconsidered and a revised version is presented in the final summary report (Edgar *et al.* in preparation). Rowell and Edgar (1983) re-examined an extensive zone of slight precious metal enrichment that had been outlined near the base of the intrusion by Dressler (1982); only background levels of Pt, Pd and Au were detected. The higher precious metal values reported by Dressler (1982) were ascribed to analytical error. Rowell and Edgar (1983) also concluded that significant precious metal concentrations occur only in a small sulphide deposit near the northern margin of the intrusion at the south end of Rathbun Lake.

The present report focuses on the platinum group element (PGE) and Au content of the Rathbun Lake deposit. In addition to determining precious metal values, the study examines the form of PGE mineralization and describes the textures and mineral associations of the constituent platinum group minerals (PGM). Using these criteria, the deposit is compared with other PGE-rich sulphide occurrences.

GEOLOGICAL SETTING

The Wanapitei intrusion is ring-shaped, centred around Portage Bay on the northeast shore of Lake Wanapitei (Figure 1). It intrudes Gowganda Formation greywacke and is cut by a Sudbury age olivine diabase dike. Approximately 98% of the intrusion is composed of gabbronorite, while the remainder consists of monzodiorite, quartz diorite, granodiorite and granite. The mineralogy of the intrusion is still pristine except in a few areas of localized hydrothermal activity. More detailed descriptions of the Lake Wanapitei - Portage Bay area geology are included in Finn *et al.* (1982) and in publications cited therein.

The Rathbun Lake sulphide deposit occurs within an outcrop of gabbronorite near the northern contact of the intrusion. Because the deposit was excavated almost 70 years ago, an *in situ* examination of the sulphide mineralization is no longer possible, and samples are only available from the nearby dump. However, based on exploration reports, Dressler (1982) concluded that the sulphides occur in a massive zone approximately 12 m long and 0.3 to 0.6 m wide. This zone is surrounded by disseminated sulphides which increase the width of the deposit to about 3 m. The deposit strikes perpendicular to the gabbronorite-greywacke contact at 135° and dips steeply to the north at 60°. Sulphide mineralization is concentrated along folds and irregularities near the contact, but does not extend beyond it into the adjacent greywacke.

MINERALOGY

Fresh Wanapitei gabbronorite is primarily composed of plagioclase laths and equigranular pyroxene. However, in all 16 sulphide-bearing samples examined, the mineralogy of the host gabbronorite has been altered by hydrothermal fluids. Silicification, chloritization, and saussuritization have reduced primary minerals to relicts in a gangue dominated by chlorite, quartz, sericite and biotite. Pyroxene accounts for <1% of the total gangue min-

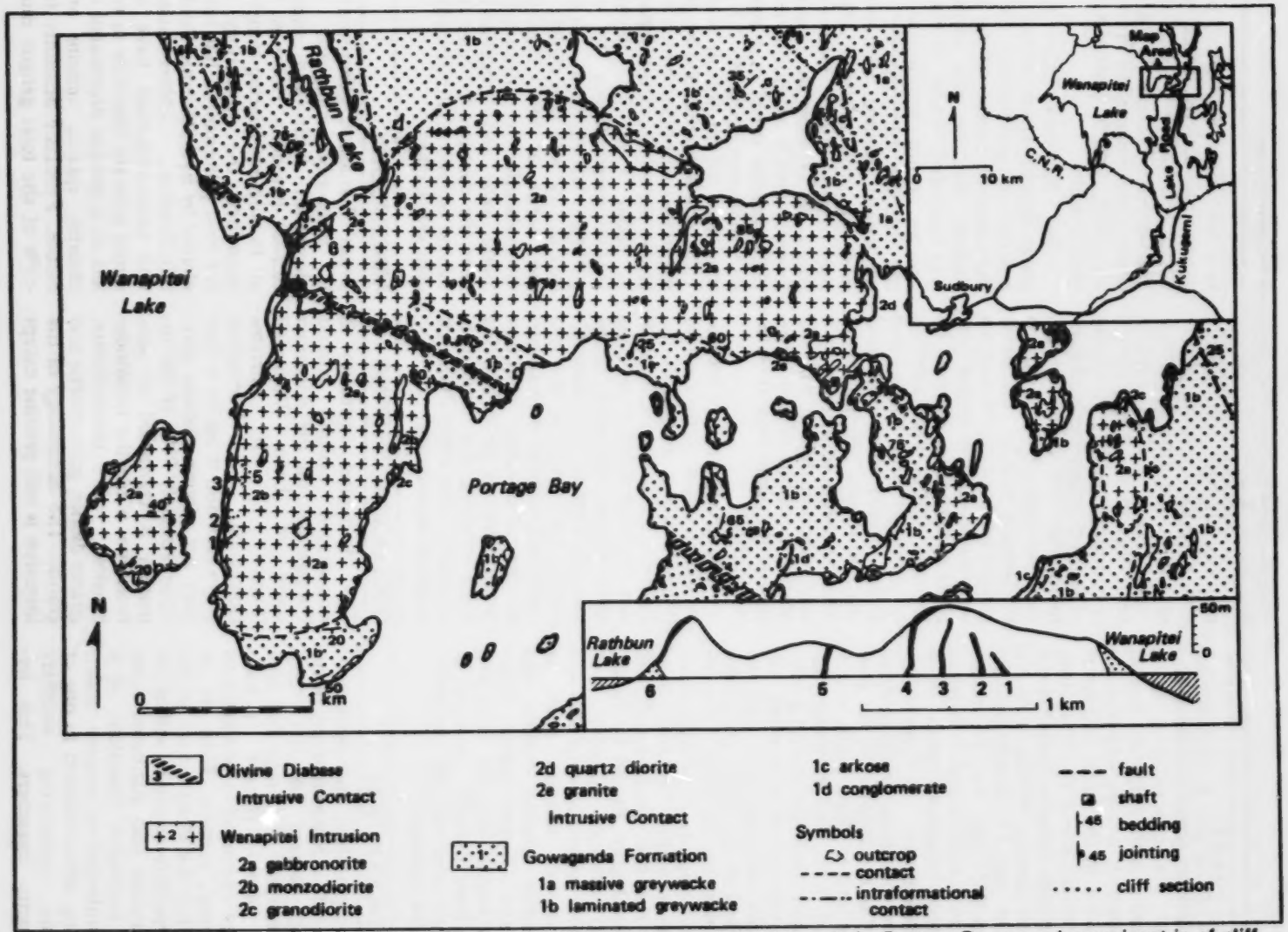

Figure 1. Geological map of the Nipissing gabbro and host rocks in the Lake Wanapitei - Portage Bay area. Lower inset is of cliff sections of unaltered gabbronorite sampled on the Lake Wanapitei side of peninsula (see Finn and Edgar 1982).

TABLE 1. ELECTRON MICROPROBE ANALYSES OF RATHBUN LAKE PLATINUM GROUP MINERALS.

	Weight Percent						
	Pt	Pd	Bi	Te	As	Sb	Total
			Sperrylite				
1	56.71	nd	nd	nd	42.73	nd	99.44
			Kotulskite				
1	nd	37.04	12.11	27.38	nd	18.56	95.09
			Merenskyite				
1	nd	22.84	15.54	53.32	0.13	0.57	92.40
2	nd	23.16	15.31	55.78	0.03	0.66	94.94
3	nd	24.32	15.63	56.68	0.08	0.74	97.45
4	nd	23.34	15.64	56.58	nd	0.72	96.28
5	nd	22.70	12.96	56.34	nd	0.53	92.52
6	nd	21.77	12.51	55.39	nd	0.48	90.14
7	nd	24.00	12.49	59.62	nd	0.85	96.96
8	nd	23.70	11.50	58.59	nd	0.70	94.49
9	nd	24.80	13.55	55.50	nd	0.60	94.48
10	nd	25.42	13.55	54.50	nd	0.41	93.88
11	nd	28.14	12.34	51.13	nd	0.53	92.14
12	nd	31.03	12.59	51.88	nd	0.56	96.06
13	nd	22.47	10.67	52.94	nd	0.75	86.83
14	nd	22.87	11.69	53.21	nd	0.81	88.58
15	nd	24.43	28.81	29.77	0.29	7.64	90.94
16	nd	23.79	15.01	48.01	nd	0.48	87.29
17	nd	25.02	13.09	57.40	nd	0.18	95.67
18	nd	22.41	11.70	58.06	nd	0.24	92.43
19	nd	23.62	9.91	58.83	nd	0.11	92.47
20	nd	24.15	12.21	57.75	nd	0.21	94.32

eralogy and plagioclase remains only as thin rims enclosing highly saussuritized cores. It is evident that both minerals have been replaced by sulphides as well as alteration silicates. Fibrous chlorite forms about 60% of the gangue, while quartz and sericite account for an additional 10% each. Biotite is scarce in all but a few samples with little sulphide mineralization.

Chalcopyrite and pyrite are the principal sulphide minerals, while millerite, arsenopyrite, violarite, magnetite and PGM occur as accessories. Traces of covellite, molybdenite and gold are present in a few samples.

Approximately 55% of the total sulphide mineralization consists of coarse patches of chalcopyrite filling the interstices between earlier formed grains of pyrite. Medium- to fine-grained euhedral pyrite forms about 40% of the sulphide mineralization and commonly contains small inclusions of chalcopyrite, pyrrhotite and magnetite. In a few pyrite grains where exsolved chalcopyrite is abundant the two minerals occur in a very fine scale myrmekitic intergrowth texture.

Millerite is the most ubiquitous, if not most abundant, accessory mineral. Typically, it occurs as fine anhedral grains associated with chalcopyrite. About half of the original millerite content has been altered to violarite by supergene fluids. Few grains have been completely altered and millerite cores rimmed by violarite are a common texture.

Arsenopyrite is present in only a few samples but is probably the most abundant accessory mineral. It is always intergrown with pyrite in medium- to coarse-grained patches associated with chalcopyrite.

PGM AND GOLD

Based on optical properties 234 PGM grains and 7 specks of gold were tentatively identified in the 16 polished thin sections of Rathbun Lake ore minerals which were examined. Because most grains were <20 μm in diameter and could not be confidently identified by optical means alone, the compositions of 22 of the largest PGM grains were determined by quantitative electron microprobe analyses using pure element standards. Although better results are achieved using synthetic standards, the compositions obtained are sufficiently accurate that 20 grains are recognizable as merenskyite ($PdTe_2$) and single grains as kotulskite (PdTe) and sperrylite ($PtAs_2$) (Table 1). While the identities of the 212 grains not probed are less certain, each has the optical properties of merenskyite. Detailed descriptions of the PGM are given in Rowell (1984). All seven specks of gold identified occurred as exsolved blebs in pyrite. Microprobe analyses of the exsolutions were not possible because of their extremely small size (i.e. <2 μm).

In PGE-rich sulphide deposits where PGM textures have been described, most grains are closely associated with sulphide minerals. In this respect the Rathbun Lake deposit is atypical as 145 of the 234 PGM grains identified are enclosed in gangue silicates. Of those that are associated with sulphides, 41 are located at chalcopyrite-silicate interfaces and 23 occur as inclusions in chalcopyrite. The remaining 24 grains are associated with pyrite, 22 as bleb-like inclusions

TABLE 2. PGE, AU, NI, CU AND S CONTENTS OF RATHBUN LAKE ORE MINERAL SAMPLES

	Wt. Percent			ppb						
	Ni	Cu	S	Pt	Pd	Rh	Ru	Ir	Os	Au
1. This Study										
R-1	0.22	19.9	23.4	1800	23000	17	<5	0.1	<3	250
R-2	0.22	9.1	19.4	74	35000	14	20	0.3	6	890
R-3	0.26	8.3	18.4	18000	37000	8	<5	0.3	11	1300
R-4	0.16	4.7	9.4	33000	19000	3	40	0.2	23	950
R-5	0.36	2.3	2.4	190	12000	23	15	28.0	3	2800
2. Dolmac Mines Report (Koulomzine, 1955)										
3	0.21	7.03		3375	23125					11250
3a		17.26		2750	29687					63
5	0.50	5.51		1187	23125					6250
5a	0.11	19.92		656	5313					
6	0.35	7.25		2812	16875					
9	0.29	1.31		2187	5000					
Mean Of 1+2	0.27	9.33	14.6	9736	20829	13.0	17.0	5.9	9.2	3053

PGE and Au contents of 5 g Chalcopyrite and Magnetite Separates

	ppb							
	Pt	Pd	Rh	Ru	Re	Ir	Os	Au
Ch-1	290	4800	7	<50	<5	<0.5	<10	300
Ch-1	6300	12000	10	50	<5	1.2	23	370
Mag-1	<5000	1200	7	<50	5	180	<15	24000

Ch - chalcopyrite
Mag - magnetite

and 2 as bordering minerals. This distribution of PGM grains suggests that many were precipitated *in situ* independently of sulphides.

Although most PGE-rich sulphide deposits are considered to be strictly magmatic in origin (Naldrett and Duke 1980), the tendency of Pt and Pd to form solution complexes with late stage volatile elements has been well documented. Extensive Pd bismuthotelluride mineralization is associated with the hydrothermal Cu ores of the New Rambler Mine, Wyoming (McCallum *et al.* 1976) and Messina, South Africa. In addition, recent studies of the Merensky Reef, South Africa (Kinloch 1982) concluded that Pt and Pd remobilized and concentrated by late stage hydrothermal fluids now resides in bismuthide, telluride and arsenide minerals. The occurrence of Pt and Pd in bismuthotelluride and arsenide minerals at Rathbun Lake provides further evidence that the two noble metals are readily mobilized and concentrated by hydrothermal fluids.

GEOCHEMISTRY

To facilitate comparisons with other PGE-rich sulphide deposits five samples of Rathbun Lake sulphide mineralization ranging from massive to sparsely disseminated were analyzed for the PGE, Au, Cu, Ni and S. In addition, two 5 g samples of chalcopyrite and a single 5 g sample of magnetite were analyzed for PGE and Au content. Cu, Ni and S analyses were performed by X-ray Assay Laboratories, Don Mills, Ontario, and PGE and Au values were determined by Neutron Activation Services, Hamilton, Ontario. The results of the analyses are listed in Table 2 along with six less complete analyses of Rathbun Lake mineralization from a Dolmac Mines Limited report (Koulomzine 1955).

The abundance of merenskyite in the Rathbun Lake deposit is evident in the results of the whole rock analyses. Pd values are relatively high in all samples and average 20,829 ppb. Pt is much more heterogeneously distributed, with values ranging from 79 to 35,000 ppb and averages 9736 ppb. Au averages 3053 ppb and, like Pt, values fluctuate markedly. In contrast to Pt and Pd, values for the other PGE are extremely low. Ratios of (Pt + Pd) to (Os + Ir + Ru) are characteristically >13 in tholeiitic hosted sulphide deposits but seldom as high as at Rathbun Lake where the ratio is 626.

The high Cu and low Ni content of the mineralization reflects the predominance of

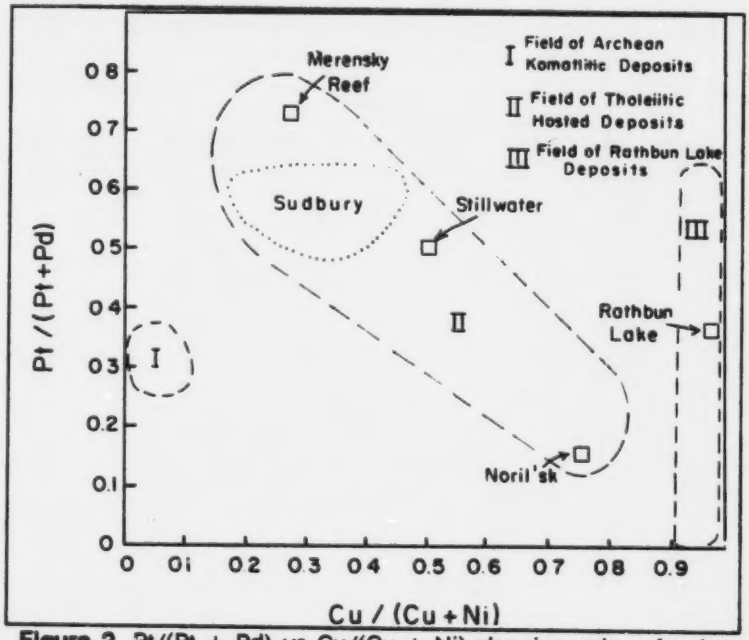

Figure 2. Pt/(Pt + Pd) vs Cu/(Cu + Ni) showing values for the Rathbun Lake deposit relative to other Cu-Ni- PGE deposits.

chalcopyrite over the Ni-bearing minerals millerite and violarite. There is no correlation between Cu or Ni and precious metal contents; a not unexpected result since most PGM are associated with gangue minerals.

The results of the chalcopyrite analyses provide further evidence that most PGM occur in the gangue as Pt, Pd and Au values are notably lower than in the whole rock analyses. While Pt and Pd values are also relatively low in the single magnetite sample analyzed, both Ir at 180 ppb and Au at 24,000 ppb are enriched (Table 2). This suggests that these two elements may be concentrated in magnetite, however, more analyses would be necessary to confirm this conclusion.

METAL RATIOS

In order to compare precious metal ratios at Rathbun Lake with those in other sulphide deposits, PGE and Au values have been recalculated to 100% sulphide using the procedure outlined by Hoffman *et al.* (1979). When applied to a deposit such as Rathbun Lake where most of the PGM grains are not associated with sulphides, 100% sulphide calculations tend to inflate precious metal values as sulphide content decreases. Fortunately, the recalculation does not substantially alter metal ratios and therefore it is still possible to make meaningful comparisons using this criteria.

In Figure 2 the Rathbun Lake deposit is compared with other sulphide deposits based on ratios of Pt/(Pt + Pd) and Cu/(Cu + Ni). Although the Rathbun Lake deposit is hosted by a tholeiitic intrusion, all samples plotted according to these ratios fall outside the tholeiitic field. The atypical plot of the Rathbun Lake deposit may be a reflection of its hydrothermal origin since all deposits within the tholeiitic field are thought to be primarily magmatic.

The Rathbun Lake deposit also appears to be atypical when compared with other tholeiitic hosted sulphide deposits on the basis of chondrite normalized 100% sulphide PGE and Au values (Figure 3). The steep slope of the graph for the precious metal enrichment trend at Rathbun Lake may be typical of hydrothermal PGE deposits as Os, Ir and Ru appear to be less soluble than Pt and Pd. This conclusion is supported by a Pd:Pt:(Os + Ir + Ru + Rh) ratio of 1800:100:1 in the hydrothermal ores of the New Rambler Mine, Wyoming (McCallum *et al.* 1976).

FLUID SOURCE AND TEMPERATURE

To determine the temperature and possible source of the ore-forming fluid, oxygen isotope analyses were conducted on two samples each of massive and disseminated sulphide and, for comparative purposes, on three samples of non-sulphide-bearing gabbronorite. R. Kerrich of the University of Western Ontario determined $\delta^{18}O$ values for each whole rock, as well as for separates of feldspar, magnetite and quartz. The results of the analyses are shown in Table 3.

For the non-sulphide-bearing gabbronorite the whole rock $\delta^{18}O$ range of +5.81 to +6.22‰ is well within the +6.5±1‰ range characteristic of unmodified basaltic

material. Temperature calculations based on the $\delta^{18}O$ values of co-existing feldspar and magnetite (Bottinga and Javoy 1975) indicate equilibration was with a magmatic fluid of 550° to 717°C.

The whole rock $\delta^{18}O$ values of +4.59‰ and +4.32‰ obtained from the massive sulphide samples fall below the range of unmodified basaltic material. Based on the $\delta^{18}O$ values of co-existing magnetite and plagioclase final equilibration was with a fluid of approximately 400°C. At this temperature Δ feldspar-water calculations yield $\delta^{18}O$ water values of +5.2‰ and +5.4‰. These values are below the field of magmatic waters and within the range of meteoric and metamorphic fluids. The absence of extensive metamorphism in the Lake Wanapitei - Portage Bay area (Finn *et al.* 1982) suggests equilibration with a fluid at least partially of meteoric origin.

In contrast to massive sulphide mineralization, disseminated sulphide samples have whole rock and quartz $\delta^{18}O$ values comparable to those of non-sulphide-bearing gabbronorite, while feldspar and magnetite values differ significantly. Since quartz becomes resistant to equilibration at temperatures ≤350°C, while the other minerals continue to undergo rapid isotopic exchange with fluids down to 100°C, these values indicate interaction with a cooler hydrothermal fluid. Disseminated sulphides may have equilibrated with a slightly cooler fluid than massive sulphides because they were further from the main channel of fluid circulation.

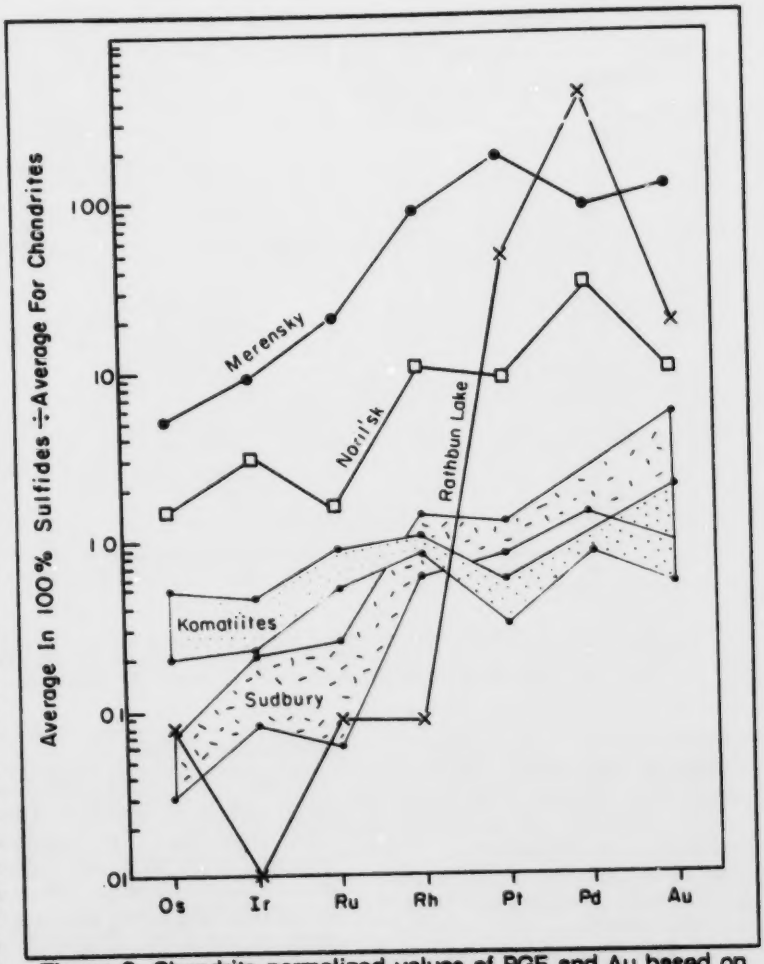

Figure 3. Chondrite normalized values of PGE and Au based on values recalculated to 100% sulphides for Rathbun Lake relative to other PGE deposits (after Naldrett et al. 1980).

TABLE 3. OXYGEN ISOTOPE COMPOSITIONS (SMOW) OF RATHBUN LAKE ORE MINERAL SAMPLES & NON-SULPHIDE-BEARING WANAPITEI GABBRONORITE

		$\delta^{18}O(‰)$					
Sulphide Content	Sample Number	Whole Rock	Quartz	Feldspar	Magnetite	Temp. °C	δ^{18} Fluid (‰)
None	NM3	5.97	9.02	6.55	0.68	549	6.56
	NM5	6.22	8.46	6.64	1.03	563	6.83
	NM6	5.81	8.93	6.67	2.64	717	7.80
Disseminated	SM1	6.13	9.47	8.45	-3.18	309	4.85
	SM2	5.58	8.22	7.75	-3.56	316	4.30
Massive	M3	4.59	10.65	7.47	-2.03	370	5.20
	M4	4.32	10.36	6.81	-1.14	429	5.50

CONCLUSION

In the Rathbun Lake Cu-Ni sulphide deposit, Pt, Pd and Au average 9736, 20,829 and 3053 ppb respectively. Pd resides in merenskyite, and to a lesser extent kotulskite, while Pt is concentrated in sperrylite. Au occurs as minute exsolutions in pyrite.

In contrast to other PGE enriched sulphide deposits, most PGM grains are situated in the gangue rather than associated with sulphides. PGM grains that are associated with sulphides occur at chalcopyrite-silicate interfaces or as inclusions in chalcopyrite and pyrite. Grains occurring as inclusions may have been exsolved during sulphide crystallization, while those in the gangue were more likely precipitated *in situ* independently of sulphides.

The deposit appears to be hydrothermal in origin and therefore is quite unusual as only two other similar deposits have been documented. Evidence supporting a hydrothermal origin includes: the spatial coincidence of altered gabbronorite and the orebody, the replacement of magmatic silicates by ore minerals, the abundance of pyrite, and the extremely large (Pt+Pd):(Os+Ir+Ru) ratio. Oxygen isotope evidence indicates that the hydrothermal fluid was at least partially of meteoric origin and at a temperature of 300 to 400°C.

ACKNOWLEDGMENTS

We thank R. Kerrich for performing the oxygen isotope studies and R.W. Hodder and R. Kerrich for discussion.

REFERENCES

Barnes, H.L.
1979: Solubilities of Ore Minerals: p.404-460 *in* Geochemistry of Hydrothermal Ore Deposits, edited by H.L. Barnes, Wiley, New York.

Bottinga, Y. and Javoy, M.
1975: Oxygen Isotope Partitioning Among the Minerals in Igneous and Metamorphic Rocks: Review of Geographies and Space Physics, Volume 13, p.401-418.

Cousins, C.A., and Vermaak, C.F.
1976: The Contribution of South Africa Ore Deposits to the Geochemistry of the Platinum Group Metals; Economic Geology, Volume 71, p.287-305.

Dressler, B.O.
1982: Geology of the Wanapitei Lake Area, District of Sudbury: Ontario Geological Survey, Report 213, p.131. Accompanied by Maps 2450, 2451, scale 1:31 680.

Finn, G.C., Edgar, A.D., and Rowell, W.F.
1982: Petrology, Geochemistry and Economic Potential of the Nipissing Diabase: Grant 100, p.43-58 in Geoscience Grant Program, Summary of Research, 1981-1982, edited by E.G. Pye, Ontario Geological Survey, Miscellaneous Paper 103.

Graterol, M., and Naldrett, A.J.
1971: Mineralogy of the Marbridge No. 3 and No. 4 Nickel-Iron Sulfide Deposit, with Some Comments on the Low Temperature Equilibrium in the Fe-Ni-S System; Economic Geology, Volume 66, p.886-900.

Hoffman, E.L., Naldrett, A.J., Alcock, R.A., and Hancock, R.G.
1979: The Noble Metal Content of Ore in the Levack West and Little Stobie Mines, Ontario; Canadian Mineralogist, Volume 17, p.437-452.

Hutchinson, R.W., Fyfe, W.S., and Kerrich, R.
1980: Deep Fluid Penetration and Ore Deposition; Minerals Science Engineering, Volume 12, p.107-118.

Innes, D.G., and Colvine, A.C.
1979: Metallogenetic Development of the Eastern Part of the Southern Province of Ontario; *in* Summary of Fieldwork, 1979, edited by V.G. Milne et al., Ontario Geological Survey, Miscellaneous Paper 90.

Keele, R.H. and Nickel, E.H.
1974: The Geology of a Primary Millerite-Bearing Sulphide Assem-

blage and Supergene Alteration; Economic Geology, Volume 69, p.1102-1117.

Kinloch, E.D.
1982: Regional Trends in the Platinum-Group Mineralogy of the Critical Zone of the Bushveld Complex, South Africa; Economic Geology, Volume 77, p.1328-1347.

Koulomzine, T.
1955: Unpublished Report on Dolmac Mines Limited Property, Rathbun Township, District of Sudbury, File 63-6035; Assessment File Research Office, Ontario Geological Survey, Toronto.

McCallum, M.E., Loucks, R.R., Carlson, R.R., Cooley, E.F., and Doerge, T.A.
1976: Platinum Metals Associated with Hydrothermal Copper Ores of the New Rambler Mine, Medicine Bow Mountain, Wyoming; Economic Geology, Volume 71, p.1420-1429.

Mostert, A.B., Hoffmeyer, P.K., and Potgieter, G.A.
1982: The Platinum-Group Mineralogy of the Merensky Reef at the Impala Platinum Mines, Bophuthatswana; Economic Geology, Volume 77, p.1385-1394.

Naldrett, A.J. and Duke, J.M.
1980: Platinum Metals in Magmatic Sulfide Ores; Science, Volume 208, p.1417-1428.

Naldrett, A.J., Innes, D.G. and Sowa, J.M.
1980: Platinum Group Element Concentration in Some Magmatic Ores in Ontario: p.171-178 in Geoscience Research Grant Program, Summary of Research 1979-1980, edited by E.G. Pye, Ontario Geological Survey Miscellaneous Paper 93.

Parthe, and Crocket, J.H.
1972: Platinum Group Minerals, *in* Handbook of Geochemistry 2-5, edited by K.H. Wedepohl, Springer-Verlag, Berlin.

Phillips, G.N., and Groves, D.I.
1983: The Nature of Archean Gold-Bearing Fluids as Deduced from Gold Deposits of Western Australia; Journal of the Geological Society of Australia, Volume 30, p.25-39.

Rahmdor, P.
1980: The Ore Minerals and Their Intergrowths; Pergamon Press, Toronto, 1205p.

Rowell, W.F.
1984: Platinum Elements and Gold in the Wanapitei-Nipissing Type Intrusion; Unpublished M.Sc. Thesis, University of Western Ontario, 86p.

Rowell, W.F., and Edgar, A.D.
1983: Petrology, Geochemistry and Economic Potential of the Nipissing Diabase; p.153-157 in Geoscience Research Grant Program, Summary of Research, 1982-1983, edited by E.G. Pye, Ontario Geological Survey, Miscellaneous Paper 113.

Grant 106 Platinum-Group Elements in Layered Intrusions

A.A. Borthwick and A.J. Naldrett

Department of Geology, University of Toronto

ABSTRACT

The Big Trout Lake layered intrusion, in northwestern Ontario, consists of peridotite overlain by anorthosite. The peridotite unit can be subdivided into lower and upper sub-units, based on contrasting major element compositions and rare earth element patterns. The lack of systematic major element and PGE trends in the lower peridotite sub-unit suggests that this unit crystallized in a magma chamber that received periodic magma influxes. The uniform chemical composition of the upper sub-unit suggests that it crystallized as a closed system, except for magma influxes marked by resorbed, re-entrant olivine. The formation of the re-entrant olivine layer is interpreted as the result of magmatic injection into a density stratified chamber, followed by magma 'roll-over' and mixing. By this process, the new magma was supercooled causing re-entrant olivine growth. Post-depositional reaction between the hot, trapped magma and the re-entrant olivine grains accounts for their resorbed boundaries.

PGE concentration decreases rapidly in the resorbed, re-entrant olivine interval suggesting this was a stagnant layer. Low Os, Ir, and Ru values in the net-textured sulphides may be attributed to their removal from the magma by chromite fractionation.

INTRODUCTION

Our first report (Borthwick and Naldrett 1982) emphasized the importance of determining the platinum-group element (PGE) distribution in layered intrusions. In this report PGE variation, with respect to magmatic processes that have been interpreted on the basis of silicate petrography and petrology, is outlined, and some mechanisms responsible for this variation are suggested.

Previous work has shown that PGE-rich ores occur at certain horizons in layered igneous complexes (Stillwater, U.S.A.; Bushveld, South Africa; Sudbury, Ontario). It is generally agreed that the sulphides separated as an immiscible sulphide liquid from a mafic magma. Sulphides have a wide range of PGE concentrations that can be attributed, in part, to the nature of their equilibration with their host silicate magma. Campbell and Naldrett (1978) showed that this can be expressed quantitatively as the ratio (R) of the mass of silicate magma to the mass of sulphide liquid. Sulphides that are rich in PGE equilibrated with a relatively large mass of silicate magma (and therefore at a high value of 'R'). A characteristic of PGE-rich sulphides in many layered intrusions is that they are located at the base of cyclic units that are believed to have been initiated by a new magma influx (Irvine and Smith 1967; Campbell 1977). Campbell *et al.* (1983) outlined a mechanism based on periodic magma injection which, under the right conditions, can achieve high 'R' values. Evidence for the arrival of new magma pulses and an understanding of factors leading to a high 'R' value could prove to be a useful tool in PGE exploration.

GENERAL GEOLOGY

The geology of the Big Trout Lake Complex was described by Hudec (1964) and Sage and Troop (1974) and is summarized in Figure 1, which includes a new interpretation of the northern limb of the syncline.

This investigation uses data collected from drill core through section A-A' and from exposures across section C-C'. The sequence of rock types and variations in mineral modal proportions with height are shown in Figures 2, 3, and 4. Peridotites are restricted to section A-A' and are capped by anorthosite. Section C-C' traverses the northern anticline. Rock types in section C-C' are dominantly magnetite-ilmenite-rich gabbro topped by quartz-bearing gabbro.

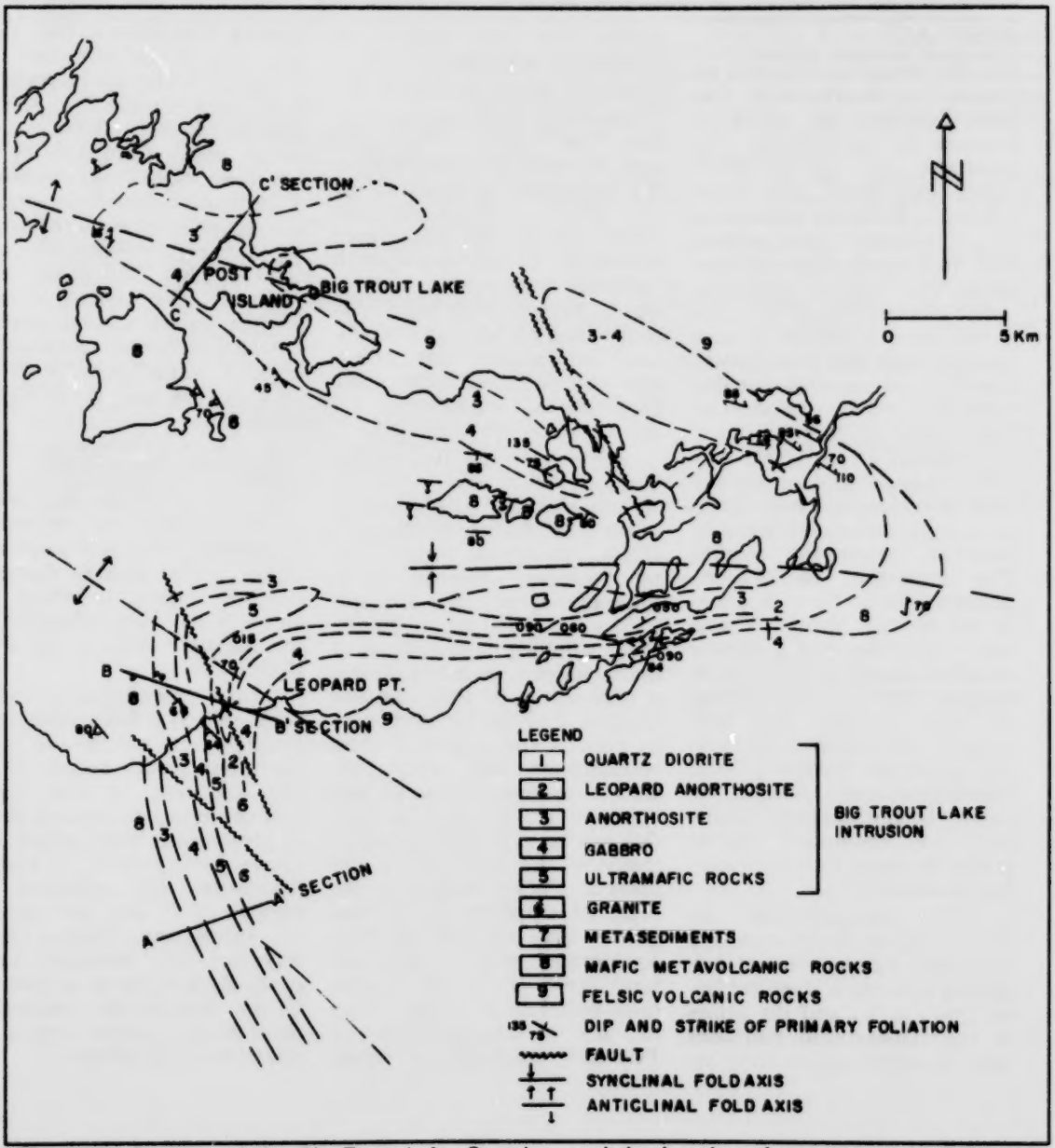

Figure 1. Geology of the Big Trout Lake Complex, and the location of traverses A-A', B-B', and C-C'.

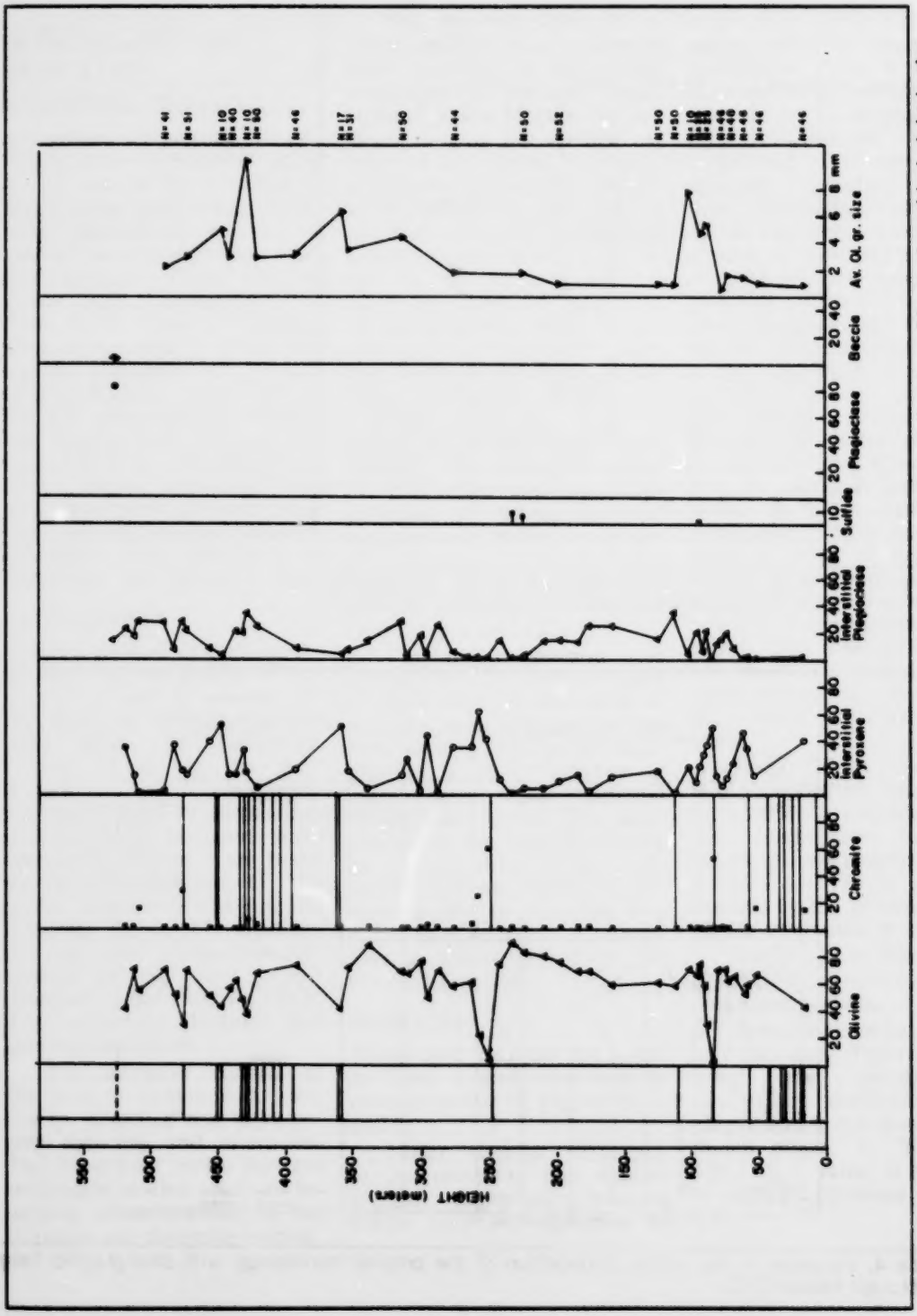

Figure 2. Variations in the modal proportion of the original mineralogy, and in olivine grain size with stratigraphic height in the peridotite unit of section A-A'. The olivine grain size is taken as the average of the long dimension, measured using a calibrated ocular; N = number of grains measured. Horizontal lines at the left of the figure represent re- entrant olivine layers, terminated horizontal lines in the sulphide column represent the modal proportion of sulphide for a particular height.

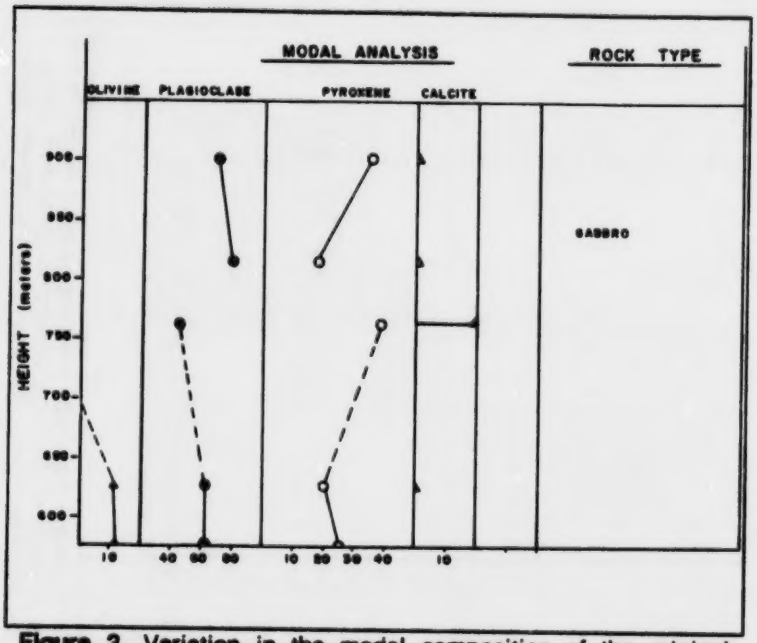

Figure 3. Variation in the modal composition of the original mineralogy with stratigraphic height in the gabbroic unit of section A-A'.

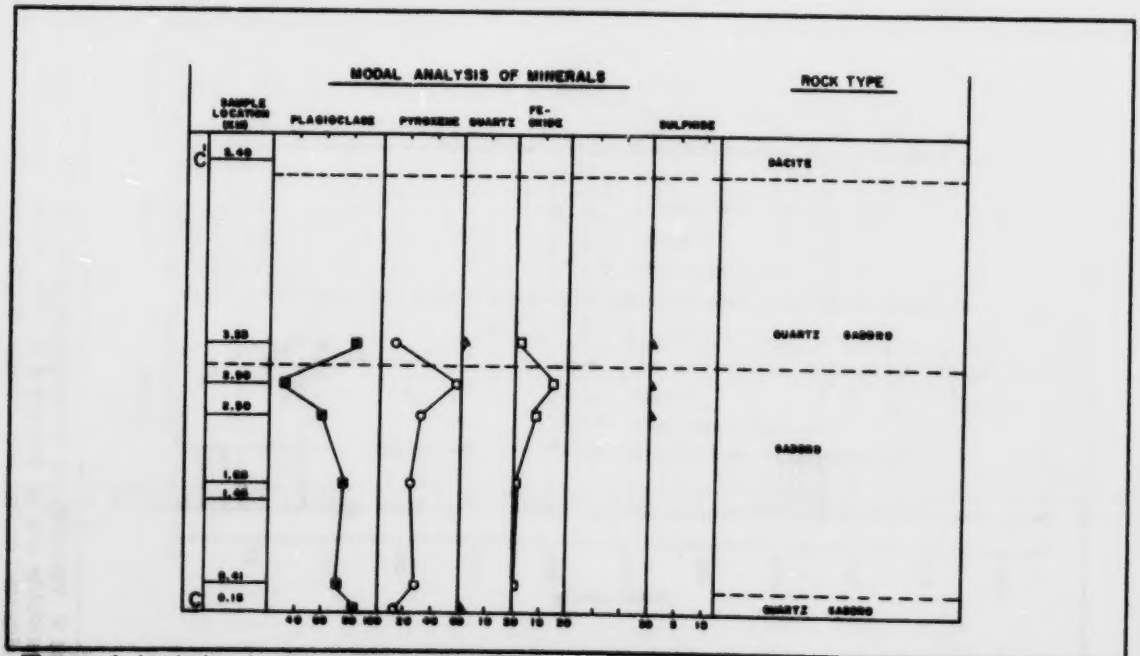

Figure 4. Variation in the modal composition of the original mineralogy with stratigraphic height through section C-C'.

PETROGRAPHY AND PETROLOGY

ANALYTICAL TECHNIQUE

Anhydrous whole-rock compositions were determined using an automated Siemens X-Ray fluorescence unit. Na_2O values were determined by instrumental neutron activation analysis (INAA). Trace element values were obtained by XRF. Rare earth element analyses were determined by INAA using the University of Toronto SLOWPOKE-II reactor following the procedure of Barnes and Gorton (1984). Since our first report on the Big Trout Lake Complex, additional PGE data have been obtained using the modified fire-assay preconcentration step described by Borthwick and Naldrett (1983).

PETROGRAPHY

Vertical profiles of sections A-A' and C-C' are shown in Figures 2, 3, and 4; detailed descriptions of these variations were given by Borthwick (1984). Olivine in the peridotites is completely pseudomorphed by serpentine, and the modal variations summarized in Figure 2 are based on the interpretation of preserved outlines of the original minerals. Details of variations in this unit have been described in our first report (Borthwick and Naldrett 1982). The important features are summarized below.

The intrusive contact at the base of section A-A' cannot be identified due to extensive shearing and alteration. The lowermost rocks that are recognized in this study as belonging unambiguously to the intrusion are chromite-bearing.

The interval from 84 to 110 m is characterized by a sharp increase in the modal proportion of olivine. These olivine grains (Figure 5) are large, ranging on average between 4 and 8 mm in length, and have a skeletal shape. Their boundaries are heavily resorbed. Layers of similar skeletal olivine grains occur at 360 m, 431 m and 448 m. They are underlain by a thin chromite layer, except in one case (360 m), where the chromite layer occurs immediately above the skeletal olivine.

The peridotite unit is capped by an anorthositic unit (Figure 3) consisting of cumulus plagioclase and interstitial pyroxene. At 760 m, the rocks are markedly richer in pyroxene. Further drilling is required to determine the complete chemical variation through this section.

The modal variation over section C-C' is shown in Figure 4. Here our interpretation of the structure (Figure 1) has been used to arrange the samples in what is believed to have been their original stratigraphic order. The mineralogy at the base is marked by cumulus ilmenite and magnetite; upwards, the rocks become poorer in pyroxene and richer in plagioclase. A quartz-bearing gabbro occurs at the top of the section.

PETROLOGY

Whole-rock analyses are given in Table 1 and illustrated in vertical profile in Figures 6, 7, and 8.

Major element variations in the peridotite unit exhibit several important features which may be explained in terms of an open or closed system at different stages of crystallization. From 50 to 84 m, MgO shows an overall increase from 26 to 33 weight percent. Over this interval, the modal proportion of olivine is fairly constant, suggesting that, over time, the magma chamber was an open system, receiving successive or continuous influxes of more primitive magma, as a result of which the olivine became progressively more forsteritic. In the interval from 84 to 110 m, MgO increases in tandem with an increase in the modal proportion of olivine. This is the portion of the section over which olivine has a skeletal morphology which is interpreted as the consequence of it having crystallized from a supercooled liquid. If this is the case, it is probable that the olivine composition is somewhat less forsteritic than it would otherwise have been. The combination of these effects can account for the overall increasing MgO trend.

From 110 to 190 m, the bulk composition remains fairly constant, consistent with there having been further influxes of new magma. The interval from 190 to 250 m is marked by the presence of sulphides interstitial to olivine.

Above 250 m, there are no significant changes in the peridotite composition.

The composition of the gabbroic unit (Figure 7) overlying the peridotite is Al_2O_3-rich confirming that plagioclase is the dominant cumulus phase. At 760 m the high MgO value is attributed to cumulus pyroxene.

TABLE 1. MAJOR, TRACE AND RARE EARTH ELEMENT DATA.

PERIDOTITE Sample	133	134	135	136	137	138	139	1312	1313	1316	1322	1327
SiO_2	44.99	49.04	47.25	45.84	42.20	41.33	39.36	40.96	42.13	41.52	40.63	39.62
TiO_2	0.06	0.06	0.15	0.27	0.17	0.12	0.15	0.23	0.19	0.06	0.09	0.06
Al_2O_3	2.18	2.32	2.48	2.83	2.24	3.13	4.54	2.84	3.81	3.32	2.78	2.02
Fe_2O_3	10.29	8.35	10.26	13.01	8.81	10.85	14.68	17.82	18.45	14.09	14.61	17.06
MnO	0.06	0.07	0.17	0.15	0.14	0.13	0.11	0.20	0.22	0.15	0.17	0.19
MgO	39.14	32.64	26.31	30.00	28.63	33.07	32.43	35.43	34.20	40.52	39.78	39.06
CaO	1.70	5.80	10.15	5.28	13.42	6.66	4.54	1.13	1.99	0.24	0.59	0.82
Na_2O	0.02	0.04	0.00	0.04	0.05	0.05	0.05	0.00	0.00	0.05	0.00	0.00
K_2O	0.03	0.04	0.04	0.05	0.04	0.04	0.03	0.05	0.06	0.05	0.02	0.02
P_2O_5	0.05	0.03	0.07	0.00	0.04	0.04	0.03	0.06	0.06	0.03	0.04	0.00
Total	98.52	98.41	96.88	97.47	95.74	95.44	95.92	98.72	101.11	100.05	98.71	98.87
S	0.99	1.22	0.90	0.60	0.47	0.80	1.32	1.66	1.63	0.49	0.69	1.62
NiO	0.33	0.29	0.42	0.22	0.28	0.60	0.46	0.43	0.38	0.18	0.24	0.37
CuO	0.05	0.21	0.22	0.05	0.14	0.02	0.09	0.13	0.16	0.02	0 07	0.30
CoO	0.02	0.02	0.02	0.01	0.02	0.03	0.03	0.02	0.02	0.02	0.02	0.02
Cr_2O_3	0.38	0.33	1.33	1.52	0.81	0.50	0.48	0.51	0.41	0.31	0.50	0.60
Total	100.29	100.48	99.77	99.87	97.46	97.39	98.30	101.47	103.71	101.07	100.23	101.78
Trace elements (ppm)												
Y	1.70	2.21	3.27	4.41	2.86	3.78	2.90	2.95	3.46	1.35	1.33	1.01
Sc	7.30	7.50	11.76	21.14	ns	9.73	11.82	15.41	12.70	8.68	8.34	7.02
Rare Earth Elements												
La	9.1	3.5	6.9	5.1	33.1	9.0	4.5	2.3	3.1	1.8	0.8	1.3
Sm	2.3	1.9	2.7	3.9	17.2	3.4	2.0	2.1	2.1	0.9	0.8	0.5
Eu	1.0	1.4	1.4	2.4	ns	1.8	1.3	4.3	2.7	1.1	0.8	0.7
Lu	1.3	1.0	1.9	1.8	1.6	1.3	1.5	1.9	1.7	1.1	1.1	nd
La/Lu	7.0	3.5	3.6	2.8	20.9	6.9	3.0	1.2	1.8	1.6	0.7	-

nd = not detected
ns = not analysed
Section A-A': lower peridotite = 133 - 138, upper peridotite = 139 - 14-258
Sample location in metres above the base of the intrusion.

TABLE 1. CONTINUED

PERIDOTITE Sample	1330	1332	1334	1336	10-142	10-230	10-365	10-464	10-650	14-90	14-258
SiO_2	35.66	38.06	38.34	38.51	41.05	42.48	42.55	42.26	41.64	44.92	45.10
TiO_2	0.08	0.09	0.06	0.22	0.10	0.10	0.08	0.16	0.09	0.09	0.20
Al_2O_3	1.39	1.80	1.73	4.29	3.95	4.14	3.86	2.95	4.18	4.36	5.17
Fe_2O_3	23.90	20.97	20.39	15.60	14.26	13.66	12.41	12.81	13.96	11.87	12.05
MnO	0.17	0.17	0.19	0.26	0.14	0.15	0.13	0.14	0.12	0.11	0.10
MgO	36.16	36.76	36.27	34.95	37.22	37.00	39.34	35.92	37.35	34.60	34.31
CaO	0.55	0.69	1.24	0.60	1.30	1.51	0.84	5.54	2.34	2.45	2.26
Na_2O	0.00	0.00	0.00	0.00	0.02	0.03	0.03	0.04	0.04	0.06	0.07
K_2O	0.02	0.03	0.01	0.02	0.07	0.03	0.04	0.04	0.03	0.07	0.07
P_2O_5	0.02	0.03	0.02	0.01	0.02	0.03	0.01	0.02	0.02	0.02	0.04
Total	97.95	98.40	100.25	94.46	98.13	99.13	99.29	99.88	99.77	98.55	99.37
S	1.27	1.86	1.87	0.11	0.04	0.05	0.05	0.06	0.11	0.21	0.03
NiO	0.27	0.37	0.31	0.18	0.14	0.16	0.18	0.13	0.15	0.21	0.29
CuO	0.16	0.30	0.31	0.00	0	0	0	0	0	0	0.30
CoO	0.02	0.04	0.02	0.01	0.01	0.01	0.02	0.01	0.02	0.02	0.02
Cr_2O_3	0.57	0.60	0.09	3.52	0.61	0.37	0.35	0.64	0.32	0.89	0.68
TOTAL	100.24	101.57	102.85	98.28	98.93	99.72	99.89	100.72	100.37	99.88	100.69
Trace elements (ppm)											
Y	1.3	1.1	1.9	3.1	1.5	1.9	2.0	3.2	2.1	3.3	3.0
Sc	7.8	na	7.8	12.1	10.4	10.2	10.5	12.7	9.8	12.2	15.0
Rare Earth Elements (chondrite normalized)											
La	0.9	2.7	1.7	2.2	1.9	2.5	0.9	2.0	0.9	3.4	3.1
Sm	0.5	0.6	1.1	2.0	1.2	1.1	1.1	1.6	1.3	2.1	1.9
Eu	nd	nd	nd	3.6	nd	nd	nd	nd	nd	nd	nd
Lu	0.7	nd	nd	nd	1.3	1.3	1.4	2.1	1.2	2.3	2.3
La/Lu	1.3	-	-	-	1.5	1.9	0.6	0.9	0.7	1.5	1.3

na = not analysed
nd = not detected

TABLE 1. CONTINUED

ANORTHOSITE-GABBRO Sample	271	273	275	279	1b	2a	3a	17	20	21	22	23
SiO_2	46.64	49.83	49.47	46.77	53.80	45.40	51.24	47.82	51.43	47.04	42.18	50.63
TiO_2	0.31	0.67	0.30	0.12	0.73	0.31	0.37	0.95	0.74	2.77	3.99	0.52
Al_2O_3	22.35	15.50	4.47	26.35	13.97	23.57	23.97	24.90	22.44	20.28	13.62	26.05
Fe_2O_3	7.02	8.93	11.51	4.34	9.15	8.00	6.62	8.59	10.35	13.29	20.66	4.68
MnO	0.08	0.16	0.15	0.09	0.09	0.09	0.08	0.08	0.09	0.17	0.23	0.10
MgO	8.56	9.48	21.21	4.75	9.36	7.75	5.03	2.57	3.88	4.41	6.93	1.32
CaO	12.62	14.51	13.42	13.69	8.99	9.77	9.95	11.65	8.27	9.92	10.51	13.02
Na_2O	0.07	0.81	0.06	2.82	3.70	1.93	3.20	2.90	3.53	3.63	2.00	3.50
K_2O	0.67	0.12	0.05	0.69	0.12	0.13	0.06	0.64	0.47	0.12	0.02	0.25
P_2O_5	0.05	0.07	0.03	0.02	0.09	0.05	0.02	0.04	0.03	0.04	0.04	0.22
Total	98.37	100.08	100.67	99.64	100.00	97.00	100.54	100.14	101.23	101.67	100.18	100.29
Trace elements (ppm)												
Zr	11	34	6	1	38	7	17	14	7	6	10	36
Y	6	15	7	3	22	7	8	7	8	5	7	13
Sr	98	68	3	141	63	111	105	205	126	180	113	207
Sc	16	38	47	17	52	na	23	20	36	na	47	13
Co	30	41	70	23	37	na	35	41	45	na	88	32
Cr_2O_3	220	515	2291	535	77	147	na	47	51	na	5	4
Rare earth elements (chondrite normalized)												
La	4.3	7.3	1.0	1.9	9.0	6.9	7.0	7.8	4.9	4.5	3.0	11.7
Ce	3.4	4.9	0.9	1.5	12.1	na	7.1	4.3	6.5	na	4.7	13.1
Sm	3.0	7.8	2.1	1.5	15.0	3.4	5.1	5.4	5.4	3.1	4.1	10.4
Eu	3.8	6.9	nd	nd	12.8	na	4.3	14.2	8.8	na	5.3	14.0
Yb	2.6	9.7	3.2	1.2	12.0	4.4	4.6	4.5	5.2	2.8	4.4	6.8
Lu	3.7	8.0	3.7	1.7	13.9	4.2	6.0	4.8	5.5	4.1	5.4	8.2
La/Lu	1.2	0.9	0.3	1.1	0.6	1.6	1.1	1.6	0.9	1.1	0.6	1.4

na = not analysed
nd = not detected
section A-A' = 271-279; section B-B' = 1a,2a,3a; section C- C' = 17,20,22,23

TABLE 1. CONTINUED

Sample	QUARTZ DIORITE 24	BASALT 1a	BASALT 25
SiO_2	64.84	51.31	54.92
TiO_2	0.52	1.02	2.20
Al_2O_3	15.65	14.90	12.98
Fe_2O_3	4.54	13.20	18.22
MnO	0.05	0.18	0.27
MgO	2.36	6.80	5.58
CaO	4.56	10.02	3.88
Na_2O	4.09	2.06	2.06
K_2O	3.19	0.11	0.27
P_2O_5	0.14	0.10	0.52
Total	99.94	99.72	100.92
Trace elements (ppm)			
Zr	158	80	370
Y	12	17	95
Sr	498	126	93
Sc	10	32	34
Co	58	62	33
Cr_2O_3	65	280	8
Rare earth elements (chondrite normalized)			
La	93.6	17.7	67.8
Ce	83.4	17.7	76.5
Sm	27.3	12.6	60.1
Eu	15.2	12.5	45.6
Yb	5.2	8.1	51.9
Lu	5.5	8.0	61.4
La/Lu	17.0	2.2	1.1

Sample 24 and 25 are from section C-C'
Sample 1a is from section B-B'

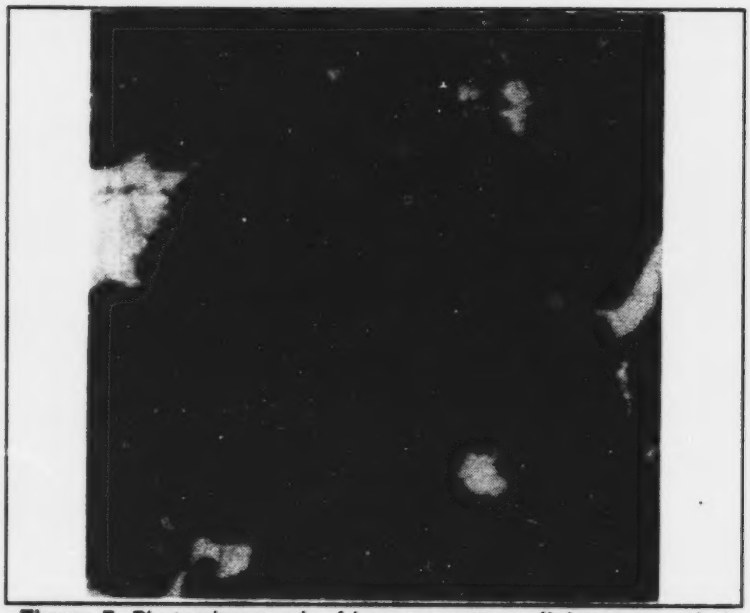

Figure 5. Photomicrograph of large re-entrant olivine surrounded by interstitial plagioclase (light) and interstitial pyroxene (dark). Notice the chromite inclusions in olivine. Diagonal field of view is 2 cm.

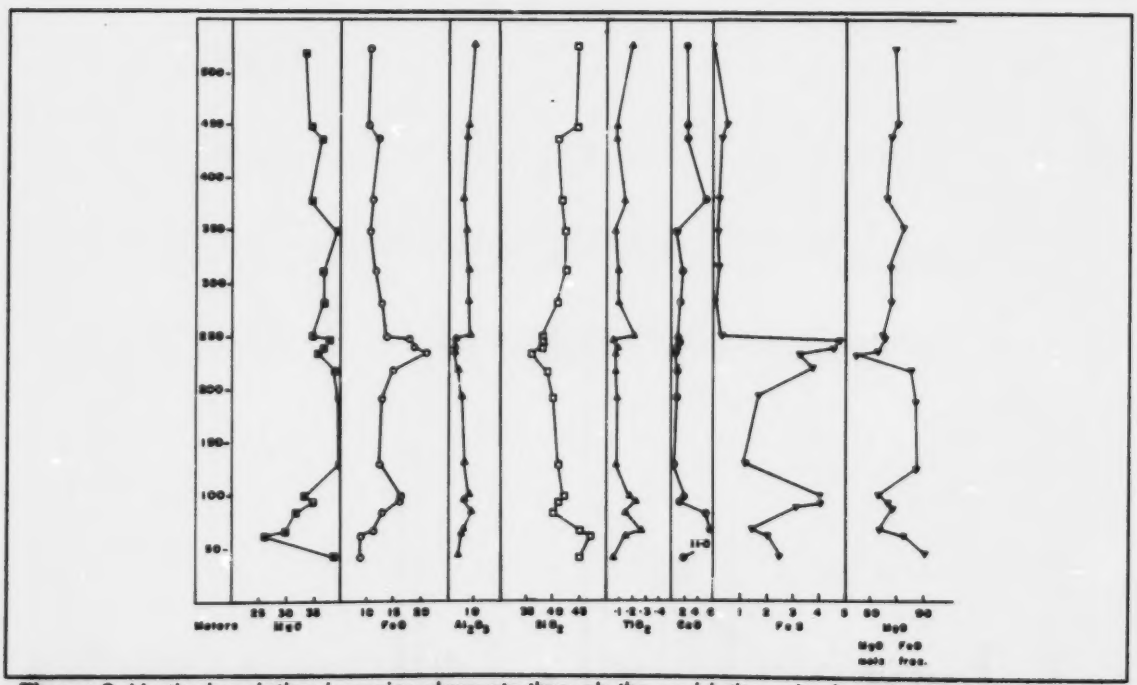

Figure 6. Vertical variation in major elements through the peridotite unit of section A-A'.

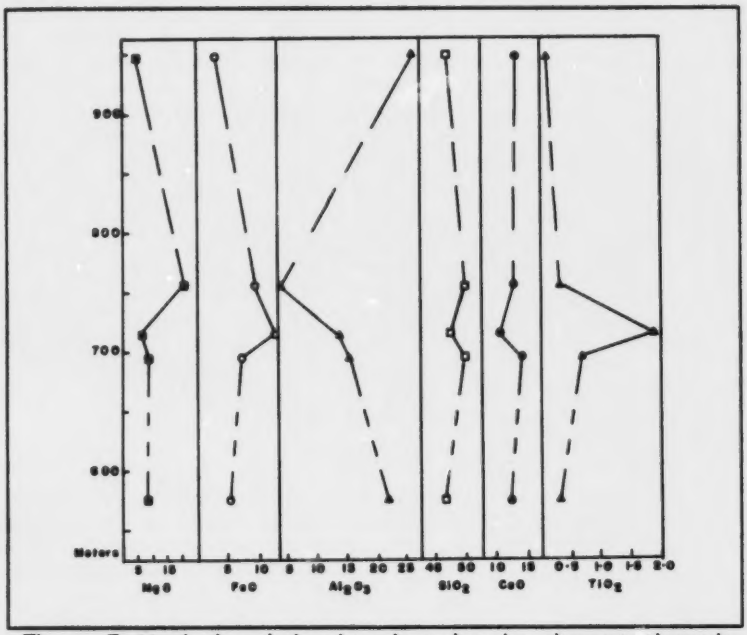

Figure 7. Vertical variation in selected major elements through the gabbro unit of section A-A'.

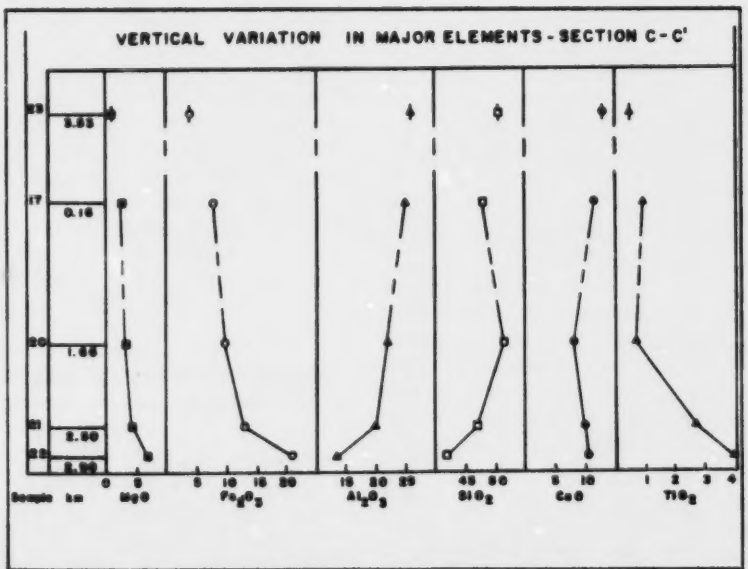

Figure 8. Vertical variation in selected major elements through section C-C'.

EVIDENCE FOR TWO CHEMICALLY DISTINCT MAGMAS

It is suggested that the Big Trout Lake peridotite unit may have formed from two magmas different in their concentrations of both major and rare earth elements.

MAJOR ELEMENT DATA

The mole fraction plot $(MgO+FeO)/Al_2O_3$ vs SiO_2/Al_2O_3 is shown in Figure 9. Points representing analyses of peridotite from below the re-entrant olivine layer plot to the right of those representing peridotite overlying this layer, suggesting that two contrasting parent magma compositions are involved. Linear regressions of these analyses are approximately parallel, each having a slope of 2:1 confirming that olivine is the only major cumulus phase.

RARE EARTH ELEMENT DATA

Rare earth element patterns from above and below 84 m are shown in Figure 10. Two parent magmas are identified by their significantly different rare earth element slopes. The lower peridotite has a rare earth element pattern with a La/Lu slope of approximately 5:1 compared to a ratio from the upper peridotite of approximately 1:1. An exception is sample 139 from the upper group which has a slope of 3:1. This sample is located at the base of the skeletal olivine layer, and may be the result of mixing between magmas responsible for the upper and lower peridotites.

Rare earth element patterns strongly suggest that two chemically distinct ultramafic magmas, derived from separate melting events, intruded the

Big Trout Lake area. Rare earth element slopes indicate that the parent magma for the lower peridotite was either the result of a lower degree of partial melting or was derived from a more fertile source than that for the upper peridotite.

MODELLING

Re-Entrant Olivine Model

The lowest re-entrant olivine layer has a relatively thick chromitite at the base, immediately overlain by very small, spherical olivine granules and chromite for a distance of 20 cm; this is overlain by 26 m of re-entrant olivine. Frequently, the larger amoeboidal re-entrant grains contain chromite inclusions. Olivine grain boundaries are strongly resorbed. Most of the interstitial space is occupied by pyroxene, plagioclase and a minor amount of sulphides. A similar olivine morphology has been described in the Tertiary Rhum pluton (Harker 1908; Wager and Brown 1951; Brown 1956; Donaldson 1974).

Major element and rare earth element data indicate a new magma influx above 84 m. It would seem reasonable, therefore, that models attempting to explain the layer of resorbed, re-entrant olivine should invoke this magma injection. They must also explain the observed layering of chromite – granular olivine + chromite – re-entrant olivine + chromite. Stokes's law can be used to calculate the settling rate of these three crystal types, re-entrant and granular olivine, and chromite.

$$V = \frac{9.g.r^2.(d_s-d_l)}{2n}$$

where d_l and d_s are the specific gravity of the magma and solid, respectively, r is radius, and n is the viscosity in poise. In using this equation a density of 5.0 g/cm^3 was assumed for chromite, 3.3 g/cm^3 for olivine, and 2.7 g/cm^3 for the liquid (McBirney and Noyes 1979). The average diameters for the re-entrant olivine grains are given in Figure 2. Histograms of measured granular olivine and chromite radii are shown in Figure 11. Values of 0.8 mm for olivine and 0.5 mm for chromite are used in the relative settling rate calculation; densities used are the same as those given above. Solving this equation shows that re-entrant olivine would settle most rapidly and chromite 1.6 times as fast as the granular olivine. The formation of chains and doublets chromite would increase its settling rate. Since the re-entrant olivine overlies the other two crystal types, it would seem that it must have crystallized last. The granular olivine may have formed at the same time as the chromite, with the latter sinking more rapidly to form the basal layer.

The following sequence of events is suggested to account for the compositional break between the upper and lower peridotite and for the chromite and re-entrant olivine that mark this break.

Prior to magma injection, the magma chamber (Figure 12) was gravity stratified (Campbell *et al.* 1983), consisting of several layers of doubly diffusive convection cells. A new magma (C) with olivine and chromite on its liquidus, was injected into the chamber (Campbell *et al.* 1983). As it was hot and therefore, more buoyant, it rose to its equivalent density level and spread out between layers A and B. Chromite and olivine settled from liquid C to form the basal chromite layer. As liquid C cooled, its density increased such that it became more dense than the underlying layer, A. Due to this density instability, perturbations at the interface A-C developed which grew into fingers that penetrated layer A. Eventually, complete convective turn-over (Campbell *et al.* 1983) occurred, resulting in the mixing of liquids A and C. This mixing of magmas resulted in supercooling which gave rise to the crystallization of the re-entrant olivine. The sulphide liquid was probably not present before the magmas mixed. Magma mixing (Irvine 1977) and/or cooling are believed to cause sulphide precipitation. Reaction between the trapped liquid and the enclosing re-entrant olivine resulted in the resorption of the olivine and the production of pyroxene.

It is postulated that each layer of re-entrant olivine corresponds to a new magma influx, similar to the model described above for the lowest layer. This interpretation is supported by the presence of chromite-rich layers at the base of each re-entrant olivine layer except in one case. This model implies that five cyclic units are present in the peridotite unit (the lower peridotite unit and four upper peridotite units) as shown in Figure 2.

GEOCHEMISTRY OF THE SULPHIDES

PGE data obtained for sulphide-bearing samples are given in Table 2 and are shown graphically in vertical profile in Figure 13. The data re-calculated to 100% sulphide (Table 3) are presented in Figure 14.

The lack of systematic variation below 84 m may be

interpreted as the consequence of repeated magma influxes due to this interval crystallizing as an open system, as is indicated by the variation in rock-forming elements.

The interval from 84 to 110 m is characterized by reentrant, resorbed olivine and interstitial sulphide droplets. The tenor of all PGE decreases systematically upwards through the section suggesting that this interval crystallized as a closed system, with the PGE being depleted rapidly as sulphides segregated.

At 110 m the sharp increase in Pt, Pd and Rh in the recalculated samples, with no major variation in the raw data except for a decrease in S, is almost certainly an artifact of sulphur loss during alteration of the samples.

The base of the interval from 110 to 250 m is characterized by a low sulphur content gradually increasing to several weight percent sulphur in the net-textured sulphides. High Pd and Pt and fairly high Rh, but very low Os, Ir, and Ru tenors, are associated with the net-textured sulphides. The low tenors of Os, Ir, and Ru are suggestive that these metals may have been removed from the magma prior to the sulphide immiscibility that gave rise to the net-textured zone. Chromite and olivine are the dominant phases in the rocks of the interval beneath this zone. Only low levels of Ir (approximately 0.1 ppb) have been detected in olivine separates (Mitchell and Keays 1982). Variable but consistently high concentrations of OPM (osmium-platinoid metals, Os, Ir, Ru) are associated with chromite (Page *et al.* 1976; Oshin and Crocket 1982; Argiorgitis and Wolf 1978). Chromite fractionation could thus account for the low OPM tenor of the sulphides of the net-textured zone.

The sharp peak at 250 m in the recalculated diagram (Figure 14) is partly attributable to sulphur loss. However, in this sample there is a high OPM content in relation to Pt and Pd. This sample is also rich in Cr suggesting a correlation between OPM and Cr.

Analyses in the interval above 256 m are characterized by very low PGE values, except at 380 m where a high PGE content is associated with low sulphur. Due to the low sulphur content of these samples, they calculate to have a high PGE tenor; this is probably spurious and the result of sulphur loss causing us to underestimate the amount of sulphide originally present. For this reason, recalculated data are not shown for this interval in Figure 14.

Platinum Group Element Patterns

The silicate chemistry suggests the peridotites lying between 84 and 256 m crystallized in a closed system. As discussed above, an interesting feature of this interval is the low OPM values in the net-textured sulphides.

Comparison of Re-Calculated PGE Patterns

Since, as has been shown, the PGE are likely to be associated with either sulphide or chromite, data for the upper peridotite has been re-calculated to 100% sulphide and 100% chromite (Figures 16 and 17 respectively). For concentrations falling below the detection limit, the convention has been adopted in constructing these diagrams of using half of the detection limit value to calculate the amount of PGE in 100% sulphide and 100% chromite. A comparison of the raw data (Figure 15) and the recalculated data to 100% sulphide shows substantially reduced vertical scatter for the bulk of the data, confirming that PGE are held in sulphides. Samples 1335 and 1336 are above most of the recalculated plots, particularly for OPM, implying that these samples are enriched in OPM compared to the norm.

Several important differences become apparent when the plots of 100% sulphide and 100% chromite are compared. PGE data re-calculated to 100% chromite define a narrow field for Os, Ir, and Ru; however the field is substantially wider for Pt, Pd, and Au. Samples 1335 and 1336 fall within the field defined by the bulk of the data for Os, Ir, Ru, and below the field for Pt, Pd and Au. This observation implies that these samples have typical OPM tenors but low Pt, Pd and Au tenor.

Comparing the standard deviations (Table 4) shows that lower standard deviations are associated with Os, Ir, and Ru, and higher standard deviations for Pt, Pd and Au when the data are re-calculated to 100% chromite in comparison with re-calculation to 100% sulphide. This observation suggests that sulphides have a major control on the distribution of Pt, Pd, and Au, whereas chromite has a significant control on Os, Ir, Ru and possibly Rh, and relatively little control on Pt, Pd and Au. This conclusion is reinforced if total Ru + Ir + Os is plotted against the Cr content of the sample, as seen in Figure 18. The high Cr samples are very much richer in the OPM.

TABLE 2. CONCENTRATION OF NOBLE METALS.

Sample	Metres	S	Cu	Co	Ni	Cr	Pt	Pd	Rh	Ru	Ir	Os	Au
133	40	0.99	0.04	0.015	0.26	0.20	48	230	8	22	5	10	27
134	41	1.22	0.17	0.013	0.23	0.21	80	267	9	28	10	12	36
135	50	0.90	0.09	0.017	0.33	0.80	86	192	11	18	10	12	17
136	53	0.60	0.04	0.015	0.21	1.01	100	245	19	<14	2	<2	na
137	58	0.47	0.11	0.013	0.24	0.56	105	295	22	<3	2	<1	na
138	80	0.80	0.02	0.022	0.50	0.32	156	257	8	13	6	8	24
139	87	1.32	0.07	0.028	0.35	0.26	98	220	14	14	3	5	12
1310	91	1.44	0.10	0.021	0.28	0.38	60	238	13	9	3	2	12
1312	95	1.66	0.10	0.021	0.28	0.59	44	265	10	<8	1	2	2
1313	101	1.63	0.13	0.027	0.35	0.27	230	163	12	<8	2	2	14
1314	102	1.60	0.10	0.031	0.31	0.26	180	182	9	<9	2	2	13
1314a	108	0.29	tr	0.017	0.20	0.64	61	67	10	1	<1	<1	na
1315	124	0.60	0.03	0.013	0.08	0.30	43	69	4	12	<1	2	8
1316	130	0.49	0.02	0.017	0.16	0.19	26	68	3	<6	<1	2	5
1317	160	0.39	0.02	0.021	0.24	0.28	34	64	3	<6	<1	2	4
1318	175	0.65	0.04	0.018	0.24	0.26	20	132	4	8	1	2	4
1319	183	1.01	0.06	0.020	0.25	0.25	42	114	5	7	<1	<1	7
1323	194	1.52	0.08	0.028	0.36	0.27	66	88	9	<8	1	2	5
1324	199	0.91	0.02	0.025	0.29	0.30	19	108	7	<8	<1	<2	6
1325	209	0.77	0.07	0.026	0.22	0.22	40	129	11	6	2	2	6
1326	214	2.12	0.10	0.033	0.31	0.26	137	112	20	12	2	<2	23
1327	219	1.62	0.24	0.027	0.32	0.39	77	136	11	<5	2	<1	16
1329	225	1.02	0.09	0.022	0.23	0.34	30	98	4	<7	<1	<1	21
1331	230	2.94	0.17	0.032	0.35	0.31	136	212	18	<11	3	<2	23
1333	241	2.46	0.10	0.020	0.28	0.05	141	476	15	<15	1	<2	19
1334	243	1.87	0.10	0.020	0.22	0.05	53	724	11	<16	<1	<2	20
1335	250	0.07	0.00	0.000	0.07	15.30	200	281	104	290	38	38	na
1336	256	0.11	0.00	0.016	0.13	2.49	16	0	4	32	4	5	1
10-142	287	0.04	0.00	0.007	0.15	0.42	nd	<20	<1	8	<1	<1	1
10-230	314	0.05	0.00	0.012	0.12	0.26	14	10	3	<1	1	<1	2
10-355	352	0.05	tr	0.014	0.14	0.23	nd	nd	nd	nd	nd	nd	1
10-454	382	0.06	0.00	0.009	0.10	0.44	50	36	12	<1	1	<1	18
10-650	442	0.11	0.00	0.010	0.12	0.23	<6	<15	<1	<3	<1	<1	1
14-90	461	0.21	tr	0.016	0.16	0.61	<8	<20	4	<7	1	2	1
14-258	520	0.03	0.02	0.015	0.23	0.47	<11	<15	10	<1	3	2	10
C-1							1021	545	200	690	540	514	152

tr = trace, nd = below detection limit. C-1 = Carbonaceous Chondrite (Naldrett and Duke 1980).
Ni, Cu, Co, Cr_2O_3 in wt percent, platinum group elements and Au in ppb.
Ni, Co, Cr_2O_3 determined by INAA at Slowpoke and Erindale Research Laboratories.
Cu and S determined by XRF by X-Ray Assay Laboratories Ltd.
Platinum group elements and Au determined by fire assay and INAA.
Samples 133 - 138 = lower peridotites.
Samples 139 - 14-258 = upper peridotites.

TABLE 3. CONCENTRATION OF NOBLE METALS IN 100% SULPHIDE.

Sample	metres	S	Cu	Co	Ni	Pt	Pd	Rh	Ru	Ir	Os	Au	alpha factor	beta factor
133	40	35.23	1.42	0.64	2.85	1708	8186	285	782	178	356	961	35.59	180
134	41	35.53	4.95	0.47	1.75	2330	7775	262	815	291	349	1048	29.12	171
135	50	33.50	3.35	0.81	7.07	3201	7146	409	670	372	447	633	37.22	45
136	53	35.16	2.34	0.82	2.93	5861	14652	1113	<820	176	117	na	58.61	36
137	58	33.62	7.91	0.94	5.76	7555	20506	1583	<216	142	<72	na	71.95	64
138	80	31.17	0.78	0.86	13.25	6078	10013	312	4870	234	311	935	38.96	112
139	87	34.40	1.82	0.73	4.95	2554	5733	365	365	78	130	313	26.06	138
1310	91	35.16	2.44	0.61	2.93	1465	5812	317	195	73	49	293	24.42	95
1312	95	35.32	2.13	0.45	2.55	936	5639	212	<170	21	43	43	21.28	103
1313	101	34.72	2.77	0.56	4.05	4899	3472	256	<170	43	43	298	21.30	133
1314	102	35.04	2.19	0.68	3.29	3942	3986	197	<197	43	43	285	21.90	138
1314a	108	34.49	2.37	2.02	4.15	7256	7970	1190	<119	<118	<118	na	118.96	56
1315	124	34.56	1.73	0.75	0.58	2475	3971	230	691	<58	115	461	57.56	120
1316	130	32.22	1.31	1.12	0.68	1710	4472	197	<396	<66	132	329	65.76	189
1317	160	33.63	1.72	1.81	6.90	2932	5519	259	<517	<86	172	345	86.23	129
1318	175	34.65	2.13	0.96	4.26	1066	7037	213	426	53	106	213	53.31	138
1319	183	35.10	2.08	0.70	3.13	1460	3962	174	243	<35	<35	243	34.75	144
1323	194	34.55	1.83	0.64	4.54	1500	2000	205	<182	23	46	114	22.73	133
1324	199	34.45	0.76	0.95	4.92	719	4069	265	<303	<38	<76	227	37.86	120
1325	209	35.20	3.20	1.19	2.74	1829	5898	503	274	91	91	274	45.72	163
1326	214	35.36	1.66	0.55	2.50	2285	1868	334	200	33	<33	384	16.68	138
1327	219	34.85	5.16	0.58	3.44	1656	2925	237	<107	43	<22	344	21.51	92
1329	225	35.33	3.12	0.76	2.42	1039	3395	138	<243	<35	<35	727	34.64	97
1331	230	35.42	2.04	0.38	2.28	1639	2555	217	133	36	<24	277	12.05	116
1333	241	35.67	1.45	0.29	1.74	2045	6902	218	<218	14	<28	275	14.50	720
1334	243	35.88	1.92	0.38	1.15	1017	13894	211	<307	<19	38	384	19.19	720
1335	250	26.13	0.00	0.00	26.13	74660	104897	38823	108257	14185	14185	na	373.30	2
1336	256	24.85	0.00	3.61	29.37	3615	6778	904	7230	904	1130	226	225.94	15
10-142	287	14.70	0.00	2.57	55.14	<367	<7352	<367	2941	<367	<367	367	367.00	-
10-230	314	18.72	0.00	4.49	44.94	5243	3745	1123	<374	374	<374	748	374.47	-
10-355	352	17.25	3.45	4.83	48.30	0	0	0	0	0	0	345	345.00	-
10-454	382	21.99	0.00	3.30	36.65	18323	13192	4397	<366	366	<366	6596	366.47	-
10-650	442	25.48	0.00	2.32	27.79	<1390	<3474	<232	<695	<232	<232	232	231.60	-
14-90	461	27.97	1.33	2.13	1.33	<1065	<2664	533	<932	133	266	266	133.20	
14-258	520	18.70	12.47	9.35	43.6	<6857	<9351	6234	<623	1870	1246	6233	623.38	-

TABLE 4. STANDARD DEVIATION OF RECALCULATED PGE DATA.

	100% SULPHIDE	100% CHROMITE
UPPER PERIDOTITE		
Os	5.84	0.70
Ir	5.35	0.32
Ru	31.90	4.20
Rh	38.68	12.40
Pt	14.52	22.53
Pd	37.65	221.84
Au	8.36	25.57
LOWER PERIDOTITE		
Os	0.29	1.67
Ir	0.16	1.04
Ru	0.47	2.54
Rh	2.77	2.22
Pt	2.31	5.44
Pd	9.60	29.45
Au	1.19	15.51

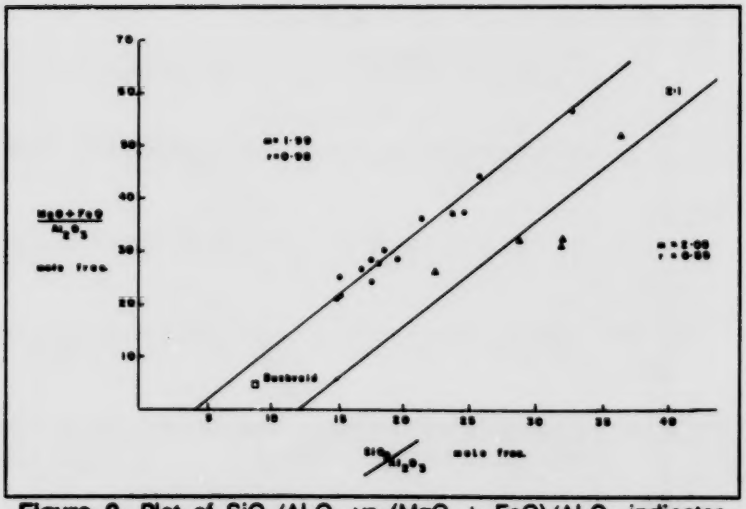

Figure 9. Plot of SiO_2/Al_2O_3 vs $(MgO + FeO)/Al_2O_3$ indicates two chemically distinct liquid compositions in the peridotite unit. Solid dots = upper peridotite unit; triangles = lower peridotite unit.

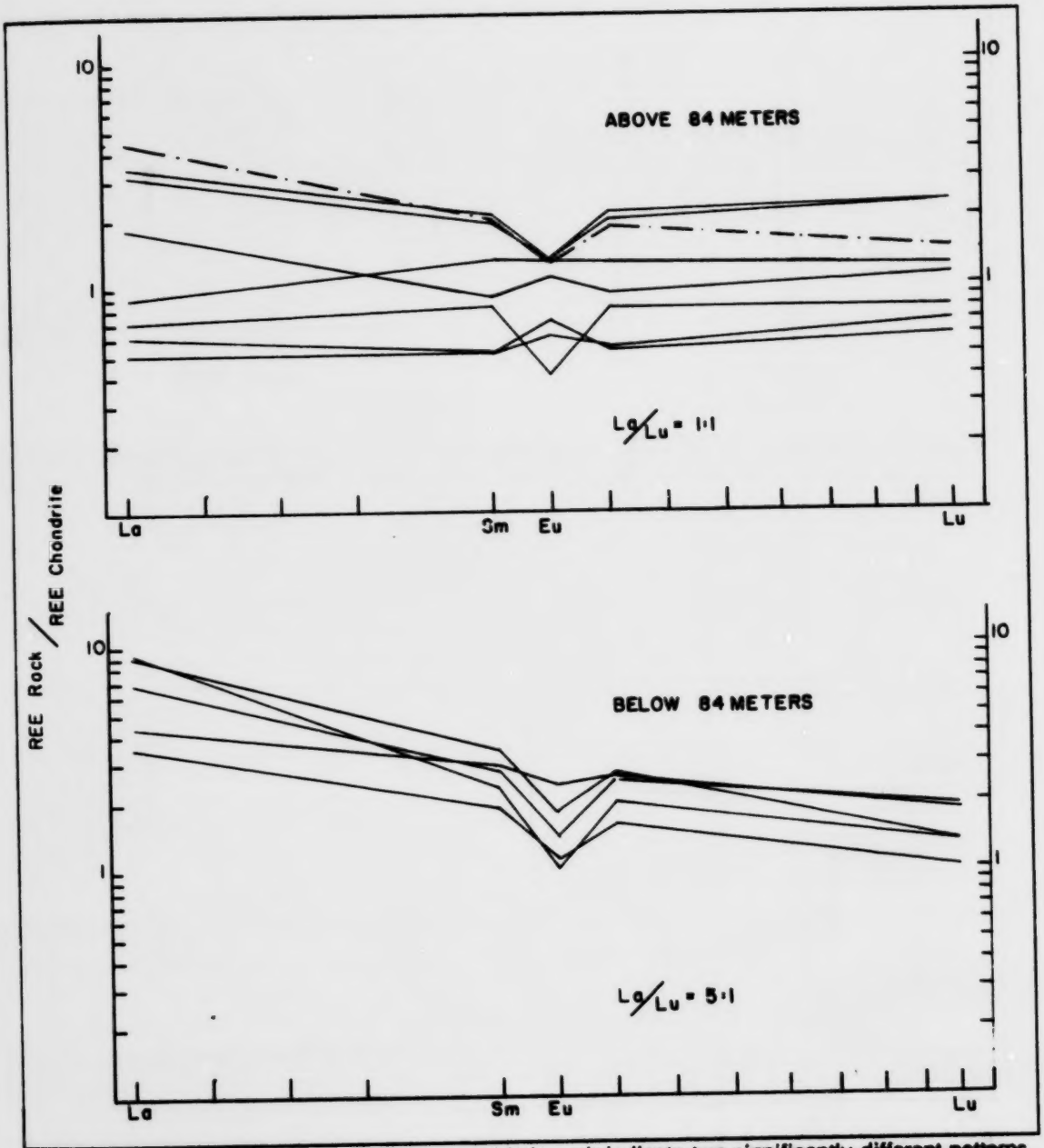

Figure 10. Plot of rare earth patterns from peridotite unit indicate two significantly different patterns and possibly a third "hybrid" pattern (dashed line).

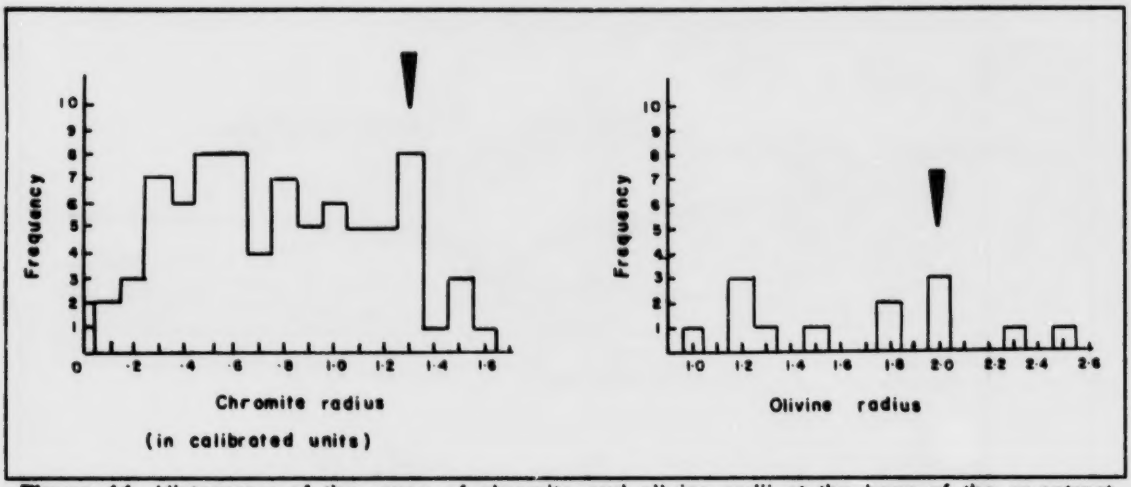

Figure 11. Histograms of the range of chromite and olivine radii at the base of the re-entrant olivine layer. Arrows indicate the radii used in the relative velocity calculation (1 unit = 0.4 mm).

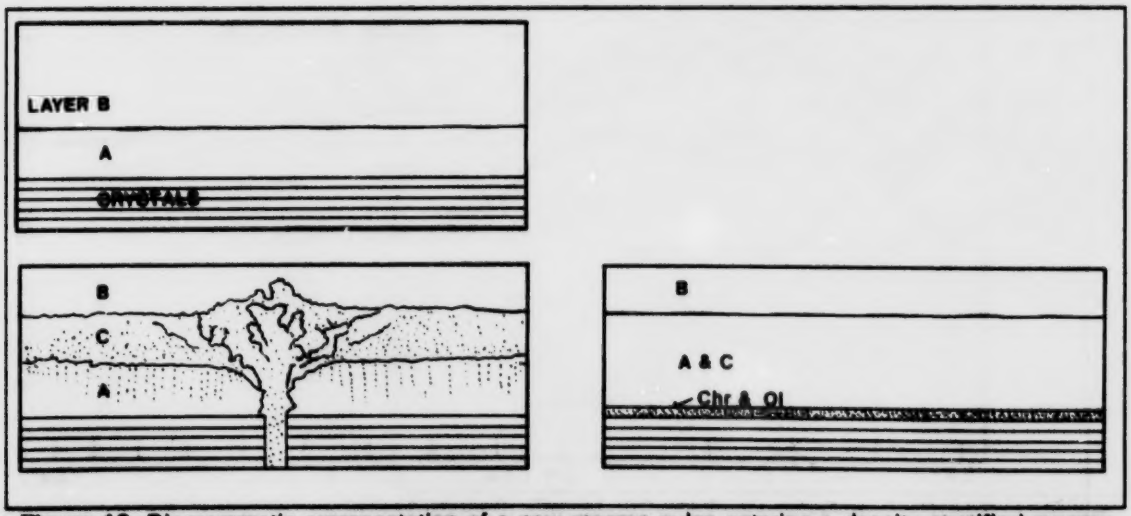

Figure 12. Diagrammatic representation of a new magma pulse entering a density stratified magma chamber. Top left: The magma chamber is stratified into layers A and B overlying the crystal pile. Lower left: The buoyant pulse of magma (C) rises until it finds its own density level, then spreads out across the chamber. Crystals on the liquidus (chromite and olivine) settle out of layer C. Right: As layer C cools it becomes more dense than the underlying layer; eventually roll-over occurs, causing layers A and C to mix. Magma mixing supercools liquid C resulting in re-entrant olivine growth and sulphide precipitation.

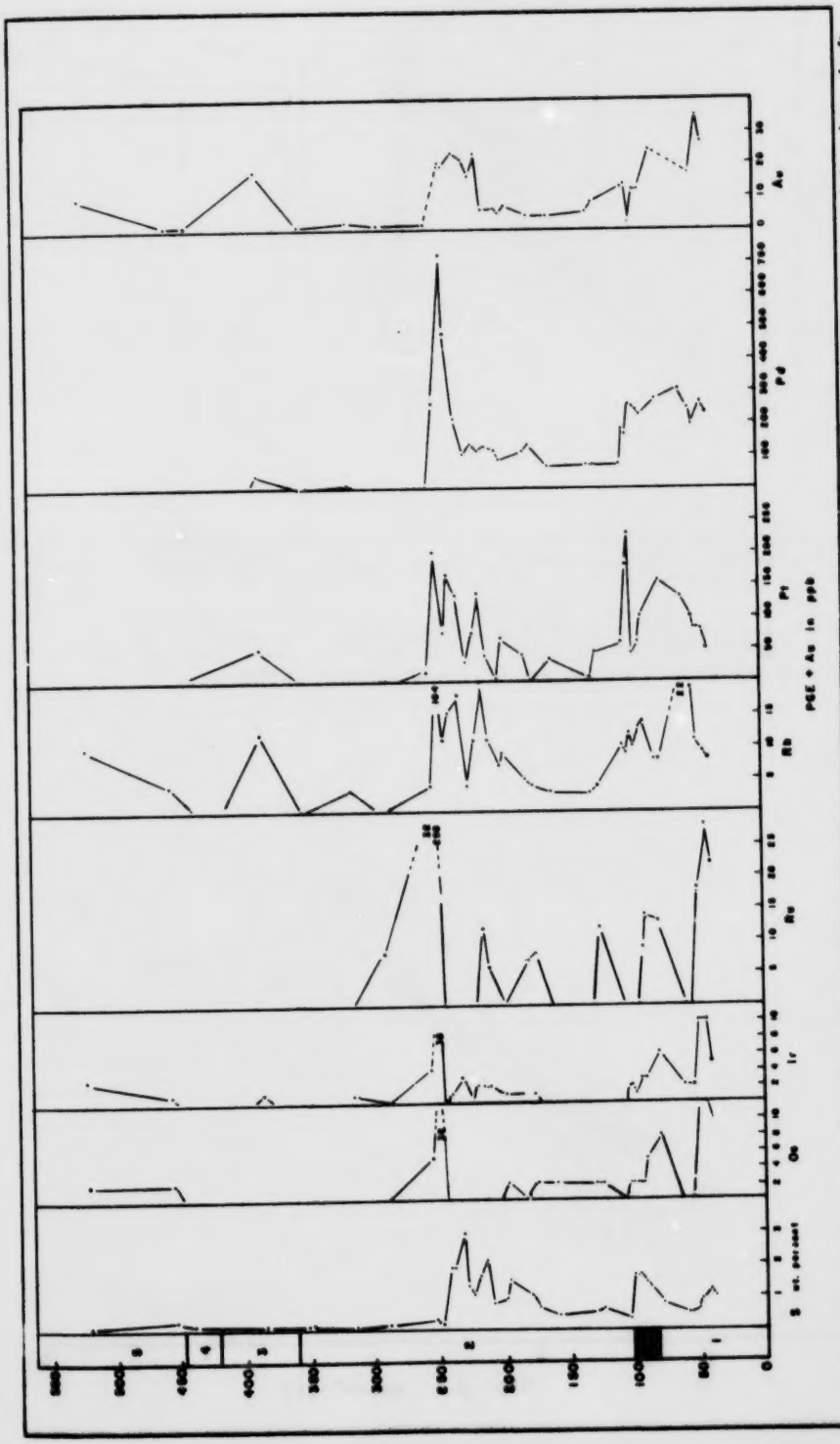

Figure 13. Vertical profile of S, PGE and Au concentrations. Low S values above 256 m are probably due to sulphur loss. Left column shows cyclic units and re-entrant layers (black lines).

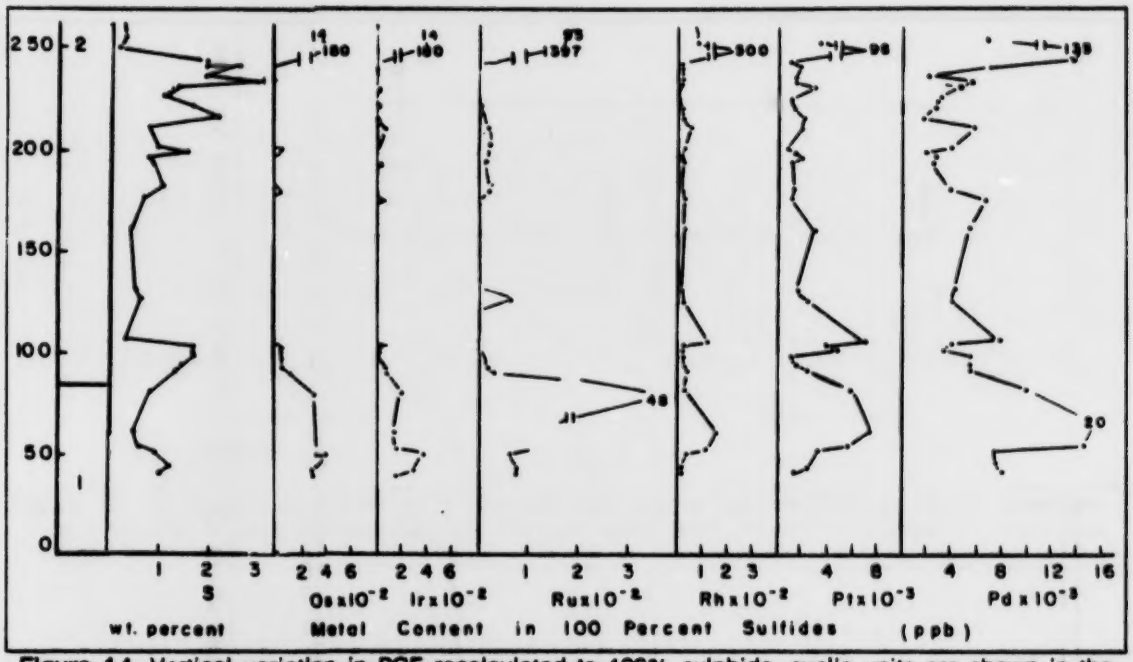

Figure 14. Vertical variation in PGE recalculated to 100% sulphide, cyclic units are shown in the far left column. Sulphur content in weight percent, metal contents in ppb.

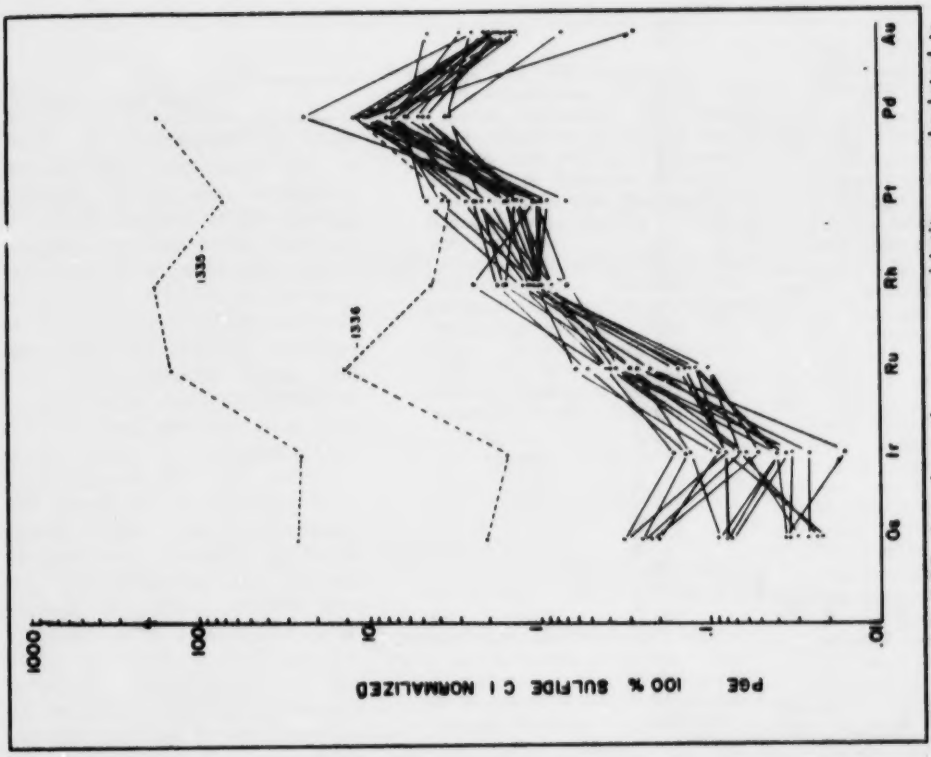

Figure 16. PGE data from the upper peridotite, re-calculated to 100% sulphide and C-1 chondrite normalized. Most of the samples define a steeply sloped field, samples 1335 and 1336 are chromite-rich.

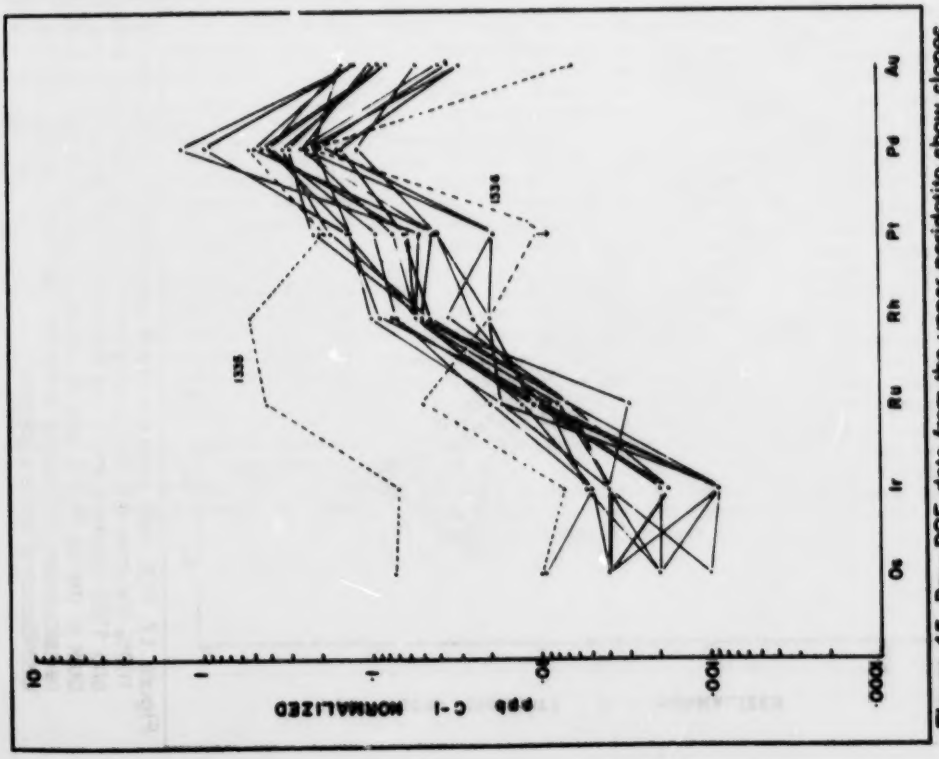

Figure 15. Raw PGE data from the upper peridotite show slopes. The shallower slopes correspond to Cr-rich samples, the steeper slopes are sulphide-chromite bearing samples.

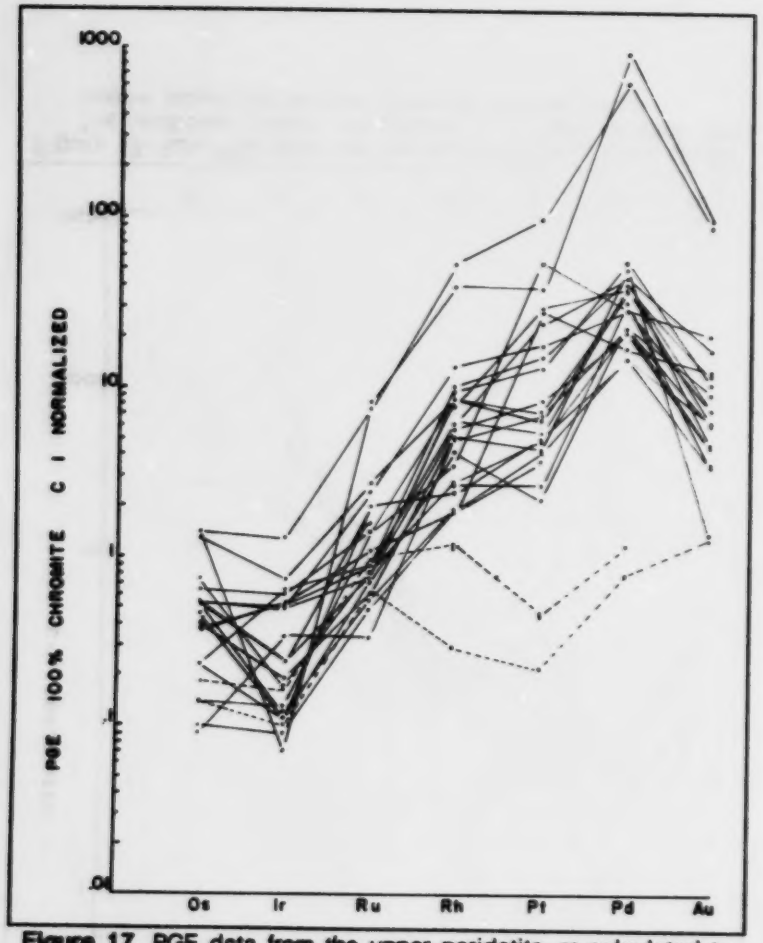

Figure 17. PGE data from the upper peridotite, re-calculated to 100% chromite and C-1 chondrite normalized. Samples 1335 and 1336 (dashed lines) fall within the field defined by the bulk of the da Pt, Pd, and Au show increased scatter in this re-calculation, indicating chromite has little control on the distribution of these elements.

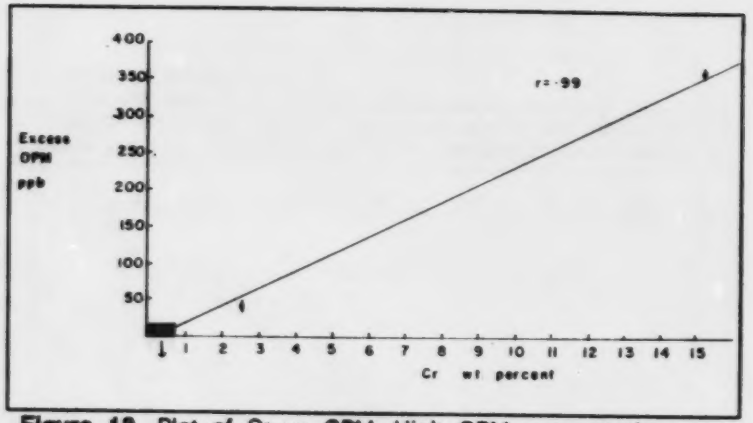

Figure 18. Plot of Cr vs OPM. High OPM concentrations are associated with Cr-rich samples.

CONCLUSIONS

PGE concentrations in sulphides are controlled by a number of factors, including the PGE content of the parent magma, the timing of the segregation of a particular batch of sulphide relative to the crystallization of silicates and oxides and the overall segregation of sulphides from the magma, and the proportion of magma that has reacted with a given batch of sulphide. Our study has shown that the upper peridotite crystallized in a closed system that fractionated olivine and chromite prior to sulphide precipitation. The resorbed, re-entrant olivine crystallized from a stagnant layer being depleted in PGE as the sulphides separated. In the net-textured sulphides, the unusually low Os, Ir and Ru values are accounted for by their removal from the magma by chromite fractionation prior to sulphide segregation.

REFERENCES

Agiorgitis, G. and Wolf, R.
1978: Aspects of Osmium, Ruthenium and Iridium Contents in Some Greek Chromites; Chemical Geology, Volume 23, p.267-272.

Barnes, S.J., and Gorton, M.P.
1984: Trace Element Analysis by Neutron Activation with a Low Flux Reactor (SLOWPOKE -II) - Results for International Standards; Geostandards Newsletter, Volume 8.

Borthwick, A.A.
1984: The Geology and Geochemistry of the Big Trout Lake Complex, Northwest Ontario; Unpublished M.Sc. thesis, University of Toronto.

Borthwick, A.A., and Naldrett, A.J.
1982: Platinum-Group Elements in Layered Intrusions, Big Trout Lake; Grant 106, p.12-19, in Geoscience Research Grant Program, Summary of Research 1981-1982, edited by E.G. Pye, Ontario Geological Survey, Miscellaneous Paper 103, 219p.
1983: Neutron Activation Analysis for Platinum-Group Elements in Chromitites; Grant 106, p.7-12 in Geoscience Research Grant Program, Summary of Research 1982-1983, edited by E.G. Pye, Ontario Geological Survey, Miscellaneous Paper 113, 199p.

Brown, G.M.
1956: The Layered Ultrabasic Rocks of Rhum, Inner Hebrides; Royal Society London, Philos. Ser.B 240, p.1-53.

Campbell, I.H.
1977: Some Problems with the Cumulus Theory; Lithos, Volume 11, p.311-32

Campbell, I.H., and Naldrett, A.J.
1978: The Influence of Silicate: Sulfide Ratios on the Geochemistry of Magmatic Sulfides; Economic Geology, Volume 74, p.1503-1506.

Campbell, I.H., Naldrett, A.J., and Barnes, S.J.
1983: A Model for the Origin of the Platinum-Rich Sulfide Horizons in the Bushveld and Stillwater Complex; Journal of Petrology, Volume 24, p.133-165.

Donaldson, C.H.
1974: Olivine Crystal Types in Harrisitic Rocks of the Rhum Pluton and Archean Spinifex Rocks; Geological Society of America, Bulletin, Volume 85, p.1721-1726.

Harker, A.
1908: The Geology of the Small Isles of Inverness-shire; Scotland Geological Survey, Memoir, p.1-20.

Hudec, P.P.
1964: Geology of the Big Trout Lake Area, District of Kenora (Patricia Portion); Ontario Department of Mines, Geological Report 23. 35p.

Irvine, T.N.
1977: Origin of Chromitite Layers in the Muskox Intrusion and Other Stratiform Intrusions: A New Interpretation; Geology, Volume 5, p.273-277.

Irvine, T.N., and Smith, C.H.
1967: The Ultramafic Rocks of the Muskox Intrusion, Northwest Territories, Canada; p.28-49 *in* Ultramafic and Related Rocks, edited by P.J. Wyllie, John Wiley and Sons, New York.

McBirney, A.R., and Noyes, R.M.
1979: Crystallization and Layering of the Skaergaard Intrusion; Journal of Petrology, Volume 20, p.487-554.

Mitchell, R.H., and Keays, R.R.
1981: Abundance and Distribution of Gold, Palladium and Iridium in Some Spinel and Garnet Lherzolites: Implications for the Nature and Origin of Precious Metal-Rich Intergranular Components in the Upper Mantle; Geochemica Cosmochemica Acta, Volume 45, p.2425-2442.

Naldrett, A.J.
1981: Nickel Sulfide Deposits: Classification, Composition and Genesis; Economic Geology, Seventy-fifth Anniversary Volume, p.628-685.

Naldrett, A.J., and Duke, J.M.
1980: Platinum Metals in Magmatic Sulfide Ores; Science, Volume 208, p.1417-1428.

Oshin, I.O., and Crocket, J.H.
1982: Noble Metals in Thetford Mines Ophiolites, Quebec, Canada. Part 1. Distribution of Gold, Iridium, Platinum and Palladium in the Ultramafic and Gabbroic Rocks; Economic Geology, Volume 77, p.1556-1570.

Page, N.J., Rowe, J.J., and Haffty, J.
1976: Platinum Metals in the Stillwater Complex, Montana; Economic Geology, Volume 71, p.1352-1363.

Sage, R.P., and Troop, W.R.
1974: Operation Winisk, Big Trout Lake Area; Ontario Division of Mines, Preliminary Map P.860, scale 1 inch to 1 mile.

Wager, L.R., and Brown, G.M.
1951: A Note on Rhythmic Layering in the Ultrabasic Rocks of Rhum; Geological Magazine, Volume 88, p.166-168.

Grant 107 Platinum Group Elements in the Eastern Gabbro, Coldwell Complex, Northwestern Ontario

David H. Watkinson, P.L. Jones, and D. Marshall

Department of Geology, Carleton University
and
Ottawa-Carleton Centre for Geoscience Studies

ABSTRACT

Magnetite-bearing layered gabbro of the Coldwell Complex, northwestern Ontario, was mapped, sampled and analyzed for Pt, Pd, Au, Cu, Ni, Co and S. No concentrations were found except in heterogeneous, marginal gabbro at the base of the section exposed on Highway 17. Platinum-group minerals were sought but not found in magnetite near the base of the layered gabbro. These results are compatible with the model that suggests that nearly all platinum-group metals were scavenged from magma by sulphur available near the base of the complex, and that little remained in the magma when it was invaded by a later pulse of new magma responsible for the layered succession.

INTRODUCTION

The occurrence of platinum-group elements (PGE) in the copper-nickel-iron sulphides at or near the contact of gabbros of the Coldwell Complex with Archean country rock has been described recently by Wilkinson (1983), Wilkinson and Colvine (1978) and Watkinson *et al.* (1983). This paper describes the continuation of the latter study into layered rocks stratigraphically above the heterogeneous gabbro: it was considered possible that concentrations of PGE might occur above the heterogeneous gabbro in early oxide-rich layers presumably related to new magma injection and mixing. The relationship of PGE content, sulphide concentration, petrology and mineral compositions will be examined in the final report.

Field work for this study of the Highway 17 cut through the gabbroic rocks and other areas of layered gabbro was carried out in June 1983. Results of the mapping are presented in Figure 1 and assay data in Table 1.

GEOLOGY OF THE EASTERN GABBRO AND ADJACENT ROCKS

General geological discussion of the Coldwell Complex and host rocks, especially in areas of economic significance for precious metals was presented by Wilkinson (1983); Watkinson *et al.* (1983) discussed the platinum-group-element potential in the Two-Duck Lake area. Mapping and sampling for this study (Figure 1) was concentrated near Highway 17.

ARCHEAN METAVOLCANIC ROCKS

Immediately adjacent to the Coldwell Complex, in the extreme southern part of the map-area, are Archean metavolcanic rocks. They consist of irregularly interdigitated light and dark agglomerates and breccias. These rocks have pale grey-green weathered surfaces and light to medium-grey fresh surfaces. The layers vary from 30 cm to 1 m thick and the fragments constitute variable amounts of each layer. The fragments vary in size, shape, composition and orientation. In some layers ovoid fragments up to 20 cm (but generally much smaller), composed predominantly of volcanic material and quartzite, are aligned, defining a penetrative foliation which strikes 161° and dips 45° to the east. In other layers, xenoliths with no predominant shape, up to 40 cm in size, are randomly oriented.

The matrix to the fragments is very fine-grained, often aphanitic except for porphyroblastic biotite up to 3 mm in size, presumably a result of contact metamorphism during emplacement of the Coldwell Complex.

Along the Lake Superior shoreline is a large rocky headland composed of breccia layers similar to those described above. This outcrop is transected by numerous quartz and feldspar veins up to 2 cm thick and dikes up to 50 cm thick (feldspar porphyries and prominent fine-grained, red-brown, apparently brecciated dikes).

COLDWELL COMPLEX

Massive Gabbro

A fine-grained massive gabbro (chilled-facies) occurs at the contact with the country rocks. It is generally rusty brown where weathered and dark grey on fresh surfaces. Extensive fracturing gives the outcrops a rubbly appearance. The grain size is variable up to approximately 2 mm. In places the fine-grained gabbro has been converted to a gossan. The sulphide content of this unit is approximately 2-3%, consisting of chalcopyrite (cpy) and pyrrhotite (po) in small interstitial clots.

Xenoliths of hornfelsed country rock, up to 7 m in diameter are not uncommon. Intrusion of gabbro by pink and green augite syenite, ap-

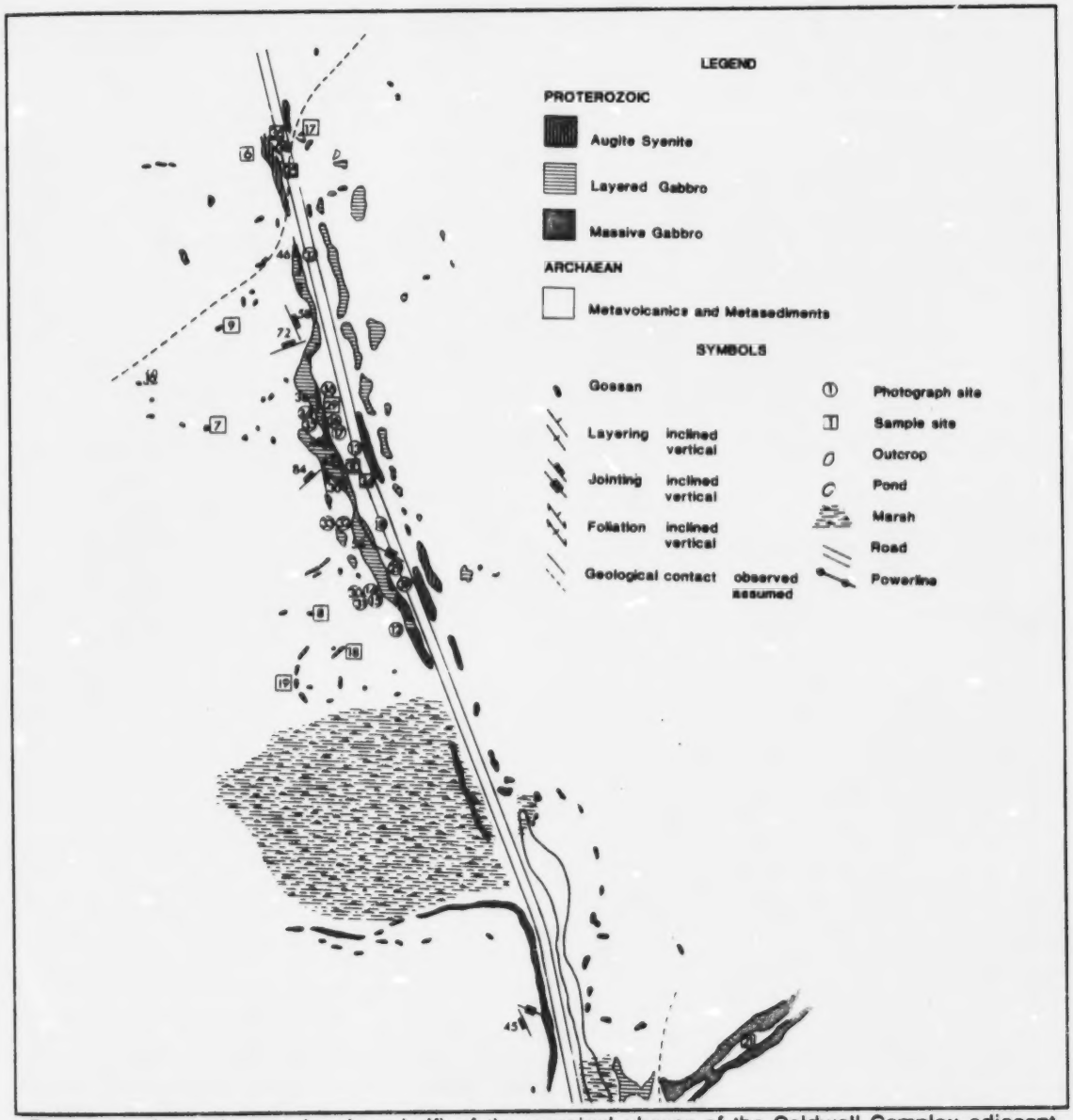

Figure 1a. Geologic map (northern half) of the marginal phases of the Coldwell Complex adjacent to Highway 17, near Marathon, Ontario.

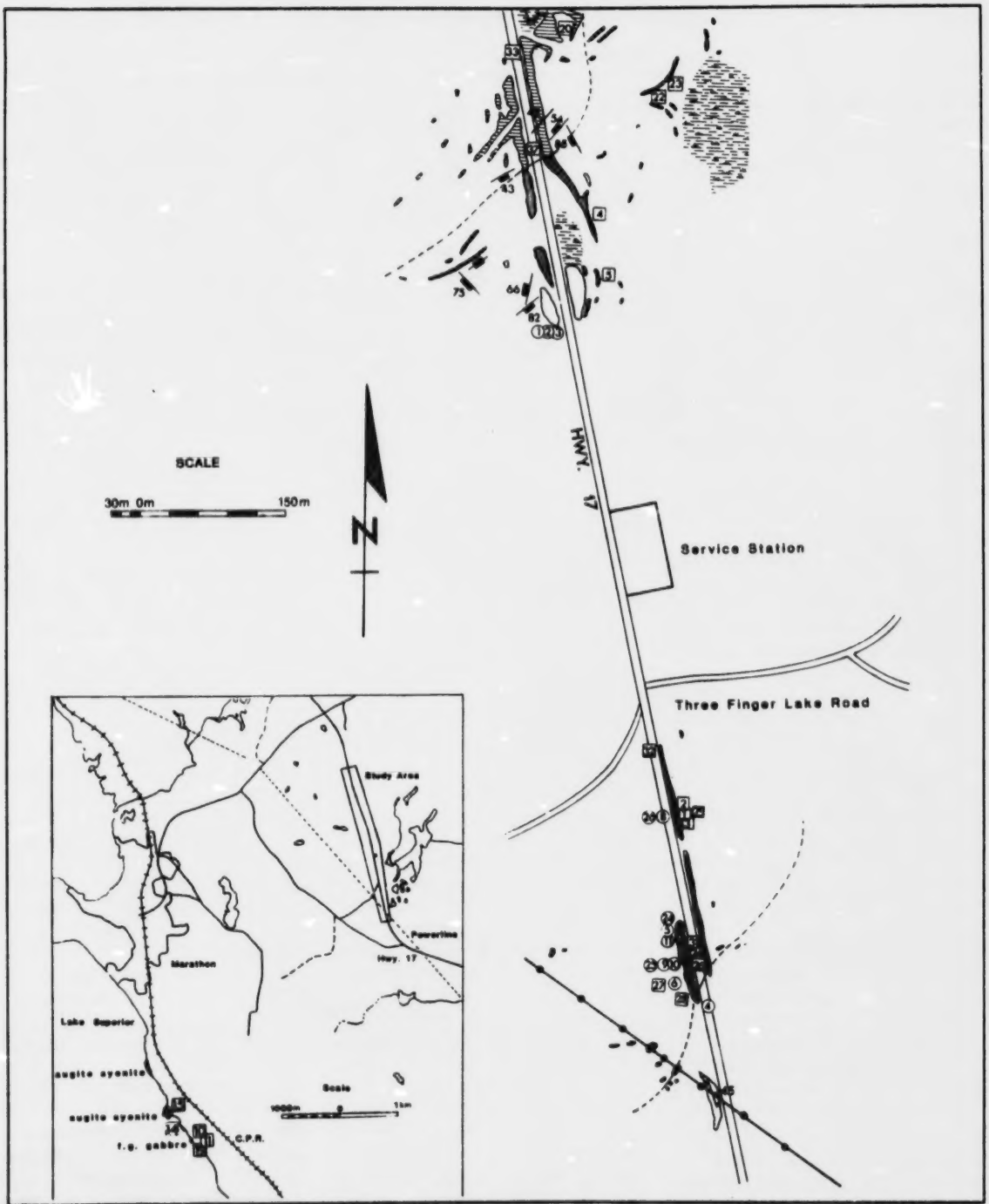

Figure 1b. Geologic map (southern half) of the marginal phases of the Coldwell Complex adjacent to Highway 17, near Marathon, Ontario.

TABLE 1. CHEMICAL ANALYSES OF SOME GABBROIC ROCKS, EASTERN COLDWELL COMPLEX.

	Cu	Ni	Co	Au	Pt	Pd	S
1	52	11	17	nd	nd	nd	900
2	46	3	37	nd	nd	nd	4100
3	40	2	29	nd	nd	nd	900
4	3190	118	50	13	nd	3	15,400
5	545	191	72	nd	nd	nd	15,800
6	3450	304	27	57	nd	3	8100
7	65	2	20	7	nd	nd	5500
8	45	2	32	4	nd	nd	1500
9	58	9	40	18	nd	nd	3800
10	14	nd	21	nd	nd	nd	3200
11	380	21	47	3	nd	nd	2100
12	176	15	26	2	nd	nd	300
13	4837	304	-	-	402	1396	-
14	2000	525	197	9	52	68	11,200

Notes. All data in ppm except Au, Pt, Pd (ppb). nd - below detection (Ni <1, Au <2, Pt <10, Pd <2). Locations on Figure 1.

Samples.

1. PCC-83-9 layered gabbro just below contact with augite syenite.
2. PCC-83-20 layered gabbro.
3. PCC-83-21 medium-grained massive gabbro.
4. PCC-83-26 fine-grained sulphide-rich gabbro with augite syenite.
5. PCC-83-27 fine-grained, supergene-altered gabbro.
6. PCC-83-28 sulphide-rich pod in fine-grained gabbro.
7. PCC-83-29 layered gabbro.
8. PCC-83-33 layered gabbro.
9. PCC-83-37 layered gabbro.
10. PCC-83-C1 chip sample, layered gabbro near location 29.
11, 12. BL-83-2,-3 layered gabbro, eastern end Bamoos Lake.
13. Average Two-Duck-Lake area trenches (Watkinson *et al.* 1983).
14. KL-83-1 grab sample of sulphide-bearing drill core, Killala Lake Complex.

parently along fractures and joints is common. The augite syenite consists of coarse-grained alkali feldspar, clinopyroxene and amphibole (up to 5 cm in size). The contact between the fine-grained gabbro and the augite syenite is often diffuse over several centimetres.

Elongate sulphide-bearing pods with irregular outline, up to 40 cm across, composed of alkali feldspar, plagioclase, pyroxene, amphibole and sulphides (cpy + po) occur in the fine-grained gabbro near the contact with the country rock. The rims of these pods, diffuse over 2 cm, are the sites of mafic mineral concentration. The sulphides, which constitute approximately 8% of the pods, occur as clots interstitial to silicates up to 1 cm across.

One large clean outcrop of fine-grained gabbro occurs along the Lake Superior shoreline. This outcrop has weathered medium grey and is apparently sulphide-free. Small patches of coarse-grained gabbro and extensive, apparently randomly oriented, quartz and feldspar veining are common. Also some coarser-grained blocks, up to 1 m in size, are included in this outcrop. A fine-grained mafic dike, 80 cm wide, has also intruded the fine-grained gabbro.

Approximately 200 m from the contact with the country rocks is the first occurrence of medium-grained gabbro, with grains as coarse as 4-5 mm. Alkali-feldspar rich, coarse-grained to pegmatitic pods (grains as large as 2 cm) are common in this unit, as are small round clots of alkali feldspar.

The medium-grained gabbro is composed of plagioclase, clinopyroxene, olivine, and magnetite. In places alkali feldspar, biotite, amphibole, quartz and sulphides also occur. Grain size is generally quite variable.

The contact between the fine-grained gabbro and the stratigraphically higher coarse-grained gabbro is generally diffuse. Large fragments of fine-grained gabbro are enveloped by the coarser-grained gabbro. Also xenoliths of hornfelsed and unhornfelsed country rock, up to 20 m across, occur throughout the coarse-grained gabbro; in particular, large blocks were observed near the contact with the stratigraphically higher, layered gabbro on Highway 17, and along the Lake Superior shoreline.

Layered Gabbro

The contact between the layered gabbro and the underlying massive gabbro is gradational over several metres. The lowermost layers, approximately 850 m from the Coldwell Complex - country rock contact on Highway 17 are alternating melanocratic and leucocratic bands composed of plagioclase, clinopyroxene, magnetite, minor olivine, biotite and rare sulphides. The outcrops are weathered dark brown and buff. The layering results from differences in the relative concentration of plagioclase and mafic minerals. These layers are 10 cm to 1 m thick and do not appear to be continuous over distances of more than several metres. They strike approximately 51° and dip 42° to the northwest. In places the layering is indistinct, the outcrop having a foliated rather than a layered appearance.

At a somewhat higher stratigraphic level, thin (up to 5 cm) magnetite layers occur. They were traced continuously

for 40 m and consist predominantly of magnetite with minor clinopyroxene; sulphides are rare. The rock is fine-grained and weathers grey-brown with the magnetite layers as prominent ridges; fresh surfaces are medium to dark grey. The layers strike 160-170° and dip 36-46° to the west. The spacing between magnetite layers varies from 2 to 25 cm. Between the magnetite layers the rock is foliated, the foliation having the same orientation as the magnetite layers.

The distance between the stratigraphically lowest and highest occurrences of layered gabbro along Highway 17 is approximately 1100 m; however, the occurrence of layered gabbro is not continuous throughout this entire distance. Much of the outcrop is composed of fine- to medium-grained massive gabbro, similar to those units already described. Contact between the layered and massive gabbro is diffuse and indistinct.

Intrusion by coarse-grained pink and medium to dark green augite syenite as dikes and irregularly shaped pods up to 20 m across is common, particularly toward the top of the layered succession (i.e. near the layered gabbro/augite syenite contact). In some cases these intrusions completely envelop layered blocks, giving parts of the outcrop a brecciated appearance. Contact between the layered gabbro and the augite syenite is sharp to diffuse over 2-3 cm. In some cases, enveloped layered gabbro fragments have been hornfelsed.

Coarse-grained to pegmatitic pods also cross-cut the magnetite layers in many places. Whether they are related to the augite syenite or perhaps to contamination is unclear; however, they are the sites of local alkali feldspar concentration, and also contain plagioclase, magnetite and clinopyroxene.

Near Bamoos Lake, approximately 8 km to the northwest of the Highway 17 study area, only small discontinuous magnetite layering was observed. Much of the outcrop is distinctly layered, but the layering is of the same type as that observed at the base of the layered series on Highway 17, i.e., phase layering composed of alternating melanocratic and leucocratic layers. No layering was observed in the gabbro along the Lake Superior shoreline.

Augite Syenite

Immediately above the layered gabbro is a thick succession of coarse-grained augite syenite. The augite syenite varies from pink to dark olive green, and consists of alkali feldspar, amphibole, clinopyroxene and magnetite. Layering was not observed along Highway 17 but very well defined, 1 m thick layers, continuous over 40-50 m were observed on large clean outcrops along the Lake Superior shoreline. The contact between the augite syenite and the underlying layered gabbro is diffuse over several metres.

PRECIOUS- AND BASE-METAL CONTENTS OF EASTERN GABBRO

Samples of massive and layered, sulphide-rich and poor, coarse- and fine-grained gabbros were taken for assay. Analyses were performed by Bondar-Clegg and Company Limited. Cu, Ni and Co were analyzed by HNO_3-HCl hot extraction and atomic absorption, the precious metals by aqua regia and fire assay/DC plasma, and sulphur by X-ray fluorescence (XRF). Results are presented in Table 1. Also shown for comparison are data from similar rocks of the nearby Killala Lake Complex. These results confirm what can be presumed from extensive, unpublished results of various mining companies; there is no indication of PGE or Au concentrations in any gabbro other than sulphide-rich rocks of the heterogeneous, marginal unit.

However, there are certainly sulphide-bearing, magnetite-rich rocks at the base of the layered succession. Wilkinson (1983) reported that one sample of magnetite-rich rock at the interface of layered and marginal gabbro contained 2200 ppb Pd and 310 ppb Pt. Clearly more sampling and analyses are necessary before these magnetite-rich layered rocks can be justifiably ignored.

When the data for the Killala Lake specimen are projected onto a Pt/(Pt + Pd) vs. Cu/(Cu + Ni) diagram, it appears that they are different from the data of Watkinson *et al.* (1983), containing relatively more Ni and Pt. However, the extent of these concentrations is apparently much less.

Cu/(Cu + Ni) values for the layered gabbro are generally consistent with data from previous work; unfortunately, precious metal values are essentially below detection. Because these values were so low, no comprehensive petrographic or mineralogic study of the magnetite-rich rocks was undertaken. Examination of a few polished sections revealed only magnetite, ilmenite ox-

yexsolution lamellae and grains, and their supergene alteration products.

CONCLUSIONS

The base-metal sulphide concentrations and their contained PGE are considered to be derived from the interaction of juvenile metals in gabbroic magma and sulphur from the footwall volcanic rocks. However, some juvenile magmatic sulphur is possible. Later injection of a second pulse of magma or a new magma, giving rise to the stratigraphically higher, layered rocks contained essentially no sulphur, and therefore no concentrations of sulphides are evident. PGE, if present above normal background levels in gabbro, were not concentrated in magnetite-rich rocks, at least in the area sampled.

ACKNOWLEDGMENTS

This project was initiated with the permisson of Anaconda Exploration Company Limited. Paul Mainwaring (Energy Mines and Resources Canada, Ottawa) provided much of the impetus for this work. Discussions with R.P. Sage, S. Wilkinson and A.C. Colvine are greatly appreciated.

REFERENCES

Watkinson, D.H., Whittaker, P.J., and Jones, P.L.
1983: Grant 107 Platinum Group Elements in the Eastern Gabbro, Coldwell Complex, Northwestern Ontario; p.183-191 *in* Geoscience Research Grant Program, Summary of Research 1982-1983, edited by E.G. Pye, Ontario Geological Survey Miscellaneous Paper 96.

Wilkinson, S.
1983: Geology and Sulphide Mineralization of the Marginal Phases of the Coldwell Complex, Northwestern Ontario; unpublished M.Sc. Thesis, Carleton University, Ottawa.

Wilkinson, S., and Colvine, A.C.
1978: Sulphide Mineralization in the Marginal Phases of the Coldwell Alkalic Complex; p.210-215 *in* Summary of Field Work, 1978, by the Ontario Geological Survey, edited by V.G. Milne, O.L. White, R.B. Barlow and J.A. Robertson, Ontario Geological Survey, Miscellaneous Paper 82, 235p.

Grant 114 Source, Correlation, and Thermal Maturation History of Hydrocarbon Deposits of Southern Ontario

J.F. Barker, R.W. Macqueen, and J. Waldron

Department of Earth Sciences, University of Waterloo

ABSTRACT

The conventional oils of southern Ontario form three geochemically distinct groups which are generally stratigraphically coincident. Cambrian-Ordovician and Silurian groups probably have local sources while the source of the Devonian group of oils is not as certain.

Ontario natural gases show considerable geochemical variation without a clear distinction between Michigan and Appalachian Basin deposits. The natural gas compositions, as well as the carbon and hydrogen isotope distributions among hydrocarbons, suggest their sources are more mature than the sediments of southern Ontario. This could indicate migration of gases from much deeper in the sedimentary basins or could be explained by degassing of dominantly methane and helium from the underlying basement rocks. It is also possible that initially-generated natural gas was not trapped while later-generated gas accumulated. This pooled gas would be "temporally mature" even though the source rocks would be thermally immature, as is the situation for the Paleozoic sequence in southern Ontario.

Geochemical studies of the possible oil shale deposits in southern Ontario have concentrated on the Collingwood Formation. Of particular interest is the geochemical environment of deposition. Preliminary geochemical and isotopic studies found no evidence that the organic richness of these carbonate rocks is associated with the onset of major anoxic ocean conditions. More detailed organic geochemical studies, utilizing pyrolysis - gas chromatographic techniques developed this year, will be undertaken to evaluate the geochemical controls of organic richness of the Collingwood and other oil shale deposits.

INTRODUCTION

This report summarizes studies of the conventional oil and gas pools and the unconventional oil shale deposits in southern Ontario. Powell *et al.* (1984) and Barker and Pollock (1984) present the conventional oil and gas studies and Barker *et al.* (1983) discussed possible oil shales. These studies are essentially geochemical in nature, and while answers to a number of geological questions have been obtained, many interesting aspects have only been recognized and are under investigation (Macqueen and Powell 1984; Churcher and Barker 1984).

OIL AND GAS DEPOSITS

Ontario's cumulative oil production from 1863 to 1980 was about 9 x 10^6 m^3. Maximum annual production was about 2 x 10^5 m^3 in 1966 while recent annual production is generally below 10^5 m^3. Although this is only a small portion of Ontario's crude oil consumption, proximity to markets, cheap exploration costs and high quality crude oil make Ontario of continuing exploration interest despite the probable small volumes of remaining, undiscovered hydrocarbons. Bailey and Cochrane (1984) present a much more optimistic picture of Ontario's conventional oil and gas potential.

Ontario oils are medium gravity and generally of low (less than 1%) sulphur content. Three families of crude oils have been identified on the basis of gross composition, n-alkane distributions, pristane to phytane ratios, carbon isotope composition of the saturate and aromatic fractions, distribution of gasoline-range hydrocarbons and ring distributions in the aromatic fractions. These families of crude oils are largely confined to the broad stratigraphic intervals of the Cambrian-Ordovician, Silurian and Devonian. A few cases of migration from Ordovician source rocks into Silurian reservoirs are recognized. The Silurian oils are the most geochemically diverse, perhaps reflecting numerous distinct, local source rock types.

Analyses of rock samples have identified likely petroleum source rocks in Ordovician and Silurian strata. Cambro-Ordovician oils can be correlated to the Collingwood Member of the Lindsay Formation on the basis of geochemical similarities of oils and rock bitumen. The Middle Silurian Eramosa Formation and perhaps other, local, organic-rich, evaporite-associated carbonates of the Guelph or Salina Formations are considered to be the source for Middle Silurian reef-hosted oils, based on a number of geochemical characteristics but particularly the occurrence of eight specific alkylbenzenes in Silurian oils and Eramosa bitumens. Although the Devonian Kettle Point and perhaps Marcellus Formations are excellent potential sources for the De-

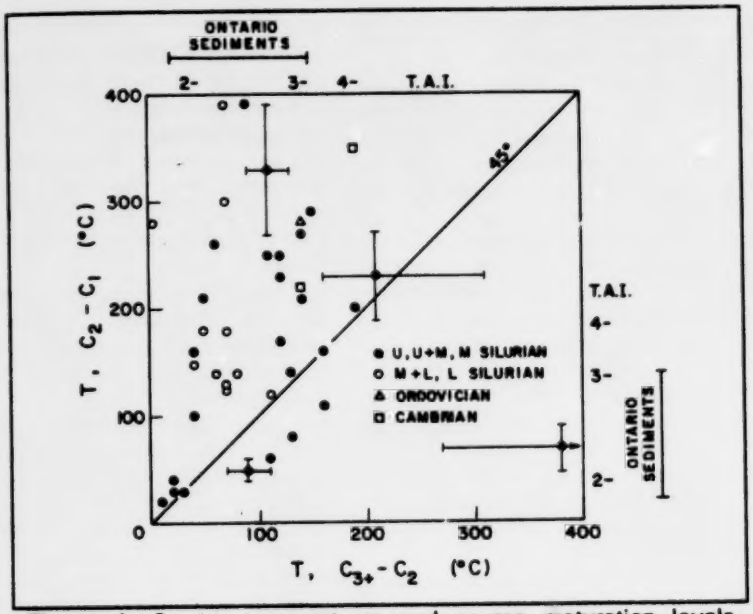

Figure 1. Source temperatures and source maturation levels derived from carbon isotope fractionation factors for pooled natural gases. Error bars indicate uncertainties in temperature estimates. T.A.I. = Thermal Alteration Index.

vonian oils, they are generally immature to only marginally mature in Ontario and so are unlikely source beds except if migration has occurred from deeper, more mature areas in the Michigan or Appalachian Basins.

More than 2 x 10^{10} m^3 of natural gas has been produced in southern Ontario since 1890. In 1980, 4.45 x 10^8 m^3 was produced from reservoirs ranging from Cambrian to Silurian in age (Booth-Horst and Rybansky 1982). Lower Silurian sandstones yield 54% and Middle-Upper Silurian reefs yielded about 40% of the 1980 production.

These natural gases generally contain more than 5% non-methane hydrocarbons and so are "wet". N_2 is the dominant non-hydrocarbon gas. Gases from the Michigan and Appalachian Basins are very similar and can be distinguished only through a ratio obtained by dividing the ethane/propane ratio by the isobutane/normal butane ratio. Although some of the chemical and isotopic maturation indicators are contradictory, most indicate a very mature to overmature source maturation level. The enclosing rocks are only immature to marginally mature. This suggests that much of the natural gas has been generated outside the sedimentary sequence of southern Ontario.

Perhaps the strongest evidence for an overmature source for much of this natural gas is the carbon isotope composition of the methane, ethane and propane plus butane fractions. James (1983) has provided a useful technique for estimating the thermal maturation level of natural gas source beds using the carbon isotopic composition of methane, ethane, and propane in the deposit. In southern Ontario, a gas source maturation level can be estimated from two indicators, the carbon isotope difference between methane and ethane (T, C_2-C_1) and between ethane and propane plus butane (T, C_{3+}-C_2). Figure 1 compares these indicators of source thermal maturation level. Scales of source temperature and Thermal Alteration Index (TAI) are shown with the TAI levels of Ontario sediments taken from Barker *et al.* (1983). A few natural gases give similar source temperature or thermal maturation indication using James' (1983) calculations, but most gases lie above the 45° correspondence line in Figure 1. That is, the indicator involving methane often yields a higher source temperature than the indicator using ethane-propane plus butane. The ethane-propane indicator is generally more reliable, in part, due to the multitude of sources of methane and its fugitive nature (James 1983). For Ontario gases, this indicator suggests most of the ethane, propane and butane could have been generated from enclosing sediments. The indicator involving methane (T, C_2-C_1) consistently indicates source temperatures well in excess of those likely attained by the enclosing or nearby sediments.

This inconsistency could be resolved if methane from a more mature source was added to wet natured gases generated from local sources. What would be the source of this more-mature methane? Methane generated at much higher maturation levels, deeper in the Michigan or Appalachian Basins would have to migrate more than 200 km judging from the rather low matura-

tion levels attained in states adjacent to Ontario. Another, somewhat speculative source of mature methane is degassing of the mantle or crust (Gold 1979). This possibility gains some support by the finding of large volumes of methane dissolved in saline groundwaters of the Canadian Shield (Fritz, Frape and Barker, current NSERC-supported study). A third option is to abandon the model of temperature-control for natural gas isotopic composition and turn to a kinetic control of isotope fractionation. In this model the natural gases in Ontario would represent accumulations of gases derived at low temperatures but late in the temporal evolution of the sediments with the earlier-formed gases escaping the trapping mechanisms.

None of these three choices is so strongly supported by the data that the others can be safely excluded. Ontario gas pools provide an ideal opportunity to test these hypotheses and so further research is planned.

OIL SHALES

The potential of organic-rich sedimentary rocks to yield oil upon retorting or pyrolysis is currently being assessed through the Hydrocarbon Energy Resources Programme of the Ontario Geological Survey. Our laboratory has been determining the organic carbon content, the yield upon pyrolysis and other assessment parameters for this project. In addition, Grant 114 permitted geochemical studies of the origin and organic-richness control for these rocks. These studies have concentrated upon the upper Ordovician Collingwood Member of the Lindsay Formation.

Useful indicators of organic matter type, depositional and diagenic environment and thermal maturation level include the distribution of normal alkanes and of the isoprenoids (branched alkanes) pristane (C_{19}) and phytane (C_{20}). These are normally determined chromatographically following solvent extraction of the sediments and extensive preparative liquid chromatography of the extracted bitumen. Our studies require many samples to be analyzed and so a more rapid, but still reproducible method was required.

A pyrolysis-gas chromatography method was developed and evaluated (J. Waldron, B.Sc. project 1984). About 10 mg of powdered rock is heated from room temperature to 300°C at 40°C/min in an inert (helium) atmosphere. The pyrolysate is trapped on Tenax and thermally desorbed into a gas chromatograph. The GC is equipped with a 60 m capillary column (DB-5) which resolves the components of the pyrolysate which are then detected by a flame ionization detector (FID).

Twenty-five samples of the Collingwood Member from the Toronto area along the subcrop/outcrop belt through Collingwood, Manitoulin Island northwest to St. Joseph Island were examined. The Carbon Preference Index (CPI) and Odd-Even Preference (OEP) varied from 0.80 to 1.30 with a slight preference for odd n-alkanes. In all but one case, pristane dominated phytane. Usually pristane and phytane were less abundant than the C_{17} or C_{18} n-alkanes although considerable variation in the isoprenoid/n-alkane ratios exists. None of these parameters varied systematically with organic richness. Further analyses are underway to provide an adequate data base for interpretation of the significance of the observed geochemical variations.

Normal marine limestones of the Lindsay Formation grade upward into organic-rich limestones and marls of the Collingwood Member. This member may represent a major shift to widespread anoxic ocean conditions. Such major differences in the diagenic/depositional environment should be reflected in variations in the types and extent of microbial processes in the sediment. In particular, anoxic, organic-rich sediments should quickly become strongly reducing and active sulphate reduction and methanogenesis should occur. Onset of these types of biological reactions should be reflected in a shift in the $^{13}C/^{12}C$ ratio of limestones, although the literature is contradictory as to what specific change should occur (Keith 1982).

The carbon isotope ratio in 15 carbonates from two boreholes near Toronto (SIS-1) and near Collingwood (CLGD 4b) were determined. All samples are from the Collingwood Member. The $\delta^{13}C$ values fall within the range for typical marine carbonates (0±2‰) and so they provide no support, but do not disprove, the concept of a large-scale anoxic event having produced the organic-rich Collingwood Member.

Berner and Raiswell (1983) suggested that an organic carbon versus pyrite sulphur plot might identify normal marine sediments, non-marine sedi-

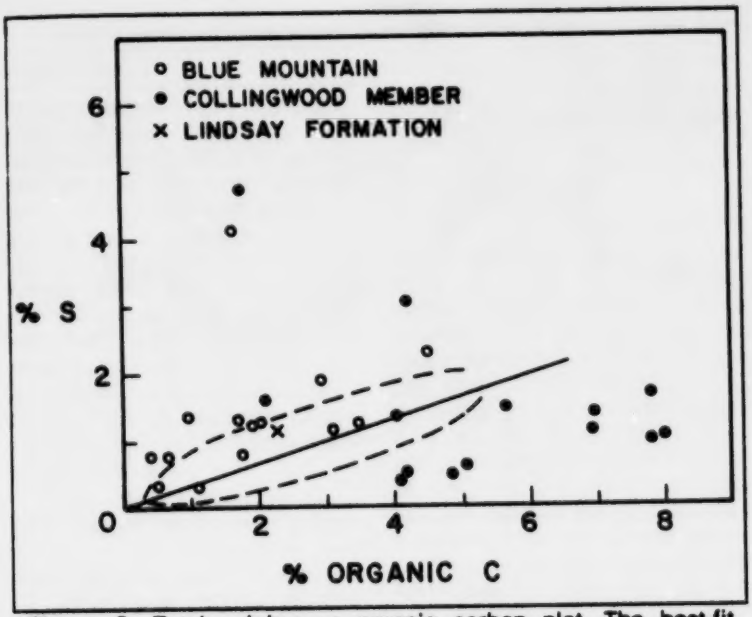

Figure 2. Total sulphur vs organic carbon plot. The best-fit straight line is for normal marine carbonates whose ratios all fall within the dashed lines (from Berner and Raiswell 1983).

ments (low S/C ratio) and anoxic, marine sediments (high S/C ratio). Figure 2 is a plot of such data from the Collingwood Member, from the overlying Blue Mountain Formation and from the underlying Lindsay Formation.

The low S/C ratio for many of the Collingwood samples cannot represent terrestrial input given the Ordovician age of these rocks. Compared to the other formations, the Collingwood appears to be enriched in organic carbon without a consistent enrichment in sulphur. Thus, neither the carbon isotopes nor the S/C ratio indicate a unique, anoxic environment during deposition of this organic-rich marl. Additional S/C data is being gathered to see if spatial variations occur along the outcrop belt of the Collingwood. These studies will continue in cooperation with the Ontario Geological Survey studies of this potential oil shale in an effort to define the environment responsible for the accumulation of this organic-rich sediment.

ACKNOWLEDGMENTS

R. Dickhout assisted with geochemical analyses. Ontario Geological Survey scientists, particularly D.J. Russell and M.D. Johnson, have assisted with sample collection and have provided considerable geological information. T.G. Powell, P. Gunther and D. Bree are co-investigators in the oil and natural gas studies.

REFERENCES

Bailey, S.M.B. and Cochrane, R.O.
1984: Evaluation of Ontario's Conventional and Potential Oil and Gas Reserves: Abstracts of the Geological Association of Canada - Mineralogical Association of Canada Joint Annual Meeting, May 14-16, 1984, Volume 9, p.44.

Barker, J.F., and Pollock, S.J.
1984: The Geochemistry and Origin of Natural Gases in Southern Ontario; Bulletin of Canadian Petroleum Geology, Volume 32, September 1984.

Barker, J.F., Dickhout, R.D., Russell, D.J., Johnson, M.D., and Gunther, P.R.
1983: Paleozoic Black Shales of Ontario - Possible Oil Shales; p.119-138 *in* Geochemistry and Chemistry of Oil Shales, edited by F.P. Miknis, and J.F. McKay, American Chemical Society Symposium Series, Volume 230.

Berner, R.A., and Raiswell, R.
1983: Burial of Organic Carbon and Pyrite Sulfur in Sediments over Phanerozoic Time: a New Theory; Geochimica et Cosmochimica Acta, Volume 47, p.855-862.

Booth-Horst, R., and Rybansky, R.
1982: Oil and Gas Exploration, Drilling and Production Summary, 1980; Ontario Ministry of Natural Resources, Oil and Gas Paper 3, 181p.

Churcher, P.L., and Barker, J.F.
1984: Geology and Geochemistry of the Collingwood "Oil Shale", Southern Ontario; Abstracts of the Geological Association of Canada - Mineralogical Association of Canada Joint Annual Meeting, May 14-16, 1984, Volume 9, p.52.

Gold, T.
1979: Terrestrial Sources of Carbon and Earthquake Outgassing; Journal of Petroleum Geology, Volume 1, p.3-19.

James, A.T.
1983: Correlation of Natural Gas by Use of Carbon Isotopic Distribution between Hydrocarbon Components; American Association of Petroleum Geologists Bulletin, Volume 67, p.1176-1191.

Keith, M.L.
1982: Violent Volcanism, Stagnant Oceans and Some Inferences Regarding Petroleum, Strata-bound Ores and Mass Extinctions; Geochimica et Cosmochimica Acta, Volume 46, p.2621-2637.

Macqueen, R.W., and Powell, T.G.
1984: Distinctive Character and Origin of Silurian Oils, Southwestern Ontario; Abstracts of the Geological Association of Canada - Mineralogical Association of Canada Joint Annual Meeting, May 14-16, 1984, Volume 9, p.86.

Powell, T.G., Macqueen, R.W., Barker, J.F., and Bree, D.G.

1984: Geochemical Character and Origin of Ontario Oils; Bulletin of Canadian Petroleum Geology. Volume 32, September 1984.

Grant 118 Surface Electromagnetic Mapping in Selected Positions of Northern Ontario

J.D. Redman, D.W. Strangway, and O.M. Ilkisik

Department of Geology, University of Toronto

ABSTRACT

In conjunction with our application of audio frequency magnetotellurics to electromagnetic mapping in northern Ontario, we have carried out measurements on the electrical resistivity of the surficial deposits (clays, silts, and sands). The conductive clays of the Abitibi clay belt, which are quite extensive in our study area, are known to be a serious impediment to the application of EM techniques in this important mining region.

The glaciolacustrine clays, silts and sands generally form a horizontally stratified section. Overburden thicknesses of 50 m and clay layer thicknesses of 30 m are not uncommon. We have characterized the 'typical' low frequency resistivities of the clays, silts, and sands and measured the frequency dependence of their resistivity in the range of 0.01 Hz to 1 MHz. We have determined the sand, silt and clay size fractions for these samples. The average DC (low frequency) resistivities are: clays (22 samples) 23 ohm metres, silts (13 samples) 72 ohm metres and sands 1000-5000 ohm metres (*in situ* measurements). *In situ* DC resistivity measurements using a Wenner array with a spacing of 0.5 m give consistently higher resistivities than laboratory measurements on samples from the same locations. We believe that this difference is due to both cracks in the near surface soil and to differences between the horizontal and vertical resistivity of the soil.

In general the samples show only a small frequency dependence in their resistivity in contrast with previous measurements on clays. The frequency effect between 5 and 50 Hz is typically less than 2.5%.

INTRODUCTION

In the previous summaries of our research we have reported on the results of audio frequency magnetotelluric (AMT) surveys. The principal aim of these surveys has been to apply the AMT technique to mapping the electrical structure of the basement buried beneath thick conductive overburden. In this report we will discuss laboratory and *in situ* measurements of the resistivity of the overburden components and their relationship to the electrical structure of the overburden.

The area in which we have concentrated our study encompasses a large part of the Abitibi clay belt shown in Figure 1. The conductive clays of the clay belt (lacustrine deposits) are a serious impediment to the application of electromagnetic (EM) techniques in this area and a better understanding of these conductive surficial deposits will be useful in the interpretation of EM data. There were two main goals in our work. One was to characterize the 'typical' resistivities of the different overburden components, that is clays, silts, and sands, and from this to derive a typical electrical section. The other was to study the frequency dependence of the resistivity. We have concentrated most of our work on characterizing the clays and silts since they are the most conductive overburden component.

OVERBURDEN DEPTHS AND STRATIGRAPHY

For the purpose of identifying 'typical' overburden depths and clay thicknesses we have reviewed the available literature on the survey area. In the Abitibi clay belt, the glaciolacustrine clays, silts and sands which were deposited in proglacial Lake Barlow-Ojibway generally form a horizontally stratified section. The clays and silts are commonly varved showing a pattern of seasonal deposition. In the northern part of the region around Cochrane, clayey and silty tills cover the clays. These were deposited during a local re-advance of the ice sheet. In other areas it is possible for the clays to be masked by sands from outwash deposits or from eskers. Clay pockets in buried bedrock valleys and between bedrock outcrops are probably quite common.

The surficial material and landforms have been mapped at a scale of 1:100,000 for the Ontario Geological Survey (Gartner *et al.* 1979). There is also a series of drift thickness maps (Baker 1979) published by Ontario Geological Survey in which the data have been obtained from assessment files (Assessment Files Research Office, Ontario Geological Survey, Toronto). The drift thickness maps presently available cover the area (region A in Figure 1) near Kirkland Lake. The distribution of overburden thicknesses for data taken from these maps is shown in Figure 2. For each of the 221 locations, we have taken the maximum depth for all drill holes near that location. The purpose of this approach was to emphasize the deepest re-

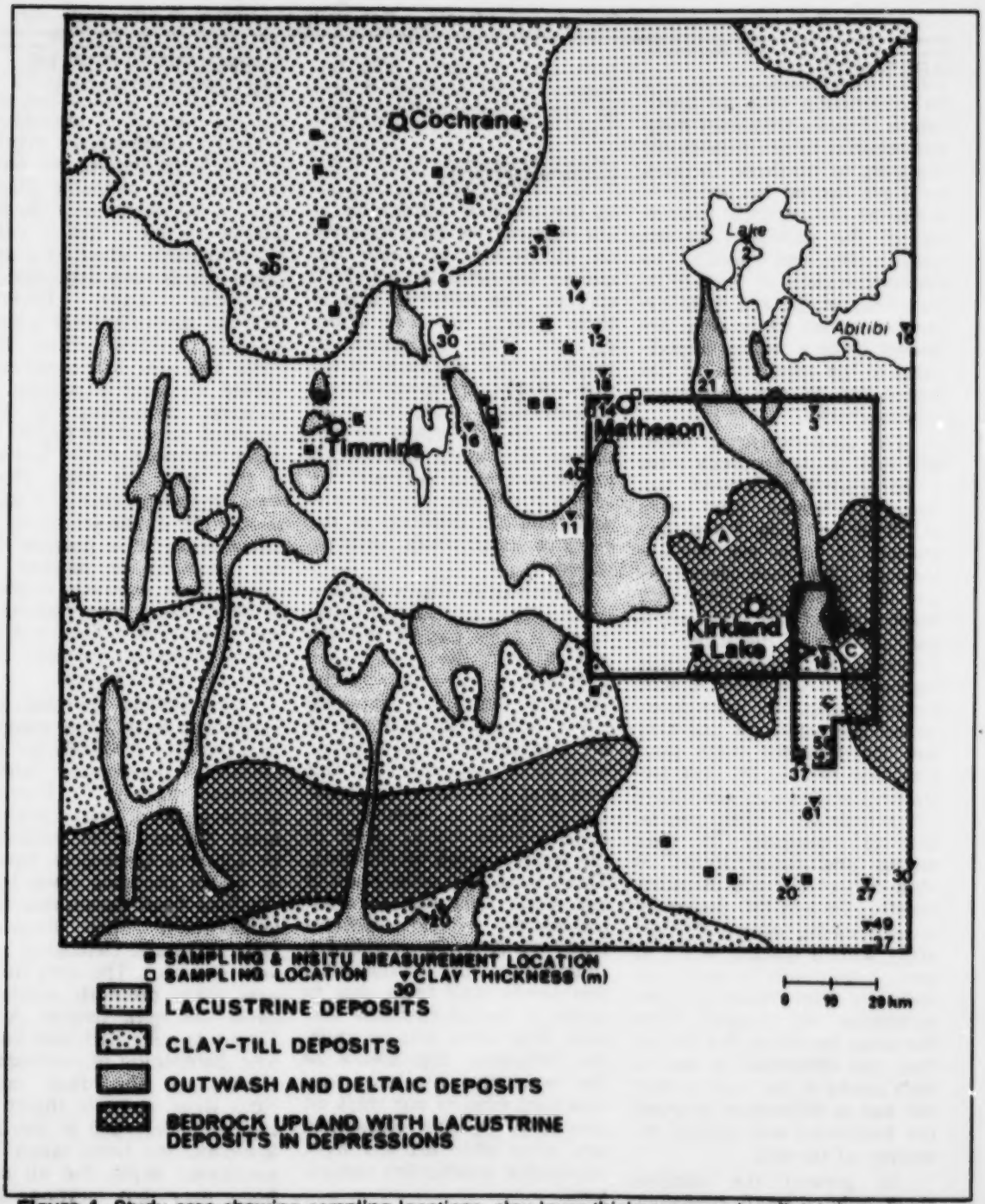

Figure 1. Study area showing sampling locations, clay layer thicknesses and surficial deposits.

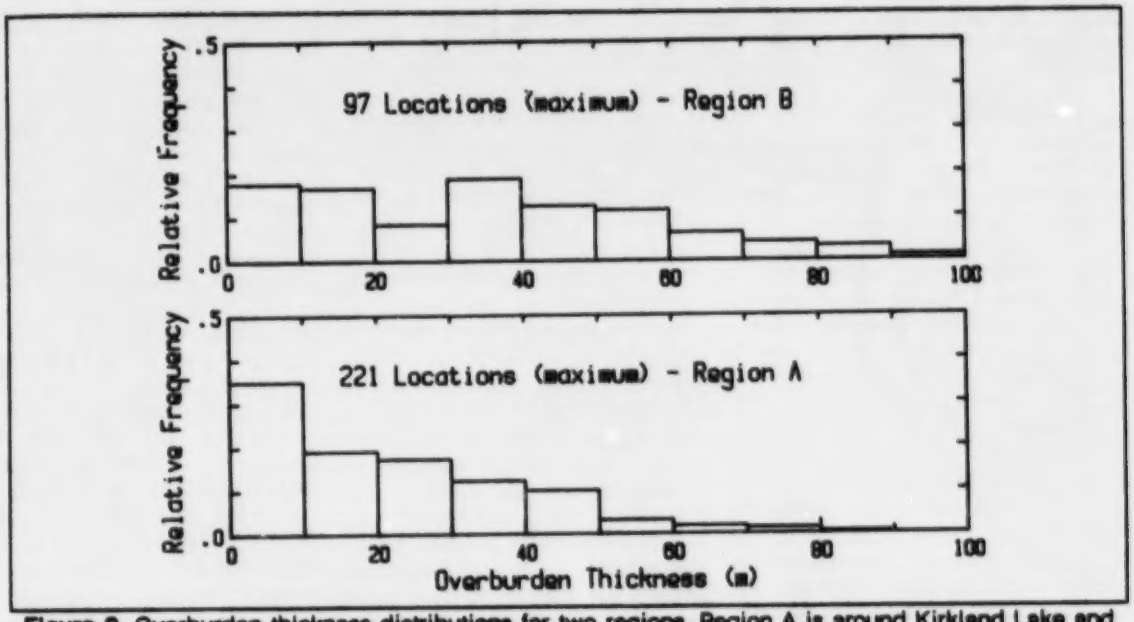

Figure 2. Overburden thickness distributions for two regions. Region A is around Kirkland Lake and region B is the remaining area outlined on Figure 1. The data were obtained from Ontario Geological Survey drift thickness maps (Maps P.2477-2480, Baker 1981) and assessment files.

gions at each locality. These results are probably still biased towards thinner overburden than is typical for the area since drilling prospects are more likely to be in areas of thinner overburden. It is clear that in this area overburden depths of greater than 50 m are not uncommon. There was one hole drilled in Gauthier Township with a depth to bedrock of 242 m. A sampling of assessment files from the rest of the area (region B) show that depths of 30 m are common.

It is the clay and silt within the overburden that predominate in limiting the depth of penetration for EM methods. Figure 1 shows typical clay and silt layer thicknesses. These data, which are taken from available literature, were obtained from drill holes and exposures. For example, near Frederick House, 93 holes were drilled giving an average clay thickness of 35 m. A reverse circulation drilling program carried out by Averill and Thompson (1981) for the Ontario Geological Survey south of Kirkland Lake (region C), where there are numerous bedrock outcrops, found a maximum overburden thickness of 73 m and maximum clay layer thickness of 58 m. The overburden sections observed in the holes in this region show that the overburden stratigraphy is quite variable. The clay and silt layers are often buried under varying thicknesses of sand. For this area in general, seismic data and drilling results show that there can often be significant bedrock relief. Thus conductive clay-filled channels and valleys may be common.

RESISTIVITY MEASUREMENT TECHNIQUE

Samples for the resistivity measurements were collected from gravel pits, road cuts and exposures along rivers at the sample sites shown in Figure 1. When collecting the samples, surface material was removed to expose unweathered and undisturbed clay. Samples were obtained by pressing a 1-inch plastic tube into the face of the clay. The samples were from homogeneous units so that even a small sample was representative of the whole unit. The samples were collected in an orientation that allowed the horizontal resistivity to be measured. They were also heat-sealed in plastic bags to preserve their original moisture content.

The magnitude and phase of the resistivity was measured

over the frequency range of 5 Hz to 1 MHz. Some measurements were also carried out in the range 0.01 Hz to 1 MHz. The Hewlett-Packard HP4192a impedance analyzer was used in these measurements for frequencies above 5 Hz. Four electrode measurements, using separate current and potential electrodes, were made from 5 Hz to 10 kHz. Above 10 kHz, a four terminal and two electrode technique was used. Platinum mesh was used for the current electrodes and platinum wire for the potential electrodes. A current density of approximately 0.1 A/m^2 was used for all measurements.

We have chosen to classify our samples according to the fraction of sand (>45 μm), silt (4 μm to 45 μm) and clay (<4 μm) size particles they contain. This grain size analysis was done by using standard techniques of sieving and sedimentation analysis. The sand size fraction is obtained by wet sieving the sample through a 45 μm sieve. The sample containing the remaining silt and clay fraction is dispersed in a column of distilled water containing a dispersant (Calgon). The mixture is allowed to settle until all particles with grain sizes greater than 4 μm have settled. The supernatent is decanted and the amount of clay in the decanted liquid is determined by evaporating the liquid in an oven and weighing the sediment. Corrections are made for the amount of dispersant in the sediment. This sedimentation process is repeated three times to remove all of the clay size fraction. The remaining sediment, in the cylinder at the end of this process, is dried to determine the silt content.

The clay size fraction typically contains 70% clay minerals. From X-ray diffraction analyses of a few of the clays it was determined that the principal clay minerals were chlorite (40%) and illite (30%). When reference is made to the amount of sand, silt or clay, we are referring to the grain size and not to the mineralogy of the sample.

LOW FREQUENCY RESISTIVITY MEASUREMENTS

The results of the low frequency (50 Hz) or DC resistivity measurements are shown in Figure 3. One measurement per site has been plotted from the widely scattered localities shown on Figure 1. The presentation of the results as both conductivities and resistivities allows details in the data to be seen at both low and high clay contents. The trend of increasing conductivity with increasing clay content along with a considerable degree of scatter for a fixed clay content is evident. This scatter is controlled primarily by the different pore water conductivities and formation factors for samples from different environments.

In Figure 4 the distribution of resistivities for silts and clays are given. For the purposes of presenting the data, the samples have been divided into three classes. Clays contain more than 35% clay (clay size fraction), silts have less than 35% clay and less than 70% sand. The resistivities of the clays are tightly grouped with an average of 23 ohm metres, whereas the resistivities of the silts are more variable. AMT surveys that we have carried out typically gave 20-50 ohm metres for the most conductive layers in the overburden section, which are presumably clays.

A relatively simple model has been given by Shainberg *et al.* (1980) to explain the dependence of the DC or low frequency conductivity (σ) of soils on pore water conductivity and surface conductivity. In this electrical model, two conductive paths in parallel are used to describe conduction in a soil. One conduction path is through the pores assuming the matrix is an insulator. The other path consists of surface conduction through the exchangeable cations on the surface of the clay particles in series with a conduction path through the pore water between the soil particles.

$$\sigma = \sigma_w F^{-1} + \sigma_s' \sigma_w (K\sigma_s' + \sigma_w)^{-1}$$

where: $\sigma_s' = \mu_+ C\rho(\theta F)^{-1}$

μ_+ - Mobility of specific cation in diffuse double layer ($cm.sec.V^{-1}.m^{-1}$)

C - Cation exchange capacity (meq/g)

ρ - Soil density (g/cm^3)

θ - Porosity

σ_w - Conductivity of pore water (mS/cm)

σ_s' - Apparent surface conductivity (mS/cm)

F - Formation factor

K - Function of fractional length of solid phase ($K \cong 0.3$)

In Figure 5 the dependence of soil conductivity on pore water conductivity is shown for two soil samples. The plot shown is based on the above model fitted to measured values which are essentially equivalent. One would expect the varved clays to show a similar dependence on pore water conductivity but to be more consolidated and thus have higher formation factors than observed in these soils. We measured a pore water conductivity of 0.13 S/m on

one of our clay samples (62% clay, 34% silt and 4% sand).

The Shainberg model implies that the scatter in the observed conductivity for a fixed clay content must be related to different pore water conductivities, formation factors and cation exchange capacities (related not to clay content but to different clay mineralogy and ionic species) for samples from different environments. The clays in the region are from a common source and were deposited in the same environment (i.e. Lake Barlow-Ojibway); therefore it is likely that the clay mineralogy is the same for all samples. Thus the scatter is related to different pore water conductivities and formation factors. Our measurements on the resistivities of the soil samples from the region are considered to be typical. Deviations from the typical values can be predicted by using the Shainberg model.

Using the drill hole logs from the overburden drilling program south of Kirkland Lake and using our laboratory resistivity measurements on silts, clays and sands and a reasonable estimate for the tills, one can estimate overburden conductances for this area (Figure 6). These results show that conductances of 1 to 2 siemens are not uncommon for the area. There have been reports of some overburden in the Abitibi region containing salt water which would clearly make a significant difference in the resistivities. Marine clays in the Hawkesbury area of Ontario have resistivities of 2 ohm metres (Dyck 1974) compared with the average of 23 ohm metres we have seen in the Abitibi clay belt.

We have also carried out *in situ* resistivity measurements using a Wenner array with a spacing of 0.5 m. The comparison between our laboratory measurements and these *in situ* measurements are shown in Figure 7a. The laboratory measurements are consistently lower than the *in situ* measurements by approximately a factor of 2. We believe that this difference is due to cracks in the near surface soil which would increase the resistivity on the large scale and to differences between the horizontal and vertical resistivity of the soil. Measurements on varved clays in this area by Chan and Kenny (1973) indicate that horizontal and vertical hydraulic conductivities can be different by up to a factor of 5, which would indicate that there could be similar differences in resistivity. A similar difference between laboratory and *in situ* measurements is shown in Figure 7b for samples taken through an exposed 2 m thick varved clay layer.

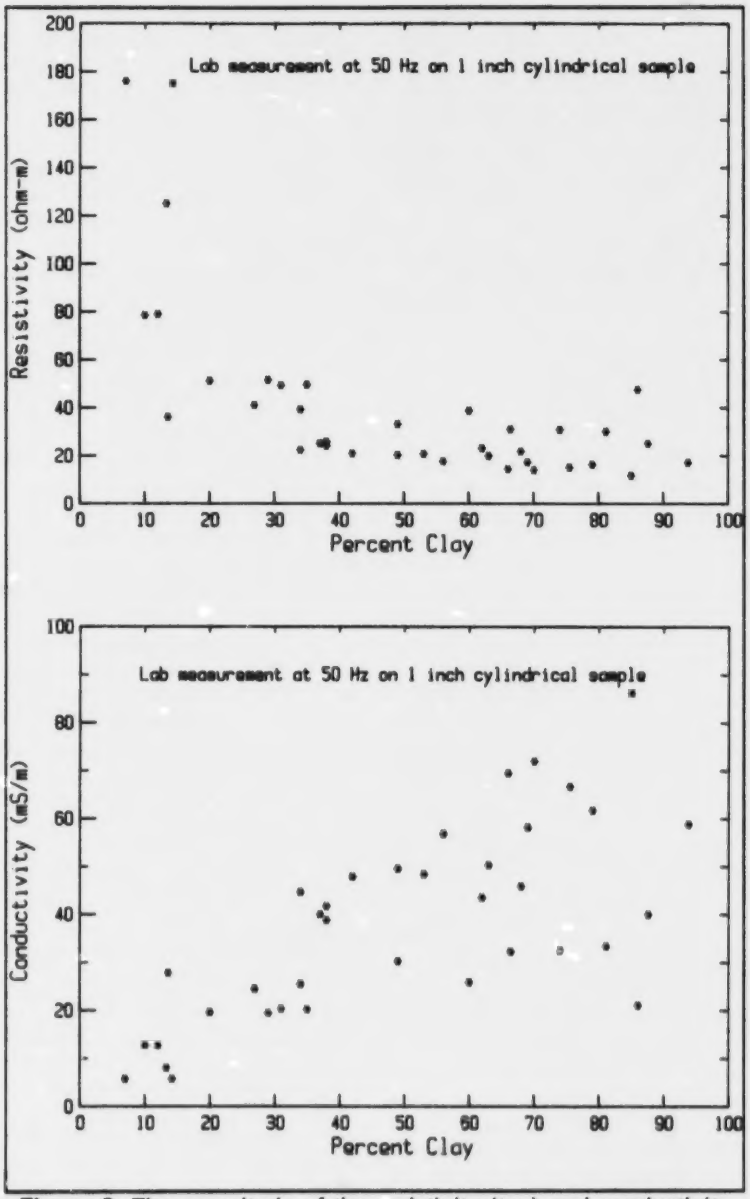
Lab measurement at 50 Hz on 1 inch cylindrical sample
Resistivity (ohm-m)
Percent Clay
Lab measurement at 50 Hz on 1 inch cylindrical sample
Conductivity (mS/m)
Percent Clay

Figure 3. The magnitude of the resistivity (top) and conductivity (bottom) at 50 Hz are plotted as a function of clay content. One data point is shown for each sampling location.

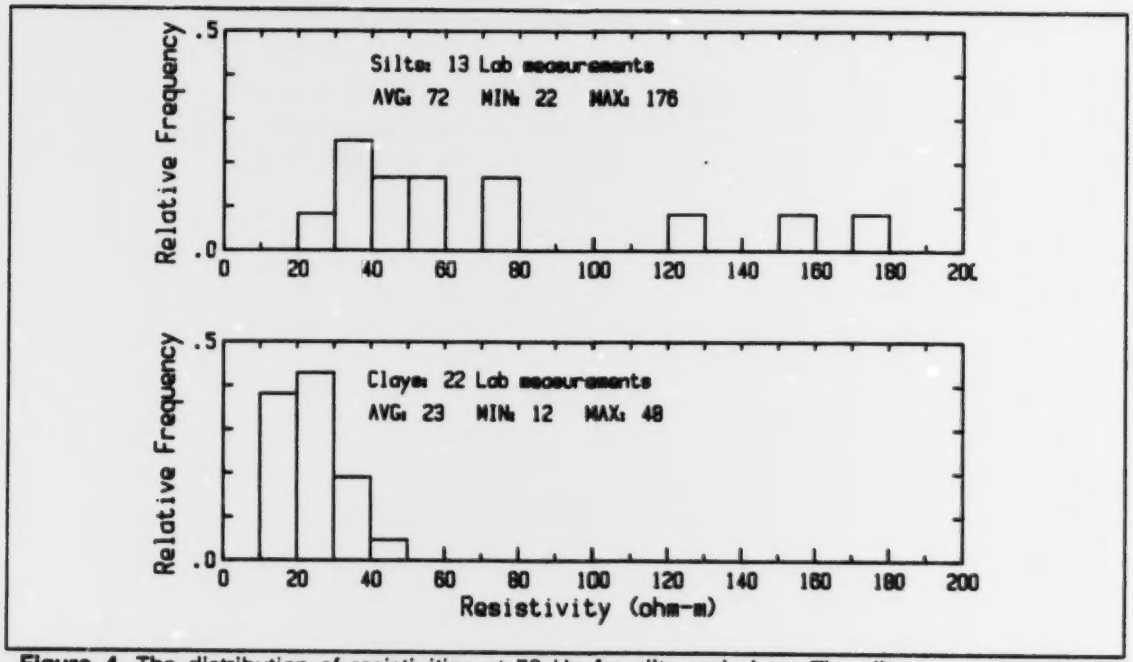
Silts: 13 Lab measurements
AVG: 72 MIN: 22 MAX: 176
Clays: 22 Lab measurements
AVG: 23 MIN: 12 MAX: 48
Relative Frequency
.5
.0
0 20 40 60 80 100 120 140 160 180 200
Resistivity (ohm-m)

Figure 4. The distribution of resistivities at 50 Hz for silts and clays. The silts are more variable and have higher resistivities.

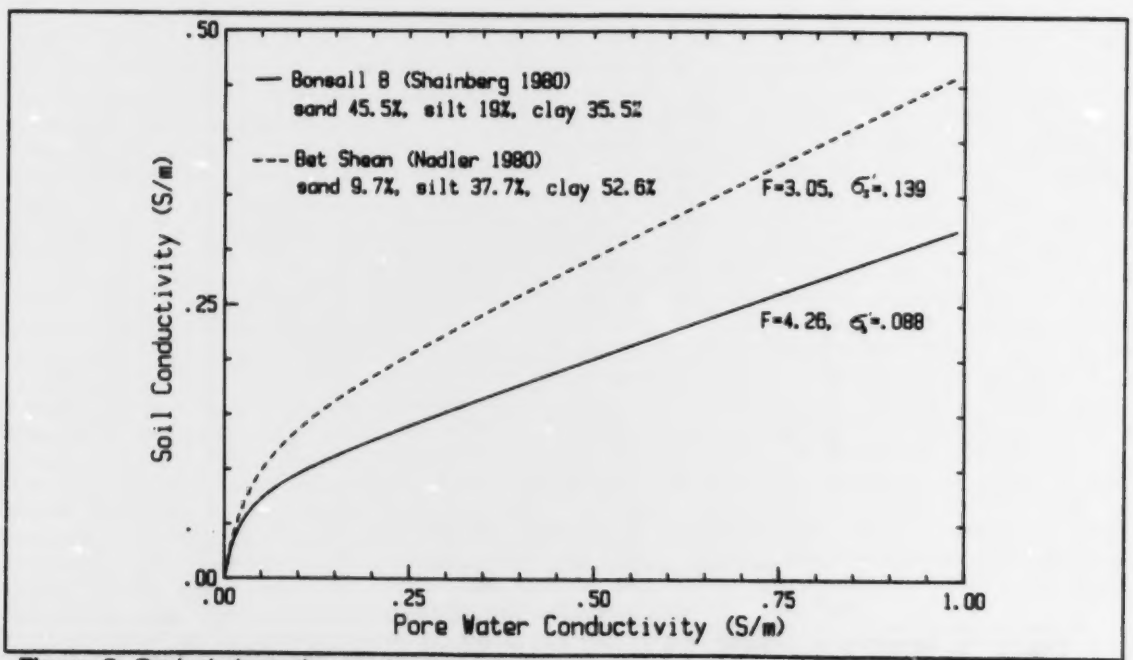

Figure 5. Typical dependence of soil conductivity on pore water conductivity for two soils (from Nadler and Frenkel 1980, and Shainberg *et al.* 1980).

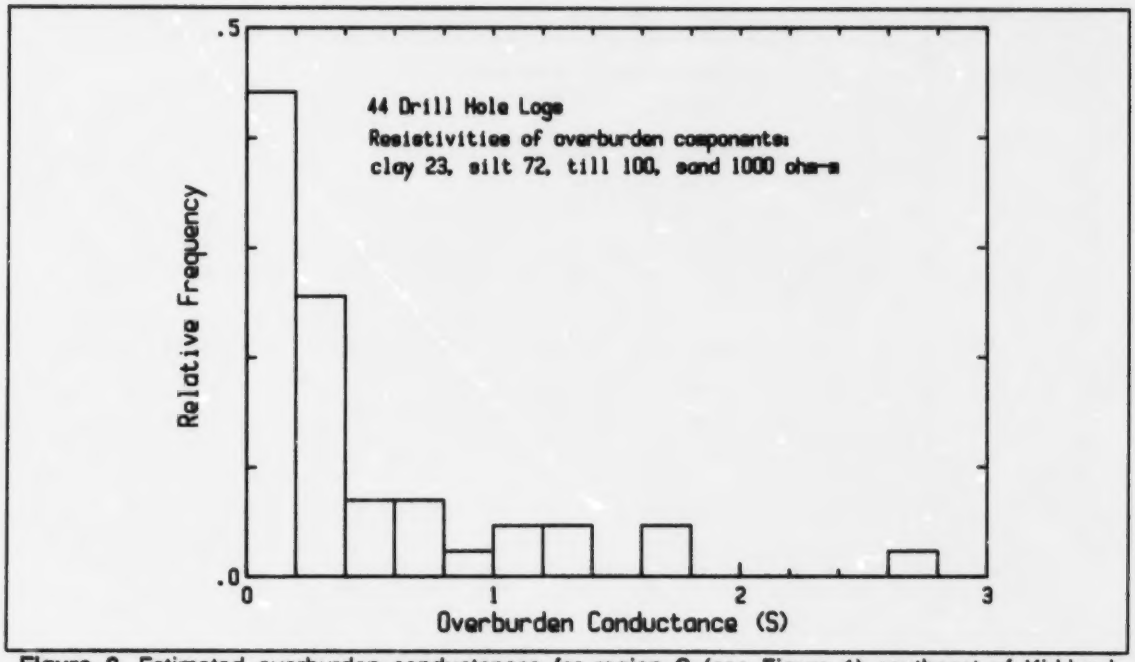

Figure 6. Estimated overburden conductances for region C (see Figure 1) southeast of Kirkland Lake.

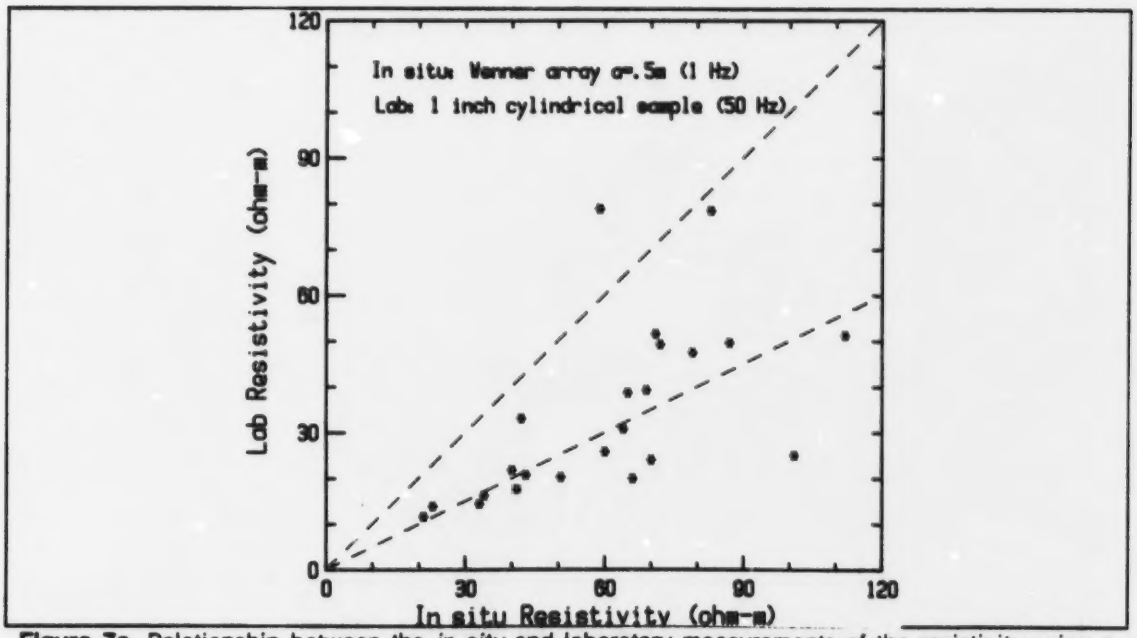

Figure 7a. Relationship between the *in situ* and laboratory measurements of the resistivity using a Wenner array with a = 0.5 m for the *in situ* measurements. The sample sites are shown on Figure 1.

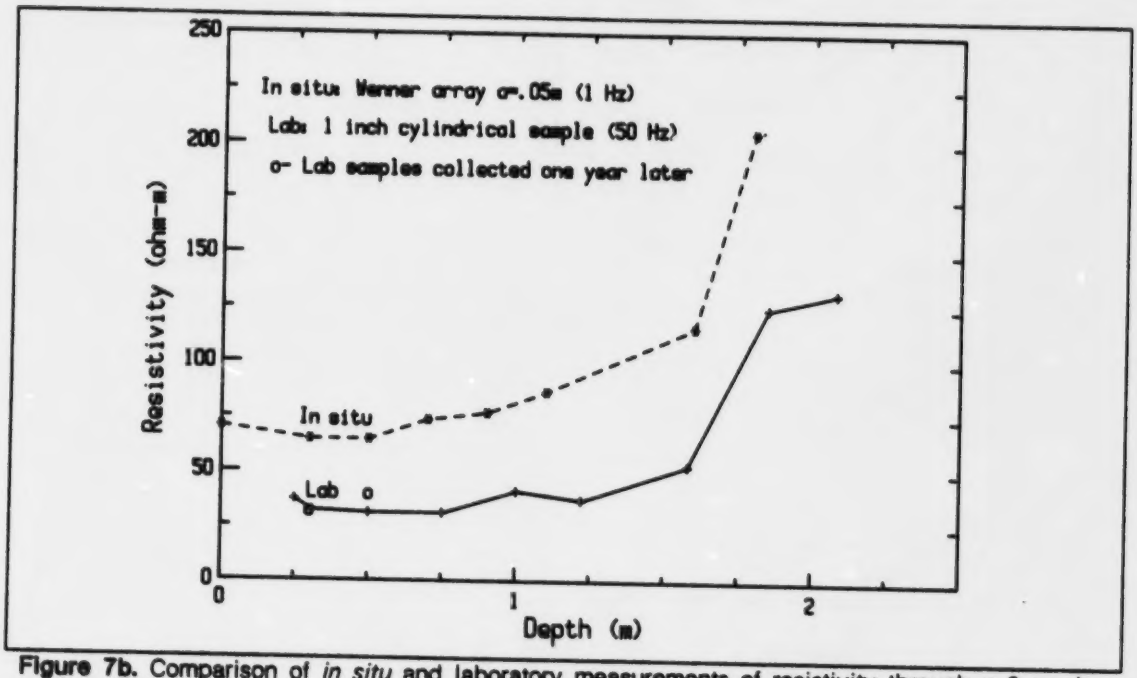

Figure 7b. Comparison of *in situ* and laboratory measurements of resistivity through a 2 m clay layer. For the *in situ* measurements a Wenner array, with a = 0.05 m, was used.

RESISTIVITY FREQUENCY DEPENDENCE

We have also measured the frequency dependence of the complex resistivity of laboratory samples. Laboratory measurements on the frequency dependence of the resistivity of kaolinite, illite and silty clay by Mehran and Arulanandan (1977) show a significant frequency dependence in the range 50 Hz to 100 kHz. Their measurements show that the magnitude of the resistivity dispersion increases with decreasing water content, electrolyte concentration and cation exchange capacity. Their measurements on silty clay gave a frequency effect of 17% between 100 Hz and 1 kHz. The dispersions that they observed are much larger than anything we have seen, our largest being 4% between 5 Hz and 50 Hz (Figure 9). In general, these samples show little dispersion in their resistivity as can be seen in Figure 8. Although, as we have reported previously (Strangway *et al.* 1983), one of our samples showed a curious negative percent frequency effect (PFE) and positive phase angle.

For the purpose of comparing directly the resistivity dispersion observed in our samples with the results of Mehran and Arulanandan (1977), we homo-ionized one of our samples with Na^+ and compared the result with another sample from the same location. The sample was homo-ionized (all exchangeable cations replaced with Na^+) by treating with 1 mol NaCl solution, followed by leaching with distilled water and then treatment with 0.01 mol NaCl solution. The frequency dependence (Figure 10) is similar to that of the untreated sample. The untreated sample has a small dispersion (negative phase peak and decreasing resistivity) at low frequencies that is not present in the treated sample. The treated sample has a higher phase response at the highest frequencies but this is simply a result of it having a lower DC resistivity. The frequency effect (between 50 Hz and 100 kHz) in the treated sample is 6% which is quite small compared with 25% obtained by Mehran and Arulanandan (1977) for an illite clay.

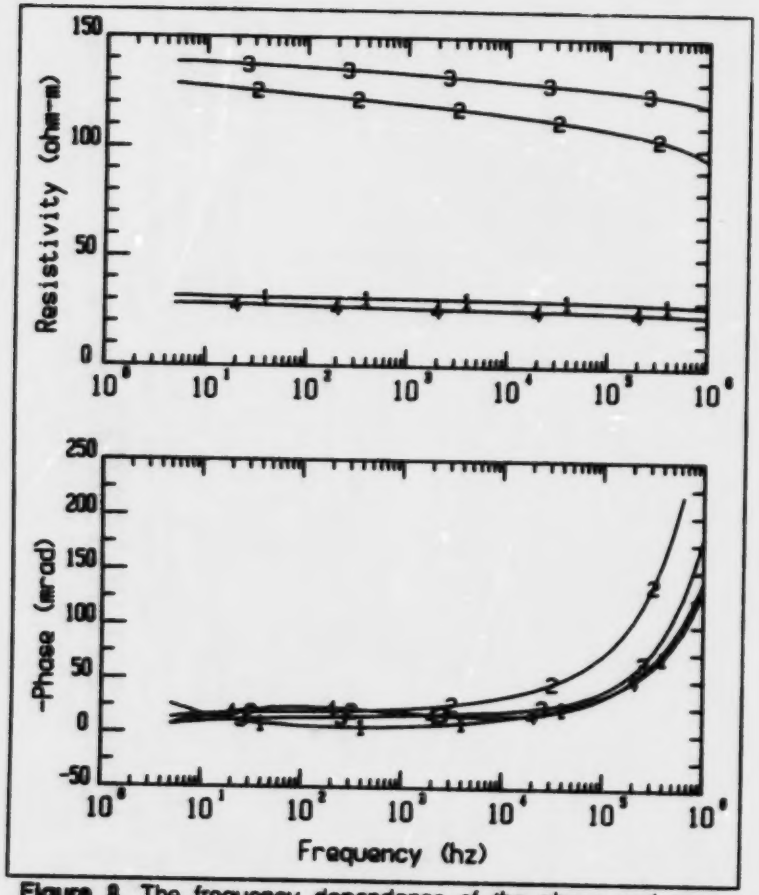

Figure 8. The frequency dependence of the phase and magnitude of the resistivity of typical soil samples. The measured data points, of which there are 10 per decade, have been joined by straight line segments. Sample 1: varved clay (clay 66%, silt 26%, sand 8%); sample 2: sandy loam (clay 14%, silt 30%, sand 56%); sample 3: varved silt loam (clay 95, silt 63%, sand 28%); sample 4: peat.

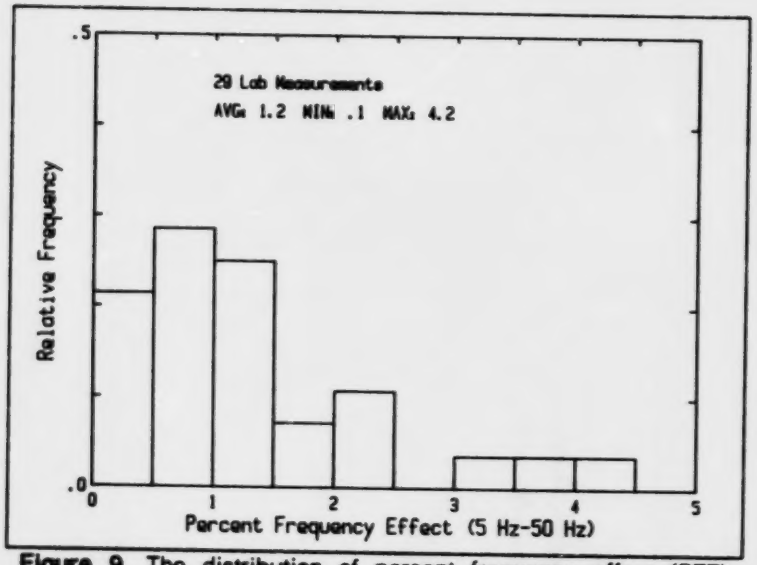

Figure 9. The distribution of percent frequency effect (PFE) observed in laboratory samples,
PFE = $(\rho_{5Hz} - \rho_{50Hz})/\rho_{5Hz} \times 100$.

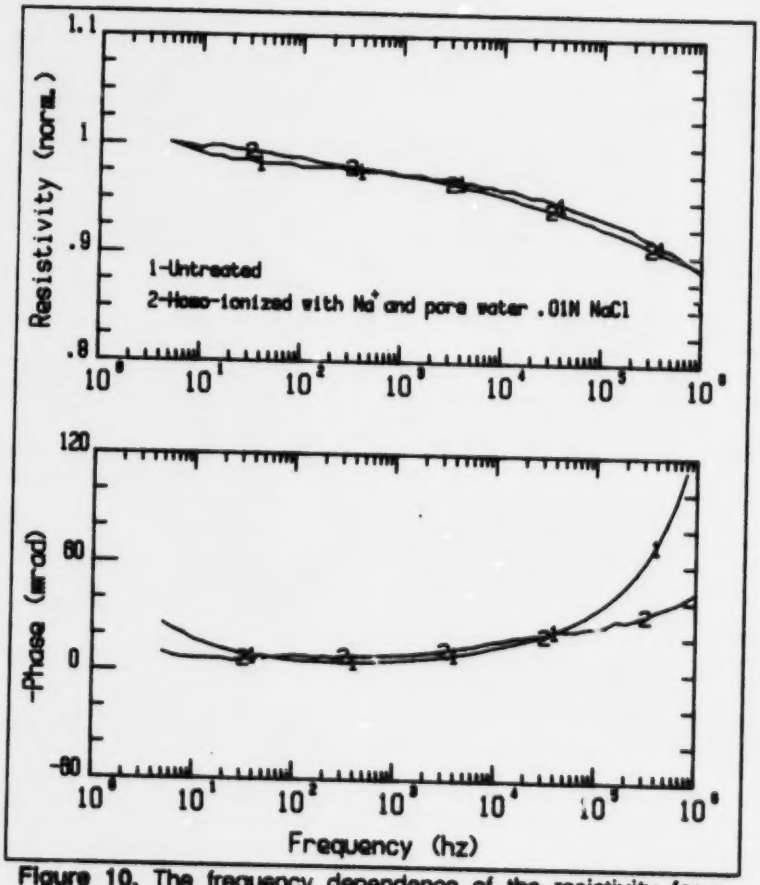

Figure 10. The frequency dependence of the resistivity for a homo-ionized and untreated clay sample. The resistivity at 5 Hz (normalizing value) is 32 ohm metres for the untreated sample and 9 ohm metres for the treated sample.

CONCLUSIONS

These resistivity measurements should be useful in predicting a typical electrical section for the overburden in this region. Our measurements show that the clays have typical resistivities of 20 ohm metres and silts typically 70 ohm metres. The relationship between the *in situ* and laboratory measurements will require more investigation to provide a satisfactory explanation for the differences observed. In general, the frequency dependence of the clays appears to be small and of little significance to most EM techniques.

REFERENCES

Averill, S.A., and Thompson, I.
1981: Reverse Circulation Rotary Drilling and Deep Overburden Geochemical Sampling in Marter, Catherine, McElroy, Skead, Gauthier and Hearst Townships, District of Timiskaming; Ontario Geological Survey, Open File Report 5335.

Baker, C.L.
1981: Drift Thickness of the Magusi River, Larder Lake, Ramore, and Kirkland Lake Areas, and the Cochrane and Timiskaming Districts; Ontario Geological Survey, Maps P.2477-P.2480, Drift Thickness Series, Scale 1:50,000, Compilation 1979-1980.

Boissonneau, A.N.
1966: Glacial History of Northeastern Ontario - I. The Cochrane-Hearst Area, Canadian Journal of Earth Sciences, Volume 3, p.559-578.

Chan, H.T., and Kenny, C.T.
1973: Laboratory Investigation of the Permeability Rates of New Liskeard Varved Soil; Canadian Geotechnical Journal, Volume 10, p.453-472.

Desaulniers, D.E.
1982: Clayey Quaternary Deposits in Northern Ontario - A Review; Atomic Energy of Canada, TR-305

Dyck, A.V.
1974: Surficial Conductivity Mapping with the Airborne Input System; Canadian Institute of Mining and Metallurgy, Bulletin, Volume 67, p.104-109.

Gartner, J.F. *et al.*
1979: Northern Ontario Engineering Geology Terrain Study Data Base Maps; Ontario Geological Survey, Maps 5000-5093, scale 1:100,000.

Hughes, O.L.
1961: Preliminary Report on Borings Through Pleistocene Deposits, Cochrane District, Ontario; Geological Survey of Canada, Paper 61-16.

Ilkisik, O.M., Hsu, D.T., Redman, J.D., and Strangway, D.W.
1982: Surface Electromagnetic Mapping in Selected Positions of Northern Ontario; *in* Summary of Research 1981-1982, edited by E.G. Pye, Ontario Geological Survey, Miscellaneous Paper 103.

Mehran, M., and Arulanandan, K.
1977: Low Frequency Conductivity Dispersion in Clay-Water-Electrolyte Systems; Clays and Clay Minerals, Volume 25, p.39.

Nadler, A., and Frenkel, H.
1980: Determination of Soil Solution Electrical Conductivity from Bulk Soil Electrical Conductivity Measurements by the Four-Electrode Method; Soil Science Society of America, Journal, Volume 44.

Roy, K.K., and Elliot, H.M.
1980: Model Studies on Some Aspects of Resistivity and Membrane Polarization Behaviour Over a Layered Earth; Geophysical Prospecting, Volume 28, p.759-775.

Shainberg, I., Rhoades, J.D., and Prather, R.J.
1980: Effect of Exchangeable Sodium Percentage, Cation Exchange Capacity, and Soil Solution Concentration on Soil Electrical Conductivity; Soil Science Society of America, Journal, Volume 44.

Strangway, D.W., Ilkisik, O.M., and Redman, J.D.
1983: Surface Electromagnetic Mapping in Selected Positions of Northern Ontario; *in* Summary of Research 1982-1983, edited by E.G. Pye, Ontario Geological Survey, Miscellaneous Paper 113.

Grant 128 Subsurface Quaternary Stratigraphy using Borehole Geophysics

R.N. Farvolden, J.P. Greenhouse and P.F. Karrow

Department of Earth Sciences, University of Waterloo

ABSTRACT

Work this year has focussed on calibration and interpretation methods for comparing geophysical logs with geological core. Calibration pits for radiation logs have been established, a fourth carefully logged borehole has been completed, and extensive experimentation with cross plotting techniques for data analysis has been undertaken. Approaching its final year, the project has already added greatly to our ability to interpret geophysical logs in terms of the lithological and hydrogeological nature of the regional overburden. The lack of sufficient core will, however, prevent us from reaching the original objectives of this project.

INTRODUCTION

Our report on this project for 1982-1983 (Greenhouse *et al.* 1983) described the background and objectives for the work we are carrying out. We describe here the progress towards those objectives in the past year.

The locations of wells referred to in this report are shown in Figure 1. At each of the well sites a borehole has been rotary-drilled to bedrock and geophysically logged. Holes have been cored two-thirds of the way to bedrock beside GB82-3, and one-third of the way to bedrock beside GB82-2. Each of the geophysically logged holes (as opposed to the cored holes) was cased with a standard casing, shown in Figure 2, following electric and caliper logging. These cased holes have then been used for repeated and careful nuclear logging with natural gamma, density and neutron tools. The primary objective of the project is to relate the geophysical logs to core logs at several sites where both sets of data are available, and thereby learn how to obtain detailed overburden stratigraphy from the (relatively inexpensive) geophysical logs alone. This stratigraphy is vital to the development of water supply in the region as well as for deciphering the Quaternary geology of the area.

PROGRESS 1983-1984

Funding was not provided for additional cored holes, so this year's work has concentrated on further analysis of the first year's data, and on establishing calibrations for physical properties and lithology versus tool response.

With reference to the objectives for 1983-1984 given in last year's report, we note the following.

1. The existing boreholes have been relogged, as many as 10 times in some cases, to establish the variability of both the tool response and of depth as recorded by the logger. The responses listed for a borehole are now the average of two or more independent runs of the tool. The responses have also been averaged over 15 cm intervals to give mean response over a typical core sample. This mean is further characterized by the variance within the interval. For example, an average taken over a transition between two response levels, say at a formation boundary, would not be typical of the materials on either side and should be treated accordingly.

2. Calibration pits have been established on the north campus of the University of Waterloo in which the radiation tools can be calibrated for clay content, density, and moisture content. A schematic of a calibration pit is given in Figure 3. The materials in the pits are calibrated by coring, and by running soil moisture and density probes down the four auxiliary boreholes around the central casing to check for lateral and vertical homogeneity. Calibration curves have been constructed by Insinna (1984).

3. Some drilling was undertaken. Drilling credits accumulated from last year were used to underwrite part of a rotary hole GB83-1 (see Figure 1), and current funding was used for shallow boreholes at two sites to improve 'stratigraphic' calibrations. One of these sites was chosen so as to intersect the two major marker horizons in the area, the Maryhill and Catfish Creek tills, at shallow depth. Two holes within 20 m of each other were cored and logged to a depth of 10 m. The core/log responses are still being analyzed. At the second site a hole was cored to 25 m beside a rotary hole GB82-2 that was logged in 1982 (see Figure 1). As noted in our 1982-1983 report, that log was interesting because - based on our knowledge of its response at that time - the Maryhill till did not appear to be present. The coring revealed that this was in fact the case. It is important to stress that the presence or absence of this prominent till cannot be established from the drillers logs; only careful inspection of the core - and now also, we believe, the geophysical logs - can identify

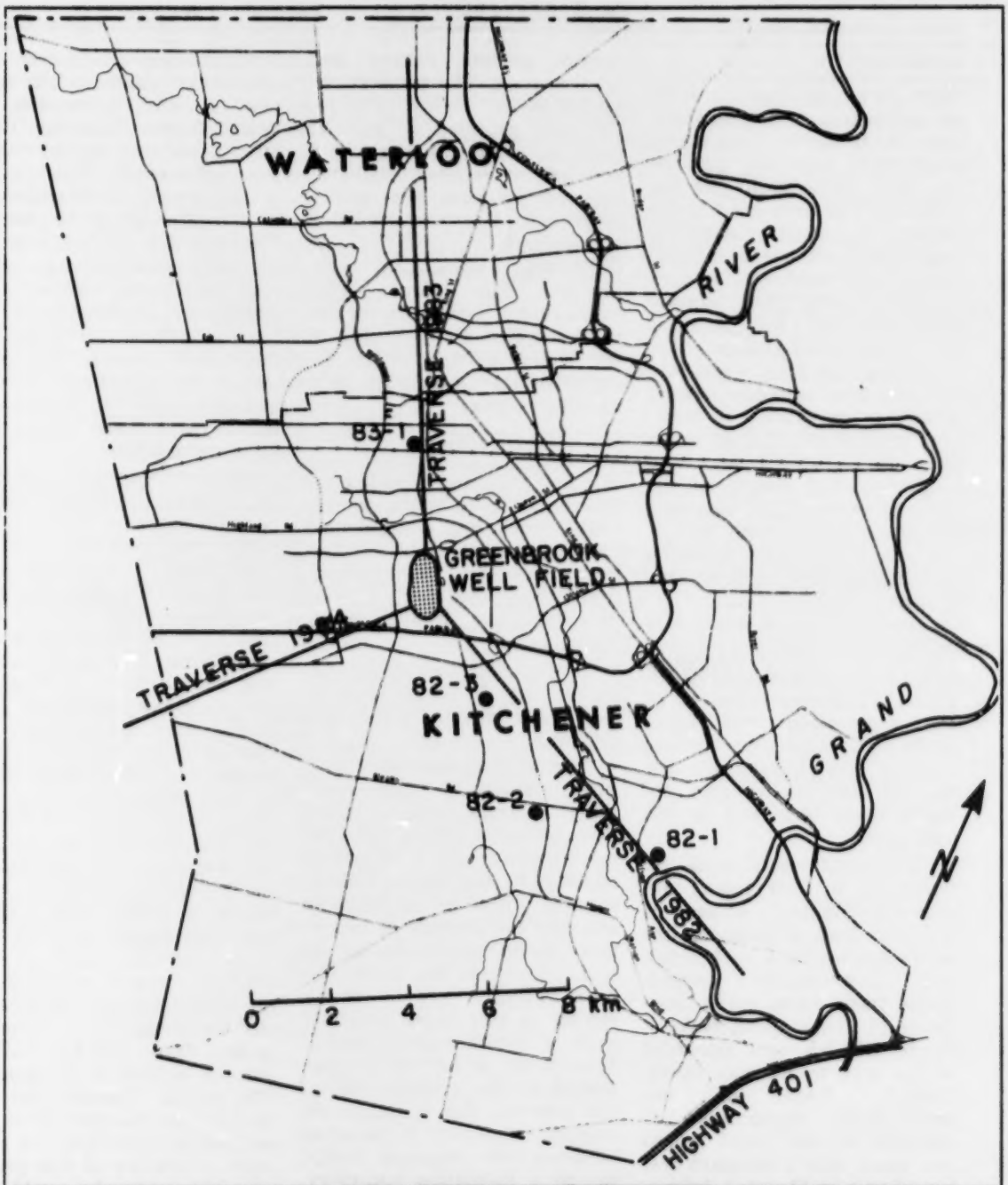

Figure 1. The area of study. The four well sites drilled to date are indicated, as are the locations of traverses along which the well sites were originally to be located.

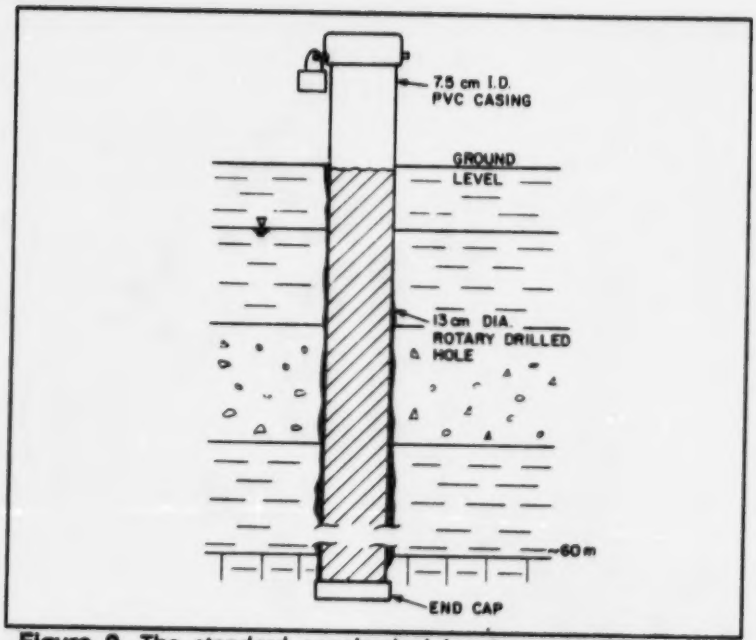

Figure 2. The standard geophysical logging environment. The casing is filled with fresh water.

the unit. The Maryhill is important for hydrogeological reasons, amongst others. It is an extremely good aquitard, preventing hydraulic connection between the heavily pumped regional aquifer beneath it and the surficial (and potentially contaminated) materials above.

4. After much experimentation a method for cross-plotting the geophysical log responses against core lithology was agreed upon, and implemented for GB82-3, the only borehole for which we have adjacent, near-complete core data. The procedure is described briefly below. The diagrams are complicated, befitting the number of parameters they must portray, and at present only available in colour. A black and white print of one of these is included here as Figure 4; all the detail of that figure is not visible but it demonstrates the approach.

a. Core samples which coincide with 'stable' geophysical responses (in the sense described in 1 above) are analyzed by particle size. The cores are further classified by their description as till or non-till.

b. With reference to Figure 4, the analysis is displayed using colour-coded pie diagrams on a neutron-gamma crossplot. The standard logging environment, shown in Figure 2, ensures that the absolute value of the response is consistent for identical materials from one hole to the next. The crossplots are also plotted for discrete ranges (slices) of density as shown schematically in Figure 5.

c. The distribution of stratigraphic and lithologic properties in this parameter space is studied for patterns. In Figure 4, for example, the materials designated as clays lie toward the lower right as expected. All samples to the right of 90 cps on the gamma scale, however, are Maryhill till. This stratigraphic unit also has a density which is markedly lower than all other units traversed by the borehole. On this basis the Maryhill has a distinctive position in response space. Within the samples on the left side of Figure 4 there is a marked distinction between the water bearing (low neutron) and hydraulically tight (high neutron) materials, allowing the separation of aquifers from compact, sandy tills such as the Catfish. The markedly high density of the Catfish also places it in a unique area of the response space.

5. The three 1982 holes and the calibration pits were logged with the gamma spectroscopy tool owned and operated by the Geological Survey of Canada. These data are still being analyzed to see if the various clays encountered are distinguishable on the basis of the energy of their gamma radiation.

6. A magnetic susceptibility tool suitable for this environment has not yet been located. We continue to inform manufacturers of logging equipment about the availability of these calibrated holes for testing their products.

7. The preliminary results of this project were presented in talks to the International Symposium on Borehole Geophysics in Toronto, and at the annual meeting of the Geological Association of Canada in London.

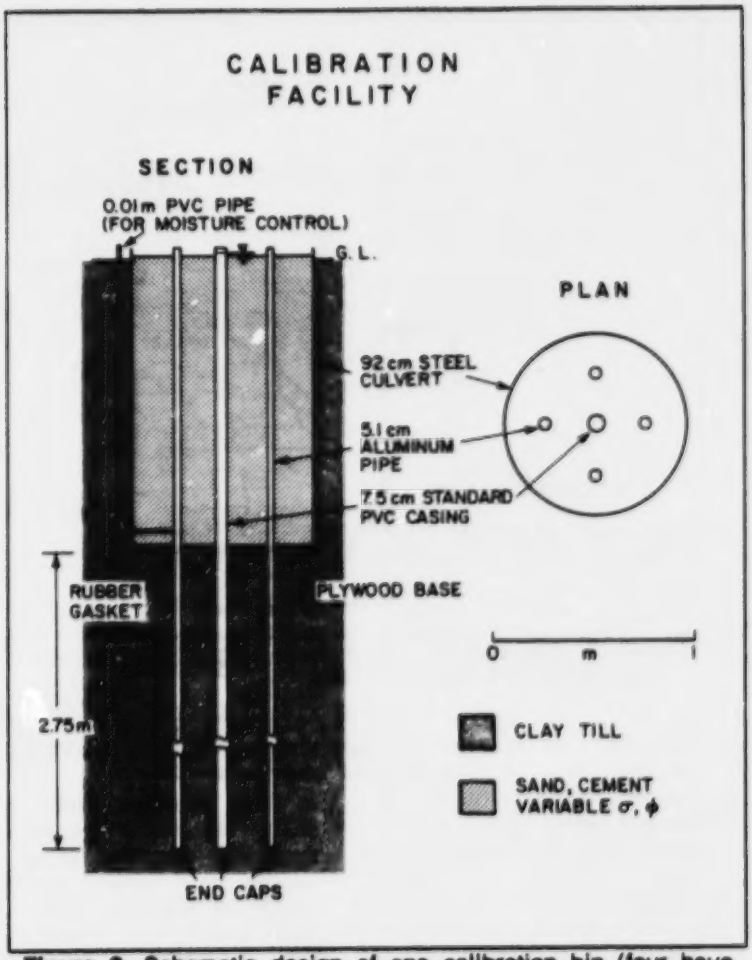

Figure 3. Schematic design of one calibration bin (four have been installed). Both the material in the bin and the clay till beneath the bin are used in the calibration. The 5.1 cm aluminum pipes surrounding the central bore are sounded with soil moisture probes to determine the calibrating materials' properties and heterogeneity.

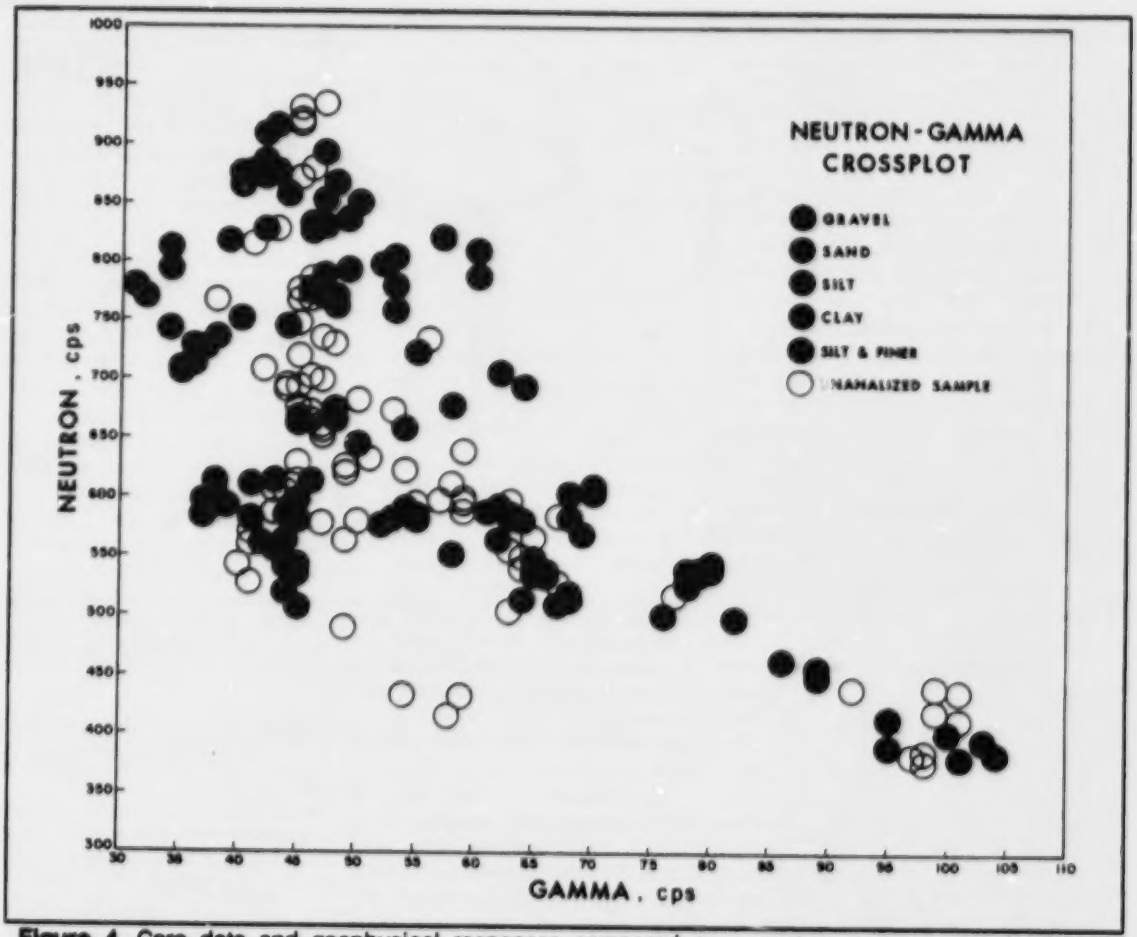

Figure 4. Core data and geophysical responses compared on a neutron-gamma crossplot for all densities. This figure is copied from a colour diagram so that only the intent of the analysis can be depicted. Black circles are actually 5 colour pie-diagrams; open circles are geophysical responses where no core was available.

FUTURE OBJECTIVES

1. We intend to complete one further core/log borehole comparison suite at the site of GB83-1 (see Figure 1).

2. The data from this suite, and from the shallow holes described in 3 above, will undergo the analysis described in section 4 above.

3. E-logs are more difficult than radiation logs to calibrate or compare from one hole to another, because they must be run quickly in the uncased hole and in a variety of mud conductivities. They do supply a largely independent parameter, however, and we intend to incorporate them into the parameter space description by correcting or normalizing their readings between holes.

4. Hydrogeological parameters such as aquifer yield or permeability, where they can be reasonably estimated, will be added to the crossplot diagrams. These parameters will come from multilevel piezometer studies currently being conducted in the Greenbrook well field. These data are not available immediately adjacent to the logged holes of this project so that a considerable extrapolation will be necessary. The results will not be definitive, but this is an important direction to take with these data.

5. The MSc thesis of P. Pehme will be completed in late summer of 1984, and the MSc project of Linda Ross in late 1985. Both reports will deal with the data obtained through this grant.

6. The final report on this program will be completed.

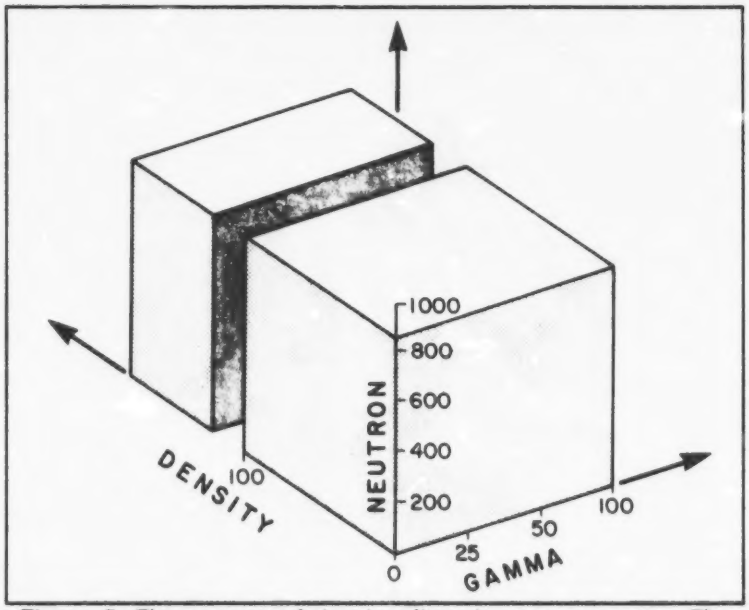

Figure 5. The concept of density slices in response space. The crossplots of Figure 4 are made for a variety of density ranges to identify the characteristic locations of various stratigraphic and lithologic units.

REFERENCES

Greenhouse, J.P., Farvolden, R.N., and Karrow, P.F.
1983: Subsurface Quaternary Stratigraphy Using Borehole Geophysics; Grant 128 *in* Ontario Geoscience Research Fund, Summary of Research 1982-1983, edited by E.G. Pye, Ontario Geological Survey, Miscellaneous Paper 113.

Insinna, A.
1984: Calibration of Radiation Logs; unpublished BSc Thesis, Department of Earth Sciences, University of Waterloo.

Grant 131 Source Rock Geochemistry of Pleistocene Tills of Southern Ontario

Uwe Brand and Jaan Terasmae

Department of Geological Sciences, Brock University

ABSTRACT

This investigation was designed to (1) develop geochemical techniques for the characterization of glacial tills and their source rocks, (2) apply these techniques to an actual glacial model, and (3) determine the usefulness of the new techniques in defining the origin and source rocks of Dummer Moraine glacial till deposits.

Approximately 400 bedrock and 100 till samples were collected in the study area northeast of Peterborough, extending across the Paleozoic-Precambrian contact as well as across the Dummer Moraine. Samples of the Ordovician Gull River, Bobcaygeon and Verulam Formations and samples of till were analysed for major, minor and trace elements, and for carbon and oxygen stable isotopes.

The three Paleozoic formations, Gull River, Bobcaygeon and Verulam, are chemically and isotopically distinct. The chemical compositions of till samples show a strong relationship to composition of the underlying bedrock formation. Correlation of till and bedrock compositions suggests that provenance of the till can be defined by Sr, Fe and Mn values.

This phase of the study has provided a data base for further refinement of geochemical techniques, an improved field sampling system, and the testing and verification of the conceptual model.

INTRODUCTION

Although several studies relating to the stratigraphic correlation of glacial deposits in southern Ontario have been carried out during the last few decades (Karrow 1974; Dreimanis 1977; Prest 1970; Terasmae 1980; Terasmae *et al.* 1972; Terasmae and Dreimanis 1976), there are still problems. In part this is due to the complex lobate configuration of the ice sheet margin during Late Wisconsinian time.

Other problems exist with respect to the genesis of the Dummer Moraine (Figure 1). Early workers suggested that the Dummer is a terminal moraine (e.g. Coleman 1937; Chapman and Putnam 1966). However, this concept has been challenged recently by Schluchter (1979), who concluded that the Dummer Moraine could have been produced by the dynamics of the retreating ice sheet. Conversely, Gadd (1980) suggested that the Dummer Moraine was formed as a consequence of its position relative to the Precambrian-Paleozoic contact, and thus is a facies equivalent of the basal till to the south. Terasmae (1980) reviewed the Dummer Moraine problem within the regional context of deglaciation and concluded that:

"It is quite possible that when the southward flowing ice of the Lake Simcoe lobe thinned over the Algonquin Highlands, large masses of ice became stagnant to the lee of these highlands and the melt-out of englacial debris resulted in the disintegration topography that characterizes the 'Dummer Moraine'".

This interpretation is in agreement with all the described characteristics of the 'Dummer Moraine'.

There also have been attempts to correlate till material with bedrock, and thus determine its provenance (Warren and Delavault 1961; May and Dreimanis 1973; Shilts 1973; Stea and Fowler 1979). A major difficulty, however, is that most tills include large amounts of quartz, feldspars, and associated minerals derived from the rocks of the Precambrian Canadian Shield. This has the effect of homogenizing tills and their geochemical properties if bulk sampling methods are employed.

The objectives of this study are to modify existing analytical methods for till samples, and to devise a model which uses sedimentological and geochemical techniques, to define the origin and the source rock of glacial deposits of the Dummer Moraine.

BEDROCK GEOLOGY

The bedrock samples were collected from outcrops along traverses that approximately parallel the ice flow direction of the last ice sheet (Figure 2). Samples of three Paleozoic carbonate formations were collected for each traverse. About 30 samples per formation per traverse were collected for a total of about 400 samples. This allows for the effects of any geochemical differentiation along ice-flow lines as well as on a regional scale.

GULL RIVER FORMATION

The Gull River Formation is a grey to light grey carbonate mudstone with variable amounts of fossils and bird's-eye structures. The Gull River samples from the contact with the underlying Shadow Lake Formation contain detrital quartz and feldspar grains. The micrite matrix of the Gull River shows signs of alteration to microspar. In one

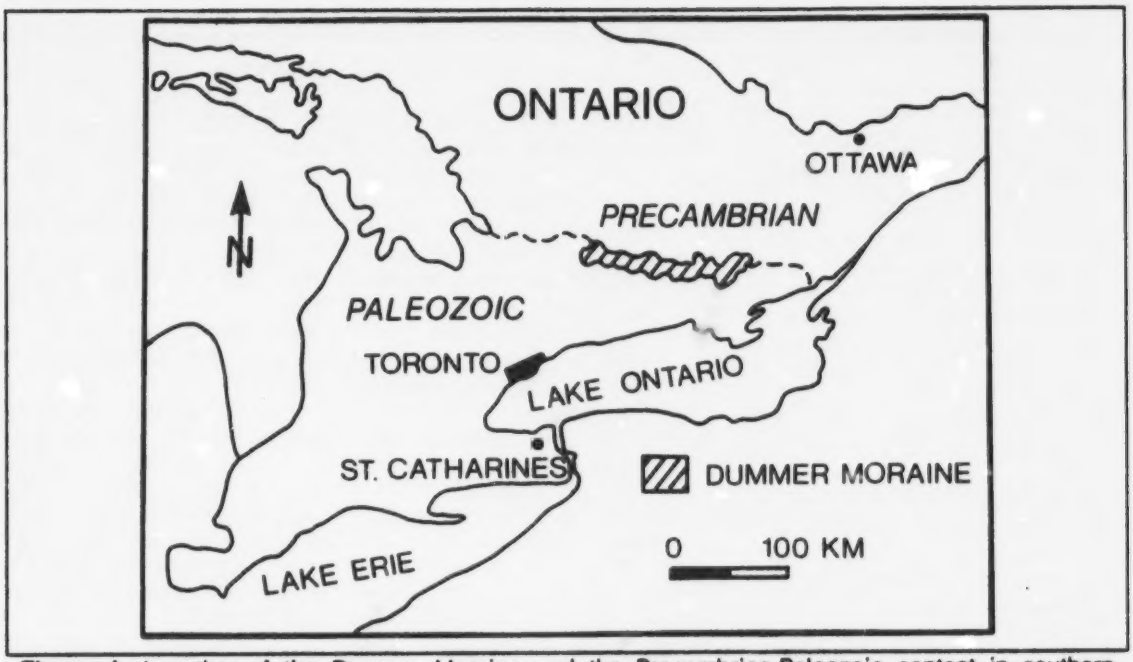

Figure 1. Location of the Dummer Moraine and the Precambrian-Paleozoic contact in southern Ontario.

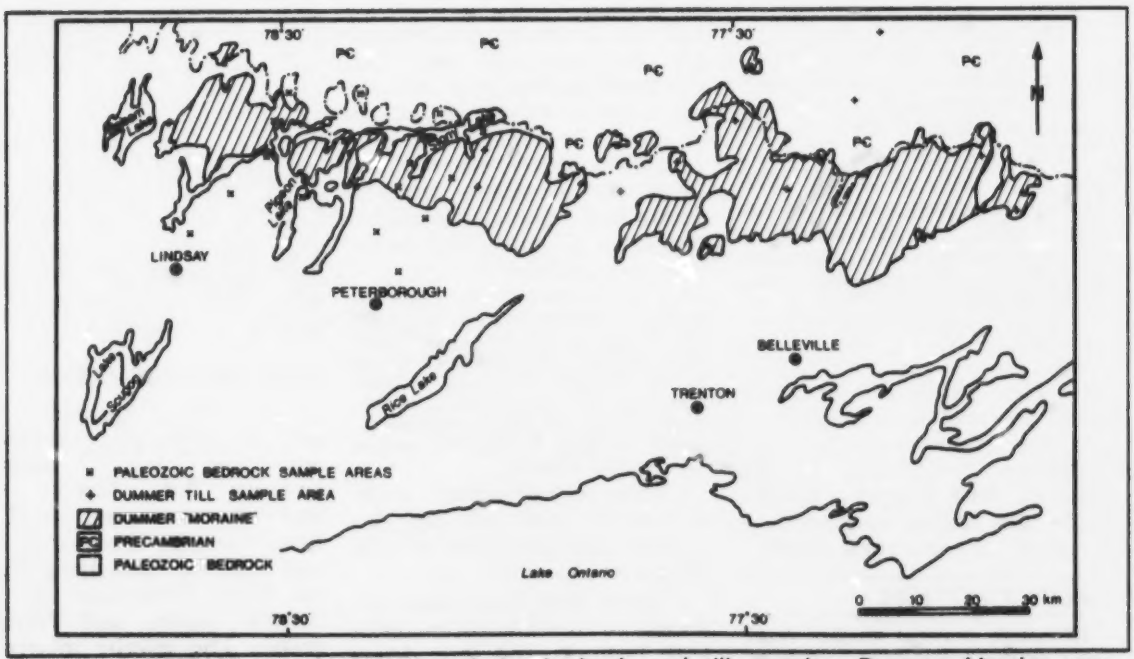

Figure 2. Location and distribution of the bedrock and till samples, Dummer Moraine area (modified after Carson 1980).

locality, the micrite is replaced by microspar-dolomite. Only minor amounts of crinoids, gastropods, and bryozoans were noted. Peloids are the most abundant allochems. Also some rip-up clasts are present in the unit.

BOBCAYGEON FORMATION

The unit overlying the Gull River Formation is the Bobcaygeon Formation. It is highly fossiliferous and grey to dark grey in colour. Its composition is that of a packstone. The most abundant allochems are peloids, coral fragments, crinoids, trilobites, and brachiopods. The peloids are preserved as micrite balls. The matrix is highly variable with a complete transition from micrite to pseudospar and sparite. However, the last two are the most abundant. Some minor silicification of the fossil allochems has occurred. Also, large rounded fossil-micrite rip-up clasts are present. Stylolite-fractures are common in the unit. These can be infilled by either calcite sparite or quartz-clay detrital material.

VERULAM FORMATION

The Verulam Formation, which overlies the Bobcaygeon Formation, is a dark grey, argillaceous packstone with shale intercalations. Fossil allochems are very abundant with gastropods, bryozoans, crinoids, trilobites, and brachiopods being the major representatives. Minor allochems are conodonts and Tetradium. Some of the fossils show replacement by chert. The matrix is mostly microspar and pseudospar, and some dolomitization of the matrix took place in selective localities. The crinoid fragments are generally rimmed by syntaxial overgrowth cement. The unit is replete with clay and silt-clay seams.

TILL GEOLOGY

North of the Dummer Moraine (and north of the limit of Paleozoic rocks) the till is generally thin and discontinuous. The landscape physiography is controlled by bedrock surface topography and the regional ice flow direction was generally from north to south. Pebble lithology of the till clearly reflects changes in bedrock types and indicates that glacial abrasion was an active process during till genesis. Till north of the Dummer Moraine is characteristically stony and has a sandy matrix.

A marked change in till characteristics occurs at the limit of Paleozoic outcrop and south of this limit in the Dummer Moraine area. Perhaps the most obvious aspect of this change is the sudden increase to predominance of Paleozoic rock fragments of all sizes in the till. The till cover becomes more continuous although its thickness varies greatly. The till surface is characterized by hummocky topography and an abundance of boulders. Clasts of Precambrian rocks are relatively rare in the 'Dummer till' which is typically very stony and has a fine sandy to silty matrix.

ANALYTICAL METHODS

BEDROCK SAMPLES

About 400 matrix samples of the Ordovician Gull River, Bobcaygeon, and Verulam Formations were cleaned and powdered for standard chemical analysis. Half a gram of each sample was leached with 18 mL of 1.8% (5% v/v) HCl for 5 hours (Brand and Veizer 1980). The samples were analyzed for Ca, Mg, Sr, Na, Mn, Fe, Zn, and Al on a Varian 1475 atomic absorption spectrophotometer with HP-85 control. For complete description of analytical techniques see Brand and Veizer (1980).

Average chemical accuracy as compared with standard rocks NBS-631 and NBS-634 and precision were better than 5 relative percent for Ca, Mg, Sr, Mn, and Fe, and better than 10 relative percent for Na, Al, and Zn (Brand and Veizer 1980). Insoluble residue (IR) was determined gravimetrically and precision was better than 7 relative percent. All chemical data are reported on a 100% carbonate basis (residue-free calculated) to facilitate intersample correlation.

Also 10 mg of each of 100 samples was reacted with 100% phosphoric acid. Carbon and oxygen were measured on a V.G. Micromass 602D Twin mass-spectrometer. Their isotopic ratios are expressed in the usual (δ) notation and are given relative to PDB in per mil. The appropriate corrections have been applied to the data.

Average accuracy and reproducibility, as compared to recommended values for COWS (University of Waterloo standard rock) were: $\delta^{18}O$ (0.2, 0.3) and $\delta^{13}C$ (0.1, 0.1) per mil. respectively. The isotopic compositions of the samples are given in Table 1.

TILL SAMPLES

Till samples are generally a mixture of various lithologies. Consequently, the leaching process devised for carbonate samples (Brand and Veizer 1980) had to be modified to fit the till lithology. An experiment was devised to test the

TABLE 1. STABLE ISOTOPE DATA OF THE THREE PALEOZOIC FORMATIONS IN THE DUMMER AREA.

Gull River Formation			Bobcaygeon Formation			Verulam Formation		
Sample	$\delta^{13}C$ ‰ (PDB)	$\delta^{18}O$ ‰ (PDB)	Sample	$\delta^{13}C$ ‰ (PDB)	$\delta^{18}O$ ‰ (PDB)	Sample	$\delta^{13}C$ ‰(PDB)	$\delta^{18}O$ ‰(PDB)
116	-1.2	-10.6	59	+2.3	-6.8	1	+1.3	-4.5
117	-1.2	-6.2	60	+2.2	-6.7	2	+0.7	-6.0
118	-0.9	-4.2	61	+2.3	-6.6	3	+1.1	-5.9
119	-0.5	-10.0	62	0.0	-9.9	4a	+1.2	-4.6
120	-0.4	-11.6	63	+2.1	-6.8	4b	+1.0	-5.5
121	-0.3	-12.9	64	+1.9	-7.0	5	+1.0	-5.7
122	0.0	-11.3	65	+2.0	-5.5	6	+0.5	-6.1
123	0.0	-10.5	66	+2.4	-5.5	7	+0.8	-5.8
124	0.0	-7.1	67	+2.4	-5.4	8	+1.1	-5.8
125	0.0	-6.8	68	+2.3	-5.4	9	+0.6	-5.9
126	-0.5	-7.2	69	+1.6	-7.0	10	+0.9	-5.2
127	+0.1	-7.9	70	+1.5	-6.7	11	+0.6	-6.3
128	+0.5	-10.3	75	+2.2	-6.3	12	+0.6	-5.8
129	+0.4	-10.3	76	+2.7	-4.8	13	+0.4	-6.1
130	+0.6	-10.1	77	+2.7	-5.0	14	+0.9	-5.4
131	+0.6	-10.3	78	+2.4	-6.0	15	+0.6	-6.2
132	+0.3	-8.4	79	+2.0	-5.5	16a	+0.8	-5.3
133	+0.3	-9.9	80	+1.8	-5.9	16b	+0.8	-5.5
134	+0.7	-10.3	81	+1.7	-6.5	17	+0.6	-5.7
135	0.0	-9.9	82	+2.1	-5.5	18	+0.5	-6.0
136	-0.1	-8.4	264	+2.1	-6.1	19	+0.2	-6.0
137	+0.1	-7.9	266	+2.9	-5.0	20	+0.4	-5.7
138	-0.2	-7.6	268	+2.4	-5.9	21	+0.3	-5.4
139	-0.1	-7.3	270	+2.1	-6.5	22	+0.5	-6.4
140	+0.2	-9.8	272	+2.3	-7.3	23	+0.6	-6.8
141	+0.3	-6.0	274	+2.4	-5.3	24	+0.7	-6.0
417	-0.5	-5.7	276	+2.0	-6.4	25	+0.5	-5.5
419	+0.1	-5.7	278	+2.2	-6.6	26	+0.8	-5.8
421	+0.3	-5.9	280	+1.6	-5.6	27	+0.8	-5.0
423	-0.6	-6.2	284	+1.6	-7.2	345	+0.6	-6.4
425	+0.5	-5.8	284a	+1.1	-6.2	349	+1.1	-5.2
427	+0.7	-5.7	286	-0.1	-6.8	353	+0.7	-6.7
429	+0.4	-6.6	288	-0.5	-5.7	357	+0.6	-6.7
			289	+0.1	-4.9			

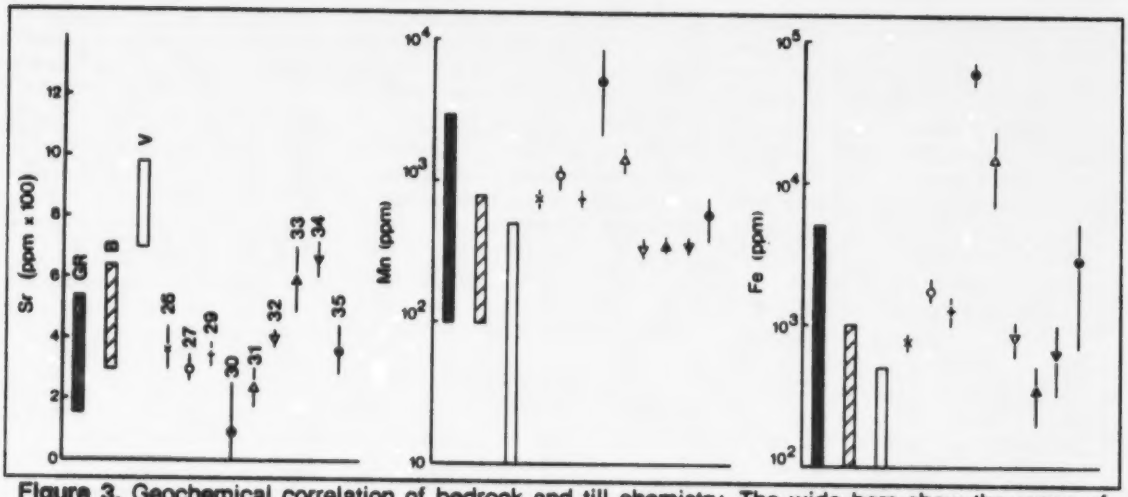

Figure 3. Geochemical correlation of bedrock and till chemistry. The wide bars show the range of composition in bedrock samples for the Paleozoic formations (GR = Gull River, B = Bobcaygeon, V = Verulam), and the symbols (with sample number) show the compositions of individual till samples.

approach. First, two till samples, one high in sand and one high in clay fraction, were sieved at 1/4 ϕ intervals. Two batches of each sample were prepared for dissolution. One sample set was leached with 18 mL (uniform volume - UV) of 1.8% (5% v/v) HCl. Another sample set was leached with variable volume (VV) of 1.8% (5% v/v) HCl. The amount of acid was calculated on the soluble portion of each till sample previously determined by leaching experiments. The insoluble residue of sandy tills (DT 290) increases less rapidly than that of clayey tills (DT 480). Furthermore, the IR trend is similar for samples leached by uniform (UV) and variable (VV) acid volume. The sandy till shows a smaller degree of elemental leaching from IR, e.g. Al, Zn, Cd, Cu are readily leached. However, this leaching can be controlled, especially for elements which are partly associated with the $CaCO_3$. Thus an element such as Sr, which is solely associated with the calcium carbonate lattice, and partly associated elements such as Fe and Mn, can be used as till-bedrock correlation tools. The chemical data of till is recalculated in a similar fashion as bedrock samples to allow intersample correlation.

A total of 40 till samples were sieved at 1/2 ϕ intervals. However, only the -2.0, -1.5, -1.0, +1.0, +3.0, and pan fraction were chosen for full geochemical analysis. The coarser fractions will be used to correlate the till to the bedrock samples. The others have been analyzed for comparison purposes.

RESULTS AND DISCUSSION

These results are based on bedrock and till samples from the Stony Lake area of the Dummer Moraine. The three Paleozoic formations, Gull River, Bobcaygeon, and Verulam, are chemically distinct lithologies (Figure 3). The till sample data can be compared to bedrock chemistry to help resolve provenance. Till sample DT 26, which is situated on the Gull River Formation, shows strong chemical affinities to this formation. This is apparent for Sr, Fe, and Mn (Figure 3). A similar affinity was determined for till samples DT 27, DT 29, and DT 32. These three tills are located on the Gull River Formation, and also show a strong chemical relationship to the underlying formation.

Till sample DT 30, based on Sr, Fe, and Mn, does not show a relationship with the Paleozoic carbonate rocks. This till is related to sands and silts derived from the Canadian Shield area to the north of the Dummer Moraine and possibly only in part to the sediments derived from the Paleozoic formations (Figure 2).

In contrast, till sample DT 31 has chemical affinities, based on Sr and Mn, to the underlying Gull River Formation (Figure 3). However, the Fe values are outside the range determined for this formation (Figure 3). Leaching from insoluble residue is probably not the dominant factor. Instead, an admixture of some till material derived from a Precambrian source could account for this anomalous Fe enrichment.

Till samples DT 33 and DT 34 were collected from exposures overlying the Gull River and Bobcaygeon Formations, respectively. This relationship is supported by the Mn and Fe data (Figure 3). However, Sr data suggest that the tills from these localities are admixed with detritus from the Verulam Formation (Figure 3).

Sample DT 35 is from an exposure of till at the top of the Bobcaygeon Formation. Only the Mn data support this relationship of superposition unequivocally (Figure 3). Conversely, the Sr and Fe data of the till sample suggest that the major portion of the till was contributed by the Bobcaygeon Formation with a minor portion being derived from the Gull River Formation (Figure 3).

A similar study showed that it was possible to determine provenance of tills by analyzing for trace elements (Leyland-Mihychuk and Brand 1982). However, a problem in that study and in others (May and Dreimanis 1973; Shilts 1973; Stea and Fowler 1979) is that the extent of leaching of elements during till digestion was not accounted for. Thus, it is possible that the observed chemical affinities of tills in those studies represent mixtures of values derived from both the carbonate and non-carbonate portions of the till samples.

In addition, the Paleozoic formations were also analyzed for carbon and oxygen isotopes (Table 1). These confirm the distinct chemical characteristics of the three formations (Figure 3). The Gull River Formation (average $\delta^{13}C$ = 0.0‰, $\delta^{18}O$ = -8.9‰), is isotopically distinct from the Bobcaygeon Formation (average $\delta^{13}C$ = +1.9‰, $\delta^{18}O$ = -6.1‰) and from the Verulam Formation (average $\delta^{13}C$ = +0.7‰, $\delta^{18}O$ = -6.0‰). Comparing samples from the Bobcaygeon and Verulam, there are large differences in the carbon isotope values, while the oxygen isotope values are similar. In contrast the oxygen isotope values of the Gull River are quite dissimilar from those of the other two formations (Table 1). The carbon isotope values probably represent original values, while the oxygen isotope values are diagenetically altered ones. In these postulated hypotheses a glacial fluid flow influence is not discounted.

CONCLUSIONS

A modified selective leaching method allows for the geochemical analysis of till samples and correlation with bedrock chemistry. This new technique is especially effective for Sr, with slightly less accurate correlations for Fe and Mn values. The correlation of till and bedrock data suggests that provenance of till materials can be resolved by these elements. In addition, extraneously derived material in the till can also be identified by this method.

ACKNOWLEDGMENTS

We thank J. Morrison and J. Pinder for assistance with chemical analyses. Also our thanks to L. Vidican for typing the manuscript.

REFERENCES

Brand, U. and Veizer, J.
1980: Chemical Diagenesis of a Multicomponent Carbonate System - 1: Trace Elements; Journal of Sedimentary Petrology, Volume 50, p.1219- 1236.

Carson, D.M.
1980: Paleozoic Geology of the Burleigh Falls-Peterborough Area, Southern Ontario; Ontario Geological Survey, Preliminary Map P.2337, Geological Series, scale 1:50 000. Geology 1979.

Chapman, L.J., and Putnam, D.F.
1966: The Physiography of Southern Ontario; University of Toronto Press, 2nd Edition, 386p.

Coleman, A.P.
1937: Geology of the North Shore of Lake Ontario; Ontario Department of Mines, Annual Report for 1936, Volume 45, Part 7, p.75-116. Accompanied by Map 45f, scale 1:316 800 or 1 inch to 5 miles.

Dreimanis, A.
1977: Correlation of Wisconsin Glacial Events between the Eastern Great Lakes and the St. Lawrence Lowlands; Geographie Physique et Quaternaire, Volume 31, p.37-51.

Gadd, N.R.
1980: Late-Glacial Regional Ice-Flow Patterns in Eastern Ontario; Canadian Journal of Earth Sciences, Volume 17, p.1439-1453.

Karrow, P.F.
1974: Till Stratigraphy in Parts of Southwestern Ontario; Geological Society of America, Bulletin, Volume 85, p.761-768.

Leyland-Mihychuk, M., and Brand, U.
1982: Sedimentology and Geochemical Analysis of Late Wisconsin Glacial Sediments and Paleozoic

Bedrock, Havelock, Ontario (Abstract); Geological Association of Canada, Program with Abstracts, Volume 7, p.63.

May, R.W., and Dreimanis, A.
1973: Differentiation of Glacial Tills in Southern Ontario, Canada, Based on Their Cu, Zn, Cr, and Ni Geochemistry; Geological Society of America, Memoir 16, p.221-228.

Prest, V.K.
1970: Quaternary Geology of Canada; p.675-764 *in* Geology and Economic Minerals of Canada, edited by R.J.W. Douglas, Geological Survey of Canada, Economic Geology Report 1.

Schluchter, C.
1979: The Dummer Moraine in Southern Ontario - Its Sedimentology and Origin (Abstract); Geological Association of Canada, Program with Abstracts, Volume 4, p.77.

Shilts, W.W.
1973: Glacial Dispersion of Rocks, Minerals, and Trace Elements in Wisconsin Till, Southeastern Quebec, Canada; Geological Society of America, Memoir 16, p.189-219.

Stea, R.R., and Fowler, J.H.
1979: Minor and Trace Element Variations in Wisconsinan Tills, Eastern Shore Region, Nova Scotia; Nova Scotia Department of Mines and Energy, Paper 79-4, 30p.

Terasmae, J.
1980: Some Problems of Late Wisconsin History and Geochronology in Southeastern Ontario; Canadian Journal of Earth Sciences, Volume 17, p.361-381.

Terasmae, J., and Dreimanis, A.
1976: Quaternary Stratigraphy of Southern Ontario; p.51-63 *in* Quaternary Stratigraphy of North America, edited by W.C. Mahaney, Dowden, Hutchinson and Ross, Stroudsburg, Pennsylvania.

Terasmae, J., Karrow, P.F., and Dreimanis, A.
1972: Quaternary Stratigraphy and Geomorphology of the Eastern Great Lakes Region of Southern Ontario; 24th International Geological Congress, Field Excursion A42 Guidebook, 75p.

Warren, H.V., and Delavault, R.E.
1961: The Lead, Copper, Zinc, and Molybdenum Content of Some Limestone and Related Rocks in Southern Ontario; Economic Geology, Volume 56, p.1264-1272.

Grant 132 Geological and Geochemical Studies of the Boston and Temagami Iron Formations and their Contiguous Volcanosedimentary Piles

J.H. Crocket, N. Blum, T. Hurley, R. Bowins, G. McRoberts, A. Fyon, R.H. McNutt, H.P. Schwarcz and C.E. Rees

Department of Geology, McMaster University

ABSTRACT

Geological mapping and isotopic - trace element studies of the Adams and Sherman mines area were concentrated on characterization of the volcanosedimentary host rocks to the iron formation. Further studies on trace heavy metal (Au, As, Sb and W) distribution in the iron formations were also undertaken.

Cyclic stratigraphic sequences of iron formation and ultramafic extrusive rocks in the Adams mine area suggest a close linkage of volcanism and iron deposition and a significant lateral extension of the iron formation environment beyond the area of economic iron formation. A dominantly volcanic origin, although not necessarily of proximal character, is implied. A volcanogenic origin of iron formation is less strongly supported on geological grounds in the Sherman mine area, but there is a close spatial association with intermediate to felsic volcanism.

These iron formations and the rocks of their associated volcanic piles are low in gold and allied metals such as arsenic. The background gold content is approximately 5 ppb in the iron formation and in the volcanic and volcaniclastic rocks in the Sherman mine area.

A significant difference in the gold content of magnetite and jasper mesobands suggests that some gold may be liberated on diagenesis and metamorphism of iron formation. Weakly anomalous gold values in sulphidized volcanic rocks immediately underlying Sherman West Pit iron formation may have resulted from such remobilization.

INTRODUCTION

In a previous report (Crocket *et al.* 1983) on the Temagami iron formation (Sherman mine area) and the Boston iron formation (Adams mine area) it was suggested that chloritic shale mesobands are the major hosts of primary sulphur in these oxide facies dominated, banded iron formations (BIF). Shale-hosted sulphur which occurs mainly as pyrite has a sulphur isotopic signature suggestive of a biogenic origin via reduction of marine sulphate. Oxide-facies-hosted pyrite has sulphur isotopic properties which indicate that volcanogenic sulphur that was leached from the volcanic pile and/or was exhaled into the depositional basin is an important source of sulphur in these rocks. Another likely source of sulphur in oxide facies mesobands is remobilized shale-hosted sulphur as suggested by occasional isotopically light sulphur in oxide facies pyrites.

Pyrite is a strong concentrator of heavy metals such as gold, arsenic and antimony compared with oxides and the distribution of sulphides is probably the major control on heavy metal abundance in both the Sherman and Adams mines BIF. Tungsten, on the other hand, is concentrated in oxide minerals. Concentrations of heavy metals in oxide facies mesobands averaged 5 to 10 ppb gold, 1 to 2 ppm arsenic and antimony and 7 to 11 ppm tungsten.

Metamorphism and diagenesis of these iron formations probably changed their primary metal distributions significantly. A distinctive low intensity metamorphic area in the Sherman West Pit is characterized by weakly anomalous heavy metal enrichment in oxide facies rocks. Metamorphism probably caused loss or redistribution of such metal from or within the iron formation. From limited data, it was found that jasper carried approximately twice the gold content of magnetite. As a ferric hydroxide gel is probably converted to magnetite during diagenesis or early metamorphism a loss of gold is implied and a further mechanism promoting metal mobility induced by metamorphism was proposed.

The geological character of the contiguous volcanosedimentary pile is discussed in the present contribution. Preliminary conclusions on the relationships between volcanism and iron formation deposition based on field mapping and some supporting geochemical data are presented. Further geochemical studies dealing with sulphur isotopes and heavy metal distribution in BIF and host rocks are presented.

GEOLOGICAL STUDIES

BOSTON IRON FORMATION AND THE ADAMS MINE

The Boston iron formation in the vicinity of the Adams mine was mapped at a scale of 1:12,000 by Lawton (1957) and recent contributions to the geology were made by Jensen (1978a). Areas mapped as part of this project are indicated in Figure 1. Mapping in the North Central, Central and Peria Pit areas was undertaken by N. Blum, and in the area west of the South Pit by G. McRoberts. It is proposed that the Adams mine includes three major BIF bands represented by the North and West Central Pits (Cycle III), the Central and North Central Pits (Cycle II), and the Peria and South Pits (Cycle I), with the latter bands representing the stratigraphically oldest BIF. The strata hosting these BIFs form the south limb of a synclinal fold which dips approximately 80° to the northwest. The synclinal axis strikes approximately 030° to 045°. The entire area has been deformed by intrusion of the Lebel syenite stock into a gently curving or arcuate configuration convex away from the Lebel stock. The extrusive rocks belong to the Larder Lake Group (Jensen 1978b).

The geology is summarized in a generalized geological section (Table 1); the rock nomenclature for the volcanic rocks is based on the Jensen cation classification (Jensen 1976). The stratigraphy is interpreted as consisting of volcanosedimentary cycles initiated by extrusive ultramafic komatiites and terminated by deposition of iron formation. Three such cycles are identified and the following generalizations recognized:

1. The ultramafic members become less magnesian and make up progressively smaller volumes of a cycle from the oldest to the youngest of the three cycles. In the first cycle, ultramafic flows make up about 50% of the cycle, while in the third cycle ultramafic members make up about 5% of the cycle.
2. The volcanic rocks of each cycle vary from ultramafic compositions at the base to mafic or intermediate compositions at the top.
3. The trend toward more silica-rich compositions at the top of a cycle is strongest in the uppermost cycle in that dacite, andesite and iron tholeiite are the terminal volcanic members of cycles III to I respectively.

The stratigraphic position of the rocks structurally underlying and in fault contact with the ultramafic flow at the base of Cycle I is uncertain. The presence of ultramafic clasts in an ultramafic matrix suggests either that these units are stratigraphically equivalent to various Cycle I rocks and have been displaced structurally or that these rocks were underlain by further BIF and ultramafic rocks lost through erosion.

Complex folding and poor exposure immediately west of the South Pit prevent unequivocal establishment of lateral continuity from the pit areas to the thin, uneconomic BIF units west of the mine area. However, mapping to the west of the South Pit has established the presence of three ultramafic komatiite flows, komatiitic basalt, magnesium and iron-rich tholeiites and at least two bands of iron formation. Thus the distinctive volcanic provenance characteristic of the mine area is continuous for at least 3 km to the west. One of the BIF bands is probably stratigraphically equivalent to the South Pit iron formation.

A genetic relationship between volcanism and iron formation is strongly suggested by the mine area stratigraphy. Specifically, episodes of volcanism which became progressively less mafic with time appear to have terminated in deposition of BIF. The general implication of this linking of BIF with volcanic evolution is that the iron formations themselves are the products of magmatic outgassing and exhalation during periods of eruptive quiescence. It is not implied, however, that volcanic centres immediately underlie the iron formations.

TEMAGAMI IRON FORMATION AND THE SHERMAN MINE AREA

The geology of the Sherman mine area and the Temagami iron formations was discussed by Bennett (1978). Areas in which mapping is in progress for this study are indicated on Figure 2. They include the volcanosedimentary sequence in west-central Strathy Township east of, and underlying, the main iron formation unit where mapping has been undertaken by A. Fyon, and the volcanic pile immediately underlying the Sherman West and North Pits being mapped by T. Hurley. In west-central Strathy Township mapping has concentrated on the dominantly mafic metavolcanic stratigraphy with emphasis on rock alteration and mineralization including two occurrences of auriferous sulphides, at Arsenic Lake and Big Dan. The following types of rock alter-

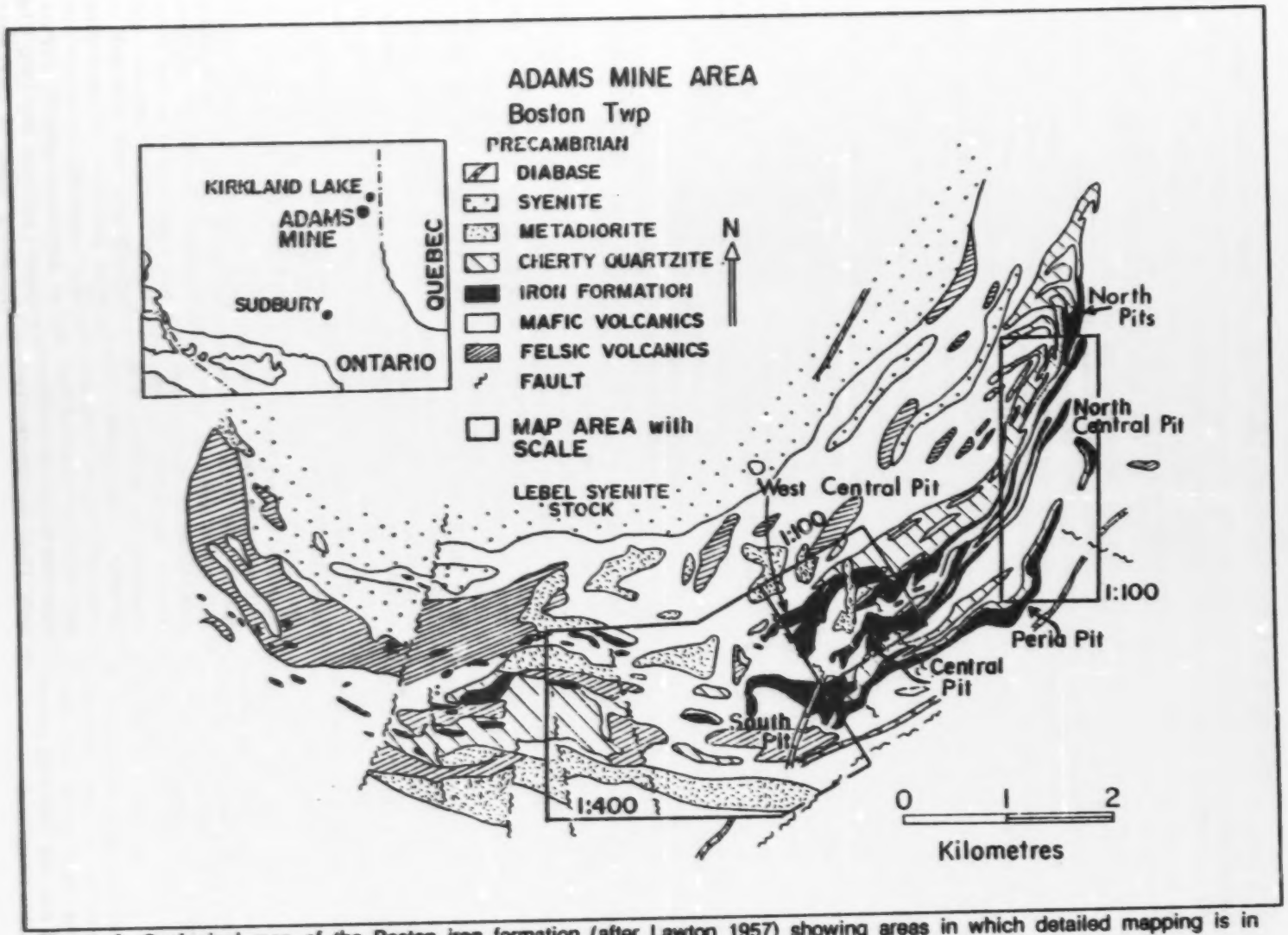

Figure 1. Geological map of the Boston iron formation (after Lawton 1957) showing areas in which detailed mapping is in progress.

TABLE 1. GENERALIZED GEOLOGICAL CROSS-SECTION SHOWING THE STRATIGRAPHIC SUCCESSION IN THE AREA OF THE PERIA, CENTRAL AND NORTH CENTRAL PITS, ADAMS MINE.

Cycle	Thickness	Lithology
III	480 m	Hanging wall - mafic volcanic rocks and cherty quartzite BIF of West Central Pit Cherty quartzite Dacite Tuffaceous sedimentary rocks and proximal, reworked conglomerate Andesite Mg Tholeiite Metadiorite, local intrusion (post Larder Lake Group) Komatiitic ultramafic flow or sill (highly sheared, 20.6 wt% MgO, constitutes about 5% of Cycle III)
II	600 m	BIF of Central Pit Andesite Rhyodacite tuff (distal, intercalated) Andesite Tuffaceous sedimentary rocks (intercalated) Fe Tholeiite Mg Tholeiite Komatiitic ultramafic flows (spinifex textured, 22.2 wt% MgO, constitutes about 20% of Cycle II) Cherty quartzite (discontinuous)
I	350 m	BIF of Peria Pit Cherty quartzite (discontinuous) Dacite to andesite flow (calc-alkaline) Fe Tholeiite flows (intercalated with graphitic, cherty beds) Mg Tholeiite Komatiitic ultramafic flows (spinifex textured, 24.8 wt% MgO, constitutes about 50% of Cycle I) fault contact Turbidite sedimentary rocks (conglomerate, sandstone, shale; ultramafic clasts, no BIF clasts, proximal) Mg Tholeiite flows (intercalated with sedimentary rocks) Turbidite sedimentary rocks (conglomerate, sandstone, shale; mafic and felsic volcanic clasts, no ultramafic clasts, few BIF clasts)

Notes.
Section is the south limb of a synclinal fold structure. Synclinal axis passes through West Central Pit BIF. Beds face northwest and dip at approximately 80° northwest.

ation listed in a tentative chronological sequence from oldest to youngest are recognized: (1) quartz, calcite and chlorite precipitation in vesicles; (2) quartz microveinlets; (3) epidote veinlets; (4) calcite veinlets or flat tension gash fillings; (5) silicification of basalt; (6) carbonatization of basalt; and (7) chloritization of shear zones.

Events 1 to 4 are common throughout the area while intense carbonatization involving both calcite and dolomite occurs preferentially near or within major east-trending shear zones such as the Link Lake shear zone where a 60 m width of basaltic rock has sustained wholesale replacement by rusty weathering dolomite. North-trending shear zones of a few metres width are characterized by intense chloritization of basalt. The Big Dan and Arsenic Lake gold mineralization are hosted in such north-trending chloritized shear zones.

Both occurrences consist of 30 to 60 m long pods or lenses of zoned auriferous sulphide. From core to margin the zonation is: arsenopyrite with traces of chalcopyrite cut by pyrite veinlets; pyrrhotite and chalcopyrite veinlets cutting chloritized basalt; disseminated pyrrhotite and pyrite. Gold is probably associated with the arsenopyrite-rich core. The Big Dan occurrence suggests that these mineralized shear structures have been active during and after volcanism. Synvolcanic activity on the shear zone is suggested by the presence of felsite dikes which cut basalt stratigraphy parallel to or within the Big Dan structure and which may represent subvolcanic feeders to felsic flows in higher stratigraphic units. The mineralization

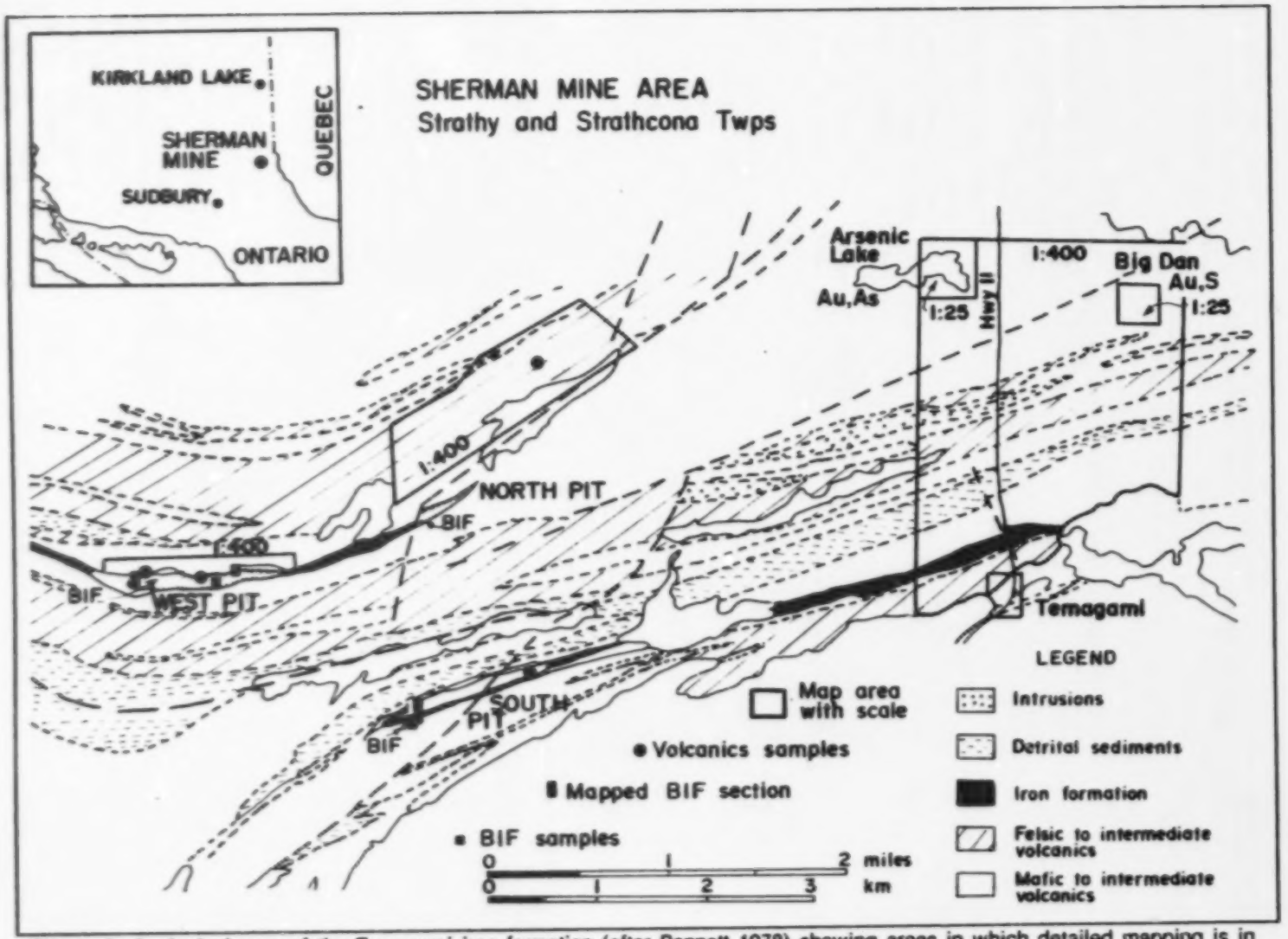

Figure 2. Geological map of the Temagami iron formation (after Bennett 1978) showing areas in which detailed mapping is in progress.

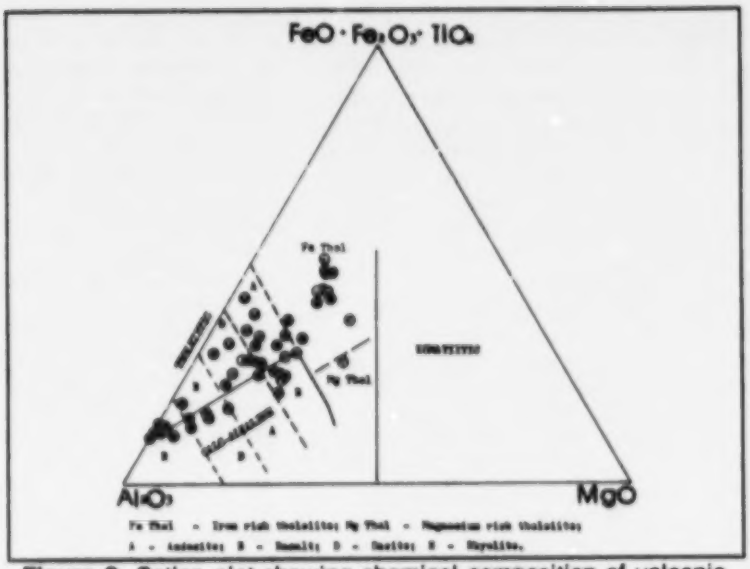

Figure 3. Cation plot showing chemical composition of volcanic, volcaniclastic and intrusive rocks stratigraphically below the Sherman West and North Pits. Solid circles - flows; open circles - volcaniclastic rocks; open circles with bar - volcaniclastic rocks within 10 m of the Sherman West Pit banded iron formation.

cross-cuts the felsic dikes and is therefore younger, suggesting post-volcanic structural reactivation during the mineralization event. A thin northwest-trending Sudbury type diabase dike known to cut volcanic and granitic rocks cuts the main shear zone on the Big Dan property and has been faulted by the shear zone. This implies reactivation of the mineralized structure after volcanism and granitic intrusion in the area. Thus, mineralization such as the Arsenic Lake and Big Dan occurrences, and probably other sulphide occurrences in north-trending shear zones, is apparently much later and presumably unrelated to BIF of the area.

Footwall Volcanic Rocks, Sherman West and North Pits

The northern band of iron formation (Figure 2) hosts the Sherman West and North Pits, and is underlain by a sequence of predominantly volcanic and volcaniclastic rocks. Detailed mapping (1:600) was carried out on a section of 5.5 km strike length by 1.5 km stratigraphic thickness which constitutes the volcanic pile immediately underlying the north band of iron formation. The section includes about 50% fragmental volcaniclastic rocks and 50% flows, flow breccia and intrusive rocks. The intrusive rocks are mainly of felsic composition and are probably synvolcanic. Felsic intrusions and flows are more prevalent in the eastern half of the area, that is to the north of the North Pit, whereas volcaniclastic rocks become the major constituents of the pile in the western half of the area, north of the West Pit. Tentatively, a focus of volcanism in the eastern portion of the area is indicated.

Rock compositions are shown on a Jensen diagram in Figure 3. Bearing in mind that volcaniclastic rocks may represent material derived from diverse sources, the rocks are mainly tholeiitic (74%); the ratio of mafic to intermediate to felsic compositions is 38 to 44 to 19. Komatiitic rocks appear to be absent, in contrast to the Adams mine setting.

Volcaniclastic rocks of dacite to andesite composition underlie the Sherman West Pit BIF. On the volcanic - BIF contact these rocks are heavily sulphidized with pyrite and some base metal minerals including sphalerite in both disseminated and massive, banded form.

GEOCHEMISTRY

ADAMS MINE VOLCANIC ROCKS

The volcanic rocks underlying and interbedded with the major BIF units (Table 1) are only moderately altered and deformed, typical of much of the Larder Lake Group. As previously noted the stratigraphy has been deformed by the intrusion of the Lebel stock, and thermal contact metamorphism of iron formation is probably responsible for formation of garnet in BIF mesobands of appropriate composition. Nevertheless, in ultramafic rocks, primary textures are commonly preserved and include spinifex and polygonal jointing; mafic rocks occasionally show easily recognizable pillows. Certain chemical parameters are also consistent with only moderate alteration. For example, mafic and ultramafic rocks consistently contain less than 0.3 weight percent CO_2 and range in loss on ignition from approximately 1 to 5%. Thus they are mod-

erately hydrated but not carbonated.

A suite of trace elements were determined by X-ray fluorescence (XRF) analysis to aid in rock classification and to evaluate base metal levels in the volcanic rocks. Average values grouped by rock type are presented in Table 2. Typically, Cr, Ni and Co contents are relatively high in komatiitic ultramafic and mafic rocks and lower in tholeiites. A significant positive correlation with MgO suggests an association of these metals with original primary ferromagnesian minerals. The base metals are generally typical of sulphur-poor mafic and ultramafic rocks. They are not significantly correlated with rock type and the relatively low Cu contents suggest very low levels of magmatic sulphide in the ultramafic rocks. Accordingly the high Ni contents probably represent original silicate-hosted Ni. Low As levels prevail as in the Adams BIFs.

SHERMAN MINE VOLCANIC ROCKS

Volcanic rocks underlying the Sherman West and North Pits were analyzed for S, Cu and Zr by XRF and Au, As and Sb by instrumental neutron activation. The results are presented in Table 3. These rocks include mainly volcaniclastic and flow rocks together with a few intrusive rocks. Sulphides occur as disseminated mineralization, mainly pyrite and pyrrhotite, and occasionally as shear controlled veinlets and clots.

Excluding the volcaniclastic rocks immediately underlying the West Pit iron formation (note 3, Table 3), the following generalizations are drawn from these data:

1. There is little difference in metal content of flows and volcaniclastic rocks of the same composition except for gold where volcaniclastic rocks carry about twice the gold content of compositionally equivalent flows.
2. The base metals Cu and Zn increase from felsic to mafic compositions as is commonly observed in volcanic rocks. As and Sb show little variation with rock type although there is a weak As trend in the same sense as Cu and Zn. Gold decreases from felsic, through intermediate to mafic compositions, a trend not usually observed in volcanic rocks (Crocket 1974).
3. There is no direct correlation of metal content with sulphur level. The suite of dacite to andesite fragmental volcanic rocks lying within 10 m of the base of the West Pit are significantly enriched in Cu, As, Sb and Au relative to other rocks. The footwall volcaniclastic rocks carry both disseminated, very fine-grained sulphides and massive banded sulphide. The suite includes two samples of the latter variety which carry high Au (69 and 24 ppb), high As (184 and 192 ppm), high Sb (15 and 6 ppm) and high Cu (314 ppm) contents. These sulphide-rich samples probably bias the averages toward higher values than are actually characteristic of the sulphide-poor fraction of the footwall suite. However, even the more restricted population within two standard deviations

TABLE 2. AVERAGE TRACE METAL CONTENTS OF ADAMS MINE VOLCANIC ROCKS.

	Rock Type[1]				
Metal ppm	UK (11,9)[2]	BK (6)	Mg Thol (9)	Fe Thol (5)	Correlation[3] with MgO
Cr	2600	3300	760	250	+
Ni	1390	1050	175	66	+
Co	90	90	60	60	+
Cu	60	50	40	50	0
Zn	80	100	85	125	0
Pb	range is 4 to 14 ppm for all rock types				0
As	range is 0 to 18 ppm for all rock types				0

Notes.
1. Rock Types: UK - ultramafic komatiite; BK - basaltic komatiite; Mg Thol - magnesium tholeiite; Fe Thol - iron tholeiite. Rock nomenclature according to Jensen cation plot.
2. Number of samples in parentheses; for UK there are 11 samples for Cr and Ni and 9 for the other metals.
3. '0' indicates no significant correlation of the metal with MgO for any rock type and + indicates a significant positive correlation of the metal with MgO in all rock types.

TABLE 3. AVERAGE TRACE METAL CONTENTS OF SHERMAN MINE VOLCANICS

Sample Description	Rock Type[1]	N[2]	S ppm	Cu ppm	Zn ppm	As ppm	Sb ppm	Au ppb
Felsic intrusions	rhyolite	6	400	5	27	4.6	0.43	4.5
Felsic flows	rhyolite, rhyodacite	4	3900	12	90	1.9	0.38	6.4
Intermediate flows	dacite and andesite	9	500	30	100	5.2	0.33	2.6
Intermediate flows*						1.4		
Mafic flows	basalt	6	400	45	175	6.7	0.50	2.2
Intermediate volcaniclastics	dacite and andesite	5	2800	32	110	3.2	0.46	5.4
Intermediate volcaniclastics**	dacite and andesite	10	300	70	67	38	2.4	13
							1.1	7.0
Mafic volcaniclastics	basalt	13	1000	45	140	6.3	0.59	6.4
Mafic volcaniclastics**						3.5		5.0

[1]Petrologic nomenclature according to Jensen cation plot.
[2]Number of samples.
* Excludes samples more than 2σ greater than the mean.
** Suite taken within 10 m of the stratigraphic base of the West Pit BIF.

TABLE 4. AVERAGE AU, AS, SB AND W IN ADAMS AND SHERMAN MINES BIF.

Sample	N	Au ppb	As ppm	Sb ppm	W ppm
Pyrite separates	19	180	120	5.0	1.5
Magnetite separates	42	4.4	1.1	1.2	6.0
Jasper mesobands	30	10.6	1.2	1.5	8.4

N = Number of samples

of the mean indicates weakly anomalous Cu, As, Sb and Au in these rocks.

Thus, the West and North Pit footwall volcanic section is characterized by weakly anomalous metal contents in rocks immediately below the iron formation, and by a trend in gold content with rock composition not commonly seen in volcanic rocks.

TRACE ELEMENTS IN BIF

It was previously reported (Crocket *et al.* 1983) that pyrite strongly concentrated Au, As and Sb relative to oxide minerals whereas the opposite trend characterized W. It was also noted that the Au content of jasper was approximately twice that of magnetite although only a small number of samples were available to support this suggestion. These data are summarized in Table 4 and apply to much larger

populations than previously reported. The data for oxide minerals are also shown in Figure 4.

The more significant generalizations drawn from these data are the following:

1. Pyrite, including separates from both shale-hosted and oxide facies mesobands, concentrates Au and As by factors of approximately 20 and 100 relative to oxides. Pyrite is a less efficient concentrator of Sb (factor of 4) relative to oxides, and is depleted in W.
2. The gold content of jasper is about twice that of magnetite, a difference found to be highly significant when tested statistically. Systematic differences in the As, Sb and W contents of these two minerals are absent.
3. The distribution of high Au and W in oxide mesobands shows a strong geographic control. All W values exceeding 4 ppm are found in the eastern half of the Sherman West Pit and in the Sherman North Pit. Many of the higher Au values are also located in the same area.
4. As and Sb are extremely low in oxide facies rocks. The 1 to 2 ppm range found in the Sherman and Adams BIF is much less than the 2800 ppm average for As in oxide facies BIF noted by Gross and McLeod (1980) although their average applies to rocks with a sulphur content of 500 ppm. The low As contents of both the Adams and Sherman mine area volcanic rocks has been noted in Tables 2 and 3.

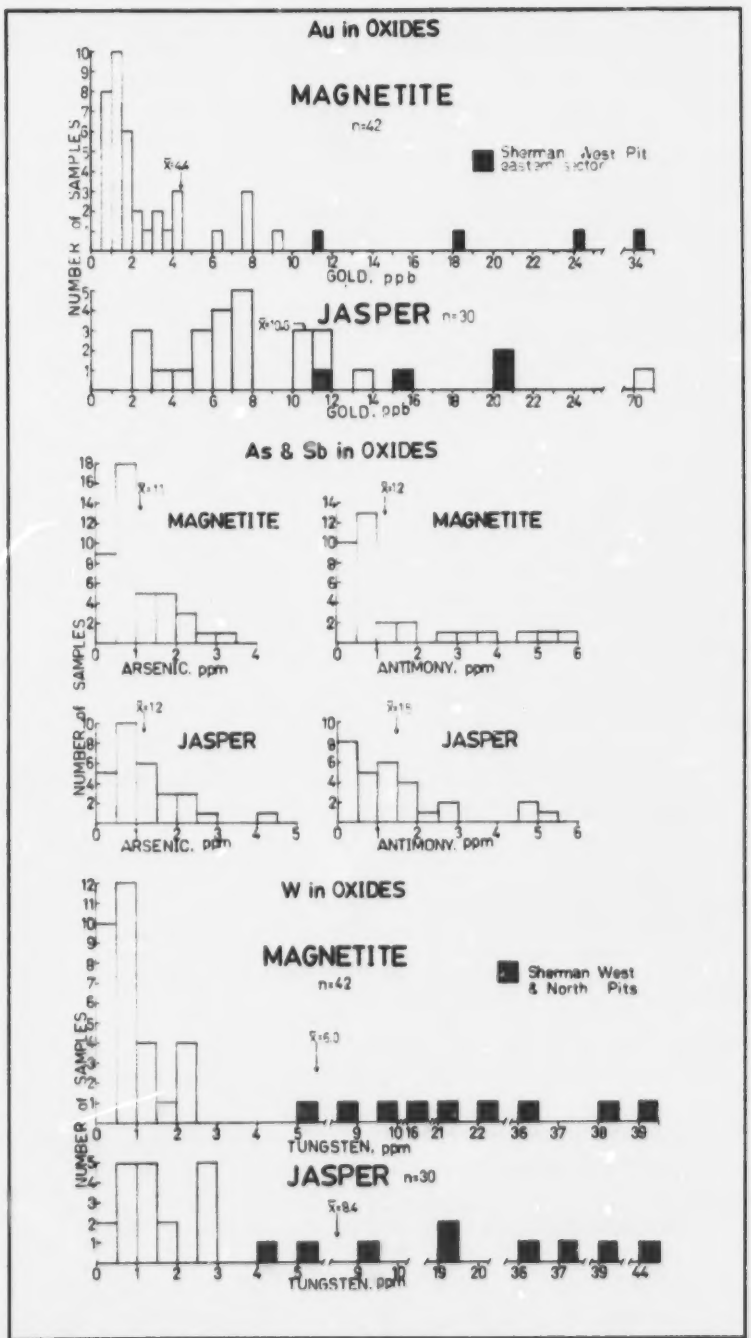

Figure 4. Histograms showing the distribution of Au (a), As (b), and W (c) in magnetite and jasper from the Sherman and Adams mines banded iron formations.

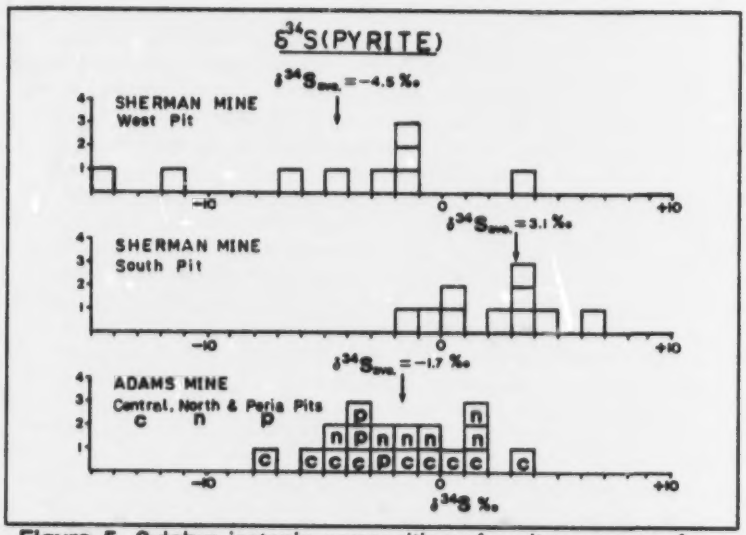

Figure 5. Sulphur isotopic composition of pyrite separates from Adams and Sherman mines banded iron formations.

One important inference from these data is that metamorphism has probably had a major effect on the metal levels in BIF. The Sherman North Pit and the eastern half of the Sherman West Pit are characterized by several features suggestive of lower metamorphism including: (1) the presence of minnesotaite rather than grunerite in silicate facies mesobands, (2) a high proportion of jasper to magnetite mesobands, (3) isotopically lighter oxygen in chert than any other Sherman or Adams BIF. While the full genetic meaning of these features, particularly the oxygen isotopic signature, is not understood, they do constitute a diverse set of distinctive and spatially restricted features which are due, in part at least, to a lower degree of metamorphic overprinting than has generally affected the iron formation. The high frequency of anomalous W and Au in oxide minerals in this area suggests that this feature too may reflect lower metamorphism. Thus the higher metal contents may represent the levels applicable to sedimentation or very early diagenesis. The higher average Au content of jasper relative to magnetite, a difference which is statistically significant at a 1% confidence level, is also considered evidence that diagenesis and/or early metamorphism has modified metal concentrations. It is suggested that a primary ferric hydroxide precipitate lost approximately half its gold content on dehydration and/or partial reduction to magnetite during early diagenesis. This gold, on the order of 5 ppb, might have been redistributed within the BIF or perhaps lost to the adjacent wallrocks.

SULPHUR ISOTOPES IN BIF

The isotopic composition of pyrite sulphur from Sherman and Adams mine BIF was previously shown to be indicative of a biogenic origin for shale-hosted pyrite. The origin of pyrite sulphur in oxide bands is not easily discerned from sulphur isotopic composition. A volcanogenic source is possible, but remobilization of shale-hosted sulphur must be considered a possible additional source. Further sulphur isotope data has been accumulated and all available data are shown in Figure 5 where data from different iron formations are distinguished.

The Adams mine BIF has a range in sulphur isotopic composition of 12‰ which is much less than the 22‰ range shown by the Sherman BIFs. The other distinctive feature is that the Sherman West Pit BIF is characterized by much lighter sulphur than the South Pit BIF. The West Pit average $\delta^{34}S$ is -4.5‰ compared to a +3.1‰ average for South Pit BIF.

The more restricted isotope range of the Adams BIFs may result from homogenization induced by metamorphism, particularly the thermal overprint and deformation caused by intrusion of the Lebel stock. If much of the sulphur was generated by biogenic reduction of marine sulphate under relatively restricted or closed basin conditions as proposed earlier (Crocket *et al.* 1983), then much of the sulphur in the sulphides will be similar in isotopic composition to the source sulphate, with the extremes in isotopic range being represented by a relatively small fraction of the total reduced sulphur. Remobilization should have mixed and ho-

mogenized the primary isotopic distribution so that the relatively smaller amounts of sulphur with very negative or very positive isotopic composition mixed with a larger pool of sulphur close in isotopic composition to the original sulphate. It is suggested, following Thode and Goodwin (1983), that the source marine sulphate had $\delta^{34}S = 0‰$. Thus an average of -1.7‰ is a reasonable mean for the homogenization process envisaged.

The significance of the distinctive variation in isotopic compositions of Sherman mine area BIF is important as such differences are not seen in the Adams mine area where higher metamorphic grade prevails, and because most of the isotopically light sulphur in the Sherman West Pit is from the sector where other distinctive geochemical and mineralogical signatures were noted. The predominance of light sulphur is suggestive of a biogenic origin where the primary isotopic character has not been strongly disturbed by metamorphic processes.

DISCUSSION

Stratigraphy in the Adams Mine area suggests that the BIFs here are of dominantly volcanogenic origin. While the chloritic, ferruginous shale mesobands probably represent fine-grained detrital sediments, the remainder of the iron-rich rocks are probably the products of fluids and exhalations outgassed from volcanic centres during volcanic quiescence at the end of well defined cycles of volcanic activity. The most persuasive geological evidence for this concept is the stratigraphic linking of each major BIF band with a cycle of volcanism, beginning with extrusion of ultramafic komatiite and evolving toward more silica-rich magmas with time. The geographic scale over which such iron deposition occurred was more extensive than the area represented by the economic BIF, because coupled BIF - ultramafic flow units are recognized 2 to 3 km west of the mine pits.

The Sherman mine BIFs are not associated with ultramafic volcanism nor with distinct cycles of volcanic activity, at least on the scale seen in the Adams area. A high proportion of volcanic rocks of intermediate to felsic composition is a distinctive regional feature (Bennett 1978). Within 1.5 km stratigraphically below the northern band of BIF, intermediate to felsic igneous rocks make up about 65% of the pile, and volcaniclastic rocks predominate. While certain aspects of the Sherman BIF such as the great lateral extent of the south band and the widespread presence of delicate, millimetre-scale microlamination suggest the unit represents a chemical sediment, geological evidence suggesting a link with volcanism seems restricted to a preferential spatial association of BIF with more felsic-rich portions of the pile.

The heavy metal content (Au, As, Sb) of both Adams and Sherman BIF is very low. Syngenetic gold probably does not exceed 5 ppb. Higher gold contents are characteristic of shale mesobands which carry abundant pyrite. Jasper rich mesobands probably average 10 ppb gold. However, both shale and jasper mesobands are minor constituents of the iron formations by comparison with magnetite mesobands. The Au and W contents of weakly metamorphosed iron formation (Sherman West Pit) indicate that diagenesis, metamorphism and deformation had a pronounced effect on levels and distribution of metals such as gold in BIF. While it seems quite probable that syngenetic gold would be redistributed by such processes and that approximately 5 ppb gold might be available, no evidence has yet been found for localized concentration of such gold in either of these BIFs. Loss of such metal from the iron formation to wallrocks is possible and the modest enrichment of gold in sulphide-rich, altered volcanic rocks immediately underlying the Sherman West Pit which carry maximum whole rock gold values of 70 ppb may reflect such redistribution.

A survey of gold and other metals in Sherman West and North Pit footwall volcanic rocks did not indicate that unusually high metal values prevail in these rocks. Similarly, the Adams mine area volcanic pile in the vicinity of the economic iron formations is relatively low in base metals and arsenic. High Cr and Ni contents do prevail in the ultramafic members, but low Cu content suggests a silicate control on the Ni and a general lack of magmatic sulphide in the ultramafic rocks.

CONCLUSIONS

The following general conclusions are drawn from the study to date:

1. Stratigraphic evidence supports a volcanogenic origin for the Adams mine BIF. Direct geological evidence that the Sherman mine BIF is volcanogenic is weaker.
2. In the Adams mine area volcanism in which iron

formation was coupled with komatiitic ultramafic extrusion was extensive well beyond the area of the economic iron formations.

3. The iron formation in general, and the major oxide facies mesobands in particular, are low in gold. The syngenetic component is probably less than 5 ppb.
4. A somewhat higher syngenetic component, perhaps 10 ppb, may have prevailed prior to diagenesis and metamorphism. Evidence that the excess metal, about 5 ppb, was locally concentrated within or adjacent to the iron formation is limited, although some sulphide-rich volcanic rocks underlying the Sherman West Pit are weakly anomalous in gold.
5. Stratigraphic units in the immediate vicinity of the iron formations do not appear to be anomalously high in precious or base metals.

ACKNOWLEDGMENTS

We thank Keith Oliver and Bob Garrett for arranging access to the Adams and Sherman properties respectively and for their wholehearted cooperation. We are also grateful to Leo Owsiaki for looking at some puzzling volcanic structures with us in Sherman mine rocks.

REFERENCES

Bennett, G.
1978: Geology of the Northeast Temagami Area, District of Nipissing; Ontario Geological Survey Report 163, 128p. Accompanied by Maps 2323 and 2324, scale 1 inch to 1/2 mile (1:31680), and 1 chart.

Crocket, J.H.
1974: Gold; Sections B-O *in* Handbook of Geochemistry, Volume II/4, edited by H. Wedepohl, Springer, Berlin.

Crocket, J.H., McNutt, R.H., Schwarcz, H.P., Rees, C.E., Blum, N., Hurley, T., Bowins, R., and Kabir, A.
1983: Isotopic and Geochemical Characterization of Archean Iron Formation and Associated Volcanic Rocks - Some Preliminary Results from the Temagami and Boston Iron Formations; p.29-40 in Geoscience Research Grant Program, Summary of Research 1982-1983, edited by E.G. Pye, Ontario Geological Survey, Miscellaneous Paper 113, 199p.

Gross, G.A., and McLeod, C.R.
1980: A Preliminary Assessment of the Chemical Composition of Iron Formations in Canada; Canadian Mineralogist, Volume 18, p.223-229.

Jensen, L.S.
1976: A New Cation Plot for Classifying Subalkaline Volcanic Rocks; Ontario Division of Mines, Miscellaneous Paper 66, 22p.

1978a: Archean Komatiitic, Tholeiitic, Calc-Alkalic and Alkalic Volcanic Sequences in the Kirkland Lake Area; p.237-239 *in* Toronto 1978, Field Excursion Guidebook, edited by A.L. Currie, W.O. Mackasey, Geological Association of Canada/Mineralogical Association of Canada.

1978b: Regional Stratigraphy and Structure of the Timmins-Kirkland Lake Area and the Kirkland Lake - Larder Lake Area; p.67-72 *in* Summary of Field Work, 1978, by the Ontario Geological Survey, edited by V.G. Milne et al., Ontario Geological Survey, Miscellaneous Paper 82, 235p.

Lawton, K.D.
1957: Geology of Boston Township and Part of Pacaud Township; Ontario Department of Mines, Annual Report, Volume 66, Part 5, 55p. Accompanied by Map 1957-4, scale 1 inch to 1000 feet.

Thode, H.G., and Goodwin, A.M.
1983: Further Sulphur and Carbon Isotope Studies of Late Archean Iron Formations of the Canadian Shield and the Rise of Sulphate Reducing Bacteria; Precambrian Research, Volume 20, p.337-356.

Grant 134 Stratigraphy and Geochemistry of Northern Ontario Carbonaceous Deposits: Onakawana Lignites

F. Murray[1], E. van der Flier[1], W.S. Fyfe[1], B.I. Kronberg[1], D.F. Long[2], C. Try[2], and C.G. Winder[1]

[1]Department of Geology, University of Western Ontario
[2]Department of Geology, Laurentian University

ABSTRACT

Detailed geochemical data are presented for coals and associated sediments from the Mattagami Formation including the Onakawana lignite area. It seems clear that the coals were deposited in a continental region in an advanced stage of weathering. In general, the lignites do not have high concentrations of environmentally undesirable elements (fluorine, arsenic, cadmium, lead, uranium). The only elements which appear to be enriched include those which form insoluble residual minerals (titanium, zirconium, rare earths) or have biological affinities (boron, germanium, gallium). There is some evidence for noble metal concentration.

GEOCHEMISTRY

The general geologic and sedimentary setting of Cretaceous coals from the Mattagami Formation of northern Ontario was described in our previous report (Fyfe *et al.* 1983). In this report we concentrate on geochemical data. The global use of coal as a fuel is expanding. At present coal provides 25% of global energy and it is anticipated that this figure will exceed 30% by next century (AECL 1984). The combustion of coal is normally associated with two main environmental problems: (1) increasing atmospheric carbon dioxide, and (2) the problems of acid rain. Another problem during coal utilization is the dispersion of trace metals which were incorporated during the transformation of plant debris to mature coal. Some of these trace metals (U, Cd, Hg, As) may exceed natural background levels by factors of 1000 x U, 1000 x Cd, 100 x Hg, 2000 x As (Fairbridge 1972). Historically, such problems have become apparent long after a given coal deposit was used. It is becoming clear that in the future, coal deposits will be assessed not only by their mass and heat of combustion, but also by their environmental quality based on sulphur and trace metal content.

Trace metals such as copper, nickel, chromium, and molybdenum are of interest with regards to gasification and liquefaction as they may act as catalysts or catalyst poisons in such technology. There is also the interesting possibility that useful metals may be extracted from coal ash. This geochemical study is thus designed to examine such factors before major use occurs.

METHODS

In this report we will concentrate on data determined by spark-source mass spectrometry, X-ray fluorescence (XRF) analysis and neutron activation for uranium, thorium and noble metals. Spark-source data are of particular value since almost all elements in the periodic table can be determined at a semi-quantitative level and hence are of great use in establishing an unusual concentration of a given element. In spark-source mass spectrometry, levels are normally compared with standard rocks so that if a given mass number appears at a level much higher than in background rocks (basalt, granite, etc.) it is immediately obvious.

In our previous report (Fyfe *et al.* 1983) some limited data were presented. Here we present more detailed data amplifying the previous data.

GEOCHEMICAL DATA

Table 1 summarizes uranium and thorium concentrations in drill holes L82-01 and J-1-2 at localities shown in Figure 1. Analyses were conducted by Neutron Activation Services, Hamilton, Ontario, on -200 mesh samples.

Table 2 describes samples used for XRF and spark source analysis. Table 3 gives major element analyses by XRF. Spark-source data are shown in Table 4. In Table 5, data are compared with crustal abundances. In Table 6, a comparison is made of data from this study with other coal ash data. Woody samples (Table 2) were ashed for spark-source analysis and these data are included in Tables 4, 5 and 6. Table 7 gives noble metal concentrations for nine sediments and lignite ashes as determined by neutron activation.

DISCUSSION

Data in Table 6 and the other tables show that the northern Ontario lignites are in general clean. The sediments associated with the lignites and minerals in the coaly material are dominated by quartz and kaolinite with some carbonates or, less frequently illite. Thus the terrain which was shedding debris into the coal basin

was at a state of advanced weathering (Kronberg *et al.* 1979) and was probably dominated by siliceous rocks. Any such environment would be trace element poor and in part this may be the reason for the low values of heavy metals in most coals and sediments. There is no geochemical evidence for the influence of marine incursions during coal formation, an influence which is normally associated with sulphur enrichment.

Particular features we noted include the following.

a. Sulphur contents are normally low except in very localized pyritic materials.

b. Uranium contents are near average crustal abundance, the highest value detected being 60 ppm but with an average for coaly material of 1.63 ppm (Table 1). In drill sections (Figure 2), uranium is in fact concentrated above and below coal seams. Average thorium/uranium ratios in the coals indicate that most of the uranium is associated with thorium and there is little evidence for specific uranium transport into the coals. The data of Figure 2 indicate that mobilized uranium (6+ ppm) may in fact be reduced and deposited in carbonaceous sediments before it reached the coal itself. We have found the same behaviour in a coal deposit in British Columbia (Figure 2). From our experience with coals in Brazil where uranium reaches ore grade, it appears that such enrichment is associated with coals near the marine interface.

c. There is significant enrichment of gold, platinum and palladium in some samples (Table 7). Work is in progress to amplify this aspect of the study.

d. In many coals fluorine is present at moderate to high levels (Brown *et al.* 1981) and this element can present an environmental hazard due to HF production during combustion. The northern Ontario lignites are very low in fluorine (Table 6).

e. Other elements of environmental concern (Pb, As, Cd) are in general at normal levels in lignite ash relative to world data (Table 6).

f. First row transition metals such as V, Cu, Zn, Co, Ni, Mn, Cr are normally depleted, again a reflection of a sediment source in a heavily weathered terrain.

g. Elements associated with refractory (insoluble) minerals are sometimes enriched. Such elements include titanium, rare earths, zirconium and thorium.

h. Some bio-essential elements such as boron, gallium and germanium are frequently enriched.

i. As some carbonate minerals and gypsum are present, some samples show enrichment in barium and strontium. Given the carbonate rocks of the Devonian, these enrichments might be associated with rising deep groundwaters.

In general, these lignites can be considered to present few serious environmental problems (except for CO_2 production) should they ever be used for energy production. With respect to their metal chemistry, they should also present few problems in conversion technologies.

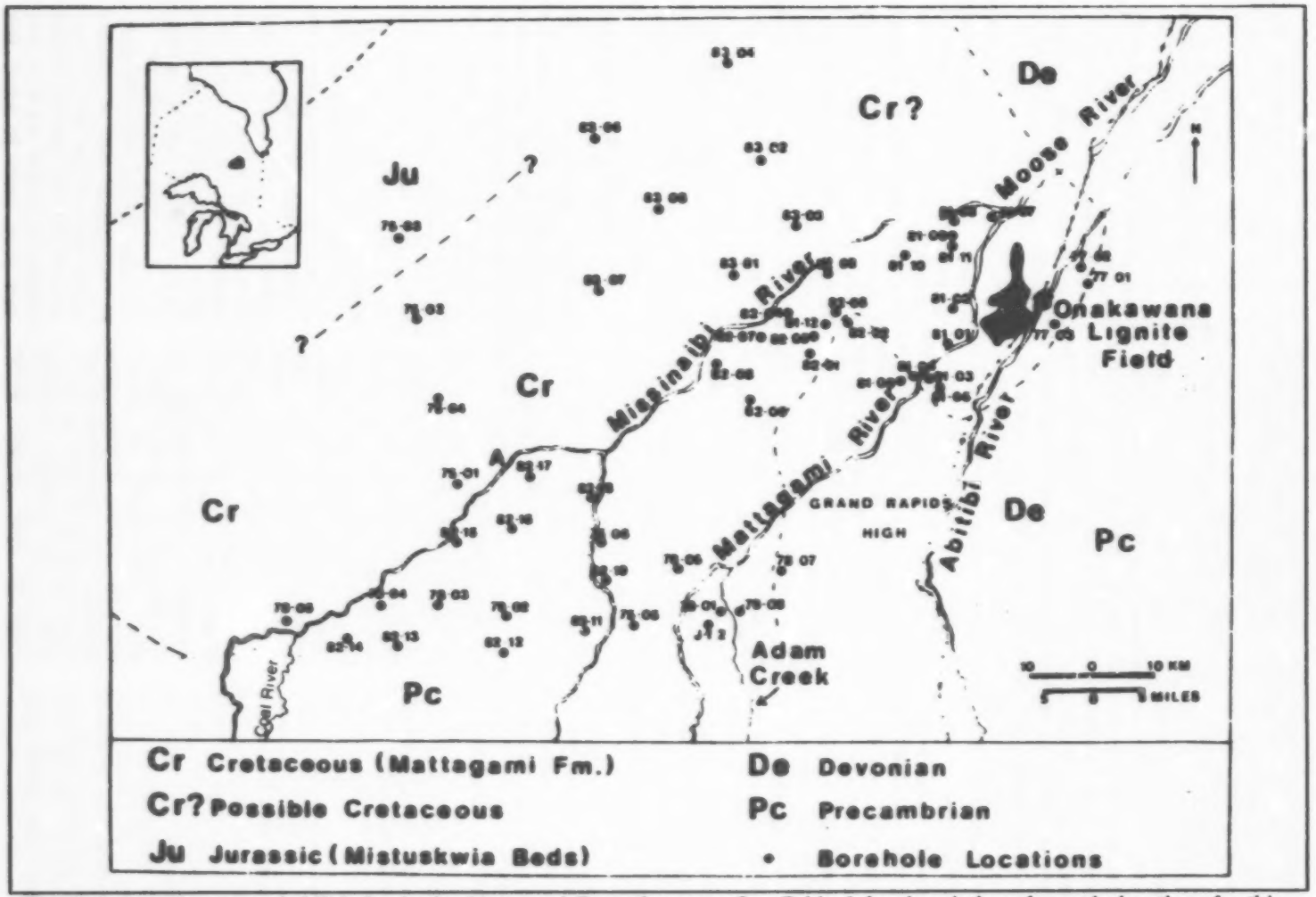

Figure 1. Location map of drill holes in the Mattagami Formation area. See Table 2 for description of sample locations for this study. (Note: location of L82-01 is approximately at drillhole 78-06.)

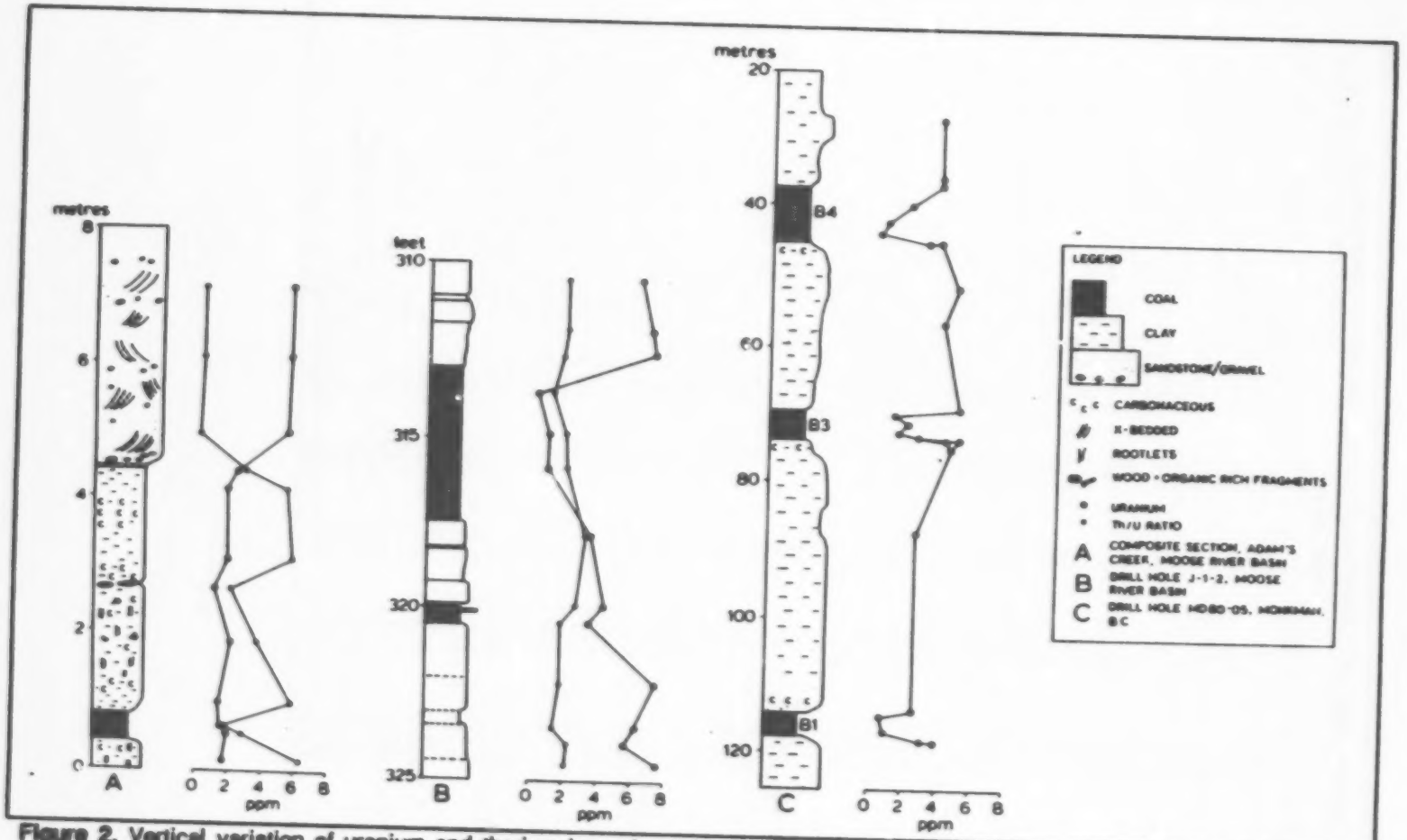

Figure 2. Vertical variation of uranium and thorium in coals of the Moose River Basin. Note the uranium depletion in the most coal-rich materials. A similar situation is shown (C) for Monkman coal, British Columbia.

TABLE 1. URANIUM AND THORIUM CONTENTS OF MATTAGAMI FORMATION COALS AND SEDIMENTS

Sample	Depth Feet	U	Th	Th/U	
		Hole L82-01			
L-1-22	172.5	1.54	5.0	3.25	quartz gravel
L-1-21	200-185	0.77	7.4	9.61	sandy gravel
L-1-19	237.1	5.34	10.0	1.87	dark grey silt (banded v.f.)
L-1-18	238.9	4.73	9.7	2.05	dark grey silt + org.mtl.
L-1-24	245.1-244.9	0.53	2.9	5.47	sandstone
L-1-23	245.6	0.14	<0.3	<2.14	lignite
L-1-25	247.1	5.25	8.2	1.56	lignite underclay
L-1-20	255.0	4.77	9.1	1.91	banded silt + orgs.
L-1-17	258.3	5.07	9.1	1.79	med.-dark grey silty clay + orgs.
L-1-16	260.0	6.36	12.0	1.89	dark grey silty clay
L-1-15	274.0	4.49	9.8	2.18	light grey silt
L-1-14	276.0	4.86	8.9	1.83	light grey silt
L-1-13	278.8	4.64	8.8	1.90	med. grey silt
L-1-12	285.8	3.91	9.4	2.40	v.f. sst (mainly silt)
L-1-11	303.5	1.82	6.6	3.63	med./fine sst + silty sst poorly sorted
L-1-10	323.5	4.15	13.0	3.13	red + green clay
L-1-9	327.9	2.85	13.0	4.56	red + green clay
L-1-8	333.1	2.08	8.1	3.89	green + yellow clay
L-1-7	342.0	3.34	6.8	2.04	yellow + green clay
L-1-5	348.2	2.32	10.0	4.31	green grey clay + orgs.
L-1-6	358.05	3.20	11.0	3.44	red + lt. green clay
L-1-4	359.1	3.83	13.0	3.39	green grey clay (little orgs.)
L-1-3	366.0	3.79	13.0	3.43	Yellow/grey clay
L-1-2	373.8	3.23	15.0	4.64	orange red clay
L-1-1	382.5	2.89	14.0	4.84	red + grey green clay
		Hole J-1-2			
L-2-27	94.0	4.27	12.0	2.81	white red green sst
L-2-28	94.8-95.1	4.31-0.00	9.8		white-yellow clay
L-2-26	226.8	10.4	12.0	1.15	brown clay + silty sst
L-2-25	228.6	6.41	14.0	2.15	med.sst (clay + org rich)
L-2-23	254.85	0.97	5.6	5.77	qtz. gravel
L-2-24	255.1	7.23	11.0	1.52	tan silt + orgs
L-2-20	297.8	0.34	2.1	6.18	white silica sst
L-2-19	298.8	0.85	3.0	3.53	tan-grey org rich sst
L-2-18	299.0-299.3	5.96	11.0	1.85	black earthy lignite + woody
L-2-17	300.0	0.80	1.3	1.63	woody lignite
L-2-16	301.8	0.52	1.2	2.31	v. woody lignite
L-2-15	302.4	2.29	6.3	2.75	earthy lignite
L-2-14	303.9	6.56	13.0	1.98	white (+ brown) clay
L-2-1	310.3	6.65	14.0	2.11	med. dk. brown clay + few orgs
L-2-2	311.7	7.25	16.0	2.21	lt. grey tan clay + orgs
L-2-3	312.5	7.49	14.0	1.87	black v. org. rich clay
L-2-4	313.6	0.51	0.7	1.37	woody + peaty lignite
L-2-5	314.8	1.18	2.5	2.12	woody + peaty lignite
L-2-6	315.8	1.09	2.4	2.20	woody + silty lignite
L-2-7	317.8	3.58	12.0	3.34	dk. grey clay + orgs
L-2-8	319.85	4.40	12.0	2.73	dk. grey original clay
L-2-9	320.35	3.54	6.5	1.84	black clay
L-2-10	322.15	7.43	14.0	1.88	org rich black clay + silt lens
L-2-13	322.85	NA	NA	NA	med. dark grey clay
L-2-11	323.4	6.28	9.1	1.45	dk. grey black clay, much wood
L-2-12	323.9	5.73	13.0	2.27	dk. + lt. grey banded clay + wood
L-2-21	324.5	7.59	16.0	2.11	med. grey clay
L-2-22	343.0	1.30	2.5	1.92	lignite earthy + silt lenses

TABLE 2. LOCATION, DESCRIPTION AND MINERALOGY OF SAMPLES FROM COAL RIVER, ADAM CREEK, ONAKAWANA, AND DRILL HOLES.

Sample	Location and/or depth below surface	Description	Major Minerals	Minor Minerals	Trace Minerals
Surface sediment from Coal River					
AC-36-82	Near Precambrian contact	Red clay, weathered from Silurian shale.	Calcite, dolomite, quartz	Feldspar	Illite, muscovite
AC-37-82	Between sample AC-36-82 and Missinaibi River.	Beige-grey clay, weathered from Silurian shale.	Quartz, Calcite	Muscovite, dolomite, feldspar	Illite
AC-07-82 to AC-10-82: from 1.10 m vertical section on Adam Creek. Cretaceous.					
AC-10-82	0-10 cm	Pyrite and wood 58.9-90.0% ash.	Pyrite		
AC-09-82	10 cm	Woody material from top of lignite seam; 10.4% ash.	Kaolinite		
AC-08-82	10-50 cm	Lignite, 'earthy' on grinding; 23.3-34.8% ash.	Quartz, Kaolinite		
AC-07-82	50-110 cm	Brown clay	Quartz, Kaolinite		
OL Series: Onakawana lignite from lignite dump mined by Manalta, OL(L) and OL(H) from same bulk sample. Cretaceous.					
OL(1)		Consolidated 'chunk'; 5.4% ash.			
OL(L)		Consolidated 'chunk'; 5.7% ash.			
OL(H)		Unconsolidated 'crumbled' lignite; 15.3% ash.			
L-1 Series: from drill hole L82-01, located approximately at drill hole 78-06 (see Figure 1). Cretaceous.					
L-1-9	327.9 ft.	Reddish brown clay, homogeneous in colour and texture.	Quartz, illite	Kaolinite	Feldspar
L-1-8	331.1 ft.	Grey clay with rust mottling.	Quartz, illite, siderite	Kaolinite	
L-1-7	342.0 ft.	Grey and rust mottled clay.	Siderite, quartz		Kaolinite, illite
L-1-6	348.2 ft.	Dark grey and purple-red mottled clay.	Quartz, illite	Hematite	
L-1-5	358.0 ft.	Dark grey homogeneous clay.	Quartz	Illite	
L-2 Series: from drill hole J-1-2, between Mattagami River and Adam Creek, 1 km north of Precambrian contact, (see Figure 1). Cretaceous.					
L-2-27	94 ft.	Slightly mottled pink clay.	Kaolinite	Hematite	Quartz
L-2-26	94.8 ft.	Beige, homogeneous clay.	Kaolinite, quartz		
L-2-25	226.8 ft.	Grey clay interspersed with coarse grains.	Kaolinite, quartz		
L-2-23	264.85 ft.	Quartzitic gravel with fine grains embedded in clay.	Quartz	Kaolinite	
L-2-19	298.8 ft.	Grey, poorly sorted unconsolidated horizon.	Quartz	Kaolinite	
1-2-18	299.3 ft.	Lignitic clay, 37.5-58.2% ash.	Kaolinite, quartz		
L-2-17	300 ft.	Lignite, 4-7-8% ash.	Quartz, kaolinite		

TABLE 3. MAJOR ELEMENT ANALYSIS (WT.%) BY XRF.

Sample	AC-36-82	AC-37-82	AC-07-82	AC-08-82	AC-09-82	AC-10-82
SiO_2	31.4	56.4	63.3	22.1	3.23	0.12
Al_2O_3	6.47	10.2	20.2	7.97	2.71	0.22
CaO	20.3	12.1	0.38	3.41	2.30	0.25
MgO	9.39	2.43	0.18	0.73	0.51	0.01
Na_2O	0.06	0.00	0.00	0.00	0.00	0.00
K_2O	3.69	5.25	0.05	0.04	0.05	0.02
Fe_2O_3	3.17	2.13	0.24	1.36	3.16	59.1
MnO	0.03	0.03	0.00	0.00	0.01	0.00
TiO_2	0.36	0.53	3.24	0.60	0.10	0.00
P_2O_5	0.20	0.13	0.04	0.25	0.02	0.00
CrO_3	-	-	-	-	-	-
LOI	24.2	10.9	11.3	65.2	89.4	41.1

Sample	L-1-6	L-1-6	L-1-7	L-1-8	L-1-9	L-2-17
SiO_2	57.8	51.8	35.2	38.9	57.1	2.60
Al_2O_3	16.4	20.0	9.32	14.3	18.3	1.86
CaO	1.16	1.14	2.34	1.09	0.67	1.30
MgO	1.63	1.34	0.90	1.16	1.44	0.33
Na_2O	0.07	0.07	<0.01	0.02	0.10	0.04
K_2O	2.31	1.52	1.17	1.94	2.58	0.01
Fe_2O_3	6.48	8.21	30.2	23.6	6.85	0.72
MnO	0.03	0.02	0.46	0.27	0.02	0.00
TiO_2	0.91	0.99	0.62	0.77	0.97	0.05
P_2O_5	0.10	0.06	0.11	0.17	0.15	0.01
CrO_3	-	-	-	-	-	0.00
LOI	14.0	15.5	20.5	18.3	11.1	92.2

Sample	L-2-18	L-2-19	L-2-23	L-2-26	L-2-27	L-2-28	crust*
SiO_2	34.4	90.5	83.5	56.9	44.4	50.9	58.4
Al_2O_3	20.1	3.94	5.77	27.8	33.5	32.2	15.8
CaO	1.02	0.11	0.12	0.26	0.24	0.19	6.5
MgO	0.31	0.11	0.13	0.23	0.24	0.24	4.6
Na_2O	0.07	0.01	0.04	0.03	0.07	0.08	3.06
K_2O	0.18	0.46	0.19	0.35	0.42	0.70	2.22
Fe_2O_3	0.94	1.26	3.80	1.13	6.96	1.36	6.5
MnO	<0.01	0.02	0.01	<0.01	<0.01	<0.01	0.14
TiO_2	0.85	0.12	0.17	1.21	1.00	0.98	1.05
P_2O_5	0.05	0.02	0.02	0.06	0.12	0.08	0.26
CrO_3	0.02	-	-	-	-	-	0.023
LOI	41.8	3.08	5.31	12.4	13.7	12.8	

*Fairbridge (1972)

TABLE 4. TRACE ELEMENT DATA BY SPARK-SOURCE, PPM.

Element	Crust[a]	AC-36-82	AC-37-82	AC-07-82	AC-08-82 (ashed)	AC-09-82 (ashed)	AC-10-82 (ashed)	OL(L) (ashed)	OL(H) (ashed)	OL(1) (ashed)
B	9	60	600	200	600	60	0.2	600	200	500
F	544	470	1290	47	470	470	47	160	470	160
S	340	24	24	24	2400	2400	12,000	7000	>7000	>13,000
Cl	126	50	395	17	50	50	17	500	1500	1500
Sc	25	4	8	37	37	37	4	12	12	33
V	136	35	120	354	354	3540	4	354	120	120
Cr	122	7	7	23	23	70	0.07	23	7	17
Mn	1060	86	260	9	90	90	3	260	260	260
Co	29	16	36	2	6	55	550	20	20	36
Ni	99	2	2	2	15	15	5	51	170	160
Cu	68	12	12	35	117	117	1	117	117	180
Zn	76	26	26	9	26	85	26	26	85	40
Ga	19	8	23	23	75	230	0.2	76	23	20
Ge	1.5	1	1	1	12	36	1	35	4	5
As	1.8	3	3	0.3	3	8	3	8	3	21
Se	0.05	0.1	0.1	0.3	0.3	0.1	0.3	0.1	0.03	0.3
Br	2.5	0.3	0.2	0.1	1	1	0.03	3	0.3	5
Rb	78	17	40	0.2	0.6	0.6	0.06	17	56	16
Sr	384	480	480	50	4800	1600	5	4800	1600	3300
Y	31	40	80	120	400	120	1	400	12	37
Zr	162	90	300	30,000	3000	900	3	300	300	190
Nb	20	14	27	135	135	40	0.4	40	14	14
Mo	1.2	0.1	0.4	1	4	4	1	36	4	11
Ag	0.08	0.05	0.05	0.05	0.05	0.5	0.05	0.07	0.07	<0.04
Cd	0.16	<0.1	<0.1	<0.1	<0.1	0.4	<0.1	<0.1	0.1	<0.1
Sn	2.1	0.5	2	5	50	5	<0.5	5	5	9
Sb	0.2	>0.3	>0.2	>0.3	>1	>0.3	>0.1	1	0.3	2
I	0.46	1	0.3	0.3	10	1	<0.1	3	<0.1	<0.1
Cs	2.6	5	5	0.1	1	1	0.03	1	5	0.3
Ba	390	560	560	187	1900	560	6	1900	1900	675
La	35	32	32	32	320	96	1	96	96	26
Ce	66	50	100	50	1500	500	2	150	150	160
Pr	9.1	6	6	2	60	19	0.2	19	6	7
Nd	40	20	20	20	600	200	2	200	60	29
Sm	7.0	7	7	7	243	73	<2	21	7	22
Eu	2.1	2	2	2	50	5	<0.5	5	0.5	7
Gd	6.1	5	5	5	50	17	<2	50	5	7
Tb	1.2	0.2	0.4	0.5	2	2	<0.1	5	0.5	1
Dy		3	5	9	27	9	<1	26	3	2
Ho	1.3	0.4	0.8	4	12	1	<0.4	4	1	1
Er	3.5	1	3	13	13	4	<1	13	4	<4
Tm	0.5	1	1	10	10	3	<0.3	3	1	<1
Yb	3.1	1	2	10	10	3	<1	10	2	<3
Hf	2.8	3	5	74	7	7	<2	73	7	<10
Tl	0.72	0.3	1	<0.3	<0.3	0.3	3	0.5	0.5	<1
Pb	13	3	9	9	31	9	3	31	31	18
Th	8.1	8	8	24	81	24	<1	24	8	6
U	2.3	2	2	60	60	20	<2	60	6	2

TABLE 4. CONTINUED

Element	Crust*	L-2-17 (ashed)	L-2-18 (ashed)	L-2-19	L-2-23	L-2-26	L-2-27	L-2-28
B	9	17	5	2	0.5	0.5	2	3
F	544	470	470	16	470	160	47	100
S	340	39,000	3960	255	1176	780	780	25
Cl	126	170	17	17	5	50	2	5
Sc	25	33	33	100	33	33	33	21
V	136	40	40	4	1	13	13	13
Cr	122	17	57	57	17	17	17	17
Mn	1060	26	26	80	8	3	3	8
Co	29	36	11	1	4	4	4	3
Ni	99	53	16	2	5	5	5	5
Cu	68	56	54	18	18	18	18	12
Zn	76	120	12	4	120	40	40	18
Ga	19	200	60	6	6	20	20	20
Ge	1.5	154	15	5	5	5	5	5
As	1.8	20	2	0.2	2	2	7	0.7
Se	0.05	0.1	0.03	0.3	0.1	0.1	0.01	0.1
Br	2.5	0.5	0.15	0.15	0.5	0.05	0.05	0.05
Rb	78	16	15	15	15	15	15	15
Sr	384	330	110	33	33	11	33	33
Y	31	123	123	1	0.4	12	12	12
Zr	162	190	190	19	57	57	190	57
Nb	20	45	135	5	14	14	45	14
Mo	1.2	33	3	3	3	1	1	1
Ag	0.08	0.1	0.06	<0.04	0.1	0.04	<0.04	<0.04
Cd	0.16	<0.1	<0.1	<0.1	0.1	<0.1	<0.1	<0.1
Sn	2.1	6	6	<3	3	3	3	3
Sb	0.2	2	1	<0.7	<0.7	0.7	0.7	0.7
I	0.46	3	<1	<1	1	<1	<1	<1
Cs	2.6	3	3	1	0.3	3	3	10
Ba	390	675	225	225	22	225	68	146
La	35	260	870	9	3	26	87	260
Ce	68	540	540	16	5	54	54	160
Pr	9.1	70	70	0.7	0.2	7	2	15
Nd	40	290	90	3	3	30	9	90
Sm	7.0	66	22	<2	2	7	2	14
Eu	2.1	19	7	<0.6	<0.7	2	0.7	2
Gd	6.1	198	66	<7	<7	7	7	20
Tb	1.2	30	3	<1	<1	1	1	3
Dy		63	6	<2	<6	2	2	6
Ho	1.3	36	2	<1	<1	1	1	4
Er	3.5	36	5	<4	11	4	<4	7
Tm	0.5	2	0.9	<0.6	2	0.6	<0.6	0.6
Yb	3.1	34	5	<3	<3	<3	<3	3
Hf	2.8	<5	<5	<5	<5	<5	<5	<5
Pb	13	18	18	5	2	5	18	18
Tl	0.72	0.5	0.5	<0.3	<0.3	<0.3	<0.3	<0.3
Th	8.1	60	60	6	<6	18	6	18
U	2.3	5	3	<2	<2	<2	2	2

TABLE 4. CONTINUED

Element	Crust*	L-1-6	L-1-6	L-1-7	L-1-6	L-1-9
B	9	5	5	5	5	5
F	544	>470	157	470	>470	470
S	340	39	39	130	39	130
Cl	126	17	5	17	5	17
Sc	25	33	110	110	33	110
V	136	133	400	400	400	133
Cr	122	17	17	17	17	57
Mn	1060	140	140	140	>1400	140
Co	29	4	4	12	12	12
Ni	99	16	16	54	54	16
Cu	70	16	16	16	16	16
Zn	19	12	12	12	38	12
Ga	1.5	7	7	7	7	20
As	1.8	2	5	2	2	2
Br	0.05	0.7	0.7	0.7	0.7	0.2
Rb	2.5	0.1	0.1	0.1	0.1	0.3
Sr	76	0.15	0.15	0.05	0.05	0.15
Y	384	16	16	16	16	47
Zr	31	33	33	110	110	110
Nb	162	12	12	37	37	12
Mo	20	60	190	570	190	190
Ag	1.2	45	45	45	45	45
Cd	0.08	0.4	1	0.4	0.4	1
Sn	0.16	0.04	0.04	0.04	<0.04	0.04
Sb	2.1	<0.1	0.1	<0.1	<0.1	0.1
I	0.2	3	3	3	3	3
Cs	0.46	0.7	0.7	0.2	0.2	0.2
Ba	2.6	<1	1	<1	<1	3
La	390	1	1	3	3	3
Ce	35	225	225	225	675	225
Pr	66	78	78	26	78	26
Nd	9.1	180	180	180	180	54
Sm	40	23	7	7	7	7
Eu	7.0	67	67	29	67	67
Gd	2.1	22	22	7	7	7
Tb	0.1	0.6	0.6	0.6	0.6	0.6
Dy	1.2	7	2	7	7	7
Ho		1	1	1	1	1
Er	1.3	4	6	0.4	1	6
Tm	0.5	0.6	1	4	1	1
Yb	3.1	1	11	0.6	11	4
Lu	0.8	5	2	1	0.6	0.6
Hf	13	5	3	5	1	1
Ta	0.72	16	5	16	5	5
Th	6.1	<0.3	0.3	<0.3	0.3	0.3
U	2.3	2	2	2	2	2

*Fairbridge (1972)

TABLE 5. TRACE ELEMENT DATA COMPARED TO CRUSTAL ABUNDANCE.

Element	Crust*	L-2-17	L-2-18	L-2-19	L-2-23	L-2-26	L-2-27	L-2-28
B	9	S	S	D	XD	XD	D	D
F	544	S	S	XD	S	D	XD	D
S	340	XXE	XE	S	E	S	S	XD
Cl	126	S	D	D	XD	S	XD	XD
Sc	25	S	S	E	S	S	S	S
V	136	D	D	XD	XXD	XD	XD	XD
Cr	122	D	S	S	D	D	D	D
Mn	1060	XD	XD	XD	XXD	XXD	XXD	XXD
Co	29	S	S	XD	D	D	D	D
Ni	99	S	D	XD	XD	XD	XD	XD
Cu	68	S	S	D	D	D	D	D
Zn	76	S	D	XD	S	S	S	D
Ga	19	XE	E	D	D	S	S	S
Ge	1.5	XXE	XE	E	E	E	E	E
As	1.8	XE	S	D	S	S	E	S
Se	0.05	S	S	E	S	S	D	S
Br	2.5	D	XD	XD	D	XD	XD	XD
Rb	78	D	D	D	D	D	D	D
Sr	384	S	D	XD	XD	XD	XD	XD
Y	31	E	E	XD	XD	S	S	S
Zr	162	S	S	D	S	S	S	S
Nb	20	S	E	D	S	S	S	S
Mo	1.2	XE	S	S	S	S	S	S
Ag	0.08	S	S	S	S	S	S	S
Cd	0.16	S	S	S	S	S	S	S
Sn	2.1	E	E	S	S	S	S	S
Sb	0.2	XE	E	S	S	E	S	E
I	0.46	S	S	S	S	S	S	S
Cs	2.6	S	S	S	D	S	S	E
Ba	390	S	S	S	XD	S	D	S
La	35	E	XE	D	XD	S	S	E
Ce	66	E	E	D	XD	S	S	S
Pr	9.1	E	E	XD	XD	S	D	S
Nd	40	E	S	XD	XD	S	D	S
Sm	7.0	E	E	D	D	S	D	S
Eu	2.1	E	E	D	D	S	D	S
Gd	6.1	XE	XE	S	S	S	S	E
Tb	1.2	XE	S	S	S	S	S	S
Ho	1.3	XE	S	S	S	S	S	E
Er	3.5	E	S	S	E	S	S	S
Tm	0.5	E	S	S	E	S	S	S
Yb	3.1	XE	S	S	S	S	S	S
Hf	2.8	S	S	S	S	S	S	S
Pb	13	S	S	S	D	S	S	S
Tl	0.72	S	S	D	D	D	D	D
Th	8.1	E	E	S	S	S	S	S
U	2.3	S	S	S	S	S	S	S

*Fairbridge (1972)

Key.
S - Similar (0.3-3 X crustal abundance)
D - Depleted (0.1-0.3 X crustal abundance)
E - Enriched (3-10 X crustal abundance)
X - 10 X (depleted or enriched)
XX - 100 X (depleted or enriched)
XXX - 1000 X (depleted or enriched)

TABLE 5. CONTINUED

Element	Crust*	AC-36-82	AC-37-82	AC-07-82	AC-08-82	AC-09-82	AC-10-82	OL(L)	OL(H)	OL(1)
B	9	E	XE	XE	XE	E	XD	XE	XE	XE
F	344	S	S	XD	S	E	XD	D	S	D
S	340	XD	XD	XD	E	S	XE	XE	XE	XE
Cl	126	S	S	D	S	S	D	E	XE	XE
Sc	25	D	D	S	S	S	D	S	S	S
V	136	D	S	S	D	XE	XD	S	XD	D
Cr	133	XD	XD	D	XD	S	XXD	D	D	D
Mn	1060	XD	D	XXD	D	XD	XXD	D	D	D
Co	29	S	S	XD	D	S	XE	S	S	S
Ni	99	XD	XD	XD	D	S	XD	S	S	S
Cu	68	D	D	S	S	S	XD	S	S	S
Zn	76	S	S	D	S	S	S	S	S	S
Ga	19	S	S	S	E	XE	XD	E	S	E
Ge	1.5	S	S	E	E	XE	S	XE	S	XE
As	1.8	S	S	E	S	E	E	E	S	E
Se	0.05	S	S	S	S	S	E	S	S	E
Br	2.5	D	XD	XD	S	S	XD	S	D	S
Rb	78	D	S	XXD	XXD	XXD	XXXD	D	S	D
Sr	384	S	S	D	XE	E	XD	XE	E	D
Y	31	S	S	E	XE	E	XD	XE	S	S
Zr	162	S	S	XXE	XE	E	XD	S	S	S
Nb	20	S	D	E	E	E	XD	S	XE	S
Mo	1.2	XD	S	S	E	E	S	XE	E	S
Ag	0.08	S	S	S	S	E	S	S	S	E
Cd	0.16	S	S	S	S	S	S	S	S	S
Sn	2.1	D	S	S	XE	S	D	S	S	E
Sb	0.2	S	S	S	E	S	S	E	S	XE
I	0.46	S	S	S	XE	S	D	E	D	D
Cs	2.6	S	S	XD	S	S	XD	E	S	D
Ba	390	S	S	S	E	S	XD	S	S	S
La	35	S	S	S	XE	S	XD	S	S	S
Ce	66	S	S	D	E	S	XD	S	S	S
Pr	9.1	S	S	S	XE	S	XD	S	S	E
Nd	40	S	S	S	XE	S	D	S	S	E
Sm	7.0	S	S	S	XE	XE	D	S	S	S
Eu	2.1	S	S	S	E	S	D	S	S	S
Gd	6.1	S	D	D	S	S	XD	S	S	S
Tb	1.2	D	D	S	E	S	D	S	S	S
Ho	1.3	D	S	E	E	S	D	S	S	S
Er	3.5	D	S	XE	XE	S	D	S	S	S
Tm	0.5	S	D	E	E	S	D	S	S	S
Yb	3.1	D	S	XE	S	S	D	S	S	S
Hf	2.8	S	D	S	D	S	E	S	S	S
Pb	13	D	S	D	XE	S	D	S	S	S
Tl	0.72	S	S	E	XE	E	S	E	S	S
Th	8.1	S	S	XE	XE	E	XE	S	S	S
U	2.3	S	S	XE	XE	E	S	XE	S	S

*Fairbridge (1972)

Key.
S - Similar (0.3-3 X crustal abundance)
D - Depleted (0.1-0.3 X crustal abundance)
E - Enriched (3-10 X crustal abundance)
X - 10 X (depleted or enriched)
XX - 100 X (depleted or enriched)
XXX - 1000 X (depleted or enriched)

TABLE 6. CONTINUED

Element	Crust*	L-1-6	L-1-6	L-1-7	L-1-8	L-1-9
B	9	S	S	S	S	S
F	544	S	D	S	S	S
S	340	D	D	S	D	S
Cl	126	D	XD	D	XD	D
Sc	25	S	E	E	S	E
V	136	S	E	E	E	S
Cr	122	D	D	D	D	S
Mn	1060	D	D	S	S	D
Co	29	D	D	S	S	S
Ni	99	D	D	S	S	D
Cu	68	D	D	D	D	D
Zn	76	D	D	D	S	D
Ga	19	S	S	S	S	S
Ge	1.5	S	E	S	S	S
As	1.8	S	S	S	S	D
Se	0.05	S	S	S	S	E
Br	2.5	XD	XD	XD	XD	XD
Rb	78	D	D	D	D	S
Sr	384	XD	XD	D	D	D
Y	31	S	S	S	S	S
Zr	162	S	S	E	S	S
Nb	20	S	S	S	S	S
Mo	1.2	D	S	D	D	S
Ag	0.08	S	S	S	S	S
Cd	0.16	S	S	S	S	S
Sn	2.1	S	S	S	S	S
Sb	0.2	E	E	S	S	S
I	0.46	S	S	S	S	E
Cs	2.6	S	S	S	S	S
Ba	390	S	S	S	S	S
La	35	S	S	S	S	S
Ce	66	S	S	S	S	S
Pr	9.1	S	S	S	S	S
Nd	40	S	S	S	S	S
Sm	7.0	E	E	S	S	S
Eu	2.1	D	D	D	D	D
Gd	6.1	S	D	S	S	S
Tb	1.2	S	S	S	S	S
Ho	1.3	S	S	D	S	S
Er	3.5	S	E	S	E	S
Tm	0.5	S	E	S	S	S
Yb	3.1	D	S	D	D	D
Hf	2.8	S	S	S	S	S
Pb	13	S	S	S	S	S
Tl	0.72	D	S	D	S	S
Th	8.1	S	S	S	S	S
U	2.3	S	S	S	S	S

*Fairbridge (1972)
Key.
S - Similar (0.3-3 X crustal abundance)
D - Depleted (0.1-0.3 X crustal abundance)
E - Enriched (3-10 X crustal abundance)
X - 10 X (depleted or enriched)
XX - 100 X (depleted or enriched)
XXX - 1000 X (depleted or enriched)

TABLE 8. COMPARISON OF TRACE ELEMENTS IN ONAKAWANA COAL ASH WITH OTHER COAL ASHES (ANALYTICAL TECHNIQUE SPECIFIED).

Element	Onakawana lignite (spark source)	North American Data[1] (spark source)	North Dakota lignite[1] (spark source)	Belgian Data[2] (neutron activation)	Global Data[3] (compilation)	American Data[4] (neutron activation spark source)	Wedepohl[5] (compilation)
B	17-600	3->500	>500		240-660		6,400
F	160-470	50-(26,000)[6]	>500				
S	2,400-39,000	up to 25,000	>500	11,000-12,000			
Cl	50-1,500	1->50	>500	1,000-3,900		185-<1,000	435-3,000
Sc	12-37	3-100	3-100	30-72		20-28	10-1,000
V	40-364	10-1,250	10-1,250	260-460	63-126	157-230	56-24,600
Cr	7-23	0.3-15	0.3-15	180-330	32-54	116-132	800
Mn	26-260			260-1,100			
Co	6-36	3-130	130	42-270		25-39	15-30
Ni	15-170	5-450	60	260-1,300	15-28	98	5-13
Cu	56-180	60-180	180	250-660	26-70	120-<500	15-500
Zn	28-120	3-400	85	550-820	36-93	210-700	430-1,000
Ga	20-200	0.5-60	20	36-58	160-320	38	6-1,000
Ge	4-154	2-5	2		23-26	476	5-10,000
As	3-21	0.5-600	600	5-74	7-28	61-70	300-700
Se	0.03-0.3	0.03-0.3	0.3	4-12	166-230	3-13	3-10
Br	0.3-5	0.2-0.5	0.2	7-30		7-12	
Rb	0.6-56	1-20	20	100-230		9-124	
Sr	330-4,800	30-3,000	650		420-660	869-1,900	420-660
Y	12,400	5-120	60				100
Zr	190-3,000	60-200	200		115	640	≤5,000
Nb	14-135	2-40	13				
Mo	4-36	3-200	200	34-130	15-26		
Ag	<.04-0.1	0.1-0.3	0.1	4-<20			<10
Cd	≤0.1	≤0.1-0.3	≤0.1	<7-<35		2	3-30
Sn	5-50	<1-10	1		5-8	740	
Sb	0.3-2	2-15	10	6-22		1-12	<40-3,000
I	≤0.1-10	≤0.3-30	1	2.5-3			142-587
Cs	0.3-5	0.3-3	3	2-6		10-14	
Ba	560-1,900	200-6,000	3,600	1,300-3,400	580-660	500-3,400	100-48,000
La	26-320	8-60	10	69-230		47-82	4
Ce	150-1,500	5-160	55	140-360		129	12
Pr	6-70	3-70	20				2
Nd	29-600	10-300	120				5
Sm	7-243	≤2-70	5	12-38		10-12	2
Eu	0.5-50	0.5-20	2	2-11		1-2	0.7
Gd	5-198	≤5-20	5				1.6
Tb	0.5-30	≤1-3	3			0.2-2	0.3
Dy	2-63	≤1-60	3	8-29		8	
Ho	1-36	≤1-12	2				0.3
Er	<4-36	≤1-10	1				0.6
Tm	≤1-10	0.5-2	1				0.1
Yb	2-34	≤1-10	3	6-12		6-9	0.5
Hf	≤5-73	≤5-15	5	7-11		6-8	
Tl	≤0.3-0.5	≤1-10	1				0.3-2.3
Pb	18-31	≤2-150	5		25-200	76-79	
Th	6-81	≤2-20	20	17-22		15-28	
U	2-60	≤2-20	20			2-12	

[1]Kronberg *et al.* (1981)
[2]Block and Dams 1975
[3]Yudovich *et al.* (1972)
[4]Carter *et al.* 1975; Sheibley 1975; Abel and Ranciselli 1975
[5]Wedepohl 1969
[6]Brown *et al.* 1981

TABLE 7. NOBLE METAL CONTENTS (ppb) IN SELECTED SEDIMENTS AND LIGNITE ASH

Sample	Au	Ru	Rh	Pt	Re	Os	Ir	Pd
RC-1	17	<20	<1	<20	<1	<3	0.1	<10
RP	6	<20	<1	<20	<1	<3	0.1	<10
PY	36	<20	<1	<20	1	<3	0.1	10
FM-1	41	<20	<1	60	3	<3	0.1	<10
FM-4	31	<20	1	50	5	<3	0.3	10
P-1	32	<20	<1	<20	<1	<3	0.5	<10
P-2	96	<20	2	35	<1	<3	0.1	250
P-3	55	<20	<1	<20	<1	<3	0.1	10
P-4	8	<20	<1	<20	<1	<3	0.3	<10
Crust*	3	0.4	0.4	2	0.5	0.4	0.4	4

Samples
P-1 - lignite
P-2 - lignite
P-3 - black clay
P-4 - green clay

RC-1 - red sst/gravel + wood
RP - red sst/gravel (pyrite rich)
PY - pyrite nodule from gravel white
FM-1 - solly lignite
FM-4 - solly/woody lignite

*Wedepohl (1969)

REFERENCES

Abel, K.H., and Rancitelli, L.A.
1975: Major, Minor, and Trace Element Composition of Coal and Fly Ash, as Determined by Instrumental Neutron Activation Analysis; p.118-138 *in* Trace Elements in Fuel, edited by S.P. Babu, American Chemical Society, Adv. Chemistry Series 141. 214p.

Atomic Energy of Canada Limited
1984: Energy in the Year 2000; Ascent, Spring 1984, p.3.

Block, C. and Dams, R.
1975: Inorganic Composition of Belgian Coal and Coal Ashes; Environmental Science and Technology, Volume 9, p.146-150.

Brown, J.R., Kronberg, B.I., and Fyfe, W.S.
1981: Semi-Quantitative ESCA Examination of Coal and Coal Ash Surfaces; Fuel, Volume 60, p.439-446.

Carter, J.A., Walker, R.L., and Sites, J.R.
1975: Trace Impurities in Fuels by Isotope Dilution Mass Spectrometry; p.74-83 *in* Trace Elements in Fuel, edited by S.P. Babu, American Chemical Society, Adv. Chemistry Series 141, 214p.

Fairbridge, R.W.
1972: The Encyclopedia of Geochemistry of Environmental Sciences; Encyclopedia of Earth Sciences Series, Volume IVA, Van Nostrand Reinhold Co., New York, 1321p.

Fyfe, W.S., Kronberg, B.I., Long, D.F., Murray, F.H., Powell, M., Try, C., van der Flier, E., Winder, C.G., and Brown, J.R.
1983: Stratigraphy and Geochemistry of Northern Ontario Carbonaceous Deposits: Onakawana Lignites; p.63-81 in Geoscience Research Grant Program, Summary of Research 1982-1983, edited by E.G. Pye, Ontario Geological Survey, Miscellaneous Paper 113.

Kronberg, B.I., Fyfe, W.S., Leonardos, O.H., and Santos, A.M.
1979: The Chemistry of Some Brazilian Soils: Element Mobility during Intense Weathering; Chemical Geology, Volume 24, p.211-229.

Kronberg, B.I., Brown, J.R., Fyfe, W.S., Peirce, M. and Winder, C.G.
1981: Distribution of Trace Elements in Western Canadian Coal Ashes; Fuel, Volume 60, p.59-63.

Sheibley, D.W.
1975: Trace Elements by Instrumental Neutron Activation Analysis for Pollution Monitoring; p.98-117 *in* Trace Elements in Fuel, edited by S.P. Babu, American Chemical Society, Adv. Chemistry Series 141, 214p.

Wedepohl, K.H.
1969: Handbook of Geochemistry; Springer-Verlag, Berlin

Yudovich, Ya., E., Korycheva, A.A., Obruchnikov, A.S. and Stepanov, Yu., V.
1972: Mean Trace-element Contents in Coals; Geochem. International, Volume 9, p.712-720.

Grant 138 Mineralogy and Geochemistry of the Chrysotile Asbestos Deposits of Ontario: Munro Mine and Garrison Deposit

F.J. Wicks, Wan Pu and K. Hedjran

Department of Geology, University of Toronto

ABSTRACT

The Munro chrysotile asbestos mine, in Munro Township, is located within the Abitibi Belt of the Superior Province. Detailed mapping in the B pit area of the Munro mine indicates that the layered ultramafic to gabbroic body usually referred to as the Munro-Beatty sill is composed of five units: a basal zone approximately 5 m thick, an olivine cumulate layer 160 m thick, a pyroxene cumulate layer 2-6 m thick, a gabbroic layer 50 m thick, and a top layer 2 m thick. The basic mineralogy and major element chemistry is similar to the differentiated komatiite flows in the area but olivine and stringbeef spinifex textures are absent. At this stage of the research program it is not certain whether the Munro-Beatty body is a sill or a flow. It is clear, however, that the olivine cumulate layer has lost calcium and that the $MgO:SiO_2$ ratio has been modified by the intense serpentinization. The rocks at the Garrison chrysotile asbestos deposit are similar to the Munro rocks but exposure is too poor to make a correlation.

The mapping in the B pit area has also illustrated the strong relationship of the chrysotile asbestos veins to intense fracturing and prograde serpentinization. The prograde event has produced limited recrystallization of the original lizardite 1T pseudomorph textures to chrysotile $2M_{cl}$ and less frequently antigorite, serrate veins. Microprobe analyses indicate an Al_2O_3 content of up to 1.4 weight percent in lizardite 1T after olivine and indicate the local mobility of aluminum during serpentinization. The prograde serpentinization at the Garrison deposit is characterized by well developed prograde chrysotile textures with variable brucite and indicates different conditions of serpentinization and chrysotile asbestos vein development.

INTRODUCTION

The ultramafic flows that occur in the Abitibi Belt, particularly the less altered ones, have been studied in some detail (Pyke *et al.* 1973; Arndt 1977; Arndt *et al.* 1977; Jensen and Pyke 1982; Barnes *et al.* 1983). The chrysotile asbestos deposits within the belt occur in some of the larger komatiite bodies that are usually described as flows or sills. These have not been studied systematically partly because none of the mines are in production and partly because the extensive alteration associated with the chrysotile asbestos development obscures the primary komatiite mineralogy and geochemistry that is of interest to most researchers. It is the object of this study to carry out a detailed study of the major chrysotile asbestos deposits. The progress during the first year of this study was given by Wicks *et al.* (1983). The present report contains some of the results of the second year of the study. The collection of data is not complete and the interpretation is not completely developed, nevertheless more interesting details have emerged.

The work on the second year of the project nas centred on the former Munro mine and the Garrison deposit (Hewitt and Satterly 1953; Vos 1971) both of which are owned by Johns-Manville Canada Incorporated. The Munro mine is located in Munro Township 16 km east of the town of Matheson. This township has been the location of much of the classic work on komatiites in Canada (Pyke *et al.* 1973; Fleet and MacRae 1975; Arndt 1977; Arndt *et al.* 1977). The Munro-Beatty komatiite occurs in the southwest corner of the township and was the host for the chrysotile asbestos deposits that were mined by Canadian Johns-Manville Company Limited from 1954 to 1964 as the Munro mine. The Garrison deposit is located in Garrison Township 38 km east of Matheson. The serpentinite that hosts the asbestos deposit lies in the northern half of the township. The asbestos zones were outlined by underground work in 1969 by Canadian Johns-Manville Company Limited and stock piles from each zone were assembled on the surface at the site.

GEOLOGY

The Munro-Beatty komatiite passes in a northwesterly direction through the southwestern corner of Munro Township up into the west-central part of Beatty Township. It was well exposed in the area that developed into the A orebody of the Munro mine (Hendry 1951; Hendry and Conn 1957), but most of this outcrop was removed during mining and only the flooded open pit remains. However, there is still excellent exposure of all units of the Munro-Beatty komatiite in the vicinity of the small open pit in the B orebody im-

mediately to the west of the A pit. Another complexly faulted but almost complete section is exposed in low outcrops 0.5 km southwest of the A pit. This section lies outside the chrysotile asbestos ore zone.

Detailed surface and underground mapping was carried out by Canadian Johns-Manville Company Limited (Hendry 1951; Hendry and Conn 1957). Hendry (1951) pointed out that the systematic and intimate relationship of the peridotite-dunite layer overlain to the northeast by a narrow pyroxenite which grades into the upper gabbro layer at the top indicates differentiation from a common magma in a sill-like body (Hendry 1951), or sill-like complex (Hendry and Conn 1957). This mapping in conjunction with diamond drilling and detailed ground geophysics outlined the ultramafic layer and located up to 29 major cross faults striking north to northeast and dipping vertically with displacements from 15 to 345 m (Hendry 1951). The most comprehensive geological maps of Munro and Beatty Townships were published by Satterly (1952) and Satterly and Armstrong (1949) respectively, and incorporated much of the Canadian Johns-Manville data.

The average strike of the Munro-Beatty komatiite is N65-70°W (Hendry 1951) and the dip is 75°N to vertical. With the exception of a major fault near the Munro-Beatty Township line that has a southward displacement, the displacement of the north- and northeast-trending cross faults is for the western block to be moved north. This gives the northwest trend to the present outcrop. In addition to cross faulting the Munro-Beatty komatiite lies between two major northwest-striking faults: the Munro fault zone immediately north of the mine, and the Pipestone fault zone to the south.

The Munro-Beatty komatiite has not been studied in detail since the importance of komatiites has been recognized. Kretschmar and Kretschmar (1982) have indicated the komatiite nature of the rocks, and Arndt (1975) after his examination of the outcrops suggested that it is a komatiite flow or sill. The detailed mapping of the B pit area during the present study presents the opportunity to study the nature of the original komatiitic rocks as well as the effect of serpentinization and the development of chrysotile asbestos veins.

The serpentinite that hosts the Garrison chrysotile-asbestos deposit lies near the northern township line striking approximately east and dipping approximately 60°N Satterly (1949). Exposure is poor with only a few outcrops of gabbro and one exposure of a chrysotile-asbestos zone in an exploration pit 855 m to the east of the exploration shaft collar. However, the stock piles of mineralized rock which had been systematically collected underground and laid out on surface provide a unique opportunity to study this deposit. Underground mapping was combined with diamond drill hole information, by Canadian Johns-Manville Company Limited to produce a map of the serpentinized ultramafic layer and the four distinct chrysotile-asbestos zones contained within it. Manville Canada has provided access to this map so that the samples collected on surface can be positioned with respect to their asbestos zones.

RESULTS

Studies have been concentrated on the petrography of the rocks both in terms of their primary and alteration mineralogy. Serpentine minerals have been identified *in situ* in thin section by Norelco X-ray microbeam camera using the procedures of Wicks and Zussman (1975). Mineral compositions have been determined using a Materials Analysis Company Model 400 electron microprobe equipped with a Kevex Model 5000A energy dispersive spectrometer following the procedures of Wicks and Plant (1983). Major element compositions of whole rocks were determined by X-ray fluorescence analysis by Domtar Incorporated, Research Centre, Senneville, Quebec, using matrix corrections developed by Lachance and Traill (1966).

MUNRO–BEATTY KOMATIITE

Mapping of the B pit area at a scale of 1:600 (Figure 1) and in the area east of the A pit at a scale of 1:1200 has revealed that what has been called the Munro-Beatty komatiite is composed of five main layers: a basal zone, an olivine cumulate layer, a pyroxene cumulate layer, a gabbroic layer (Figure 2) and a top layer.

The basal zone is approximately 5 m thick and is fairly strongly affected by carbonate and talc alteration along the contact so that the primary features are somewhat obscured. The composition of the basal zone particularly at the contact is variable from locality to locality but it consistently contains clinopyroxene either as equant to slightly elon-

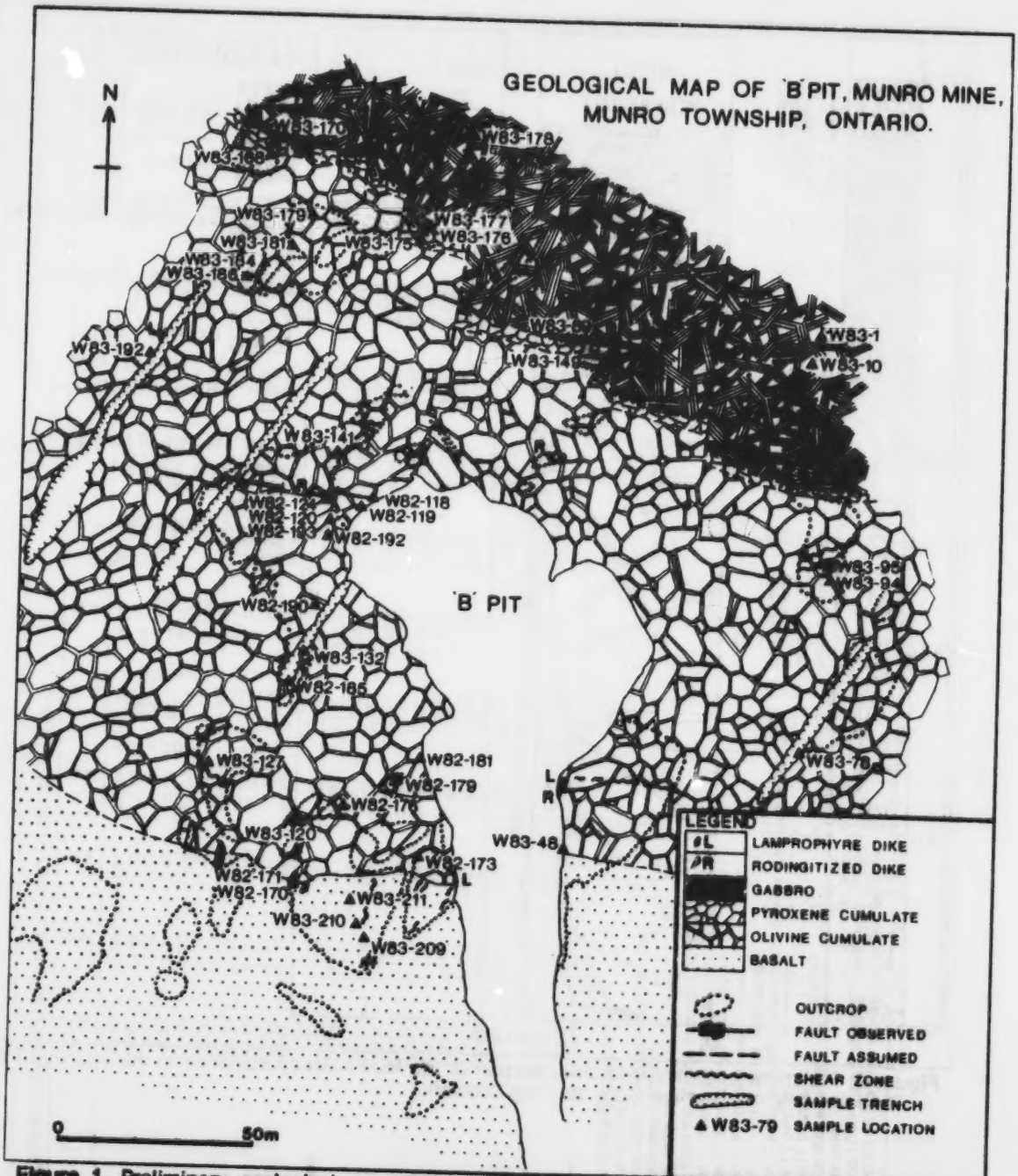

Figure 1. Preliminary geological map of the Munro-Beatty komatiite in the vicinity of the B pit, Munro mine.

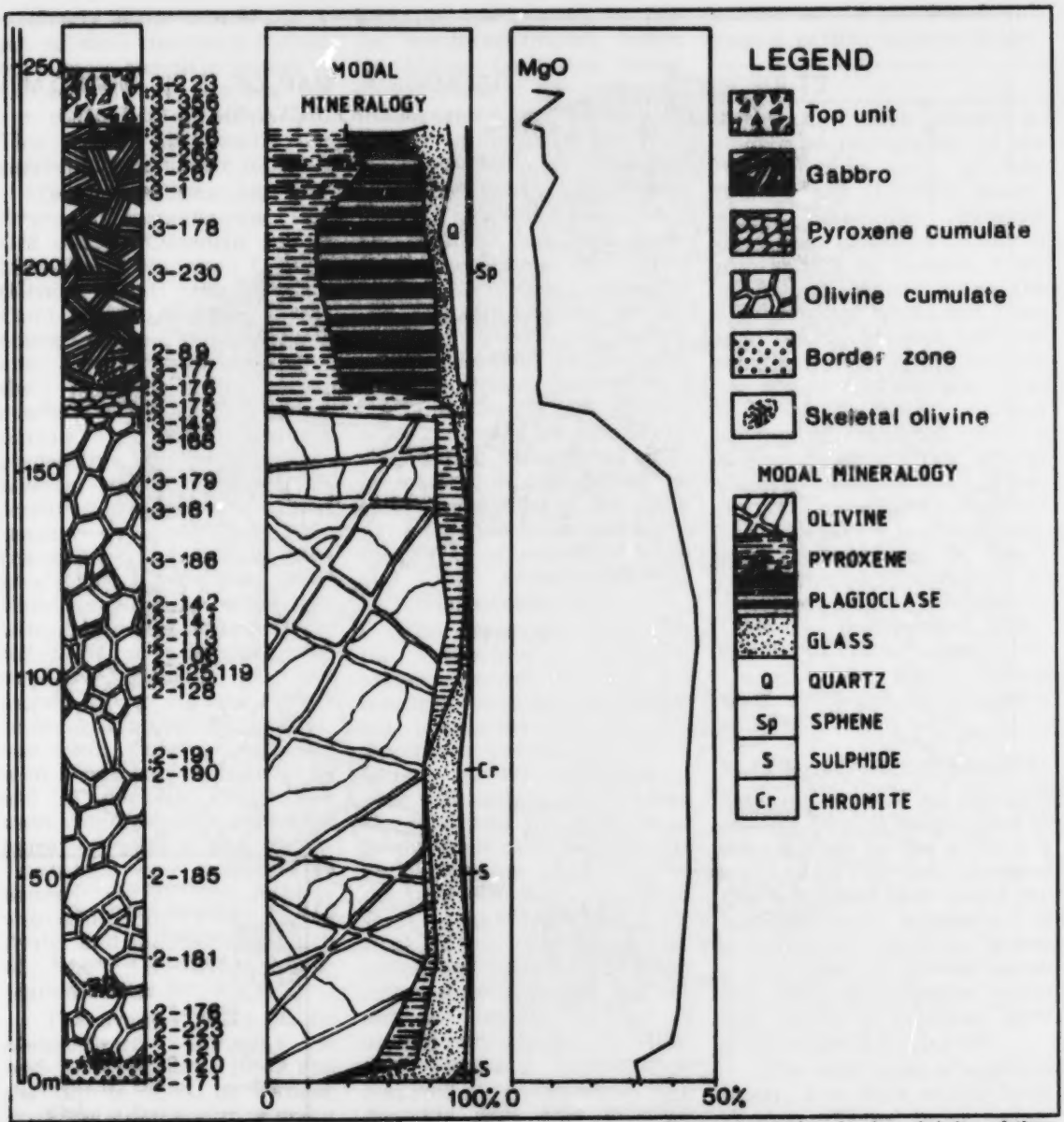

Figure 2. Preliminary, generalized cross-section of the Munro-Beatty komatiite in the vicinity of the B pit showing modal mineralogy and MgO content.

TABLE 1. ELECTRON MICROPROBE ANALYSES OF VARIOUS MINERALS.

Sample	1	2	3	4	5	6	7	8	9	10	11	12	13
n	4	3	4	3	3	3	3	3	7	3	3	9	3
SiO_2	48.93	52.66	54.61	40.97	41.33	40.20	39.93	40.06	40.19	39.83	39.48	41.40	41.61
TiO_2	0.81	0.45	0.23	0.05	0.07	0.10	0.09	0.12	0.10	0.10	0.13	0.07	0.06
Al_2O_3	4.41	2.32	1.60	0.18	1.08	0.58	0.95	1.35	1.44	1.84	2.15	0.79	1.18
Cr_2O_3	0.22	0.56	0.35	0.11	0.08	0.13	0.25	0.30	0.38	0.31	0.72	0.11	0.32
FeO*	11.85	5.60	10.01	12.03	1.78	2.20	4.20	4.18	2.46	2.02	2.91	3.18	2.17
MnO	0.20	0.11	0.20	0.16	0.09	0.10	0.05	0.08	0.06	0.09	0.07	0.13	0.09
MgO	13.07	16.73	31.50	46.94	41.07	40.82	40.39	40.24	40.06	40.54	38.74	39.68	40.64
CaO	20.00	19.89	2.14	0.20	0.02	0.02	0.03	0.02	0.01	0.01	0.02	0.02	0.06
Na_2O	0.46	0.00	0.00	0.00	0.00	0.00	0.00	0.00	0.00	0.00	0.00	0.01	0.00
K_2O	0.15	0.04	0.02	0.00	0.04	0.02	0.03	0.03	0.00	0.03	0.03	0.00	0.01
Total	100.09	100.55	100.65	100.63	86.54	84.15	85.91	86.40	84.72	84.77	84.25	85.39	86.16
					Calculated Formulae								
No. of oxygen	(6)	(6)	(6)	(4)	(14)	(14)	(14)	(14)	(14)	(14)	(14)	(14)	(14)
Si	1.850	1.915	1.921	1.006	3.921	3.894	3.835	3.826	3.870	3.828	3.836	3.969	3.927
Ti	0.023	0.012	0.006	0.001	0.005	0.007	0.008	0.009	0.007	0.007	0.009	0.005	0.006
Al	0.197	0.099	0.066	0.005	0.120	0.066	0.107	0.152	0.164	0.208	0.246	0.089	0.131
Cr	0.008	0.016	0.010	0.002	0.004	0.010	0.019	0.022	0.029	0.024	0.055	0.009	0.024
Fe	0.375	0.177	0.294	0.247	0.141	0.178	0.336	0.334	0.198	0.163	0.237	0.254	0.171
Mn	0.007	0.003	0.006	0.003	0.007	0.008	0.004	0.008	0.005	0.007	0.005	0.010	0.007
Mg	0.737	1.015	1.651	1.719	5.808	5.895	5.783	5.726	5.753	5.808	5.611	5.658	5.717
Ca	0.810	0.775	0.080	0.005	0.002	0.002	0.003	0.002	0.001	0.001	0.002	0.002	0.006
Na	0.034	0.000	0.000	0.000	0.000	0.000	0.000	0.000	0.000	0.000	0.000	0.001	0.000
K	0.007	0.002	0.001	0.000	0.005	0.002	0.003	0.004	0.000	0.003	0.004	0.000	0.002
Total	4.046	4.015	4.036	2.989	10.014	10.062	10.098	10.080	10.027	10.050	10.006	9.988	9.991
					Calculated Formulae (Fe+Mg+Ca = 100%)								
Fe	19.5	9.0	14.5	12.5	2.4	2.9	5.5	5.5	3.3	2.7	4.1	4.3	2.9
Mg	38.3	51.6	81.5	87.5	17.6	97.1	94.5	94.5	96.7	97.3	95.9	95.7	97.1
Ca	42.2	39.4	4.0	-	-	-	-	-	-	-	-	-	-

Notes.

n Number of points analysed.
* Total iron as FeO.
1. Clinopyroxene from basal zone, W83-48.
2. Clinopyroxene, W83-120.
3. Enstatite, W83-120.
4. Olivine, from the olivine cumulate, W83-78.
5. Lizardite 1T mesh rim after olivine.
6. Lizardite 1T mesh centre after olivine.
7. Lizardite 1T mesh rim after olivine.
8. Lizardite 1T mesh centre after olivine.
9. Lizardite 1T hourglass after olivine from olivine cumulate, W83-94b.
10. Lizardite 1T bastite.
11. Lizardite 1T bastite.
12. Chrysotile $2M_{cl}$ asbestos, cross-fibre vein from olivine cumulate, W83-192.
13. Antigorite vein.

2,3,5,6 and 10 all from a skeletal patch in the olivine cumulate, W83-120.
7,8,11 and 13 all from the olivine cumulate, W83-95a.

TABLE 2. ANHYDROUS BULK ROCK COMPOSITION OF THE MUNRO-BEATTY KOMATIITE

	1	2	3	4	5	6	7	8	9	10
SiO_2	45.12	42.04	42.81	40.73	41.48	44.09	42.60	51.31	51.83	47.82
TiO_2	0.32	0.15	0.31	0.15	0.13	0.11	0.13	0.31	0.85	0.43
Al_2O_3	6.11	3.28	5.46	2.92	2.88	2.61	2.68	4.21	14.43	16.41
Cr_2O_3	0.40	1.29	0.84	2.17	2.07	1.46	0.75	0.54	0.01	0.11
Fe_2O_3*	11.68	10.76	11.17	12.10	9.42	7.55	10.58	11.39	13.76	8.65
MnO	0.16	0.17	0.20	0.18	0.16	0.08	0.13	0.24	0.02	0.16
MgO	31.53	41.23	29.59	41.94	42.40	45.22	42.97	19.75	6.19	10.61
CaO	4.30	0.32	8.50	0.00	0.00	0.00	0.00	12.58	12.35	14.09
Na_2O	0.32	0.08	0.42	0.68	0.58	0.20	0.00	0.44	0.32	2.23
K_2O	0.05	0.01	0.04	0.04	0.05	0.02	0.01	0.05	0.51	0.21
P_2O_5	0.02	0.01	0.02	0.01	0.01	0.00	0.00	0.02	0.07	0.02
Total	100.01	99.36	99.36	100.90	99.18	101.34	99.85	100.84	100.53	100.74
L.O.I.**	9.1	11.67	7.65	11.60	11.87	12.53	11.96	3.40	2.80	2.92

* Total iron as Fe_2O_3
** Loss on ignition to 1000°C
1. Basal zone, W82-171
2. Olivine cumulate, W82-176
3. Skeletal patch in olivine cumulate, W83-120
4,5,6. Olivine cumulate, chrysotile-asbestos ore zone, W83-132, W83-185, W83-113
7. Olivine cumulate, W82-179
8. Clinopyroxene cumulate, W83-175
9,10. Gabbro layer, W83-177,W83-247

gate cumulate crystals, strongly zoned elongate coarse crystals or elongate fine crystals ($Wo_{42}En_{38}Fs_{20}$, Table 1). Cumulate olivine, now altered to serpentine, may be present or absent at the contact but it increases in abundance rapidly and the basal zone grades into the olivine cumulate zone (Figure 2). Glass, now altered to chlorite, occurs in interstitial zones in most samples, and varying amounts of sulphides, mainly pyrrhotite (Grubb 1962), produce a net texture in some parts of the contact. These zones have been trenched by Johns-Manville for bulk sampling of the sulphides (Figure 1). The altered nature of the contact makes it difficult to find a suitable sample for analysis. A sample part way up the basal zone shows the effect of increasing olivine content (Table 2).

The olivine cumulate layer is 155 to 160 m thick in the B pit area (Figure 1). Serpentinization has been intense (see below) and few relict primary minerals remain unaltered. However, in almost all cases serpentinization has produced excellent pseudomorphs so that most of the primary minerals and primary features can be recognized. Cumulate olivine dominated the mineralogy (Figure 2) with lesser pyroxene and glass, minor chromite and traces of biotite and hornblende. Olivine occurred as subhedral to euhedral, equant or slightly elongate grains, and has been completely altered to lizardite 1T mesh or hourglass textures (Wicks *et al.* 1977) and minor secondary magnetite. Rare relict olivine grains (Fo_{87}, Table 1) are occasionally found in some mesh centres.

Pyroxene occurs as anhedral grains interstitial to the olivine. Almost all the pyroxene has been altered to lizardite 1T bastite. The nature of the bastites (Wicks and Whittaker 1977) suggest that the original pyroxene was a clinopyroxene, presumably similar to augites in other komatiites (Arndt 1977; Barnes *et al.* 1983) but minor orthopyroxene commonly found in other flows would go unrecognized because of the advanced serpentinization in the Munro-Beatty komatiite. Primary clinopyroxene ($Wo_{39}En_{37}Fs_{24}$, Table 1) and enstatite ($Wo_4En_{81}Fs_{15}$) are preserved in some patches of skeletal textures and glass, which are similar to those described by Barnes *et al.* (1983) and are irregularly distributed within the lower part of the olivine cumulate layer.

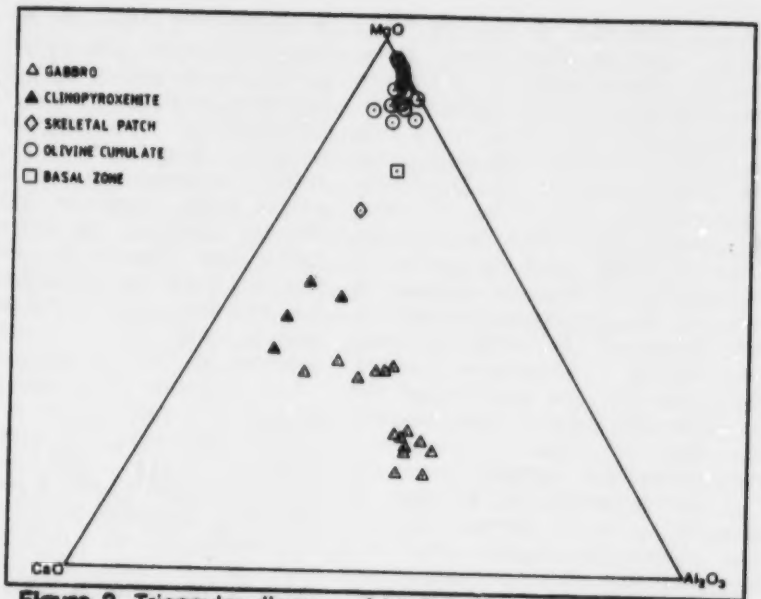

Figure 3. Triangular diagram of MgO-CaO-Al_2O_3 variation in the Munro-Beatty komatiite.

Glass occurred interstitially to the olivine grains particularly in the lower half of the olivine cumulate layer (Figure 2) but has recrystallized completely to fine-grained chlorite with occasional accessory tremolite.

The pyroxene cumulate layer varies between 2 and 6 m in thickness in the B pit area (Figure 1). The lower contact with the underlying olivine cumulate is sharp and is marked by the sudden absence of cumulate olivine. The upper contact is gradational with the overlying gabbro. This layer is dominated by cumulate euhedral clinopyroxene but also may or may not contain minor devitrified glass, hornblende, plagioclase (Figure 2) and possibly minor orthopyroxene. Alteration to fine-grained chlorite, talc, amphibole and epidote varies from moderate to very intense.

The gabbro layer is up to 50 m thick in the B pit area (Figure 2). It is composed mainly of slightly elongate laths of clinopyroxene and plagioclase with interstitial quartz and glass, now altered to chlorite, minor hornblende and, in places, skeletal sphene. Alteration of the plagioclase to very fine-grained mass of epidote and opaque material is abundant. The grain-size of the gabbro varies from medium to coarse, but with no distinct pattern. Plagioclase tends to be more abundant towards the bottom of the layer and clinopyroxene is more abundant towards the top. The clinopyroxene often has elongate habit, particularly towards the top of the layer but also in irregular zones lower down in the layer. In extreme cases the length to width ratio reaches 20 to 1. These crystals are gently bent.

The unit that caps the sequence, the top layer, is approximately 2 m thick and it is not well understood at this time. Limited exposure of the top layer occurs both in the B pit area and in the area east of the Munro mine, but it is frequently obscured by the intrusion of a later gabbro or by shearing. In the eastern exposure the Munro-Beatty komatiite is overlain by a basaltic komatiite flow with a rubbley brecciated base. It was difficult to determine the position of the top of the Munro-Beatty komatiite in the field and whether or not it is brecciated, without detailed petrographic work. In the B pit area brecciation was not observed during the 1983 mapping but subsequent petrographic studies revealed what appears to be a fine scale brecciation. The exact nature of the top layer is critical in determining whether or not the Munro-Beatty komatiite is sill or a flow. The petrographic and chemical studies carried out after the 1983 mapping will provide the basis for solving this problem during the 1984 field season.

The results of major element analyses by X-ray fluorescence analysis of selected samples from the major layers of the komatiite are given in Table 2. The komatiitic nature and the similarity of this suite of rocks to Fred's flow described by Arndt (1977), is illustrated by Figure 3. The olivine cumulate layer in the Munro-Beatty komatiite is thicker and was richer in olivine than Fred's flow and thus plots at higher MgO values (Figure 3). The intense serpentinization associated with the chrysotile asbestos development in the Munro-Beatty komatiite has removed most of the calcium from the ultra-

mafic rocks so that most of the olivine cumulate analyses plot on the MgO-Al_2O_3 join at zero CaO (Figure 3). This migration of calcium has produced the rodingites in the olivine cumulate layer described earlier in this study (Wicks *et al.* 1983). The sample from the basal zone plots at a fairly MgO-rich part of the trend. This sample is approximately 1 m above the contact and contained some cumulate olivine grains. Thus it does not represent the initial liquid but is an intermediate composition between the initial liquid and the olivine cumulate (Figure 3).

The analyses of samples from the pyroxene cumulate layer plot to the CaO-rich side of the general trend of analysis as was found by Arndt (1977) for Fred's flow. Similarly, the gabbro analyses plot in the same position as the gabbros from Fred's flow.

The plot of MgO vs SiO_2, as well as other related plots, is often used to illustrate whether or not magnesium and silicon have migrated during alteration (Beswick 1982; Barnes *et al.* 1983). Often analyses plot along a trend suggesting olivine fractionation and minor or no migration of elements. The plot of many of the Munro-Beatty analyses in Figure 4, lie along a crude olivine fractionation trend. However, the analyses of the olivine cumulate layer, particularly the most intensely serpentinized samples from the chrysotile-asbestos ore zone, lie on a trend normal to the olivine fractionation trend and aligned with the stoichiometric serpentine composition. This suggests that serpentinization has produced some migration.

The olivine cumulate layer is highly serpentinized and as a result behaves very differently under stress than the much more competent pyroxene cumulate layer, gabbro layer and enclosing volcanic rocks. The prominent widely-spaced north-trending faults that are readily recognized in the competent rocks cannot be traced directly through the serpentinite (see Figure 1). East-trending shearing or faulting is not well developed in the competent rocks but is a major feature in the serpentinite. Close examination of the serpentinite reveals that it is intensely shattered into steeply dipping north- and east-trending fractures and a set of flat lying fractures. Minor sets of fractures in other directions also occur. The chrysotile-asbestos ore zone is bounded by two intense east-trending shear zones, one approximately 40 m above the base of the flow and one approximately 35 m below the top of the serpen-

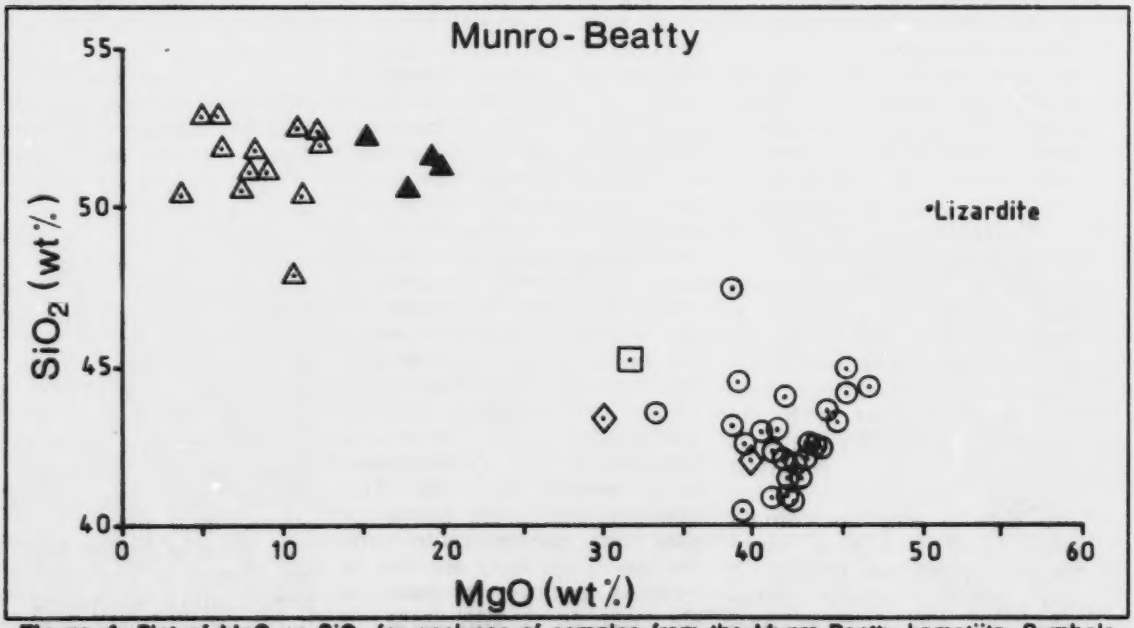

Figure 4. Plot of MgO vs SiO_2 for analyses of samples from the Munro-Beatty komatiite. Symbols are the same as on Figure 3.

tinized olivine cumulate layer (Figure 1). Within these two shear zones in a zone 90 m wide the shattering of the serpentinite is very intense and closely spaced. Cross-fibre chrysotile-asbestos veins with or without associated non-fibrous picrolite occupy the fractures. Many of the fracture surfaces are coated with non-fibrous, slip-picrolite and occasionally slip-chrysotile asbestos indicating movement along the fractures.

Cross-fibre chrysotile-asbestos is the main ore, occurring as a stockwork in most cases. The horizontal set of veins with fibre up to 2.5 cm long is the principal ore, the north-trending set of veins is secondary, and the east-trending set is tertiary. The fibres in the latter two are 0.6 cm or less in length. Locally the east-trending veins dominate to produce ribbon fibre zones.

Serpentinization outside the ore zone is characterized by the alteration of the olivine to lizardite 1T mesh textures and pyroxene to lizardite 1T bastites. The mesh texture is composed of lizardite 1T as α-serpentine in the mesh rims and isotropic serpentine in the mesh centres. The bastites are usually composed of lizardite 1T as γ-serpentine parallel to the original pyroxene cleavage but some in an α-serpentine orientation also occurs. The assemblage represents a typical retrograde type 3 serpentinization (Wicks and Whittaker 1977).

Lizardite 1T is also the dominant polytype within the chrysotile-asbestos ore zone, occurring as lizardite 1T mesh rims with lizardite 1T hourglass mesh centres or as lizardite 1T hourglass texture. Chrysotile $2M_{cl}$ occurs as hourglass textures and serrate veins that have replaced the lizardite 1T mesh rims and mesh centres. In one chrysotile hourglass texture minor chrysotile $20r_{cl}$ occurs in association with chrysotile $2M_{cl}$, but with this one exception chrysotile $2M_{cl}$ is the dominant polytype. Antigorite occurs less frequently than chrysotile, either as serrate veins after lizardite 1T mesh rims or as randomly oriented blades replacing lizardite 1T mesh centres. The extensive development of lizardite 1T hourglass and chrysotile $2M_{cl}$ hourglass and serrate veins indicates a prograde serpentinization which would be classified as type 5 by Wicks and Whittaker (1977). The presence of antigorite indicates a fairly high grade of prograde serpentinization of type 7 although the limited development of antigorite indicates a limited period of high grade metamorphism.

A minor amount of antigorite also occurs in association with the talc-carbonate alteration along the basal contact in the B pit area. To the east at the east end of the A pit talc-carbonate alteration is extensively developed in a keel-shaped zone around and replacing the main A chrysotile asbestos ore body (Hendry and Conn 1959).

The cross-fibre chrysotile-asbestos veins are the dominant type of vein in the ore zone. Some of them have been slightly deformed and may be cut by or developed in association with a non-fibrous picrolite. These are abundant fractures coated with thin veneers of slip picrolite that may also contain fine cross-fibre or minor slip-fibre chrysotile-asbestos. Chrysotile $2M_{cl}$ is the dominant polytype in the asbestos veins. Chrysotile $20r_{cl}$ occurs in minor amounts in some veins and very minor parachrysotile was detected in two locations.

Outside the ore zone chrysotile-asbestos veins are rare, fracturing is less intense, and non-fibrous picrolite is dominant. Picrolite is commonly composed of lizardite 1T, or a mixture of lizardite 1T and chrysotile $2M_{cl}$. Antigorite rarely has formed picrolite veins.

The microprobe analyses in Table 1 are fairly typical serpentine mineral analyses. The composition of the lizardite 1T mesh textures varies mainly in iron content. In some cases there is a small difference between mesh rim and centre, in others there is no difference. The lizardite 1T hourglass has a very uniform composition throughout a thin section. An unusual feature of this lizardite formed after olivine is its variable but unusually high Al-content of up to 1.44 weight percent Al_2O_3.

The lizardite 1T bastites generally have slightly higher Al-contents than the lizardite after olivine, a reflection of the high Al-content of the host pyroxene. In general the serpentine in veins whether chrysotile-asbestos, antigorite or lizardite has lower Fe content than the enclosing host serpentines, although all have significant Al-contents (Table 1).

GARRISON KOMATIITE

The Garrison chrysotile-asbestos deposit occurs in the northern part of Garrison Township 23 km east of the Munro Mine (Satterly 1949; Hewitt and Satterly 1953, MacRae 1969). The major serpentinite is approximately 800

m thick at its widest point and contains 5 fibre zones outlined by Canadian Johns-Manville: the north fibre, van fibre and open pit fibre zones towards the north contact, and the Bird fibre and Bird west extension fibre zones along the southern contact.

Gabbro and pyroxenite are exposed in scattered outcrops in an east-trending zone north of the exploration shaft collar. The serpentinite is only exposed around the small open pit and thus the stockpiles of rock brought up from underground fibre zones form the most important source of samples.

The ultramafic rock at the Garrison asbestos deposit is intensely serpentinized and relict primary minerals other than chromite are extremely rare. However, the primary textures are well preserved in places and strong textural similarities to the Munro-Beatty komatiite are evident. In the fibre zones sampled underground, the compositions varied from 84 to 91% olivine, 3 to 12% pyroxene, 1 to 10% glass and 2 to 3% chromite. The surface showing in the open pit, was composed of 67% olivine, 18% pyroxene, 12% glass, and 3% chromite.

Two stages of serpentinization are evident. The first stage is characterized by pseudomorphic lizardite 1T mesh textures after olivine and bastites after pyroxene, and is a retrograde serpentinization (Wicks and Whittaker 1977). The second stage is characterized by chrysotile ± brucite + magnetite nonpseudomorphic textures, and is a prograde event that has recrystallized the earlier retrograde textures and completely serpentinized any relict primary minerals. This prograde serpentinization is more widespread and extensive than at the Munro-Beatty komatiite and is mineralogically more varied. In the fibre zones near the northern contact prograde chrysotile is moderately abundant but brucite is absent or present in minor amounts up to 6%. In the southern fibre zones the prograde event was more intense with abundant chrysotile and brucite in amounts from 4 to 25%. Carbonate with some talc alteration is well developed along the southern contact limiting the size of these fibre zones.

DISCUSSION

At this stage of the study extensive discussion is premature as the laboratory work in progress needs to be completed, and the field work finished before comprehensive interpretations can be made. However, even at this stage certain points can be noted.

The Munro-Beatty komatiite does display some similarities to Fred's flow in the northern part of Munro Township as well as some differences. The large scale layered structure is similar as is the general chemical composition although the olivine cumulate layer at the Munro-Beatty komatiite appears to have been slightly more olivine-rich. Some elongate clinopyroxene crystals occur in the gabbro layer of the Munro-Beatty komatiite and some skeletal clinopyroxenes occur in the basal zone and in skeletal patches within the olivine cumulate, however, the olivine and clinopyroxene stringbeef spinifex of Fred's flow are absent.

The intensive serpentinization that has accompanied the development of the chrysotile-asbestos ore has produced some significant changes in the $MgO:SiO_2$ ratio of the olivine cumulate. Thus in cases of intense serpentinization the $MgO:SiO_2$ ratio of the rock appears to be controlled by the serpentine composition and not the olivine composition of the original rock (see Figure 4). In less intensely serpentinized olivine cumulate this relationship will not be as well developed. The loss of calcium from the intensely serpentinized olivine cumulate is virtually complete and leads to the development of rodingites reported on earlier (Wicks *et al.* 1983). It also indicates that the use of the $CaO:Al_2O_3$ ratio to define komatiites must be restricted to unserpentinized or only very mildly serpentinized ultramafic rocks. The presence of up to 1.4 weight percent Al_2O_3 within lizardite 1T pseudomorphs after olivine, at least a ten-fold increase over the primary olivine, indicates that, at least on a thin section scale, aluminum has a significant mobility during serpentinization.

The importance of shearing and faulting as an essential step in the formation of chrysotile-asbestos veins is demonstrated by the detailed mapping. The chrysotile-asbestos ore body is limited to the north and to the south by strong east-trending shear zones. The serpentinite between the two shear zones is intensely shattered, essentially along three sets of fractures: a horizontal set, a north-trending vertical set and an east-trending vertical set. These are the host fractures to the principal cross-fibre chrysotile-asbestos veins. In contrast to the response of the incompetent serpentinite, the

competent volcanic rocks and the clinopyroxenite and gabbro layers that enclose the serpentinite and were subjected to the same stress field, failed in a different fashion. In these rocks well-spaced, north-trending vertical faults dominate and only minor east-trending fractures and shears occur.

Studies on the Garrison chrysotile-asbestos deposit indicate several similarities to the Munro-Beatty komatiite. However, the prograde serpentinization has been more intense at the Garrison deposit and in the fibre zones along the south contact brucite is quite abundant. This indicates a significant difference in the conditions during prograde serpentinization compared to conditions at the Munro-Beatty deposit.

As a result of the present study on Ontario chrysotile-asbestos deposits, some well characterized samples have been produced. This has presented the opportunity of other associated studies not anticipated in the original research plan. A preliminary study of the distribution of boron in serpentinites and serpentine minerals is now under way (Higgins *et al.* 1984).

ACKNOWLEDGMENTS

We are very grateful to F.J. Eveleigh, Johns-Manville Canada Incorporated, Matheson, Ontario for his assistance while we were working at the Munro Mine and the Garrison chrysotile-asbestos deposit, and to W.C. Streib, Manville Service Corporation, Denver, Colorado for his support of the project. Our thanks is extended to R. Mason for draughting the figures and Mary Anne Chalmers for typing the manuscript.

REFERENCES

Arndt, N.T.
1975: Ultramafic Rocks of Munro Township and their Volcanic Setting; Ph.D. Thesis, University of Toronto, Toronto, Canada.
1977: Thick, Layered Peridotite-Gabbro Lava Flows in Munro Township, Ontario; Canadian Journal of Earth Sciences, Volume 14, p.2620-2637.

Arndt, N.T., Naldrett, A.M., and Pyke, D.R.
1977: Komatiitic and Iron-rich Tholeiitic Lavas of Munro Township, Northeast Ontario; Journal of Petrology, Volume 18, p.319-364.

Barnes, S.J., Gorton, M.P., and Naldrett, A.J.
1983: A Comparative Study of Olivine and Clinopyroxene Spinifex Flows from Alexo, Abitibi Greenstone Belt, Ontario, Canada; Contributions to Mineralogy and Petrology, Volume 83, p.293-308.

Beswick, A.E.
1982: Some Geochemical Aspects of Alteration and Genetic Relations in Komatiitic Suites; p.283-308, *in* Komatiites, edited by N.T. Arndt and E.G. Nisbet, George Allen and Unwin, London, 526p.

Fleet, M.E., and MacRae, N.D.
1975: A Spinifex Rock from Munro Township, Ontario; Canadian Journal of Earth Sciences, Volume 12, p.928-939.

Grubb, P.L.C.
1962: Serpentinization and Chrysotile Formation in the Matheson Ultrabasic Belt, Northern Ontario; Economic Geology, Volume 57, p.1228-1246.

Hendry, N.W.
1951: Chrysotile Asbestos in Munro and Beatty Townships, Ontario; Canadian Institute of Mining and Metallurgy, Transactions, Volume 54, p.28-35.

Hendry, N.W., and Conn, H.K.
1957: The Ontario Asbestos Deposit of Canadian Johns-Manville Company Limited; *in* Geology of Canadian Industrial Mineral Deposits, 6th Commonwealth Mining and Metallurgical Congress, p.36-45.

Hewitt, D.F., and Satterly, J.
1953: Asbestos in Ontario; Ontario Department of Mines, Industrial Mineral Circular 1, revised edition.

Higgins, M.D., Ozoray, J., and Wicks, F.J.
1984: Boron in Serpentinite and Serpentine Minerals; Abstract, Geological Association of Canada - Mineralogical Association of Canada, Joint Annual Meeting Program with Abstracts 9, p.73.

Jensen, L.S., and Pyke, D.R.
1982: Komatiites in the Ontario Portion of the Abitibi Belt; *in* Komatiites, edited by N.T. Arndt and E.G. Nisbet, George Allen and Unwin, London, 526p.

Kretschmar, U., and Kretschmar, D.
1982: Talc, Magnesite and Asbestos Deposits in the Kirkland Lake - Timmins Area; Ontario Geological Survey, Open File Report 5391.

Lachance, G.R., and Traill, R.J.
1966: A Practical Solution to the Matrix Problem in X-ray Analysis; Canadian Spectroscopy, Volume 11, p.43-47.

MacRae, N.D.
1969: Ultramafic Intrusions of the Abitibi Area, Ontario; Canadian Journal of Earth Sciences, Volume 6, p.281-301.

Pyke, D.R., Naldrett, A.J., and Eckstrand, O.R.
1973: Archean Ultramafic Flows in Munro Township, Ontario; Geological Society of America, Bulletin, Volume 84, p.955-978.

Satterly, J.
1949: Geology of Garrison Township; Ontario Department of Mines, Annual Report, Volume 58, Part 4.
1952: Geology of Munro Township; Ontario Department of Mines, Annual Report, Volume 60, Part 8.

Satterly, J., and Armstrong, H.S.
1949: Geology of Beatty Township; Ontario Department of Mines, Annual Report, Volume 56, Part 7.

Vos, M.A.
1971: Asbestos in Ontario; Ontario Department of Mines and Northern Affairs, Industrial Minerals Report 36.

Wicks, F.J., and Plant, A.G.
1983: The Accuracy and Precision of Routine Energy-Dispersive Electron Microprobe Analysis of Serpentine; X-ray Spectrometry, Volume 12, p.59-66.

Wicks, F.J., Schandl, E.S., Ozoray, J., and Wan Pu

1983: Mineralogy and Geochemistry of the Chrysotile Asbestos Deposits of Ontario; Grant 138 in Geoscience Research Grant Program, Summary of Research 1982-83, edited by E.G. Pye, Ontario Geological Survey Miscellaneous Paper 113, p.177-182.

Wicks, F.J., and Whittaker, E.J.W.
1977: Serpentine Textures and Serpentinization; Canadian Mineralogist, Volume 15, p.459-488.

Wicks, F.J., Whittaker, E.J.W., and Zussman, J.
1977: An Idealized Model for Serpentine Textures After Olivine; Canadian Mineralogist, Volume 15, p.446-458.

Wicks, F.J., and Zussman, J.
1975: Microbeam X-ray Diffraction Patterns of the Serpentine Minerals; Canadian Mineralogist, Volume 13, p.244-258.

Grant 140 Direct Trace Elemental Analysis of Solid Samples by Techniques of Atomic Spectrometry

Jon C. Van Loon, R. Kanipayor, C.M. Nimjee and R.R. Barefoot

Department of Geology, University of Toronto

ABSTRACT

A method is being developed for the injection of solids into flames and plasmas for direct trace element analysis by the techniques of atomic emission, absorption and fluorescence spectrometry. A graphite furnace is used to produce an aerosol (vapour) of the solid by ramping the temperature up to a maximum of 2800°C. The aerosol thus produced is carried into the flame or plasma atomizer in a stream of argon. Experimental considerations such as carrier gas flow rate, thermal program and prevolatilization treatments have been investigated. A study has been made to optimize the interface between the furnace and the plasma. Background absorption and matrix dependency problems have been examined. Calibration techniques have been investigated. Analytical procedures have been developed for some relatively straightforward samples.

INTRODUCTION

In trace element analysis, minimal sample handling and chemical pretreatment are very important in order to avoid contamination and/or losses. A variety of strategies has been proposed for the direct analysis of solids by means of atomic absorption, atomic fluorescence and atomic emission spectroscopy. With the exception of arc/spark optical emission spectroscopy, no approach to the direct determination of trace elements in solid samples has received widespread acceptance.

Solids have been placed directly in flames for flame emission analysis. Spark excitation is the most popular industrial method for direct trace analysis of solids. This method is applicable with good results only to conducting samples. Arc excitation, although applicable to a wide range of sample compositions, yields results of relatively poor repeatability and accuracy. Minor variations in sample composition cause variation in the excitation conditions, making a close matching of samples and standards necessary.

Furnace atomic absorption spectrometry has been used for the direct trace element analysis of solids. A number of problems exist with this approach including:

1. Generally sample size must be less than 1 mg;
2. High levels of nonspecific background signal are encountered;
3. Skeletal remains of the sample can block the optical beam;
4. Problems with standardization occur.

In the method described here, a commercially available graphite furnace is used to generate an aerosol (vapour) of a solid sample which is then swept in a stream of inert gas into a flame or plasma atomizer. Of the available atomizers, the inductively coupled plasma shows greatest potential for direct solids analysis.

EXPERIMENTAL

EQUIPMENT

Emission System

An Applied Research Laboratories 34000 Quantometer equipped with an ICP source and a PDP 11 computer was used. Operating conditions for the ICP spectrometer are given in Table 1.

The output from the spectrometer was connected to a strip chart recorder. The channel to be monitored was designated by means of a computer command. Attenuations of 0-0.1 or 0-1 volts full scale were selected according to the quantity of metal in the sample or standard.

A Perkin-Elmer HGA 2100 graphite furnace was mounted beneath the plasma torch in place of the nebulizer. The furnace was connected to the torch by means of a J-shaped quartz tube secured in a gas tight graphite bushing at one end of the furnace. Gas flows to the plasma torch and through the furnace to the torch were metered and controlled by means of high precision valves. A stopcock and a T connection in the quartz tube allowed the gas flow through the furnace to be interrupted while the furnace was opened. The flow of argon (carrier gas) through the bypass line maintained the plasma. A pressure reduction system completed the interface. Figure 1 is a photograph of the equipment.

Atomic Absorption System

A Perkin-Elmer 603 atomic absorption spectrometer equipped with a deuterium arc for background correction, a three-slot

burner head, and a Perkin-Elmer model 56 recorder were employed. An electrothermal atomizer (Perkin-Elmer model HGA 2000) was used for dry sample aerosol production. Both end windows of the furnace were removed. At one end of the furnace an adaptor for the gas inlet tube was inserted and a continuous stream of argon was passed through the furnace. At the other end of the furnace a graphite support for the quartz T-tube was inserted. The support was precisely machined to fit within the graphite cone and around the quartz T-tube. A schematic of this modification for the HGA 2000 is shown in Figure 2. The T-tube used was constructed of 2.0 mm thick quartz. The bottom of the "T" was 20 cm long (OD - 8 mm) and the top of the "T" was 8 cm long (OD - 16 mm). A slot (8 x 2 mm) was made at the bottom of the top of the "T" for the flame gases to enter.

The volatilized sample from the furnace was swept into the quartz tube by the carrier gas. The quartz tube was positioned in such a way that the optical beam passed through the top of the "T". This section of the quartz tube was heated by an air-acetylene flame supported on a three-slot burner head. A portion of the flame gases enters the quartz T-tube through the slot at the bottom. The active chemical environment in the tube improves dissociation of the analyte and matrix species during the atomization step. The atomic absorption measurements were then made.

Graphite furnace tubes and platforms were tantalum coated. New tubes and platforms were conditioned by repeating the heating cycle a sufficient number of times to reduce the "empty furnace" response for the particular element to a very low value.

REAGENTS

Stock standard solutions of metals were prepared from spec pure material dissolved in minimum volumes of "Instra-Analyzed" nitric acid (J.T. Baker Company). Very dilute working solutions were prepared as required.

Dilute hydrofluoric acid was prepared from equal volumes of reagent grade 48% acid and water.

PROCEDURES

Atomic Absorption

Geological solid samples were contained in 'L'vov Type' graphite platforms (L'vov 1976) (which can handle up to 50 mg of samples) and placed in the furnace. The samples were weighed together with the platforms and inserted into the graphite tube. Standard solutions (when used) were injected directly into the tube through the sample port or on to the platform placed inside the tube. In all cases the drying temperature was 100°C. The D_2 arc background corrector used in this work could correct background absorbances up to about 100 µL of a saturated $(NH_4)_2SO_4$ solution on to the samples prior to drying. Most results were obtained by measuring the height of the analyte peak absorbance on the strip chart recorder.

Atomic Emission

A volume of 30 µL of 1:1 hydrofluoric acid was pipeted onto the sample on the platform before the platform was placed in the furnace. The J tube was wrapped with heating tape, and sufficient heat

TABLE 1. OPERATING CONDITIONS FOR ICP SPECTROMETER.

Incident power	1300 W
Reflected power	<10 W
Coolant gas pressure	50 psi
Plasma gas pressure	35 psi
Carrier gas flow rate	0.3 litres min^{-1}
Sample sweep gas flow rate	0.4 litres min^{-1}

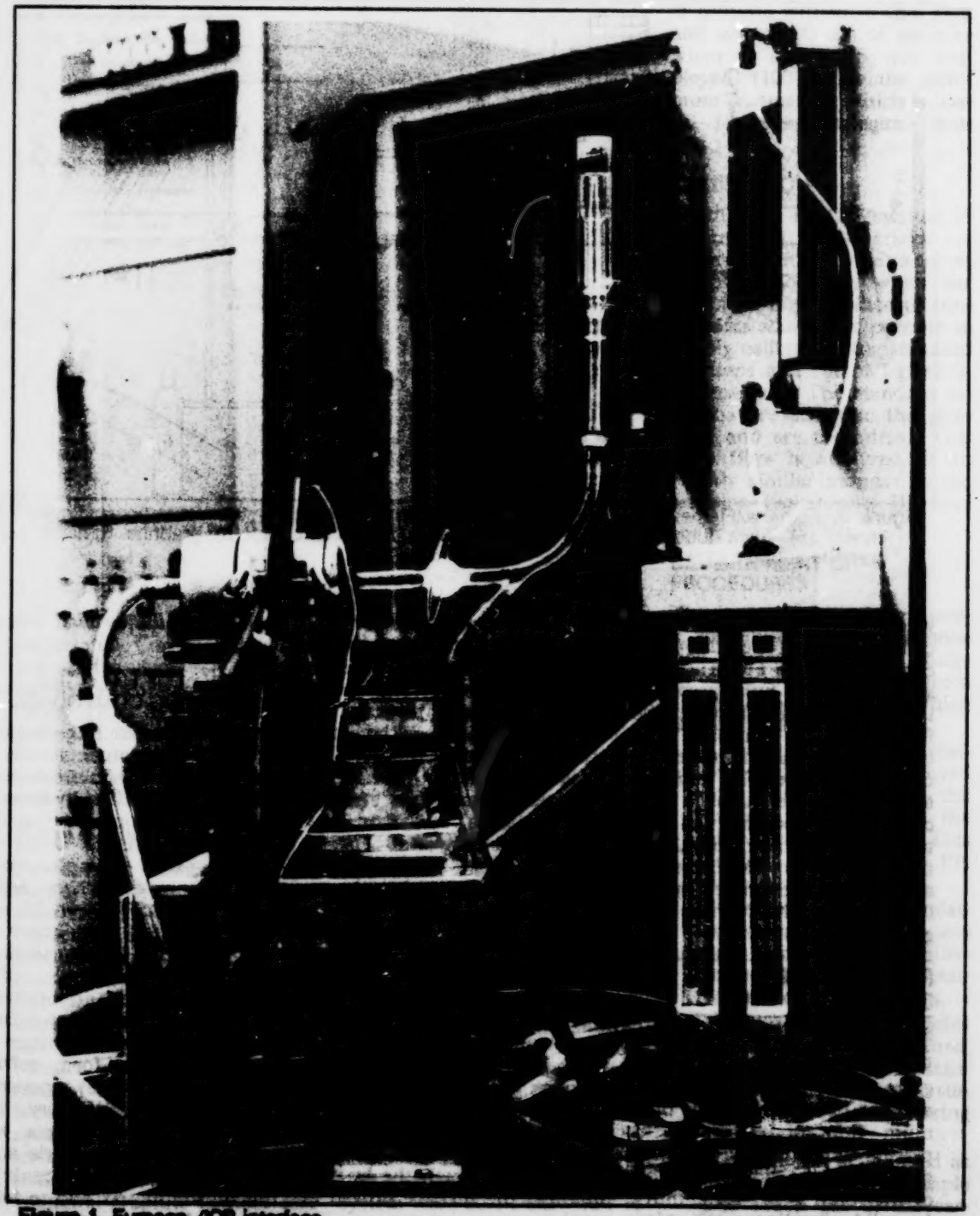

Figure 1. Furnace /ICP interface.

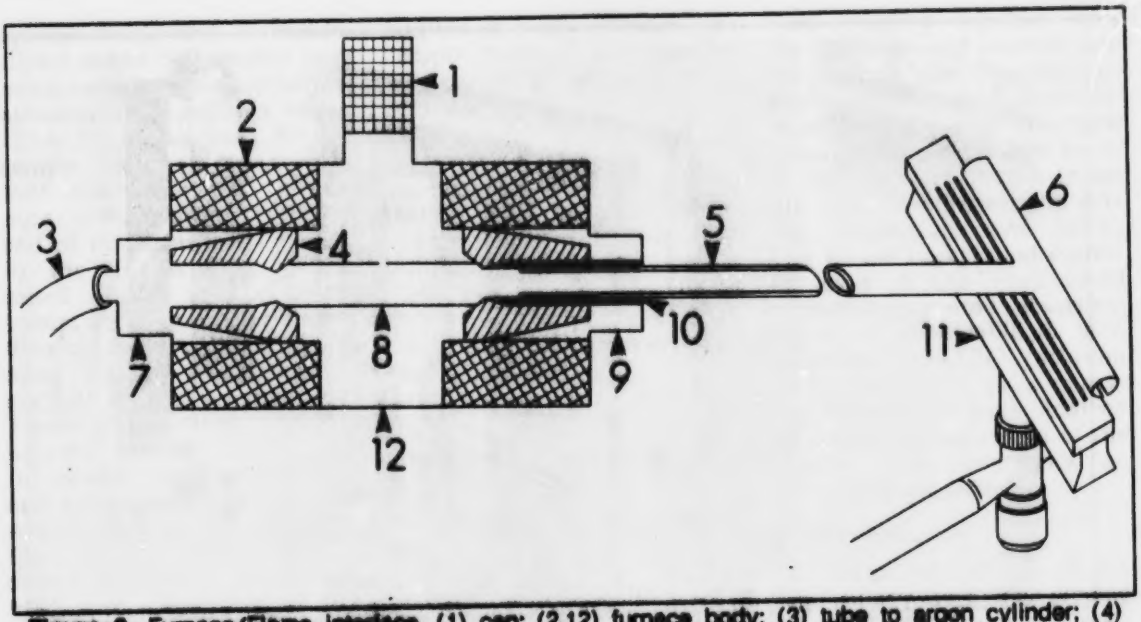

Figure 2. Furnace/Flame interface. (1) cap; (2,12) furnace body; (3) tube to argon cylinder; (4) cones; (5) silica tube; (6) silica tube atomizer; (7,9) end caps; (8) graphite furnace; (10) graphite support; (11) burnerhead.

was applied to prevent any condensation of liquid. Argon containing 0.5% Freon 23 was substituted for pure argon as the gas flowing through the furnace. The platform was centred in the furnace by means of a specially designed tool. After the furnace was closed, the stopcock in the transfer line was opened, and the argon flow was increased slowly to the designated rate of 0.4 L min^{-1}. The furnace program was initiated.

RESULTS AND DISCUSSION

FURNACE ICP INTERFACE

Figure 3 is a schematic diagram of the optimised furnace and gas flow system. The optimum flow of argon to the plasma torch through the sample line i.e. the central channel of the torch is 0.7-1.0 L min^{-1}. In solid sampling work, plasma stability must be maintained while the furnace is open to the atmosphere during loading. Argon plasmas are sensitive to the presence of oxygen, and they will be extinguished by surges of air or air/argon entering the torch. In order to maintain stability of the plasma, the argon flow is divided into two streams as shown in Figure 3. While the furnace is being loaded, the argon flow through the furnace is interrupted by closing the valve of flowmeter F_1. Stopcock T_1 is closed. Argon continues to flow to the plasma through the by-pass line. After the furnace has been closed, T_1 is opened, and the argon flow through the furnace is restored by opening the control valve F_1 slowly. As a result of an experimental program, the best flow rates through the by-pass line and the furnace proved to be 0.3 and 0.4 L min^{-1} respectively.

ADDITION OF HALOGEN CONTAINING COMPOUNDS

The volatilization of geologically important elements such as vanadium in electrothermal analyzers is difficult because of the formation of refractory oxides and carbides. Using vanadium as an example, recoveries improved when argon containing 0.5% Freon 23 was substituted for pure argon in the furnace. Other workers have reported that halocarbon/argon atmospheres in electrothermal atomizers have increased sensitivities of elements which form refractory oxides. Since recoveries were still unsatisfactory, the sample on the platform was treated with hydrofluoric acid. The objective was to break up the silicate matrix and to form volatile silicon fluoride.

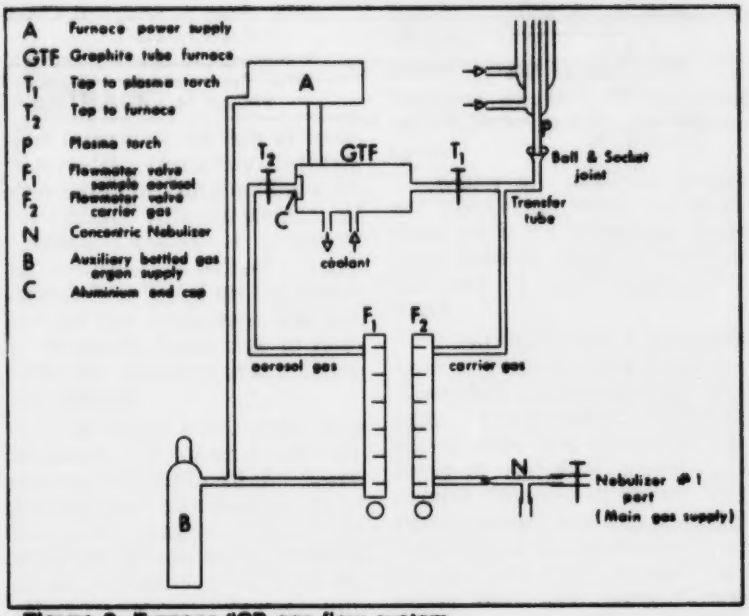

Figure 3. Furnace/ICP gas flow system.

The volume of acid was important. Concentrated acid reacted too vigorously with the sample. A volume of 30 μL of dilute (1:1) hydrofluoric acid and an atmosphere of 0.5% Freon 23 in argon were necessary to obtain the satisfactory recoveries of vanadium.

THERMAL PRE-TREATMENT

Non-specific absorption noted during the direct analysis of solid samples results from the molecular absorption of both inorganic and organic species produced from the sample matrix. Some of the most common interfering inorganic species in conventional graphite furnace atomic absorption are salts of the halides. The non-specific absorption from such species was found to be much lower in the proposed system than those reported for conventional graphite furnace and with Woodriff's (Nichols *et al.* 1978) isothermal furnace atomic absorption methods (about 3 and 2 orders of magnitude respectively). A similar study of organic species such as benzene, hexane and methanol showed that the non-specific absorption generated by the proposed method were 1 to 2 orders of magnitude lower than those reported for the Robinson graphite-T atomizer (Robinson and Walcott 1975).

The background absorption recorded with and without a char step for samples with a high organic content was obtained. The results showed that if no char step was used, by far the greater contributions to the non-specific background absorption were from the organic species (volatiles). The levels of non-specific absorption produced by the proposed system were sufficiently low to allow the use of about 10 mg of samples without a char step and about 100 mg of samples when a char step was employed. (100 mg is the minimum sample size which is useful for most geological samples.)

CALIBRATION

Much work is still essential in determining valid methods for calibration for a wide range of samples. However, when the sample is high in siliceous constituents it appears possible to simply calibrate using standard solutions and "blank" glass fibre material. The standard solutions are added to the glass fibre and are then dried. This glass fibre is analyzed in an exactly similar manner to the samples (using the HF and Freon treatments).

DEVELOPMENT OF PROCEDURES

The procedures used for atomic absorption and plasma emission spectrometry direct analysis of solid samples are given above. Important steps which should be noted are:

1. L'vov type graphite platforms should be employed to prevent fusion of the sample residue to the graphite tube walls. This greatly extends tube life time.
2. Tantalum coating of platforms and tubes is also very beneficial in improving signal shape and platform and tube life times.
3. When lower boiling point elements are determined, addition of $(NH_4)_2SO_4$ solution should be made to stabilize the element during the char step.
4. Hydrofluoric acid added as a μL droplet to the sample and Freon gas in the carrier gas stream are benefi-

cial when working with most elements.

The procedures are now being investigated on a wide range of sample types.

REFERENCES

L'vov, B.V.
1976: *Paper in* Talanta, Volume 23, p.109.

Nichols, J.A., Jones, R.D., and Woodriff, R.
1978: *Paper in* Analytical Chemistry, Volume 50, p.207.

Robinson, J.W., and Walcott, D.K.
1975: *Paper in* Anal. Chimica Acta, Volume 74, p.43.

Grant 145 Ontario Field Tests and Instrumentation of Cross-Hole Magnetometric Resistivity

B.B.H. Lo, R.N. Edwards, and S. Cheesman

Geophysics Laboratory, Department of Physics, University of Toronto

ABSTRACT

The cross-hole variant of magnetometric resistivity (MMR), developed in conjunction with Newmont Exploration of Canada Limited, is a simple inexpensive borehole technique. It is based on the detection of low frequency, low level magnetic fields due to non-inductive currents injected into the ground.

The down-hole probe is a sensitive coil tuned to the operating frequency of 7.5 hertz. Twenty-four thousand turns of No. 28 magnet wire are wrapped in ten equal sections about a ferrite core with an effective magnetic permeability of 204. Cascaded tuned amplifier stages are used to amplify the received signal before its transmission up hole in a 1 km long, shielded, two conductor, Kevlar reinforced signal cable.

When all amplifier stages are used, the signal to noise ratio for a 0.1 nanotesla magnetic field signal at 7.5 hertz is 580 with a band width of 1 hertz.

Field data from a site near Ignace, Ontario, and from the Cavendish geophysical test site near Gooderham, Ontario, shows that the system is capable of detecting lateral conductive features at depth. The signal quality and repeatability is good and the anomalies seen in the data from Ignace correlate well with some Crone down-hole Pulse EM data collected in the same boreholes.

An integral equation technique using a bendable lamella (program MMRPlate) may be used for anomaly interpretation. The response from Cavendish can be modelled using a 100 by 20 m plate dipping at 45 degrees.

INTRODUCTION

In a previous paper (Edwards *et al.* 1983), a review of the theory and a case history from the southwestern United States using the cross-hole MMR method were presented.

The ideal cross-hole MMR method described by Edwards *et al.* (1983), is illustrated in Figure 1. A current bipole is set up in a vertical borehole to inject currents into the ground. A receiver probe measures the borehole magnetic component in a separate vertical borehole as a function of depth. Using symmetry arguments, the injected currents from the current poles in either a half-space or a layered earth, are independently axially symmetric about the injection point. From Ampere's Circuital Law, the magnetic field due to the injected currents is entirely horizontal. The magnetic field of the vertical current wire is also horizontal. In the presence of a conductor which channels or distorts current, a vertical magnetic field is produced. The magnitude and geometric form of this component may be interpreted to indicate the position and physical properties of the conductor. A more conductive body produces greater horizontal current channelling, resulting in a more enhanced anomaly.

When either the receiver probe or the transmitter bipole is non-vertical, a correction for the non-ideal geometry has to be made. The inclined wire

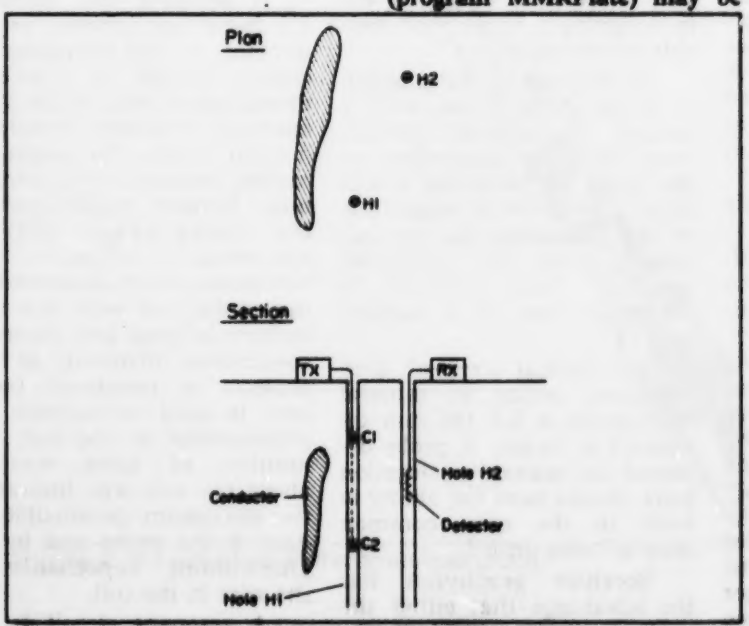

Figure 1. Geometry of the cross-hole MMR method.

connecting the current source and sink would, in this case, produce a vertical component of the magnetic field, which would masquerade as an 'anomaly'. Further, the magnetic field detected by the non-vertical probe does contain a component of the horizontal magnetic field.

Edwards *et al.* (1983) showed that an integral equation numerical routine (program MMRPlate) may be used for theoretical investigation of the form of MMR anomalies. The program uses a thin bendable lamella to model a thin conductor. The currents flowing in the sheet are represented by a distribution of current dipoles distributed into smaller elements which make up the sheet. Each small element can be assigned a different conductivity.

Numerical modelling results, presented by them, showed that conductive overburden reduces the surface horizontal electric field. A greater portion of the injected currents would be flowing in the overburden. The net result is to reduce the horizontal current flow and the anomaly caused by local conductors.

They also modelled the effects of using either a moving receiver or a moving transmitted current source. Studies presented show that the coupling between the local conductor and the receiver to be more important than the coupling between the conductor and the current bipole for anomaly strength. Either surface electrodes or down-hole electrodes with the probe being lowered down-hole would yield larger anomaly signals than surface measurements with a down-hole source.

At the time of the first publication (Edwards *et al.* 1983), field data from Ontario were not yet collected and the instrumentation presently being developed under the OGRF grant was not described. The present paper will consequently concentrate on the development of suitable, simple instrumentation for the method. In addition, field surveys conducted near Ignace, and at the Cavendish geophysical test range in Ontario are described.

The two papers form a set, with the first being concerned principally with theory and response computation.

SCALE OF THE PROBLEM

The down-hole sensor must meet certain sensitivity, size, signal cable and pressure design criteria to operate in a borehole. A study of the scale of the problem and the geometries involved is needed to aid in designing a sensor with suitable sensitivity.

If the scale of the problem is to be about 1 km, with 1 ampere of injected current, then magnetic anomalies on the order of picoteslas would arise. The order of magnitude of the anomalies can be calculated from the horizontal magnetic field ($100\,I/R$ in picoteslas) due to a current pole.

The typical sizes of deep boreholes drilled in mineral exploration is EX (36 mm diameter) or larger. A probe designed for mineral exploration work should have the ability to work in the most common sizes of holes drilled.

Borehole geophysics has the advantage that either the excitation source and/or the receiver probe is near the region of interest. The system must be able to operate to the typical depths to which deep boreholes are drilled.

A Kevlar reinforced, two conductor shielded cable is used to carry the received signal back up-hole. This cable is mounted on a manual winch system with a counter calibrated in tenths of a metre. One kilometre of cable is available for lowering the probe down hole.

INSTRUMENTATION

DESIGN CRITERIA AND SOLUTION

Design criteria of the down-hole probe are:

1. maximum diameter of 36 mm to permit its use in EX (36 mm) sized holes;
2. an operational depth in the order of 1 km in water filled holes;
3. ability to detect picotesla strength magnetic fields.

A sensitive coil tuned to 7.5 hertz was chosen as the detector. A high operating frequency results in a shorter measurement time while a low operating frequency avoids induction effects. The chosen operating frequency is a compromise. Further, modification of our existing surface MMR instrumentation is feasible. Magnetometers were considered for the probe, but were not used because of time and monetary constraints involved in the project. A powdered ferrite core is used to increase the permeability of the coil. The number of turns wrapped about the coil was limited by the maximum permissible radius of the probe and by the interwinding capacitance of the wire in the coil.

A resonant circuit is formed between the self capacitance and the inductance of the coil. To ensure stability

Figure 2. Pre-amplifiers in the down-hole probe.

and linear response, the coil must operate in the linear range below the resonant frequency. This is achieved by decreasing the interwinding capacitance to increase the resonant frequency.

The coil is wound in sections to reduce the interwinding capacitance. Twenty-four thousand turns of No. 28 magnet wire was wound in ten equal sections about a 101 cm long ferrite core. This produced a coil with an inductance of 52.2 henries and a capacitance of 0.125 microfarads.

SIGNAL AMPLIFICATION

Figure 2 shows the electronics which are built into the probe casing. The output is amplified in stages using active resonant filters in cascade to allow for the possibility of changes in gain and to minimize the settling time of a circuit with high quality factor, Q. The output of the first stage is resonated in series with capacitors of total capacitance of 8.63 microfarads. A simple feedback filter using the resistance of the wire in the coil as the input resistance makes up the first stage. Four identical stages of active tuned circuits each with a gain of 10 and a 3 decibel passband of 3.75 hertz centred about the operating frequency of 7.5 hertz follow the first stage. The supply voltage of each stage is individually regulated by 5 volt voltage regulators.

If all five stages are used, the 3 decibel passband is 0.84 hertz wide and the gain is 115 decibels. With such a narrow passband, the output closely approximates a simusoid of 7.5 hertz frequency. The signal output from the sensor is phase shifted in the calibration

process to yield the magnetic field at the sensor location.

With a calibration of 35.5 volts per nanotesla, the system can then measure magnetic fields of 0.2 picotesla variation with a dynamic range of 150 picotesla. Greater dynamic range is obtained at the expense of signal amplification by using fewer amplifier stages for signal amplification. Each amplifier stage not used results in a ten-fold increase in the dynamic range at the expense of 20 decibels of gain.

Electric field pick-up from the sensor could mask the magnetic response measurements or cause the amplifiers to saturate. It is avoided by grounding the electronics only at the input and running separate signal and signal ground wires to the surface.

The current consumption of all the stages together is 22 milliamperes. With the use of four 9 volt transistor batteries as 9 volt positive and negative voltage supplies, the system has an operating time of about 9 hours.

INSTRUMENT NOISE

Internal noise of the system arises from two major sources. The first is thermal noise of the copper mass in the wire windings. Noise from the amplifiers also contributes to the total noise in the system. Thermal noise could not be easily reduced unless either the mass or the operating temperature was significantly decreased. Amplifier noise is reduced by using high quality, low noise, precision operational amplifiers (model OPA 27GT from Burr-Brown Research Corporation) in the first stages.

Theoretical calculations of the instrument noise compares favourably with the noise (6 millivolts rms/$Hz^{1/2}$) as measured in an electromagnetically shielded room at the Erindale Campus of the University of Toronto. With a 0.1 nanotesla signal at 7.5 hertz, and a bandwidth of 1 hertz, the signal to noise ratio is 580 using any number of the last four amplifier stages.

REMAINING INSTRUMENTATION

The remaining instrumentation of a cross-hole survey consists of slightly modified surface MMR equipment which was available. It includes the following.

1. A University of Toronto designed, crystal oscillator controlled, transmitter used to inject a square wave into the ground. A Kohler motor generator set provides the operating power.
2. The MMR receiver (University of Toronto designed) constructed for surface MMR surveys. Through careful calibrations, this digital portable receiver can also be used for cross-hole MMR surveys. Conversion of the probe signal to a magnetic response is done by measuring the response of a known field (usually from a very long current source). Phase reference with the transmitter is maintained through the use of a second crystal, matched to the one in the transmitter.

SURVEY METHOD AND GEOMETRY

Although the survey configuration for a cross-hole MMR survey is basically what is shown in Figure 1, in practice, the drill holes are seldom vertical. After data have been collected in the drill hole, a geometry correction has to be made. From dip and tropari (azimuth) measurements of the drill hole, the relative locations and orientation of the probe with the electrodes and the current wire can be used to make this correction.

Electrode contact with the earth is not a problem if the electrode is located on the surface. Aluminum foil and copper stakes along with salt are used in setting up the surface electrodes when good electrical contact is needed. Down-hole electrodes are placed near mineralized zones even when the holes are water filled. If the host rock is very competent, with little or no fracturing, good electrode contact is difficult to achieve in the absence of conductive fluid.

Readings are taken at 10 m intervals for deep drill holes, unless a rapid change in the observed readings occurs. In such cases 5 m intervals or less are used to log the sections. Shorter reading intervals (less than 1 m) are used for short drill holes such as the one in Cavendish.

Once the transmitting bipole is set up, a kilometre long borehole logged at 5 m intervals with shorter spacings near anomalies can be logged in several hours.

FIELD SURVEYS

Two separate sets of tests have been done to date. The first was done on Noranda Exploration Company Limited property near Sturgeon Lake, during July of 1983. The second data set was obtained at the Cavendish geophysical test range near Gooderham, Ontario, during December of 1983. Data collected at the Noranda property used down-hole current electrodes, while surface sour-

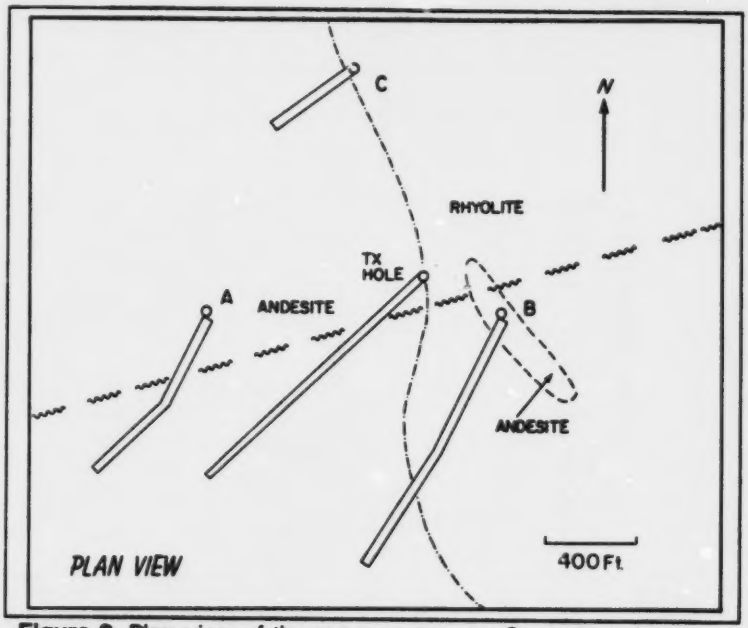

Figure 3. Plan view of the survey area near Sturgeon Lake.

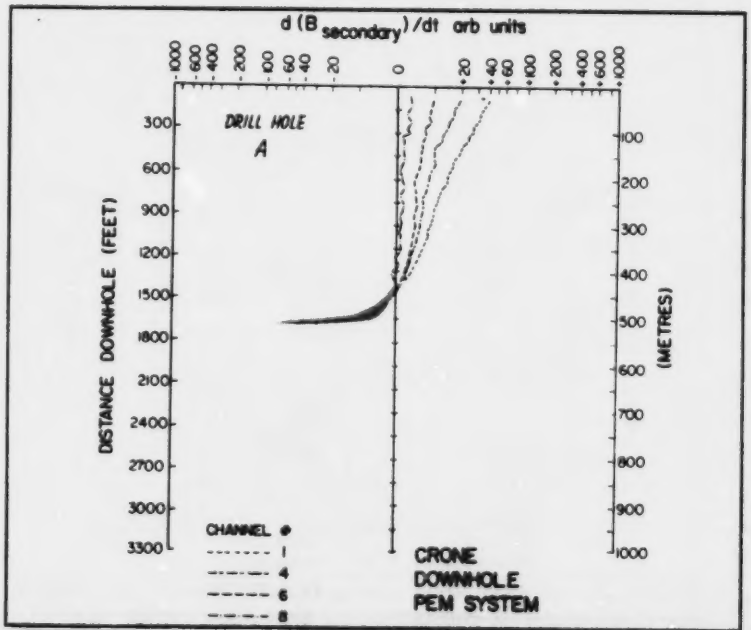

Figure 4a. Plots of several channels of Crone Pulse EM data for drill hole A (Figure 3). Shaded portions of curves are areas where the various channels cannot be distinguished.

ces were used at the Cavendish site. Both sets of data are presented.

STURGEON LAKE TEST

Geology and Previous Surveys

Noranda Exploration Company Limited provided the first drill holes for the cross-hole MMR tests. The site is located near Sturgeon Lake north of Ignace, Ontario. Access to the site is by a winter road which, in the summer, is drivable to within a kilometre of the drill holes used. Topographic relief is slight, and most of the survey area was swampy with about 5 m of overburden. Figure 3 is a plan view of the survey area showing the boreholes used.

Major rock types are andesite and rhyolite. Several different andesites and rhyolites can be distinguished. Up to 5% magnetite is found in one of the andesite units.

Previous borehole geophysical work in these holes included Crone drill-hole Pulse EM surveys. The data is presented in Figures 4a,b,c.

Interpretation of the Pulse EM data for drill hole 'A' shows a partially developed off-hole response at the end of the hole. Drill hole 'B' has in-hole responses at 731 and 769 m which corresponds with known mineralization. A weak in-hole response is detected near the bottom of drill hole 'C'.

Survey Configuration

A current bipole was used as the transmitting source in the survey conducted on the Noranda property. It is marked as the 'TX hole' on Figure 3. One electrode was placed at the top of the drill hole while the other was

placed 750 m down-hole. Three drill holes were logged and are labeled 'A', 'B', and 'C' on Figure 3. All were water filled and were BX sized (59 mm diameter) drill holes.

Data

Errors in the data were calculated by treating each reading as an independent measurement. For all three holes the plotted error bars are lost in the thickness of the plotted lines. It demonstrates the ease with which MMR data may be obtained. No errors were assumed for the location along the borehole as the calibrated counter returned to the same reading (within a metre) after each hole was logged.

Figures 5a,b,c show the data plotted to the same vertical scale as the Crone Pulse EM data. The dotted line represents the data scaled to 1 ampere of transmitted current. Effects of geometry, or transmitter-receiver coupling are shown by the dashed line. Finally, the solid curve is the corrected data. In all three cases, the geometry corrections are as large in magnitude as the collected data.

Comparison of the cross-hole MMR logs and the Crone Pulse EM logs shows that both detect anomalies at the same place. Due to the lack of a complete anomaly curve, fitting the data collected with the program MMRPlate in drill holes 'A' and 'B' can be achieved with a plate dipping between 20 and 60 degrees towards the drill holes and striking in the approximate direction of the andesite-rhyolite contact. Drill hole 'C' shows a more complicated response. In the interval between 175 and 350 m, there is high spatial frequency data probably caus-

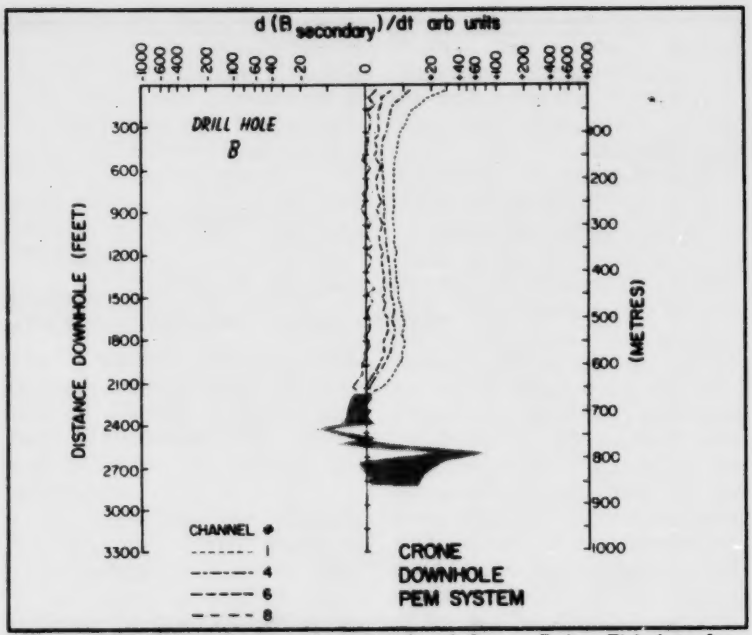

Figure 4b. Plots of several channels of Crone Pulse EM data for drill hole B (Figure 3). Shaded portions of curves are areas where the various channels cannot be distinguished.

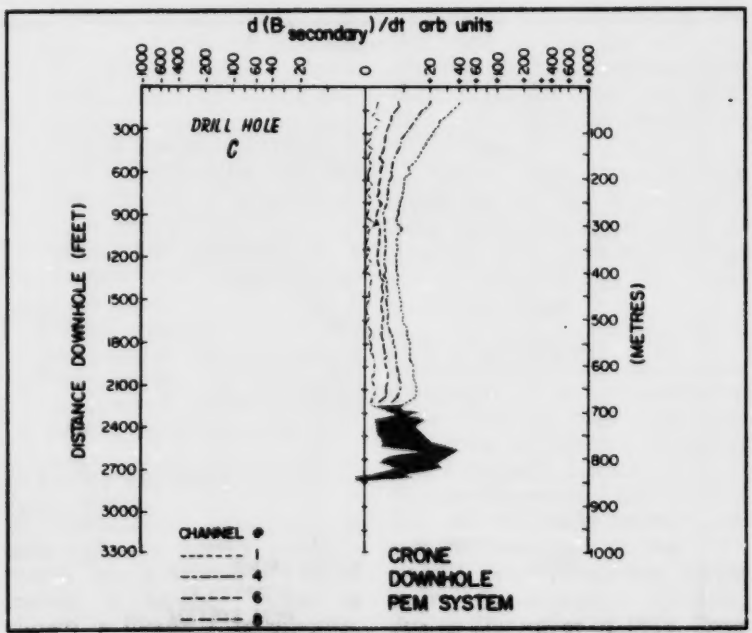

Figure 4c. Plots of several channels of Crone Pulse EM data for drill hole C (Figure 3). Shaded portions of curves are areas where the various channels cannot be distinguished.

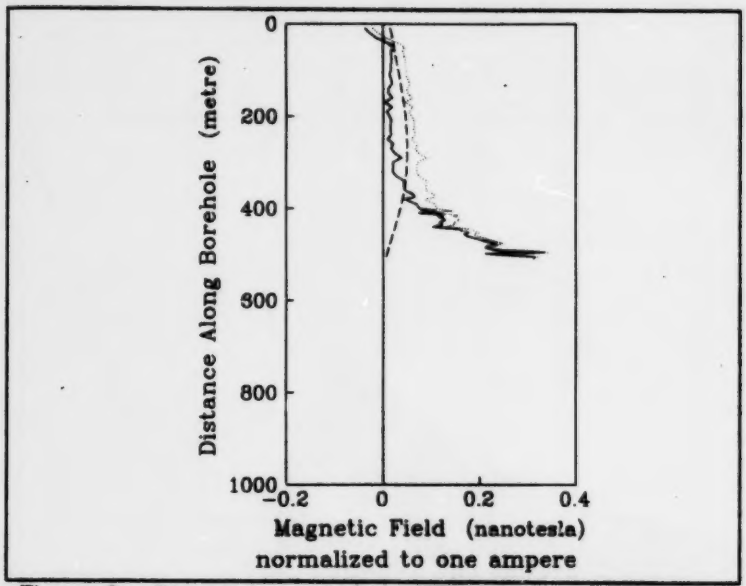

Figure 5a. Plot of the cross-hole MMR data for the Sturgeon Lake survey (drill hole A) normalized to 1 ampere of transmitted current. Uncorrected data - dotted line, correction for non-vertical hole effects - dashed line, anomalous magnetic field - solid line.

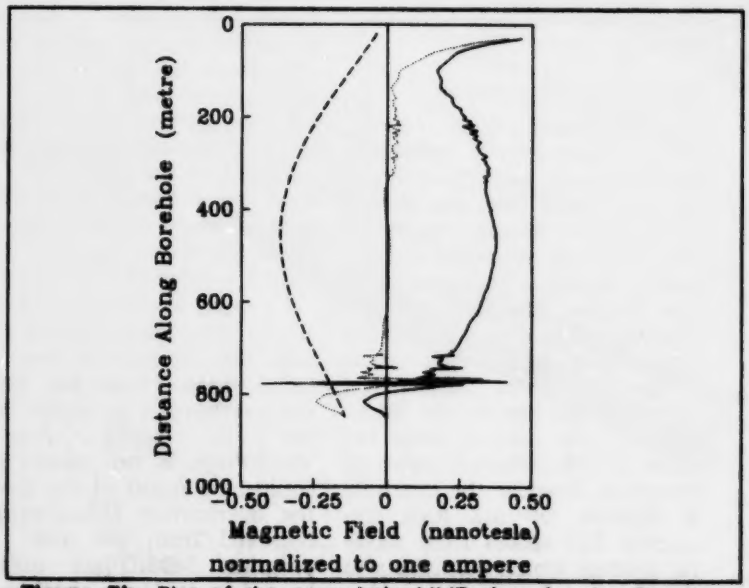

Figure 5b. Plot of the cross-hole MMR data for the Sturgeon Lake survey (drill hole B) normalized to 1 ampere of transmitted current. Uncorrected data - dotted line, correction for non-vertical hole effects - dashed line, anomalous magnetic field - solid line.

ed by magnetic minerals in the andesitic rocks. Magnetic minerals create a magnetic flux gathering effect to create a MMR anomaly. This effect cannot be distinguished from current gathering. The large amplitude spikes near the mineralization zones are probably caused by very local current channelling in the region of the borehole. A satisfactory fit using the program MMRPlate to model the data for drill hole 'C' had not been accomplished at the time of writing this report. A more complete interpretation of this data will be available in a University of Toronto, M.Sc. thesis by B.B.H. Lo (1984).

CAVENDISH TEST

Geology and Previous Surveys

Access to the Cavendish Township geophysical test range is by Salmon Lake Road, off Highway 507. Various private roads off Salmon Lake Road run through the established grid. The Geological Survey of Canada drilled 33 short holes in the area during 1973 (Williams *et al.* 1975). Figure 6 is a geologic map of the survey area (from Williams *et al.* 1975).

The basement rocks in the survey area are in the Grenville structural province of the Canadian Shield. Mafic gneiss, crystalline limestone, and granitic gneiss are overlain by several metres of overburden.

Figure 7 is a geologic section along line C and shows drill hole DDH15+80C which was used for this survey. The hole intersected 4.3 m of overburden, 14.8 m of biotite gneiss, 11.7 m of granitic gneiss, and 4.3 m of biotite-hornblende gneiss.

Mineralization consisting of 10% sulphides (pyrrhotite-pyrite) was intersected between 10.3 and 13.4 m. Bracketing this interval is an outer zone of 2% mineralization which starts at 4.3 m and extends to 19.1 m. Mineralization occurs as disseminations and as stringers parallel to the foliation.

Previous geophysical work in the area has been extensive. Practically every geophysical instrument suitable for massive sulphide exploration has been calibrated at this location. Of particular interest is the borehole work reported by Mansinha and Mwenifumbo (1983). They performed a mise-a-la-masse survey of the survey area and logged three holes (among them, DDH15+80C), with a resistivity probe. The main sulphide zone was logged at 1 siemen with the sulphide halo logged at an average apparent conductivity of 5×10^{-4} siemen/metre. The surrounding granitic gneiss averaged 1×10^{-4} siemen/metre.

Survey Configuration

Only one borehole, DDH15+80C, was logged at the Cavendish geophysical test site. Surface electrodes were used with two different electrode configurations for the same drill hole. The results from only one of the electrode configurations are presented in this paper. One electrode was placed 5 km down Salmon Lake Road and is a very good approximation to being an infinity electrode. The near electrode was located on Line A, 13W (see Figure 6). This electrode is a culvert which passes underneath Salmon Lake Road. The lie of the current wire is along Salmon Lake road.

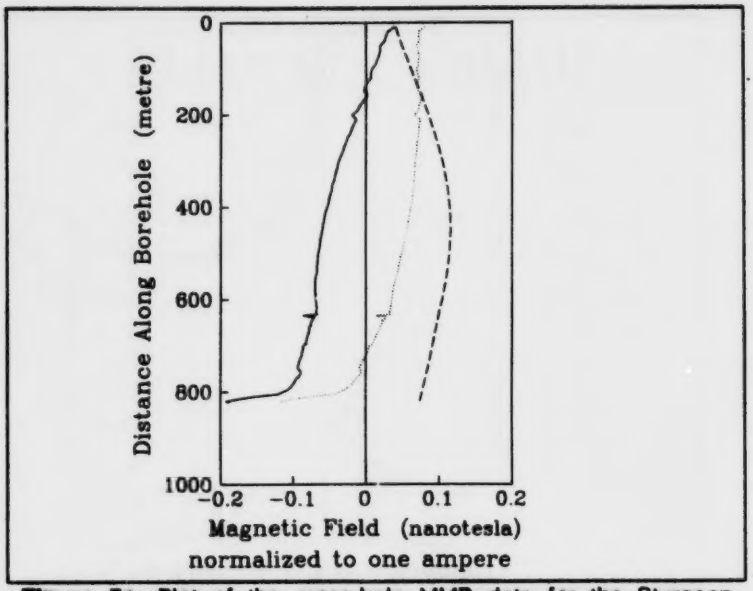

Figure 5c. Plot of the cross-hole MMR data for the Sturgeon Lake survey (drill hole C) normalized to 1 ampere of transmitted current. Uncorrected data - dotted line, correction for non-vertical hole effects - dashed line, anomalous magnetic field - solid line.

Spacings of 0.5 m were used in the readings with electrode at Line A, 13W.

Data and Interpretation

The collected data (dotted line), geometry correction (dashed line), and the corrected data (solid line) are shown in Figure 8. Measurement errors of these tests are significantly higher than those from the deeper boreholes of the Sturgeon Lake site. The plotted error bars are larger than those in Figures 5a,b,c, but they are still lost in the thickness of the plotted lines because of the different scales of the plots. Because the borehole is shallow (30 m), high frequency EM spikes from natural sources which contribute to the noise of the system are not attenuated as much as in the Sturgeon Lake data.

A 100 m long by 20 m wide dipping plate, perpendicular to the survey lines, centred about line 'C' was used to model the conductive zone. The plate dips 45° to the east and the top edge is 3.5 m below the surface. Two conductivity thickness products were assigned to the plate. The top 4 m has a conductivity thickness product of 0.03 siemens while the remaining part is assigned a value of 0.08 siemens.

Figure 9 presents the corrected field data (dotted line) and the theoretical response (solid line). From just below the overburden to about 10 m the fit using program MMRPlate is not good. This could be a result of not having the overburden effect entirely removed from the data. The program MMRPlate uses a bent lamella in a half-space. Effects of conductive overburden on the response, or effects of direct electrical contact of the plate with the overburden,

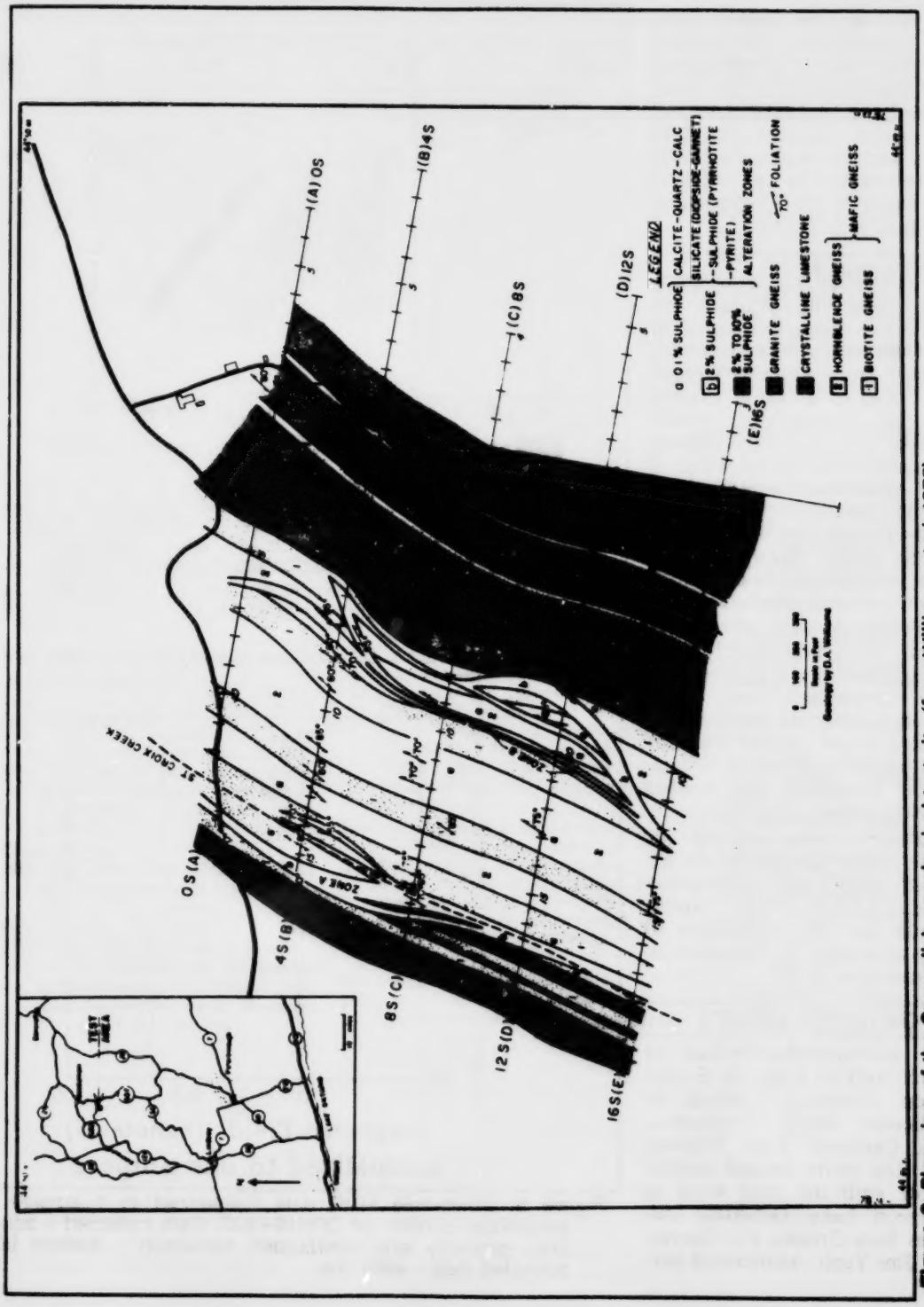

Figure 6. Plan view of the Cavendish geophysical test site (from Williams *et al.* 1975).

are not as yet incorporated into MMRPlate. Differences between the conductivity-thickness product of the body as modeled by MMRPlate and the results reported by Mansinha and Mwenifumbo (1983) may be caused by the overburden masking effect reported by Edwards *et al.* (1983).

CONCLUSION

The cross-hole variant of MMR has been developed at the University of Toronto with support from Ontario Geoscience Research Fund, Grant 145. An inexpensive, simple logging tool capable of operation under 800 m of water is now available. Current channelling caused by anomalous conductivities can be detected by the probe. Several sets of field results have been collected and partially interpreted.

Problems such as the removal of overburden effects and inclined probe and current wire corrections are being solved. Numerical routines exist for these corrections but they are hampered by a lack of the positional data needed to make these corrections.

Future work should include further studies on the inclined probe and overburden effects. More field studies should also be undertaken to fully determine the capabilities of cross-hole MMR.

ACKNOWLEDGMENTS

The authors would like to thank staff of Noranda Exploration Company Limited; in particular, Roger Pemberton, Don Carriere, Paul Nielsen, and Rod Swire helped considerably with the field work at Sturgeon Lake. Graduate students Ross Groom, Pat Garces, and Jim Yeoh volunteered sev-

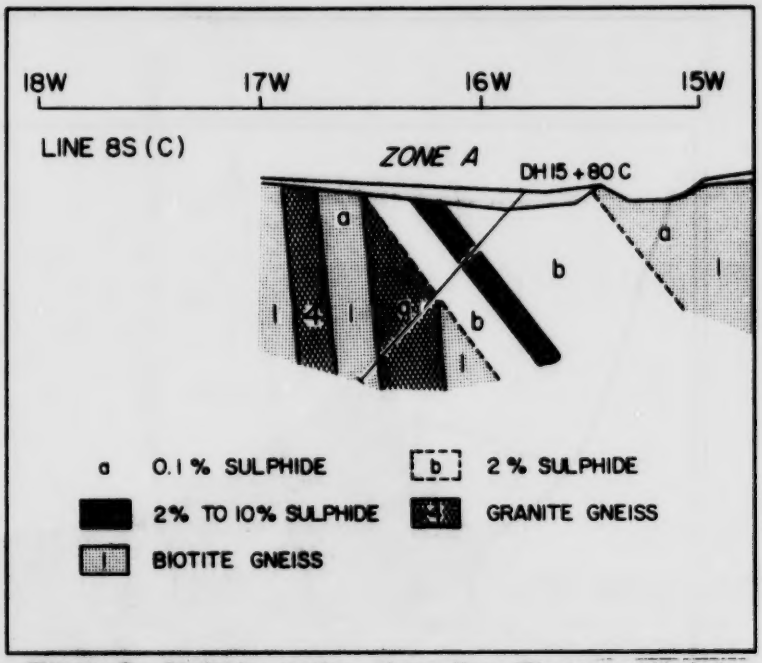

Figure 7. Geologic section along line 'C' near drill hole DDH15+80C (from Williams *et al.* 1975).

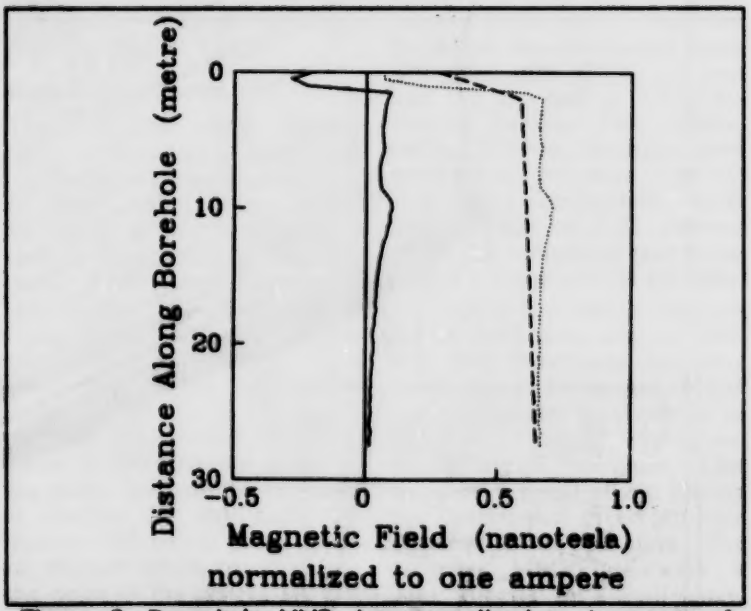

Figure 8. Down-hole MMR data normalized to 1 ampere of transmitted current for DDH15+80C. Data collected - dotted line, geometry and overburden correction - dashed line, corrected data - solid line.

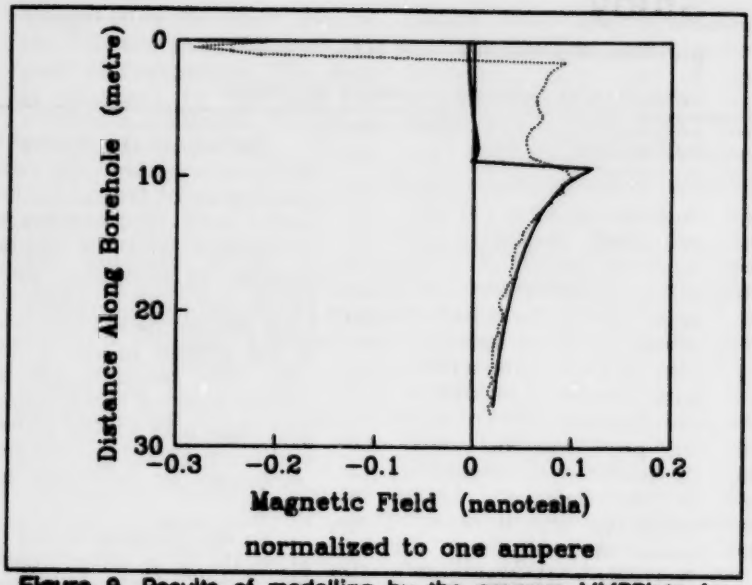

Figure 9. Results of modelling by the program MMRPlate for Cavendish data. The dotted line is the corrected data; the solid line is the model's fit of the data.

eral days of their time to assist in this project.

REFERENCES

Acosta, J.E., and Worthington, M.H.
1983: A Borehole Magnetometric Resistivity Experiment; Geophysical Prospecting, Volume 31, p.800-809.

Cheesman, S.J.
1983: The Cross-Hole MMR Response of a Bent Lamella; B.A.Sc. Thesis, University of Toronto.

Edwards, R.N.
1974: The Magnetometric Resistivity (MMR) Method and Application to the Mapping of a Fault; Canadian Journal of Earth Sciences, Volume 11, p.1136-1156.

1983: An Approximate Model of the Magnetometric Resistivity (MMR) and Magnetic Induced Polarization (MIP) Response of Dipping Dikes Beneath a Conductive Overburden; Bulletin of the Australian Society of Exploration Geophysicists, Volume 14, p.30-35.

Edwards, R.N. and Gomez-Trevino, E.
1980: MMR2D - A Programme for the Computation of Magnetometric Resistivity (MMR) Anomalies of Two-Dimensional Structures; Macquarie University, School of Earth Sciences, North Ryde, Australia.

Edwards, R.N. and Howell, E.C.
1976: A Field Test of the Magnetometric Resistivity (MMR) Method; Geophysics, Volume 41, p.1170-1183.

Edwards, R.N. and Nabighian, M.N.
1981: Extensions of the Magnetometric Resistivity (MMR) Method; Geophysics, Volume 46, p.459.

Edwards, R.N., Lee, H., and Nabighian, M.N.
1978: On the Theory of Magnetometric Resistivity (MMR) Methods; Geophysics, Volume 43, p.1176-1203.

Edwards, R.N., Lo, B., Cheesman, S., Nabighian, M., and Opplinger, G.
1983: Cross-hole Magnetometric Resistivity (MMR); *in* Ontario Geoscience Research Grant Program, Summary of Research 1982-1983, edited by E.G. Pye, Ontario Geological Survey, Miscellaneous Paper 113.

Gomez-Trevino, E., and Edwards, R.N.
1979: Magnetometric Resistivity (MMR) Anomalies of Two-Dimensional Structures; Geophysics, Volume 41, p.1170-1183.

Lo, B.B.H.
1984: On the Development of the Down-Hole Magnetometric Resistivity; Unpublished M.Sc. thesis, University of Toronto.

Mansinha, L., and Mwenifumbo, C.J.
1983: A Mise-a-la-Masse Study of the Cavendish Geophysical Test Site; Geophysics, Volume 48, p.1252-1557.

Nabighian, M.N., Opplinger, G., Edwards, R.N., Lo, B. and Cheesman, S.
1984: Cross-Hole Magnetometric Resistivity (MMR); Geophysics, in press.

Pai, D., and Edwards, R.N.
1983: Programme MMR2DFD: Finite Difference Modelling of MMR Anomalies; Reports in Applied Geophysics Number 25, University of Toronto, Department of Geophysics.

Williams, D.A., Scott, W.J., and Dyck, A.V.
1975: Cavendish Township Geophysical Test Range: 1973 Diamond Drilling; Geological Survey of Canada, Paper 74-62.

Grant 146 Crustal Contamination in the Sublayer, Sudbury Igneous Complex: a Combined Trace Element and Strontium Isotope Study

B.V. Rao, A.J. Naldrett, and N.M. Evensen

Department of Geology, University of Toronto

ABSTRACT

All of the Ni-Cu ore deposits of the Sudbury structure, Ontario, are associated with the Sublayer, a series of distinctive masses of rock of gabbroic to quartz dioritic composition along the outer margin of the Main Mass of the Sudbury Igneous Complex. The $(^{87}Sr/^{86}Sr)_{i=1.849G_a}$ ratios of Sublayer samples from the South Range (mean value = 0.70742) and North Range (mean value = 0.70454) are similar to those for the Main Mass norites from the two ranges and suggest contamination to different extents in the two locations. Further, when the trace element contents are compared with $(^{87}Sr/^{86}Sr)_{i=1.849G_a}$ ratios, the Sublayer samples from the North and South Ranges plot on two separate trends. These differences are also apparent amongst the Sublayer samples from Levack West, Strathcona, and Little Stobie deposits.

Model calculations suggest that the observed chemical and isotopic trends can be produced by a combined assimilation and fractional crystallization (AFC) process. In the context of such a model, the differences between the North and South Ranges and variation trends within both groups may be explained by varying degrees of coupled assimilation and fractional crystallization. These differences may have caused the large compositional variation in the sulphide liquids responsible for different Sudbury ore deposits.

INTRODUCTION

The Ni-Cu sulphide ores of the Sudbury district, Ontario, are principally associated with the Sublayer, which is considered to be a separate series of intrusions along the outer margin of the Sudbury Igneous Complex (SIC). Irvine (1975) and subsequently Naldrett and MacDonald (1980) attributed the prevalence of Ni-Cu ores at Sudbury to contamination of the Sublayer magma by silica-rich crustal rocks. They based their argument on the fact that silicification of mafic magmas depresses the solubility of Fe-rich sulphides.

Further, the SiO_2-rich nature of the Main Mass of the SIC as a whole has also been stressed by Naldrett and MacDonald (1980) and Naldrett and Hewins (in press). The high initial strontium isotopic composition of the Sudbury border norites, the high rare earth element (REE) abundances, and the significant enrichment of the light rare earths as demonstrated by their high $(La/Yb)_N$ ratios, and the complementary nature of the cumulus norites and granophyres, are all suggestive of significant contamination of the Sudbury magma by crustal components before it was emplaced into its present position.

The major role of crustal contamination in the genesis of suites of igneous rocks, and its effects on trace element trends and isotope systematics of the evolving liquids, have been emphasized by Carter *et al.* (1978), James (1981, 1982), Myers *et al.* (1984), and Dupy and Dostal (1984).

The aim of this project has been to evaluate the nature and degree of crustal contamination in the Sudbury magmas in general, and the Sublayer magmas in particular, and to assess the role, if any, that such contamination has played in the genesis of the Sudbury ores. This research will have implications for Ni-Cu exploration elsewhere in the province and for evaluating other mafic intrusions as potential hosts for ore.

In the previous report (Rao *et al.* 1983) we have presented the major and trace element (including REE) data for Sublayer samples collected from various locations around the Sudbury structure. The conclusions that we reached were: (1) the Sublayer magma experienced extensive contamination probably through bulk assimilation, and (2) recognisable differences exist between Sublayer samples of the North and South Ranges of the Sudbury structure. The major question at issue has been the nature and degree of this contamination.

In this report, strontium isotope data for the previously reported sublayer samples are presented. In addition, trace element (Th, Hf, Ta, Zr, Rb, Sr, Y, Sc, Ba, and the REE) and strontium isotope data for selected samples from the Strathcona and Levack West (McCreedy) deposits on the North Range and the Little Stobie deposit on the South Range are also presented. Data for selected samples of the mafic norites (North Range) and quartz-rich norites (South

Range) from the Main Mass of the SIC are given for the purpose of comparison. The data is discussed in the light of coupled assimilation fractional crystallization (AFC) processes (Taylor 1980; DePaolo 1981).

SUBLAYER

The Sublayer occurs around the outer margin of the SIC as discontinuous lenses and offset dikes. It occupies depressions and embayments in the footwall of the complex and protrudes into the footwall. A notable characteristic of the Sublayer is the presence of inclusions of footwall affinity and of an exotic suite of gabbros, pyroxenites, and peridotites. The samples for this study have been chosen from zones showing the smallest abundance of these inclusions. Inclusions identifiable with the naked eye were removed before the samples were crushed.

PETROGRAPHY

The Sublayer matrix consists of fine- to medium-grained interlocking laths of plagioclase (40-55%), prismatic to subophitic grains of clinopyroxene and orthopyroxene (20-35%), varying proportions of biotite (mostly enclosing and rimming iron-titanium oxides), hornblende, quartz, and occasional microcline. The samples studied are mostly fresh in appearance. Although the same minerals are present in the Sublayer samples from the three deposits - Levack West, Strathcona, and Little Stobie - there are differences in modal abundances, grain size, and fabric. Further, the textural character of the Sublayer from Little Stobie has a striking similarity with the overlying quartz-rich norites of the Main Mass, whereas the Sublayer from the Levack West and Strathcona deposits exhibits considerable differences from that of the overlying mafic norites of the North Range. The overall textural character of the Sublayer suggests *in situ* crystallization of magma.

CHEMISTRY

The major and trace element chemistry of the Sublayer was described in detail in the previous report (Rao *et al.* 1983) as well as in Naldrett *et al.* (in press). Only plots of SiO_2 vs major oxides and a few trace elements are presented in Figure 1 for the purpose of discussion. The fractionation trends shown in the figure are broadly similar to those of continental tholeiites and are indicative of fractionation of plagioclase and clinopyroxene. MgO is relatively depleted and the Al_2O_3 remains constant in a large number of the more evolved Sublayer samples from the North and South Ranges. This may be indicative of some olivine fractionation. The lack of smooth trends in SiO_2 vs major oxide and trace element plots suggests that not all the samples are the products of a single fractionating liquid.

COUNTRY ROCKS

On the North Range, the footwall rocks for the Sublayer are essentially the rocks of the Levack Gneiss Complex which are highly variable in composition, ranging from diorite or quartz diorite to quartz monzonite and containing appreciable amounts of mafic material. The isotopic studies of Fairbairn *et al.* (1965) indicated an initial $(^{87}Sr/^{86}Sr)_{\sim 2.5Ga}$ ratio of 0.706 ±0.001 for the rocks of this complex. In the Strathcona and Levack West mines, the immediate footwall country rock is quartz-plagioclase-augite gneiss of the Levack Complex which has a widely varying chemical composition. The chondrite-normalized rare earth patterns of this rock show a very strong positive Eu anomaly and significant fractionation of both light and heavy rare earths (La/Yb ratio is as much as 30).

The footwall rocks on the South Range consist of metabasalts and metasediments of the Elliot Lake Group of the Huronian Supergroup (2.3-2.4 Ga) and Creighton and Murray granites. In the Little Stobie mine, metabasalts and granites constitute the immediate footwall. The metabasalts are subalkaline to tholeiitic with high K_2O and have initial strontium isotope ratios of 0.7048 ± 0.0014 (Knight 1967). They are also characterized by very high REE abundance and significant enrichment of the light rare earths. The Huronian metasediments have initial isotopic compositions ranging from 0.7072 to 0.7203 with a weighted average of 0.712 (Fairbairn *et al.* 1968). They are characterized by significant enrichment of the light rare earths. The younger formations of this Supergroup show negative Eu anomalies and the older formations (McKim pellites) show no Eu anomalies (McLennan *et al.* 1977). The Murray and Creighton granites have very high initial strontium isotopic composition (0.7211, Gibbins and McNutt 1975) and their chondrite-normalized rare earth element patterns are similar to those of the upper crustal rocks of the Precambrian Canadian Shield (Shaw *et al.* 1976).

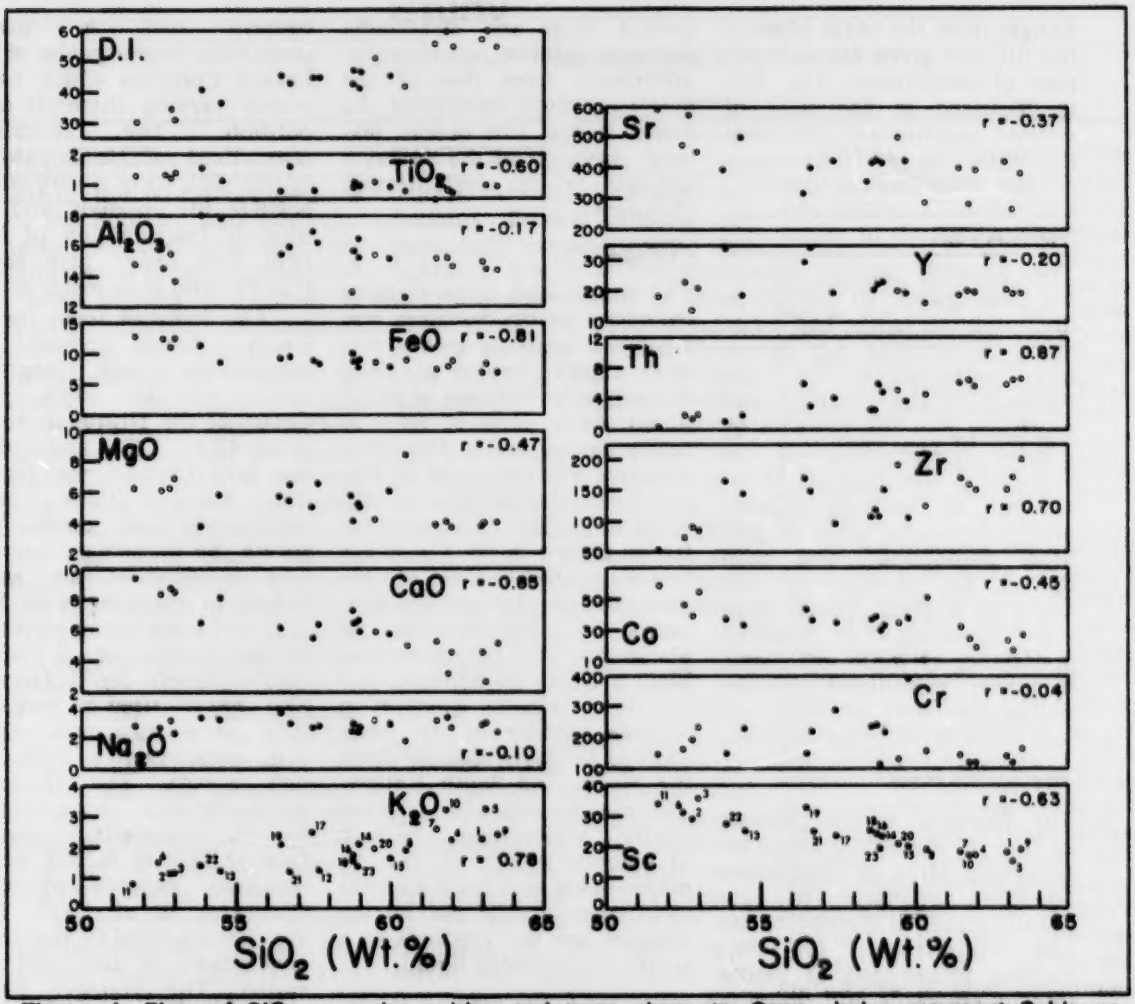

Figure 1. Plots of SiO_2 vs major oxides and trace elements. Open circles represent Sublayer samples from the North Range and filled circles from the South Range. The numbers refer to sample numbers in Tables 1 and 2 of Rao *et al.* (1983).

TABLE 1. STRONTIUM ISOTOPE DATA FOR SUBLAYER.

Sample No.	Locality	Rb	Sr	Rb/Sr	$^{87}Rb/^{86}Sr$	$^{87}Sr/^{86}Sr$	$(^{87}Sr/^{86}Sr)_0$
North Range							
12/Lev/BVR/84	Levack West	36.02	377.4	0.09544	0.27673	0. 71146 (±4)	0.70410
10/Lev/BVR/84	Levack West	27.84	356.4	0.078114	0.22649	0. 71010 (±3)	0.70408
4/Lev/BVR/84	Levack West	25.96	477.4	0.054357	0.15761	0. 70901 (±6)	0.70481
6/Lev/BVR/84	Levack West	34.53	416.5	0.082905	0.24038	0. 71037 (±2)	0.70398
13/Lev/BVR/84	Levack West	7.95	511.7	0.015536	0.04504	0. 70449 (±17)	0.70330
3/Lev/BVR/84	Levack West	7.20	469.6	0.015331	0.04445	0. 70477 (±4)	0.70360
7/Lev/BVR/84	Levack West	13.10	522.4	0.025076	0.07271	0. 70573 (±2)	0.70360
6B/Stn/BVR/83	Strathcona	40.0	249	0.16064	0.46578	0. 71909 (±16)	0.70670
3B/Stn/BVR/83	Strathcona	9.4	449	0.02093	0.06070	0. 70658 (±7)	0.70496
7B/Stn/BVR/84	Strathcona	9.9	456	0.02161	0.062675	0. 70628 (±17)	0.70461
8B/Stn/BVR/83	Strathcona	15.5	449	0.03452	0.10009	0. 70741 (±9)	0.70475
8D/Stn/BVR/83	Strathcona	28.3	229	0.12356	0.123581	0. 71562 (±4)	0.70609
BVR-2/82	Norman	24	580	0.04136	0.11998	0. 70790 (±1)	0.70471
BVR-3/82	Norman	28	456	0.06140	0.17803	0. 70962 (±2)	0.70488
BVR-4/82	Norman	45	387	0.11628	0.33715	0. 71512 (±2)	0.70615
BVR-6/82	Norman	43	477	0.09015	0.26139	0. 71131 (±3)	0.70435
BVR-5/82	Whistle Offset	65	263	0.24715	0.71661	0. 72236 (±2)	0.70330
BVR-7/82	Foy Offset	70	398	0.17586	0.50996	0. 71878 (±5)	0.70522
BVR-8/82	Bowell	68	288	0.23611	0.68460	0. 72233 (±1)	0.70412
BVR-9/82	Bowell	55	379	0.14512	0.42060	0. 71883 (±6)	0.70440
BVR-11/82	Capreol	21	602	0.03490	0.10114	0. 70815 (±2)	0.70346
BVR-20/82	McLennan	36	496	0.07258	0.21045	0. 71205 (±3)	0.70646
South range							
2/Lstb/BVR/84	Little Stobie	50.5	396.6	0.12765	0.37010	0.71729 (±10)	0.70744
3/Lstb/BVR/84	Little Stobie	46.0	246.6	0.18654	0.54080	0.72209 (±10)	0.70770
4/Lstb/BVR/84	Little Stobie	47.0	398.4	0.11797	0.34200	0.71670 (±7)	0.70760
17/Lstb/BVR/84	Little Stobie	37.0	476.1	0.07786	0.22580	0.71374 (±14)	0.70773
7/Lstb/BVR/84	Little Stobie	22.3	433.5	0.05144	0.14915	0.71101 (±10)	0.70705
6/STB/BVR/82	Little Stobie	34	456.1	0.07298	0.21150	0.71201 (±5)	0.70610
1B/Lstb/BVR/84	Little Stobie	4.8	456.1	0.01052	0.03051	0.71152 (±3)	0.71078
BVR-13/82	Denison	43	484	0.08880	0.25769	0.71338 (±13)	0.70683
BVR-14/82	Denison	67	323	0.20743	0.60144	0.72208 (±2)	0.70610
BVR-15/82	Denison	54	427	0.12646	0.3667	0.71594 (±1)	0.70620
BVR-16/82	Denison	57	418	0.13636	0.3954	0.71576 (±1)	0.70520
BVR-17/82	Denison	143	425	0.33650	0.97565	0.73320 (±23)	0.70725
BVR-18/82	Denison	50	356	0.1405	0.40723	0.71736 (±3)	0.70653
BVR-19/82	Denison	76	315	0.24127	0.69960	0.72659 (±12)	0.70796
BVR-21/82	McKim	44	388	0.11340	0.3288	0.72243 (±2)	0.71358
BVR-22/82	McKim	41	393	0.10432	0.3025	0.72550 (±2)	0.71745
BVR-23/82	Creighton	56	428	0.13084	0.3794	0.71675 (±2)	0.70666

Note. Initial isotopic ratios ($(^{87}Sr/^{86}Sr)_0$) are calculated using a common age of 1.849Ga (Krogh *et al.* 1982).These are referred to as $(^{87}Sr/^{86}Sr)_{t=1.849Ga}$ in the text. Rb and Sr concentrations were determined by XRF. Errors are 2-sigma mean and correspond to the last significant digits.

TABLE 2. RARE EARTH AND OTHER TRACE ELEMENT DATA FOR SUBLAYER SAMPLES.

	Levack West							
Sample Number	10/Lev/ BVR/84	7/Lev/ BVR/84	12/Lev/ BVR/84	3/Lev/ BVR/84	13/Lev/ BVR/84	9/Lev/ BVR/84	4 /Lev/ B VR/84	6/Lev/ BVR/84
La	18.6	11.8	24.5	12.4	12.0	20.2	16.9	13.1
Ce	39.7	23.8	52.0	28.5	25.7	41.7	34.7	25.0
Nd	17.7	10.3	24.8	13.3	-	19.2	13.3	12.1
Sm	3.4	2.15	4.84	2.9	2.64	3.54	2.73	2.36
Eu	0.85	0.62	1.04	0.9	0.77	0.86	0.73	0.71
Tb	0.55	0.27	0.47	0.39	0.50	0.59	0.28	0.24
Yb	1.2	0.74	1.50	1.65	0.92	1.33	0.85	0.89
Lu	0.17	0.12	0.20	0.24	0.10	0.21	0.14	0.13
Σ REE	82.17	49.80	109.35	60.28	42.63	87.63	69.63	54.53
Th	3.3	1.3	3.5	1.0	1.5	3.9	2.5	2.4
Hf	2.0	1.0	2.9	0.71	1.5	1.8	1.6	1.6
Ta	0.38	0.13	0.35	0.13	0.22	0.33	0.23	0.21
Ba	345	428	597	597	352	423	430	456
Sc	23	17	26	43	26	23	19	22
Co	67	67	79	43	57	61	70	51
Cr	-	-	648	366	137	790	791	910
Ni	-	-	-	107	271	336	-	239
Zr	91	45	123	45	65	93	70	62
Y	14	9	19	17	12	13	10	10
Ratios								
$(La/Sm)_N$	3.30	3.36	3.07	2.61	2.78	3.50	3.75	3.37
$(La/Yb)_N$	10.1	10.4	10.8	5.0	8.65	10.03	13.1	9.65
Zr/Y	6.50	5.0	6.47	2.64	5.49	7.0	6.9	6.14
Zr/Hf	45.5	45.0	42.4	63.0	43.5	51.4	44.0	39.0
Th/Ta	8.7	10.0	10.0	7.7	6.8	11.8	10.9	11.4
Hf/Ta	5.3	7.7	8.3	5.5	6.8	5.4	7.0	7.6
Th/La	0.18	0.11	0.14	0.08	0.12	0.19	0.15	0.18
Ba/La	18.5	36.0	24.4	48.0	29.0	20.9	25.4	34.0
Zr/Rb	3.25	3.46	3.42	6.25	8.16	4.2	2.7	1.81
Y/Sr	0.04	0.02	0.05	0.036	0.02	0.03	0.02	0.024

TABLE 2. CONTINUED

	Strathcona				
Sample Number	**6B/Stn/ SVR/83**	**7B/Stn/ SVR/83**	**3B/Stn SVR/83**	**9D/Stn/ SVR/83**	**9E/Stn/ SVR/83**
La	19.5	17.0	11.3	21.1	20.0
Ce	43.0	31.0	33.0	31.6	28.0
Nd	13.8	7.2	11.9	13.7	7.8
Sm	3.4	2.2	2.8	2.6	2.0
Eu	0.88	0.87	0.86	0.70	0.90
Tb	0.32	0.36	0.60	0.30	0.23
Yb	1.4	1.2	1.3	1.5	1.05
Lu	0.23	0.12	0.2	0.16	0.12
Σ REE					
Th	3.3	1.0	1.2	1.6	1.1
Hf	2.65	1.1	1.2	2.3	1.6
Ta	0.20	0.1	0.1	0.12	0.1
Ba	332	282	206	297	320
Sc	24	36	56	21	23
Co	75	90	66	229	84
Zr	103	40	40	78	41
Y	15	9	14	11	9.5
Ratios					
$(La/Sm)_N$	3.48	4.54	2.2	4.96	6.0
$(La/Yb)_N$	9.5	8.8	5.8	9.4	15.3
Zr/Y	6.9	4.2	2.85	7.2	4.36
Zr/Hf	38.9	35.4	33.3	34.0	25.6
Th/Ta	13.9	8.3	14.0	11.8	11.78
Hf/Ta	6.97	4.78	12.0	10.45	11.42
Th/La	0.25	0.11	0.12	0.12	0.08
Ba/La	15.7	16.6	18.4	14.1	16.0
Zr/Rb	2.57	3.93	4.25	2.76	2.64
Y/Sr	0.06	0.02	0.03	0.046	0.02

TABLE 2. CONTINUED

Sample Number	2/Lstb/ BVR/84	4/Lstb/ BVR/84	6/Lstb/ BVR/84	7/Lstb BVR/84	17/Lstb/ BVR/84	11B/Lstb BVR/84	1B/Lstb/ BVR/84
	Little Stoble						
La	24.3	22.40	20.3	20.6	29.8	31.7	23.5
Ce	58.0	56.40	46.6	39.8	56.3	69.0	52.3
Nd	23.5	23.40	14.3	16.8	23.3	33.5	19.5
Sm	4.8	4.45	3.94	3.1	4.04	5.8 4	4.53
Eu	1.35	1.23	1.06	1.08	1.15	1.7 2	1.33
Tb	0.95	1.01	0.78	0.54	0.64	-	0.75
Yb	2.2	1.89	2.20	1.55	1.82	1.0 3	2.43
Lu	0.37	0.32	0.38	0.25	0.31	0.2 0	0.38
Σ REE	115.47	111.10	89.56	83.72	117.36	142.9 9	104.72
Th	8.1	9.3	6.3	3.3	5.0	1.8	7.1
Hf	2.2	2.4	2.6	2.5	1.03	1.9	1.3
Ta	0.67	0.58	0.55	0.37	0.64	0.0 7	0.53
Ba	575	542	570	482	457	863	-
Sc	21	20	23	20	18	19	23
Co	43	60	172	49	32	71	84
Cr	499	511	-	411	471	657	223
Ni	286	-	-	325	374	830	921
Zr	66	58.6	84	83	81	86	116
Y	23	20.7	19.7	14.5	18.3	13.4	23.4
Ratios							
$(La/Sm)_N$	3.06	3.09	3.16	4.03	4.54	3.30	3.26
$(La/Yb)_N$	7.2	7.8	6.2	8.9	11.1	20.20	6.4
Zr/Y	2.87	2.8	4.26	5.75	4.4	6.4	4.9
Zr/Hf	30.0	24.4	32.3	33.4	78.0	45.0	89.0
Th/Ta	12.1	16.0	11.5	8.92	7.8	25.7	13.4
Hf/Ta	3.3	4.1	4.7	6.7	1.6	27.0	2.45
Th/La	0.33	0.42	0.31	0.16	0.17	0.06	0.30
Ba/La	23.7	24.2	28.1	23.4	15.3	27.2	-
Zr/Rb	1.34	1.24	1.92	3.75	2.35	3.3	24.1
Y/Sr	0.056	0.049	0.07	0.03	0.037	0.06	0.05

TABLE 1. REE AND OTHER TRACE ELEMENT ANALYSES OF NORITES FROM THE MAIN MASS OF THE SUDBURY IGNEOUS COMPLEX (VALUES ARE IN PPM).

	North Range (Mafic Norites)								
Sample	55-SDB	56-SDB	57-SDB	58-SDB	59-SDB	62-SDB	6 3-SDB	1-STN	8-STN
La	24.50	23.40	26.40	19.70	27.00	21.40	26.00	28.80	24.30
Ce	41.90	40.70	48.00	-	49.60	42.40	49.00	78.60	70.20
Nd	13.30	17.90	21.80	17.20	18.80	20.00	17.30	20.50	17.20
Sm	2.85	3.72	4.30	3.00	4.20	3.46	4.10	3.10	4.16
Eu	0.65	0.82	0.88	-	0.99	0.81	0.97	1.46	1.16
Yb	0.72	1.60	1.70	1.30	1.37	1.50	1.60	1.35	1.35
Lu	0.10	0.21	0.29	0.11	0.18	0.23	0.21	0.21	0.23
Σ REE	84.02	88.35	103.37		102.14	86.34	99.18	134.02	118.60
Th	7.0	5.2	5.5	-	5.7	5.3	5.7	6.0	6.7
Hf	2.8	2.6	2.3	-	2.1	2.7	2.3	3.2	3.7
Ta	0.39	0.37	0.44	-	0.46	0.43	0.55	0.36	0.23
Zr	112	95	117	111	112	97	114	110	120
Y	8	16	17	14	15	15	16	15	16
Sr	349	280	285	459	468	255	282	444	236
Rb	26	39	46	42	45	39	47	37	41
Co	60	96	104	-	46	84	102	112	84
Cr	2300	2000	1725	-	360	1220	2450	1825	1450
Sc	15	24	22	-	16	23	22	28	31
Ratios									
Zr/Y	14.0	5.9	6.7	7.93	7.47	6.4 7	7.1	7.3	7.5
Zr/Hf	40.0	36.5	50.9	-	53.3	35.9	49.6	34.4	32.4
Th/Ta	17.9	14.0	12.5	-	12.4	12.3	10.4	16.7	29.0
Hf/Ta	7.2	7.03	5.2	-	4.56	6.3	4.2	8.9	16.1
Th/La	0.28	0.22	0.21	-	0.21	0.2 5	0.22	0.21	0.28
Zr/Rb	4.31	2.44	2.54	2.64	2.5	2.5	2.41	2.97	2.93
Y/Sr	0.023	0.057	0.06	0.03	0.03	0.0 6	0.057	0.034	0.068

TABLE 3. CONTINUED

	South Range (Quartz-Rich Norites)									
Sample	**9 QN/ BVR/84**	**8 QN/ BVR/84**	**7 QN/ BVR/84**	**1 QN/ BVR/84**	**2 QN/ BVR/84**	**3 QN/ BVR/84**	**4 QN/ B VR/84**	**5 QN/ BVR/84**	**6 QN/ BVR/84**	**10 QN/ BVR/84**
La	20.2	28.1	24.7	20.6	22.4	18.3	19.2	18.2	19.5	21.9
Ce	34.0	53.8	46.4	47.7	53.8	40.5	43.2	44.2	38.9	44.5
Nd	14.5	21.4	17.1	19.4	20.4	15.4	18.3	16.1	16.3	17.4
Sm	3.07	4.37	3.5	3.53	3.74	2.8	3.04	3.1	3.04	3.5
Eu	0.77	1.2	1.1	1.04	1.1	0.97	1.11	0.98	0.91	0.97
Tb	0.38	0.6	0.42	0.44	0.46	0.42	0.34	0.37	0.37	0.41
Yb	1.3	1.8	1.54	1.89	1.5	1.25	1.5	1.7	1.32	1.25
Lu	0.22	0.27	0.28	0.26	0.3	0.23	0.24	0.26	0.2	0.21
Σ REE	74.44	111.54	95.04	94.88	103.70	79.8 7	84.93	84.91	80.54	90.14
Th	7.8	5.1	5.6	5.7	5.3	4.6	5.1	4.7	5.7	5.3
Hf	4.5	2.9	3.7	2.6	1.7	1.7	2.0	2.1	2.2	2.9
Ta	0.63	0.43	0.47	0.47	0.38	0.45	0.45	0.37	0.33	0.36
Be	454	504	550	519	563	545	436	397	520	442
Sc	23	22	22	17	16	16	17	17	16	16
Co	43	47	48	31	32	35	33	32	28	31
Cr	841	648	644	336	410	388	324	361	314	305
Ni	196	136	128	59	62	63	74	84	73	70
V	131	116	112	97	87	95	91	100	97	84
Zr	166	86	139	82	59	71	64	84	96	112
Y	16	18	17	17	16	14	15	17	14	16
Sr	174	395	387	451	462	479	485	462	412	517
Rb	82	39	39	42	39	40	36	46	50	43
Ratios										
Zr/Y	10.37	4.65	8.17	4.91	3.69	5.07	4.27	4.94	6.86	7.0
Zr/Hf	37.2	29.65	37.30	31.5	35.1	41.8	32.0	40.0	43.60	38.6
Th/Ta	12.4	11.86	11.90	12.1	13.9	10.2	11.3	12.5	17.3	14.7
Hf/Ta	7.06	6.74	7.90	5.53	4.42	3.78	4.4	5.7	6.7	8.05
Th/La	0.39	0.18	0.23	0.28	0.24	0.25	0.26	0.26	0.29	0.24
Ba/La	22.5	17.9	22.3	25.1	24.7	29.80	22.7	21.90	26.70	20.20
Zr/Rb	2.02	2.21	3.53	1.96	1.5	1.78	1.75	1.83	1.91	2.57
Y/Sr	0.09	0.05	0.044	0.037	0.033	0.02 8	0.031	0.037	0.034	0.031
$(^{87}Sr/^{86}Sr)_M$			0.71511 (±5)	0.71402 (±9)	0.71358 (±10)	0.71429 (±6)		0.71511 (±5)	0.71574 (±21)	
$(^{87}Sr/^{86}Sr)_o$			0.70726	0.70687	0.70723	0.70818		0.70747	0.70633	

Note: $(^{87}Sr/^{86}Sr)_M$ are the measured strontium isotopic compositions and $(^{87}Sr/^{86}Sr)_o$ are the calculated initial isotopic compositions using a common age of 1.849 Ga. Errors are two-sigma mean and correspond to the last significant digits.

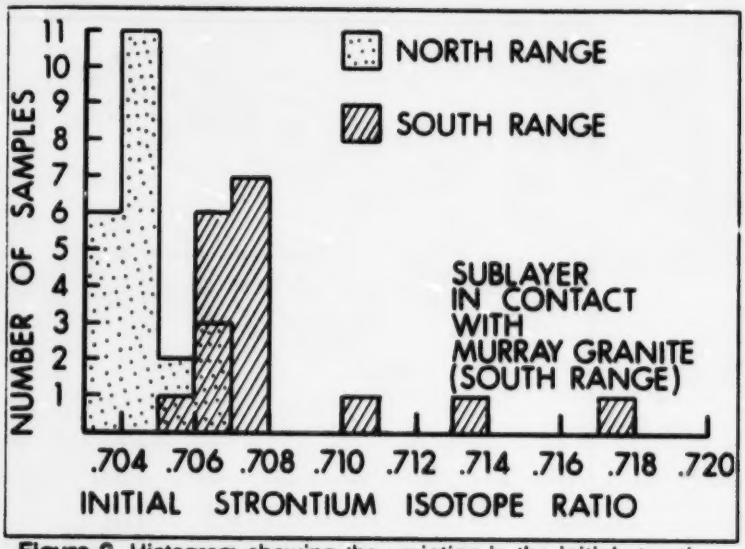

Figure 2. Histogram showing the variation in the initial strontium isotopic composition of the Sublayer.

RESULTS

The strontium isotope results are presented in Table 1. The trace element data for the Sublayer samples from the three deposits - Strathcona, Levack West (McCreedy), and Little Stobie - are given in Table 2, and the trace element data for the border norites of the Main Mass of the Sudbury Igneous Complex (SIC) are listed in Table 3. The strontium isotope data for the quartz-rich norites are also included in Table 3.

The variation in the initial strontium isotopic compositions of the Sublayer are illustrated in the histogram in Figure 2. The $(^{87}Sr/^{86}Sr)_{i=1.849Ga}$ values vary between 0.7033 and 0.7078. Anomalously high values are noticed in three samples which were collected from zones adjacent to the Murray Granite. A spatial dependence of the isotopic ratios is obvious. The Sublayer from the North Range shows initial strontium isotopic ratios ranging from 0.7033 to 0.706 (mean value is 0.70454) and the Sublayer from the South Range has values ranging from 0.705 to 0.7078 (mean value is 0.70742). The initial strontium isotope ratios of the Sublayer are similar to those determined by Gibbins and McNutt (1975), and in this study as well, for the norites of the Main Mass of the complex from the two ranges and suggest contamination to different extents in the two locations. This confirms a similar observation by Ding and Schwartz (1984) on the basis of oxygen isotope data from the norites of the Main Mass.

The strontium isotope data for the Sublayer samples from Levack West, Strathcona, and Little Stobie deposits are plotted on an isochron diagram in Figure 3. The data apparently define pseudo-isochrons and indicate successively higher initial ratios for the three deposits respectively. Unless it is confirmed by Sm-Nd isotope study (in progress), we regard these as artifacts of some complex igneous process rather than indicative of actual ages. One sample from the Little Stobie mine, which is very much different in textural character and modal mineralogy from the rest of the samples, shows higher $(^{87}Sr/^{86}Sr)_{i=1.849Ga}$ ratio. The data obtained in this study do not show any correlation of initial strontium isotope ratios with SiO_2. Ding and Schwartz (1984) also did not notice any such correlation with $\delta^{18}O$ values.

The chondrite-normalized rare earth element $(REE)_N$ patterns are shown in Figure 4. The general characteristics of the REE in the Sublayer samples of this study are similar to those described previously (Rao *et al.* 1983). The samples from all locations have strikingly similar patterns although their absolute abundances (Σ REE) vary widely. All are characterized by significant light rare earth enrichment (LREE) with no Eu anomalies. Although there is no significant fractionation of the heavier rare earths (HREE) in the samples from Little Stobie deposit, the samples from Levack West and Strathcona deposits show considerably fractionated HREE patterns. This is also true of the norites from the Main Mass of the North Range. Kuo and Crocket (1978) consider that these represent the liquid composition parental to the Sudbury Igneous Complex and suggest that extensive crustal contamination of magma was responsible for the LREE enrichment.

The incompatible element ratios (element/Yb ratios are used to minimize the effects of partial melting and crystal fractionation) normalized to corresponding ratios of chondrites show patterns parallel to that of Precambrian Canadian Shield (Shaw *et al.* 1976), as is the case with Precambrian Coppermine River basalts and other continental tholeiites contaminated by crustal components (Dupy and Dostal 1984). Crustal features characterized by depletion of Ta and enrichment of Th relative to La are seen in these patterns shown in Figure 5.

In plots of pairs of strongly incompatible elements (SIE), the variations in concentrations in the Sublayer samples seem to be completely unsystematic (as is evident from large variation in such ratios, see Table 2). Minister and Allegre (1978) have shown that the concentration ratios of two such elements is constant during partial melting and crystallization process and equals the concentration ratio in the source. In plots of pairs of such elements, rocks from a common source and affected only by partial melting and fractional crystallization will plot on a straight line through the origin.

When $(^{87}Sr/^{86}Sr)_{t=1.849Ga}$ values are plotted against 1/Sr in Figure 6, no simple correlation is evident. The absence of correlation eliminates simple processes such as crystal fractionation, magma mixing, and crustal contamination acting alone as being responsible for the genesis of Sublayer magmas. The relationships of Sr and other strongly incompatible elements (SIE) Rb, La, Th, and Zr with initial strontium isotopic compositions do not suggest appreciable linear cor-

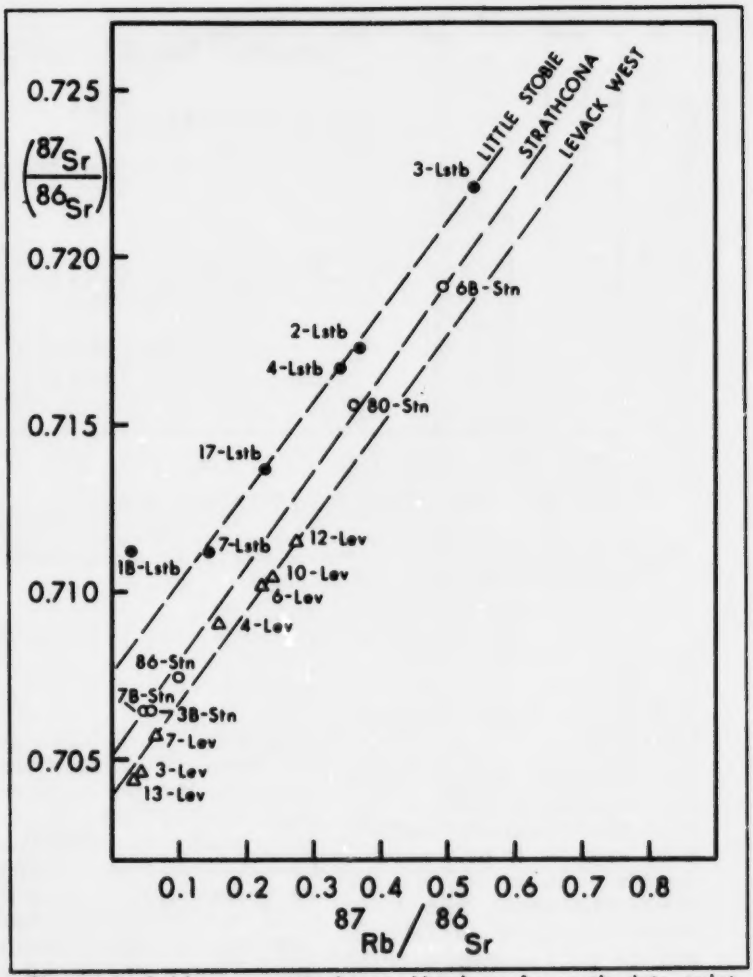

Figure 3. Sublayer scatterchrons. Numbers for each data point refer to the sample numbers in Table 1. The data for each locality are fitted with regression lines (dashed lines).

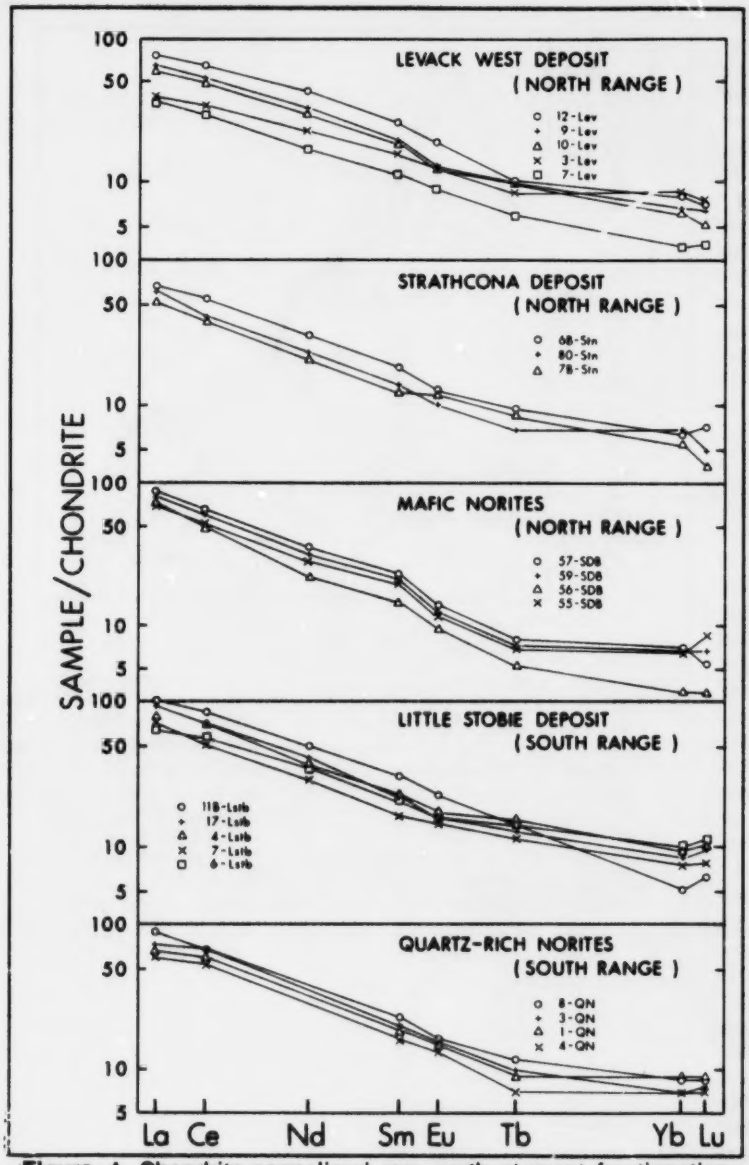

Figure 4. Chondrite-normalized rare earth element fractionation patterns for the Sublayer samples from various locations. Fractionation patterns for the border norites for the Main Mass of the Sudbury Igneous Complex are also shown for comparison. Numbers indicated for each pattern refer to the sample numbers in Tables 2 and 3.

relation in the combined data. But when the samples are divided into two groups, a large part of samples from the South Range seem to follow trends steeper than the trends for samples from the North Range (see below).

EVOLUTION OF TRACE ELEMENT TRENDS AND ISOTOPE CHARACTERISTICS

Crystal fractionation alone could not have produced the observed chemical and isotopic variability and trends in the Sublayer from a single parental magma. Therefore, a more complex process must be invoked to account for the observed compositional variability and trends. The trace element abundances and the initial strontium isotopic composition of the Sublayer rocks suggest the major role of crustal contamination. Such contamination processes vary widely in their nature. These may be classified essentially into three variants:

1. Simple binary-type mixing with a fixed contaminant (Langmuir *et al.* 1978);

2. Mixing by multiple contaminants having different trace element and isotopic signatures;

3. Contamination of the above two types accompanied by concurrent fractional crystallization (Taylor 1980; DePaolo 1981).

The isotopic and chemical character of the hybrid liquids resulting from the above contamination processes depend on (1) the isotopic compositions of the end members, and (2) the relative mixing proportions of the two end members. On plots of $^{87}Sr/^{86}Sr$ vs various trace element, the compositions of the hybrid liquids

should define hyperbolic mixing curves, their curvature depending on the ratio of trace element concentration in the contaminant to that in the parental magma. However, subsequent fractionation of the hybrid liquids would modify the trace element character substantially, without affecting the strontium isotope composition. Clearly, the Sublayer data do not define a single mixing hyperbola with a constant curvature. Therefore, process (1) i.e. simple mixing, above can be eliminated. As a result of compound mixing process (2) above, additional sets of mixing curves are produced. Certainly, the scatter in the data points can be explained by this process. But Figure 7 shows that the Sublayer samples from the North Range would require a contaminant with a Sr concentration much lower than in the Levack gneiss, which is the most probable contaminant. Although local assimilation of contaminants (included as xenoliths) of widely varying compositions has certainly played a role in modifying the liquid composition, the overall isotope vs trace element trends require some other process as an explanation. Because the major and trace element variations suggest a significant fractionation of plagioclase and clinopyroxene (and probably olivine), and the trace element and strontium isotope characters indicate the dominant role of crustal contamination, we analyze the Sublayer data in the light of coupled assimilation - fractional crystallization (AFC) processes. These models are more realistic than simple mixing models because the AFC process represents a situation in which the latent heat released by crystallization is

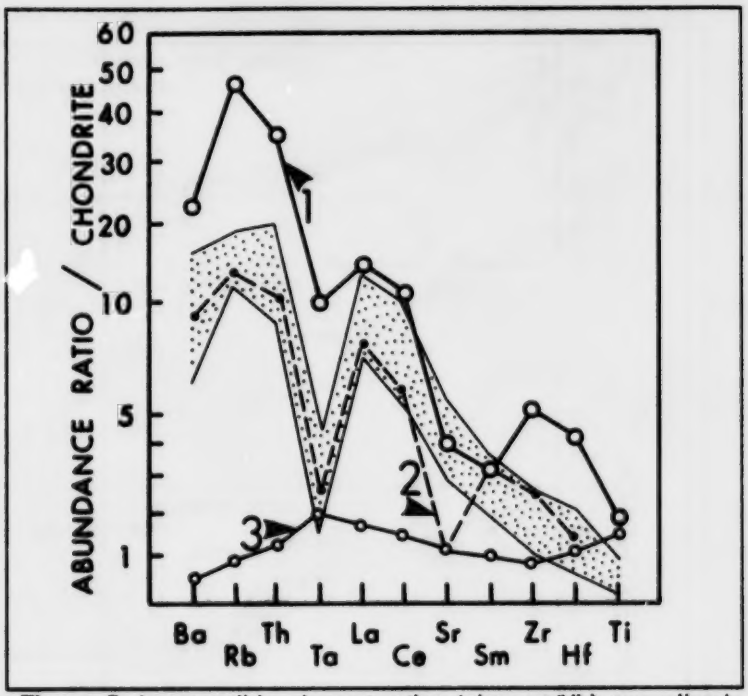

Figure 6. Incompatible element ratios (element/Yb) normalized to chondrites. The stipled area represents the range in Sublayer rocks. The patterns are for the Precambrian Canadian Shield (1), Precambrian Coppermine River basalts, Canada (2), and P-type MORB (3) (data from Dupy and Dostal 1984). The normalizing values are from Thomson *et al.* (1982).

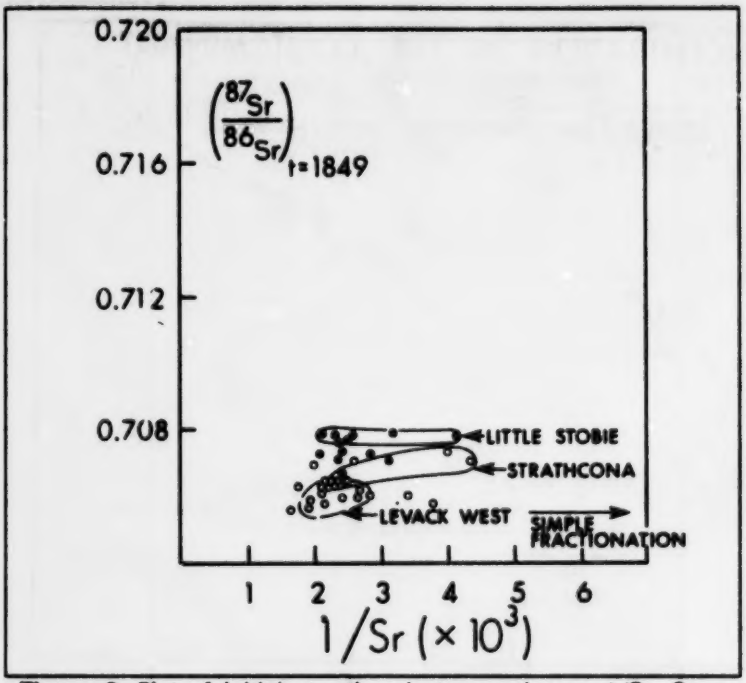

Figure 6. Plot of initial strontium isotope ratios vs 1/Sr. Open circles represent Sublayer samples from the North Range and filled circles Sublayer samples from the South Range. Since crystallization cannot induce variation in strontium isotope ratios, simple fractionation of Sr-bearing phases (plagioclase and pyroxene) causes the liquids to evolve along a horizontal line. The fields for Sublayer samples from the three deposits Levack West (r = +0.3), Strathcona (r = +.9), and Little Stobie (r = +0.44) are indicated. The apparently high correlation in the Strathcona samples is essentially due to the two highly contaminated samples 6B/Stn and 80/Stn (see Table 1).

utilized for fusing crustal material and thus accounts for the heat-balance. We are still in the process of acquiring data, so only qualitative models are proposed here.

The effects of the AFC processes on isotope ratios and trace element concentrations differ markedly from those produced by either two-component mixing or fractional crystallization operating singly, since the crystallization of phases can substantially alter the concentration of elements such as Sr in magma. These effects are illustrated in Figure 8. The calculations are made with the assumptions that: (1) the cumulate formed is removed instantaneously (Rayleigh crystallization) or crystals which remain in liquid maintain equilibrium with the melt, (2) the ratio (r) of assimilated material to the magma crystallized (cumulate) remains constant during magmatic evolution, and (3) the bulk partition coefficients (D) of the crystallizing phases also remain constant throughout the evolution. For the purpose of illustrating the effects of the AFC process, calculations have been performed for two contaminants with different Sr concentrations. As illustrated in Figure 8, if 'r' becomes small (approaches zero), the AFC trends approach the behaviour of simple fractional crystallization. If 'r' becomes large (approaches infinity), the AFC trends collapse towards the simple mixing trajectories. In other words, as 'r' increases, the shifts in $^{87}Sr/^{86}Sr$ become greater for a given shift in Sr concentration. Further, for the same amount of fractionation (fraction of magma remaining, F), the process with higher 'r' produces greater shifts in both

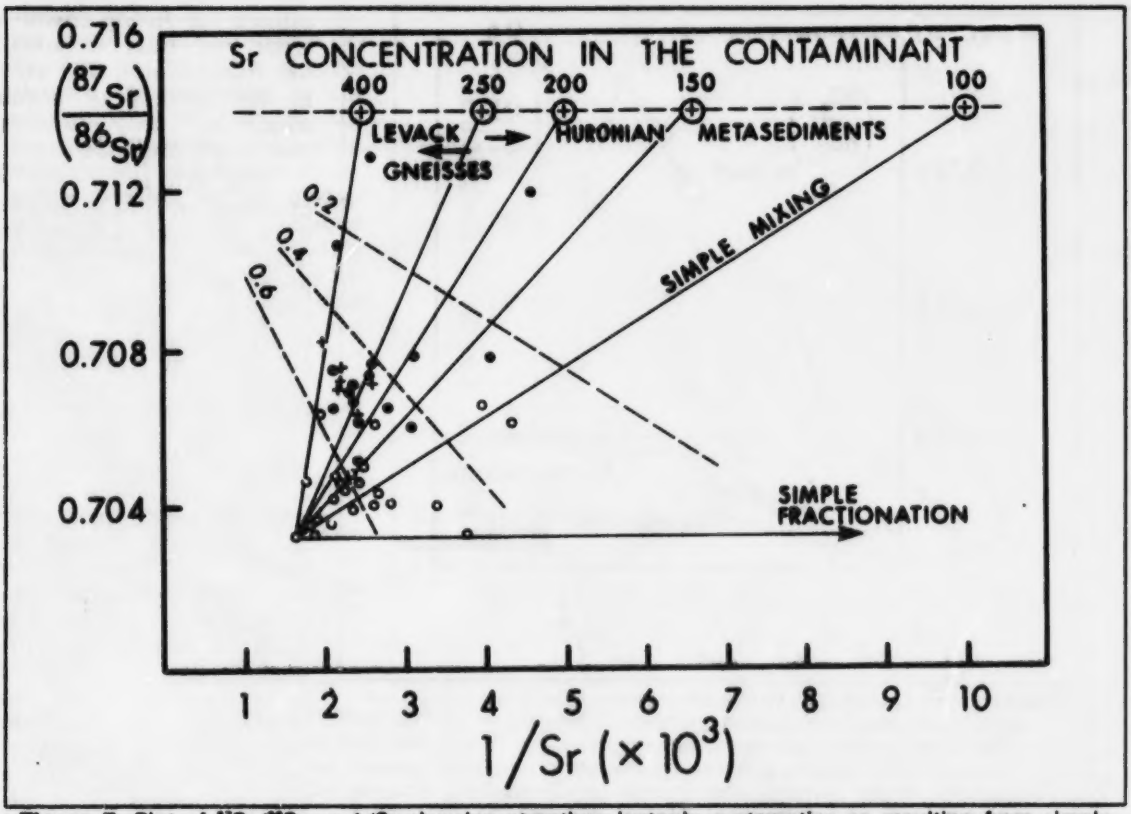

Figure 7. Plot of $^{87}Sr/^{86}Sr$ vs 1/Sr showing strontium isotopic systematics as resulting from simple mixing (with multiple contaminants). In this diagram mixing lines plot as straight lines between end members. They are labelled with the concentration of Sr in the contaminant. The initial $^{87}SR/^{86}Sr$ ratio in the contaminant is 0.714 and that in the parent magma is 0.7035. Dashed lines with negative slopes are contours of constant contaminant to magma ratio. The data for the Sublayer samples from the North Range (open circles) and South Range (filled circles) are plotted. The data for the quartz-rich norites (+) are also indicated. In a general way, the North Range samples appear to have been contaminated with material having lower Sr concentration than the contaminant of the South Range. The concentration of Sr in the two possible contaminants (Levack gneisses and Huronian metasediments) tend to vary in the direction pointed by the arrows.

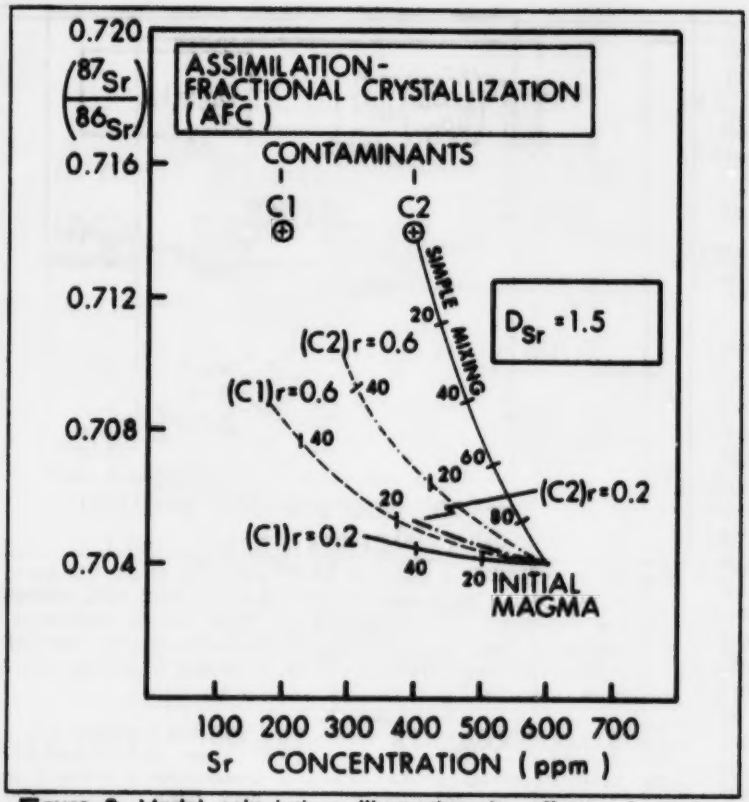

Figure 8. Model calculations illustrating the effects of varying degrees of coupled assimilation and fractional crystallization (AFC) on strontium isotopic and trace element compositions and trends (see text). The numbers by the side of tick-marks on each curve represent the degree of fractionation (weight percent magma crystallized). Calculations are made with the assumption that plagioclase and pyroxene crystallize in the ratio 1:1 (bulk partition coefficient D_{Sr} = 1.5). See text for discussion.

Sr and Sr-isotopic compositions.

Model calculations are presented in Figures 9 and 10 to explain the observed trends in the Sublayer samples. Because of the uncertainties in the composition of the principal contaminant, a composition that closely approximates the upper crustal composition of the Precambrian Canadian shield (Shaw *et al.* 1978) has been used in the calculations. Experimentally determined partition coefficients are used here. A crystallizing assemblage of clinopyroxene and plagioclase in the ratio 1:1 was chosen for the calculations. The best qualitative fit to explain the differences between the North and South Ranges and the variation trends within each group seem to be that given by variable rates of assimilation coupled with varying degrees of crystal fractionation. This conclusion applies to Sr ($D > 1$) as well as incompatible elements with $D << 1$. As seen from Figures 9 and 10, the Sublayer samples from the South Range conform to trends with $r = 0.6$ and higher with the degree of fractionation (see figures for explanation) varying from 15-25 weight percent. The samples from the North Range follow trends that result from lower r values.

Although a larger data base and other controls such as Sm-Nd isotope characteristics are necessary to propose quantitative models, from the discussion presented above the following differences are apparent in the Sublayer from Levack West, Strathcona, and Little Stobie deposits.

1. The Sublayer from the Levack West is less contaminated than Sublayer from the

Strathcona and Little Stobie deposits, but is more fractionated than the Sublayer from the Little Stobie deposit.

2. The degree of fractionation experienced by the Sublayer from Levack West and Strathcona appears to be more or less the same.

3. The Sublayer of the Little Stobie deposit is the most contaminated of all the three.

CONCLUSIONS

The combined study of trace elements and strontium isotopes suggests that the Sublayer magmas of the North and South Ranges of the Sudbury structure have undergone different degrees of assimilation and fractional crystallization. The reasonable agreement between the calculated and the observed trends indicates that the broad differences between the two groups, as well as within group variations, may be accountable by different degrees of crustal assimilation with concurrent fractional crystallization of varying magnitude. Naldrett (1981) has shown that the sulphide liquids responsible for different Sudbury ore deposits vary widely in their composition. He has suggested that these compositional variations are due to separation of sulphides from different batches of a single magma that experienced different degrees of contamination and fractional crystallization during magmatic evolution. The differences in the Sublayer from various locations indicated in this study may be responsible for the large compositional variation of the resulting sulphide liquids.

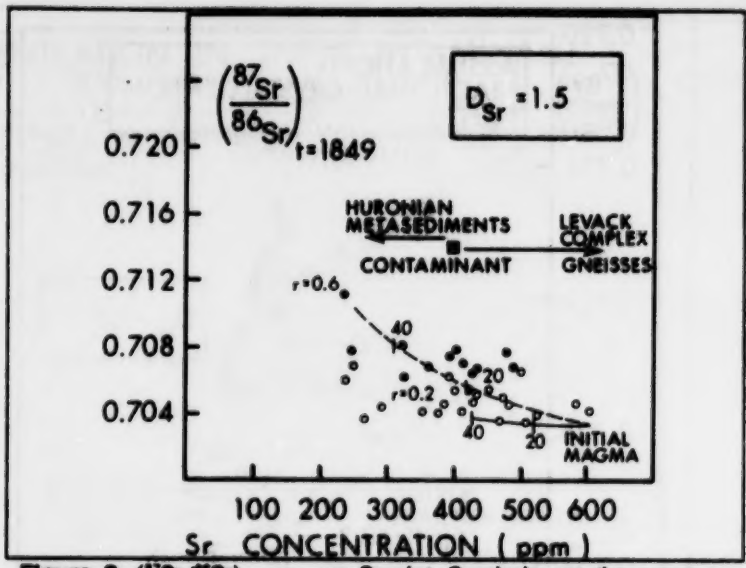

Figure 9. $(^{87}Sr/^{86}Sr)_{t=1.849Ga}$ vs Sr plot. Symbols are the same as in Figure 7. Calculated trends resulting from AFC processes are indicated. The numbers on each curve represent the degree of fractionation (magma crystallized). Notice that the bulk partition coefficient (D) is >1 and the curves are concave upwards.

ACKNOWLEDGMENTS

The help received from Dr. B.O. Dressler (Ontario Geological Survey), Dr. W.V. Peredery (INCO Limited), and Mr. P. Snajdr (Falconbridge Limited) throughout the course of this research is appreciatively acknowledged.

REFERENCES

Campbell, I.H. and Naldrett, A.J.
1979: The Influence of Silicate: Sulfide Ratios on the Geochemistry of Magmatic Sulfides; Economic Geology, Volume 74, p.1503-1505.

Carter, S.R., Evensen, N.M., Hamilton, P.J., and O'Nions, R.K.
1978: Neodymium and Strontium Isotope Evidence of Crustal Contamination of Continental Volcanics; Science, Volume 202, p.743-747.

DePaolo, D.J.
1981: Trace Element and Isotopic Effects of Combined Wall-Rock Assimilation and Fractional Crystallization; Earth and Planetary Science Letters, Volume 53, p.189-202.

Ding, T.P., and Schwartz, H.P.
1984: Oxygen Isotopic and Chemical Composition of Rocks of the Sudbury Basin, Ontario; Canadian Journal of Earth Science, Volume 21, p.305-318.

Dupy, C., and Dostal, J.
1984: Trace Element Geochemistry of some Continental Tholeiites; Earth and Planetary Science Letters, Volume 67, p.61-69.

Fairbairn, H.W., Hurley, P.M., and Pinson, W.H.
1965: Re-examination of the Rb-Sr Whole-Rock Ages at Sudbury; Geological Association of Canada Proceedings, Volume 12, p.41-66.

1968: Rb-Sr Whole-Rock Age of the Sudbury Lopolith and Basin Sediments; Canadian Journal of Earth Sciences, Volume 5, p.707-714.

Gibbins, W., and McNutt, R.H.
1975: The Age of the Sudbury Nickel Irruptive and the Murray Granite; Canadian Journal of Earth Science, Volume 12, p.1970-1989.

Irvine, T.N.
1975: Crystallization Sequences of the Muskox Intrusion and Other Layered Intrusions - II. Origin of Chromatite Layers and similar Deposits of other Magmatic Ores; Geochimica et Cosmochimica Acta, Volume 39, p.991-1020.

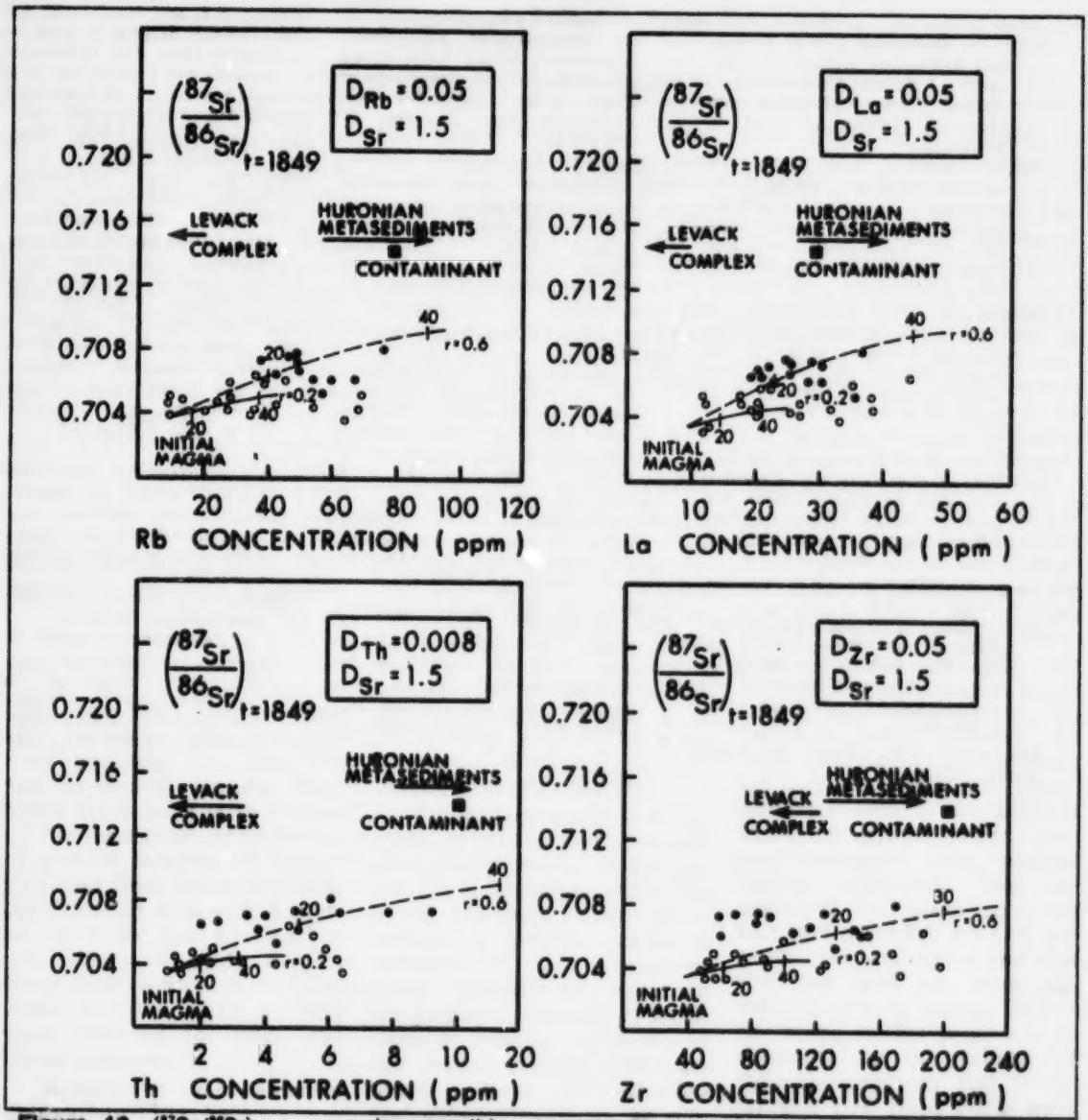

Figure 10. $(^{87}Sr/^{86}Sr)_{t=1.849Ga}$ vs incompatible elements Rb, La, Th, and Zr with bulk partition coefficients <<1. Notice that the curves are convex upwards. Symbols are the same as in Figure 7.

James, D.E.
1981: The Combined Use of Oxygen and Radiogenic Isotopes as Indicators of Crustal Contamination; Annual Review of Earth and Planetary Science, Volume 9, p.311-344.
1982: A Combined O, Sr, Nd, and Pb Isotopic and Trace Element Study of Crustal Contamination in Central Andean Lavas, I. Local Geochemical Variations; Earth and Planetary Science Letters, Volume 57, p.47-62.

Knight, C.J.
1967: Rubidium-Strontium Isochron Ages of Volcanic Rocks of the North Shore of Lake Huron, Ontario, Canada; Unpublished Ph.D Thesis, University of Toronto.

Kuo, H.Y., and Crocket, J.H.
1978: Rare Earth Elements in the Sudbury Nickel Irruptive: Comparison with Layered Gabbros and Implications for Nickel Irruptive Petrogenesis; Economic Geology, Volume 79, p.590-605.

Langmuir, C.H., Vocke, R.D., Hanson, G.N., and Hart, S.R.
1978: A General Mixing Equation: Applied to the Petrogenesis of Basalts from Iceland and Reykjanes Ridge; Earth and Planetary Science Letters: Volume 37, p.380-392.

McLennan, S.M., Fryer, B.J., and Young, G.M.
1977: Rare Earth Elements in Huronian (Lower Proterozoic) Sedimentary Rocks: Composition and Evolution of Post-Kenoran Upper Crust: Geochimica Cosmochimica Acta, Volume 43, p.375-388.

Minister, J.F., and Allegre, C.J.
1978: Systematic Use of Trace Elements in Igneous Processes, Part III, Inverse Problem of Batch Partial Melting in Volcanic Suites; Contributions to Mineralogy and Petrology, Volume 68, p.37-52.

Myers, J.D., Krishna Sinha, A., and Marsh, B.D.
1984: Assimilation of Crustal Material by Basaltic Magma: Strontium Isotopic and Trace Element Data from the Edgecumbe Volcanic Field, SE Alaska; Journal of Petrology, Volume 25, p.1-26.

Naldrett, A.J.
1981: Nickel Sulfide Deposits: Classification, Composition, and Genesis; Economic Geology, 75th Anniversary Volume, p.628-685.

Naldrett, A.J., Hewins, R.H., Dressler, B.O., and Rao, B.V.
(in press): The Sublayer of the Sudbury Igneous Complex; *in* The Geology and Ore Deposits of the Sudbury Structure, Ontario Geological Survey, Special Volume 1.

Naldrett, A.J., and MacDonald, A.J.
1980: Tectonic Settings of some Ni-Cu Sulfide Ores: The Importance in Genesis and Exploration; Geological Association of Canada, Special Paper 20, p.633-657.

Rao, B.V., Naldrett, A.J., Evensen, N.M., and Dressler, B.O.
1983: Contamination and Genesis of the Sudbury Ores; Grant 146, p.139-152 *in* Geoscience Research Grant Program, Summary of Research 1982-83, edited by E.G. Pye, Ontario Geological Survey, Miscellaneous Paper 113, 199p.

Shaw, D.M., Dostal, J., and Keys, R.R.
1976: Additional Estimates of Continental Surface Precambrian Shield Composition in Canada; Geochimica et Cosmochimica Acta, Volume 40, p.73-83.

Taylor, H.P. Jr.
1980: The Effects of Assimilation of Country Rocks by Magmas on $^{18}O/^{16}O$ and $^{87}Sr/^{86}Sr$ Systematics in Igneous Rocks; Earth and Planetary Science Letters, Volume 47, p.243-254.

Thomson, R.N., Dickin, A.P., Gibson, I.L., and Morrison, M.A.
1982: Elemental Fingerprints of Isotopic Contamination of Hebridean Palaeocene Mantle-Derived Magmas by Archean Sial; Contributions to Mineralogy and Petrology, Volume 79, p.159-168.

Grant 148 Geochemical Study of the Salina Formation of Southern Ontario — Isotopes, Major and Minor Elements

M.C. Miles, P. Fritz, S.K. Frape, D.E. Lawson, and E.C. Appleyard

Department of Earth Sciences, University of Waterloo

ABSTRACT

The purpose of the research was to establish geochemical evidence in support of paleoenvironmental interpretations, to investigate the nature and genesis of brines within the salt formations, to contribute to a data base for the study of Canadian Shield saline brines and to provide modern analogue chemical data for Precambrian evaporite investigations. Isotopic and chemical analyses have been carried out on sampled sections from the Salina Formation as represented at the Sifto Salt mine, Goderich, Canadian Salt Company mine, Windsor, Domtar gypsum mine, Caledonia, and Consumers' Gas holes 33406 and 33411, Fletcher Field, Ontario. Two-hundred and seventy carbonate samples were analysed for carbon-13 and oxygen-18; samples from active brine leaks were analysed for deuterium, tritium and oxygen-18; samples of brines, rock and fluid inclusions from the Goderich area were analysed for major and selected minor elements; and samples from shale sequences at Caledonia and the Fletcher Field were analysed for trace and minor elements.

Results to date indicate that carbon-13 cycles were present in the Silurian sea during Salina deposition and may reflect carbon budget fluctuations within the Michigan Basin and that the entire marginal facies of the Michigan Basin must have been above sea level during the deposition of the B-Anhydrite. Contemporaneous dolomite deposition at Goderich and the Fletcher Field show remarkably different oxygen-18 compositions which may be related to different crystallization processes. Brines sampled are typical Michigan Basin brines; they were not formed by the direct dissolution of salts, and are not the direct remnants of fossil sea water. Tritium discovered in Goderich brines indicates that minor amounts of fresh water have mixed with the brines at this location.

INTRODUCTION

This is the initial report on a geochemical study of the Salina Formation in Ontario. The study was initiated in April, 1983, after M.C. Miles (1982) noted interesting isotopic trends associated with the sedimentary sequence at the Domtar gypsum mine in Caledonia. Work will be continuing through 1984-1985.

The general purpose of the study is to further evaluate geochemical trends in the entire Salina sequence elsewhere in the Michigan Basin and to provide a greater statistical certainty for this evaluation. Major emphasis was placed on the paleoenvironment of deposition in relation to theories of salt deposit genesis. Other interests include dolomitization and diagenetic effects on geochemical and isotopic parameters.

Isotope and trace element geochemistry have potential as tools for the exploration and the exploitation of saline deposits. Recently, carbon isotopic fluctuations in the rock record have been shown to be associated with oceanic anoxic events. Scholle and Arthur (1980), after a study of Cretaceous chalks, suggested that the interpretation of $\delta^{13}C$ fluctuations is potentially useful for the precise timing of the preservation of organic matter in deep sea and continental-margin sediments. Carbon-13 studies may aid in estimating potential hydrocarbon resources, using carbon mass balance calculations. In our study, an interpretation has been made of carbon isotopes in the Michigan Basin.

Active brine leaks are periodically encountered in mine workings in the Salina Formation, and are of concern to the companies that operate the mines (Canadian Salt Company, Windsor, and Sifto Salt Divison of the Domtar Chemicals Group, Goderich). It has generally been assumed by these companies that the leaks are local in origin and represent remnants of the original fluids which were trapped during deposition and evolved during diagenesis. This assumption was based upon the fact that the leaks are only periodically encountered and that the flow rates are never significant or long lasting. Part of the scope of this study was to comment on the validity of these assumptions and to determine how these fluids have evolved from an assumed hypersaline precursor, through rock-water interaction. Such an understanding would be significant for discussion on the origin and movement of these brines and would be invaluable to studies of the saline brines found in the Canadian Shield (Frape and Fritz 1981, 1982). An understanding of their gen-

esis is of relevance to the Canada Nuclear Waste Management Program.

GEOLOGICAL BACKGROUND

Since outcrops of the Salina Formation are scarce, most structural, stratigraphic and lithological information is obtained from drill core. The first hole to penetrate the Salina of Ontario was drilled in 1866. Stratigraphic descriptions and nomenclature were first published in 1945 (Landes 1945) and numerous studies followed which described the various Salina units in more detail, e.g., Roliff (1949), Grieve (1955), Caley (1946), Sanford (1962, 1965, 1969), Hewitt (1962), Dellwig (1953), Guillet (1964), Brigham (1971), Briggs (1958), and Nurmi and Friedman (1977).

The Salina Formation is Upper Silurian in age and consists of dolostone, shale, gypsum, and salt. Maximum regional dip for these rocks is less than 1 degree (Brigham 1971). Dips and thicknesses increase towards the centre of the basin. In subcrop the formation is variable in thickness, averaging 98 m in the Caledonia area and gradually increasing to over 670 m at the centre of the basin. The thinning of the formation from basin centre to basin margin is due principally to the disappearance of halite and the thinning of carbonate beds (Guillet 1964).

The Salina of Ontario represents marginal facies of two barred evaporitic basins, the Michigan Basin centred to the northwest and the Alleghany Trough centred to the southeast (Figure 1). The two basins are separated by the Algonquin Arch which trends northeast across southern Ontario. In Ontario, Goderich and Sarnia are the areas closest to the centre of a basin, and yet occupy only a marginal facies or interpinnacle shelf facies as shown by Nurmi and Friedman (1977).

SAMPLING PROCEDURE

Samples for this study were obtained from a complete core through the Salina from Consumers' Gas holes 33411 and 33406 in the Fletcher Field. This core was sampled extensively to establish complete isotopic data for this area. The Fletcher Field occupies the northern flank of the Algonquin Arch and its oil reserves are found in the Guelph-Salina zone and in Guelph reefs below. The cores sampled are from an inter-reef area.

The lithology of core 33411 and 33406 records a prograding Sabkha sequence through A-1 to B-anhydrite, similar in nature to that described by Nurmi and Friedman (1977). Some examples of typical sedimentary structures found in this core are shown in Figures 2 and 3. Nurmi and Friedman (1977) described this lithological sequence (prograding Sabkha) as proximal to their interpinnacle shelf facies and contemporaneous with the basin centre laminated carbonate-anhydrite layers, A-1, A-2, and B-Salt Members.

Other cores sampled include cores from Domtar's gypsum mine in Caledonia, Ontario. One core was sampled by M.C. Miles in 1982 and another one was selected in 1983. Other cores at Caledonia were sampled by E.C. Appleyard for his area of study. Caledonia represents another Sabkha sequence on the very marginal flanks of the Michigan Basin.

Other samples came from the Sifto Salt Mine workings in the A-2 Salt Member of the Salina Formation. A 4.6 m section was sampled from a 21 m exposure. Mainly the unique horizontal bands were sampled. The bands are composed of euhedral to subhedral dolomite and anhydrite; the petrography of the bands from this mine has yet to be described. Dellwig (1953) briefly described the petrography of the Goderich deposit and indicated that the salt had not retained its original sedimentary features.

Of particular interest was the discovery during this study of idiomorphic authigenic quartz crystals within the halite-dolomite layers. In Denmark and Germany, authigenic quartz has been shown to be a sensitive indicator of local stratigraphic and facies variations (Schettler 1968). In addition, fluid inclusions within the quartz have been used to determine temperature and pressures to which the salt deposits have been exposed during quartz crystal formation (Fabricius 1984). Temperatures obtained from analysis of fluid inclusions in quartz have been shown to be more reliable than those derived from fluid inclusions in halite (Fabricius 1984).

Only one determination of temperature and chemical compositions of fluid inclusions has been done to date because of the time-consuming nature of selecting appropriate crystals, which are on the order of 0.25 to 0.50 mm in size. The halite-dolomite bands were analysed for major and selected minor elements in or-

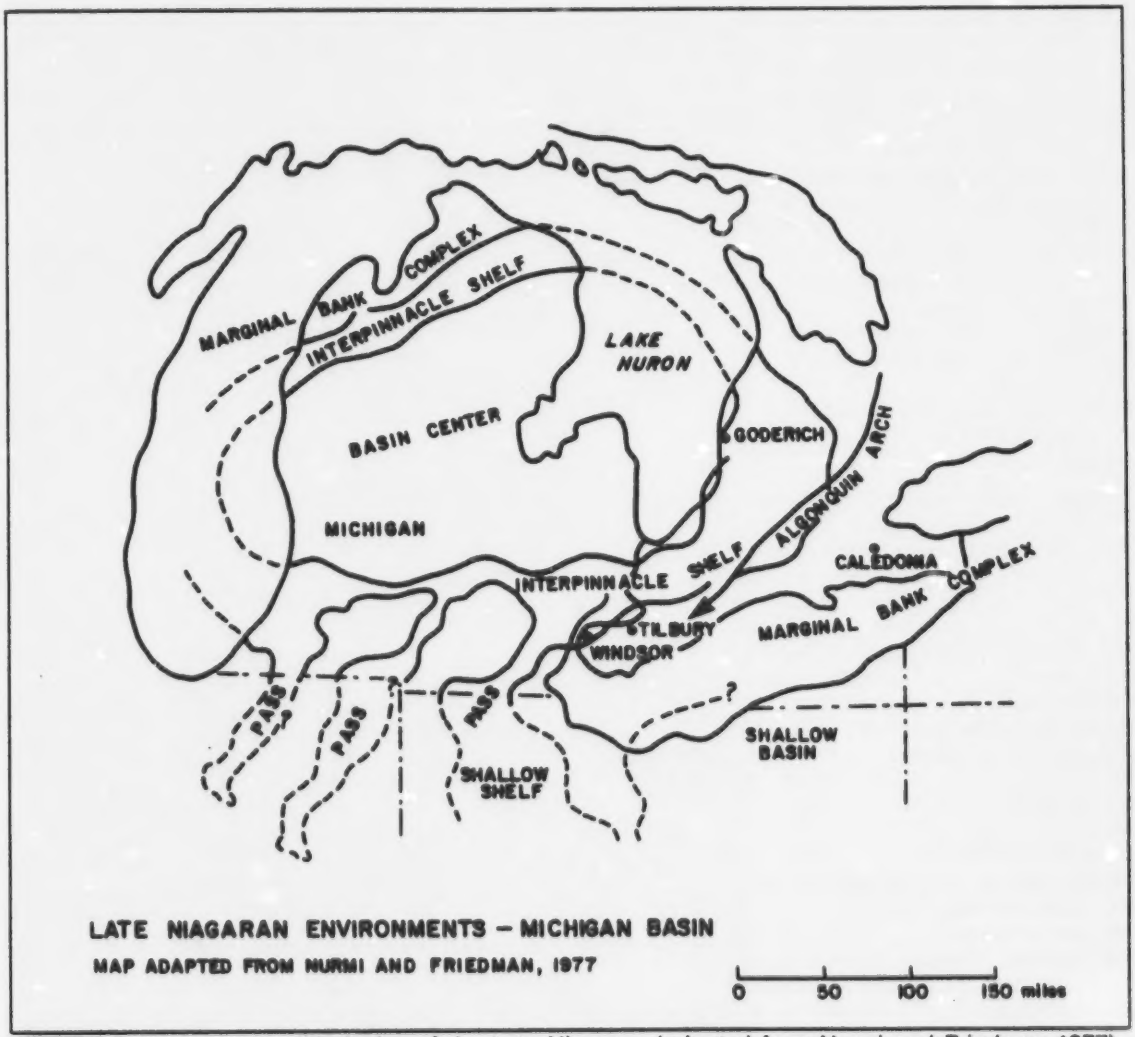

Figure 1. Map showing lithofacies of the Late Niagaran (adapted from Nurmi and Friedman 1977) and locations of the sites sampled in this study.

der to compare the composition of the rocks with the composition of the fluids and to see if there were geochemical trends that would correspond to isotopic trends.

Other samples were obtained from the Canadian Salt Company mine workings which are located in the F-Salt Member. A 2.0 m section was sampled from a 4.5 m exposure, in the same way as at Goderich and similar data was retrieved.

ANALYTICAL RESULTS

Figures 4, 5, and 6 summarize the carbon and oxygen analyses to date. Tables 1 and 2 summarize the brine analyses. Table 3 summarizes the rock salt chemistry at Goderich. Data not included in this report (but summarized in Figure 7) are the chemical analyses of the marl units. No sulphur-34 data was available at time of writing.

DISCUSSION

CARBON–13

Figure 4 depicts the isotopic compositions as correlated to the stratigraphic section at the Fletcher Field. Of note is the remarkable shift from positive to negative $\delta^{13}C$ values at the lower contact of the B-Anhydrite. The $\delta^{13}C$ of the A-1 horizon from hole 33411 averages 2.5‰ (PDB) which correlates with values from the A-1 of hole 33406 where the average value is 2.4‰. The A-1 to A-2 contact on Figure 4 is marked by a very gradual but systematic decline in $\delta^{13}C$ values.

A minor cycle back toward positive $\delta^{13}C$ values in the A-2 is abruptly terminated at the B-Anhydrite contact. The very negative $\delta^{13}C$ values in the B-

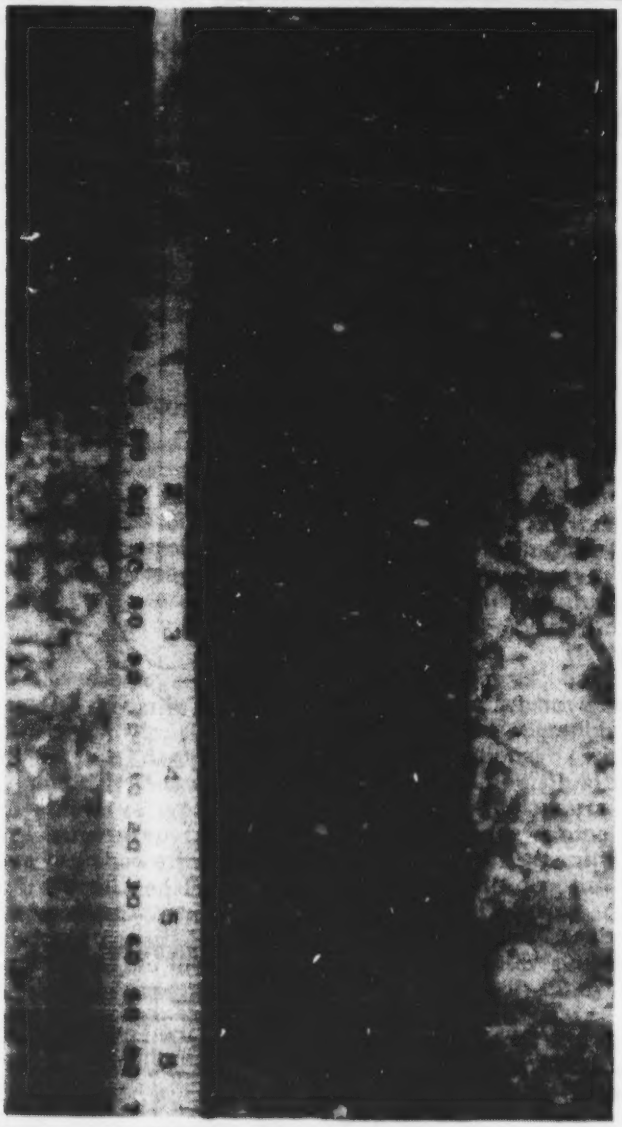

Figure 2. Algal structure from Consumers' Gas core 33411, Fletcher Field, Ontario.

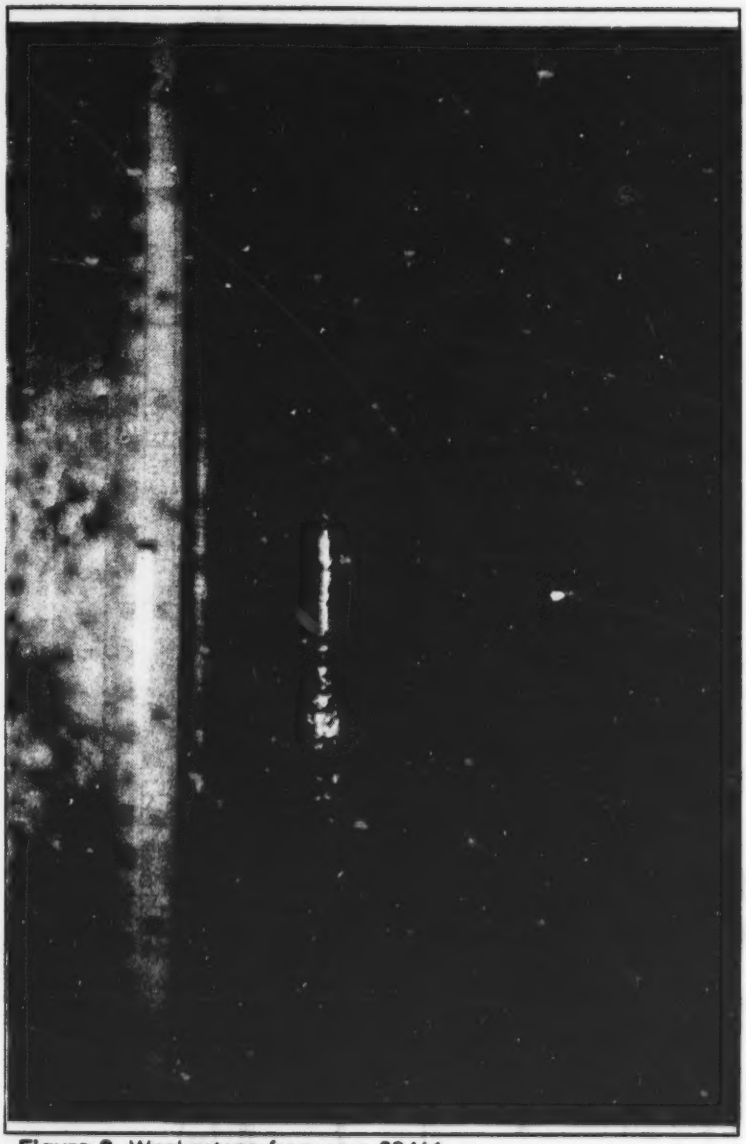

Figure 3. Wackestone from core 33411.

Anhydrite are indicative of the participation of organic CO_2 in the formation of the carbonate present here. The participation of organic CO_2 usually signifies subareal exposure, the development of a soil and/or the presence of photosynthetically active algae, i.e., any terrestrial or restrictive marine environment (Land 1980; Plummer *et al.* 1976; Gross 1964). The shift to these very negative values is also seen in core 33406 and in the core from the Domtar Gypsum mine at Caledonia sampled by Miles (1982).

Therefore the entire marginal facies of the Michigan basin must have been above sea level for a significant time during the deposition of the B-Anhydrite in order to account for the considerable shifts in the $\delta^{13}C$ composition of the carbonates.

Post-depositional secondary changes in carbon-13 contents cannot *a priori* be excluded. However, the contribution of post-depositional processes on the carbon-13 shifts is probably negligible because lithological and petrographical information indicates that the majority of the carbonates are 'primary' or very early diagenetic dolomite and are well preserved. Post-depositional changes are also unlikely because of the relative insolubility of CO_2 which therefore limits the carbon reservoir which could have come in contact with these sediments. In addition, the data clearly show regular, systematic and correlatable fluctuations. As noted, there is a high degree of correlation in ^{13}C fluctuations between core 33411 and core 33406 (Figures 4 and 8).

Also of interest is that after the B-Anhydrite 'episode', the $\delta^{13}C$ values of the

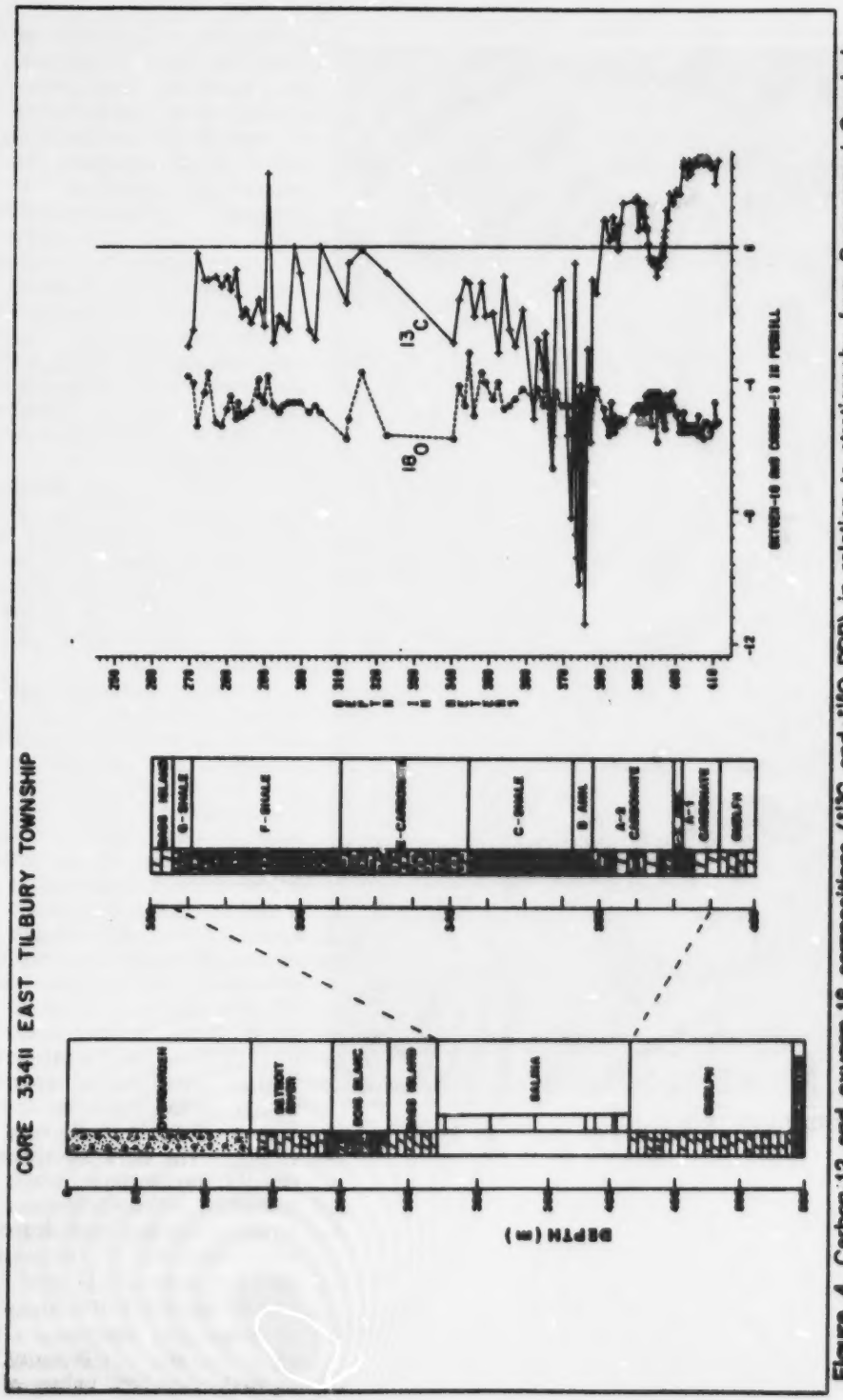

Figure 4. Carbon-13 and oxygen-18 compositions ($\delta^{13}C$ and $\delta^{18}O$ PDB) in relation to stratigraphy from Consumers' Gas hole 33411, Fletcher Field, Ontario.

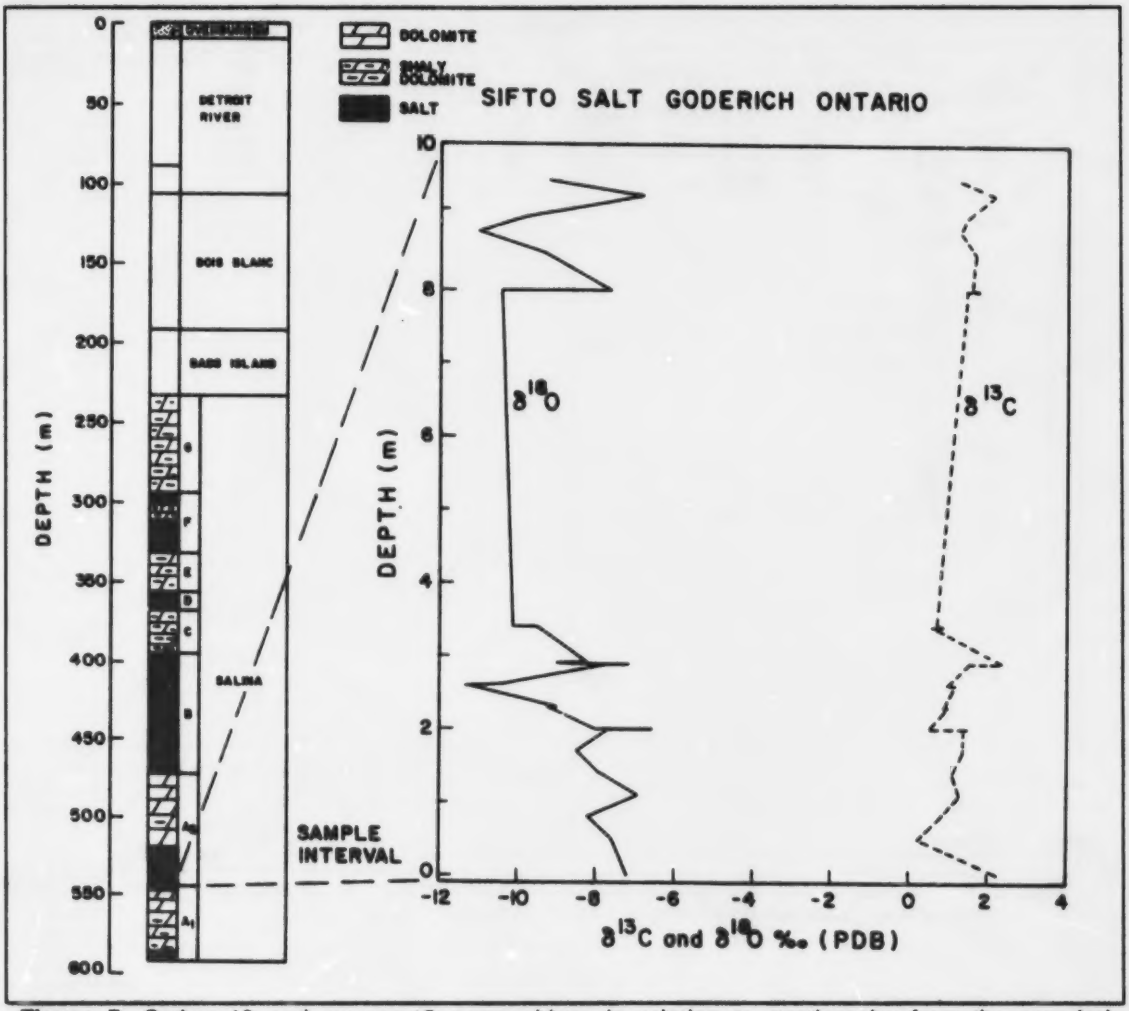

Figure 5. Carbon-13 and oxygen-18 compositions in relation to stratigraphy from the sampled section at the Sifto Salt mine, Goderich.

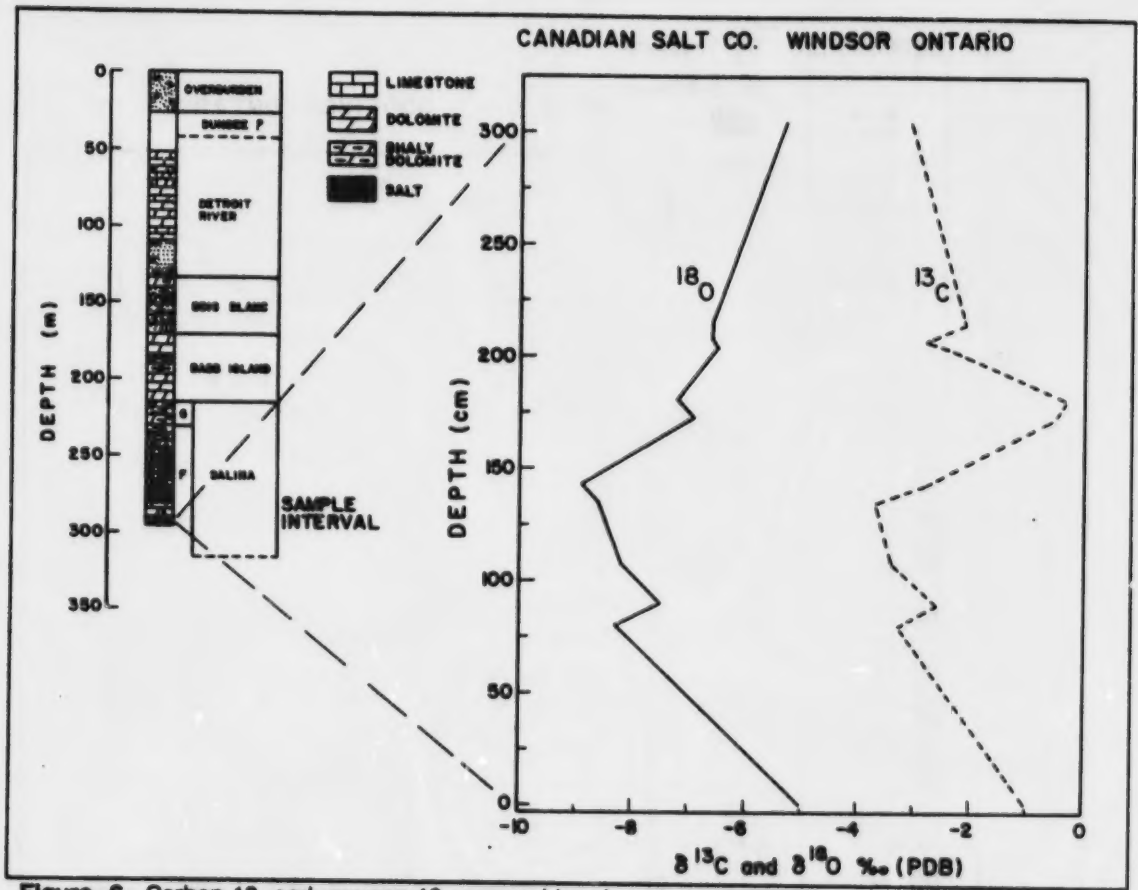

Figure 6. Carbon-13 and oxygen-18 composition in relation to stratigraphy from the sampled section at the Canadian Salt Company mine, Windsor.

TABLE 1. BRINE CHEMISTRY.

Sample	Na mg/L	Mg mg/L	Ca mg/L	K mg/L	Cl mg/L	SO_4 mg/L	Sr mg/L	Br mg/L	B mg/L	Ba mg/L
Sea Water	10925	1314	417	391	19854	2728	8.2	62	-	-
Sifto Drip	33400	18600	48400	5000	232000	110	1620	3220	108	3
Sifto Pool	33600	16200	46800	6400	232000	106	1620	3214	110	3
Canadian Salt	100000	2850	8200	2600	207000	750	214	587	77	3

TABLE 2. INTERPRETIVE BRINE CHEMISTRY.

Sample	Ionic Strength	Na/Cl*	Mg/Ca*	Sr/Ca*	TDS mg/L	Cl/Br	NaCl Log SI	$CaSO_4.2H_2O$ Log SI
Sea Water	0.7	0.85	5.19	$0.9x10^{-2}$	35600	320	-2.2	1.07
Sifto Drip	7.9	0.22	0.57	$1.5x10^{-2}$	340000	72	-0.6	1.7
Sifto Pool	7.9	0.22	0.57	$1.5x10^{-2}$	340000	72	-0.6	1.7
Canadian Salt	5.8	0.74	0.57	$1.0x10^{-2}$	322000	350	-0.2	1.8

Notes.
*Molar ratios
Saturation indices (SI) were calculated assuming activity coefficients were equal to 1 with no ionic complexing.

TABLE 3. ROCK SALT ANALYSES, GODERICH, ONTARIO. ALL ELEMENTS WERE NORMALIZED TO SODIUM AND ARE EXPRESSED IN PPM HALITE.

	K	Ca	Mg	Mn	Sr	Fe	SO_4	Na	Cl	ELEV	SAMPLE
1	101.5	2212.2	100.2	2.7	27.1	17.1	3468.4	393373	664081	-	E-1
2	-	34923.8	213.0	4.8	539.2	11.5	82704.2	393373	663936	-	G-24
3	111.8	4077.6	3.7	2.2	23.7	15.8	6956.0	393373	657220	-	RET
4	105.9	3618.1	105.9	2.2	51.5	14.1	5779.2	393373	679903	0.5	G-22
5	81.3	881.3	77.9	3.0	21.2	17.8	609.0	393373	608971	0.8	G-21
6	74.0	5113.8	62.9	2.4	55.1	16.7	8024.8	393373	652999	1.1	G-20
7	75.8	1176.4	69.9	2.0	18.4	15.5	1384.1	393373	611913	1.4	G-19
8	86.2	2341.5	84.3	2.2	42.3	18.0	2847.3	393373	670607	1.7	G-18
9	82.5	2760.1	80.9	2.5	48.8	15.9	3744.6	393373	635448	2.0	G-15
10	81.2	2415.8	68.0	2.3	44.0	16.0	-	393373	-	2.0	G-17
11	86.0	3644.5	86.4	2.8	31.2	17.4	5514.9	393373	647908	2.3	G-13
12	76.8	2345.1	73.8	2.8	22.1	16.6	3252.9	393373	658143	2.3	G-14
13	86.2	2261.0	90.1	2.8	22.8	16.7	-	393373	-	2.6	G-11
14	73.3	1991.1	73.8	2.6	16.8	14.1	2039.7	393373	656621	2.6	G-12
15	89.6	4011.6	83.0	2.8	36.9	17.5	5861.1	393373	654323	2.9	G-4
16	504.3	10036.0	349.0	2.6	133.1	17.9	16967.6	393373	640491	2.9	G-7
17	119.5	5245.0	139.5	2.3	39.3	14.2	8559.5	393373	611913	5.0	G-25
18	140.5	4616.1	134.5	2.3	36.5	15.3	7546.3	393373	654283	5.0	G-26
19	108.6	2577.5	105.6	2.2	19.1	15.5	4420.7	393373	588185	5.8	G-30
20	108.8	4392.0	116.5	2.4	34.9	16.2	6855.3	393373	656894	6.3	G-31
21	92.8	5826.4	85.4	2.5	50.1	14.5	9945.6	393373	645725	6.5	G-32

rest of the sequence remain for the most part negative. The A-1 and A-2 Carbonates average 2.5‰ and 0.4‰ (PDB), but above the B-anhydrite, the $\delta^{13}C$ values generally average -2.0‰. The carbonate from the A-2 Salt at Goderich averages 1.4‰ in agreement with an A-1 to A-2 transition from positive to negative $\delta^{13}C$ values found at the Fletcher Field. The carbonate from the F-Salt layer at Windsor averages -2.3‰ (PDB), correlating with an average $\delta^{13}C$ of -1.5‰ for the same stratigraphic unit from the Fletcher Field.

Our opinion at this time, which is subject to corroboration from the pending sulphur-34 results and the examination of basin centre cores, is that with the exception of the B-Anhydrite 'episode', the $\delta^{13}C$ fluctuations between the A units and the rest of the Salina sequence are carbon-budget

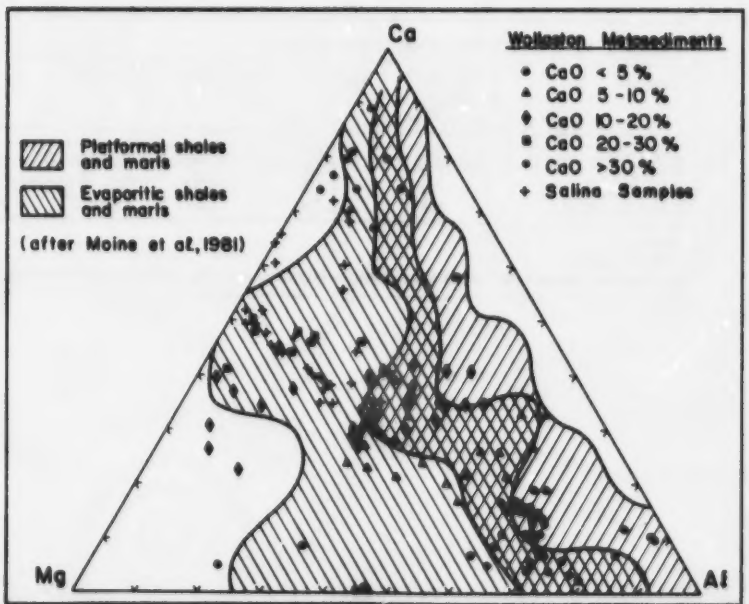

Figure 7. Ternary diagram depicting the Salina marl units in relation to geochemical facies and Wollaston (meta-evaporite?) Metasediments, Saskatchewan (Moine et al. 1981).

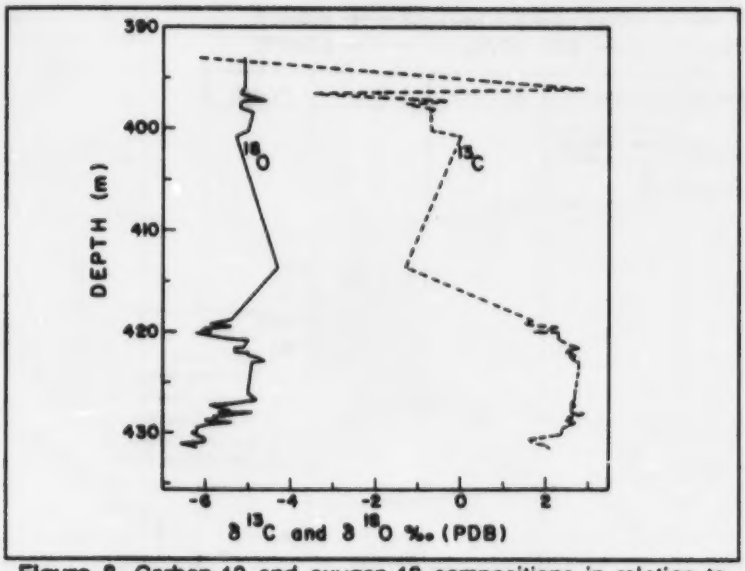

Figure 8. Carbon-13 and oxygen-18 compositions in relation to stratigraphy from Consumers' Gas hole 33406, 8 km north of hole 33411. Note the A-1, A-2 and B-Anhydrite trend in carbon-13 values correlative to core 33411.

controlled. There appear to be minor cycles within the sequence and one megacycle. The minor cycles are still quite difficult to assess. The megacycle is more easily explained.

The megacycle referred to is the shift from positive $\delta^{13}C$ values in the A units to the generally negative $\delta^{13}C$ values of the C-D-E-F-G units. This can be explained by reference to Figure 9 (from Matthews and Egleson 1974). Based on Br profiles from salt units within the centre of the Michigan Basin, Matthews and Egleson (1974) proposed an evolutionary history for the Michigan Basin. The A to B rock units represent a period of time during which the originally deep basin filled, upon precipitation of basinal evaporites. This concept has implications on previously determined subsidence rates and the tectonic history of the Michigan Basin.

The deep basin period was an anoxic event as the waters were hypersaline (potash facies in the A-1 Salt) and most likely density stratified. Flow out to the ocean was restricted but inflow kept the basin more or less water filled until the B-Anhydrite deposition. Hence positive or 'normal' marine $\delta^{13}C$ values are recorded in the carbonate deposited during this time, either on the marginal banks or deeper in the basin. The question remains however: Do the $\delta^{13}C$ values of the A units reflect burial of organic carbon or do they reflect an open marine situation?

This question may be clarified by sulphur-34 analyses; however, one qualitative observation is offered to support carbon-balance control. The observation is that the A units at the Fletcher Field are quite organic rich. Some layers grade 10% total organic carbon (TOC), whereas the succeeding C to G units are generally less than 0.5% TOC. Therefore there is a gross correlation between the organic content of the units and their ^{13}C composition.

Matthews and Elgeson (1974) proposed that after deposition of the B-Anhydrite, the basin was virtually filled and subsequent filling was subsidence controlled. The younger sediments became progressively thinner and the brine involved in the deposition of the later evaporites became smaller in volume. The basin was now shallower, less saline and as a result more oxidizing. Hence, organic carbon produced would be oxidized giving the trend to more negative $\delta^{13}C$ values, as detected in this study. An increase in biological respiration as the result of the basin being shallower and perhaps more restricted could also be a factor in this trend. Regardless of the interpretation, however, two different basinal environments are represented by the carbon-13 data.

Future work involves obtaining core material from deeper in the basin, to evaluate this carbon balance theory. If similar trends can be found then facies effect on ^{13}C can be ruled out and perhaps carbon budget calculations can be made for the Michigan Basin.

OXYGEN–18

The interpretation of oxygen-18 compositions from carbonates is more difficult since the oxygen of the carbonate is readily exchangeable with the oxygen of water. There is some controversy as to the usefulness of ^{18}O values ob-

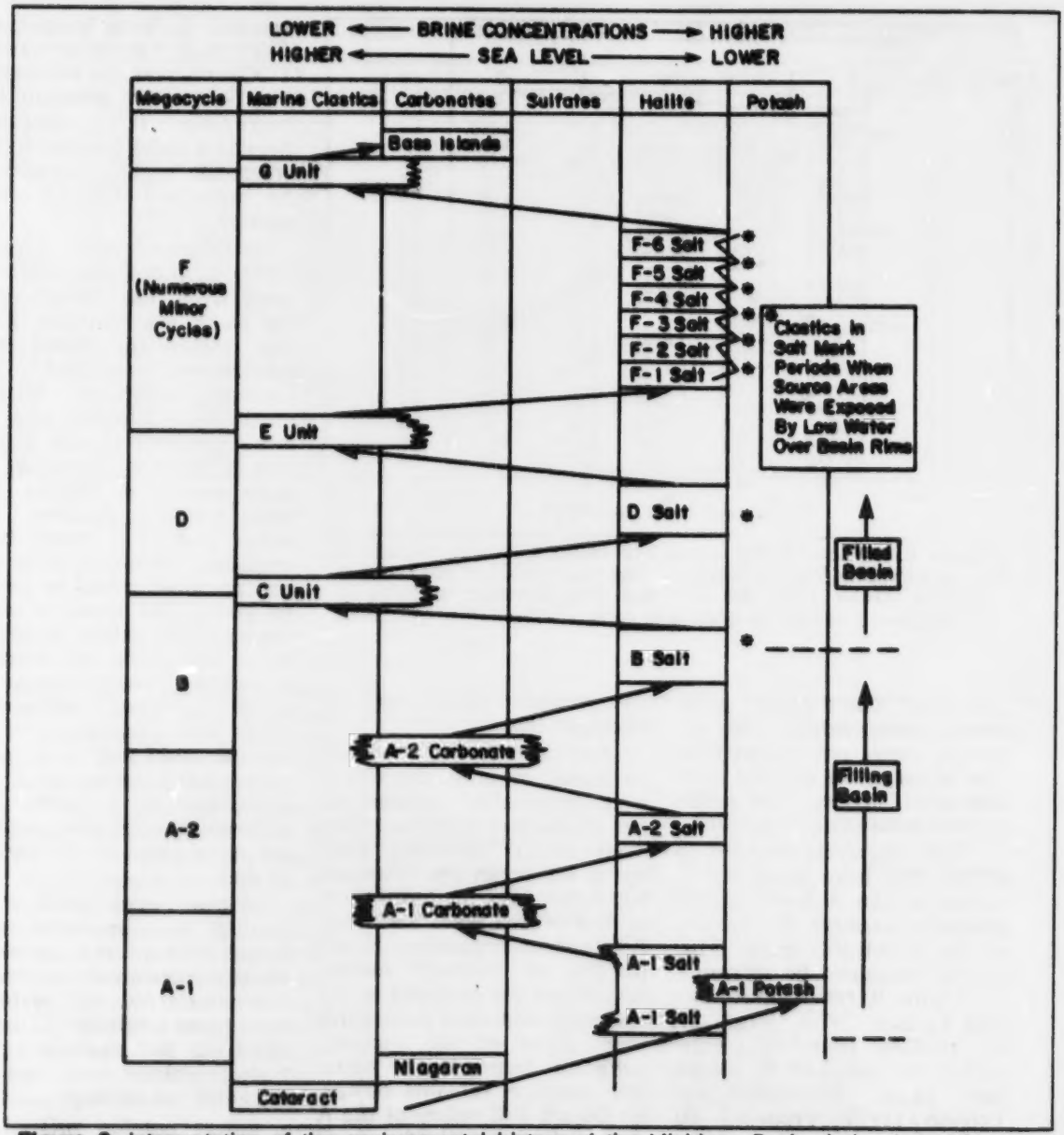

Figure 9. Interpretation of the environmental history of the Michigan Basin during Late Niagaran time (from Matthews and Egleson 1974). Our data supports their interpretation.

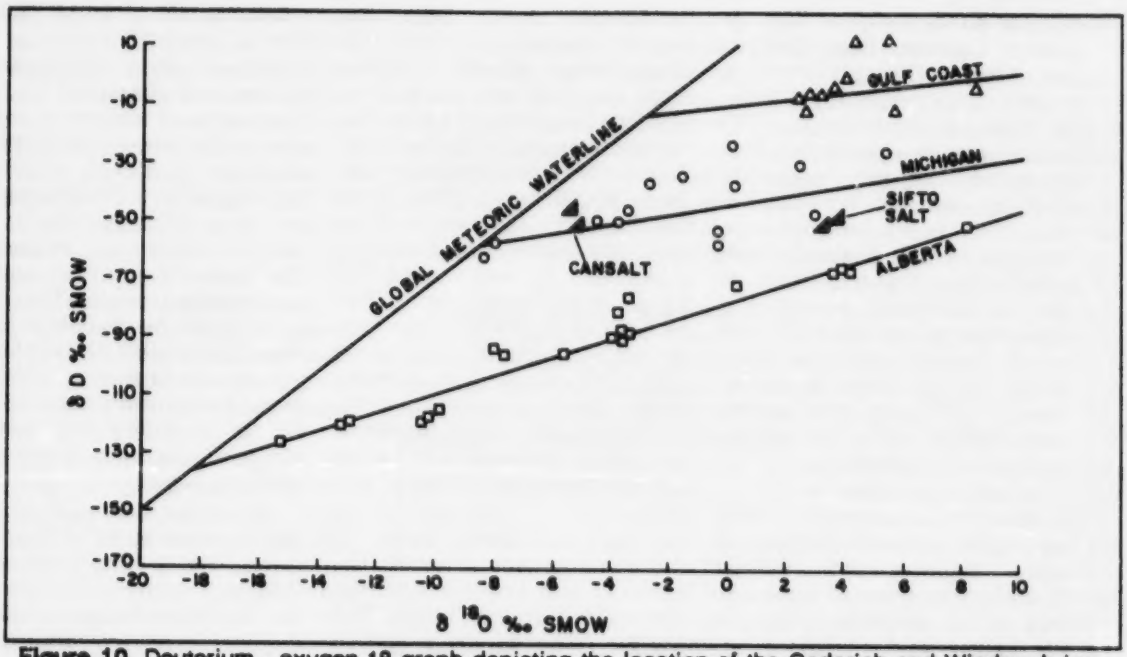

Figure 10. Deuterium - oxygen-18 graph depicting the location of the Goderich and Windsor brines in relation to other known basin brines and meteoric waters.

tained from ancient carbonates. Land (1980) maintained that the early chemical and oxygen isotopic composition of carbonates has been largely but not completely erased by later processes. However, Fritz and Jackson (1972) concluded from ^{18}O compositions and petrography that the ^{18}O composition of Devonian seas were different from today's.

It can be seen at first glance that the ^{18}O values from most of our locations display rather uniform values: for example, the mean $\delta^{18}O$ from core 33411 is -5.0‰ (PDB) with a standard deviation of only 0.6‰. The mean from core 33406 is -5.3‰ (PDB) also with a standard deviation of 0.6‰. Oxygen-18 values from Goderich and Windsor are less uniform and more depleted in ^{18}O. At Goderich the mean $\delta^{18}O$ is -8.7‰ (PDB) with a standard deviation of 1.3‰. At Windsor the mean is -7.1‰ with a standard deviation of 1.2‰. These differences are probably primary in nature and not the result of secondary exchange, i.e., recrystallization processes. The principal mineral phase of the carbonate at Goderich and Windsor is calcite, whereas at the Fletcher Field it is dolomite. The distinction between the two carbonates is based on X-ray diffraction traces, in accordance with Clayton *et al.* (1968). However, the isotopic differences between the dolomite and the calcite as represented at the different localities may represent the isotopic fractionation between calcite and dolomite.

Calcite enclosed in the water-'impermeable' halite deposits of Windsor and Goderich has ^{18}O compositions that require either a high temperature (50-60°C), or a seawater depleted with respect to modern water. The alternative to these conditions is the possibility that the salt is not impenetrable to meteoric water i.e. secondary ^{18}O loss. Another possibility, from consideration of sulphate and SiO_2 ^{18}O data, is that $^{18}O/^{16}O$ fractionation factors are affected by high salinity solutions.

At 25°C, the water that precipitated the Goderich calcite (enclosed as bands in halite from a supposed deeper basin environment) would have to have been 6.5‰ lighter than seawater today, unless one considers the other previously mentioned factors. At Windsor the value is 2.4‰ lighter with respect to modern ocean water.

If the Windsor deposit (part of the F unit) is considered to represent a shallow deposit (Matthews and Elgeson 1974; Dellwig 1953) possibly

similar to deposits at Ojo de Liebre Lagoon, Baja California, Mexico (Phleger 1969), a higher temperature (51°C) can be imposed, such that the ^{18}O results are in agreement with predicted values assuming modern seawater ^{18}O compositions. This is not believed to be the case in that shallow water sedimentary features such as detrital dolomite, quartz and other detrital minerals are not found. Subareal exposure similar to Ojo de Liebre is not indicated either in the isotope compositions or in the petrography of the deposit.

Exchanges with brines at elevated temperatures could also cause minor shifts toward more negative ^{18}O values. However, this would probably lead to an homogenization of ^{13}C values and therefore appears as a process of unlikely significance.

BRINES

The brines in the mine workings at Goderich and Windsor have a very large dissolved solid load and are Ca-Na-Cl brines. They contain the same order of magnitude of total dissolved solids (TDS) as do some deep seated Canadian Shield brines and many Michigan Basin brines. Isotopically, the brines also resemble other Michigan Basin brines (Figure 10). The brines found in the Michigan Basin and in this study do not chemically resemble Canadian Shield brines. The chemical distinction lies primarily in the Mg values and the Cl/Br ratios. Also, Canadian Shield brines have significantly different ^{2}H and ^{18}O values than brines found in the Michigan Basin.

Chemically, the Goderich Ca-Na-Cl-Mg brine resembles brines found in the Sylvania Sandstone, Middle Devonian, State of Michigan, and the Niagara Group, Middle Silurian, State of Michigan, as well as closely resembling formation waters from above in the Stray Sandstone, Late Mississippian, State of Michigan. Data from Graf *et al.* (1966) were used in the comparison. The Goderich brine in no way resembles brines taken from the Salina by Graf *et al.* (1966). This may be understandable since Graf may have obtained his samples from active brining wells. Therefore, his brines represent secondary dissolution of Salina salt members by meteoric waters.

The Goderich brine is more saline, has more K, Ca, and Mg and less Na and SO_4 than the Windsor brine. The Mg/Ca ratios of the Goderich and Windsor brines are identical. Isotopically, the Goderich brine is further removed from the Global Meteoric Water Line (GMWL) (see Figure 10) than is the Windsor brine. The GMWL is a line which represents a linear fit to world-wide observations of the deuterium-oxygen-18 values found in precipitation and groundwaters. The Windsor brine possesses a higher Cl/Br ratio which indicates a component of halite solution. This is also reflected in the higher Na and SO_4 concentrations.

The Goderich brine has a low Cl/Br ratio, suggestive of either a connate water unrelated to the bitterns residual to the crystallization of salt rock (Holser 1965) or a formation water that is residual after precipitation of halite (Graf *et al.* 1966). Since the overall chemical composition of the Goderich brine is more related to Michigan Basin formation waters and less to evaporated seawater, the former conclusion is favoured.

Based upon consideration of the rock chemistry and the chemical and isotopic composition of the brines, the brine at Goderich (a deeper, more central region of the Michigan Basin) is a Michigan Basin formation water not related to the halite formation and of controversial origin. The brine at Windsor (a shallower, more marginal region of the Michigan Basin) is also a Michigan Basin formation water, however, its chemical and isotopic compositions have a signature of halite solution.

A major 'discontinuity' in the interpretation arises from the discovery of tritium in the Goderich brine. The presence of ^{3}H (created in significant quantities in the atmosphere during the 1960s H-bomb tests) is indicative of the mixing of young meteoric water. A minor amount of meteoric water must be involved because the chemical compositions, the ^{2}H and the ^{18}O values are very different from local meteoric waters. In addition no halite solution is indicated. At Windsor, where solution appears to have had an effect on the chemical composition, the ^{2}H and the ^{18}O values, no tritium was found. One can only conclude that the Windsor solution 'event' was not related to modern meteoric water. Tritium must have been introduced into the Goderich sample either during sampling or during the recent mining activities.

AUTHIGENIC QUARTZ

Authigenic idiomorphic quartz crystals were discovered within the carbonate-sulphate-halite bands present at Goderich and Windsor. Due to the difficult

nature of isolating good fluid inclusions in the quartz grains, only one chemical composition and temperature measurement from one crystal from Goderich have been done to date. The fluid inclusion is principally $CaCl_2$ with an enclosing temperature determined to be 115°C. Oxygen isotopic composition of the quartz crystals yield excessively low values, averaging +4‰(SMOW) on three samples. Most detrital, igneous and metamorphic quartz averages 10-30‰ (SMOW).

At this time we have no adequate explanation for the oxygen isotope results from quartz. What is known is that the quartz could not have precipitated in equilibrium with either seawater or the brines that are presently found in the Salina. The temperature of fluid inclusion formation of 115°C is also too high a temperature since it has long been considered that the maturation level of the Salina is mature to submature (i.e.<65°C, Heroux *et al.* 1979). Perhaps a short thermal event was recorded by these crystals. The crystals also would appear to record the intrusion of a Ca-Cl brine into Salina rocks. Such brines may be similar to those found in the Canadian Shield.

MARL

A reconnaissance study of the major and trace elements compositions of shales, marls and argillaceous carbonates was completed on 40 samples collected from two sites, a suite of 10 boreholes at the Caledonia Gypsum Mine and Hole 33411 near Tilbury. The samples can be classified as dolomitic argillite (5-10% CaO), dolomitic marl (10-20% CaO), argillaceous carbonate (20-30% CaO) and carbonate (>30% CaO). For the most part, corresponding lithologies from the two sites have very similar compositions in accordance with the similar depositional setting as in Nurmi and Friedman's (1977) marginal bank complex. Higher F and Sr values are present at Caledonia than at the Fletcher Field.

Evaporite related argillites, marls and, to a lesser extent, carbonates possess unique geochemical characteristics which serve to distinguish them from analogous sediments formed under normal marine conditions (Moine *et al.* 1981). Hypersaline characteristics of the Salina samples include B/Al ratios >0.006, MgO/(MgO + FeO) >0.85, K/Al >0.4, Li usually >100 ppm, combined with high Li/Mg, Sr >1000 ppm in sulphate-bearing sediments, F frequently >1000 ppm and up to 3400 ppm, Br/Cl = 0.022.

The lithogeochemistry of shales, marls and carbonates from the Caledonia and Fletcher Field sites differs principally in the higher F and Sr values at Caledonia. These relationships indicate that water of lower salinity was present at Caledonia than at the Fletcher Field according to Jeans (1978) facies models for the Keuper Marl of England and western Europe.

FUTURE WORK

Some questions arising from the first year's work may be resolved by pending studies. Sulphur-34 and oxygen-18 analyses of anhydrite from the Fletcher Field and elsewhere are ongoing. Some cores from the central part of the basin are being selected for an isotopic survey of carbonate and sulphate, quartz crystals and clay minerals.

A major thrust of future work is to analyse the marl units of the Salina with a view to characterizing their environment of deposition as specifically related to the salinity. Work by Jeans (1978) on the Keuper Marl of England has determined specific suites of clay minerals with varying salinities. Trace and minor element composition forms an important facet of the mineralogical study of the marls. After further data are collected from the marl units, more precise sea inlet and outlet locations may be determined. The clay mineral study in conjunction with the other work should provide a better understanding of the environments and history of the Salina Formation.

ACKNOWLEDGMENTS

Gratitude is expressed to Domtar Chemicals Group, Sifto Salt Division, and their mine geologist, Don Dickie, for permission to sample and tour their Goderich and Caledonia facilities. Equal gratitude is expressed to the Canadian Salt Company and their geologist, Dr. Nordau Goodman, mine superintendant, Bob Giegerich, and mine engineer, Ray Holliday, whose help during the sampling was greatly appreciated. Cores 33411 and 33406 were provided through the generous auspices of the Consumers' Gas Company. As well, thanks go to Dr. J. Guha, Universite du Quebec a Chicoutimi, for the analysis of the quartz fluid inclusions and to Dr. R. Kerrich, University of Western Ontario, for the oxygen-18 analyses of the quartz. Final thanks go to all the technicians at the Isotope

Geochemistry Laboratory, University of Waterloo and to Mike Jones and Glen McGill, summer assistants on this project's first year.

REFERENCES

Brigham, R.J.
1971: Structural Geology of Southwestern Ontario and Southeastern Michigan; Ontario Department of Mines and Northern Affairs, Petroleum Resources Section, Paper 71-2.

Briggs, L.I.
1958: Evaporite Facies; Journal of Sedimentary Petrology, Volume 28, Number 1, p.46-56.

Caley, J.F.
1946: Paleozoic Geology of the Windsor-Sarnia Area, Ontario; Geological Survey of Canada, Memoir 240.

Clayton, R.N., Jones, B.F., and Berner, R.A.
1968: Isotope Studies of Dolomite Formation Under Sedimentary Conditions; Geochimica et Cosmochimica Acta, Volume 32, p.415-432.

Dellwig, L.F.
1953: Origin of the Salina Salt of Michigan; Journal of Sedimentary Petrology, Volume 25, p.83-110.

Fabricius, J.
1984: Studies of Fluid Inclusions in Halite and Euhedral Quartz Crystals from Salt Domes in the Norwegian-Danish Basin; Sixth Symposium on Salt, Northern Ohio Geological Society, Volume 1, p.15-35.

Frape, S.K., and Fritz, P.
1981: A Preliminary Report on the Occurrence and Geochemistry of Saline Groundwaters on the Canadian Shield; Atomic Energy of Canada Ltd., Technical Report 136, 71p.
1982: The Chemistry and Isotopic Composition of Saline Groundwaters from the Sudbury Basin, Ontario; Canadian Journal of Earth Sciences, Volume 19, Number 4, p.645-661.

Fritz, P., and Jackson, S.A.
1972: Geochemical and Isotopic Characteristics of Middle Devonian Dolomites from Pine Point, Northern Canada; 24th International Geologic Congress, Section 6.

Graf, D.L., Meents, W.F., Friedman, I, and Shimp, N.F.
1966: Origin of Saline Formation Waters, III: Calcium Chloride Waters; Illinois State Geological Survey, Circular 397.

Grieve, R.O.
1955: Leaching (?) of Silurian Salt Beds in Southwestern Ontario as Evidenced in Wells Drilled for Oil and Gas; Canadian Institute of Mining and Metallurgy, Transactions, Volume 58, p.10-16.

Gross, M.G.
1964: Variations in the $^{18}O/^{16}O$ and $^{13}C/^{12}C$ Ratios of Diagenetically Altered Limestone in the Bermuda Islands; Journal of Geology, Volume 72, p.170-194.

Guillet, G.R.
1964: Gypsum in Ontario; Ontario Department of Mines, Industrial Mineral Report, Number 18.

Hewitt, D.F.
1962: Salt in Ontario; Ontario Department of Mines; Industrial Mineral Report 6.

Heroux, Y., Chagnon, A., and Bertrand, R.
1979: Compilation and Correlation of Major Thermal Maturation Indicators; American Association of Petroleum Geologists Bulletin, Volume 63, p.2128-2144.

Holser, W.T.
1965: Bromide Geochemistry of Salt Rocks; Second Symposium on Salt, Northern Ohio Geological Society, Volume 1, p.248-276.

Jeans, C.V.
1978: The Origin of the Triassic Clay Assemblages of Europe with Special Reference to the Keuper Marl and Rhaetic of Parts of England; Philosophical Transactions of the Royal Society of London, Volume 289, series A, p.549-637.

Land, L.S.
1980: The Isotopic and Trace Element Geochemistry of Dolomite: The State of the Art; Society of Economic Paleontologists and Mineralogists (SEPM), Special Publication 28, p.87-110.

Landes, K.K.
1945: The Salina and Bass Island Rocks in the Michigan Basin; United States Geological Survey, Preliminary Map 40.

Matthews, R.D., and Egleson, G.C.
1974: Origin and Implications of Mid-Basin Potash Facies in the Salina Salt of Michigan; Fourth Symposium on Salt, Northern Ohio Geological Society, Volume 1, p.15-35.

Miles, M.C.
1982: A Study of the Isotopic Composition of the Salina Formation Gypsum Deposit at Caledonia, Ontario; Unpublished B.Sc. Thesis, University of Waterloo.

Moine, B., Sauvan, P., and Jarousse, J.
1981: Geochemistry of Evaporite-Bearing Series: A Tentative Guide for the Identification of Meta-Evaporites; Contributions to Mineral Petrography, Volume 76, p.401-412.

Nurmi, R.D., and Friedman, G.M.
1977: Sedimentology and Depositional Environments of Basin-centre Evaporites, Lower Salina Group (Upper Silurian), Michigan Basin; *in* Reefs and Evaporites - Concepts and Depositional Models, American Association of Petroleum Geologists, Studies in Geology Number 5.

Phleger, F.B.
1969: A Modern Evaporite Deposit in Mexico; American Association of Petroleum Geologists Bulletin, Volume 53, Number 4, p.824-829.

Plummer, L.N., Vacher, H.L., MacKenzie, F.T., Bricker, O.P., and Land, L.S.
1976: Hydrogeochemistry of Bermuda: A Case History of Groundwater Diagenesis of Biocalcarenites; Geological Society of America Bulletin, Volume 87, p.1301-1316.

Roliff, W.A.
1949: Salina-Guelph Fields of Southwestern Ontario; American Association of Petroleum Geologists, Bulletin, Volume 33, Number 2, p.153-188.

Sanford, B.V.
1962: Sources and Occurrences of Oil and Gas in the Sedimentary Basins of Ontario; Geological Association of Canada, Proceedings, Volume 14.
1965: Salina Salt Beds - Southwestern Ontario; Geological Survey of Canada, Paper 65-9.
1969: Silurian of Southwestern Ontario; Ontario Petroleum Institute, Technical Report 5.

Schettler, H.
1968: The Stratigraphic Significance of Idiomorphic Quartz Crystals in the Saline Formation of the Weser-Ems Area, Northwestern Germany; p.111-127 *in* Geology of Saline Deposits; Proceedings of the Hanover Symposium, United Nations Educational, Scientific and Cultural Organization (UNESCO), Earth Sciences, Volume 7.

Scholle, P.A., and Arthur, M.A.
1980: Carbon Isotope Fluctuations in Cretaceous Pelagic Limestones:

Potential Stratigraphic and Petroleum Exploration Tool; American Association of Petroleum Geologists. Bulletin, Volume 64. p.67-87.

Grant 149 Structural Signature and Tectonic History of Deformed Gold-Bearing Rocks in Northwestern Ontario

H. Hugon and W.M. Schwerdtner

Department of Geology, University of Toronto

ABSTRACT

Deformed variolites, xenoliths, pillows, mineral grains and polycrystalline aggregates show that foliation surfaces are approximately normal to the trajectories of maximum total shortening throughout most of the Red Lake greenstone belt. Regional foliation surfaces within greenstone roughly follow the boundaries of the oval granitoid bodies. The foliation pattern, together with a prevailing down-dip stretch lineation, strongly suggest that the strain in this belt was mainly accumulated during the rise and expansion of the surrounding plutonic rocks. Departures from the trend of the regional foliation occur around the Dome and Keg Lake stocks. Here the total strain includes a large component of late transcurrent shear, and the foliation patterns have been strongly influenced by the horizontal deformation.

In the Madsen and Starratt-Olsen areas, left-lateral displacement is indicated by the large-scale pattern of foliation and by many zones of sinistral ductile shear at the outcrop scale. Discrete shear zones of which the Austin Shear Zone (ASZ) is by far the largest, also occur on an intermediate scale.

Ductile shearing, regional metamorphism, local rock alteration and batholith emplacement have a close spatial and temporal relationship. Because the richest gold ore is found in those portions of the ASZ that are most-strongly foliated it may be possible to correlate ore grade with the intensity of total deformation.

Specimens of Madsen ore exhibit lenticles of free gold that are less elongate than adjacent highly stretched sulphide lenses. Apparently, the gold lenticles are less deformed than aggregates of massive sulphides. This in turn suggests that the free gold crystallized no earlier than in the late stages of sinistral shearing.

INTRODUCTION

Prior to initiation of this project, the Madsen and Starratt-Olsen orebodies were regarded as strata-bound deposits hosted by heterogeneous, highly-altered tuff units (Durocher 1983). The largest unit containing the Madsen "main ore zone" was called the Austin Tuff (Horwood 1945; Ferguson 1965, 1968).

This contribution will show that, no matter what the actual protolith of the Austin 'tuff', it is now composed of highly-strained metamorphic rocks that fall into a discrete band of severe ductile deformation, the Austin Shear Zone. We made a field-based structural study in 1983 of the Austin Shear Zone, and are attempting to comprehend the deformational history of the Madsen area and its vicinity. The rocks of the Austin Shear Zone have a characteristic structural signature, which will be described in the following section. Unfortunately, we were unable to study the gold deposits underground, and had to be content with analyzing unoriented samples.

GENERAL GEOLOGY

The geology of the Red Lake belt is shown in simplified form in Figure 1a; a more detailed map of the Madsen area is shown in Figure 1b. Three volcanic cycles have been recognized (Wallace 1982) and have been dated by the zircon U-Pb method. The first cycle has been dated at 2990 to 2925 Ma, the second at 2840 to 2800 Ma, and the third at 2760 to 2740 Ma (F. Corfu, Geochronologist, Jack Satterly Geochronology Laboratory, Royal Ontario Museum, personal communication, 1984). The latest event was the emplacement of batholiths and stocks which took place about 2720-2700 Ma. The Killala-Baird batholith which has an age ranging from 2710 to 2700 Ma (preliminary results of U-Pb dating, F. Corfu, 1984, personal communication) represents the youngest granitoid body known in the Red Lake belt. Batholiths and stocks appear to young from north to south. The following dates are available: 2718 Ma for the Dome and McKenzie stocks and between 2710 and 2700 Ma for the Killala-Baird batholith (preliminary results of U-Pb dating, F. Corfu 1984, personal communication). Accordingly, diapir-related strain within volcanic rocks is youngest in the southern part of the belt, i.e., in the Madsen and Starratt-Olsen areas (Figure 1a). Thus considerable amounts of late stage strain, associated with the rise and expansion of batholiths must have occurred in the Madsen and Starratt-Olsen areas.

The rocks of the Madsen area (Figure 1b) can be divided

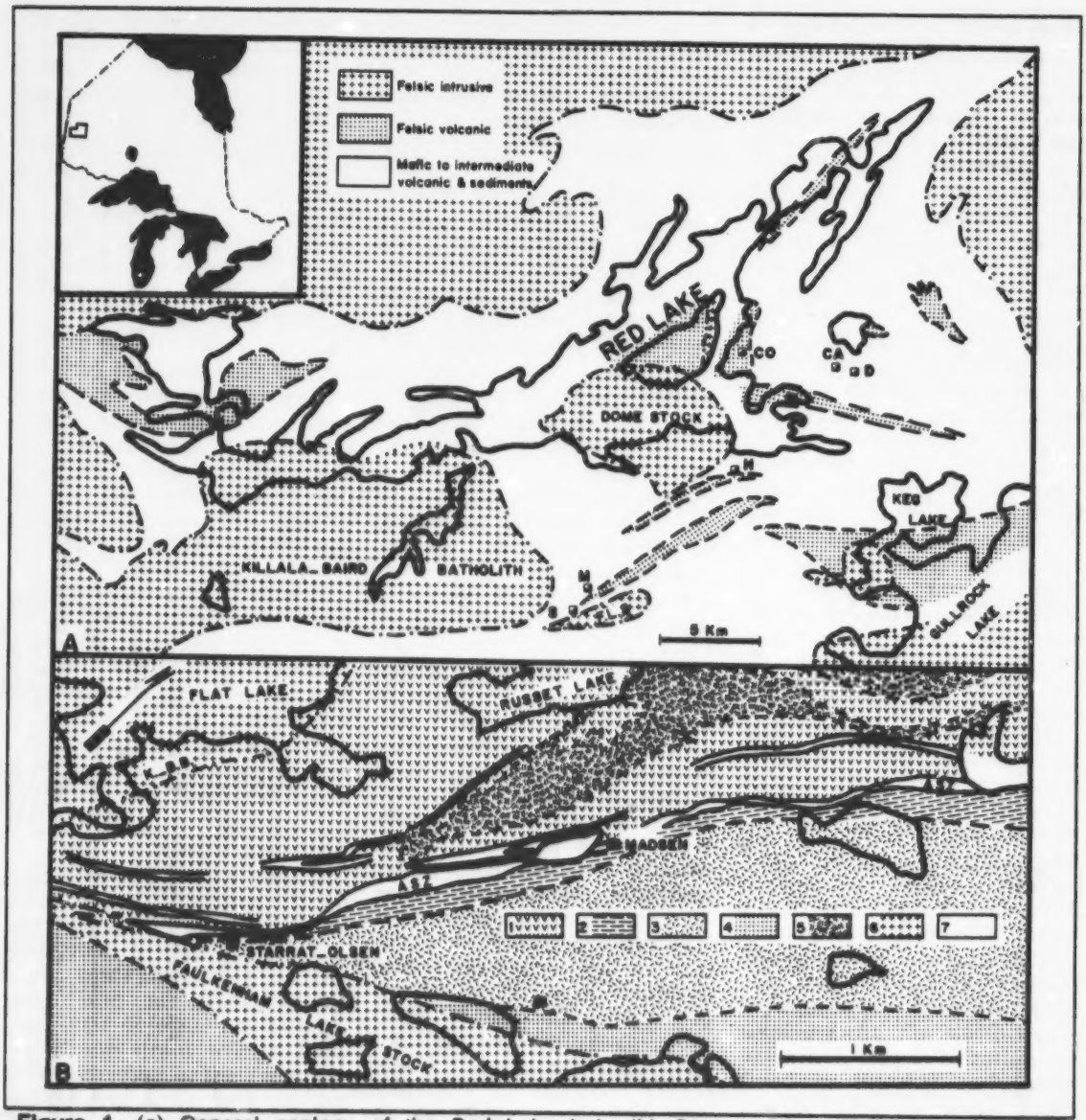

Figure 1. (a) General geology of the Red Lake belt. (b) Geology of the Madsen area. S = Starratt-Olsen Mine, M = Madsen Mine, H = Howey-Hasaga Mine, D = Dickenson Mine, CA = Campbell Mine, CO = Cochenour Mine, F.L.S. = Faulkenham Lake Stock. Geologic legend for Madsen area: (1) mafic and ultramafic rocks, (2) felsic pyroclastic rocks (includes quartz and feldspar porphyry units), (3) felsic flow and mafic to intermediate volcanic rocks, (4) felsic volcanic rocks, (5) gabbro sills, (6) granodiorite, (7) highly altered and deformed rocks. ASZ = Austin Shear Zone.

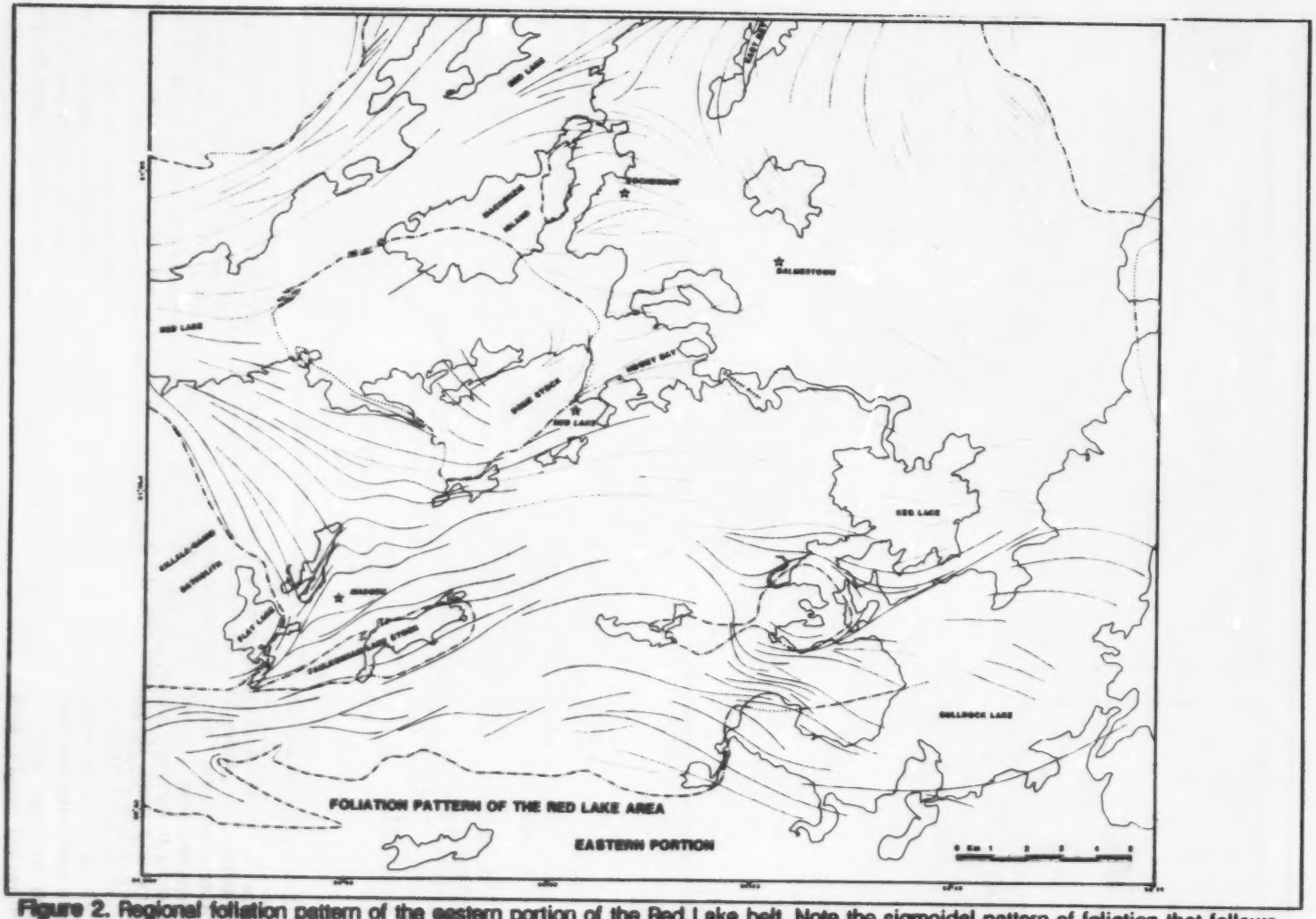

Figure 2. Regional foliation pattern of the eastern portion of the Red Lake belt. Note the sigmoidal pattern of foliation that follows the southeast edges of Dome and Keg Lake stocks. Note also an apparent triple junction of foliation northeast of the Dome stock. The open Z geometry of foliation trend suggests a component of right-lateral displacement along a line Cochenour - Campbell - Dickenson Mines. (Data from Horwood 1945 and Pirie and Kita 1979).

into two major sequences (see Durocher 1983 for further details): a lower tholeiitic to komatiitic sequence adjacent to the Killala-Baird batholith, and an upper calc-alkalic sequence beginning 1 km east of the Madsen mine. Lithological boundaries as well as highly altered and deformed rocks (formerly described as 'tuffs', Horwood 1945, Ferguson 1965, 1968) define a gently sigmoidal pattern (Figure 1b).

The hanging wall of the main ore zone is composed of quartz and feldspar porphyries. These porphyries have a unique structural signature among the host rocks of the Madsen deposit. The quartz porphyry unit has a U-Pb age of 2744 Ma (F. Corfu, Royal Ontario Museum, 1984, personal communication). Therefore, the structural features in this unit analyzed in 1983 provide information about the late increment of the total strain recorded in the Red Lake belt.

REGIONAL FOLIATION PATTERN

Strained pillows, xenoliths, variolites and fabrics yield trajectories of maximal finite shortening and maximal finite elongation throughout the Red Lake belt. Depending on the age of the rock units involved and their deformation history, this finite strain will be total or incremental in the evolution of the Red Lake belt. In the following paragraphs, it will be assumed that foliation and/or schistosity surfaces are normal to the maximum shortening trajectories, be they incremental or total.

At the scale of the Red Lake belt (Figure 2) foliation trajectories near granitoid bodies are generally concordant to the granite-greenstone contacts. Presumably, the space required by the rising plutons was provided by sinking and associated ductile deformation of the greenstone material. The foliation trajectories concordant to the granitoid-volcanic contacts indicate that a large increment of the total strain accumulated in the supracrustal material was due to the rise and expansion of the surrounding batholiths. The presence of a triple junction of foliation trajectories (cf. Brun *et al.* 1981) northeast of Dome Stock strongly supports this hypothesis.

Throughout the belt, the prevalence of down-dip stretch lineations gives further support to this interpretation of the regional foliation pattern. However, departures from this regional trend occur around the Dome and Keg Lake stocks. Foliation trajectories around the Dome stock suggest that this stock behaved like a rigid-modulus inclusion during a later deformation of regional scale. Broad sigmoidal and Z-shaped trajectories of foliation define large-scale ductile shear zones which delineate a crudely conjugate pattern. The most obvious shear zones show a sinistral component of displacement following, and in continuity with, the southeast edges of the Dome and Keg Lake Stocks. Smaller-scale conjugate shear zones have been described by Horwood (1945) in the Dome Stock. This suggests that a regional deformation event is responsible for the increment of the total strain accumulated in the supracrustal and plutonic rocks of the Red Lake belt. This regional scale deformational event will be discussed later in the light of the results obtained in the Madsen area.

FOLIATION PATTERN AND MINOR STRUCTURES IN THE MADSEN AREA

Foliation trajectories in the area between the Killala-Baird batholith and the Dome and Faulkenham Lake stocks (Figure 3) corroborate the strong component of sinistral shear that is reflected in the regional foliation pattern. The foliation trajectories define two main ductile shear zones, one following the main ore horizon of the Madsen mine, the other following the east shore of Russet Lake. At the outcrop scale, the penetrative tectonic fabric (schistosity in the Madsen area) is related to local ductile shear zones ranging in horizontal width from 1 to 100 m. The zones have two main trends, N10-20E and N40-50E. The Austin 'tuff' which hosts the main orebodies of the Madsen deposits is by far the largest, being up to 100 m wide and about 9 km long (Durocher 1983; Durocher and Hugon 1983). The geometric relationship between schistosity and shear plane in the Madsen area (cf. Ramsay and Graham 1970; Berthe, Choukroune and Gapais 1979; Berthe, Choukroune and Jegouzo 1979 for the terminology used in this contribution) is indicative of a left-lateral displacement. The distinct subhorizontal stretch-lineation defined by mineral corrugation in the Madsen shear zones confirms this subhorizontal relative displacement (Figure 4). The network of the small-scale shear zones points to heterogeneous finite strain and delineates a deformation zone (cf. Durocher and Hugon 1983) which extends from the Starratt-Olsen area to Howey Bay.

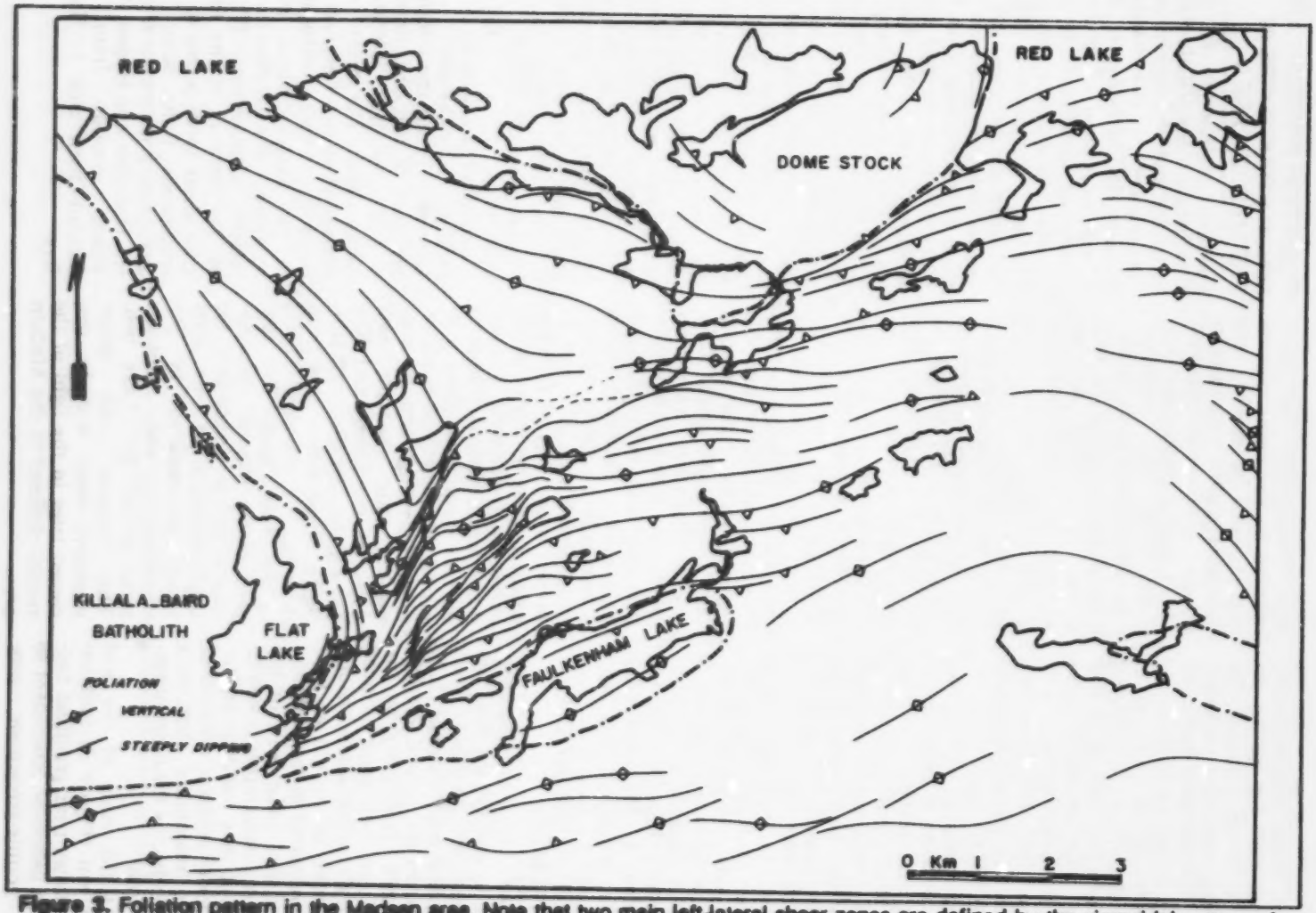

Figure 3. Foliation pattern in the Madsen area. Note that two main left-lateral shear zones are defined by the sigmoidal pattern of the foliation trend. One follows the lithological boundary at the Madsen Mine, the second follows the eastern shore of Russet Lake.

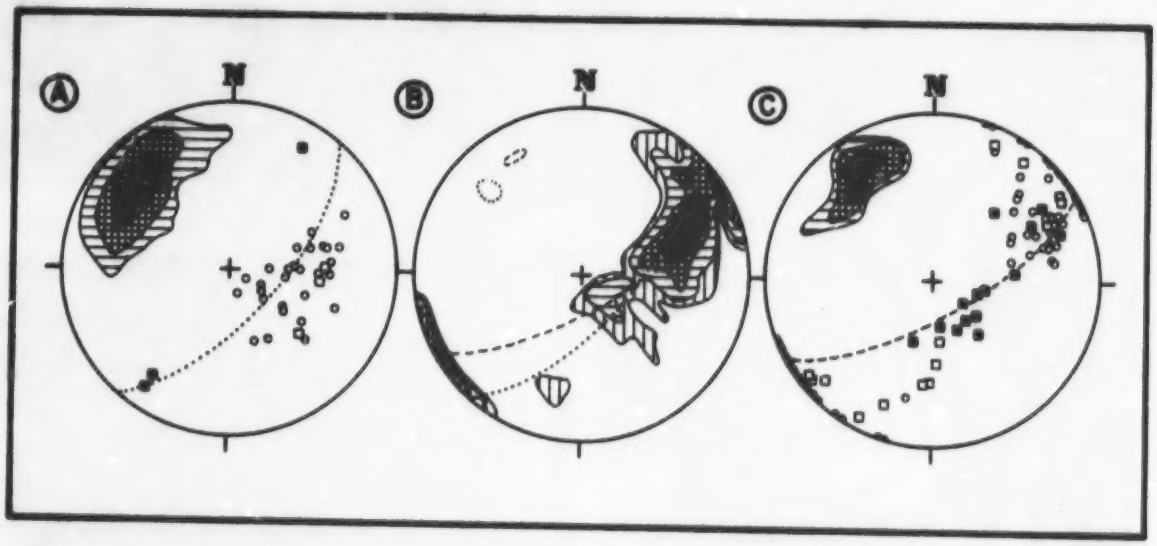

Figure 4. Equal area stereograms (lower hemisphere). (a) Statistical distribution of poles to foliation and shear planes from weakly deformed domains of the Madsen area. Contours at 2, 10, 20 and 25% of 170 measurements contained in 1% of the hemisphere area. The dotted line represents the average foliation plane corresponding to the foliation maximum. The circles represent the measured stretch lineations. Solid squares represent the constructed shearplane/foliation intersections. The open squares are the normals to these intersections within the shearplanes and are equivalent to stretch lineations, which give the direction of displacement. This stereogram demonstrates that in weakly deformed domains the displacement has been mainly subvertical. This is shown by the down-dip stretch lineation, the subhorizontal shearplane/foliation intersections, the shape of the foliation maximum, which indicates the variation in foliation dips. (b) Statistical contours at 2, 5, 10, 15 and 20% of 52 stretch lineation measurements from the whole Madsen area. Note that the distribution of the stretch lineations is asymmetric and restricted to the NE quadrant of the stereogram. Also plotted are the traces of the average foliation planes from weakly deformed domains (dotted line) and strongly sheared domains (dashed line), with corresponding maximum of foliation poles. (c) Statistical contours at 2, 10, 20 and 25% of 54 poles of foliation and shear planes from strongly deformed domains of the Madsen area. The dashed line represents the trace of the average foliation plane corresponding to the maximum of foliation poles of these domains. Other symbols are the same as in (a). This stereogram demonstrates that in the strongly deformed domains of the Madsen area, i.e. in the Austin Shear Zone, the adjacent quartz porphyry and shear zones with 1 m width, the displacement has been mainly subhorizontal. This is shown by the subhorizontal stretch lineations, the subvertical shearplane/foliation intersections and the shape of the maximum of foliation poles, which indicates the variation in strike of the foliation planes.

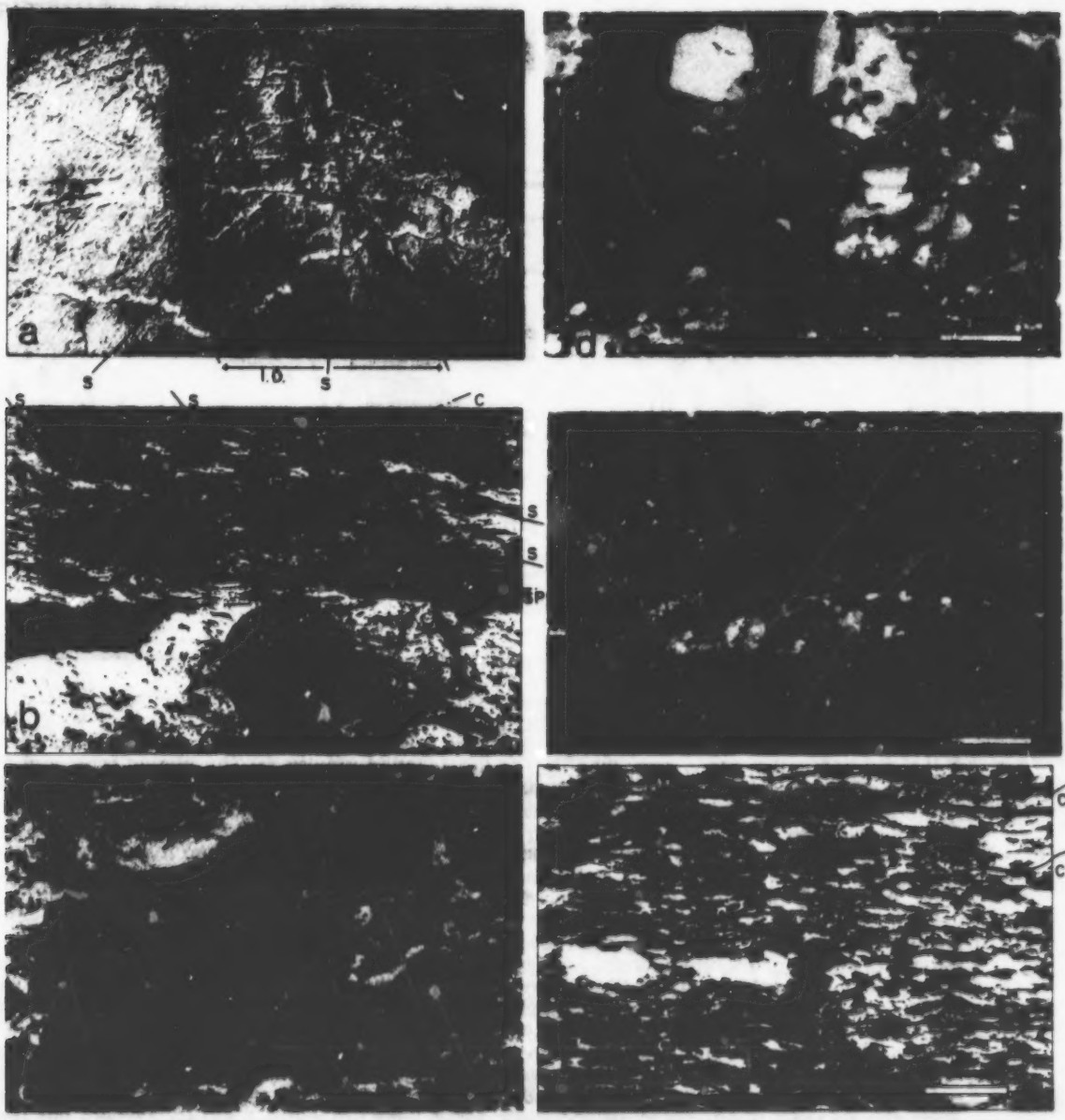

Figure 5. (a) Quartz-feldspar porphyry crosscut by an incompetent dike. The folds are Z-shaped within the dike and S-shaped outside the dike. Foliation (S) is axial planar in both cases. This indicates that shearing has mainly been absorbed within the incompetent dike (I.D.) (see Figure 7). Coin is 22 mm in diameter. (b) Left-lateral small-scale ductile shear zone showing C planes in early stages of development. Note the progressive conversion of quartz grains into ribbons giving rise to a well layered fault rock. This could have happened at a larger scale with pillowed lava flows. S - foliation/schistosity trace. SP - shear plane trace. Coin is 22 mm in diameter. (c) Ultramylonitic features in the same porphyry as shown in (a), near the contact of the so-called "Austin Tuff". The coin is 22 mm in diameter. (d) Photomicrograph of slightly deformed quartz-feldspar porphyry, showing plastic deformation of subgrains of a primary quartz phenocryst. Note also the strong state of alteration (sericitization) of a feldspar crystal in left half of the photo. Scale bar, 1.00 mm. (e) Photomicrograph of strongly deformed quartz aggregate (subgrains) elongated in the foliation and showing plastic deformation of subgrains. Note that the feldspars have disappeared from the matrix which is quartzo-sericitic in the present state of high strain. Scale bar, 1.00 mm. (f) Photomicrograph showing how quartz, under extremely high strain, grew along the foliation plane which corresponds to the shear plane. This can be deduced from the presence of C planes (cf. Berthe, Choukroune and Gapais 1979). Scale bar, 0.25 mm.

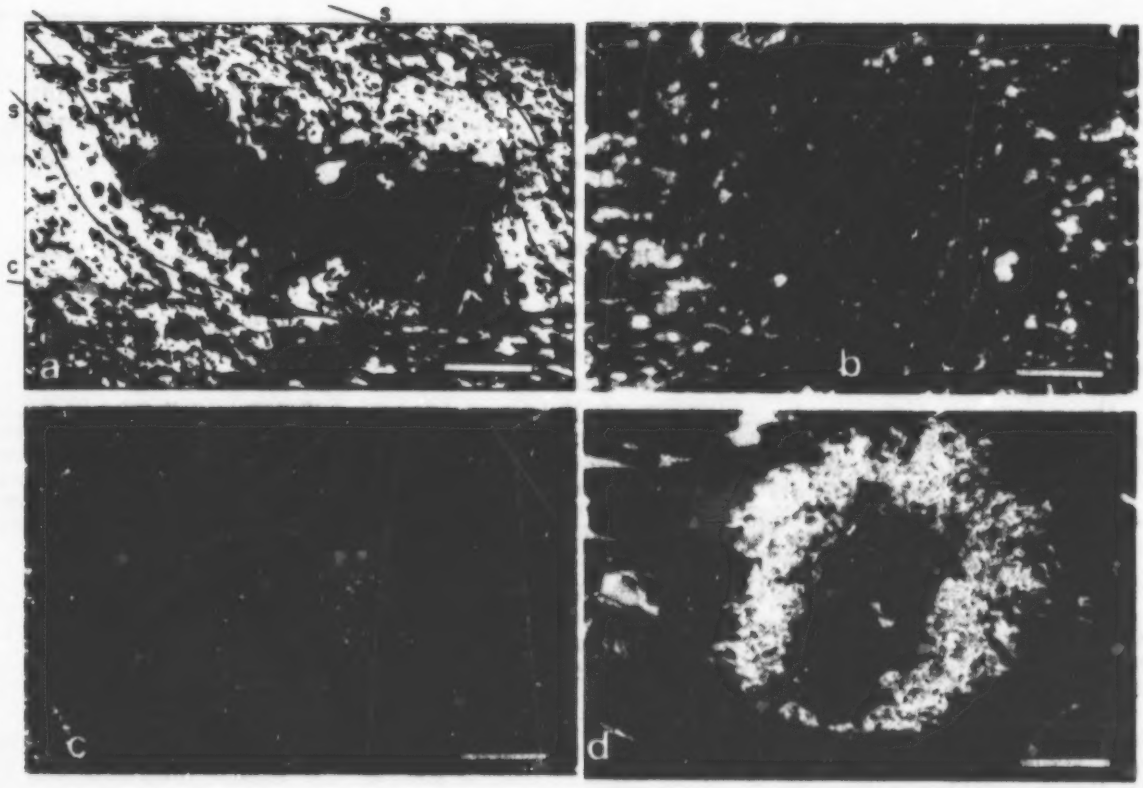

Figure 6. (a) Photomicrograph of deformed garnet crystals showing an asymmetric strain shadow (SS) consistent with the sense of shear revealed by the curvature of schistosity traces (S) toward C planes. All the evidence indicates the same sense of displacement. Scale bar, 1.00 mm. (b) Photomicrograph showing sigmoidal inclusion trails in a garnet porphyroblast, indicative of anticlockwise rotation. Scale bar, 1.00 mm. (c) Sigmoidal inclusion trails within an altered andalusite porphyroblast. Scale bar, 1.00 mm. (d) Photomicrograph showing sigmoidal inclusion trails within staurolite pseudomorphic after cordierite. The trails are consistent with the asymmetry of the strain shadow. Overall foliation trace is parallel to long edges of photograph. Scale bar, 0.12 mm. (b), (c) and (d) are taken from oriented thin sections.

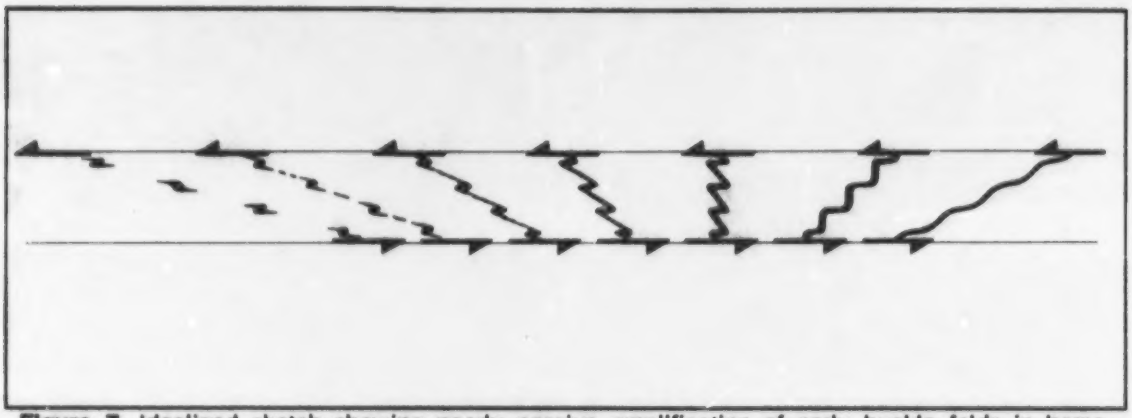

Figure 7. Idealized sketch showing nearly passive amplification of early buckle folds in homogeneous sinistral simple shear. Progressive deformation is illustrated from right to left. The dextral equivalent would be a mirror image of the illustration. The Z asymmetry of the fold develops in the late stages of deformation in spite of left-lateral shear. The thickness variation in the folds may also be misinterpreted. Ramsay *et al.* (1983) suggested a similar, nearly passive amplification of earlier buckle fold at a larger scale.

Field observations in the Madsen area indicate that a down-dip stretch lineation occurs mainly in domains between minor or major shear zones. A progressive variation of the orientation of the stretch lineation from down-dip outside shear zones to intermediate, at shear zone boundaries, to subhorizontal within the shear zones is also observed. Figure 4c shows a concentration of the stretch lineation only in the northeast quadrant. This suggests that the transcurrent shearing was either contemporaneous with, or took over from, a component of subvertical shear. Indeed, if a transcurrent shear is superimposed successively on a vertical shear, or vice versa, a symmetric dispersion of the stretch lineation about the plunge of the average-plane of foliation should be expected. In turn, a penetrative fabric due to subhorizontal displacement indicates that, at least at the scale of the shear zone, vertical shear had ceased. It is therefore concluded that the transcurrent shear progressively took over from the subvertical shear in the Madsen area. The progressive variation of the rake of the stretch lineation together with the left-lateral displacement suggests an asymmetric southward-directed expansion and mushrooming of the Killala-Baird batholith. The northward dip of the foliation surfaces, just south of the Killala-Baird batholith, supports this hypothesis.

Typical shear zones contain (1) buckled quartz veins, indicative of ductile-brittle rock behaviour, (2) passively folded quartz veins and layers (Figure 5a), (3) smaller-scale ductile shear zones (Figure 5b) (C planes of Berthe, Choukroune and Gapais 1979), (4) stretch lineations and (5) strain shadows about rigid-modulus inclusions (Figure 5b and Figure 6). The latest quartz veins (some of which are rich in gold, Horwood 1945) represent folded subvertical tension gashes that are subperpendicular to foliation. Their sigmoidal geometry attests to a horizontal component of late left-lateral displacement. The earliest quartz veins display fold geometries that are largely due to amplification of earlier buckle folds (Figure 7). Their Z-shaped asymmetry (cf. Figure 5a and Figure 7) is inconsistent with all other kinematic indicators of left-lateral displacement. This sense of displacement is also revealed by the sigmoidal asymmetry of the folded contact between the quartz and feldspar porphyries and the Austin 'tuff' (Figure 7).

Number and width of small-scale left-lateral ductile shear zones (C planes) in the porphyry unit increase toward the main Madsen ore zone. These narrow shear zones are subparallel to each other and occur in swarms. Viewed on a scale of hundreds of metres, the shear zones are akin to secondary shear planes (C planes of Berthe, Choukroune and Gapais 1979, and Berthe, Choukroune and Jegouzo 1979), typically appearing in the middle region of shear zones with high shear intensity. At its contact, the porphyry displays features of ultramylonitization (Figure 5c). The shearing converted the porphyry into a schistose mylonitic rock. The rock matrix is quartzo-sericitic and becomes finer-grained as the deformation level increases. Remnants of quartz aggregates show strong plastic deformation (Figure 5d, e, f). The stretch lineation is strongest in the finest-grained schists. Thin sections reveal that C' planes (Berthe, Choukroune and Jegouzo 1979) started to form in schistose material (Figure 5f). All this evidence is indicative of a high degree of strain incurred by the unit formerly called the Austin Tuff, which includes the main ore horizon of the Madsen mine. In other words, the Austin 'tuff' is the end product of the mylonitization or ultramylonitization of unknown protoliths. These observations led Durocher and Hugon (1983) to propose the name "Austin Shear Zone" (ASZ).

Other field observations and geochemical data (Durocher and Hugon 1983) suggest that ASZ was produced by tectonic conversion of quartz and feldspar porphyries as well as mafic flows. However, relics of primary volcanoclastic units may be present in the Madsen area and could play an important role in the localization of the ASZ.

Apparently, the main ore zone is located in a tectonic mixture of ultramylonitized porphyries and/or mafic flows. The horizontal disposition of the orebodies within the main ore zone (Figure 8a) is strikingly similar to anastomosing shear zones (cf. Simpson 1983, Figure 2). According to Horwood (1945) these orebodies were mined in the most foliated parts of the Austin 'tuff'.

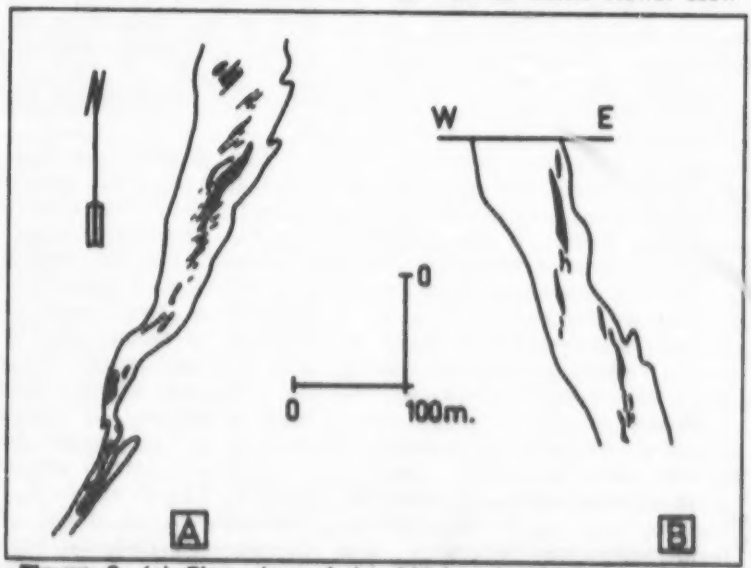

Figure 8. (a) Plan view of the 800-foot level of the Madsen mine. (b) Cross-section of the Madsen mine. Note the *en echelon* disposition of ore zones and of orebodies within ore zones. This geometry is similar to the networks of shear zones observed in granitoid rocks deformed heterogeneously by transcurrent shearing (cf. Simpson 1983, Figure 2).

DEFORMATION, ALTERATION AND METAMORPHISM

Study of thin sections indicates that left-lateral displacement in the ASZ occurred in the realm of regional metamorphism. Thus garnet and staurolite porphyroblasts provide a remarkable record of the progressive deformation in the Austin Shear Zone (see Figure 6). Looking down-dip in thin sections cut normal to foliation and parallel to the horizontal stretch lineation, inclusion trails within these porphyroblasts are clearly sigmoidal (S-shaped, see Figure 6). This reveals that the porphyroblasts rotated in a sinistral sense within a ductile matrix. The sinistral sense is confirmed by the strain shadows around the same porphyroblasts. Gradual transition from well-preserved pillow lavas to their strongly altered and strained equivalents (Durocher and Hugon 1983) reveals that the alteration was syn-shearing. However, the mineral assemblage found in the rocks points to a metasediment rather than mafic flow and suggests that alteration

preceded the peak of metamorphism (cf. Durocher and Hugon 1983). This implies that alteration took place in the early stages of shearing, whereas the porphyroblasts grew at a later stage of the same progressive deformation.

The amphibolite isograd follows the Killala-Baird batholith but curves towards the northeast, south of Russet Lake, to outline the major and minor shear zones of the Madsen area (M.E. Durocher 1984, personal communication). Thus, relatively unstrained, unaltered and less metamorphosed domains are found between major shear zones. This suggests that hot fluids and heat flow emanating from the plutonic bodies were preferentially channelled towards the evolving shear zones. This, in turn, would have had a strain softening effect on the rock material (cf. White *et al.* 1980) which increased the strain rate within the shear zone while the stress level remained constant.

Bleaching by hot fluids would explain the alteration and peculiar metamorphic assemblage of mafic flows (garnet, staurolite, andalusite, chloritoid). It would also explain the rapid growth of the metamorphic porphyroblasts that recorded the progressive deformation within the shear zone.

DISCUSSION AND SUMMARY

The Madsen and Starratt-Olsen gold deposits are located in a prominent zone of left-lateral ductile shearing. Sinistral displacement has also occurred in the Howey-Hasaga area where orebodies may be akin to strained and transposed tension gashes. Accordingly, all of these deposits fall within a belt of sinistral shear, the Flat Lake - Howey Bay deformation zone.

Alteration and transcurrent shearing occurred during regional metamorphism, as revealed by the microstructural behaviour of metamorphic minerals. A new theoretical analysis of the creation and development of shear zones within a compressive stress field (P.Y.F. Robin, in preparation) indicates that in most cases shear zones create a low pressure domain and attract fluids. The presence of conjugate shear zones at all scales suggests that the Red Lake belt has been subjected to overall compression in a north-south direction. Fluids within a shear zone create a strain softening (hydrolitic softening, cf. White *et al.* 1980) as well as a stress softening (Robin 1982; personal communication 1984). Therefore a snow-ball effect is created, i.e., fluids assist in a rapid development of shear zones which in turn attract pore fluids, and so on. The amphibolite-facies metamorphic aureole around the Killala-Baird batholith and around the major and minor shear zones in the Madsen area, together with the peculiar mineral assemblage occurring in the shear zones, indicate that circulating fluids in these shear zones were related to the batholith emplacement. Based on the evidence provided by the metamorphic-kinematic indicators, the authors conclude that deformation, metamorphism, alteration/mineralization and batholith emplacement had a very close temporal and spatial relationship.

Concerning the tectonic history of the Red Lake belt, an important point to consider is the existence of conjugate shear zones at all scales within the belt (cf. Horwood 1945, Durocher and Hugon 1983, Durocher and Burchell 1983). The shearing must have outlasted the granite plutonism or it must be a late deformation increment in the Red Lake belt as it affects the 2744 Ma quartz porphyry of the Madsen area. Apparently the sinistral shear occurred while the batholiths solidified, i.e., roughly between 2720 and 2700 Ma. Two hypotheses can explain the origin of the apparent conjugate shear zones in the belt. The first hypothesis holds that the shear zones were caused by the rise and expansion of large plutonic bodies. This would imply that the geometry of the conjugate shear zones be restricted to the Red Lake belt. The second hypothesis holds that the large-scale shear zones are an expression of a regional deformation event. According to the second hypothesis, similar patterns should be found elsewhere in northwestern Ontario.

The Madsen study indicates that at least one shear zone, the ASZ, was active during the emplacement of the youngest batholith known in the belt. Concerning the first hypothesis two main facts have to be reconciled: (1) the gravitational instability does not disappear when a plutonic body solidifies, (2) the late-stage growth of plutonic bodies is mainly by lateral expansion (Dixon 1975, Brun *et al.* 1981, Schwerdtner, in press). Thus supracrustal material between three or four large growing diapirs may have recorded late horizontal shear that either is superimposed on or progressively took over from previous vertical flow effects (Brun *et*

al. 1981). Therefore, the existence of conjugate shear zones within the belt or within the Dome stock (older than the Killala-Baird batholith) is not a sufficient proof for a regional-scale deformation event. The only possible way of discriminating between the two hypotheses is to conduct a detailed structural study of the youngest batholith in the area. It should be pointed out that, regardless of whether it is local or regional character, the tectonic event responsible for development of transcurrent shear zones occurred around 2700 Ma.

The highly auriferous rocks of the Madsen deposit, formerly called the Austin Tuff, have been severely altered and deformed. According to Ferguson (1965), most of the gold occurs in the native state as minute (4-5 μm) inclusions in silicate minerals, and to a lesser extent as coating on sulphide minerals. In view of the state of large strain and of metamorphism in the highly altered shear zones of the Madsen area, it is improbable that primary gold would have stayed at a steady state in such a stream of mineralized hot fluids channelled within the shear zones. One way of demonstrating whether matrix-hosted gold has been deformed is to measure the gold fabric with a texture goniometer. This should indicate if a preferred orientation of gold lattice does exist or not (P.Y.F. Robin, Erindale College, University of Toronto, personal communication, 1984). In turn this would indicate whether or not the gold recorded the left lateral shearing. Free gold observed in samples (Resident Geologist's collection, Ontario Ministry of Natural Resources, Red Lake) is apparently far less stretched than adjacent aggregates of massive sulphides. It is thus suggested that gold crystallized no earlier than in the late stages of sinistral shearing. At the present stage of knowledge, the possibility that highly auriferous rocks of the Madsen deposit are of pyroclastic origin and that the concordant Madsen shear zone developed preferentially along an incompetent tuff horizon cannot be ruled out. Regardless of protolith, the fact remains that the highest-grade ore occurred in the most-strongly foliated domains (Horwood 1945) of the Austin Shear Zone.

A narrow zone of hydrothermal alteration (Durocher 1983) follows the Flat Lake - Howey Bay deformation zone (Durocher and Hugon 1983). This shows clearly that there is a spatial association between highly-strained rocks, hydrothermal alteration and mineralization. (This association has also been noted elsewhere: Higgins 1971, p.39). Whatever the source of the gold in highly auriferous rocks, the economic deposits are now located in highly-strained rocks. If these rocks had pyroclastic protoliths then they were particularly prone to deformation because of their intrinsically low competence. Preliminary study of other gold deposits in northwestern Ontario suggests that matrix-hosted gold deposits occur mainly at the intersections between shear zones and the amphibolite/greenschist facies boundary zone. This relationship will be further investigated in the Red Lake and Hemlo greenstone belts.

ACKNOWLEDGMENTS

The authors would like to thank M.E. Durocher (former Resident Geologist, Ontario Ministry of Natural Resources, Red Lake), Ray Church (Chief Geologist, Campbell Mine), James Rogers (Chief Geologist Dickenson Mine) and Ebe Scherkus (former Manager, Cochenour Mine, Willanour Resources Limited) for guidance in the field and helpful discussions. The authors also wish to thank A.C. Colvine, A.J. Andrews and Henry Wallace (Ontario Geological Survey) for logistical support in the field and stimulating discussions.

REFERENCES

Berthe, D., Choukroune, P., and Gapais, D.
1979: Orientations Preferentielles du Quartz et Orthogneissification Progressive en Regime Cisaillant: L'exemple du Cisaillement Sud-Armorican; Bulletin de Mineralogie, Volume 102, p.265-272.

Berthe, D., Choukroune, P., and Jegouzo, P.,
1979: Orthogneiss, Mylonite and Non-Coaxial Deformation of Granites: The Example of the South-Armorican Shear Zone; Journal of Structural Geology, Volume 1, p.31-42.

Brun, J.P., Gapais, D., and Le Theoff, B.
1981: The Mantled Gneiss Domes of Kuopio (Finland): Interfering Diapirs; Tectonophysics, Volume 74, p.283-304.

Dixon, J.M.
1975: Finite Strain and Progressive Deformation in Models of Diapiric Structures; Tectonophysics, Volume 28, p.89-124.

Durocher, M.E.
1983: The Nature of Hydrothermal Alteration Associated with the Madsen and Starratt-Olsen Gold Deposits, Red Lake Area; Ontario Geological Survey, Miscellaneous Paper 106, p.123-140.

Durocher, M.E., and Burchell, P.
1983: Structural Geology, Hydrothermal Alteration, Metamorphism and Gold Mineralization in the

Pipestone Bay - St. Paul Bay Deformation Zone, Red Lake; Ontario Geological Survey, Miscellaneous Paper 116, p.220-223.

Durocher, M.E., and Hugon, H.
1983: Structural Geology and Hydrothermal Alteration in the Flat Lake - Howey Bay Deformation Zone, Red Lake Area; Ontario Geological Survey, Miscellaneous Paper 116, p.216-219.

Ferguson, S.A.
1965: Geology of the Eastern Part of Baird Township, District of Kenora; Ontario Department of Mines, Geological Report 39, 47p. Accompanied by Map 2207, scale 1:12 000 or 1 inch to 1000 feet.
1968: Geology of the Northern Part of Heyson Township, District of Kenora; Ontario Department of Mines, Geological Report 56, 54p. Accompanied by Map 2125, scale 1:12 000 or 1 inch to 1000 feet.

Higgins, M.W.
1971: Cataclastic Rocks; United States Geological Survey, Professional Paper 687, 97p.

Horwood, H.C.
1945: Geology and Mineral Deposits of the Red Lake Area; Ontario Department of Mines, Annual Report for 1940, Volume 49, part 2.

Pirie, J., and Kita, J.H.
1979: Byshe Township, District of Kenora (Patricia Portion); Ontario Geological Survey, Preliminary Map 2213, scale 1 inch to 1000 feet.

Ramsay, J.G., and Graham, R.H.
1970: Strain Variation in Shear Belts; Canadian Journal of Earth Sciences, Volume 7, p.786-813.

Ramsay, J.G., Casey, M., and Kligfield, R.
1983: Role of Shear in Development of the Helvetic Fold-Thrust Belt of Switzerland; Geology, Volume 11, p.439-442.

Robin, P.Y.F.
1982: Fluid Migration Within Shear Zones (Abstract); Program with Abstracts, Joint Annual Meeting, Geological Association of Canada and Mineralogical Association of Canada, May, 1982, Winnipeg, Volume 7, p.76.

Schwerdtner, W.M.
in press: Foliation Patterns in Large Gneiss Bodies of the Archean Wabigoon Subprovince, Southern Canada Shield; Geodynamics.

Simpson, C.
1983: Strain and Shape Fabric in Ductile Shear Zones; Journal of Structural Geology, Volume 5(1), p.61-72.

Wallace, H.
1982: Red Lake Synoptic Project, District of Kenora; Ontario Geological Survey, Miscellaneous Paper 106, p.5-7.

White, S.H., Burrows, S.E., Carreras, J., Shaw, N.D , and Humphreys, F.J.
1980: On Mylonites in Ductile Shear Zones; Journal of Structural Geology, Volume 2, p.175-187.

Grant 167 Resedimentation Associated with the Gold-Bearing Banded Iron Formation in the Geraldton-Beardmore Area

T.J. Barrett[1] and P.W. Fralick[2]

[1]Department of Geology, University of Toronto
[2]Department of Geology, Lakehead University

ABSTRACT

Archean iron formation (IF) typically occurs over 5-15 m intervals within predominantly arenitic sedimentary rocks in the Beardmore-Geraldton greenstone belt. The IF consists primarily of dark laminated magnetite (chemical component) with intercalated siltstone/sandstone beds (clastic component) which range in thickness from less than a millimetre to tens of centimetres. Sedimentary structures in the IF, which include graded bedding, parallel lamination, and load casts, indicate deposition of clastic beds, together with some magnetitic material, by turbidity currents. Within intervals of alternating magnetite, siltstone and sandstone, the clastic component may coarsen and thicken upward over a scale of metres, and eventually pass vertically into a 100% clastic succession. This upward transition suggests progradation of submarine fan clastic sediment lobes (with a minor magnetite component) into an environment where essentially iron-rich sediment (the magnetite precursor) was otherwise being deposited as background chemical rainout. Variations in thickness and coarseness of clastic beds in different sections within the IF are interpreted as reflecting proximal through to distal locations relative to channel feed systems.

INTRODUCTION

Occurrences of Archean iron formation (IF) containing interbedded clastic sediments have been reported in recent years from a number of localities on the Canadian Shield in Ontario. In the northwestern part of the province, they are present in the Spirit Lake and Rainy Lake areas (Wood 1980), Lake St. Joseph region (Meyn and Palonen 1980), and Manitou Straits area (Teal and Walker 1977); in northeastern Ontario they have been recorded in the Abitibi Belt (Hyde 1980).

The purpose of the present study is to closely examine three typical IF-bearing stratigraphic sections from the Beardmore-Geraldton area (Figure 1), north of Lake Superior. This region, which contains numerous vein-type gold deposits in close spatial association with the IF, has been of economic interest since early in the century (Colvine 1983). Detailed mapping has been carried out by Pye (1952) and Mackasey (1975, 1976), and recently extended by the Ontario Geological Survey (Mason and Macdonald 1983; Mason and McConnell 1983; Macdonald 1983). Using this background field information, we chose our sections to cover a spectrum of sediment associations that range from an almost purely chemical end-member to an entirely clastic end-member. In this paper, we document the characteristic sedimentary structures and sequences in these sections, and interpret these features in terms of a general model which may be applicable to other occurrences of Archean clastic-bearing IF.

GENERAL FIELD RELATIONS

The Beardmore-Geraldton belt, which extends continuously in an east-west direction for some 100 km, displays numerous features typical of Archean greenstone belts on the Canadian Shield. Mafic to felsic volcanic rocks are associated with tuffaceous and clastic units, all of which have been metamorphosed to greenschist facies, and are surrounded by granitic to gneissic-migmatitic terrains (Figure 1). Two characteristics of the Beardmore-Geraldton belt are (i) the high proportion of clastic sedimentary rocks, which consist primarily of feldspathic arenite and greywacke with lesser conglomerate and slate, and (ii) the general occurrence of IF within these clastic lithological units.

Fold structures are typically isoclinal, parallel to lithological belts, and have hinge spacings of hundreds of metres. On the outcrop scale, bedding is generally sub-vertical and small isoclinal fold hinges are commonly present. We have tried to avoid such areas in our measured sections, and in fact did not recognize obvious repetitions in stratigraphy on a metre scale. Nevertheless there remains the possibility that some centimetre-scale repetition is present.

STRATIGRAPHIC ASPECTS OF THE SECTIONS

Three measured sections are illustrated in Figure 2 (note different vertical scales). Detailed measurements of another 10

sections throughout the Beardmore-Geraldton belt have also been made, but those of Figure 2 have been selected as they are representative of both the range of stratigraphic variation and the range of observed sedimentary structures. Section 1 is basically a magnetite-rich interval with interbedded siltstones, section 2 a sandstone-rich interval with thin magnetite-bearing intercalations, and section 3 an upward-coarsening transition from a magnetite-rich interval with thin interbedded siltstones, through sandstones with thin magnetite-rich intercalations, to an entirely clastic succession.

SECTION 1

On an island in Barton Bay, Lake Kenogamisis, IF is exposed around a shallow pit and in a north-trending trench 50 m west of the pit. On the east side of the pit is a 9 m thick, glacially smoothed section. Reddish jasper occurs only in the northernmost metre. The remainder of the section consists of 0.5-2 m thick intervals of magnetite-rich sedimentary rock, separated by compound siltstone units up to 80 cm thick. The magnetite-rich sedimentary rock also contains variable proportions of thin intercalated siltstones. We term the distinctive association of magnetite-rich sedimentary rock and thin siltstone beds *Lithofacies Association* a, or LA-a (e.g. Figure 3a). Within the trench, which cannot be directly correlated with the pit, the frequency of siltstone/sandstone beds increases southwards over a distance of several tens of metres until a 100% clastic section is attained.

SECTION 2

The Hutchison Lake section, located several hundred metres northeast of the east shore of the lake, is clastic-dominated, with compound sandstone beds up to 0.5 m thick (or occasional single beds up to 0.3 m thick) separated by thin magnetite-rich intervals. Sandstone laminae (<1 cm) are present within the latter intervals. In the basal 2 m of section, sandstones are whitish. Above this, they are frequently dark greenish, particularly where they occur as thin single beds or laminae intercalated within magnetite-rich intervals (Figure 3b).

SECTION 3

The section exposed in the Leitch Mine trench begins with 7 m of finely laminated, magnetite-rich sedimentary rock containing occasional dark siltstone and reddish jas-

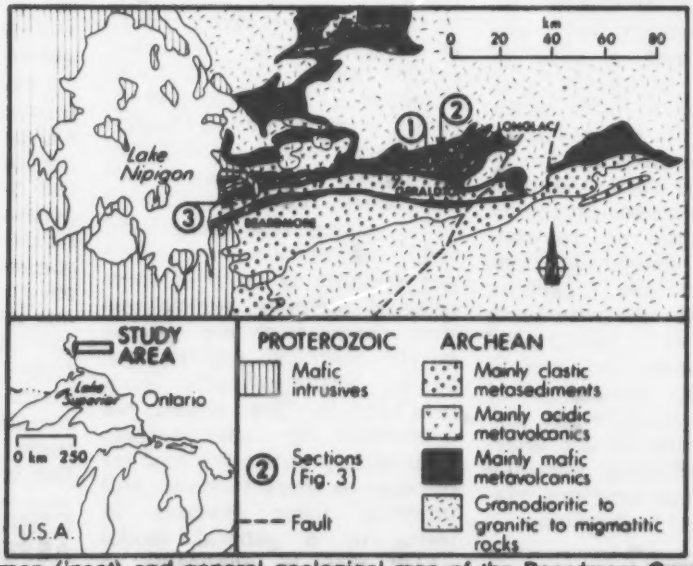

Figure 1. Location map (inset) and general geological map of the Beardmore-Geraldton area, north of Lake Superior. Based on Ontario Geological Survey Map 2199. Locations of three sections of Archean IF and clastic sedimentary rocks which were examined in detail are indicated by the arrows. Several major east-striking faults in this area have been omitted for clarity.

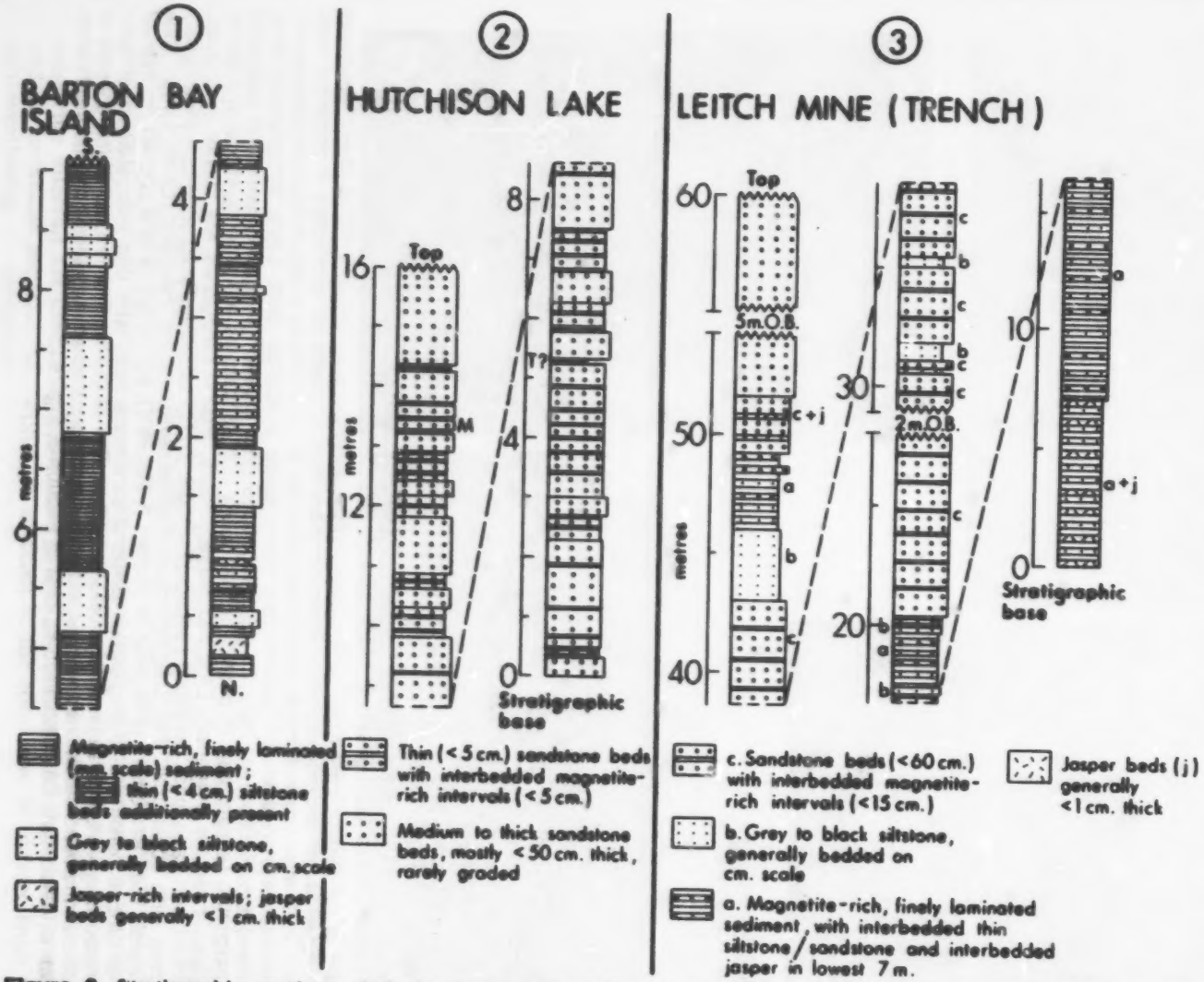

Figure 2. Stratigraphic sections of three occurrences of IF and associated clastic sedimentary rocks within the Beardmore-Geraldton belt. Locations given in Figure 1. Note different vertical scales. Younging direction is known from graded beds in sections 2 and 3, but is uncertain in section 1. The letters a, b, and c in section 3 refer to distinct sediment lithofacies associations, and are discussed in the text; the letter "j" indicates the presence of jaspery beds. The symbol "T?" in section 2 indicates a possible tuffaceous bed.

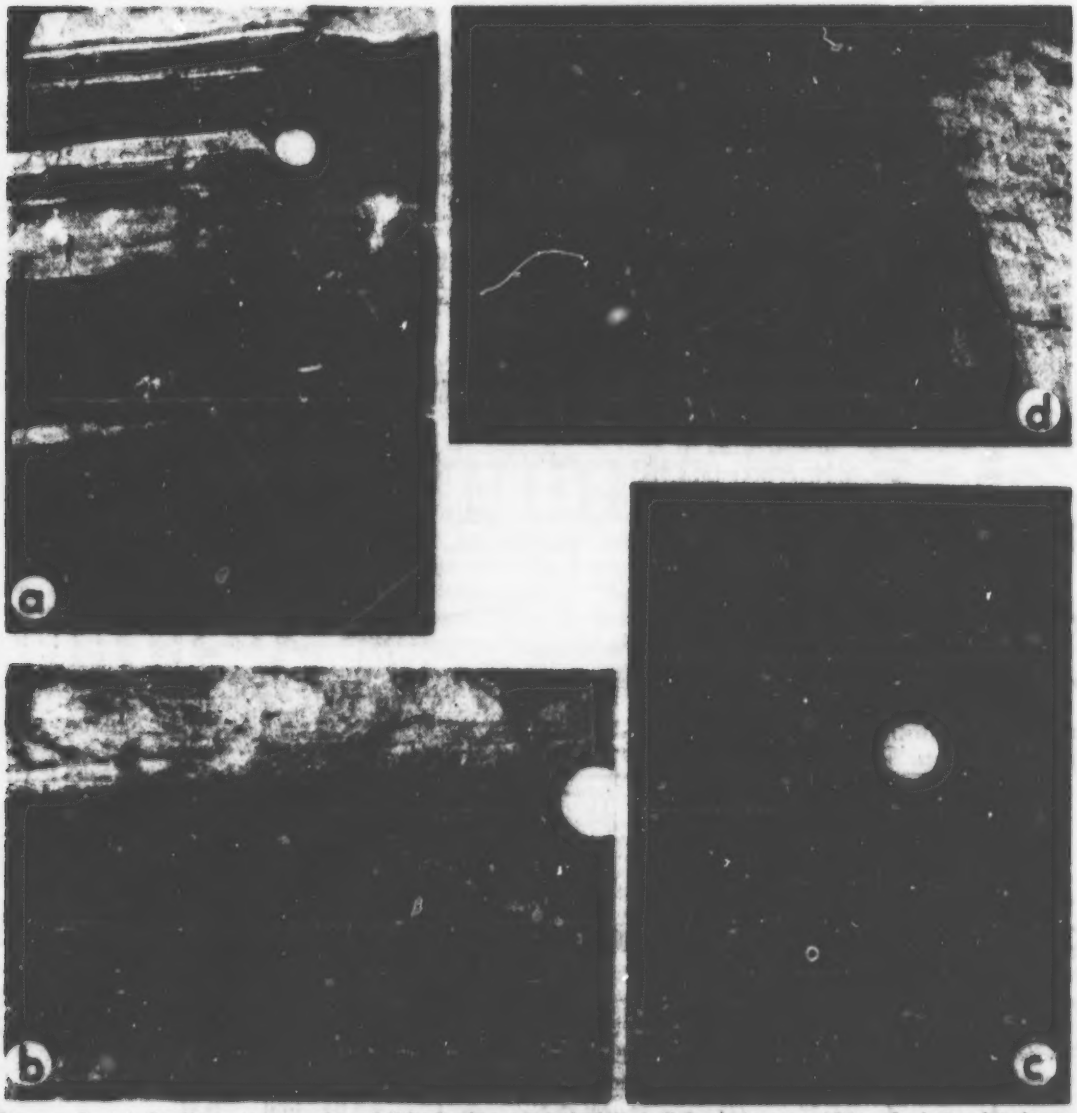

Figure 3. (a) Sedimentary rocks of lithofacies association a (LA-a). Lower 40% of photo: laminated magnetite-rich sedimentary rock; laminations are rich in clastic silt and range in thickness from <1 to 5 mm. Upper 60% of photo: several siltstone beds, 1 to 4 cm thick, with intervening laminated magnetite-rich sedimentary rock. Island in Barton Bay, Lake Kenogamisis, near Geraldton (Section 1, Figure 2). (b) Interbedded dark greenish thin sandstones and laminated magnetite (central part of photo); lighter quartz-rich sandstones are present above and below this. These are essentially LA-c sedimentary rocks, though sandstones are thinner than usual. Hutchison Lake, near Geraldton (Section 2, Figure 2). (c) Laminated magnetite-rich sedimentary rock with occasional, thin, sharply-bordered siltstone/sandstone interbeds (LA-a). Leitch Mine trench, near Beardmore (9 m level in Section 3, Figure 2). (d) To left of lens cap: 40 cm interval of LA-b consisting of thin greenish siltstone/sandstone beds with thin intercalations of laminated magnetite-rich sedimentary rock. On either side of this interval is LA-c which consists of thick compound sandstone beds seperated by distinctly thinner magnetite-rich intervals. Leitch mine trench, near Beardmore (35 m level in Section 3, Figure 2).

per intercalations. This is overlain by 13 m of LA-a (Figure 3c): laminated magnetite-rich sedimentary rock which lacks jasper beds but contains occasional thin sandstone in addition to siltstone intercalations (clastic strata are <2 cm thick). Within this lithofacies association, the intercalated siltstones, which may be graded, occasionally form compound units consisting of two or more contiguous beds. Where these compound units are thick enough to form a mapoable unit at our scale of section, i.e., greater than 0.3 m, we term them LA-b (immediately right of centre in Figure 3d). This lithofacies association is essentially composed of thin compound siltstone beds, either contiguous or separated by laminae of magnetite-rich sediment.

At the 20 m level of the section, thick light-weathering sandstone units 0.2 to 0.6 m thick appear; these are separated by magnetite-rich intervals up to 15 cm thick. Thin (centimetre-scale) greenish sandstone/siltstone beds are also present within the latter intervals. We term this whole association of beds LA-c (immediately left of centre in Figure 3d). The transition from LA-a to LA-c is rather abrupt, taking place between 19 and 20 m in the section.

Section 3 represents an essentially coarsening-upwards sequence over the 0-30 m interval. LA-c continues until 43 m, with the exception of a few thin occurrences of LA-b in the 30-35 m interval. Over the next 9 m, a fining upwards succession (c–b–a) is followed by a coarsening upwards succession. Above the 52 m level, magnetite intervals are absent, and an unbroken sequence of light-weathering sandstone beds (generally compound) is present to the top of the section. Recent field work in other areas of the Geraldton-Beardmore belt has demonstrated that upward thickening and coarsening cycles are common within magnetite - siltstone - sandstone - bearing sections; typically the cycles have thicknesses in the order of metres, with rather gradual upward trends but sharp terminations.

Having defined LA-a to LA-c we can now consider Section 2 (which consists primarily of medium-bedded sandstone with centimetre-scale magnetite-rich intercalations) as a variant of LA-c, the main difference being the generally thinner nature of the sandstone intervals in Section 2.

OTHER SECTIONS

Two IF-bearing successions contain quite different lithologies from those described above. On the southern shore of Barton Bay (Geraldton), coarse- to very coarse-grained sandstone beds up to 3 m thick are separated by intervals of laminated IF up to 15 cm thick. Grading in the sandstones is usually present only near their tops, where the grain size may decrease to fine-grained sand. Some of the thick clastic beds contain abundant intraformational rip-up clasts composed of laminated siltstone and magnetite.

The second unusual outcrop occurs in the central portion of the study area near the eastern shore of Watson Lake. Here, thin units of IF and gravelly conglomerate (each up to 30 cm thick) occur within a dominantly coarse sandstone succession. The IF lies either within or adjacent to the conglomeratic units. Although spatial proximity between IF and conglomerates was noted at various other locations, the Watson Lake occurrence was the only one where interbedding was observed.

SEDIMENTOLOGY

In terms of sediment composition, the majority of clastic strata in the sections we have examined are feldspathic arenites. However, some beds contain up to 20% muscovite and/or 20% carbonate and/or 10% magnetite, hence they would be quartz-intermediate greywackes according to Crook (1974). Although rock fragments are not obvious, it is possible that some of the muscovite has been derived from metamorphism of pre-existent rock fragments. Carbonate is mainly developed around the Geraldton area. Strong tectonic deformation and quartz-carbonate veining (Macdonald 1982) suggest that it is of secondary origin. The carbonate occurs within the clastic beds as scattered pinkish grains, often coarser than the adjacent siliciclastic minerals. No evidence for primary carbonate layers has been found. Muscovite is the dominant sheet-silicate mineral, and is either distributed more or less evenly throughout beds, or is concentrated within laminae related to internal sedimentary structures. Magnetite is secondary where it forms euhedral grains distinctly coarser than the siliciclastic grains in the bed (this is mainly developed in siltstone beds).

It is worth noting that the occurrence of centimetre-scale chert bands is quite limited within IF of the Beardmore-Geraldton area. In this respect, the IF differs from the more

characteristic magnetite - (hematite) - chert interbanding of Algoma-type iron formation of greenschist or lower metamorphic grade (Gross 1965; Eichler 1976). Chert bands in the Beardmore-Geraldton area are generally <1 cm thick. They are almost always reddish, due to a significant iron oxide content, and are more appropriately termed jasper (hematitic bands may also be associated with the jasper). In addition to the uncommon centimetre-scale chert bands, cherty microbands less than a millimetre thick occur within magnetite-rich intervals of the IF. These microbands, which are not visible on the outcrop scale, probably originated as primary chemical precipitates (see "Discussion").

BARTON BAY

Near-black, magnetite-rich intervals dominate this section. On the outcrop scale, these intervals are commonly finely laminated on a millimetre scale. This produces a "ribbed" appearance on the weathered surface; the ribs that stand marginally higher in relief have the higher magnetite content. These millimetre-scale ribs display hair-thickness microlamination, which thin sections reveal to be due to alternating magnetite and chert microbands. Thin sections also indicate that the furrows between the "ribs" contain silt-sized (or finer) siliciclastic grains, together with dispersed magnetite. Clearly-defined clastic beds within the section are thin and generally sharply-bounded; they commonly show faint parallel lamination, and rarely display grading and/or load casts. The clastic beds weather to a pinkish colour due to the presence of (secondary) Fe-bearing carbonates.

HUTCHISON LAKE

Both the thick and the thin sandstone strata in this section may show grading, but this is mainly restricted to the lowermost and uppermost portion of each bed. Occasionally, tops of dark greenish sandstones grade quite smoothly through a few millimetres into an overlying magnetite-rich bed. Fine-grained sandstones commonly display millimetre-scale lamination.

LEITCH MINE TRENCH

The compound sandstone units (LA-c) are typically 0.2-0.6 m thick, and consist of a random sequence of graded, parallel-laminated, or structureless beds (<1 cm to a few centimetres thick). Thin-bedded siltstone-rich intervals (LA-b) and laminated magnetite-rich intervals (LA-a) within the Leitch Mine trench show the same sedimentological features as described for these lithologies in the previous section.

SEDIMENT MICROFEATURES

Thin section prints and photomicrographs of the laminated magnetite-rich rock (LA-a) reveal a variety of fine sedimentary structures. Figure 4a shows a central, clearly graded, siltstone bed (1 cm thick) with increasing amounts of fine-grained magnetite towards the top. This bed displays parallel lamination over its upper 2 mm. It is overlain and underlain by discrete quartz-magnetite-rich laminae (1 to 2 mm thick) which show hints of grading. On the outcrop scale, these laminae would not be distinguishable as thin clastic intercalations. Generally, they would appear (on the weathered surface) as "furrows" between magnetite-rich "ribbings".

In Figure 4b, the central third of the photo shows a complex graded unit containing several alternating quartz-rich and magnetite-rich laminae which exhibit an overall upward fining trend (over 1.5 mm). This graded unit is capped by 0.5 mm of dense, clastic-free magnetitic material, above which, with sharp contact, is a siltstone lamination (followed by a siltstone bed). Figure 4c illustrates a central, fine-grained clastic bed which is graded and faintly parallel-laminated. This bed has a coarser erosive base, and becomes finer and more magnetite-rich upwards (dark clots in upper part of photo are recrystallized magnetite). Below this bed is dense, clastic-free magnetitic sedimentary rock. In Figure 4d, the central clastic bed (0.6 mm thick) shows a distinct separation into a quartz-rich lower part and a magnetite-bearing finer top. Dense, clastic-free magnetitic material flanks this bed both below and above.

In Figure 5a, an example of a chert-jasper bed (0.6 cm thick) is shown. The chert-jasper is microcrystalline, shows traces of microbanding, and totally lacks the discrete (and larger) quartz grains of the clastic strata. Figure 5b shows a thin (3 mm thick) siltstone bed overlying magnetite-rich sedimentary rock. In thin section, the latter can be resolved into alternations (0.2-0.5 mm thick) of clastic-rich and magnetite-rich material. Figures 5c and 5d are enlargements of the lower part of Figure 5b. At these magnifications, the fine-grained clastic-rich laminae are clearly visible. On the outcrop scale,

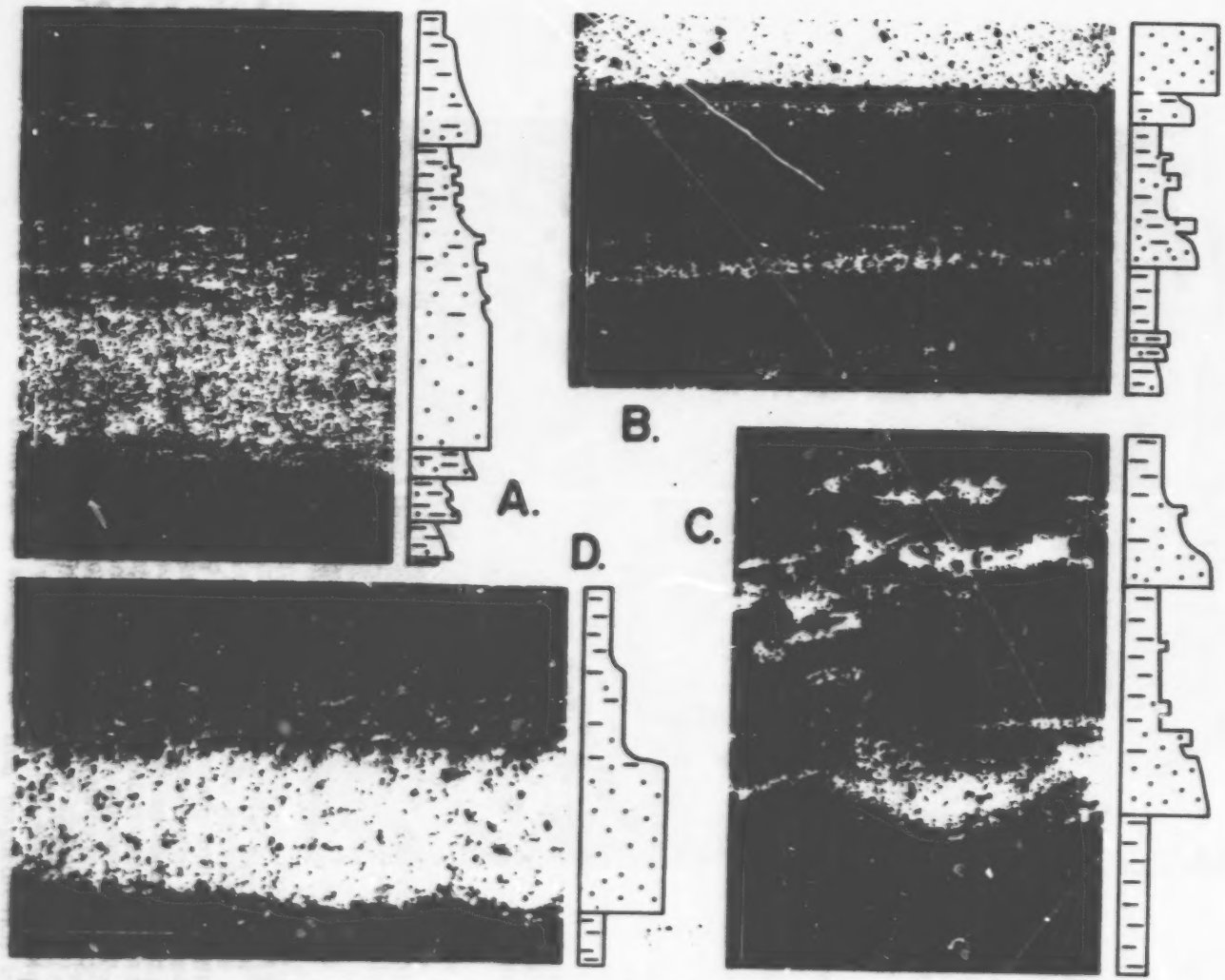

Figure 4. Photomicrographs of fine-grained sandstone and siltstone associated with laminated magnetite-rich sedimentary rock (LA-a). Logs to right of photos outline borders of beds and laminae, and schematically illustrate grain size variations (dots and dashes represent the clastic and magnetite components, respectively). See text for discussion. Scale bars: (a) 5.0 mm, (b) 2.0 mm, (c) 3.0 mm, (d) 2.0 mm; crossed nicols. (a) - (c): Section 1, Figure 2: (d): Section 3, Figure 2.

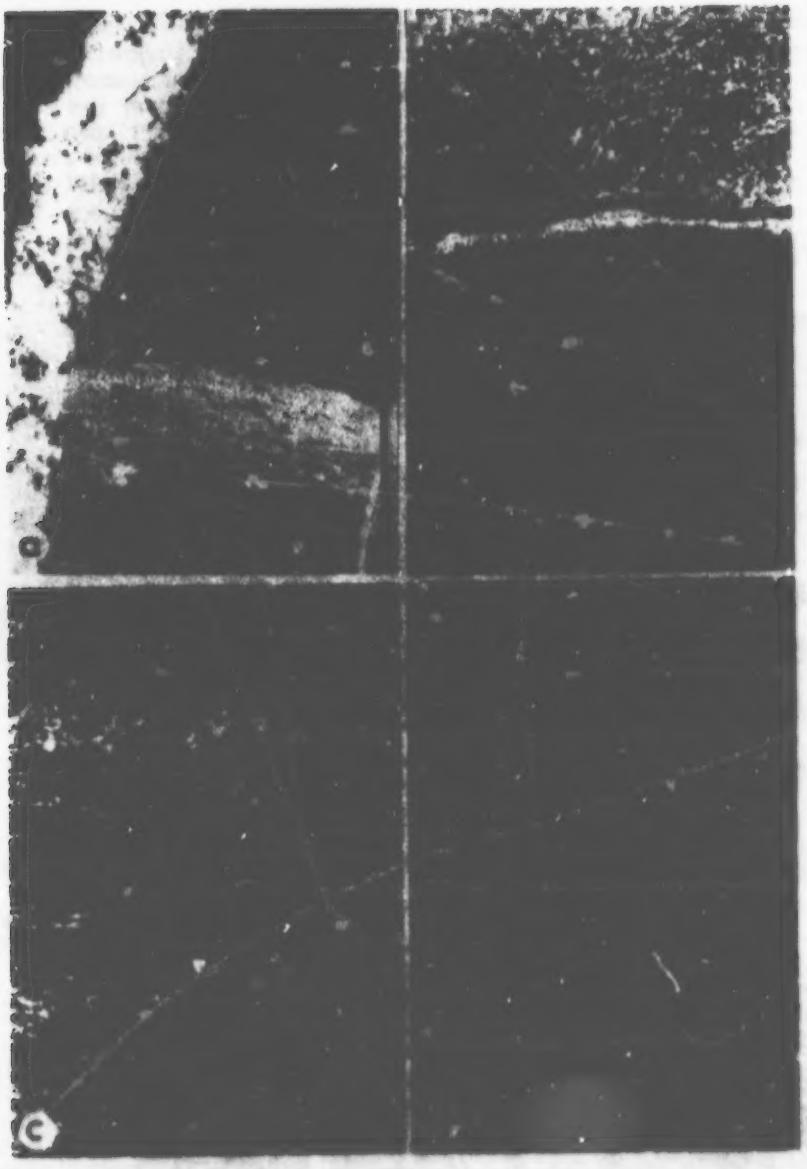

Figure 6. (a) Photomicrograph of jasper-chert bed. Dark, upper part of bed contains hematite dust and appears reddish on the outcrop; light, lower part is cherty and pale red in outcrop. Note semi-continuous microbanding, which is more distinct in upper than in lower sublayer. (Scale bar: 2.0 mm; plane light; Section 3, Figure 2.) (b) Photomicrograph showing base of clastic siltstone lamination (upper 40% of photo) and very thin clastic siltstone laminae separated by dark clastic-free magnetite-rich intervals (lower 60% of photo). (Scale bar: 2.0 mm; crossed nicols. Location as in (a).) (c) Enlargement of (b), showing two thin siltstone laminae immediately below the thick siltstone lamination. Note that these laminae are separated above and below by intervals of clastic-free microbanded chert-magnetite. (Scale bar: 0.5 mm; plane light.) (d) Enlargement of (c), showing chert-magnetite microbands between the two siltstone laminae. (Scale bar: 0.2 mm; plane light.)

these clastic-rich laminae would generally appear as "furrows" between "ribbings" in typical magnetite-rich sedimentary rock. In Figure 5b, the near-black magnetite-rich laminae can be further resolved into alternating chert and magnetite microbands, both of which are typically <0.1 mm in thickness. On the outcrop scale, these magnetite-rich laminae, which stand in relief as "ribbings", display hair-thickness microlaminations. These microlaminations appear to correspond directly to the chert-magnetite microbands seen in thin section. (See Trendall and Blockley (1970) for a discussion of very similar chert-magnetite microbanding in the Hamersley Basin IF of Western Australia). The ease with which the cherty microbands can be observed in thin section depends on their magnetite content. If they contain significant amounts of finely disseminated magnetite, they will appear nearly black, and will only be microscopically resolvable from the magnetite microbands by using high light intensities.

INTERPRETATION

CLASTIC COMPONENT

A number of the sedimentary structures we have observed in the magnetite-rich and siltstone-rich lithofacies associations (a and b) are characteristic of fine-grained distal turbidites (Piper 1972, 1978). First, intercalated thin siltstone beds (in both LA-a and LA-b) may display parallel lamination and size grading; commonly a component of magnetitic sediment is present within the upper portions of these beds (see Figure 4). In these cases, we interpret the siltstone beds together with their magnetite-bearing tops, even where only millimetre-scale in thickness, as fine-grained turbidites. The magnetitic sediment is inferred to have been transported with the clastic material as some type of Fe-oxyhydroxide which subsequently underwent post-depositional diagenetic modification (see next section).

A second feature to be noted is the thin (generally <5 cm) bundles of alternating quartz-silt and magnetite-rich laminae, which exhibit complex upward-fining and upward-thinning trends (see Figure 4b). These are strongly analogous to structures recently described from various fine-grained turbidite sequences (Stow and Bowen 1980, p.32; Hesse and Chough 1980, Figures 5 and 6, Chough and Hesse 1980, Figures 3 and 4; Stow and Shanmugan 1980, Figures 4 to 6). Although somewhat different mechanisms have been suggested by these authors for the deposition of the alternating laminations, there is agreement that each bundle of laminations represents sediment laid down by the passing of a single, slow, low-density turbidity current. Low-density turbidity currents are responsible for building portions of the natural levees of deep-sea channels and submarine fan valleys (Hesse and Chough 1980) and the thick interchannel deposits on fans of the outer continental margin (Stow 1979; Stow and Bowen 1980). These fine-grained deposits result primarily from the spillover of upper parts of large channelized turbidity currents. With regard to the common siltstone and sandstone beds which have sharp bases both below and above, we note that the grain-size of such beds is near-uniform throughout. Hence, these beds may represent clastic material which has undergone previous sorting (e.g. in a shallow water environment) prior to redeposition. We interpret these beds as thin mass flow deposits emplaced by mechanisms more closely related to fluidized flow than to true turbidity currents.

With reference to the coarsening and thickening upwards IF-clastic cycles (e.g. Leitch Mine) we interpret these thicker, metre-scale successions as resulting from progradation of clastic-rich sediment lobes on a submarine fan into relatively quiet, low energy environments (water depths unspecified). At times when little detritus was being supplied, magnetite-rich sequences developed (e.g. Barton Bay section). As the clastic input increased, the succession slowly changed from chemical-dominated to clastic-dominated. As individual sand lobes continued to build outwards, some sequences became totally clastic (e.g. traversing southwards through the Leitch Mine trench) and all deposition of chemical sediment terminated.

We interpret the thickest clastic sediment beds, in LA-c, as having been deposited on fan lobes nearest the source channels. LA-a, consisting mainly of magnetite with intercalated thin siltstones, would represent the most channel-distal sediments. These appear to have been deposited in a low energy basin-plain type of environment, wherein chemical sediment accumulation was periodically interrupted by influxes of fine clastic material. LA-b, consisting mostly of siltstones (compound or separated by thin magnetite-rich intervals),

is interpreted as having formed in an intermediary location, either just distal to the toes of sandy fan lobes, or as interchannel deposits between active channels on the fan itself.

The two sections containing magnetite interbedded with coarse-grained clastics or conglomerates (Barton Bay and Watson Lake respectively) may represent areas where magnetite was episodically deposited in a shore-proximal environment. The thick-bedded, very coarse-grained sandstones present on the shore at Barton Bay represent fluidized-flow deposits, some of which contain abundant rafted, intraformational clasts. It is doubtful that the clay-poor nature of these sandstones could have been maintained after prolonged flow over a muddy (magnetite-clay-rich) bottom, as mud from the substratum would tend to become incorporated in the flow. Hence, these deposits may represent slumps which originated off fluvial feed points in a shallow marine environment, but came to rest in a deeper marine low energy environment. The occurrence of such events may have been favoured by the existence of a very narrow continental shelf, as postulated in the model of Meyn and Palonen (1980). The observation that some IF occurs stratigraphically proximal to sandstones and conglomerates of possible fluvial origin (Devaney 1983) suggests that lateral facies transitions to continental sediments may have been rapid. However, a major stratigraphic hiatus separating the possible subaerial and the marine sediments cannot be ruled out.

CHEMICAL COMPONENT

As noted earlier, the main chemical component on the outcrop scale is laminated magnetite. Reddish jaspery to hematitic beds (up to 1 cm thick) are rather uncommon, and light-coloured chert bands of centimetre-scale thickness have not been observed. The dense magnetite-rich sedimentary rock which occurs below sharply-based siltstone (or thin sandstone) strata is interpreted as having formed from interturbidite chemical rainout material (see Figures 4c,d). This dense magnetite-rich material may also be present above the magnetite-bearing tops of the graded beds. It is distinguishable from the tops through its virtual absence of clastic silt, and is also considered to represent a strictly chemical, post-turbidity current sediment. As noted earlier, the purely chemical sediments generally can be resolved microscopically into alternating magnetite and chert microbands.

The development of magnetite in iron formations of the Lake Superior region has been discussed by LaBerge (1964), who concluded that "the bulk of the magnetite was formed under low-grade metamorphism by oxidation of the primary ferrous-iron minerals, siderite and greenalite." However, the mineralogical and textural aspects of the Superior-type IFs he examined are fundamentally different from the Archean IFs of northwestern Ontario, and thus do not necessarily apply. One major feature of the latter IFs is the very fine sedimentary structures preserved by the magnetite: grading in the upper part of some centimetre-scale clastic beds, the millimetre-scale alternations between clastic- and magnetite-rich laminae, and, finally, the microbanding of the purely chemical layers. These features suggest that much of the magnetite is either primary or early diagenetic; if metamorphic in origin, it has entirely replaced the original Fe-bearing component and has done so on a remarkably fine scale and without affecting sedimentary structures. We favour an early replacement model, such as that of Drever (1974). In this model, the possible primary minerals in IF are, according to availability of oxygen at the time of deposition, amorphous $Fe(OH)_3$ or FeO(OH) (goethite), siderite, and pyrite. With diagenesis of the oxide facies sediments, hematite results. However, if sufficient organic carbon was present at the time of sediment deposition, "the ferric hydroxide in the sediment would have been partly reduced and the product of the diagenesis would have been magnetite" (Drever 1974). Because of the reduced densities of colloidal Fe-rich precipitates relative to siliciclastic grains, a ferric hydroxide precursor to the magnetite would also help to explain the presence of fine-grained magnetite in the upper, rather than the lower parts of certain clastic turbidite beds. With regard to the uncommon jasper beds and the chert component of the magnetite-chert microbanding, we have no evidence to allow us to select between an organic (Laberge 1973) or an inorganic origin (Cloud 1973).

ACKNOWLEDGMENTS

Grateful appreciation is expressed to J.K. Mason and the geological staff of the Thunder Bay offices of the Ontario

Ministry of Natural Resources, and to A.J. Macdonald and the Ontario Geological Survey for providing both logistical support and enlightening discussions on the geology of the Geraldton-Beardmore area. The project was supported by Grant 167 from the Ontario Geological Survey of the Ministry of Natural Resources.

REFERENCES

Chough, S.K., and Hesse, R.
1980: The Northwest Atlantic Mid-Ocean Channel of the Labrador Sea: III. Head Spill vs Body Spill Deposits from Turbidity Currents on Natural Levees; Journal of Sedimentary Petrology, Volume 50, p.227-234.

Cloud, P.E.
1973: Paleoecological Significance of Banded Iron Formation; Economic Geology, Volume 68, p.1135-1143.

Colvine, A.C. (Ed.)
1983: The Geology of Gold in Ontario; Ontario Geological Survey, Miscellaneous Paper 110, 278p.

Crook, K.A.W.
1974: Lithogenesis and Geotectonics: the Significance of Compositional Variation in Flysch Arenites (Greywackes); p.304-310 *in* Modern and Ancient Geosynclinal Sedimentation, edited by R.H. Dott, Jr and R.H. Shaver, Society of Economic Pal. Min., Special Publication 19.

Devaney, J.
1983: The Stratigraphy of the Volcan Lake Metaconglomerate: Archean Braided River Deposits; University of Toronto, unpublished B.Sc. thesis.

Dimroth, E.
1976: Aspects of the Sedimentary Petrology of Cherty Iron-Formation, p.203-254 *in* Handbook of Stratabound Ore Deposits, edited by K.H. Wolf, Elsevier, New York, Volume 7.

Drever, J.I.
1974: Geochemical Model for the Origin of Precambrian Banded Iron Formations; Geological Society of America, Bulletin, Volume 85, p.1099-1106.

Eichler, J.
1976: Origin of the Precambrian Banded Iron-Formations; p.159-201 *in* Handbook of Stratabound Ore Deposits, edited by K.H. Wolf, Elsevier, New York, Volume 7.

Gross, G.A.
1965: Geology of Iron Deposits in Canada: General Geology and Evaluation of Iron Deposits; Geological Survey of Canada, Economic Geology Report 22, Volume 1, p.181.

Hesse, R., and Chough, S.K.
1980: The Northwest Atlantic Mid-Ocean Channel of the Labrador Sea: II. Deposition of Parallel Laminated Levee-Muds from the Viscous Sublayer of Low Density Turbidity Currents; Sedimentology, Volume 27, p.697-711.

Hyde, R.S.
1980: Sedimentary Facies in the Archean Timiskaming Group and their Tectonic Implications, Abitibi Greenstone Belt, Northeastern Ontario, Canada; Precambrian Research, Volume 12, p.161-195.

LaBerge, G.L.
1964: Development of Magnetite in Iron-Formations of the Lake Superior Region; Economic Geology, Volume 59, p.1313-1342.
1973: Possible Biogenic Origin of Precambrian Iron-Formations; Economic Geology, Volume 68, p.1098-1109.

Macdonald, J.A.
1982: The MacLeod-Cockshutt and Hard Rock Mines, Geraldton, Examples of an Iron-Formation Related Gold Deposit; Ontario Geological Survey, Miscellaneous Paper 106, p.188-191.
1983: The Iron Formation - Gold Association: Evidence from the Geraldton Area; p.75-83 *in* Geology of Gold in Ontario, edited by A.C. Colvine, Ontario Geological Survey, Miscellaneous Paper 110.

Mackasey, W.O.
1975: Geology of Dorothea, Sandra and Irwin Townships, District of Thunder Bay; Ontario Division of Mines, Geological Report 122.
1976: Geology of Walters and Leduc Townships, District of Thunder Bay; Ontario Division of Mines, Geological Report 149.

Mason, J.K., and Macdonald, A.J.
1983: Mining and Exploration Activities, and Gold Studies in the Geraldton-Beardmore Belt; p.191-193 *in* Summary of Field Work, 1983, edited by J. Wood et al., Ontario Geological Survey, Miscellaneous Paper 116.

Mason, J.K., and McConnell, C.D.
1983: Gold Mineralization in the Beardmore-Geraldton Area; p.75-83 *in* Geology of Gold in Ontario, edited by A.C. Colvine, Ontario Geological Survey, Miscellaneous Paper 110.

Meyn, H.D. and Palonen, P.A.
1980: Stratigraphy of an Archean Submarine Fan; Precambrian Research Volume 12, p.257-285.

Piper, D.J.W.
1972: Turbidite Origin of some Laminated Mudstones; Geological Magazine, Volume 109, p.115-126.
1978: Turbidite Muds and Silts on Deep Sea Fans and Abyssal Plains; *in* Submarine Canyon and Fan Sedimentation, edited by D.J. Stanley and G. Kelling, Dowden, Hutchinson and Ross, Stroudsburgh, Pa.

Pye, E.G.
1952: Geology of Errington Township, Little Long Lac Area, Thunder Bay District; Ontario Department of Mines, Annual Report for 1951, Volume 60, Part 5, 140p.

Stow, D.A.V.
1979: Distinguishing between Fine-Grained Turbidites and Contourites on the Deep-Water Margin off Nova Scotia; Sedimentology, Volume 26, p.371-387.

Stow, D.A.V., and Bowen, A.J.
1980: A Physical Model for the Transport and Sorting of Fine-Grained Sediment by Turbidity Currents; Sedimentology, Volume 27, p.31-46.

Stow, D.A.V., and Shanmugam, G.
1980: Sequence of Structures in Fine-Grained Turbidites: Comparison of Recent Deep-Sea and Ancient Flysch Sediments; Sedimentary Geology, Volume 25, p.23-42.

Teal, P.R., and Walker, R.G.
1977: Stratigraphy and Sedimentology of the Archean Manitou Group, Northwestern Ontario; Geological Survey of Canada, Paper 77-1A, p.181-184.

Trendall, A.F., and Blockley, J.G.
1970: The Iron Formations of Western Australia, with Special Reference to the Associated Crocidolite; West Australia Geological Survey, Bulletin 119, 353p.

Wood, J.
1980: Epiclastic Sedimentation and Stratigraphy in the North Spirit Lake and Rainy Lake areas: A Comparison; Precambrian Research, Volume 12, p.227-235.

Grant 168 Petrogenesis of Mineralized Horizons in Uchi Lake Metavolcanics

S.R. Noble[1], N.M. Evensen[1], and T.E. Krogh[2]

[1]Department of Geology, University of Toronto
[2]Jack Satterly Geochronology Laboratory, Royal Ontario Museum

ABSTRACT

The Uchi-Confederation Lakes area presents a unique opportunity to study both the evolution of early Archean crust and the origin of base metal mineralization associated with greenstone belt volcanism. Three cycles of mafic-to-felsic volcanism, spanning 220 Ma, are spatially associated with a complex granitoid terrane displaying a multi-stage history. Mineralization is found only in the latest volcanic cycle, associated with distinctive rare earth patterns which appear to reflect characteristics of the source magma chamber, and are possibly produced by contamination.

Both the volcanic rocks and the associated granitoid rocks are being studied petrologically, geochemically and isotopically to understand possible temporal and petrogenetic relations between the volcanic cycles and the multiple granitoid lithologies, as well as the origin of the characteristic geochemistry of the mineralized volcanic rocks. At least three distinct episodes of plutonism have been recognized from field relations, and are being dated by U-Pb zircon analysis. Initial Nd and Hf isotopic ratios will also be used to correlate lithologies and to assess the geochemical characteristics and evolution of their source areas.

INTRODUCTION

The Uchi-Confederation Lakes greenstone belt, in the Uchi Subprovince of the Superior Province (Figure 1), is unique in demonstrating three major cycles of mafic to felsic volcanism (Goodwin 1967; Pryslak 1971) which have been dated by U-Pb in zircons at 2959, 2794 and 2738 Ma (Nunes and Thurston 1980). Geochronology in the Red Lake greenstone belt, tentatively correlated with the Uchi-Confederation Lakes belt (P.C. Thurston, Ontario Geological Survey, personal communication, 1984), reveals a similar set of ages (F. Corfu, Jack Satterly Geochronology Laboratory, Royal Ontario Museum, personal communication, 1984). Both the relatively great age of the older cycles and the 220 Ma time span of volcanism at a single location render the Uchi-Confederation Lakes volcanic rocks fundamentally important in understanding crustal growth during Archean time.

Furthermore Thurston (1982) found at Uchi Lake, and Campbell *et al.* (1982) demonstrated in other areas worldwide, a correlation between the occurrence of base metal mineralization and the rare earth element (REE) patterns of the associated felsic volcanic rocks (at Uchi Lake, cycle III, the latest cycle, is the only one to show mineralization). Light REE enriched patterns without Eu anomalies are associated with barren horizons, and flat patterns showing negative Eu anomalies are associated with mineralization. Despite its great potential significance, the mechanism underlying this correlation remains unclear.

However Campbell *et al.* (1981) suggested that large magma chambers may be centrally important both in ore genesis and in trace element evolution in greenstone belt volcanic rocks. Thurston and Fryer (1983) presented evidence that the Uchi-Confederation Lakes volcanic rocks were derived from a succession of large, compositionally zoned magma chambers of the type described by Hildreth (1979) and Smith (1979), and proposed that the cycle III mineralization is a consequence of the evolution of the magma chambers beneath a progressively thickening crust. These concepts lead to consequences that can be geochemically, and in particular, isotopically, tested.

We are therefore using a variety of geochemical tools, together with field and petrographic observation, to understand the origin of the mineralized horizons in the Uchi-Confederation Lake volcanic rocks, and their relation to the granitoid rocks of the Trout Lake region, which may include the magma chamber differentiates associated with the greenstone belt volcanic rocks. This represents an opportunity to examine both a significant question of direct economic relevance, and an area of unique interest in Archean crustal evolution.

The geochemical techniques being applied in this study include major and trace element (including REE) analysis by X-ray fluorescence (XRF) and instrumental neutron activation analysis (INAA); precise geochronology by U-Pb dating of zircons; and analysis of Nd, Sr and Hf isotopic ratios in whole rocks and minerals.

Careful geochronology and the use of geochemical tracers, particularly Nd and Hf isotopes, should demonstrate

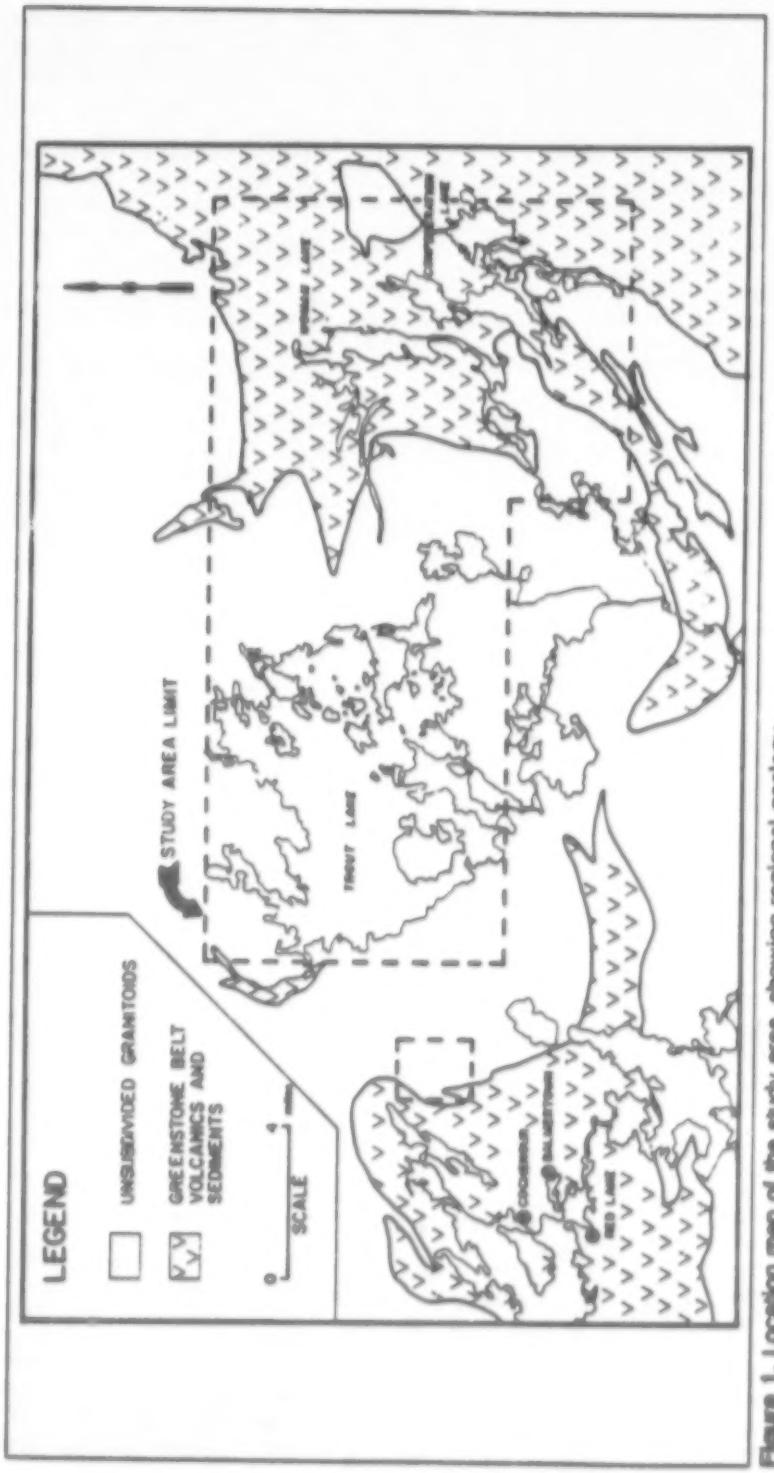

Figure 1. Location map of the study area, showing regional geology.

what temporal and petrogenetic relationships exist between the volcanic rocks and plutonic rocks in the area, and whether the mineralized horizons originate from a geochemically and isotopically distinctive source area. Crustal assimilation has been suggested as a possible origin for the distinctive REE patterns of the mineralized volcanic rocks (Thurston and Fryer 1983), and can be tested by isotopic criteria, including the possible presence of inherited zircons. Furthermore, magma chamber evolution may be critically important in ore genesis in associated volcanic rocks (Campbell *et al.* 1981), and can potentially be followed through analysis of the mini-cycles within the cycle II volcanic rocks.

To date, field work and extensive sampling have been carried out in the volcanic rocks and granitoid rocks, and geochemical analysis is in its early stages.

ANALYTICAL FACILITIES

The analytical facilities for high precision U-Pb dating in zircons are operational in the geochronology laboratory operated by T.E. Krogh under Ontario Geological Survey sponsorship at the Royal Ontario Museum, and the initial isotopic work is focussed on this aspect.

The Sr and Nd techniques have been developed in laboratory space at the Royal Ontario Museum. Modern clean laboratory facilities in the Mining Building (Department of Geology, University of Toronto) have now been completed and all Sr and Nd chemistry will be performed there. Rb and Sr are separated by the standard technique of HCl elution on cation exchange resin; this initial separation also yields the rare earth elements (REE) as a group. Sm and Nd are then separated by HCl elution on columns packed with teflon powder coated with bis-(2-ethylhexyl) hydrogen phosphate, in a modification of the technique of Richard *et al.* (1976). This yields excellent separations of Sm from Nd and uses easily obtainable and readily purified reagents.

A solid source mass spectrometer (VG Isotopes 354) at the Royal Ontario Museum is used for all Sr and Nd analyses and for some Pb analyses. It is fully automated, with a sixteen sample turret and five collectors. The new chemistry laboratories have been designed to process samples at a rate commensurate with the very high throughput of this machine. For Sr and Nd, the multiple collectors are used in conjunction with peak switching, which allows the rapid analysis and extremely high precision of the multiple collector configuration to be realized, while avoiding the uncertainties of amplifier calibration encountered in purely static multi-collection. Sr and Nd analyses are being performed with a precision (2σ) of 100 ppm or better.

We have obtained isotopic spikes and standards for Lu-Hf analysis, begun experiments using the Slowpoke reactor to determine Lu/Hf ratios by neutron activation, and investigated the possibility of a simpler technique for chemical separations than that of Patchett *et al.* (1981). A major difficulty in the chemistry is the tendency of Hf (and Zr) to polymerize in solution, rendering them almost impossible to separate. Treatment with H_2SO_4 inhibits polymerization and could form a component of a useful technique. In any event, Hf analysis will not be done until fairly late in the program; in the interim, Hf-bearing solutions will be saved from the dissolved zircon fractions for future separation and analysis, using well tested and established techniques.

TROUT LAKE GRANITOID ROCKS

Reconnaissance of the Trout Lake granitoid rocks has resulted in significant modification in the classification and subdivision of intrusive phases. Previous mapping (Donaldson and Jackson 1969) suggested that the terrane is composed of several discrete granodioritic intrusions which enclose several screens of paragneiss presumably derived from adjacent greenstone belts (cf. Glikson 1979). However, a variety of gneiss types and a range of intrusive phases from trondhjemite to granite were encountered.

The granitoid lithologies identified in the course of field work for this project are summarized in Table 1, and the distribution of the major lithologic units is illustrated in Figure 2. The lithologic boundaries shown in Figure 2 have only been slightly modified from those in recent compilation maps (e.g. Thurston and Bartlett 1981). Classification of the granitoid rocks is based on the criteria of Ayres (1972).

GNEISSES

The oldest granitoid rocks in the area are multiply deformed trondhjemite gneisses (unit 1, Figure 2). The gneisses occur as an enclave distinct from the enclosing trondhjemite-granodiorite batholith. The enclave is bounded by intrusive

TABLE 1. SUMMARY OF PRINCIPAL LITHOLOGIES OF THE TROUT LAKE GRANITOID ROCKS

1. (a) Hornblende-biotite trondhjemite gneiss. Equigranular, fine- to medium-grained, gneissic structure defined by 1-5 cm thick biotite- and hornblende-rich layers. Gneisses contain mafic xenoliths ranging in size from 10 cm to 2 m.
   (b) Leucocratic medium- to coarse-grained trondhjemite dikes, cutting 1a, discordant or locally concordant.
2. Granodiorite gneiss. Uncertain age relationships with unit 1a and 1b. Well banded, with 1-10 cm bands composed of quartz - plagioclase - biotite - hornblende and quartz - plagioclase - K-feldspar. Occurs as xenoliths in unit 3.
3. Foliated biotite trondhjemite-granodiorite, and minor diorite. Unit 3 dominates the map area, forming the bulk of the batholith. Foliation development is variable from weak to moderate. Contains mafic schlieren and xenoliths of units 1 and 2.
4. Mafic dikes. Dikes range from 2 cm to >2 m. Dikes are fine grained, composed of plagioclase, hornblende, chlorite, and quartz. Mafic dikes have a wide range of ages spanning biotite gneiss formation, to some late dikes cutting late felsic dikes (unit 5).
5. Equigranular unfoliated quartz monzonite. Occurs as irregular bodies up to 10 x 10 m. Main bodies have associated irregular discordant felsic and pegmatitic dikes.

contacts and has been invaded by discordant dikes which can be clearly traced in outcrop to the batholith. Gneiss mineralogy is dominated by quartz, oligoclase, biotite, hornblende, epidote, microcline and sphene. The texture is medium grained, seriate to equigranular, and gneissosity is defined by mafic clots and layers composed of biotite, hornblende, sphene and epidote. In outcrops where gneissosity is relatively poorly developed, a foliation parallel to gneissosity is outlined by biotite.

The gneiss enclave is host to a variety of mafic xenoliths and dikes ranging from 0.5 to 2 m wide. Amphibolite xenoliths usually exhibit sharp contacts, although they are frequently invaded by quartz-feldspar veins originating from the gneiss. Xenolith mineralogy includes medium-grained hornblende, biotite, oligoclase-andesine, sphene and epidote, with the biotite and hornblende outlining a foliation parallel to the trondhjemite gneissosity. In some cases the enclaves can be directly related to deformed mafic dikes (as with some enclaves in the Morton Gneiss; Nielsen and Weiblen 1980). However, the origin of the enclaves is generally ambiguous; they may be related to earlier greenstones (cf. the Amitsoq Gneiss; McGregor and Mason 1977).

Predominantly discordant mafic dikes are ubiquitous in the area, but are especially common in the gneiss enclave. The dikes span at least one major period of deformation within the gneisses; pre- and syn-deformation dikes are now present as amphibolite boudins, lenses and related mafic schlieren foliated parallel to the host gneissosity. Post-tectonic dikes generally show relict chilled margins and coarser equigranular cores. Primary mineralogy in the dikes is entirely absent; the dikes are now composed of hornblende, andesine, epidote, sphene, and biotite.

A second major gneiss enclave (unit 2, Figure 2) has been recognized northwest of tne trondhjemite gneiss enclave. This second enclave is composed of alternating granodiorite and amphibolite layers ranging from 1 to 10 cm thick. Age relationships with the trondhjemite gneiss enclave are uncertain, but the granodiorite gneiss is clearly older than the enclosing trondhjemite-granodiorite plutons, since gneiss xenoliths commonly occur in the trondhjemite-granodiorite.

TRONDHJEMITE–GRANODIORITE–DIORITE

The bulk of the Trout Lake granitoid rocks are relatively homogeneous, medium-grained trondhjemite and granodiorite. This unit clearly post-dates the gneisses, as evidenced by consistent cross-cutting relationships and different degrees of deformation and development of foliation.

Only minor mineralogical differences are observed in the trondhjemites examined along the entire eastern shore of Trout Lake, compounding the problem of subdividing the batholith into discrete plutons. The trondhjemites are composed of medium-grained quartz, albite-oligoclase, microcline, epidote, sphene, biotite and hornblende. Biotite/hornblende ratios are variable and usually greater than 1, and hornblende is generally absent in samples from the area near the greenstone belt contact.

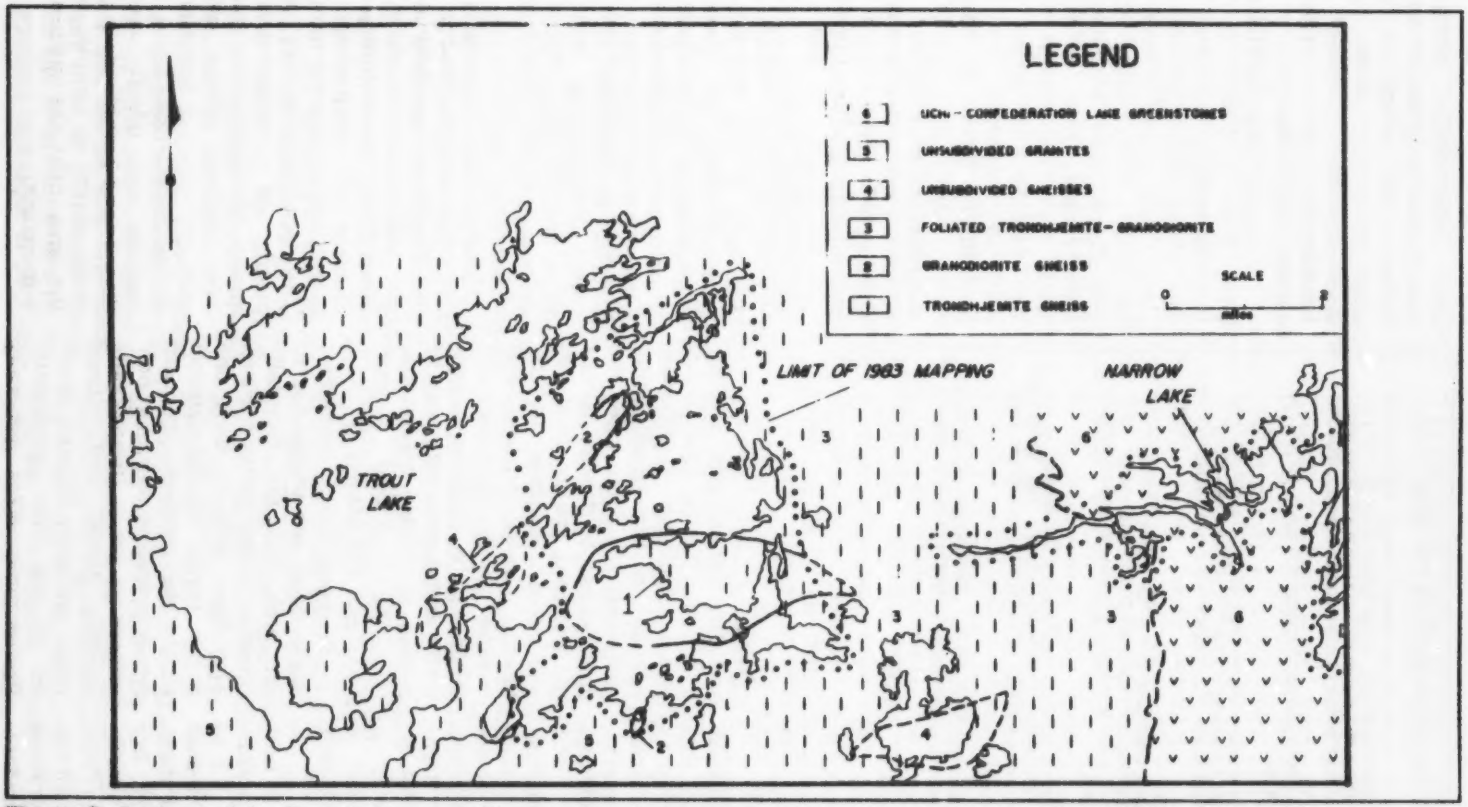

Figure 2. Geology of the Trout Lake granitoid rocks. Lithological contacts after Thurston and Bartlett (1981) and this study.

Foliation is most obvious adjacent to the greenstone belt, and is outlined by aligned biotite and lenticular quartz. The trondhjemites in the central Trout Lake region are characterized by a weaker foliation coupled with a more equigranular fabric.

Mafic enclaves in the trondhjemites are most common adjacent to the metavolcanic rocks. This suite of enclaves is unambiguously related to the Uchi-Confederation Lakes metavolcanic rocks. Unlike enclaves in the gneiss, relict volcanic textures are often present, and occasional reaction zones are present between the trondhjemite-granodiorites and the xenoliths.

POST–DEFORMATION GRANITES

A variety of late granodiorites and granites post-date the main Trout Lake granitoid phases but are of limited extent and hence are not shown in Figure 2. Two varieties are common: aplitic to coarse-grained felsic dikes, and granitic pegmatites.

The felsic dikes are intrusive into both the foliated trondhjemites and gneisses. The dikes are unfoliated and undeformed, and often can be traced to outcrop-sized irregular granodiorite intrusions which are likewise unfoliated. The dikes range in composition from granodiorite to granite, with a fine- to medium-grained seriate texture.

Pegmatites are less common and are generally separate from the felsic dikes. The pegmatites are most common at the contact between the trondhjemite batholith and the Uchi-Confederation Lake metavolcanic rocks, forming irregular bodies along the contact, and pods in the adjacent foliated trondhjemites. The principal minerals in the pegmatites are microcline, albite and quartz, with minor muscovite. Pegmatite pods also occur in the foliated trondhjemites well removed from the greenstone contact. The pods are unzoned and dominated by euhedral 3 to 7 cm microcline crystals in a medium- to coarse-grained quartz-albite matrix, with accessory garnet and muscovite. As with the felsic dikes, the pegmatites are undeformed, excepting minor brittle fracture of the larger mineral grains, subsequently infilled by quartz and albite.

GEOCHEMISTRY AND GEOCHRONOLOGY

Laboratory based studies are now in progress. Major and trace element contents of samples from the granitoid rocks and volcanic rocks are being determined by X-ray fluorescence and instrumental neutron activation analysis at the University of Toronto. Complete major and minor element analyses representative of an entire rock suite were not available at the time of writing.

To date, three zircon samples from the Trout Lake granitoid rocks have been prepared and are being analyzed at the geochronology laboratory of the Royal Ontario Museum. Two samples from the trondhjemite gneisses and one from the late felsic dikes have been chosen to give a maximum spread in granitoid ages. It is suspected that the gneiss enclave is similar to gneisses dated at 2950 Ma (U-Pb in zircons) adjacent to the Favourable Lake volcanic complex (F. Corfu, Royal Ontario Museum, personal cummunication, 1984; Hillary and Ayres 1980), while the late felsic intrusions are probably of similar age to the post-tectonic plutons in the Uchi-Confederation Lakes belt (2729.6 ±1.3 Ma, Nunes and Thurston 1980). The zircon populations in both rock types contain relatively few crack-free, clear grains of the type needed to provide concordant or nearly concordant analyses. The bulk of the zircons in the least magnetic fractions of both rock types are stubby brown variably-zoned crystals with short prism faces, although in the gneiss fine clear needles comprise a distinct group which are also being analyzed (Figures 3 and 4). Therefore, extensive use of abrasion techniques is in progress to obtain useful data from the cores of the zoned crystals.

Two felsic volcanic samples collected from the Cycle II mini-cycles (Thurston 1980; Thurston and Fryer 1983) were prepared for U-Pb dating. Although 70 kg samples from both the top and bottom of the mini-cycles were processed, neither sample provided sufficient numbers of good quality zircons for analysis. The zircons recovered from both samples were unusual in that they were dominantly clear crystal fragments of variable size, with only occasional subrounded grains preserved. Since dating the time interval of volcanism in the mini-cycles is important for understanding the temporal development of Cycle II, additional rhyolite samples with more abundant quartz and feldspar phenocrysts have been obtained from the lowermost mini-cycle and a felsic crystal tuff overlying the mini-cycles. Since phenocryst content is roughly correlated with zircon abundance, these should prove

more suitable for zircon analysis.

CONCLUSIONS AND FUTURE OBJECTIVES

The following conclusions can be drawn based upon field data obtained thus far.

1. The Trout Lake granitoid rocks have a more complex temporal and tectonic history than has previously been reported. The lithologies examined indicate that a minimum of three major igneous events have occurred in the region. It is at least possible, based on the tentative correlations with well-dated lithologies discussed above, that the total time span represented in the Trout Lake granitoid rocks is comparable to that of the Uchi-Confederation Lake metavolcanic rocks.

2. The early trondhjemite gneiss enclave is probably orthogneiss based on field and petrographic observations. However, the age and origin of the granodiorite gneiss enclave are enigmatic. These should be clarified by the chemical and isotopic studies now in progress.

3. The gneiss enclaves and foliated trondhjemite-granodiorite have been metamorphosed to amphibolite facies based upon the metamorphic grade of mafic inclusions and post-intrusion mafic dikes.

The principal objectives for the immediate future are completion of field work, continuation of the geochemical analysis of the granitoid rocks and volcanic rocks, and dating 3-5 samples from the granitoid rocks immediately before and after the field season. Before the end of 1984 the first Sm-

Figure 3. Representative zircons from the trondhjemite gneiss enclave. The two dominant zircon types are stubby rounded grains (centre) and grains with well-developed prism faces (right). A grain fragment is on the left. All grains were picked from final non-magnetic fraction before air abrasion.

Figure 4. Representative zircons from late undeformed granitic intrusion associated with late felsic dikes. Three populations are: (left) grains with well developed prism faces; (centre) large stubby grains; and (right) small rounded grains. All grains are from final non-magnetic fractions before air abrasion.

Nd analyses of Cycle II and III volcanic rocks will be available. Ten weeks of field work will concentrate on: (a) collecting a suite of Cycle I volcanic samples from the Uchi Lake area for a U-Pb date in the uppermost felsic unit and Sm-Nd analyses from a series of subvolcanic gabbroic to dioritic sills; and (b) examining and sampling approximately five small areas in the Trout Lake granitoid rocks.

ACKNOWLEDGMENTS

We are grateful to P.C. Thurston of the Ontario Geological Survey for invaluable assistance in planning and executing the field work, and for sharing his knowledge of volcanology with us. We also thank M.E. Durocher, Resident Geologist, Ontario Ministry of Natural Resources, Red Lake, and A.J. Andrews of the Ontario Geological Survey for help in the logistics. Isotope facilities at the Royal Ontario Museum and the University of Toronto are supported by funds from NSERC, the Ontario Geological Survey, and the University of Toronto.

REFERENCES

Ayres, L.D.
1972: Guide to Granitic Rock Nomenclature Used in Reports of the Ontario Division of Mines: Ontario Geological Survey, Miscellaneous Paper 52, 14p.

Campbell, I.M., Coad, P., Franklin, J.M., Gorton, M.P., Scott, S.D., Sowa, J., and Thurston, P.C.
1982: Rare Earth Elements in Volcanic Rocks Associated with Cu-Zn Massive Sulphide Mineralization: A Preliminary Report; Canadian Journal of Earth Sciences, Volume 19, p.619-623.

Campbell, I.M., Franklin, J.M., Gorton, M.P., Hart, T.R., and Scott, S.D.
1981: The Role of Subvolcanic Sills in the Generation of Massive Sulfide Deposits; Economic Geology, Volume 76, p.2248-2253.

Donaldson, J.A. and Jackson, G.D.
1969: Geology, Trout Lake, Ontario; Map 1200A, Geological Survey of Canada, scale 1:253 440.

Glikson, A.Y.
1979: Early Precambrian Tonalite-Trondhjemite Sialic Nuclei; Earth Science Reviews, Volume 15, p.1-73.

Goodwin, A.M.
1967: Volcanic Studies in the Birch-Uchi Lakes Area of Ontario; Ontario Department of Mines, Miscellaneous Paper 6, 96p.

Hildreth, W.
1979: The Bishop Tuff: Evidence for the Origin of Compositional Zonation in Silicic Magma Chambers; p.43-75 *in* Ash-Flow Tuffs, edited by G.E. Chapin and W.E. Elston, Geological Society of America, Special Paper 180.

Hillary, E.M., and Ayres, L.D.
1980: Trondhjemitic Basement Enclave near the Archean Favourable Lake Volcanic Complex, Northwestern Ontario, Canada; Canadian Journal of Earth Sciences, Volume 17, p.652-667.

McGregor, V.R., and Mason, B.
1977: Petrogenesis and Geochemistry of Metabasaltic and Metasedimentary Enclaves in the Amitsoq Gneisses, West Greenland; American Mineralogist, Volume 62, p.887-904.

Nielsen, B.V., and Weiblen, P.W.
1980: Mineral and Rock Compositions of Mafic Enclaves in the Morton Gneiss; p.95-103 *in* Selected Studies of Archean Gneisses and Lower Proterozoic Rocks, Southern Canadian Shield, edited by G.B. Morey and G.H. Hanson, Geological Society of America, Special Paper 182.

Nunes, P.D., and Thurston, P.C.
1980: Two Hundred and Twenty Million Years of Archean Evolution: A Zircon U-Pb Age Stratigraphic Study of the Uchi-Confederation Lakes Greenstone Belt, Northwestern Ontario; Canadian Journal of Earth Sciences, Volume 17, p.720-731.

Patchett, P.J., Kouvo, O., Hedge, C.E., and Tatsumoto, M.
1981: Evolution of Continental Crust and Mantle Heterogeneity: Evidence from Hf Isotopes; Contributions to Mineralogy and Petrology, Volume 78, p.279-297.

Pryslak, A.P.
1971: Corless Township, District of Kenora (Patricia Portion); Ontario Department of Mines and Northern Affairs, Preliminary Map P.634, scale 1:15 840.

Richard, P., Shimizu, N., and Allegre, C.J.
1976: $^{143}Nd/^{146}Nd$, a Natural Tracer: An Application to Oceanic Basalts; Earth and Planetary Science Letters, Volume 31, p.269-278.

Smith, R.L.
1979: Ash-Flow Magmatism; p.43-75 *in* Ash-Flow Tuffs, edited by G.E. Chapin and W.E. Elston, Geological Society of America, Special Paper 180.

Thurston, P.C.
1980: The Volcanology and Trace Element Geochemistry of Cyclical Volcanism in the Archean Confederation Lake Area, Northwestern Ontario; Unpublished Ph.D. Thesis, University of Western Ontario, 553p.
1982: Economic Evaluation of Archean Felsic Volcanic Rocks Using REE Geochemistry; Geological Society of Australia, Special Publication 7, p.439-450.

Thurston, P.C., and Bartlett, J.R.
1981: Trout Lake - Birch Lake Sheet, Kenora District; Ontario Geological Survey, Preliminary Map P.2386, scale 1:126 720.

Thurston, P.C., and Fryer, B.J.
1983: The Geochemistry of Repetitive Cyclical Volcanism from Basalt Through Rhyolite in the Uchi-Confederation Greenstone Belt, Canada; Contributions to Mineralogy and Petrology, Volume 83, p.204-226.

Grant 172 Strength Testing of Reservoir Strata in the Grimsby Formation (Lower Silurian) of Southwestern Ontario

P.E. Holm

Department of Geology, University of Windsor

ABSTRACT

Unconfined and confined compressive tests have been conducted on 38 mm by 19 mm test cores from sandstone units from seven Lake Erie exploration wells in the Grimsby Sandstone. The Grimsby is a major oil and gas producer in southern Ontario. Porosity, permeability, petrologic, and petrographic data for the tested samples are to be correlated with the deformational test results. Analysis of the strength data is incomplete, but initial results show a range of unconfined compressive strengths of 60-150 MPa with E values of 20-30 x 10^3 MPa. Application of 10 MPa confining pressure results in a 40-60% increase in compressive strength. There is a significant correlation between decreasing porosity and increasing strength.

INTRODUCTION

The strength and deformational behaviour of samples from the Lower Silurian Grimsby Sandstone have been investigated under unconfined and confined test conditions. The Grimsby, consisting of quartz arenites and subordinate shales, is a major source of natural gas and crude oil production in southern Ontario. Gas and liquid flow in the Grimsby is poorly understood, and hydraulic fracturing to enhance flow is not always successful. The data should aid in the modelling of flow and fracture characteristics of this unit for enhanced recovery and future gas storage prospects.

GENERAL GEOLOGY

The Grimsby Sandstone is part of the Lower Silurian Medina Formation. The stratigraphy and sedimentology of the Grimsby and the Medina Formation have been described by Fisher (1954) and Martini (1971), and the petrology of the Grimsby was discussed by Lumsden and Pelletier (1969). The Grimsby outcrops along the base of the Niagara escarpment and extends into the subsurface beneath Lake Erie where it is a gas and oil producer. It characteristically consists of red hematitic sandstones and shales/siltstones with some light green and mottled red and green sandstones. The Grimsby was deposited during a westward regression as deltaic and littoral to sublittoral sands and muds. Thus, the sandstones occur as isolated lenses or elongated bar or channel fill deposits enclosed by the shales which form the seal for accumulated hydrocarbons.

TESTING PROGRAM

Slabbed cores of the Grimsby in the core storage laboratory at the University of Windsor were examined and seven were selected that would provide adequate test material and a representative variety of sandstone lithologies. Cores are from Consumers' Power exploration wells in Lake Erie south of Norfolk County, Ontario, in the vicinity of the Clear Creek gas field. Sampled sandstone layers were generally 1-2 m thick. Thinner units or those with numerous clay laminae would not provide adequate test material.

Vertical and horizontal 19 mm diameter plugs were obtained from all sampled sections for porosity and permeability measurements. Multiple plugs were obtained from thick sections or those that showed internal variability to ensure a close correspondence to the location of strength test cores. Approximately 70 mercury porosimeter and gas permeameter measurements were made. Vertical and horizontal thin sections were produced from the vicinity of the plugs for petrographic analysis. Test cores, 38 mm by 19 mm, were obtained from the sandstone units. Duplicate tests on each unit or different portions of thicker units were conducted at 0, 10, and 20 MPa confining pressure, dry, at room temperature, and a strain rate of 10^{-5}/sec. When possible, cores oriented other than vertical were tested to check for strength anisotropy effects. The test program was conducted at the Rock Deformation Laboratory, University of Illinois at Urbana-Champaign.

EXPERIMENTAL RESULTS AND DISCUSSION

Petrographic examination showed that the sandstones have subangular to subrounded grains consisting of 80-90% quartz with subordinate feldspar, lithic fragments, calcite, and opaques. They tend to be fine-grained and closely packed with a predominance of planar and concavo-convex contacts. Grains are hematite coated and quartz overgrowths, marked by dusty hematitic inclusions, are common. Porosity generally varies from 10 to 15% with highly variable per-

meabilities ranging from <1.0 md to >20 md. Lower permeability samples had a greater proportion of secondary quartz overgrowths.

Initial results of the deformation tests show a range of unconfined compressive strengths of 60-150 MPa with typical E values of 20-30 x 10^3 MPa. Application of 10 MPa confining pressure resulted in a 40-60% increase in compressive strength. There appears to be a statistically significant correlation between increasing strength and decreasing porosity, but not between permeability and strength. An average Poisson's ratio of 0.16 was determined in an earlier study (Rogers 1982) by use of a dilatometer attached to the pressure vessel. The Grimsby samples display limited dilatant behaviour, typical of most rocks, unlike the extreme dilatancy of some high porosity sandstones (Rogers and Holm 1983). Due to mechanical and recalibration problems with the testing apparatus, the analysis of the strength data is incomplete. The detailed data with petrologic and petrographic correlations, appear in the final report.

REFERENCES

Fisher, D.W.
1954: Stratigraphy of Medina Group, New York and Ontario; Bulletin of the American Association of Petroleum Geologists, Volume 38, p.1979-1996.

Lumsden, D.N., and Pelletier, B.R.
1969: Petrology of the Grimsby Sandstone (Lower Silurian) of Ontario and New York; Journal of Sedimentary Petrology, Volume 39, p.521-530.

Martini, I.P.
1971: Regional Analysis of Sedimentology of Medina Formation (Silurian), Ontario and New York; Bulletin of the American Association of Petroleum Geologists, Volume 55, p.1249-1261.

Rogers, C.T.
1982: The Influence of Petrographic Factors on the Strength and Deformational Behaviour of Some Quartz-Rich Sandstones; Unpublished M.Sc. Thesis, University of Windsor, 172p.

Rogers, C.T., and Holm, P.E.
1983: Interrelationship of Petrologic Factors and the Deformational Behaviour of Sylvania and Grimsby Sandstone Samples at Low Confining Pressure; Geological Society of America, Abstracts with Programs, Volume 15, Number 4, p.259.

Grant 173 Sedimentary Rocks and Stratabound Mineralization in the Cobalt Region

J.A. Donaldson[1], M.D. Goodz[1], F.A. Michel[1], P. Mustard[1], R. Rainbird[1], B.R. Rust[2], D.H. Watkinson[1], and B. Wilson[1]

Ottawa-Carleton Centre for Geoscience Studies
[1]Department of Geology, Carleton University
[2]Department of Geology, University of Ottawa

ABSTRACT

The principal objectives of this project are to re-examine sedimentary strata of the Cobalt Group (uppermost component of the Huronian Supergroup) in the light of recently published sedimentological models, to improve the data base for these strata on the basis of field mapping, to investigate the nature of the Archean-Proterozoic unconformity, and to evaluate possible controls of ore emplacement in Proterozoic strata and underlying Archean basement rocks of the Cobalt region. Of particular interest from an economic point of view is the possible stratiform/stratabound relationship of some concentrations of base metals (especially Cu, Zn, Pb) and precious metals (Ag, Au) to specific beds in the Coleman Member of the Cobalt Group.

Detailed mapping (1:2000 scale) combined with stratigraphic, fabric, paleocurrent, and petrographic studies have provided a data base for reinterpretation of the lower Gowganda (Coleman Member) in the Cobalt area. Here, gently dipping strata comprise, in ascending order: basal breccia (periglacial and/or subglacial in origin); basal diamictite (primary till); an upward-coarsening sequence of rhythmically laminated argillite, siltstone, and fine-grained sandstone, overlain by interbedded medium- to coarse-grained sandstone and pebble-granule orthoconglomerate (prograding subaqueous outwash fan deposits); and bedded heterolithic diamictite resulting from subaqueous sediment gravity flows. The Gowganda Formation at Cobalt fits an inner-shelf grounded ice sheet model. Substantial subaqueous deposition occurred in either a glaciolacustrine or a glaciomarine tidewater environment.

Systematic studies of joints at Cobalt have revealed a preponderance of NNE and NW trends. The NNE-trending joints predominate, but most ore veins are parallel to the NW-trending joints. The latter set of joints is tentatively interpreted to be of shear origin, created by NW-SE compression (responsible also for creating major NE-trending reverse faults in the Cobalt camp).

Studies of sulphur isotopes from the Beaver-Temiskaming mine have revealed two distinct trends: (1) the isotopic ratios decrease (lighten) from the syngenetic basement sulphides to the epigenetic vein-related sulphides; (2) regardless of sulphide type or mineral separate, the $\delta^{34}S$ content decreases from the wallrocks to the vein centres. These trends support a model of mixing of basement sulphur and vein sulphur.

INTRODUCTION

Although much of the mineral wealth of the Cobalt region (Ag, Pb, Zn, Cu, Pt, Co) has been derived from Proterozoic and Archean sedimentary rocks, few detailed sedimentological studies have been carried out in this region. Whereas considerable research efforts have been directed at mineralogy, structure, metamorphism and relationship of the ore deposits to emplacement of the Nipissing diabase (e.g. Jambor 1971), most sedimentary studies of the Cobalt Group have been directed at regional syntheses (see Young 1973). The present research project involves systematic studies of stratigraphic components of the Cobalt Group and subjacent Archean basement rocks (Figure 1), as well as the regolith at the Archean-Proterozoic unconformity (Patterson 1979, Rainbird 1980). The principal aims are to establish criteria for recognizing specific lithofacies, to infer depositional environments and to evaluate possible associations of mineral deposits with these facies.

The underlying premise for this study is that the provision of new insights into relationships between sedimentology/stratigraphy and ore deposits will elicit renewed interest, and generate new approaches to mineral exploration, in this promising region of the Canadian Shield.

GOWGANDA FORMATION

Lindsey (1967) reaffirmed glacial origin for the Gowganda Formation, attributing northern occurrences of the Gowganda (including those of the Cobalt area) to continental glaciation and southern occurrences to glaciomarine deposition. More recently, Miall (1983) has suggested that all of the Gowganda sediments were deposited in a glaciomarine environment.

Detailed mapping (1:2000 scale) of a 6 km^2 area (including the town of Cobalt), combined with measurement

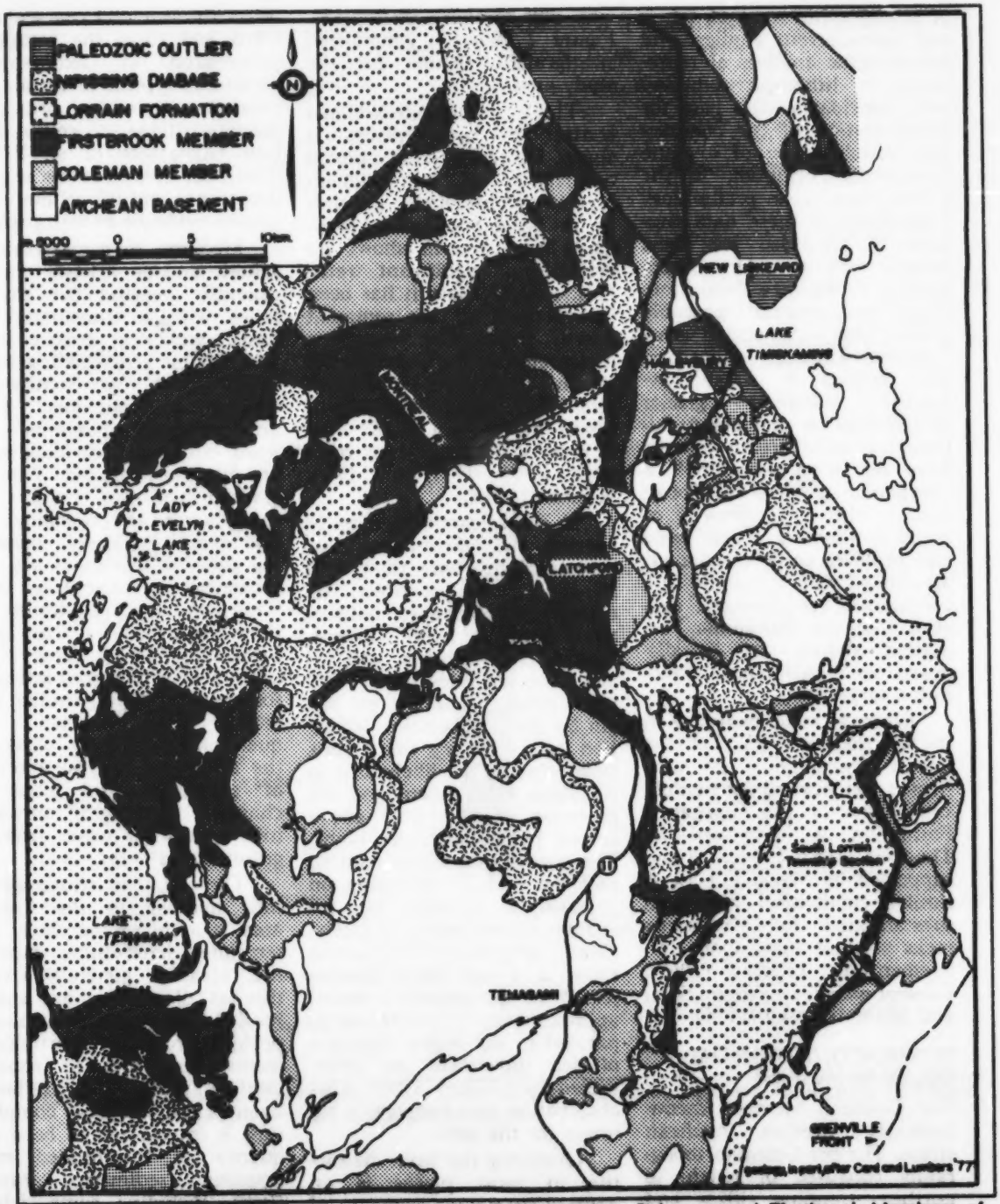

Figure 1. Distribution of Huronian rocks in the Cobalt region: Coleman and Firstbrook Members of the Gowganda Formation, Lorrain Formation and Nipissing Diabase.

of stratigraphic sections, fabric and paleocurrent studies, and petrographic analysis of representative lithologic samples, have provided a data base for interpretation of the complex sedimentology of the Gowganda Formation in the Cobalt area. Our preliminary assessment of these data supports a grounded ice sheet model, with a major component of subaqueous deposition. This environment probably graded into a lacustrine environment, although sedimentation related to a shallow-marine tidewater glacier should also be considered. Although braided stream deposits have not been recognized in Gowganda strata of the Cobalt area, the presence of meltwater-derived coarse sand and pebble-granule conglomerate, linked with proximity to a continental environment, suggests that the Gowganda Formation should not be dismissed as a paleoplacer exploration target.

Regional reconnaissance in the northeastern part of the Cobalt Embayment has confirmed justification for twofold subdivision of the Gowganda Formation as suggested by Thomson (1957; 1964a,b,c) and supported by Wood (1979). A similar subdivision has been substantiated for Gowganda rocks west of the Cobalt Embayment by Lindsey (1969), Card *et al.* (1973), Wood (1973) and Siemiatkowska (1978).

SEDIMENTOLOGY OF THE COLEMAN MEMBER

The Coleman Member unconformably overlies Archean strata. The pre-Coleman topography consisted of north- to northeast-trending ridges and valleys with moderate relief (Legun 1984). Coleman strata are generally subhorizontal, with dips rarely exceeding 15°. Figure 2 shows a generalized stratigraphic section for the study area.

The Coleman-Archean contact in most places is sharp. However, some isolated occurrences of non-Coleman breccia are preserved, generally in paleotopographic lows. This basal breccia shows no evidence of significant transport, except where it has been incorporated in rare sediment gravity flows. The breccia is interpreted to be a periglacial regolith (Patterson 1979, Rainbird 1980). Some component of freeze-thaw action at the base of grounded ice also may have been involved (Legun 1984, Scammell 1984).

A basal diamictite directly overlies the unconformity or breccia along more than 60% of the exposed contact. Its massive, structureless, nonsorted nature, areal extent, stratigraphic position, and facies relationships to other units strongly support an origin by direct subglacial deposition as a primary till. Debris flow origin is not likely, due to the large areal extent and the presence of this unit above several paleotopographic highs. The high silt and clay content and the lack of slumping on paleoslopes renders an ice rainout interpretation unlikely. Clast long-axis orientations show a non-random pattern (clasts are statistically oriented approximately north-south, parallel to the major direction of ice movement as determined by Lindsey 1967). This observation also supports a till origin for the unit.

Overlying the basal diamictite in most places is an upward-coarsening sequence of rhythmites, sandstones and orthoconglomerates. The rhythmites thicken and coarsen upward and show the complete progression of sedimentary structures typical of distal, intermediate and proximal glaciolacustrine rhythmites (see Gustavson *et al.* 1975). This unit also contains sparse dropstones and till pellets, conclusive evidence of ice-rafting.

Medium- to coarse-grained arkose and/or arkosic wacke generally overlies the rhythmites with a transitional or (less commonly) erosive contact. Planar crossbedding indicates south to southwest-flowing paleocurrents. This unit generally coarsens upward, but some individual beds are normally graded. Pebble-granule (and rare boulder) orthoconglomerates cap much of this sequence. These coarsening upward sequences are interpreted as subaqueous outwash fan deposits similar to those described by Rust and Romanelli (1975). Individual units cannot be traced laterally for great distances; similar but laterally unconnected sequences in different parts of the map area suggest a series of subglacial and englacial channels discharging outwash into a body of water from a grounded ice-sheet.

The highest stratigraphic unit mapped in the Cobalt area is a thick, complexly intercalated heterolithic diamictite. Massive, generally structureless diamictites are interbedded with discontinuous pebble-granule orthoconglomerates, fine- to coarse-grained arkoses, and rare laminated siltstones. This complex unit is interpreted to be a sequence of interbedded subaqueous sediment gravity flows, including some debris flows, density-modified grain flows, high-density turbidity flows and liquefied/fluidized

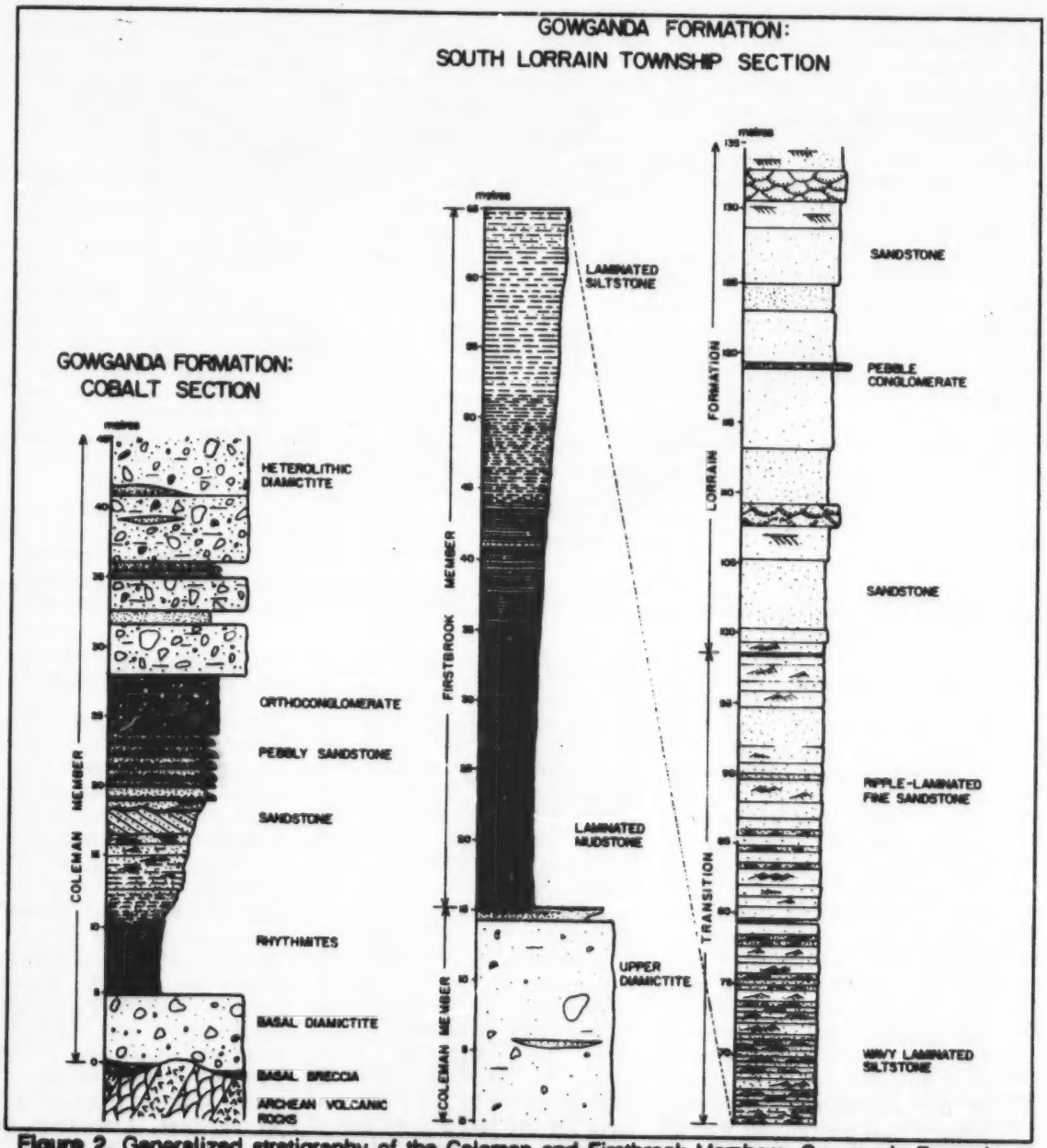

Figure 2. Generalized stratigraphy of the Coleman and Firstbrook Members, Gowganda Formation, based on measured sections in the Cobalt region.

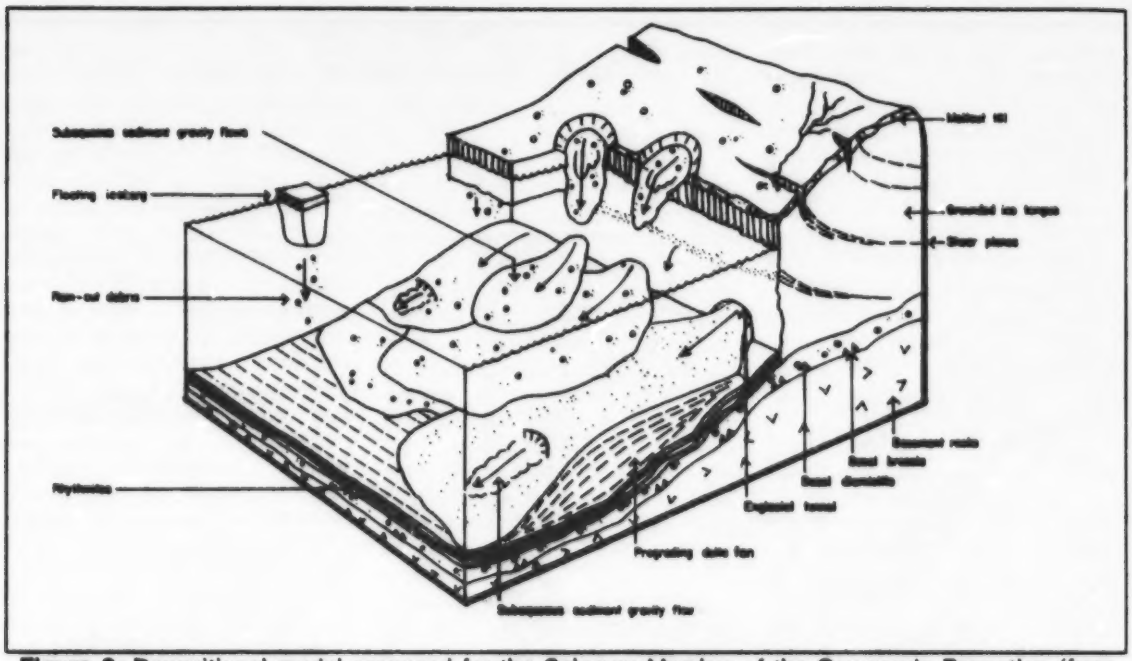

Figure 3. Depositional model proposed for the Coleman Member of the Gowganda Formation (from Scammell 1984).

flows (terminology of Lowe 1982). The close association with subaqueous outwash fans suggests that failure on fan slopes may have initiated some of these flows. Flows into the basin of water-saturated supraglacial melt-out debris during slow retreat or stagnation of the ice sheet may also have been an important source for these sediments. Although ice rainout from an ice shelf cannot be completely ruled out, the discontinuous nature of the subunits and the apparent lack of correlation between flow directions and paleoslopes of the Archean unconformity suggest that ice rainout was no more than a minor component of sedimentation in the Cobalt area.

A possible depositional model is shown in Figure 3. Deposition appears to have occurred in an inner shelf environment (in the sense of Gravenor *et al.* 1984, where lacustrine or marine conditions are not specified). The relatively small areal extent of the rhythmites and close similarity to Quaternary glaciolacustrine varves are suggestive of freshwater deposition. Although glaciomarine varve-like sediments are recorded in the literature, their resemblance to glaciolacustrine varves generally is superficial. A detailed examination of lateral facies relationships and small-scale sedimentary structures should serve to distinguish these types. An exception may be sedimentation by tidewater glaciers for the facies associations described by Powell (1981), which in many respects resemble facies associations in the Coleman Member at Cobalt.

SEDIMENTOLOGY OF THE FIRSTBROOK MEMBER

The Firstbrook Member (see Figure 1) is a laterally continuous unit that extends from the town of Gowganda southeastward to Temagami. It reaches a maximum thickness of greater than 500 m in the region between Lady Evelyn Lake and northern Lake Temagami, but thins rapidly toward the margins of the embayment. Measured sections in South Lorrain Township indicate a thickness of less than 60 m, whereas in Nicol Township, east of Gowganda, the Firstbrook Member is no more than 25 m thick. Firstbrook strata are absent in the region north and west of Temagami, and southeast of the Cobalt townsite. Deposition in these regions was likely precluded by proximity to topographic highs of Archean basement.

The Firstbrook Member conformably overlies the Coleman Member (the contact is well exposed in a single locality within South Lorrain Township). Firstbrook strata are typically subhorizontal, with dips less than 15 degrees. The Firstbrook Member is distinguished from similar Coleman Member rocks by greater lateral extent, lack of dropstones and lack of other features indicative of deposition in a glacial environment. A generalized stratigraphic section based on exposures in South Lorrain Township summarizes the lithologic components of the Firstbrook Member, Coleman Member and overlying Lorrain Formation (Figure 2). Similar coarsening-upward sequences have been measured in several other localities within the study region.

The lower portion of the Firstbrook Member consists mainly of dark green thinly laminated shaly mudstones. The basal layers are draped over cobbles and boulders that protrude from the top of the Coleman Member. In thin section the laminae show consistent normal grading (fine silt to clay), suggesting deposition by distal turbidity currents. East of Lady Evelyn Lake, this lower section is distinctively black to grey-black. Gradational with the lower strata is the middle and most extensive component of the Firstbrook Member, comprising medium- to thick-laminated red and green variegated siltstones. Red colouration, typically confined to the coarser laminae, presumably is the result of early diagenetic hematite formation; the green colouration is due to chlorite in the finer laminae (reverse variegation also occurs, but is rare). Variegation of this type can be explained by differing degrees of intrastratal alteration of Fe-Mg silicates and dehydration of Fe oxyhydroxides (Aspler and Donaldson 1984).

In Firstbrook and Barr Townships, red colouration is ubiquitous throughout most of the section. Several authors have suggested that this red colouration marks the beginning of significant O_2 accumulation in the Earth's atmosphere (Roscoe 1969, Frarey and Roscoe 1970). This "oxyatmoversion" (terminology of Roscoe 1973) could be significant in that sedimentary strata which postdate it may contain paleoplacers of gold exhibiting features of enrichment comparable to geologically younger deposits (Mossman and Harron 1983). Wood (1979, 1980) concluded that the Lorrain red beds are diachronous, and suggested that strata in northern parts of the Cobalt Embayment are younger than similar strata to the south.

Up section, overall grain size increases and ripple bed forms begin to predominate. The upper part of the Firstbrook Member is typified by wavy and ripple cross-laminated mudstone and siltstone separating thin beds of fine-grained pink sandstone. Ripple cross-lamination indicates predominantly unidirectional currents toward the south, although some reversals have been noted. As the overlying Lorrain Formation is approached, sand content and bed thickness increase, and rippled mud laminae decrease. Ball-and-pillow structures and slump folds are common in this transition zone.

The basal part of the Lorrain Formation mainly consists of massive fine- to medium-grained grey and maroon arkose. Trough crossbeds are characteristic of most sections, and they indicate unidirectional transport toward the south. The Firstbrook-Lorrain coarsening-upward sequence is interpreted as the record of a prograding delta (initial deposition of mudstone and siltstone, perhaps in a shallow marine environment, giving way to deposition of arkose which shows features suggestive of a braided fluvial environment). A similar model was proposed by Lindsey (1969) for deposition of the upper Gowganda Formation in the Whitefish Falls area. The sequence also records rapid amelioration of the climate from frigid conditions implied for deposition of the Coleman Member to humid and possibly subtropical conditions as proposed for the Lorrain Formation by Wood (1970) and by Young (1970, 1973).

SULPHIDE MINERALIZATION

Sedimentary rocks of the Coleman Member of the Gowganda Formation host most of the native silver and Co-Ni arsenide mineralization at Cobalt. Several hundred samples have been collected to determine the types, percentages and isotopic ratios of the various sulphides, which in close association with the arsenides, are widely disseminated throughout the sedimentary rocks. Most of the samples were taken in the vicinity of Little Silver Vein, Coniagas-Tretheway Open Pit, Vein 64, MacDonald Vein, Cobalt Vein, the east end of Kerr Lake Arch, numerous smaller surface workings, and from the

Langis Mine in Casey Township (20 km north of Cobalt).

Preliminary polished section work has identified chalcopyrite, sphalerite, galena, bornite, covellite, cobaltite(?), pyrrhotite, pyrite, native silver and at least six other species yet to be determined. These metallic minerals appear to partially replace other minerals, and for the most part occupy interstices between clastic grains. Within most samples, one or two sulphide minerals predominate, and other metallic minerals are subordinate.

The abundance of sulphide minerals varies between different rock types and from place to place within the Cobalt camp. In some places, sulphides appear to be abundant adjacent to mined-out veins, such as Little Silver Vein. Within a few metres of this vein-cut, coarse-grained sandstone contains up to several percent chalcopyrite. Farther away, the sandstone contains much less sulphide (the concentration tapers off to visibly undetectable levels about 7-10 m away from the vein). One silt-rich layer, about 10-20 cm thick, contains a white metallic mineral, possibly cobaltite or arsenopyrite, which also is most abundant near the vein.

Laminated siltstones and massive orthoconglomerates do not show a noticeable increase in sulphide content near the old workings. Unfortunately, the rock immediately next to the vein was not available for sampling, because it was mined out along with the vein decades ago. At other sample sites the vein-cuts are wider than at Little Silver Vein, and evidence of sulphide enrichment near the veins probably has been removed.

Sulphides are present to some degree in most of the sedimentary rocks, but it is not clear whether they are detrital, as suggested by Kim (1980), or if they were introduced by hydrothermal solutions such as may be the case for the sulphides adjacent to Little Silver Vein.

At the eastern end of Kerr Lake Arch near Drummond Cairn, sulphides are abundant both adjacent to vein-cuts and in strata tens of metres away. Preliminary investigations have not yet shown any consistent pattern of sulphide distribution in this area.

STRUCTURAL CONTROLS OF MINERALIZATION

Approximately 80% of the silver mined at Cobalt has come from veins that occur for the most part in steeply dipping joints and faults in the Coleman Member (Moore 1942). Attitudes of faults and joints in the Coleman Member and the underlying Archean volcanic rocks were measured to assess the possible relationship between silver veins and fracture patterns in the host rocks (Figure 4). These measurements were obtained from an area of about 1 km^2 selected for detailed study on the east shore of Cobalt Lake.

Two types of joints are recognized: quartz-filled extension joints and ubiquitous tight joints. The extension joints are generally sparse, but are locally abundant within scattered areas of a few square metres. These joints are filled with fibrous quartz crystals, the long axes of which are perpendicular to the joint walls. The tight joints are planar to sub-planar; some curve slightly and some show wave-like undulations. Systematic joint attitudes were measured only where at least three parallel to sub-parallel fractures occur within a distance of less than 6 m. In most outcrops, several sets of joints with distinctly different orientations were observed.

The abundance of systematic joints is dependent on the type of host rock. Field mapping indicates that the Coleman Member has well-developed joints in almost every exposure, whereas joints in the Archean volcanic rocks are much less abundant, and commonly absent, even in outcrops exposed for tens of metres.

The joint frequency also differs among rock types of the Coleman Member. Systematic joints in the orthoconglomerates are commonly spaced about 1 m apart, whereas most joints in the laminated siltstones are 10-15 cm apart. Where these two rock types are in contact, the joints in the siltstone extend only a few decimetres into the orthoconglomerate, or end abruptly at the contact. Only 10-20% of the joints in the siltstone pass completely into the orthoconglomerate. In some places, slight differences in joint frequency were noticed between orthoconglomerate, sandstone and diamictite.

Most of the tight joints are steeply dipping (70-90°). The central part of Figure 4a shows that systematic joints in the Coleman Member are oriented in two main sets: a major NNE-trending set, and a more dispersed NW-trending set. Figure 4b shows the almost random orientation of systematic joints in the Archean volcanic rocks.

Some silver veins occupy faults, but most occur in narrow and steeply dipping fractures which may be dilated

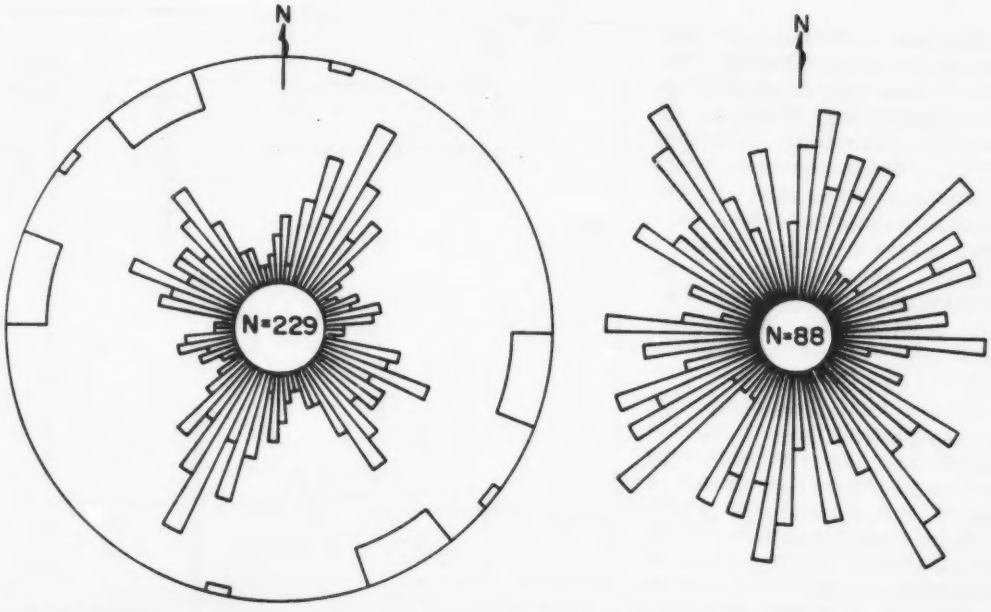

Figure 4. (a, left) Rose diagram showing frequency distributions of joint orientations (inner cluster) and ore vein orientations (plotted inward from circumference of outer circle) in Coleman Member of Gowganda Formation. (b, right) Rose diagram showing frequency distribution of joint orientations in Archean volcanic rocks in the Cobalt region.

joints. Two lines of evidence suggest that the silver-bearing veins follow pre-existing systematic joints: (1) the similarity in orientations of the silver-bearing veins (outside rim of Figure 4a) and the NW-trending joints indicates that the veins probably are dilated and infilled joints; and (2) open-to-surface mine workings northeast of Cobalt reveal that numerous ore shoots within the thinly bedded siltstones do not extend into the overlying orthoconglomerates (a pattern similar to that for the systematic joints). If the veins follow pre-existing joints, joints must be at least as old as the vein mineralization, which is probably slightly younger than the diabase (Jambor 1971, Thorpe 1974).

Three major reverse faults are recognized in the Cobalt area (Cobalt Lake fault, Valley fault, and Contact fault: see Thomson 1964). These three faults trend northeasterly and dip 10-70°, suggesting that they were produced by NW-SE compression. This compressive event probably also produced the NW-trending joints. The spread in orientation of the NW-trending joints (Figure 4a) suggests that they may be shear joints (cf. McClay 1984).

At least some movement along the Cobalt Lake fault occurred after emplacement of the Nipissing diabase (Thomson 1957). Ore veins cut across some of the reverse faults (Knight 1924), establishing a post-fault age for the mineralization.

West of the Cobalt Lake fault, a few silver-bearing veins are parallel to the NNE-trending joints. Assuming that the silver-bearing veins occupy pre-existing joints, the NNE-trending joints must have formed before mineralization. The NNE-trending joints are difficult to explain in terms of NW-SE compression, because the NNE-trending joints and the direction of inferred compressive stress are almost perpendicular to each other. The NNE-trending joints possibly developed before both the reverse faults and the NW-trending joints, as a result of a different pattern of stress orientation, or perhaps they developed during relaxation of the NW-SE compression.

Although the NNE-trending joints are the most abundant (Figure 4a), predominant vein orientations are parallel to the NW-trending joints. Possibly this was due to a continuous or renewed NW-SE compression during silver mineralization, resulting in the NW-trending joints being more favourable for extension and mineral infilling than the compressed NNE-trending joints.

Additional evidence for this possibility is provided by brecciated veins within the Cobalt Lake fault zone, indicating renewed movement (Jambor 1971). Paleomagnetic data (Symons 1970) suggest that the Nipissing diabase may have been slightly folded about a NE-SW axis, indicating the possibility of post-diabase NW-SE compression that could have caused reactivation of the Cobalt Lake fault.

Additional field work will be conducted to determine whether these relationships are consistent throughout a wider region, and the joints will be examined more closely to establish whether there is any shear component, and to assess age relationships among the various joint trends.

SULPHUR ISOTOPES: RELEVANCE TO MINERALIZATION

A combined geological and isotopic study of silver deposits in the Cobalt area was initiated to place constraints on the source and the mechanism that controlled ore deposition (Goodz 1984). The sulphur isotope studies were supplemented by petrographic examination of samples from more than 200 localities within the Beaver-Temiskaming and Pan Silver mines and the Vein 65 occurrence. This discussion will focus on sulphides from the Beaver-Temiskaming mine.

Silver mineralization in the Beaver-Temiskaming mine is restricted to quartz-calcite sulpharsenide veins and brecciated vein wallrocks within Archean pillowed to massive mafic volcanic flows and interflow sedimentary rocks. This mineralization, below the Nipissing diabase sill (Figure 5), hosts two types of sulphides:

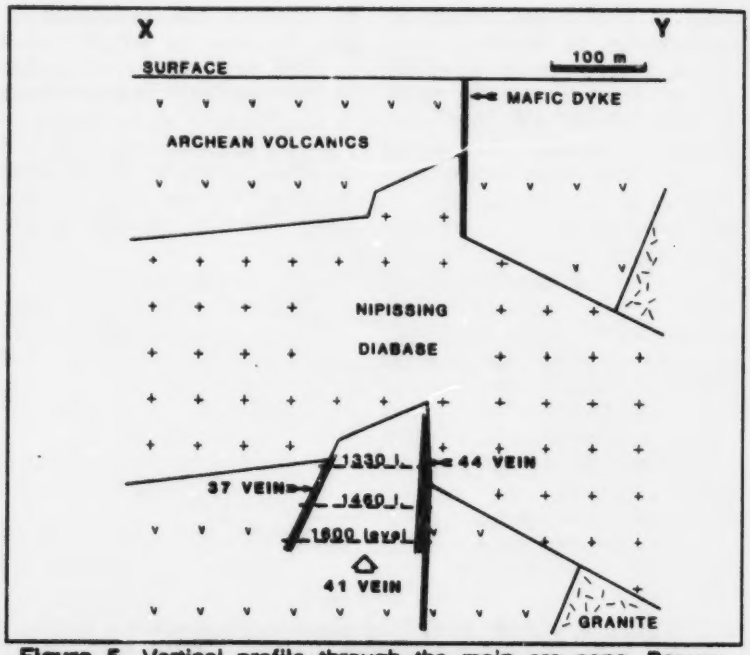

Figure 5. Vertical profile through the main ore zone, Beaver-Temiskaming mine.

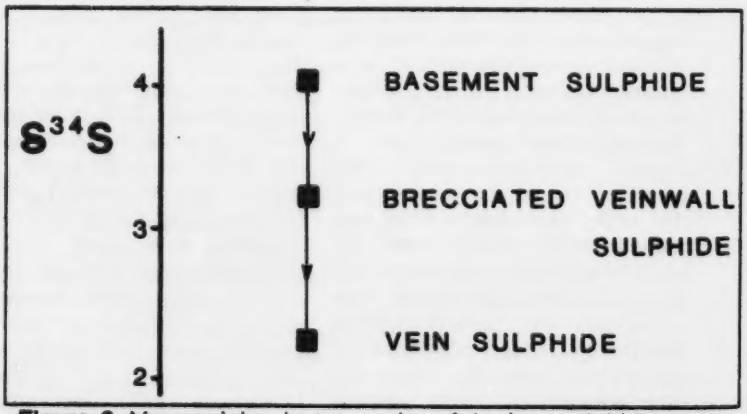

Figure 6. Mean sulphur isotope ratios of the host sulphide types.

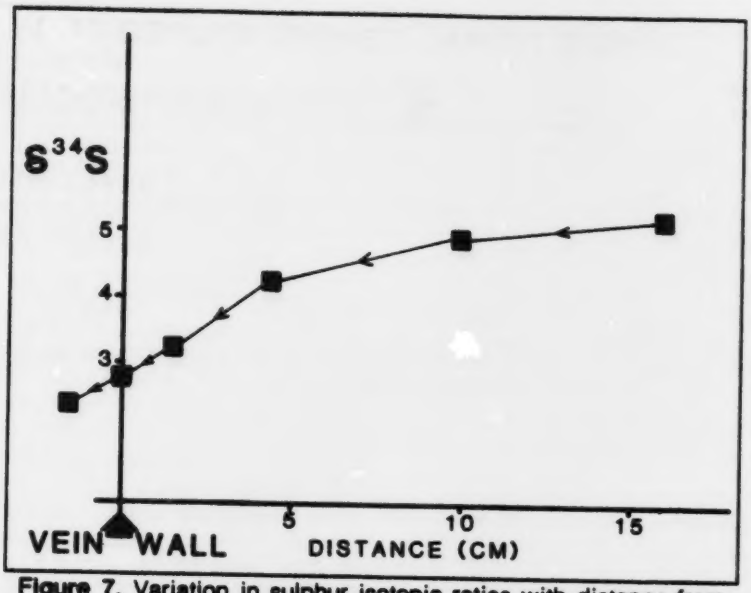

Figure 7. Variation in sulphur isotopic ratios with distance from the vein centre.

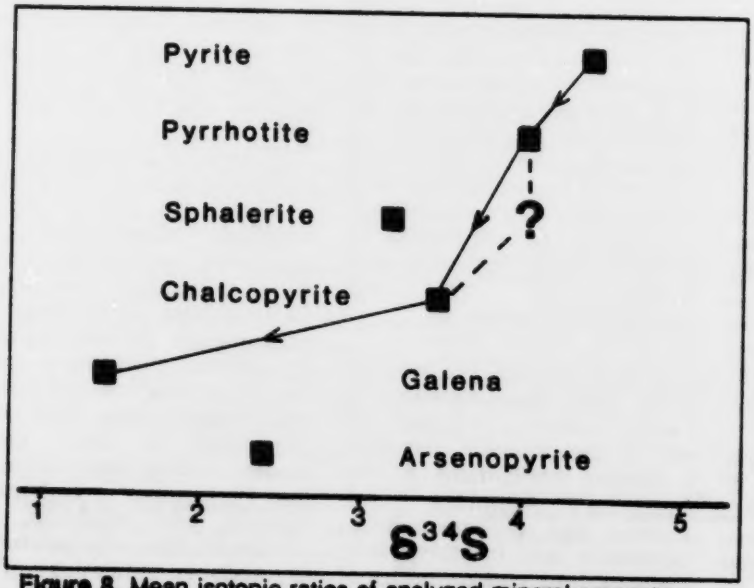

Figure 8. Mean isotopic ratios of analyzed mineral separates.

"syngenetic" basement sulphides of Archean age deposited with the volcanic flows and interflow sediments; and Proterozoic "epigenetic" vein-associated sulphides.

The summary presented here, based on 106 sulphur isotope analyses, is an overview of the detailed descriptions and proposed models presented in a paper by Goodz *et al.* (in press).

Mean sulphur isotopic compositions for the sulphide types and the isotopic variations with respect to distance from the vein wall are shown in Figures 6 and 7. These figures demonstrate two key points. First, the isotopic ratios decrease (lighten) from the syngenetic basement sulphides to the epigenetic vein-related sulphides. Second, regardless of sulphide type or mineral separate, the $\delta^{34}S$ content decreases from the wallrocks to the vein centres. These trends support a model of mixing of basement sulphur and vein sulphur.

Figures 8 and 9 show the mean isotopic compositions of mineral separates and the calculated equilibrium temperatures of deposition. Note that sphalerite, which should be isotopically similar to pyrrhotite, falls off the equilibrium tie line for the sulphides, suggesting that either equilibrium was not attained or that some of the sphalerite was not deposited contemporaneously with the other sulphides. Note also that the difference in isotopic compositions between galena, chalcopyrite and pyrrhotite yields a depositional temperature range of 130-227°C. The higher temperatures for brecciated wallrock sulphides suggest a slight-

ly earlier deposition from warmer ore fluids.

On the basis of textural and isotopic (both S and Pb) studies of sulphide minerals, most sulphides in wallrocks adjacent to the veins are inferred to have been deposited by the hydrothermal fluids that were responsible for Ag-vein formation. The dominant vein and wallrock sulphur-bearing minerals are Pb, Cu, Fe and Zn sulphides, sulpharsenides and Cu-Ag sulphosalts. Vein-related sphalerite in the Beaver-Temiskaming mine is comparatively minor; however, it is a common syngenetic basement sulphide closely associated with pyrrhotite and pyrite. This explains the isotopic disequilibrium character of sphalerite in the veins of this deposit.

In summary, Goodz *et al.* (in press) suggest that for the deposits studied:

1. hydrothermal fluids associated with the Ag-vein formation were enriched in the base metals Pb, Cu and to a lesser extent Zn;
2. the bulk of Pb and Cu mineralization in the wallrocks adjacent to the veins was deposited epigenetically from these ore fluids;
3. certain sulphides can be used as a thermometer, perhaps yielding more realistic temperatures of silver deposition;
4. textural, fluid and isotopic evidence support a model of leaching of the Ag-sulpharsenide elemental association from both the Archean basement rocks and the Coleman Member rocks, and subsequent concentration in vein deposits emplaced within the Proterozoic strata at about 2150 Ma; and
5. although it has been argued that the basement rocks were not the source of metals (because of "an apparent lack of base metal enrichment" associated with the formation of Ag-veins), an appreciable amount of base metal has been shown to have been mobilized, transported and deposited together with the elemental association of the Ag-sulpharsenide veins.

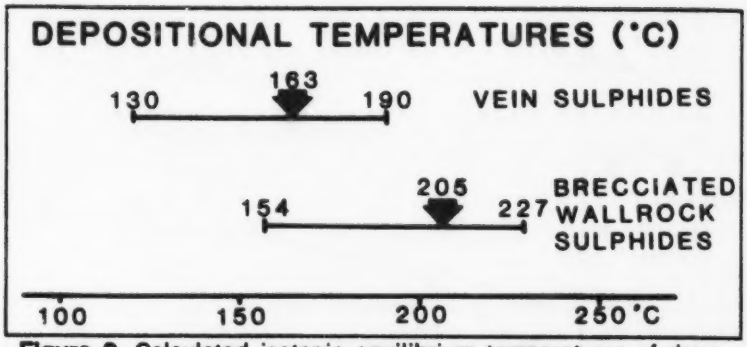

Figure 9. Calculated isotopic equilibrium temperatures of deposition of sulphide minerals within and adjacent to silver veins.

The Coleman sedimentary rocks that host Ag-veins in Castle-Tretheway Open Pit and at Drummond Cairn show a similar enrichment of Pb-Cu-Fe-Zn sulphides, sulphosalts and sulpharsenides in permeable and fractured sedimentary host rocks. Studies of trace element chemistry by Kim (1980) and by Ross (1980) show enrichment of Pb and Cu in permeable beds at Little Silver Vein, whereas the Zn content remained constant. At Drummond Cairn and Castle-Tretheway Open Pit, the sedimentary rocks are enriched in Zn and Fe, as well as in Pb and Cu.

Intensive petrographic and isotopic studies of other deposits within the Cobalt Camp is required to assess whether the epigenetic base metal enrichments noted above are typical. Because base metal-silver sulphosalts are difficult to identify without microprobe analyses, their presence and relative abundances may have been overlooked in many earlier studies. Initial studies of C, O and Pb isotopes in carbonates, silicates and sulphides, and studies of the vein geochemistry and ore mineralogy of the Beaver-Temiskaming silver mine have been completed (Goodz 1984); additional studies of ores and spatially asso-

ciated Archean rocks are now underway.

ACKNOWLEDGMENTS

J.A. Donaldson and B.R. Rust express thanks to B.O. Dressler, A.C. Colvine and John Wood, Ontario Geological Survey, for their helpful advice during preliminary planning of this project. Leo Owsiacki, Resident Geologist, Ontario Ministry of Natural Resources, Cobalt, together with his staff, provided invaluable advice and access to their library and laboratory facilities.

Zaira Arias, David Bethune, Elaine Dodd, and Robert Scammell provided cheerful assistance in the field. Part of Robert Scammell's B.Sc. thesis (Scammell 1984) has contributed to our Gowganda interpretations.

The effort, time and accessibility to the Beaver-Temiskaming and Langis mines provided by Agnico-Eagle Mines Limited, Cobalt, was greatly appreciated. Special thanks are extended to Douglas Robinson and David Marek, the mine geologists for these two mines. Gratitude also is extended to the Isotope Geochemistry Laboratory, Geological Survey of Czechoslovakia, for sulphur isotope analyses. Field work was supported in part by NSERC Grants A5536 (J.A. Donaldson), A2646 (F.A. Michel) and A7874 (D.H. Watkinson).

REFERENCES

Aspler, L.B., and Donaldson, J.A.
1984: Origin of Variegated Red Beds in the Nonacho Basin (abstract); Geological Association of Canada, Program with Abstracts, p.43.

Card, K.D., and Lumbers, S.B.
1977: Sudbury-Cobalt, District of Algoma, Manitoulin, Nipissing, Sudbury and Timiskaming; Ontario Geological Survey, Map 2361, Geological Compilation Series, Scale 1:243 440.

Card, K.D., McIlwaine, W.H., and Meyn, H.D.
1973: Geology of the Maple Mountain Area, Operation Maple Mountain, Districts of Timiskaming, Nipissing, and Sudbury; Ontario Division of Mines, Geological Report 106, 160p. Accompanied by Maps 2256, 2257, 2258, 2259, Scale 1 inch to 1 mile and Map 2260, scale 1 inch to 1/2 mile.

Frarey, M.J., and Roscoe, S.M.
1970: The Huronian Supergroup North of Lake Huron; p.143-157 *in* Symposium on Basins and Geosynclines of the Canadian Shield, edited by A.J. Baer, Geological Survey of Canada Paper 70-40.

Goodz, M.D.
1984: The Geology and Isotope Geochemistry of the Beaver-Temiskaming Silver Mine, Cobalt, Ontario; Unpublished M.Sc. Thesis, Carleton University, Ottawa.

Goodz, M.D., Watkinson, D.H., Smejkal, V., and Pertold, Z.
In press: Sulphur Isotope Geochemistry and Physicochemical Parameters of Ore-Forming Fluids at the Beaver-Temiskaming Silver Mine, Cobalt, Ontario; Canadian Journal of Earth Sciences.

Gravenor, C.P., Von Brunn, V., and Dreimanis, A.
1984: Nature and Classification of Waterlain Glaciogenic Sediments, Exemplified by Pleistocene, Late Paleozoic and Late Precambrian Deposits; Earth-Science Reviews, Volume 20, p.105-166.

Gustavson, T.C., Ashley, G.M., and Boothroyd, J.C.
1975: Depositional Sequences in Glaciolacustrine Deltas; p.264-280 *in* Glaciofluvial and Glaciolacustrine Sedimentation, edited by A.V. Jopling and B.C. McDonald, Society of Economic Paleontologists and Mineralogists, Special Publication 23.

Jambor, J.L.
1971: General Geology; p.12-33 *in* The Silver-Arsenide Deposits of the Cobalt-Gowganda Region, Ontario, edited by L.G. Berry, Canadian Mineralogist, Volume 11.

Kim, W.S.
1980: Sulphide Mineralization in the Coleman Member, Cobalt, Ontario; Unpublished M.Sc. Thesis, Carleton University, Ottawa, 112p.

Knight, C.W.
1924: Geology and the Mine Workings of Cobalt and South Lorrain Silver Areas; Ontario Department of Mines, Annual Report for 1922, Volume 31, Part 2.

Legun, A.
1984: Stratigraphy and Sedimentation in the Cobalt Area; Ontario Geological Survey, Open File Report 5508, 60p.

Lindsey, D.A.
1967: The Sedimentology of the Huronian Gowganda Formation, Ontario, Canada (with Special Reference to the Whitefish Falls Area); Ph.D. Thesis, Johns Hopkins University, Baltimore, 296p.
1969: Glacial Sedimentology of the Precambrian Gowganda Formation, Ontario, Canada; Geological Society of America, Bulletin, Volume 80, p.1635-1702.

Lowe, D.R.
1982: Sediment Gravity Flows: II. Depositional Models with Special Reference to the Deposits of High-density Turbidity Currents; Journal of Sedimentary Petrology, Volume 52, p.279-297.

McClay, K.R.
1984: Mapping Geological Structures; Geological Association of Canada, Cordilleran Section, Short Course Number 2, Part 1.

Miall, A.D.
1983: Glaciomarine Sedimentation in the Gowganda Formation (Huronian), Northern Ontario; Journal of Sedimentary Petrology, Volume 53, p.477-491.

Moore, E.S.
1942: Cobalt, Ontario; *in* Ore Deposits as related to Structural Features, edited by W.H. Newhouse, Princeton University Press, Princeton, New Jersey.

Mossman, D.J. and Harron, G.A.
1983: Origin and Distribution of Gold in the Huronian Supergroup, Canada - The Case for Witwatersrand-Type Paleoplacers; Precambrian Research, Volume 20, p.543-583.
1984: Witwatersrand-Type Paleoplacer Gold in the Huronian Supergroup of Ontario; Geoscience Canada, Volume 11, p.33-40.

Patterson, G.C.
1979: Metallogenetic Relationships of Base-Metal Occurrences in the Cobalt Area; p.222-229 *in* Summary of Field Work 1979, by the Ontario Geological Survey, edited by V.G. Milne, O.L. White, R.B. Barlow, and C.R. Kustra, Ontario

Geological Survey, Miscellaneous Paper 90, p.222-229.

Powell, R.D.
1981: A Model for Sedimentation by Tidewater Glaciers; Annals of Glaciology, Volume 2, p.129-134.

Rainbird, R.H.
1980: The Geology of an Area Straddling the Archean-Proterozoic Unconformity near Cobalt, Ontario; Unpublished B.Sc. Thesis, Carleton University, Ottawa, 52p.

Roscoe, S.M.
1969: Huronian Rocks and Uraniferous Conglomerates; Geological Survey of Canada, Paper 68-40, 205p.
1973: The Huronian Supergroup, Paleoaphebian Succession Showing Evidence of Atmospheric Evolution; p.31-47 *in* Huronian Stratigraphy and Sedimentation, edited by G.M. Young, Geological Association of Canada, Special Paper 12.

Ross, G.M.
1980: Petrogenesis of Disseminated Sulphides in the Little Silver Vein Area, Cobalt, Ontario; Unpublished Directed Study, Carleton University, Ottawa.

Rust, B.R., and Romanelli, R.
1975: Late Quaternary Subaqueous Outwash Deposits near Ottawa, Canada; p.177-192 *in* Glaciofluvial and Glaciolacustrine Sedimentation, edited by A.V. Jopling and B.C. McDonald, Society of Economic Paleontologists and Mineralogists, Special Publication 23.

Scammell, R.J.
1984: The Geology of Precambrian Strata East of Cobalt, Ontario; Unpublished B.Sc. Thesis, Carleton University, Ottawa, 71p.

Siemiatkowska, K.M.
1978: Geology of the Endakai Lake Area, District of Algoma; Ontario Geological Survey Report 178, 79p. Accompanied by Map 2399, Scale 1:31,680.

Symons, D.T.A.
1970: Paleomagnetism of the Nipissing Diabase, Cobalt Area, Ontario; Canadian Journal of Earth Sciences, Volume 7, p.86-90.

Thomson, R.
1957: Cobalt Camp; p.377-388 *in* Structural Geology of Canadian Ore Deposits: Volume 2, Canadian Institute Mining and Metallurgy, Sixth Commonwealth Mining and Metallurgy Congress, 1957, Montreal.
1964a: Geological Map of the Cobalt Silver Area, Northern Sheet; Ontario Department of Mines, Map 2050, scale 1 inch to 1,000 feet.
1964b: Geological Map of the Cobalt Silver Area, Southwestern Sheet; Ontario Department of Mines, Map 2051, Scale 1 inch to 1,000 feet.
1964c: Geological Map of the Cobalt Silver Area, Southeastern Sheet; Ontario Department of Mines, Map 2052, scale 1 inch to 1,000 feet.

Thorpe, R.
1974: Lead Isotope Evidence on the Genesis of the Silver-Arsenide Vein Deposits of the Cobalt and Great Bear Lake Areas, Canada; Economic Geology, Volume 69, p.777-791.

Wood, J.
1970: Evidence for a Tropical Climate and Oxygenic Atmosphere in Upper Huronian Rocks of the Rawhide Lake - Flack Lake Area, Ontario (abstract); 16th Annual Institute Lake Superior Geology, Thunder Bay, May 1970, p.45-46.
1973: Stratigraphy and Depositional Environments of the Upper Huronian Rocks of the Rawhide Lake - Flack Lake Area, Ontario; p.73-95 *in* Huronian Stratigraphy and Sedimentation, edited by G.M. Young, Geological Association of Canada, Special Paper 12.
1979: Regional Geology of the Cobalt Embayment, Districts of Sudbury, Nipissing and Temiskaming; p.79-81 *in* Summary of Field Work, 1979, Ontario Geological Survey, edited by V.G. Milne, O.L. White, R.B. Barlow and C.R. Kustra, Ontario Geological Survey, Miscellaneous Paper 90.
1980: Regional Geology of the Cobalt Embayment, Districts of Sudbury, Nipissing and Temiskaming; p.61-63 *in* Summary of Field Work, 1980, Ontario Geological Survey, edited by V.G. Milne, O.L. White, R.B. Barlow, J.A. Robertson and A.C. Colvine, Ontario Geological Survey Miscellaneous Paper 96.

Young, G.M.
1970: Widespread Occurrence of Aluminous Minerals in Aphebian Quartzites (Abstract); 16th Annual Institute on Lake Superior Geology, Thunder Bay, May 1970, p.47-48.
1973: Tillites and Aluminous Quartzites as Possible Time Markers for Middle Precambrian Rocks of North America; p.97-127 *in* Huronian Stratigraphy and Sedimentation, edited by G.M. Young, Geological Association of Canada, Special Paper 12.

Grant 175 Structural Geology of Northern Dome and Southern McDonough Townships, Red Lake Area, Ontario

P.M. Berger and J.M. Summers

Department of Geological Sciences, Queen's University

ABSTRACT

Detailed mapping of structures within northern Dome and southern McDonough Townships, in the Red Lake area, was carried out during the 1983 field season.

The area is underlain by a sequence of mafic to ultramafic metavolcanic rocks, grading upward to clastic metasedimentary rocks. The metavolcanic to metasedimentary sequence is crosscut by felsic to intermediate intrusive bodies. All of the supracrustal rocks have been metamorphosed to greenschist facies and have locally undergone carbonatization, silicification, and sericitization.

Three distinct deformation fabrics have been recognized within the study area. Based on relative predominance of each fabric, the study area has been divided into Southern, Central, and Northern Zones.

The earliest fabric can be observed in all zones, but is predominant within the Central Zone. This east-trending flattening fabric is axial planar to minor folds within the metasedimentary units.

The Northern Zone is marked by the appearance of a northeast-trending fabric associated with subparallel transcurrent sinistral shear zones. These shear zones cross-cut and rotate the earlier east-trending fabric.

The rocks of the Southern Zone are characterized by a third penetrative fabric which trends southeast. The southeast-trending fabric ceases to be the dominant fabric at the "boundary" between the Southern and Central Zones. It becomes a discontinuous, poorly developed, spaced fabric northwestward through the study area. This penetrative fabric cross-cuts and locally deforms both the east- and northeast-trending fabrics in the Central and Northern Zones.

It is suggested that the area was subject to a bulk shortening oriented north-south, which resulted in the east-trending fabric and associated folds. Later, possibly during the same deformational event, northeast-trending sinistral shear zones developed over the northern portion of the area. Further study is planned which will help to determine the nature and tectonic significance of the southeast-trending fabric.

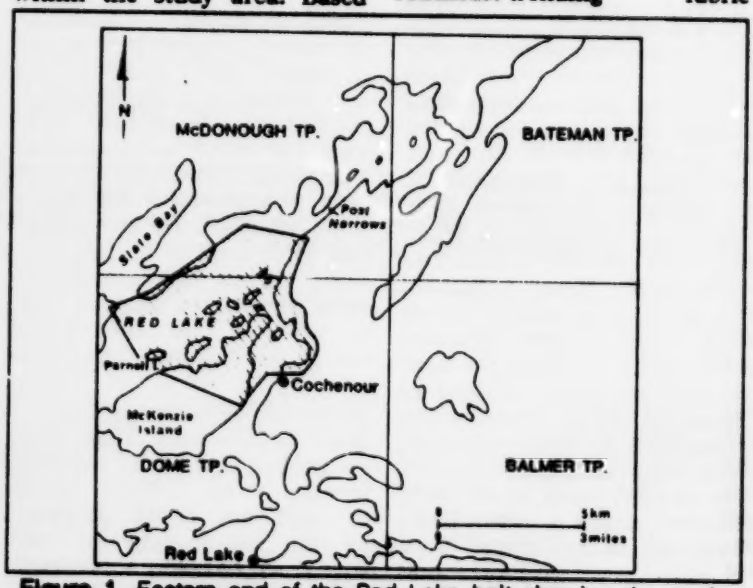

Figure 1. Eastern end of the Red Lake belt showing the study area.

INTRODUCTION

The study area (Figure 1), located in northern Dome and southern McDonough Townships near Red Lake, Ontario, extends from the town of Cochenour to Slate Bay, including the northern quarter of McKenzie Island, the Parnell Islands and smaller islands to the northeast, and the lakeshore extending from Cochenour to the southern end of Post Narrows.

This study is being done in conjunction with a continuing program of research in the Red Lake district initiated by the Ontario Geological Survey (Andrews and Wallace 1983). The general aim of this program is to determine the geological relationship of alteration, metamorphism, and

structural patterns to gold mineralization in the eastern portion of the Red Lake metavolcanic-metasedimentary belt. The area discussed in this report was chosen on the basis of lithologic and structural mapping by Pirie (1981), and Andrews and Wallace (1983) indicated that two regionally dominant structural trends intersect in the area (Figure 2). The specific objective of this research is to elucidate the structural and tectonic significance of this intersection zone in relation to the structural trends of the eastern Red Lake belt.

Mapping was carried out during the 1983 field season, at a 1:1000 scale over the entire area and at a 1:10 scale on selected outcrops. This paper summarizes observations and conclusions to date. Continued thin section analysis and mapping of adjoining areas of interest during the 1984 field season will add to the conclusions reached here.

GENERAL GEOLOGY

The first comprehensive map of the Red Lake greenstone belt, including the study area, was produced by Horwood (1945). Dome and McDonough Townships were mapped at a scale of 1:12,000 by Ferguson (1966), Pirie (unpublished data, 1978), and Pirie and Sawitzky (1977). The area is underlain by rocks included within Pirie's (1981) Lower Mafic Sequence. All of the supracrustal rocks have been metamorphosed to greenschist facies and are locally carbonatized, silicified, and/or sericitized. Rock types distinguished within the map-area are: mafic metavolcanic rocks, ultramafic metavolcanic rocks, felsic metavolcanic rocks,

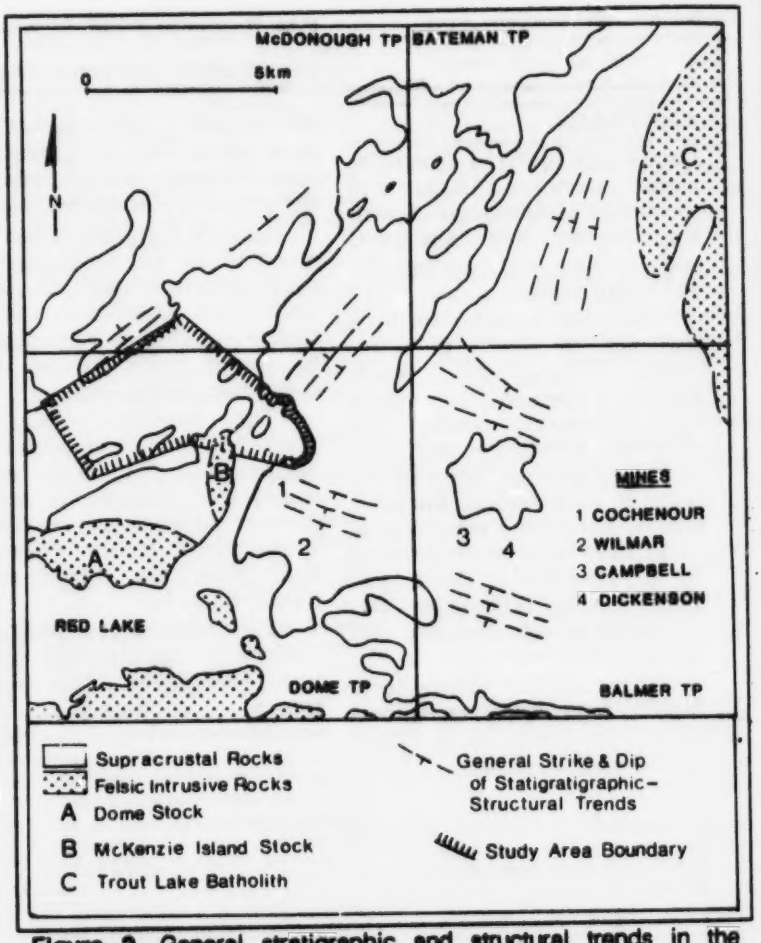

Figure 2. General stratigraphic and structural trends in the eastern half of the Red Lake belt (after Andrews 1983) and their relationship to the study area.

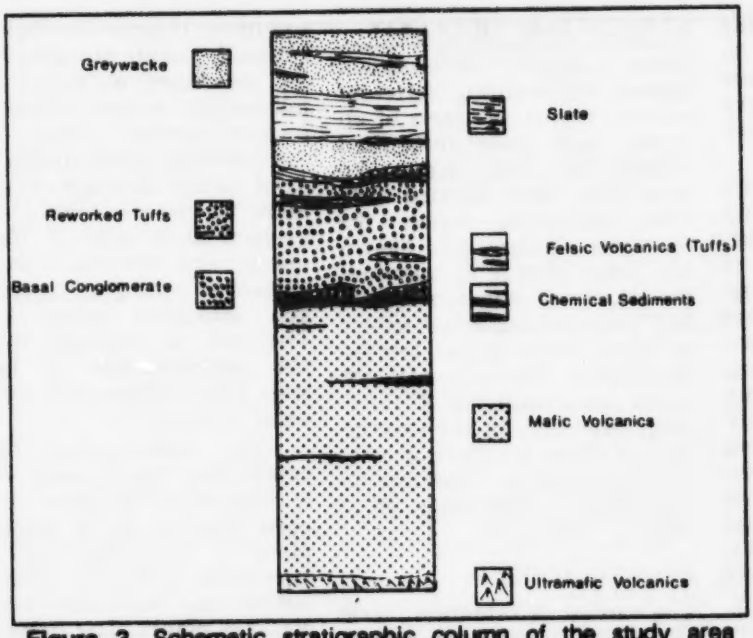

Figure 3. Schematic stratigraphic column of the study area showing the relationship between, and relative thicknesses of different rock types.

clastic metasedimentary rocks, chemical metasedimentary rocks, and felsic to intermediate intrusive rocks (Figure 3). Interbedding and graded contacts between stratigraphically adjacent rock types are commonly observed. Individual units cannot be traced with confidence for distances greater than 100 m because of lack of outcrop and marker units, and because of intense alteration and the presence of structural complexities in the area.

Stratigraphically the lowest unit, mafic metavolcanic rocks dominate the area, making up about 50% of outcrops mapped. Flows are fine- to very fine-grained and may be massive or pillowed, each type equally abundant throughout the area. Younging directions were determined, with confidence, from only three pillowed outcrops due to alteration, deformation, weathering, or lack of sufficient exposure. Varioles characterize the majority of the mafic metavolcanic outcrops and are usually, though not exclusively, associated with pillowed flows.

Ultramafic metavolcanic rocks are interlayered with the mafic volcanic rocks and make up about 5% of the area mapped. These rocks, composed almost completely of tremolite and actinolite, have been classified by Pirie (1981) as basaltic komatiites and are considered to be the metamorphic equivalents of pyroxenite. Pillowed, variolitic units were observed in about 60% of outcrops and spinifex textures were recognized at one location.

Carbonatization, silicification, and to a lesser extent, sericitization, affect all mafic and ultramafic metavolcanic exposures to some degree. Carbonate, quartz, and sericite may take the form of veins or may occur as a pervasive replacement. Staining has shown the dominant carbonate to be Fe-bearing calcite in relatively undeformed rocks and ferroan dolomite and ankerite in rocks with a strong penetrative fabric. Silicification has affected most exposures, and recrystallized quartz may compose up to 50% of a sample. Sericite alteration, and the occurrence of green muscovite, is generally confined to relatively highly deformed rocks, primarily within shear zones.

Clastic metasedimentary rocks compose about 35% of exposures mapped, are divided into a lower reworked felsic tuff and an overlying, more mature sequence of slates, argillites, and greywackes. The reworked tuff unit is separated from the mafic metavolcanic unit by a relatively thin, discontinuous layer of ironstone. Directly overlying the ironstone is a conglomerate composed of up to 80% subangular to sub-rounded clasts of tuffaceous material set in a fine-grained matrix of quartz, feldspar, and sericite. Up to 10% of the clasts are composed of chert and mafic metavolcanic fragments. Reworked tuff outcrops are fine to coarse grained, and composed of subrounded to subangular quartz and feldspar grains set in a very fine-grained quartz-sericite matrix. Graded bedding can be observed in nearly all outcrops and cross beds were observed at two locations. Isolated pods of tuff containing pummice fragments are found near the base of this unit, suggesting contemporaneous extrusion, deposition, and reworking of tuffaceous material.

Carbonatization, occurring primarily as a pervasive replacement by ferroan dolomite and ankerite, affects only the relatively highly deformed metasedimentary rocks.

Mineralogically the slates and greywackes are nearly identical to the reworked tuff and are distinguished by a greater degree of maturity. Massive or layered exposures are well sorted, often displaying graded and cross bedding, load casts, clastic dikes, rip-up structures, and convolute bedding. Fe-rich calcite is present in the majority of exposures. However ferroan dolomite and ankerite, as in the mafic and ultramafic metavolcanic rocks, are limited to the relatively highly deformed rocks.

Chemical metasedimentary rocks, dominantly massive chert, layered chert and magnetite, and conglomeratic ironstone occur in about 5% of exposures mapped. They are found as discontinuous layers, 5 cm to 10s of metres thick. Silicification affects most exposures and is most commonly observed as pervasive, subparallel sets of millimetre to centimetre thick veinlets. Ferroan dolomite and ankerite are found in only the most intensely deformed outcrops.

Felsic to intermediate stocks, sills, and dikes intrude the supracrustal sequences, making up about 5% of exposures mapped. The largest intrusive body within the map-area is the McKenzie Island Stock, a zoned intrusion with a quartz diorite core and an outer layer of augite diorite. Other smaller intrusions were observed throughout the area. None of the observed exposures of the intrusive rocks had been carbonatized.

STRUCTURAL GEOLOGY

Three distinct deformation fabrics, representing different tectonic events, or stages of an event, have been recognized within the study area. The area has been divided into three structural zones, the Southern, Central, and Northern Zones (Figure 4), based on the degree of development of, and cross-cutting relationships between, these planar fabrics. Boundaries between adjacent zones are gradational. Terminology used here in the description of these fabrics and associated structures conforms to that used by Borradaile *et al.* 1982.

CENTRAL ZONE

The earliest deformation fabric recognized in the study area is the dominant fabric observed in the Central Zone. The fabric dips steeply to vertically throughout the zone and varies continuously in strike from 090 to 110 to 075 to 090 northwestward across the zone (Figure 5). The nature and intensity of this fabric varies spatially and by lithology from continuous to anastomosing to spaced cleavage. In general, continuous cleavages are developed in metavolcanic and fine-grained clastic metasedimentary rocks. Coarser-grained clastic metasedimentary and chemical metasedimentary rocks are characterized by anastomosing to spaced cleavages, with a continuous, penetrative cleavage developed in the most intensely deformed exposures. Variation of relative fabric intensity within one rock type may occur on the scale of an individual outcrop or up to 10s of metres.

Primary layering dips steeply to vertically and varies in strike from northeast to southeast (Figure 5). Tight to isoclinal, steeply plunging folds are developed at macro and microscopic scales within the metasedimentary units. The east-trending fabric forms the axial planar cleavage of these folds. Large-scale folds can be mapped at a scale of 10s of metres and inferred from reversals of younging directions and associated minor folds. The lack of exposure makes the determination of large-scale fold configuration impossible.

The east-trending fabric dominating the Central Zone is interpreted to have developed parallel to a principal plane of flattening, with the maximum extension plunging steeply to vertically within cleavage planes. The flattening is recorded by pillows, varioles, and clasts elongated in a vertical and east-west direction. Microscopic evidence is provided by the distribution of pressure shadows developed around quartz, feldspar, epidote, and pyroxene grains. The orthorhombic symmetry of pressure shadows and of quartz and mica beards developed within them, as well as the general orthorhombic symmetry of the anastomosing fabric and the presence of sub-horizontal microfractures containing phyllosilicates oriented normal to the fracture boundaries, indicates that the deformation is irrotational (i.e. the direction of tectonic shortening remained relatively constant with reference to the deforming rock system and north-south with respect to the present attitude of rocks in the map-area).

NORTHERN ZONE

The transition from the Central to the Northern Zone is characterized by a progressive

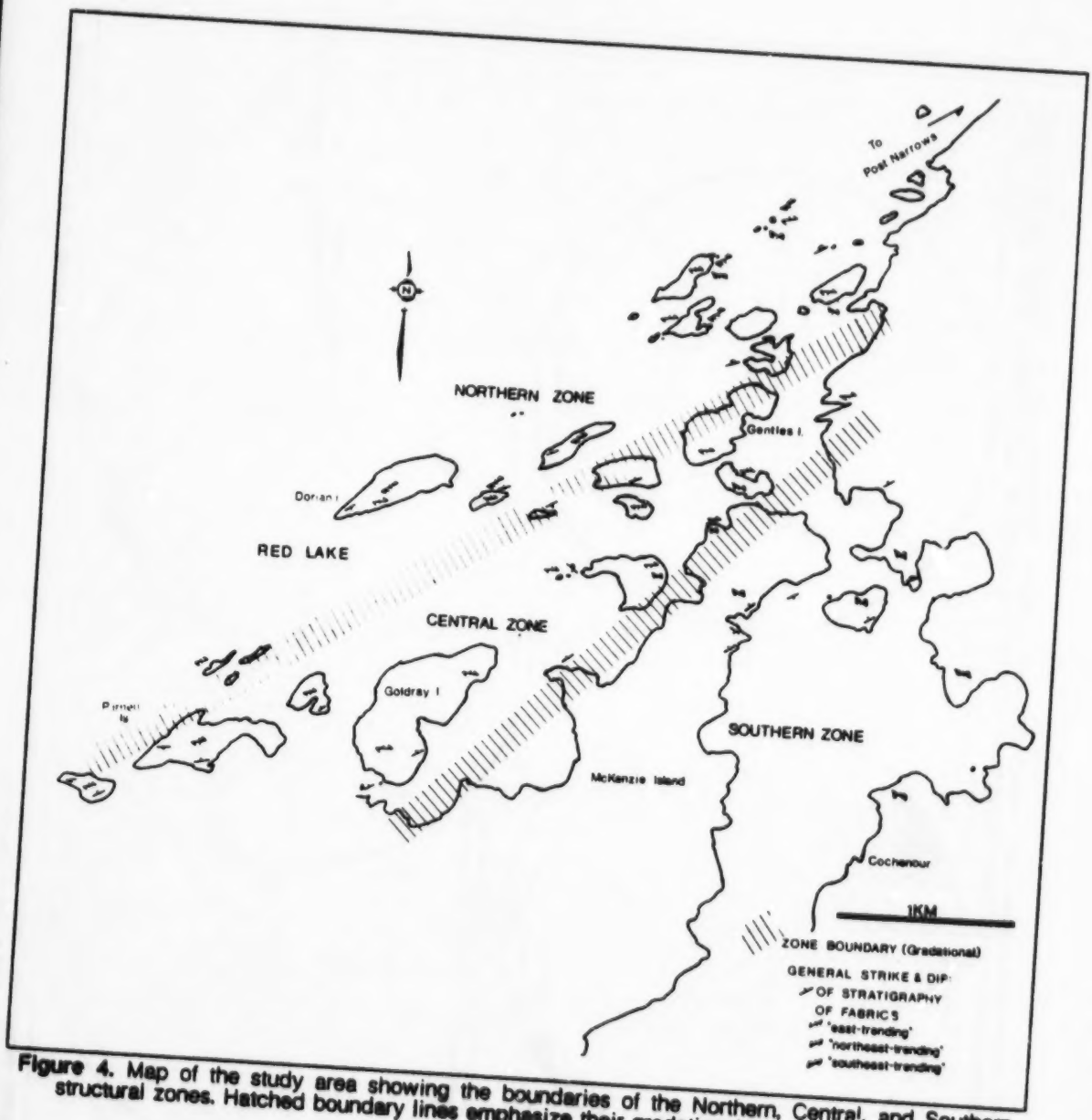

Figure 4. Map of the study area showing the boundaries of the Northern, Central, and Southern structural zones. Hatched boundary lines emphasize their gradational nature.

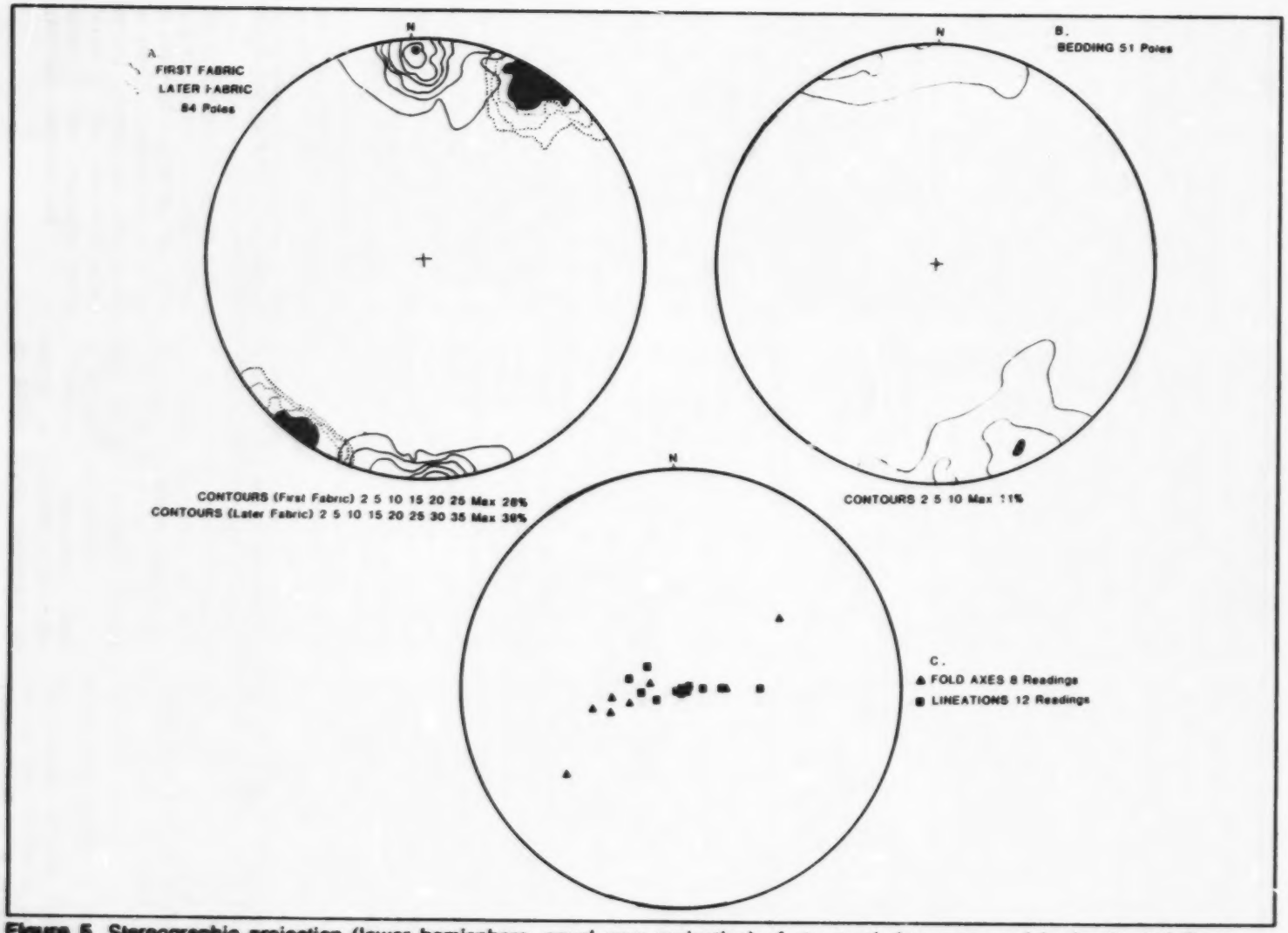

Figure 5. Stereographic projection (lower hemisphere, equal area projection) of structural data measured in the Central Zone. Lineations include stretching and mineral lineations.

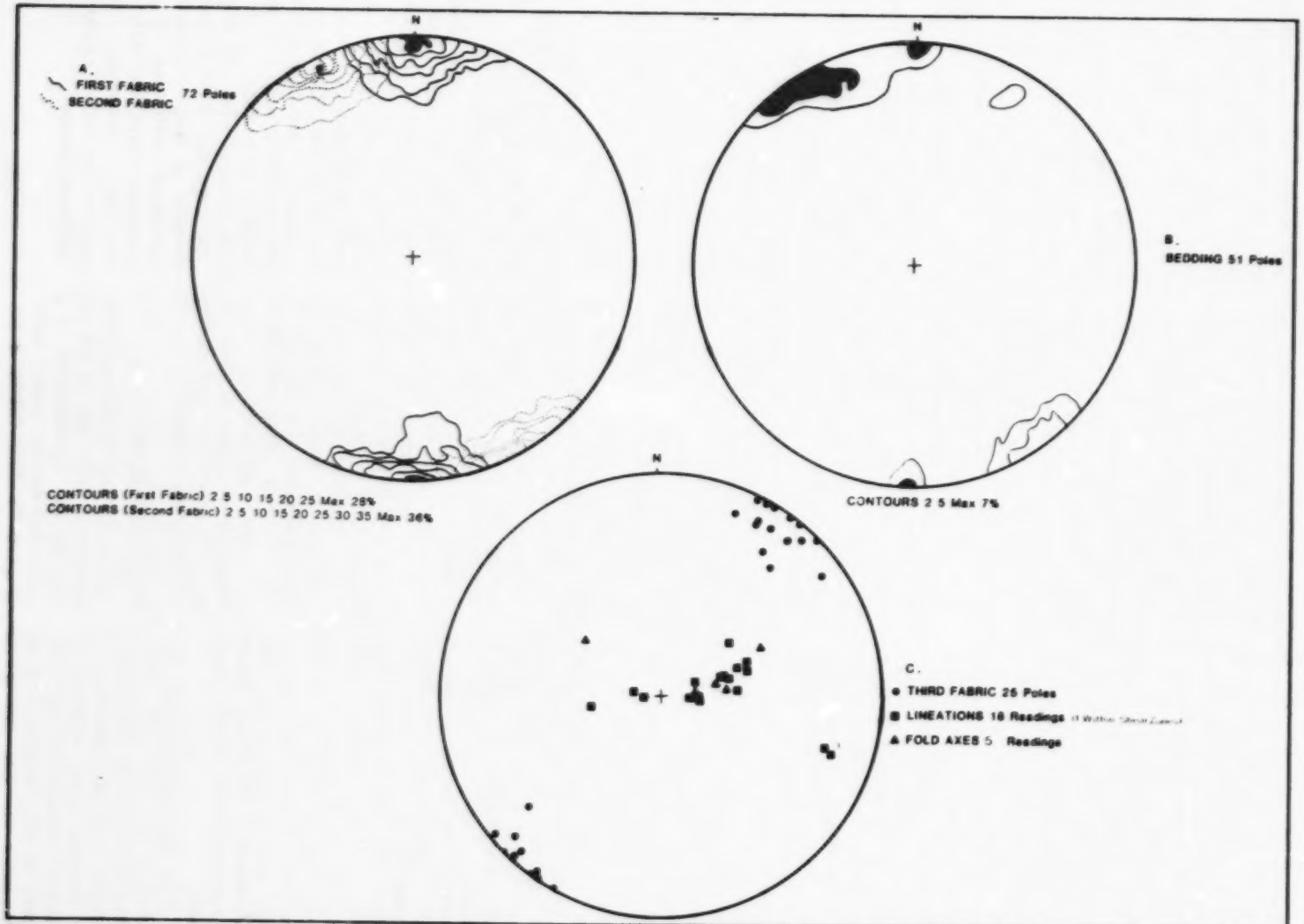

Figure 6. Stereographic projection (lower hemisphere, equal area projection) of structural data measured in the Northern Zone. First and second fabrics were differentiated only where observed together. Lineations include stretching and mineral lineations.

increase in the degree of development of a steeply dipping fabric which strikes 045 to 075 (Figure 6). Near the southern boundary of the zone, this fabric occurs as a weakly developed, discontinuous spaced cleavage which crosscuts and commonly displaces sinistrally the east-trending fabric. This northeast-trending fabric increases in intensity northwestward through the zone, to become a strong, penetrative cleavage which totally overprints the east-trending fabric.

The deformation event producing this fabric is interpreted to have involved a major component of horizontal simple shear along sub-vertical shear planes trending to the northeast. The fabric is developed as a more penetrative structure within northeast-trending shear zones, most commonly developed in massive, unlayered outcrops. Where boundaries can be observed they vary from 2 cm to 2 m in width. They may possibly reach greater widths in areas where the penetrative shear fabric is developed but shear zone boundaries are unexposed. The continuous to anastomosing fabric developed within shear zones, is oriented subparallel to the shear zone boundaries. The sense of rotation of the earlier, east-trending fabric outside of the shear zones is sinistral. Variole stretching directions change from sub-vertical within the east-trending flattening plane to sub-horizontal within shear zones.

The sinistral rotation and overprinting of the east-trending fabric by shear zone parallel cleavage observed at an outcrop scale, appears to provide a small-scale representation of the structural characteristics in the northwest section of the study area as a whole. The change in trend of the east-trending fabric to a more northeasterly strike, and the progressive intensification of the northeast-trending shear fabric to become the dominant penetrative fabric in the northern part of the map-area, provides evidence for the existence of a major northeast-trending zone of transcurrent sinistral shear. This structure has been named the "Post-Narrows Deformation Zone" by Andrews and Durocher (1983). The southeastern boundary of this zone coincides with the boundary between the Central and Northern Zones defined here. Reconnaissance mapping in the vicinity of Slate Bay shows that this area is dominated by a steeply dipping penetrative fabric striking 045 to 060. It has not been determined whether this fabric is related to the sinistral "deformation zone", or whether it is a northeast-trending flattening fabric corelatable with that of the Central Zone.

Most primary layering trends are east to northeast within the Northern Zone (Figure 6). Minor "S" folds, with subvertical fold axes, formed by the trancurrent shear of layered units, are observed at a few locations. The northeast-trending penetrative cleavage is axial planar to these folds, but it is difficult to determine if these structures represent pre-existing folds modified by sinistral shear or if they were developed during the shearing episode.

SOUTHERN ZONE

The rocks within the southern structural zone are characterized by the development of a third, sub-vertical planar fabric (Figure 7). This fabric is present in all zones but predominates in the southeastern portion of the map-area. It overprints and deforms both the east- and northeast-trending fabrics of the Central and Northern Zones (Figure 8a). Striking 120 to 150, the general southeast-trending attitude of this fabric is consistent throughout the study area.

The boundary between the Central and Southern Zones is positioned, somewhat subjectively, where the southeast-trending fabric ceases to be the dominant structure. The nature and intensity varies with rock type. It occurs as a continuous to anastomosing cleavage through metavolcanic and clastic metasedimentary rocks. It forms well developed pressure shadows around garnets in metasedimentary rocks adjacent to the McKenzie Island Stock. The fabric takes the form of a spaced cleavage in chemical metasediments and portions of the McKenzie Island Stock.

The southeast-trending fabric is axial planar to outcrop-scale, open to tight folds with axes which plunge 50 to 70° northwest. These folds are found predominantly within the Southern Zone but were observed at four locations throughout the rest of the area. Evidence for a larger scale fold structure with an east- to northeast-trending axial plane, is provided by younging reversals and changes in bedding orientation. Individual fold closures with this orientation were not observed but the attitude of these structures is consistent with that of folds associated with the early east-trending flattening fabric mapped in the Central and Northern Zones.

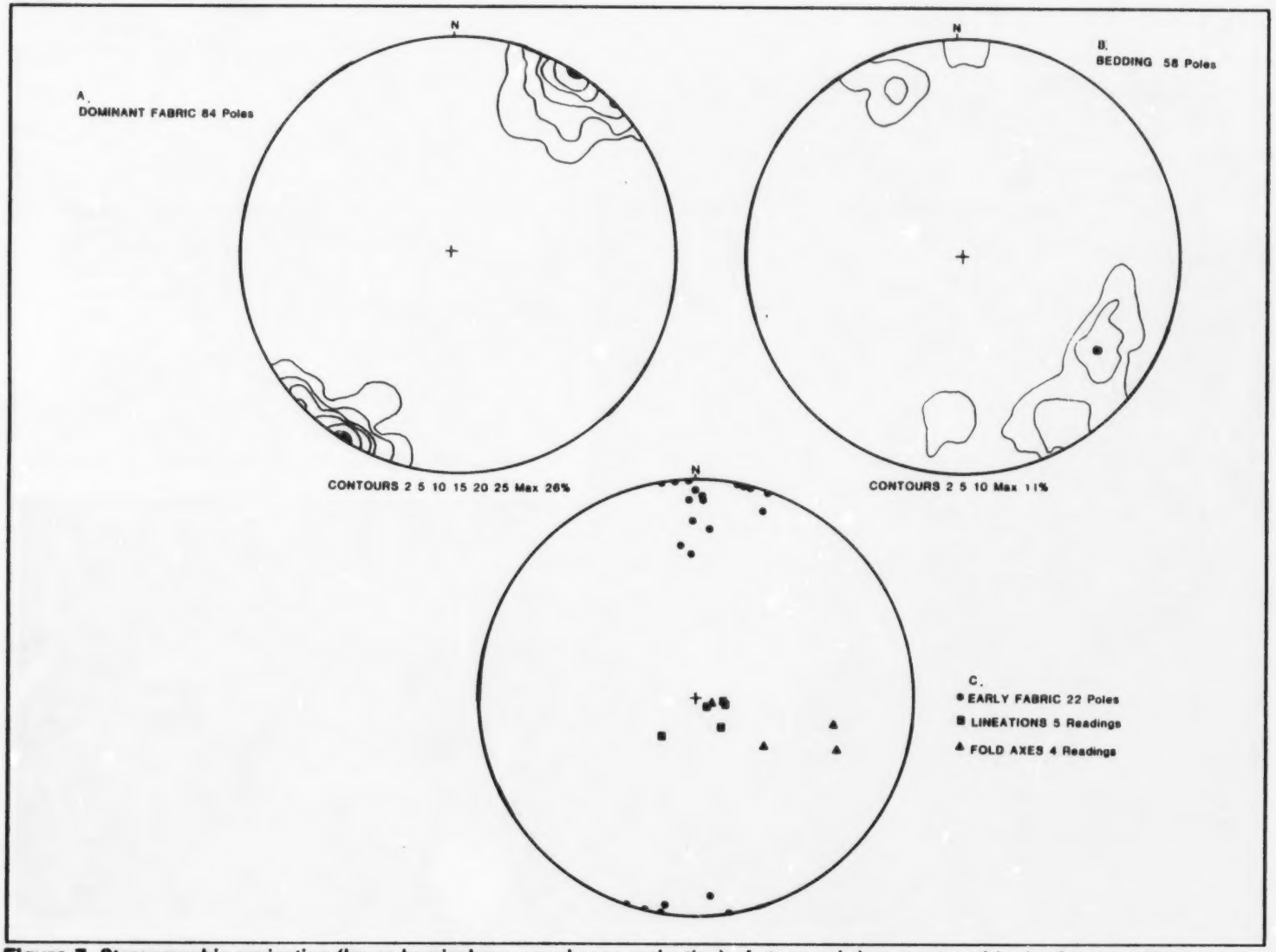

Figure 7. Stereographic projection (lower hemisphere, equal area projection) of structural data measured in the Southern Zone.

Figure 8. (a, above left) East-trending elongated varioles and penetrative cleavage are cross-cut by a southwest-trending spaced cleavage. Pressure solution has taken place along both cleavage planes (Central Zone). (b, above right) Cleavage is refracted sinistrally through coarse- to fine-grained reworked tuff layers. Bedding strikes northeast (Northern Zone). (c, right) Bedding and an early penetrative cleavage strike east in an exposure of reworked tuff. The early cleavage (S_1) is refracted to the northeast in fine-grained layers. A later, northwest-trending cleavage (S_2) is developed within the coarser-grained units (Northern Zone).

The southeast-trending fabric becomes more discontinuous, less penetrative, and much more localized in development northwestward through the map area. It is most commonly observed, in both Central and Northern Zones, as a weak, poorly developed, spaced cleavage, which is locally developed as a crenulation cleavage.

SUMMARY AND CONCLUSIONS

The earliest fabric observed within the study area trends 075 to 110. It is interpreted to be an irrotational flattening fabric which formed normal to a direction of maximum shortening oriented generally north-south.

Reconnaissance mapping in surrounding areas as well as structural studies in portions of the Campbell Red Lake, Dickenson (Rigg and Helmstaedt 1981), and Wilmar Resources properties (Rigg and Sherkus 1983), and other regional studies (Bruce Wilson, Graduate Student, Queen's University, Kingston, Ontario, personal communication, 1983) suggest this east-trending fabric is regionally developed over the eastern half of the Red Lake belt. It is locally rotated or overprinted by later structural features.

A northeast-trending fabric cross-cuts and generally displaces sinistrally the east-trending fabric in the northern portion of the study area. This fabric is the penetrative cleavage formed within outcrop-scale transcurrent sinistral shear zones which also trend to the northeast. The occurrence of this fabric marks the southeast boundary of the "Post-Narrows Deformation Zone" defined by Andrews and Durocher (1983). These zones are interpreted to have formed by dominantly simple shear along northeast-trending planes, possibly during a later phase of the north-south compressive event. Structures observed within this shear zone are similar to those documented in the northeast-trending, sinistral shear zone known as the "Flat Lake - Howey Bay Deformation Zone" (Hugon and Schwerdtner, this volume).

Both northeast- and east-trending fabrics are cross-cut and locally crenulated by a later, southeast-trending fabric which dominates the southern portion of the study area and postdates the McKenzie Island Stock. This fabric becomes more discontinuous, spaced, and weakly developed northwestward through the area. Further study of this fabric during the 1984 field season will be directed toward an understanding of the kinematics of this fabric and associated structures, as well as its relationship to the "Cochenour-Dickenson Deformation Zone" (Andrews and Durocher 1983).

REFERENCES

Andrews, A.J.
1983: Alteration, Metamorphism, and Structure Associated with Archean Volcanic-Hosted Gold Deposits, Red Lake District; p.211-215 *in* Summary of Field Work 1983, edited by J. Wood et al., Ontario Geological Survey, Miscellaneous Paper 116.

Andrews, A.J., and Durocher, M.E.
1983: Gold Studies in the Red Lake Area; p.207-210 *in* Summary of Field Work, 1983, edited by J. Wood et al., Ontario Geological Survey, Miscellaneous Paper Number 116.

Andrews, A.J., and Wallace, H.
1983: Alteration, Metamorphism, and Structural Patterns Associated with Archean Gold Deposits - Preliminary Observations in the Red Lake Area; p.111-122 *in* Geology of Gold in Ontario, edited by A.C. Colvine, Ontario Geological Survey, Miscellaneous Paper 110.

Borradaile, G.J., Bayley, M.B., and Powell, C.M. (editors)
1982: Atlas of Deformational and Metamorphic Rock Fabrics; Springer-Verlag, New York, 551p.

Ferguson, S.A.
1966: Geology of Dome Township, District of Kenora; Ontario Department of Mines, Geological Report 45, 98p. Accompanied by Map 2074, scale 1:12,000.

Horwood, H.C.
1945: Geology and Mineral Deposits of the Red Lake Area, Ontario; Ontario Department of Mines, Annual Report for 1940, Volume 49, Part 2, 231p.

Pirie, J.
1981: Regional Geological Setting of Gold Mineralization in the Red Lake Area, Northwestern Ontario; p.71-93 *in* Genesis of Archean, Volcanic-Hosted Gold Deposits, edited by E.G. Pye and R.G. Roberts, Ontario Geological Survey, Miscellaneous Paper 97.

Pirie, J., and Sawitzky, E.
1977: McDonough Township, District of Kenora (Patricia Portion); Ontario Geological Survey, Preliminary Map P.1240, Scale 1:12,000.

Rigg, D.M., and Helmstaedt, H.
1981: Relationship Between Structures and Gold Mineralization in Campbell Red Lake and Dickenson Mines, Red Lake Area, Ontario; p.111-127 *in* Genesis of Archean, Volcanic-Hosted Gold Deposits, edited by E.G. Pye and R.G. Roberts, Ontario Geological Survey, Miscellaneous Paper 97.

Rigg, D.M., and Sherkus, E.W.
1983: Geology of the Wilmar Mine, Red Lake Area; p.159-173 *in* Geology of Gold in Ontario, edited by A.C. Colvine, Ontario Geological Survey, Miscellaneous Paper 110.

Grant 179 Petrogenesis and Metallogenesis of the Atikwa-Lawrence Volcanic-Plutonic Terrane

G.R. Edwards[1] and D.W. Davis[2]

[1]Earth and Atmospheric Science, York University
[2]Royal Ontario Museum

ABSTRACT

A compositionally diverse group of batholiths in the Wabigoon Subprovince is surrounded by contemporaneous, equally diverse metavolcanic rocks. Trondhjemite to granodiorite at the south margin of the group of batholiths, near the rhyolite-hosted Straw Lake Beach Mine, is host to some small gold occurrences. In this area, rhyolite and andesite are closely related spatially and chemically to trondhjemite to granodiorite and quartz diorite intrusions, respectively. A layered basic intrusion at the northwest margin of the group of batholiths is partly surrounded by chemically related quartz diorite and trondhjemite. The central portion of the group of batholiths is occupied by biotite trondhjemite that is chemically unrelated to the marginal phases.

Gold in the granitoid rocks near Straw Lake was emplaced with quartz in fault zones, perhaps by late magmatic fluids in a subvolcanic environment, or by metamorphic fluids arising from metamorphism and partial melting deep in the crust. Basaltic magma, which was parental to the layered basic intrusion, also differentiated to form diorite (andesite) and the south marginal phase trondhjemite to granodiorite (rhyolite), and provided the heat to partially melt deep crustal rocks to form the biotite trondhjemite at the centre of the group of batholiths.

INTRODUCTION

Research on the chemical evolution and petrogenetic modelling of Archean rocks has centred on relatively complex supracrustal sequences from which there has been significant metal production. For example: metavolcanic sequences in the Timmins-Kirkland Lake and Abitibi areas have resulted from complex magma evolution and an obscure crustal history (Gelinas *et al.* 1984, Jensen 1981, Pyke 1981, Goodwin 1977, De Rosen-Spence 1976, Jolly 1975, Ridler 1970). The Uchi-Confederation Lakes supracrustal sequence has chemically complex, cyclic volcanism and a long crustal history (Thurston and Fryer 1983).

Emerging from this research is evidence that the primary chemistry of felsic volcanic rocks in the vicinity of massive sulphide deposits is distinct from the chemistry of felsic volcanic rocks of barren areas (Thurston 1982, Campbell *et al.* 1982). Magma chamber processes therefore, may have a critical but as yet poorly understood role in the genesis of ore deposits (Campbell *et al.* 1982; see also Hildreth 1979).

Most of the work in this field has been concerned with the volcanic part of the magma system or with small intravolcanic, subvolcanic plutons associated with mineral deposits (Severin 1982, Campbell *et al.* 1981, and Franklin *et al.* 1977). The batholiths tend to be ignored because they are generally not directly associated with base metal or gold deposits.

This is the first year of a study of the petrochemical relationship of volcanism and plutonism in the Atikwa-Lawrence volcanic-plutonic terrane of western Wabigoon Subprovince. A preliminary model is presented for the field and petrochemical relationships of volcanism and plutonism, and for the genesis of gold occurrences near Straw Lake.

GEOLOGY OF THE ATIKWA-LAWRENCE TERRANE

The Atikwa-Lawrence volcanic-plutonic terrane (Figure 1) has central composite batholiths which range in composition from mafic to felsic. Layered and composite basic to ultrabasic intrusions and attendant diorite to quartz diorite are sparsely distributed at the contact between the batholiths and the volcanic rocks. The cores of the batholiths are mainly trondhjemite to granodiorite.

Metavolcanic rocks exhibit a range of compositions similar to the batholiths, comprising basalt at the base overlain by andesite and less common rhyolite.

The current project is concerned with the south and west parts of the terrane.

STRAW LAKE – LAWRENCE LAKE

There is a close link between volcanic and plutonic rocks at the south end of the Lawrence Lake batholith, at Straw Lake. Volcanic rocks in the contact

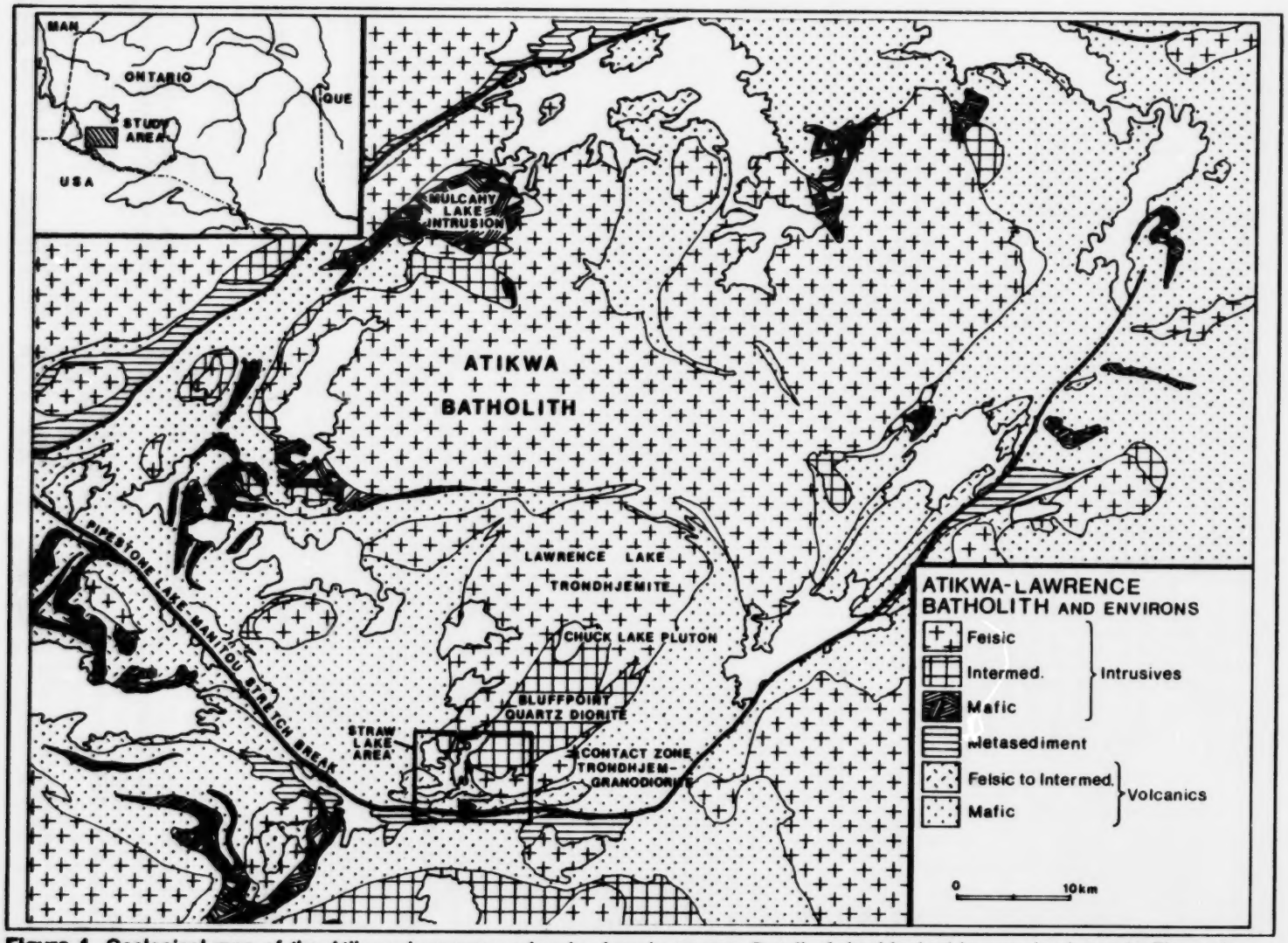

Figure 1. Geological map of the Atikwa- Lawrence volcanic-plutonic terrane. Detail of the blocked-in area is shown in Figure 2. (Modified from Ontario Geological Survey Map 2443.)

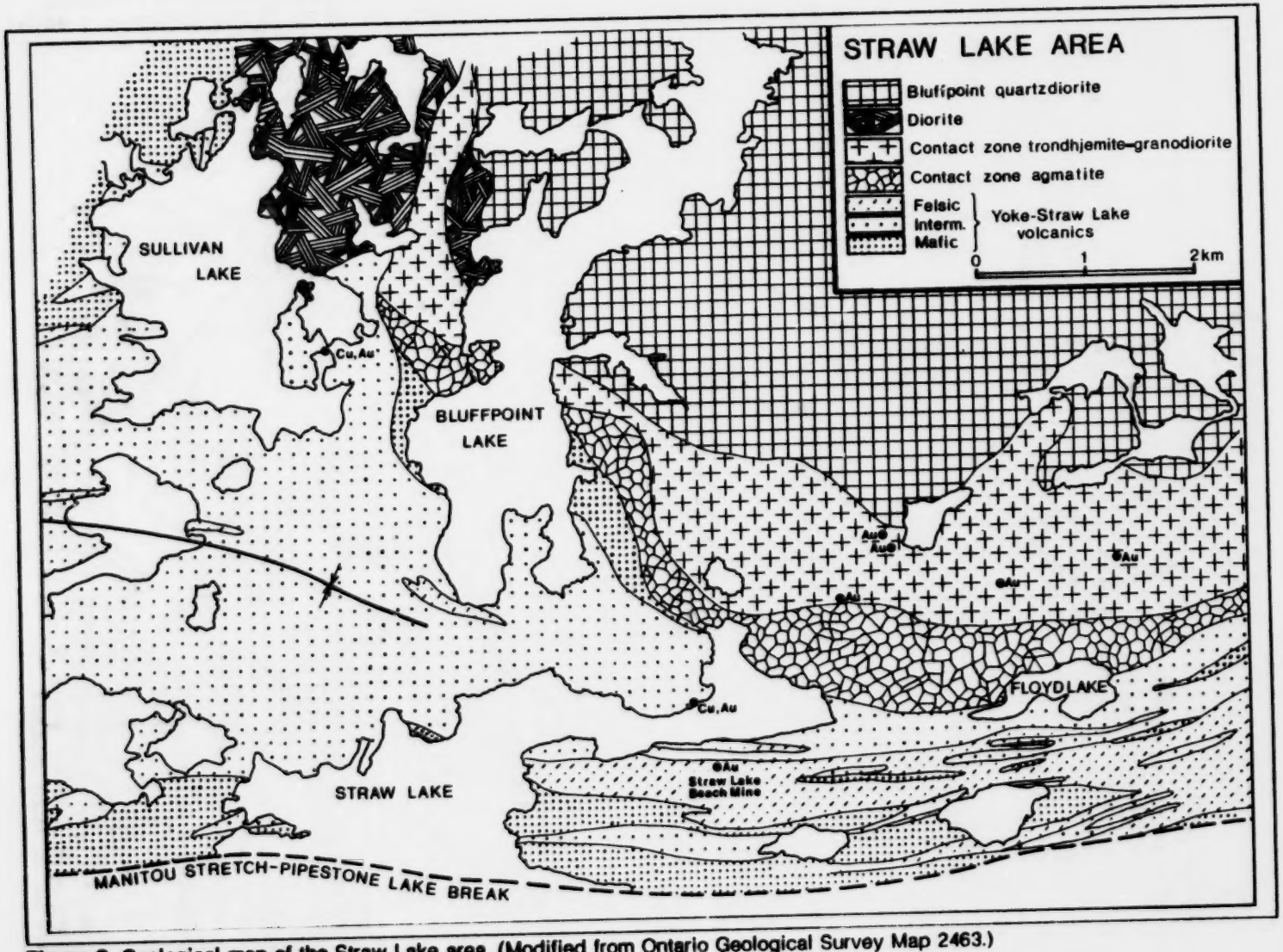

Figure 2. Geological map of the Straw Lake area. (Modified from Ontario Geological Survey Map 2463.)

zone (Figure 2) are strongly metasomatized. A broad zone of felsic intrusive rocks at the contact are fine grained and porphyritic but grade northward into the contact zone biotite trondhjemite to granodiorite (CZT) (Figure 2).

North of the contact zone, the Bluffpoint diorite to quartz diorite occupies much of the southern part of the Lawrence Lake batholith (Figures 1, 2). Its contact with CZT is nebulous suggesting that the magmas were contemporaneous liquids. At Sullivan Lake the medium-grained Bluffpoint diorite grades into andesite flow at the base of a sequence of andesite flows and pyroclastic rocks (Figure 2).

Two intimately related subphases of fine- and medium-grained biotite trondhjemite to granodiorite called the Lawrence Lake trondhjemite (LLT), comprise the bulk of the Lawrence Lake batholith north of, and intruding, the Bluffpoint diorite (Figures 1, 2). These sub-phases are in contact with basalt and they exhibit no close link to equivalent volcanic rocks.

Volcanic rocks south of the contact with the Lawrence Lake batholith at Straw Lake (Figure 2) are mainly rhyolite flows and pyroclastics with intercalated andesite flows. Along strike to the west, at Yoke Lake, andesitic volcanic rocks are more common and rhyolite is scarce. Here andesite overlies tholeiitic and high-alumina basalts that are the basal platform upon which the intermediate and felsic volcanic rocks were deposited.

MULCAHY LAKE

The northwest contact between the Atikwa Batholith and the volcanic belt is occupied partly by the well-preserved Mulcahy Lake layered basic intrusion (MLI) (see Figure 1). Where the layered intrusion is in contact with the basaltic volcanic rocks, pyroxene and amphibole hornfelses are developed. The intrusion also tends to have pegmatitic patches in areas adjacent to the volcanic rocks. The layered intrusion is partly surrounded by quartz diorite and trondhjemite to granodiorite of the Atikwa Batholith. Sparse mafic dikes, possibly representing chilled primary magma related to the basic intrusion, intrude the quartz diorite.

The granitoid and mafic phases appear to have exerted a profound effect on each other. In some outcrops, blue quartz and magnetite in the granitoid phase appear to have originated from the adjacent layered basic intrusion. In other areas the layered intrusion appears to grade into granitoid rocks through a diffuse pegmatite-rich zone. Temporal relations between these intrusive rocks are contradictory. Layered intrusion-like rocks are included in the quartz diorite and trondhjemite to granodiorite in some outcrops but in other areas the granitoid rocks are mixed with or incorporated with the layered intrusion. It remains to be seen whether these features are a result of partial fusion or magma mixing but it appears from the field evidence that intrusive events in this area were contemporaneous.

MINERAL OCCURRENCES

GOLD

Gold occurs in the volcanic and the plutonic environments in the Straw Lake area. The volcanic-hosted Straw Lake Beach Mine (past producer) is located in schistose, sericitic, silicified, pyritized and locally chloritized rhyolite (Figure 2). The gold occurs in quartz veins, 5 to 65 cm wide, and locally in the host sericitic schist. Varying amounts of pyrite, chalcopyrite, tetradymite, galena, magnetite and sphalerite were present in the gold ore (Thomson 1936). The quartz lode is approximately parallel to the regional schistosity.

Gold also occurs in CZT northeast of Straw Lake (Figure 2). Here the gold is in pyritized and sericitized or locally hematitized rocks and quartz veins adjacent to faults transecting the area. The foliation of the host rock is usually strongly contorted in the fault zones. One of the faults, if projected southeastward, intersects the volcanic rocks in the vicinity of the Straw Lake Beach Mine.

GEOCHRONOLOGY

The contemporaneity of volcanic and plutonic events in the Atikwa-Lawrence terrane is supported by high precision, zircon U-Pb isotope geochronology. The ages determined to the present (Davis *et al.* 1982, Morrison *et al.* 1984 and this study) are:

2734.8 (+4.0/-3.1) Ma - rhyolite, south of Wabigoon Lake

2732.2 (+2.9/-2.9) Ma - trondhjemite, south of Wabigoon Lake

2742.8 (+1.4/-1.2) Ma - rhyolite at Eagle Lake

2731.8 (+1.6/-1.3) Ma - trondhjemite at Eagle Lake

2733.2 (+1.0/-0.9) Ma - gabbro, Mulcahy Lake intrusion

2732.4 (+2.1/-1.8) Ma - Bluffpoint diorite

With the exception of the rhyolite sample from Eagle Lake, these ages indicate a very rapid evolution for much of the Atikwa-Lawrence volcanic-plutonic terrane. Dating elsewhere in the Savant Lake - Crow Lake belt (Davis and Trowell 1982) has demonstrated a chronological correlation of the Atikwa-Lawrence terrane with the Neepawa group (2732.7 +1.2/-1.1 Ma) in the Sioux Lookout area and the base of the South Sturgeon Lake volcanics (2733.8 +1.7/-1.3 Ma). The base of the Handy Lake volcanics, at 2745.2 +1.9/-1.8 Ma, however is only slightly older than the rhyolite at Eagle Lake.

GEOCHEMISTRY

Major element analyses were done by X-Ray Assay Laboratories Limited and trace element analyses for lanthanides (rare earth elements), U, Th, Ba, Au, As, Cr, Hf, Ni, Sc, Ta, Co, Zn, and Cs were done using the facilities at the University of Toronto. Analyses for the trace elements Rb, Sr and Zr were done by X-Ray Assay Laboratories Limited. Tables 1 and 2 summarize the analytical data. Chondrite-normalized rare earth element abundances are plotted in Figures 3 to 7.

STRAW LAKE – LAWRENCE LAKE

Intermediate Volcanic Rocks and Bluffpoint Quartz Diorite

The intermediate volcanic rocks (Table 1) exhibit a range in silica content from 54.16 to 65.33%. They vary from high-alumina to low-alumina andesite but all samples have low nickel abundances relative to more modern low-K orogenic andesites (Ewart 1982). Chrome varies within a wide range that seems to be independent of silica content. The general tendency for CaO to increase with decreasing silica is probably a primary rather than a secondary feature because most of the andesites in this area are relatively well preserved.

Bluffpoint quartz diorite (Table 2) has silica contents in the upper end of the range exhibited by the andesites. Otherwise, their overall chemical composition is very similar.

Rhyolite and Contact Zone Trondhjemite to Granodiorite

The rhyolite typically exhibits decreasing alumina with increasing silica (Table 1). Chondrite-normalized rare earth elements for some samples exhibit La/Yb ratios and total abundances similar to the andesites but a negative Eu anomaly is evident with increasing differentiation in the rhyolites.

The major and trace element trends of CZT (Table 2) are very similar to those of the rhyolite. Most samples of the medium-grained trondhjemite to granodiorite have well developed negative Eu anomalies. Some of its finer grained equivalent phases at the contact with volcanic rocks have similar overall chemical attributes but have a positive Eu anomaly. Sample S6 has an unusually high abundance of LREE, a high silica and low alumina content and may represent the end stage of differentiation of this group.

Lawrence Lake Trondhjemite to Granodiorite

Like the CZT, the Lawrence Lake intrusion (LLT) exhibits a decrease in alumina with increased silica but the trend is not so pronounced (Table 2). LLT also has higher Fe and Sr, but lower Th, Hf, Sc, and Zr, than CZT. La/Yb ratios for LLT are greater, because of low HREE abundances.

Mulcahy Lake

Rare earth element trends of rock samples taken from the Mulcahy Lake intrusion (MLI) and its enveloping quartz diorite and trondhjemite support a close relationship between mafic and felsic plutonic rocks in this area. As shown in Figure 7, REE patterns from quartz diorites adjacent to the MLI are similar to the nearby MLI gabbro. Biotite trondhjemite that appears in some areas to be gradational with the quartz diorite also shows similar REE trends. In contrast, biotite trondhjemite from the core of the Atikwa Batholith, like Lawrence Lake trondhjemite has high La/Yb ratios.

DISCUSSION AND CONCLUSIONS

GOLD DEPOSITION

Gold is found both in altered rhyolite at the site of the past-producing Straw Lake Beach Mine and in CZT that has been altered adjacent to faults (see Figure 2). In both environments, the gold is closely associated with sericitization and pyritization accompanying quartz veins in deformed rock.

The source of the gold is not immediately evident. However, there is a slight correlation between HREE and gold abundance in three samples of CZT, suggesting that gold may have been concentrated by a late magmatic fluid phase in the CZT. It may be possible that arguments extended by Campbell *et al.* (1982) for the association: HREE enriched rhyolites with negative Eu anomalies - massive sulphide

TABLE 1. MAJOR AND TRACE ELEMENT ABUNDANCES OF VOLCANIC ROCKS NEAR STRAW LAKE.

	SL9	SL19A	SL5	SL12	SL15	SL22	S48
SiO_2	75.11	74.92	73.34	73.31	71.43	71.07	69.01
Al_2O_3	10.21	11.93	11.26	13.01	13.78	15.60	15.73
CaO	3.37	3.84	3.34	1.67	2.15	2.02	2.78
MgO	1.47	1.01	1.84	0.53	0.57	0.57	1.34
Na_2O	4.56	3.66	5.04	4.19	5.83	3.24	4.80
K_2O	0.65	0.90	0.48	3.24	1.75	3.55	2.11
Fe_2O_3	3.84	3.12	4.06	3.51	3.75	3.56	3.61
MnO	0.13	0.05	0.14	0.05	0.07	0.06	0.07
TiO_2	0.52	0.47	0.43	0.41	0.56	0.23	0.42
P_2O_5	0.15	0.09	0.07	0.06	0.09	0.08	0.12
(LOI)[2]	(5.00)	(1.16)	(3.77)	(0.77)	(2.23)	(3.23)	(1.77)
Rb	8	15	20	100	40	100	52
Sr	160	520	160	230	260	160	490
Ba	140	560	400	720	520	1250	490
Cs	<1	<1	<1	1	1	2	1
U	<1	1	1	1	1	1	1
Th	4	6	5	6	7	7	3
Hf	3	7	5	7	6	7	3
Ta	<1	1	1	1	1	1	<1
Sc	6	8	7	9	10	4	6
Ni	<1	1	1	4	6	<1	<1
Co	3	4	3	2	2	3	7
Cr	3	4	2	3	<1	4	6
Zn	60	40	185	65	64	90	65
Zr	140	300	240	320	270	310	150

Notes.
1. Major elements in weight percent recalculated to 100%; trace elements are in ppm.
2. Loss on ignition not included in recalculated analyses.
Samples.

SL9	Rhyolite, south of Straw Lake
SL19A	Rhyolite flow breccia, Yoke Lake
SL5	Rhyolite hyaloclastite, south of Straw Lake
SL12	Rhyolite lapilli tuff, Yoke Lake
SL15	Rhyolite, Yoke Lake
SL22	Rhyolite, Yoke Lake
S48	Rhyodacite, Yoke Lake

TABLE 1 CONTINUED

	SL6	SL14	SL13	SL10	S41	SL16	S40	SL11
SiO_2	61.03	60.27	59.76	59.25	58.47	57.31	54.87	54.16
Al_2O_3	16.13	15.07	15.61	14.76	16.06	16.34	18.86	17.95
CaO	4.42	6.00	6.48	5.25	7.52	6.58	7.12	7.57
MgO	1.73	4.13	4.63	4.09	4.49	4.92	4.01	4.00
Na_2O	3.96	4.07	2.85	4.32	2.95	4.11	3.41	4.50
K_2O	1.36	1.18	1.04	0.12	0.83	0.73	0.99	0.97
Fe_2O_3	9.53	8.04	8.41	10.44	8.67	8.82	9.33	9.53
MnO	0.08	0.11	0.09	0.13	0.11	0.12	0.12	0.14
TiO_2	1.46	0.91	0.91	1.37	0.74	0.88	1.05	0.94
P_2O_5	0.29	0.23	0.21	0.27	0.14	0.19	0.23	0.22
(LOI)	(6.08)	(1.85)	(2.85)	(5.54)	(2.77)	(2.54)	(6.08)	(2.70)
Rb	37	36	19	<10	20	20	50	35
Sr	220	280	330	340	270	360	360	480
Ba	255	250	255	35	155	250	240	255
Cs	2	<1	<1	<1	<1	<1	<1	<1
U	<1	<1	<1	1	<1	<1	<1	<1
Th	2	3	3	2	2	3	2	3
Hf	4	3	3	4	3	3	3	3
Ta	<1	<1	<1	<1	<1	<1	<1	<1
Sc	23	17	18	23	20	20	20	21
Ni	1	3	3	2	3	2	2	1
Co	32	25	27	27	30	30	25	31
Cr	13	125	155	15	120	105	98	25
Zn	95	90	75	95	50	100	115	95
Zr	190	180	180	180	110	120	160	120

Samples.

SL6	Andesite, south of Straw Lake
SL14	Andesite, Yoke Lake
SL13	Andesite, coarse-grained, Yoke Lake
SL10	Andesite, south of Straw Lake
S41	Andesite, medium-grained, Sullivan Lake
SL16	Andesite, pillowed, Yoke Lake
S40	Andesite, pillowed, Sullivan Lake
SL11	Andesite, pillowed, Yoke Lake

TABLE 1 CONTINUED

	S50	S71	S79	S42	S56	S43	S44
SiO_2	65.33	63.02	60.42	58.56	57.72	57.59	57.32
Al_2O_3	14.50	16.16	16.00	16.62	16.57	16.31	18.04
CaO	4.60	6.10	6.20	7.38	7.59	6.96	7.18
MgO	2.45	2.76	4.06	3.54	3.80	5.87	3.11
Na_2O	4.16	3.74	3.20	3.71	3.54	2.94	3.95
K_2O	1.54	1.12	1.54	0.30	0.66	0.85	0.96
Fe_2O_3	6.28	6.30	7.51	8.47	8.74	8.65	8.13
MnO	0.10	0.09	0.11	0.12	0.12	0.15	0.10
TiO_2	0.84	0.57	0.79	1.06	1.03	0.57	0.99
P_2O_5	0.19	0.13	0.17	0.24	0.24	0.12	0.22
(LOI)	(2.08)	(.47)	(1.77)	(2.77)	(2.70)	(2.70)	(2.47)
Rb	ND	50	45	10	27	22	25
Sr	320	290	370	380	390	280	410
Ba	380	330	315	90	155	215	290
Cs	<1	1	2	<1	<1	1	1
U	<1	<1	<1	<1	<1	<1	<1
Th	4	3	2	2	3	2	2.5
Hf	3	3	3	3	3	2	3
Ta	<1	<1	<1	<1	<1	<1	<1
Sc	14	14	16	19	21	17	18
Ni	2	1	3	1	3	5	3
Co	16	19	23	22	26	29	21
Cr	40	65	105	57	93	275	40
Zn	70	95	90	80	100	80	85
Zr	180	140	120	130	160	90	120

Samples.

S50	Dacite lapilli tuff, Yoke Lake
S71	Andesite, Upper Lawrence Lake
S79	Andesite, Lawrence Lake
S42	Andesite, Sullivan Lake
S56	Andesite, Yoke Lake
S43	Diorite, medium-grained, subvolcanic, NE of Sullivan Lake
S44	Andesite, Sullivan Lake

TABLE 2. MAJOR AND TRACE ELEMENT ABUNDANCES OF PLUTONIC ROCKS OF THE ATIKWA-LAWRENCE TERRANE.

	S23	S35	S62	S32	PC7	PL2	PC5	PC1
SiO_2	64.57	63.90	61.85	60.29	76.17	75.47	75.44	75.06
Al_2O_3	15.05	16.48	16.82	17.17	13.10	12.82	13.99	13.20
CaO	5.14	5.44	6.12	6.57	0.38	1.43	0.09	0.23
MgO	2.60	2.18	2.18	2.95	0.32	0.33	0.37	0.15
Na_2O	4.02	4.42	3.94	4.05	5.79	5.64	5.03	6.44
K_2O	1.26	1.16	1.18	1.22	1.17	1.22	2.06	1.15
Fe_2O_3	6.48	5.66	6.86	6.90	2.75	2.79	2.72	3.47
MnO	0.11	0.08	0.10	0.11	0.03	0.02	0.00	0.02
TiO_2	0.72	0.56	0.74	0.59	0.25	0.24	0.24	0.26
P_2O_5	0.15	0.13	0.18	0.15	0.04	0.04	0.06	0.03
Rb	30	30	45	30	15	40	45	20
Sr	360	450	390	360	160	170	30	140
Ba	330	310	240	250	415	415	550	500
Cs	<1	1	2	1	<1	1	1	<1
U	<1	<1	<1	<1	1	1	2	1
Th	3	1	2.5	2.5	6	9	9	6
Hf	4	2	4	2.5	8	8	9	7
Ta	<1	<1	<1	<1	1	1	1	1
Sc	13	11	12	15	7	8	7	6
Ni	2	2	1	2	<1	1	<1	1
Co	15	14	16	20	1	2	2	2
Cr	40	13	17	43	4	1	2	2
Zn	65	60	95	80	40	10	30	60
Zr	210	110	220	90	360	390	410	360

Notes.
1. Major elements in weight percent, recalculated to 100%; trace elements are in ppm.
Samples.

S23	Bluffpoint quartz diorite
S35	Bluffpoint quartz diorite
S62	Bluffpoint quartz diorite
S32	Bluffpoint quartz diorite
PC7	Contact zone trondhjemite
PL2	Contact zone trondhjemite
PC5	Contact zone granodiorite
PC1	Contact zone trondhjemite

TABLE 2 CONTINUED

	PC3	PL7	PL6	S6	S25	S11	S13	S14C
SiO_2	73.60	73.54	73.74	79.82	74.39	72.31	64.32	62.78
Al_2O_3	12.28	13.41	13.42	11.76	12.72	14.48	15.63	15.67
CaO	1.68	1.96	1.78	2.04	0.64	3.17	5.30	4.99
MgO	1.58	0.69	0.71	0.19	0.38	0.84	2.27	2.70
Na_2O	3.37	4.39	4.41	4.86	5.20	6.15	5.49	4.05
K_2O	2.65	2.73	3.25	0.51	2.55	0.49	0.96	1.97
Fe_2O_3	4.51	2.85	2.51	0.47	3.82	1.94	5.19	6.88
MnO	0.04	0.02	0.03	0.00	0.02	0.02	0.06	0.07
TiO_2	0.24	0.34	0.35	0.21	0.24	0.49	0.65	0.74
P_2O_5	0.04	0.07	0.07	0.04	0.04	0.10	0.13	0.14
Rb	95	80	75	14	70	10	20	50
Sr	70	200	210	230	50	250	330	380
Ba	475	550	710	180	510	200	400	660
Cs	2	2	<1	1	<1	<1	<1	1
U	1	1	1	1	1	1	1	<1
Th	5	8	8	7	5	6	6	1
Hf	8	5	5	7	7	5	4	2
Ta	1	1	1	<1	1	<1	<1	<1
Sc	7	6	6	5	8	8	12	1
Ni	<1	<1	<1	1	<1	1	2	<1
Co	8	6	4	1	2	21	9	1
Cr	1	2	3	3	<1	7	37	3
Zn	115	25	40	-	20	28	70	25
Zr	360	230	210	310	340	280	160	110

Samples.

PC3	Contact zone granodiorite
PL7	Contact zone granodiorite
PL6	Contact zone granodiorite-quartz monzonite
S6	Contact zone quartz porphyry
S25	Contact zone granodiorite
S11	Contact zone fine-grained, clotty trondhjemite
S13	Contact zone clotty trondhjemite
S14C	Contact zone clotty trondhjemite

TABLE 2 CONTINUED

	S8	S14A	S9	S18	S91	S82	S22	S95
SiO_2	78.88	74.61	74.22	75.01	74.33	73.87	73.32	71.82
Al_2O_3	11.87	13.54	14.20	13.98	14.38	14.73	15.80	15.91
CaO	1.90	2.30	2.28	1.76	2.49	2.11	0.99	2.15
MgO	0.51	0.49	0.51	0.18	0.41	0.33	0.67	0.41
Na_2O	5.69	4.53	6.30	4.89	4.56	5.03	6.46	5.51
K_2O	0.22	2.29	0.49	2.30	1.80	2.39	1.83	2.53
Fe_2O_3	0.68	2.20	0.99	1.73	1.82	1.32	0.77	1.37
MnO	0.01	0.02	0.02	0.03	0.02	0.02	0.01	0.02
TiO_2	0.19	0.35	0.53	0.09	0.16	0.15	0.10	0.22
P_2O_5	0.03	0.06	0.07	0.02	0.02	0.04	0.04	0.06
Rb	10	30	25	65	85	55	50	70
Sr	210	260	350	160	250	270	710	560
Ba	150	740	180	750	620	820	650	610
Cs	<1	<1	<1	1	2	2	1	1
U	<1	1	1	<1	<1	<1	<1	1
Th	7	6	5	5	4	4	1	3
Hf	5	6	6	2	3	2	2	2
Ta	<1	1	1	<1	<1	<1	<1	<1
Sc	3	5	6	1	2	2	1	2
Ni	<1	10	1	1	2	<1	<1	<1
Co	<1	3	1	1	3	2	1	2
Cr	2	5	<1	2	3	2	3	2
Zn	6	45	15	62	53	50	25	65
Zr	260	270	250	70	100	80	80	90

Samples.

S8	Contact zone quartz porphyry
S14A	Contact zone fine-grained granodiorite
S9	Contact zone plagioclasite
S18	Lawrence Lake granodiorite
S91	Lawrence Lake trondhjemite
S82	Lawrence Lake granodiorite
S22	Lawrence Lake trondhjemite
S95	Lawrence Lake granodiorite

TABLE 2 CONTINUED

	T8	S82A	T14A	T1	T14B	S95	S84	S96
SiO_2	67.72	71.90	72.35	72.05	71.94	71.82	71.78	67.28
Al_2O_3	16.63	15.51	15.09	14.89	15.07	15.91	15.40	15.92
CaO	4.54	2.91	3.15	3.23	3.17	2.15	2.70	3.87
MgO	0.96	0.56	0.57	0.68	0.71	0.41	0.66	1.77
Na_2O	4.34	5.23	4.64	4.39	4.64	5.51	4.92	5.01
K_2O	1.46	1.63	1.65	1.66	1.34	2.53	1.94	2.04
Fe_2O_3	3.78	1.93	2.19	2.69	2.74	1.37	2.22	3.54
MnO	0.05	0.02	0.03	0.04	0.04	0.02	0.03	0.05
TiO_2	0.41	0.24	0.25	0.28	0.26	0.22	0.26	0.40
P_2O_5	0.11	0.06	0.07	0.08	0.08	0.06	0.07	0.11
Rb	70	70	45	30	68	70	50	65
Sr	320	420	260	260	240	560	340	760
Ba	620	710	500	640	265	610	590	900
Cs	1	2	1	1	2	1	2	1
U	1	1	<1	1	1	1	<1	<1
Th	3	3	3	8	6	3	5	3
Hf	5	3	3	4	4	2	3	3
Ta	<1	<1	<1	<1	1	<1	<1	<1
Sc	6	3	2.5	3	3	2	2	6
Ni	<1	1	<1	8	<1	<1	1	13
Co	7	4	4	6	8	2	4	11
Cr	2	7	4	6	6	2	3	33
Zn	85	65	60	70	70	65	70	60
Zr	270	120	160	190	170	90	120	110

Samples.

T8	Lawrence Lake trondhjemite
S82A	Lawrence Lake trondhjemite
T14A	Lawrence Lake trondhjemite
T1	Lawrence Lake trondhjemite
T14B	Lawrence Lake trondhjemite
S95	Lawrence Lake granodiorite
S84	Lawrence Lake granodiorite
S96	Lawrence Lake granodiorite

deposits, may also apply to gold deposits. A similar fluid phase may have been mobile enough to have deposited gold in quartz veins of the Straw Lake Beach Mine, that is, less than 900 m from the contact zone.

Alternatively, and equally viable at this stage of the investigation, gold may have been introduced after the main magmatic activity ceased. The gold-bearing quartz veins at the Straw Lake Beach Mine were introduced parallel to schistosity in the rhyolite. If the veins postdate regional deformation, then it is feasible that the gold has a metamorphic origin. Perhaps the process of partial melting and accompanying metamorphism of deep crust that gave rise to the Lawrence Lake trondhjemite also produced the gold-bearing fluids in this area. These possibilities will be assessed with the results of ongoing research.

PETROGENESIS OF VOLCANIC AND PLUTONIC ROCKS

Formulation of a model for the petrogenetic evolution of the Atikwa-Lawrence volcanic-plutonic terrane requires a detailed knowledge of the field and chemical relationships among the plutonic rocks, and between the plutonic rocks and the volcanic rocks. Field evidence for the relationship between these rock types is largely derived from mapping at the south end of the Lawrence Lake batholith where the relation is most intimate.

At Sullivan Lake, Bluffpoint diorite grades into andesite flow (Figure 2), an observation borne out by their similar chemical composition. At Straw Lake, CZT, which hosts the gold occurrences, grades "upward" into quartz

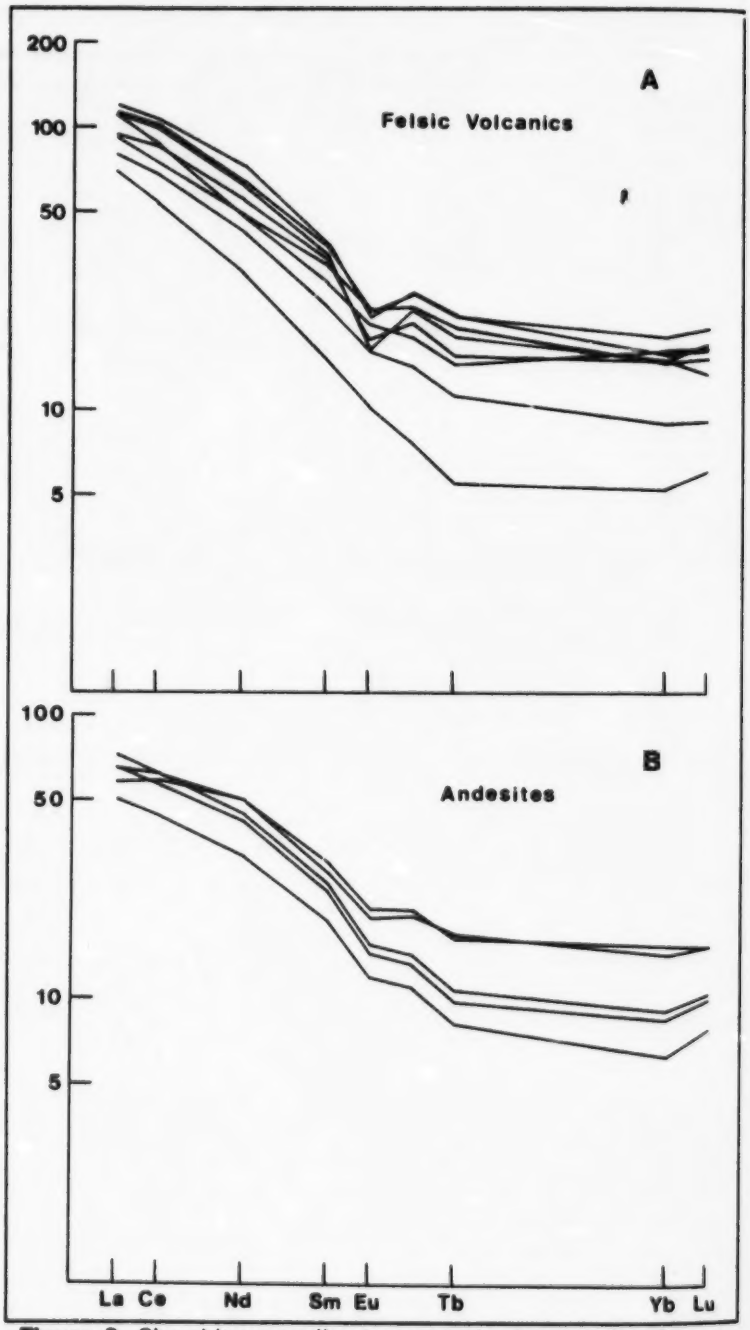

Figure 3. Chondrite-normalized rare earth element abundances in felsic metavolcanic rocks and andesites near Straw Lake.

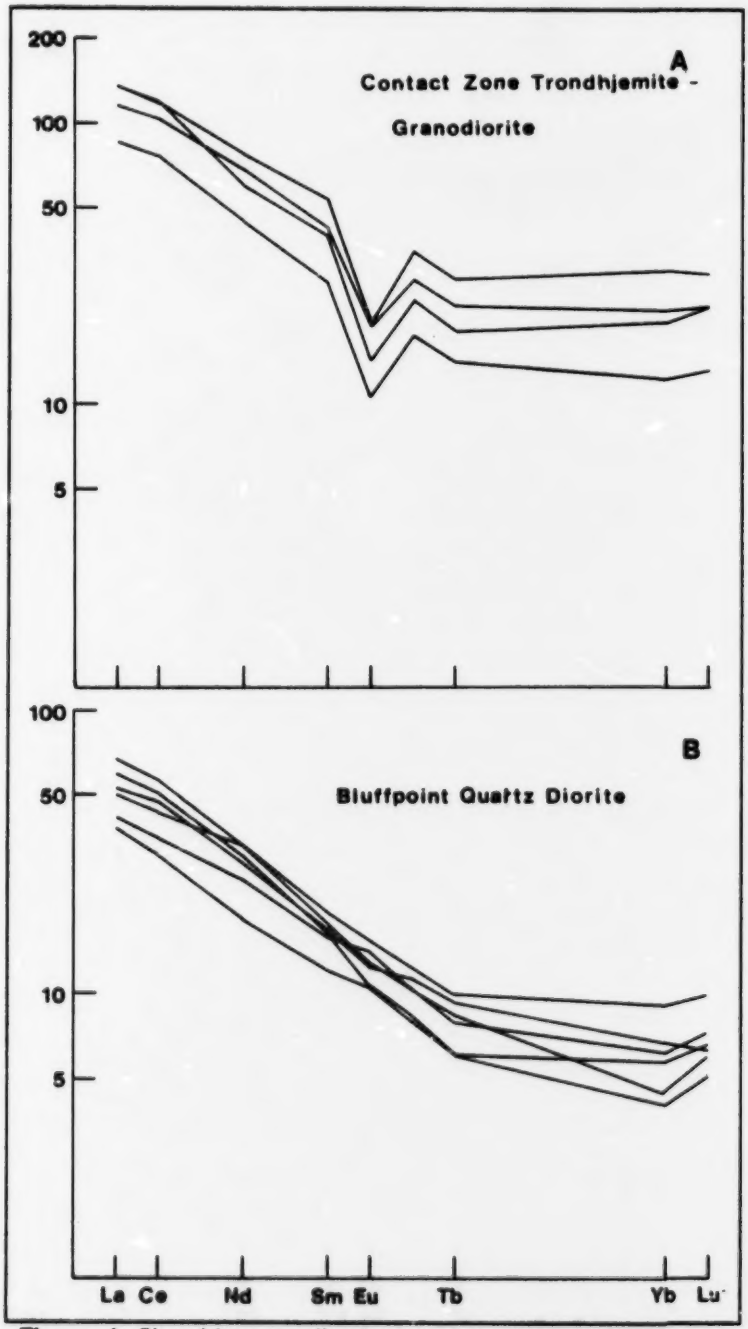

Figure 4. Chondrite-normalized rare earth element abundances in contact zone trondhjemite to granodiorite (CZT) and Bluffpoint quartz diorite.

porphyry and other related contact zone phases which bear a close spatial and chemical relationship to the Straw Lake rhyolite flows.

The preliminary interpretation of the chemical data, supported by field evidence is:

1. Contact zone trondhjemite (CZT) and Bluffpoint diorite are the intrusive counterparts of the rhyolite and andesite, respectively, at Straw Lake.
2. CZT evolved from Bluffpoint diorite by the removal of amphibole, calcic plagioclase and some clinopyroxene and the concomitant accumulation of sodic plagioclase and quartz.
3. Bluffpoint diorite is a crustally contaminated or direct derivative of basic magma similar to that forming Mulcahy Lake intrusion (MLI). Diorite and trondhjemite adjacent to MLI formed in the same way.
4. Lawrence Lake trondhjemite (LLT) was formed by the partial melting of basalt leaving a clinopyroxene- and amphibole-rich residue. It was intruded as a result of heat added to the lower part of a predominantly basaltic crust by the continuous introduction of new basaltic magma in systems like those that fed MLI.
5. MLI primary magma, rich in iron, produced high-iron tholeiitic basalts such as those (undated) at the top of the Eagle Lake - Wabigoon Lake sequence to the northeast. The MLI has a zircon U/Pb isotope age (2733.2 + 1.0/-0.9 Ma, Morrison *et al.* 1984) within error of the zircon age determined for a subvolcanic, iron-rich gabbro in the Katimiagamak basalts west of Straw lake (2734.9 +3.0/-2.8 Ma, Edwards and Davis, in preparation.)

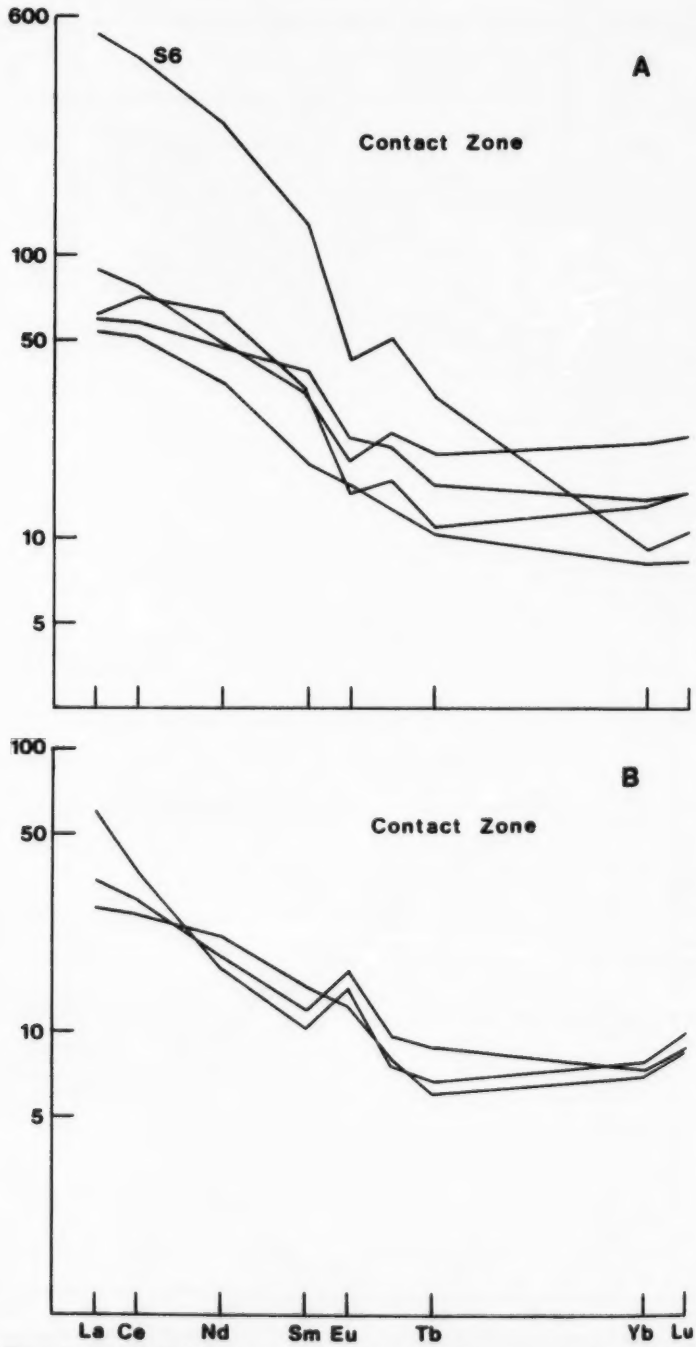

Figure 5. Chondrite-normalized rare earth element abundances in contact zone fine-grained and porphyritic intrusive rocks with (a) zero or negative Eu anomalies and (b) positive Eu anomalies. S6 is the contact zone quartz porphyry.

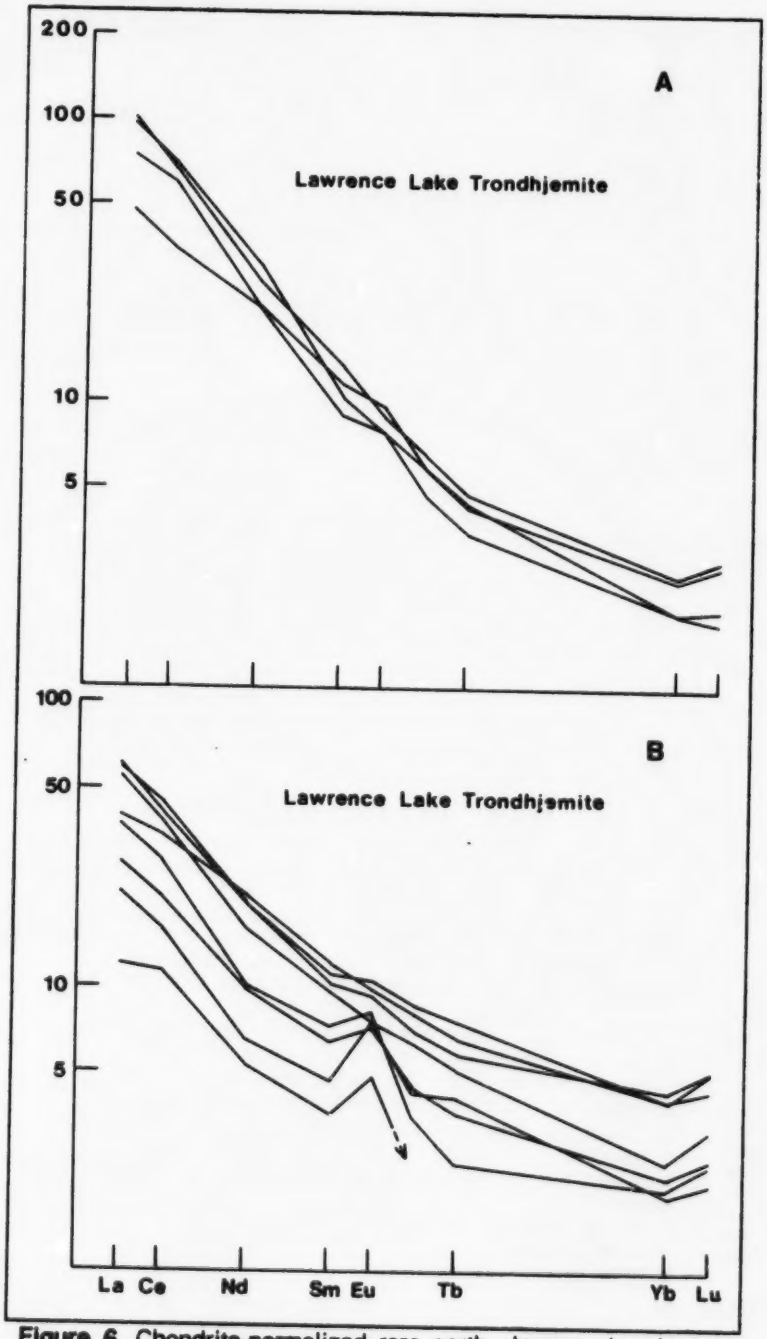

Figure 6. Chondrite-normalized rare earth element abundances in Lawrence Lake trondhjemite to granodiorite with (a) large La/Yb ratios and (b) without large La/Yb ratios.

ACKNOWLEDGMENTS

The authors would like to thank Rob Mason for his assistance in preparing the maps for this report; Nick Keehn and Barbara Every prepared some of the drawings.

REFERENCES

Campbell, I.H., Franklin J.M., Gorton, M.P., Hart, T.R. and Scott, S.D.
1981: The Role of Subvolcanic Sills in the Generation of Massive Sulfide Deposits: Economic Geology, Volume 76, p.2248.

Campbell, I.H., Coad, P., Franklin, J.M., Gorton, M.P., Scott, S.D., Sowa, J., and Thurston, P.C.
1982: Rare Earth Elements in Volcanic Rocks Associated with Cu-Zn Massive Sulphide Mineralization: A Preliminary Report: Canadian Journal of Earth Sciences, Volume 19, p.619.

Davis, D.W., Blackburn, C.E., and Krogh, T.E.
1982: Zircon U-Pb Ages from the Wabigoon-Manitou Lakes Region, Wabigoon Subprovince, Northwest Ontario: Canadian Journal of Earth Sciences, Volume 19, p.254.

Davis, D.W., and Trowell, N.F.
1982: U-Pb Ages from the Eastern Savant Lake - Crow Lake Metavolcanic-Metasedimentary Belt, Northwest Ontario: Canadian Journal of Earth Sciences, Volume 19, p.868.

De Rosen-Spence, A.F.
1976: Stratigraphy, Development and Petrogenesis of the Central Noranda Volcanic Pile, Noranda, Quebec: Unpublished Ph.D. Thesis, University of Toronto, 166p.

Ewart, A.
1982: The Mineralogy and Petrology of Tertiary-Recent Orogenic Volcanic Rocks: with Special Reference to the Andesitic-Basaltic Compositional Range; p.25 *in* Andesites: Orogenic Andesites and Related Rocks, edited by R.S. Thorpe, John Wiley and Sons, New York.

Franklin, J.M., Gibb, W., Poulson, K.H., and Severin, P.
1977: Archean Metallogeny and Stratigraphy of the South Sturgeon Lake Area, Mattabi Trip: 23rd Annual Meeting, Institute Lake Superior Geology, 73p.

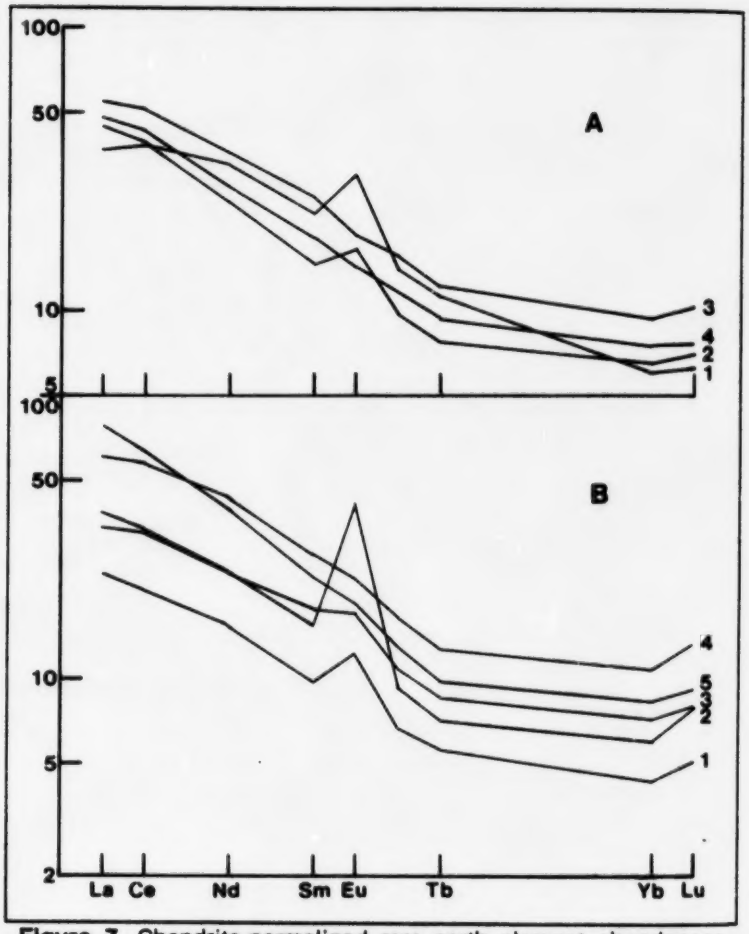

Figure 7. Chondrite-normalized rare earth element abundances in Mulcahy Lake intrusion and adjacent rocks.
(a) Section across the contact between the Mulcahy Lake intrusion and adjacent quartz diorite.
1. gabbro 30 m inside the Mulcahy Lake intrusion
2. gabbro 15 m inside the Mulcahy Lake intrusion
3. quartz diorite 15 m from the Mulcahy Lake intrusion
4. quartz diorite 45 m from the Mulcahy Lake intrusion
(b) Mulcahy Lake layered intrusion and surrounding rocks.
1. gabbro, 18 m inside the Mulcahy Lake intrusion
2. quartz diorite 12 m south of contact with the Mulcahy Lake intrusion
3. biotite trondhjemite
4. quartz diorite
5. 'blue quartz' granodiorite

Gelinas, L. Trudel, P., and Hubert, C.
1984: Chemostratigraphic Division of the Blake River Group, Rouyn-Noranda Area, Abitibi, Quebec; Canadian Journal of Earth Sciences, Volume 21, p.220.

Goodwin, A.M.
1977: Archean Volcanism in Superior Province, Canadian Shield; p.205 *in* Volcanic Regimes in Canada, Geological Association of Canada, Special Paper 16.

Hildreth, W.
1979: The Bishop Tuff: Evidence for the Origin of Compositional Zonation in Silicic Magma Chambers; p.43 *in* Ash Flow Tuffs, edited by C.E. Chapin and W.E. Elston, Geological Society of America, Special Paper 180.

Jensen, L.S.
1981: Gold Mineralization in the Kirkland Lake - Larder Lake Area; p.59-65 *in* Genesis of Archean Volcanic Hosted Gold Deposits, Symposium held at the University of Waterloo, March 7, 1980, Ontario Geological Survey, Miscellaneous Paper 97, 175p.

Jolly, W.T.
1975: Subdivisions and Origin of the Archean Lavas of the Abitibi Area, Canada, from Fe-Mg-Ni-Cr Relations; Earth and Planetary Science Letters, Volume 27, p.200.

Morrison, D.A., Davis, D.W., Wooden, J.L., Bogard, D., Maczuga, D.E., Phinney, W.C., and Ashwal, L.D.
1984: Age of the Mulcahy Lake Intrusion, NW Ontario, and Implications for the Evolution of Greenstone-granite Terranes; Submitted to Earth and Planetary Science Letters.

Pyke, D.R.
1981: Relationship of Gold Mineralization to Stratigraphy and Structure in Timmins and Surrounding Area; p.1-15 *in* Genesis of Archean, Volcanic Hosted Gold Deposits, Symposium held at the University of Waterloo, March 7, 1980, Ontario Geological Survey, Miscellaneous Paper 97, p.175.

Ridler, R.H.
1970: Relationship of Mineralization to Volcanic Stratigraphy in the Kirkland Lake-Larder Lake Area, Ontario; Geological Association of Canada, Proceedings, Volume 21, p.33.

Severin, P.W.A.
1982: Geology of the Sturgeon Lake Copper-Zinc-Lead-Silver-Gold Deposit; Canadian Institute of Mining and Metallurgy, Bulletin, Volume 75, p.107.

Thomson, J.E.
1936: Geology of the Rowan-Straw Lakes Area; Ontario Department of Mines, Annual Report for 1935, Volume 44, Part 4, p.1-28, accompanied by Map 44e.

Thurston, P.C.
1982: Economic Evaluation of Archean Felsic Volcanic Rocks Using REE Geochemistry; Geological Society of Australia, Special Publication 7, p.439.

Thurston, P.C., and Fryer, B.J.
1983: The Geochemistry of Repetitive Cyclical Volcanism From Basalt Through Rhyolite, in the Uchi-Confederation Greenstone Belt, Canada; Contributions to Mineralogy and Petrology, Volume 3, Number 83.

Grant 187 Sedimentology of the Cambro-Ordovician Sandstones of Eastern Ontario

Rainer R. Wolf and Robert W. Dalrymple

Department of Geological Sciences, Queen's University

ABSTRACT

Sandstones of the Cambro-Ordovician Potsdam Group which outcrop on the Frontenac Axis, north and east of Kingston, Ontario, can be subdivided into the 'Covey Hill' and overlying Nepean Formations. Isolated outliers of pebbly arkose and feldspathic conglomerate that are preserved within down-faulted blocks northeast of Big Rideau Lake are tentatively correlated with the Covey Hill Formation of Quebec. The well-sorted quartz arenites of the Nepean Formation outcrop more extensively, providing excellent exposures for study.

Two terrestrial and two marine facies have been identified from these units. The poorly-sorted, and commonly cross-bedded, pebbly arkoses and conglomerates of the 'Covey Hill' formation are interpreted to represent a proximal braided fluvial environment. The sequence of structures suggests that sedimentation was influenced by movement on the nearby Rideau Lake Fault. The second terrestrial facies is characterized by very large, simple cross beds composed of medium-grained, well sorted and rounded quartz grains, interbedded with thin, unsorted conglomerates. The cross beds display a variety of small features including adhesion ripples, wave ripples and arthropod crawling traces (*Protichnites*), and are considered to represent a coastal dune complex that was locally cut by fluvial channels, and periodically flooded by marine waters.

The third and most extensively-developed facies is composed of cyclically-interbedded cross-bedded and bioturbated quartz arenites. A typical cycle is 1-3 m thick and consists of a basal erosion surface overlain by small-scale cross-bedding and ripple cross-lamination, which passes upward into totally bioturbated sandstone. The sequence of structures suggests that these cycles represent the repeated progradation of a subtidal to intertidal-flat environment. The final facies includes all of the scattered outcrops of marine sandstone which do not fit into the third facies. It includes trough cross-bedded and parallel-bedded quartz arenites, and represents an (at present) undifferentiated nearshore facies in which beach, foreshore, tidal inlet and offshore bar deposits may be present. Initial results from this study suggest that the second and third facies have the greatest potential for high quality silica.

INTRODUCTION

OBJECTIVES

Sandstones of the Cambro-Ordovician Potsdam Group of eastern Ontario have long been considered as a possible source of silica (Cole 1923). Over the last few years renewed interest in these sandstones has led to considerable drilling and sampling by both government agencies and industry (Powell and Klugman 1979; Klugman and Yen 1980; Collings and Andrews 1983; Kingston and Papertzian 1983), and in 1982, the W.R. Barnes Company Limited removed 30,000 tonnes of silica sandstone from their Storrington Township (Frontenac County) quarry, north of Kingston, for processing in their plant at Waterdown, Ontario (Kingston and Papertzian 1983). Silica has many industrial applications: it is a primary ingredient in the production of glass, concrete products, enamel paint, ferrosilicon and silicon carbide, and is an abrasive agent in soap and scouring pads (Vos 1981). Canadian consumption totalled more than 3.5 million tonnes in 1980. Less than 2.3 million tonnes of silica ore was mined in Canada so that more than $10 million worth of silica was imported (Boyd 1982).

The study summarized here was initiated to assist in the evaluation of the silica sand potential of the Potsdam Group sandstones by determining the depositional processes and environments which produced them. The determination of the geographic and stratigraphic distribution of the environmental facies will also aid in extending and predicting occurrences of high quality silica sand.

STUDY AREA

The area under investigation extends north and east of Kingston, Ontario, and occupies the roughly triangular area between Kingston, Brockville, and Big Rideau Lake (Figure 1). This area straddles the Frontenac Axis and includes the southwestern margin of the Ottawa Valley. The Paleozoic rocks in this region have been examined recently by the Ontario Geological Survey (Carson 1982a,b; Wolf and Williams 1984a,b). These maps, with certain revisions required by the additional work reported here, provide the basis for this study. Natural and man-made exposures of the Potsdam Group sandstones are scattered and sparse

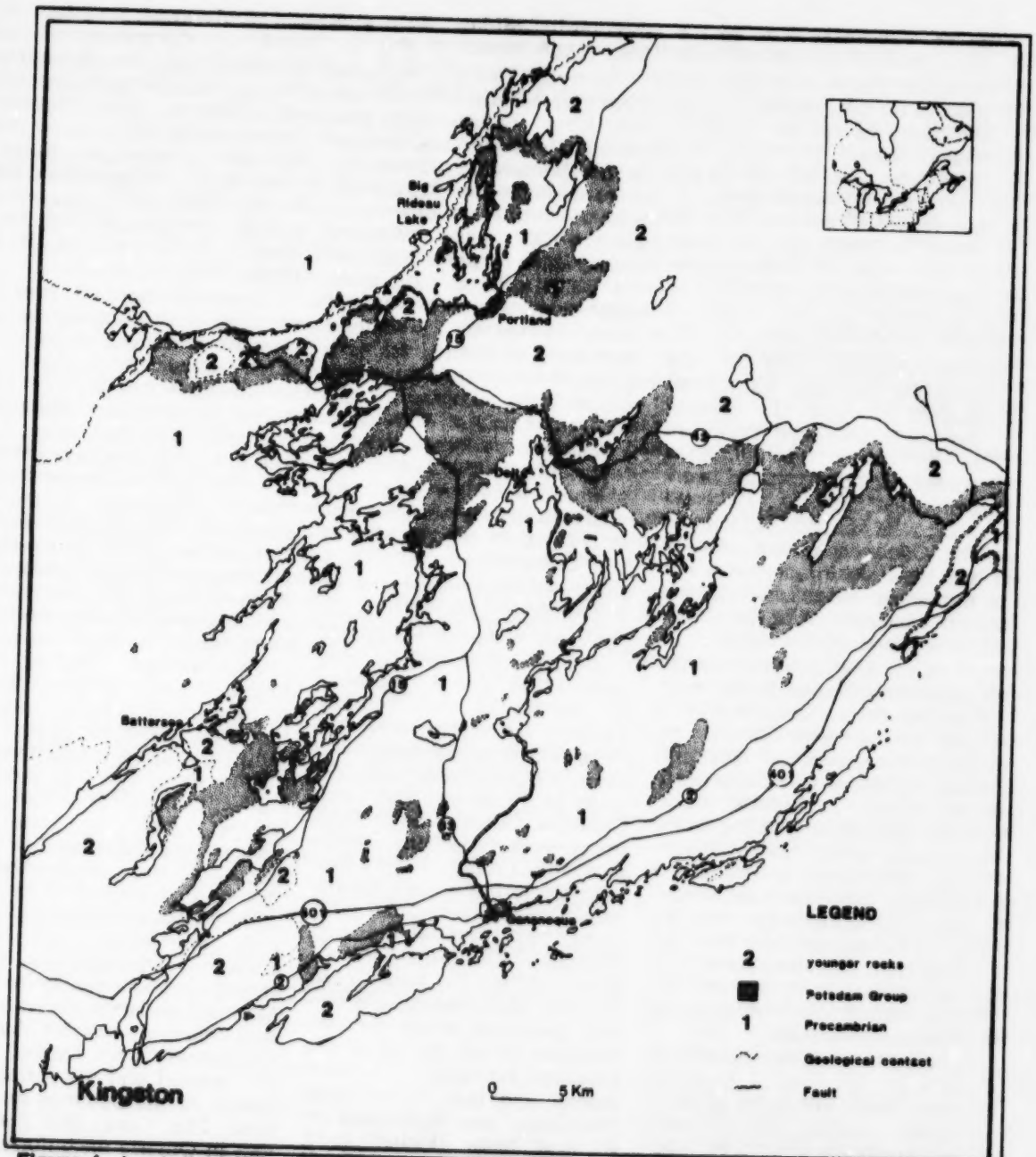

Figure 1. Areal distribution of the Potsdam Group in the study area (modified from Carson 1962a,b and Wolf and Williams 1984a,b). X - Mill Pond Quarry.

on the Frontenac Axis in the southern and central portions of the map-area, and most exposures do not exceed 2 m in thickness, except in the Battersea area. In the northeastern part of the map-area, however, continuous exposure, which exceeds 20 m in height in many places, exists along the Precambrian-Paleozoic contact.

METHODOLOGY

Approximately 70% of the available outcrops have been studied in detail; the remainder have also been examined in an earlier reconnaissance survey. Detailed studies were conducted in the Battersea area, west and east of Delta, in the Gananoque area, and in the Big Rideau Lake area. The remaining areas of exposure will be examined in the second field season of this study.

Over 130 outcrops showing more than 2 m of section were measured and described on a bed by bed basis. The data recorded included: bed thickness and its lateral variability; vertical trends in bedding thickness; nature of bedding plane contacts; grain size and sorting; variations in grain size through the beds; grain roundness and mineralogy, especially in the gravel sizes; rock colour; and the nature of any sedimentary structures present. The description of physical structures included: size of structures and vertical trends in size; direction of cross-bed dips; shape and orientation of ripple marks and other bedding-plane structures; lateral variations of structures within beds; and vertical changes in the types of structures present. In addition, biological structures were recorded, including the degree of bioturbation in each bed and the nature of any body and trace fossils found.

Samples were collected from representative locations for X-ray radiographs, geochemical analysis, and petrographic examination. From the more than 200 samples collected, 45 thin sections were made. Of these, detailed petrographic analyses, including point counts, have been made on 15 thin sections (Dorr 1984). An initial 20 samples have been submitted for geochemical analysis, with each sample being analyzed for silica, iron, calcium, aluminum, magnesium, sodium, potassium, and titanium. Approximately 25 slabs from apparently structureless sandstones will be X-rayed to search for any fine structures.

GENERAL GEOLOGY

The term 'Potsdam Sandstone' was first introduced by Emmons (1838) for a succession of sandstones in Potsdam County, New York, and Logan (1863) extended the term to include lithologically similar rocks in Frontenac and Leeds Counties, Ontario. Since then, many workers in both Canada and the United States have used the term Potsdam for any basal Cambro-Ordovician sandstone, regardless of lithology (Wright 1923; Keith 1949; Liberty 1972). In New York, Quebec, and Ontario, the current practice is to use the term Potsdam Group for all of the Cambro-Ordovician sandstones, and then to subdivide the Group into formations on a local basis (Fisher 1977; Globensky 1981, 1982a,b; Wolf and Williams 1984a,b)

The Potsdam Group forms the basal Paleozoic unit in eastern Ontario, unconformably overlying the Precambrian and conformably overlain by sandy dolostones and dolostones of the Beekmantown Group (Table 1). In eastern Ontario the Potsdam Group can be divided into two formations based on distinct lithological differences, the lower, 'Covey Hill' formation and the overlying Nepean Formation (Williams and Wolf 1982) (Table 1).

Several isolated outcrops in the Big Rideau Lake area, most of which are found in a down-faulted block, have been tentatively assigned to the Covey Hill Formation, a formation originally described from the Montreal area (Clark 1966). The Big Rideau Lake outcrops consist of massive to poorly stratified, arkosic conglomerates and cross-stratified pebbly arkoses, similar to exposures of the Covey Hill Formation near Montreal. Earlier workers were either unable to correlate these outcrops (Wilson and Dugas 1961), or believed them to be equivalent to the Middle Ordovician Shadow Lake Formation (Wynne-Edwards 1967). Based on its stratigraphic position in water-well records, and the lack of Phanerozoic lithologies in the clasts of the conglomerates, this unit is considered by the authors to be post-Grenville and pre-Nepean in age. Though lithologically and stratigraphically similar to the Montreal outcrops, the correlation remains tentative due to the distance from Quebec and the isolated and discontinuous nature of the outcrops in Ontario. The 'Covey Hill' formation in Ontario unconformably overlies the Precambrian and, while the upper contact is not exposed at Big Rideau Lake, an exposure of a similar conglomerate at Jones Falls is unconformably overlain by

quartz arenites of the Nepean Formation.

The Nepean Formation was introduced by Wilson (1946) for the quartz arenites which lie directly on the Precambrian in the Ottawa area where the 'Covey Hill' formation is generally absent, due to either pre-Nepean erosion or non-deposition. The Nepean Formation was named for Nepean Township where large quarries were developed for the building stone which was used for the Parliament Buildings in Ottawa. Because these quarries have been either partially or totally filled, Greggs and Bond (1972, 1977) proposed that the nearby roadcut on the Queensway (Highway 417), west of Ottawa, be designated as a principal reference section. Later, Brand and Rust (1977a,b) recognized the contact between the Nepean Formation and the overlying March Formation in this section, and proposed that it be designated as the type section for the Nepean Formation.

In the immediate Kingston area it is more difficult to divide the Potsdam Group due to the more variable and scattered nature of the outcrops. The rocks in this area, however, are all quartz arenites and, thus, can be assigned to the Nepean Formation. As will be seen later in this report, the sedimentary structures within the quartz arenites in the Kingston area are very different from the structures found in the typical Nepean Sandstone of the Ottawa - St. Lawrence Lowlands. Further study may result in further subdivision of the Nepean Formation.

In eastern Ontario the upper portion of the Nepean Formation is Lower Ordovician (Tremadocian) in age, based on a sparse conodont fauna (Brand and Rust 1977a), whereas the stratigraphically-equivalent unit in northern New York State (Keeseville Formation) is Upper Cambrian (Canadian) in age, based on trilobite assemblages (Fisher 1977). This indicates that at least the upper part of the Potsdam Group is diachronous (changes age) northward from New York to Ontario. The exact position of the Cambrian-Ordovician boundary in Ontario cannot be precisely determined due to the lack of diagnostic fossils in the lower portion of the Potsdam Group.

TABLE 1. CAMBRO-ORDOVICIAN STRATIGRAPHY OF THE OTTAWA-ST. LAWRENCE LOWLANDS (AFTER WOLF AND WILLIAMS 1984A,B).

Middle Ordovician	Ottawa Group	
	Chazy Group	
Lower Ordovician	Beekmantown Group	Oxford Formation
		March Formation
Upper Cambrian	Potsdam Group	Nepean Formation
		'Covey Hill' formation
PRECAMBRIAN		

DEPOSITIONAL ENVIRONMENTS

The sandstones of the Potsdam Group have long been regarded simplistically as an undifferentiated blanket of nearshore sandstones, produced during the marine transgression of the Precambrian surface. During the initial field season, examination of outcrops has shown that the Potsdam Group in eastern Ontario is actually a complex mosaic of several different terrestrial and marine facies. Two terrestrial and two marine environments have been identified to date, each of which can be further subdivided into distinct components. A summary of the results has recently been presented (Wolf and Dalrymple 1984); these provisional findings are presented below.

FACIES 1 – PEBBLY ARKOSES AND CONGLOMERATES

This facies is restricted to the 'Covey Hill' formation, and is dominantly found in the Big Rideau Lake area, although a few additional outcrops are scattered throughout the study

area (Figure 2). A readily accessible quarry located near the Mill Pond Conservation Area, on lot 6, concessions II and III of South Burgess Township in Leeds County (Figure 1), provides a representative section over 13 m thick (Figure 3). The Mill Pond quarry, like most outcrops of this facies, is found in a down-faulted block that includes Big Rideau Lake, and which is bounded by the Rideau Lake Fault (Wynne-Edwards 1967) on the northwest and by the Briton Bay Fault (Wolf and Williams 1984a) to the east. A detailed study of this quarry formed the basis for a B.Sc. thesis by Dorr (1984) under the supervision of the authors. Some of these results, together with additional observations, are summarized below.

Description

This facies is characterized by poorly sorted, massive to cross-stratified, feldspathic conglomerates and cross-stratified pebbly arkoses. The Mill Pond quarry section can be divided into five erosionally-bounded units, based on grain size and sedimentary structures (Figure 3). These units are organized into two generally fining upwards sequences, each with a discrete, unimodal paleocurrent orientation, based on pebble imbrication and cross-bed dips: units 1 to 3 with an easterly flow; and units 4 and 5 with a northerly paleocurrent direction (Figure 3). The lower sequence also displays a minor coarsening upwards sequence in unit 2.

The pebble to cobble conglomerates of units 1, 4, and the upper part of unit 2 consist of poorly-sorted, dominantly subround to round clasts of quartzite set in a matrix of feldspathic coarse sand and fine pebbles. Unstable lithologies such as feldspathic gneiss, marble, and schist compose, on average, about 12% of the clasts in unit 1, but decrease in abundance up section to 5-6% in unit 4 (Figure 3). Similarly, the matrix of these conglomerates also becomes more mature (less potassium-feldspar, plagioclase, and lithic fragments) up section. Sedimentary structures in the conglomerates range from massive (no structures) to crude horizontal bedding and cross-stratification.

The sandy lower portion of unit 2, and units 3 and 5, are characterized by poorly-sorted, pebbly arkoses. As in the conglomerates, the unstable components decrease in abundance up section (Figure 3). In unit 2, the sandstones are horizontally stratified and grade upwards into the overlying horizontally stratified conglomerates. Large-scale (0.5 to 1.9 m thick) planar cross beds occupy the lower portion of unit 3, and are erosionally overlain by smaller-scale trough cross beds.

Interpretation

The presence of poorly stratified conglomerates, the size of the cross beds, the consistently uni-directional paleocurrents, and the poorly sorted, immature character of the sediments all suggest that this facies was formed in a setting transitional between a distal, flow-dominated alluvial fan and a proximal braided fluvial environment. The fining upward sequences visible in the Mill Pond quarry also show a strong similarity to the braided river facies models of Miall (1977, 1978) and Rust (1978). A beach to nearshore origin is incompatible with the poor sorting, immature mineralogy, and the type and scale of the sedimentary structures.

The massive to stratified conglomerates of units 1 and 4 are considered to represent longitudinal bars formed during high flood stage. The cross-stratified conglomerates of unit 4 probably represent the preserved lee faces of these bars, whereas the structureless to crudely horizontally-stratified beds may be due to high rates of deposition by a rapidly waning flow which did not allow significant sorting. The imbrication of the cobbles in these deposits indicates the paleoslope at the time of deposition better than cross beds do (Collinson 1970); therefore, the general paleoslope was eastward in unit 2 and northward in unit 4. Miall (1977) noted that longitudinal bar formation occurs most commonly in proximal, gravelly braided rivers.

The planar cross beds of units 3 and 5 are interpreted to have been formed by the migration of transverse bars in a more distal setting (Miall 1977). In unit 3, the upward transition from planar to trough cross beds, and the corresponding decrease in set size, suggests either that water depth over the top of the underlying transverse bar was sufficient to allow sinuous bedforms to form on it (Miall 1977), or that channels filled with sinuous bedforms cut across the top of the transverse bars at a later time. Unit 5 probably represents the deposits of smaller transverse bars driven over the longitudinal bar of unit 4 in the manner described by Cant and Walker (1978). The coarsening-upward sequence of horizontal stratification in unit 2 may represent a channel fill formed under upper flow re-

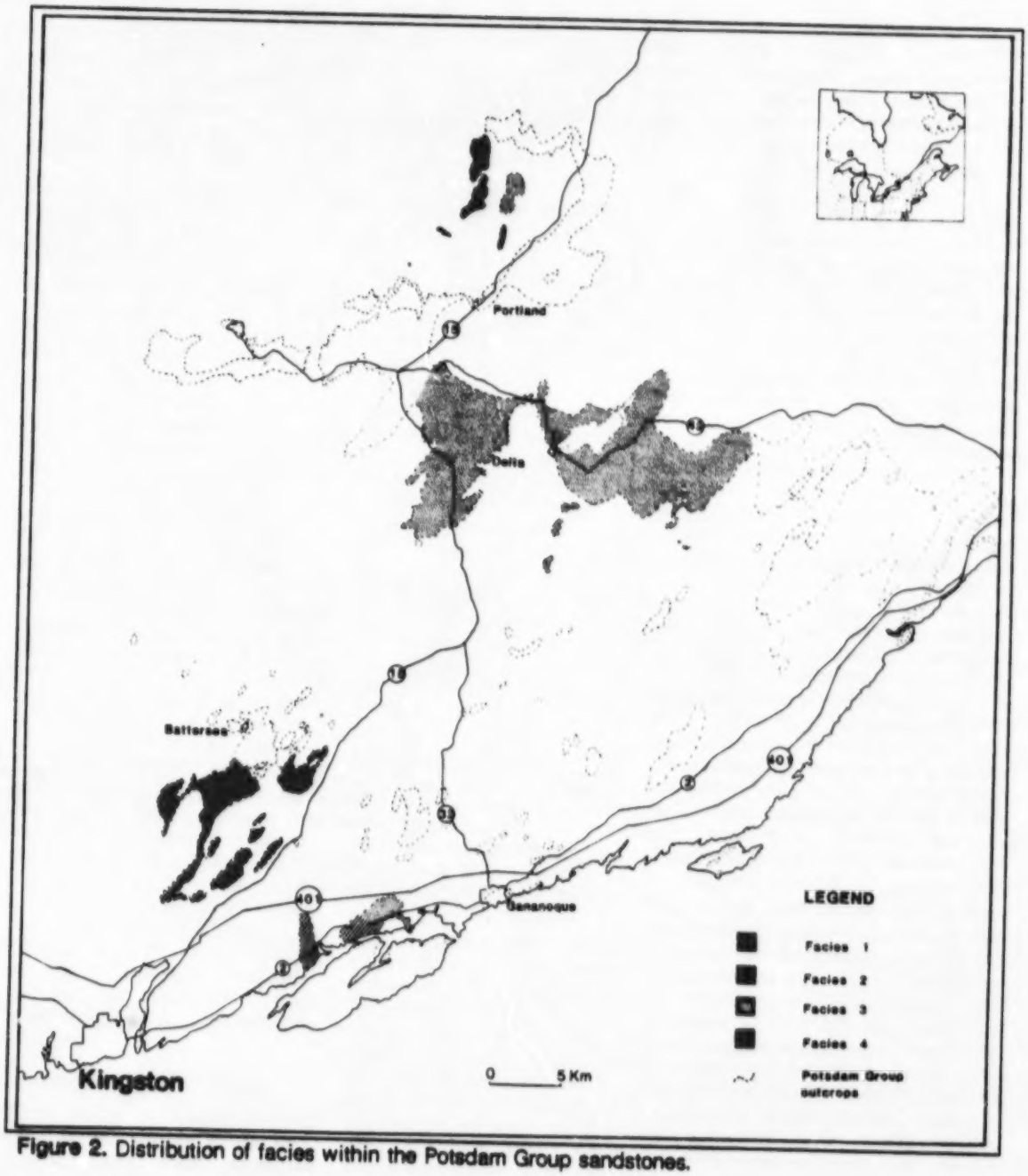

Figure 2. Distribution of facies within the Potsdam Group sandstones.

gime conditions. The upward increase in grain size may be due to either a progressive increase in flow velocity as the channel was re-occupied, or to rejuvenation of the source area.

The upward-fining sequences of units 1 to 3 and 4 to 5, the immaturity of the rock fragments, and the close proximity to the major Rideau Lake Fault system strongly suggest that deposition of this facies was controlled by movement of the fault. Repeated uplift would explain the repetition of the sequences. Initial uplift would cause deposition of the coarse-grained, proximal conglomerates, and then, as the source area became subdued, the decreasing relief would result in a transition to more distal, sandy environments (Steel *et al.* 1977). Alternatively, the sequences could result from the avulsive switching of alluvial fan lobes and their subsequent, gradual abandonment (Steel and Aasheim 1978). The upward increase in sediment maturity indicates that less first-cycle debris was supplied to the fluvial system, and that the amount of reworking increased through time.

A paleohydraulic reconstruction, based on the grain size and the scale of the sedimentary structures observed, suggests a channel depth on the order of 4 m. The resulting fluvial system would have had a drainage basin approximately half the size of the present day Saskatchewan River system (Dorr 1984). The large size of the river system and the apparently-contradictory, proximal nature of the sediments is presumably the result of local fault control on sedimentation. The large river size also suggests that the 'Covey

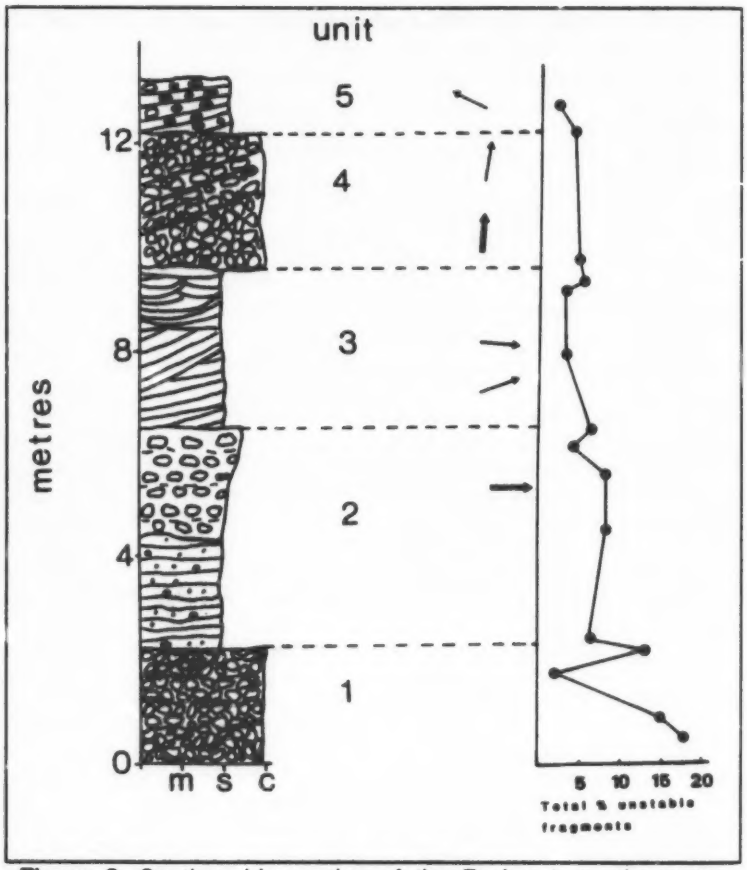

Figure 3. Stratigraphic section of the Facies 1 conglomerates and sandstones in the Mill Pond quarry (modified from Dorr 1984). Paleocurrent directions shown by arrows: thick arrows - pebble imbrications; thin arrows - cross-bed dips. At the base of the stratigraphic column, grain size: m = mud, s = sand, and c = conglomerate.

Hill' formation would originally have covered a much more extensive portion of eastern Ontario, and beyond. The scarcity of such outcrop today is due to either pre- or post-Nepean erosion.

FACIES 2 – VERY LARGE–SCALE CROSS–BEDDED SANDSTONE

A large area of exposure of Facies 2 occurs northeast of Kingston, in the Battersea area, with smaller outcrops around Delta (Figure 2). This facies is provisionally placed in the Nepean Formation on the basis of its quartz content, although its distinctive characteristics might allow it to be considered as a separate unit. In most places where it is exposed, this facies immediately overlies the Precambrian and sits in low areas between Precambrian highs; this is especially noticeable in the Delta area. In one exposure east of Battersea, a unit of apparently marine sandstone is in fault contact with rocks of Facies 2, which are situated on the presumed down-thrown side of the fault. This indicates that Facies 2 may overlie the marine beds at least locally. Throughout most of the study area however, it would appear that the rocks of Facies 2 lie stratigraphically below typical marine Nepean Sandstone, though no exposures have been found to date to substantiate this.

Description

This facies is dominated by very large, simple cross beds which have long sweeping toesets and bottomsets; in general, only the toe and bottomsets are exposed, and less commonly the lower portion of the foresets. The thickness of individual sets ranges from 2 to 10 m, but they were undoubtedly larger as the maximum thickness is generally controlled by the height of the available outcrop. Most of the sets are transitional in shape between planar and trough cross beds; some of the planar sets may, however, be part of very large troughs, as some troughs over 20 m wide have been measured. Cross-bed dip and trough axis orientations indicate a dominant paleocurrent flow toward the southwest. Approximately one-quarter of the set boundaries show little or no change in grain size or sorting from one set to the next. More commonly though, thin quartz-pebble horizons occur either at the top of the underlying set or at the base of the overlying set. In a few cases, lenses and thin sheets of poorly-sorted and unstratified, polymictic conglomerate separate the cross beds. At one locality, the uppermost 5 to 7 cm of a set is deep purple, in sharp contrast to the normal white to cream colour.

The cross beds are composed of very regular laminae of well-sorted, well-rounded, medium-grained quartz. Individual laminae can sometimes be traced for several 10s to 100s of centimetres. In places where there is clean, relatively unweathered exposure, faint, low-angle, climbing translatent laminae (Hunter 1977a,b) were observed. Small reverse faults with displacements of a few centimetres are common in the bottomsets of some of the larger cross-bed sets. Bedding-plane exposures of bottom and toesets locally display several significant features including: slightly sinuous, wave ripple marks; the trace fossil *Protichnites*, a crawling trace formed by a large arthropod; and, closely associated with this trace in one place, wart-like, low-amplitude ripple marks which are similar to the adhesion structures described by Kocurek and Fielder (1982).

Interpretation

The features observed in this facies suggest that these very large scale, cross-bedded quartz arenites were deposited in an aeolian dune complex. The size and style of the cross beds is similar to aeolian dune structures described from both modern (Tsoar 1982) and ancient (McKee 1979) examples. The climbing translatent structures which are formed by climbing wind ripples (Hunter 1977a,b), and the adhesion ripples (features formed when wind-blown sand is deposited on a wet surface; Kocurek and Fielder 1982) provide confirmation of the aeolian origin of these cross beds. Grain flow and avalanche deposits, which Hunter (1977a,b) described as being characteristic of aeolian deposits, are absent, but this may be because these structures normally form in the upper part of foresets which are not preserved in the outcrops studied to date.

The conglomeratic lenses present between the cross beds are interpreted to have been formed by small streams which occupied the interdune areas. The larger sheets of conglomerate may have been deposited by flash floods. Reworking of the fluvial deposits by the wind would produce a deflation lag of quartz pebbles which would then line the set boundaries after the next sand dune had advanced over the lag surface. A long period of interdune weathering might also be responsible for the dark purple zone at the top of

one of the cross-bed sets, although this colouration might also be diagenetic in origin.

The occurrence of wave ripple marks and marine arthropod crawling traces can be reconciled with the aeolian interpretation by suggesting that the dunes constituted a coastal dune complex in which some of the interdune areas were periodically flooded by sea water. The close association of the crawling traces with the adhesion ripples suggest that the arthropod may have been stranded on the lower dune surface when the marine waters receded. Further work is needed to substantiate this as the occurrence of a subaerial arthropod trace of Late Cambrian - Early Ordovician age has significant implications for the paleoecological tolerances of these primitive organisms.

The only reasonable alternative to an aeolian origin for these cross beds is that they are the deposits of large, shallow marine sand waves, such as those described from the North Sea, Georges Bank, and the east coast of southern Africa (Allen 1980). Recent studies of modern (Dalrymple 1984) and ancient (Allen and Homewood 1984; Blakey 1984) sand waves, as well as theoretical models (Allen 1980), have shown, however, that the internal structures of marine sand waves are highly complex, reflecting the fluctuating nature of the tidal and storm currents which generate them. In addition, marine sand waves would not contain climbing translatent strata or adhesion ripples. Thus, based on the various features observed in this facies, the aeolian interpretation is favoured.

FACIES 3 – ALTERNATING CROSS–BEDDED AND BIOTURBATED SANDSTONES

Facies 3 represents those rocks which are typically regarded as the Nepean Formation. Within the study area this facies occurs predominantly in the northeast, along the margin of the Ottawa - St. Lawrence Lowlands around Delta (Figure 2). Commonly, a thin, discontinuous horizon of quartz pebble and cobble conglomerate with a matrix of well-rounded, medium-grained, quartz arenite immediately overlies the Precambrian at the base of this facies. The quartz-rich nature of these conglomerates distinguishes them from those of Facies 1.

Description

Facies 3 consists of laterally continuous beds of quartz arenite which show a cyclic alternation between cross-bedded and bioturbated sandstone. The cross-bedded units begin with a sharp, erosional base and pass gradationally upwards into totally bioturbated beds. Complete cycles are 1 to 3 m thick, though in many cases the cycles are incomplete. The cross-bedded portion of the cycle is usually whiter, thicker, and more resistant to weathering than the bioturbated intervals. This gives the outcrops of this facies a distinctive repetition of dark-coloured recessive units and lighter, resistant beds. Both the cross-bedded and bioturbated beds are composed of fine- to medium-grained, well-sorted and well-rounded, quartz grains cemented by silica. In cycles higher in the formation, calcareous and dolomitic cements are also present, particularly in the bioturbated units.

The lower portion of each cycle is characterized by small-scale (30 to 50 cm) planar and trough cross beds which generally pass abruptly upwards into ripple cross-laminated sandstone. Formsets of megaripples are present in some sections. The cross beds commonly display bipolar, 'herringbone', cross-bed dips, usually oriented east-west. Reactivation surfaces are abundant within the cross beds, and several may occur in a single set, spaced several 10s of centimetres apart. Discrete vertical burrows of *Skolithos* sp., *Diplocraterion* sp., and *Monocraterion* sp. commonly penetrate the cross beds. In cases where a cycle terminates at this level, the upper surface may have areas covered by symmetrical wave ripple marks.

In complete cycles, the degree of burrowing increases rapidly upwards. The degree of bioturbation in the upper part of the cycles varies from approximately 50% by volume to almost 100% so that all sedimentary structures are obliterated. No identifiable trace fossils have yet been recovered from these highly burrowed intervals. On some bedding plane surfaces disarticulated lingulid brachiopods were found. Rarely, distinct erosional surfaces separate the bioturbated beds. At one locality near Phillipsville, a zone of disrupted laminae caps the burrowed beds. The nature of the laminae suggests collapse into small cavities.

Interpretation

The vertical sequence of structures, the herringbone cross beds, the reactivation surfaces and the trace and body fossils indicate that this facies was deposited in a marine environ-

ment influenced by tidal currents. Each cycle is interpreted to represent a minor transgression, which is preserved only as an erosional surface, followed by progradation of a sandy tidal flat environment. A subtidal to lower intertidal setting is envisioned for the lower portion of the cycle. Here, megaripples and/or sand waves capped by ripples formed under the influence of the tidal currents. As progradation continued and the water depth shallowed, energy levels and the rate of sediment movement decreased allowing organisms to colonize the sandy substrate in greater numbers. The completely bioturbated sandstones probably represent deposition under such quiet conditions in an upper intertidal environment. The disrupted laminae which cap the cycle at the Phillipsville locality may represent the collapse of overlying sand into cavities formed by the dissolution of evaporites, such as gypsum or halite (B.W. Selleck, Colgate University, personal communication 1983), which might have formed in the supratidal zone (Thompson 1968). The next cycle would begin with another minor transgression, which might erode some of the upper sediments of the previous sequence.

Most of the facies models proposed for tidal flat progradation contain significant amounts of mud in the upper intertidal zone (Reineck 1972; Reineck and Singh 1980). The lack of shale in Facies 3 does not detract seriously from the above interpretation however, as the absence of mud-sized terrigenous clastics is a feature that is common to many Cambro-Ordovician sequences on the North American craton (Byers and Dott 1981), and many other deposits of this age, which are interpreted as intertidal in origin, also lack shale (Barnes and Klein 1975; Jansa 1975).

FACIES 4 – HORIZONTAL AND TROUGH CROSS–STRATIFIED SANDSTONE

This final facies groups those outcrops which cannot be assigned to Facies 3. In general, these outcrops are scattered and poorly exposed, and most occur in the southern part of the map-area; exposures between Kingston and Gananoque, as well as some south of Delta, are placed in this facies (Figure 2). These outcrops generally have not been investigated in detail, but the variety of structures and sequences already seen ensure that this facies will be subdivided further after more study. Only two of the more widespread subfacies will be described.

Description

The most extensive subfacies is a trough cross-bedded quartz arenite. The individual sets vary from 0.3 to 0.5 m in thickness, and occur in co-sets several metres thick, which are separated by thin, continuous, quartz pebble horizons. Measurements of the trough axes indicate a uni-directional paleocurrent flow to the south-southwest. Discrete burrows of *Skolithos* are present, and small lenses of ripple cross lamination occur between the trough cross beds in a few places. West of Gananoque this subfacies usually rests on the Precambrian and is overlain by burrowed quartz arenites of Facies 3 (Figure 2).

A second subfacies occurs west of Gananoque, underlying trough cross-bedded sandstone. This subfacies consists of horizontally-bedded quartz arenite, with occasional ripple and megaripple formsets randomly interbedded. No dominant paleocurrent direction was determined from the few measurements taken. Thin, continuous layers of quartz granules and pebbles subdivide this subfacies into several similar units. No trace fossils have been observed.

Interpretation

Due to the variable nature of the several subfacies and the lack of detailed observations, this facies is provisionally considered to be an undifferentiated nearshore deposit. The trough cross-bedded sandstone might have accumulated in tidal inlet and/or offshore bar settings, while the horizontally-bedded sandstone could be a beach to foreshore deposit. Undoubtedly, this facies will be subdivided into a variety of nearshore environments with more study.

SUMMARY AND DISCUSSION OF SILICA POTENTIAL

The sandstones of the Potsdam Group can be divided into four facies representing two terrestrial environments (braided fluvial and aeolian), and at least two marine environments (subtidal to intertidal and nearshore), which are organized into a complex depositional mosaic. Alluvial fan/braided fluvial sequences, the deposition of which was locally influenced by syn-depositional tectonic activity, mantled portions of the Precambrian surface prior to the Late Cambrian transgression. Along the advancing shoreline, a coastal dune complex, that was cut by gravelly

streams, developed in the arid to semi-arid climate that is indicated by the possible evaporite-dissolution features in Facies 3. As the transgression progressed, coastal erosion reworked most of these terrestrial sediments into the various marine sandstones described above, and only locally have the terrestrial deposits survived. If the aeolian-on-marine stratigraphy is confirmed by further work, then at least one period of relative sea level fall is indicated; such an event is also suggested by the presence of silcrete breccias in the Potsdam sandstones of northern New York State (Selleck 1978). This sea-level fluctuation would raise the possibility of additional, complex interfingering of the depositional environments. A close modern analogue, in which the sea is transgressing over an irregular bedrock surface, is the Atlantic coast of Nova Scotia (Boyd *et al.* 1983). The general suite of environments is similar in the two cases, but differences exist because of the presence of mud, vegetation and a humid climate in the Nova Scotia example.

Figure 2 shows the geographic distribution of the four facies as known to date. From this it appears that the terrestrial facies are preferentially preserved along the crest of the Frontenac Axis, whereas the marine facies are exposed primarily along the flanks, and especially to the northeast. This configuration could be interpreted to suggest that the crest of the axis was not transgressed until later in the Ordovician. It is likely, however, that these terrestrial deposits preferentially escaped erosion by the transgressing sea because of their sheltered position in topographic or structural depressions, and that subsequent erosion has removed any overlying marine sandstones that were once present on the axis. The large area of marine sandstone that occurs on the western flank of the Frontenac Axis in upper New York State (Selleck 1975) supports this alternative.

Very little work has yet been undertaken on the relationship between the depositional facies and silica-sand potential, but a few preliminary comments are possible. Correlation of the sample locations of various published chemical analyses (Cole 1923; Keith 1949; Powell and Klugman 1979) with the known facies distribution (Figure 2) indicates that the highest silica values are found in Facies 2 (aeolian) and Facies 3 (subtidal to intertidal). In addition, the W.R. Barnes Company Limited's silica quarry in Storrington Township is located in the large-scale aeolian cross beds of Facies 2, while the proposed Angelstone Company Limited operation near Delta is in Facies 3 sandstones. It is clear from the petrographic examination of the Facies 1 fluvial sandstones that the initial sediment derived from the Canadian Shield was immature, and that a portion, but not all, of the quartz enrichment was accomplished by fluvial action. The final purification must, therefore, have taken place either in an aeolian environment and/or in the nearshore region of the transgressing sea. The relative role of these environments in the production of quartz-rich sandstones may be clarified when the stratigraphic relationship between the aeolian and marine facies is established. It may be that aeolian sands derived from marine sediments, which were themselves reworked from fluvial deposits, are the purest quartz sandstones.

FUTURE STUDY

Approximately 30% of the significant outcrops in the study area remain to be examined in detail: the main areas to be studied are located around Brockville and Westport, and in the region between Gananoque and Delta. The major concerns will be to complete the delineation of the facies distributions (Figure 2) and to provide a satisfactory subdivision and interpretation of Facies 4 (undifferentiated nearshore). Evidence to confirm and/or modify the provisional interpretations of the other facies will also be sought in the remaining outcrops.

When the facies subdivision and interpretation is complete, the emphasis will switch to a more rigorous evaluation of the factors controlling silica content. Systematic sampling of all of the facies for geochemical analysis will continue, to complement those samples already being processed. Further thin section analyses will also be undertaken. The geochemical and petrographic data will then be integrated with the environmental interpretations to determine the influence of depositional processes on silica distribution. These data should lead to the development of a set of guidelines to be used in the exploration for silica deposits.

ACKNOWLEDGMENTS

Grateful appreciation is extended to the landowners in the study area who cheerfully granted permission to study exposures on their property. The various quarry owners are especially thanked. We would

also like to thank members of the Engineering and Terrain Geology Section of the Ontario Geological Survey, and particularly D.A. Williams, for informative discussions on stratigraphy. Dr. G.M. Narbonne of Queen's University, and Dr. B.W. Selleck, Colgate University, are gratefully acknowledged for their comments in the field regarding the various environmental interpretations presented here.

REFERENCES

Allen, J.R.L.
1980: Sand Waves: a Model of Origin and Internal Structure; Sedimentary Geology, Volume 26, p.281-328.

Allen, P.A., and Homewood, P.
1984: Evolution and Mechanics of a Miocene Tidal Sandwave; Sedimentology, Volume 31, p.63-81.

Barnes, J.J. and Klein, G. deV.
1975: Tidal Deposits in the Zabriskie Quartzite (Cambrian), Eastern California and Western Nevada; p.163-169 *in* Tidal Deposits: a Casebook of Recent Examples and Fossil Counterparts, edited by R.N. Ginsburg, Springer-Verlag, Berlin, 428p.

Blakey, R.C.
1984: Marine Sand-wave Complex in the Permian of Central Arizona; Journal of Sedimentary Petrology, Volume 54,, p.29-51.

Boyd, B.W.
1982: Silica; p.405-409 *in* Canadian Minerals Yearbook, 1980, Energy, Mines and Resources Canada, Mineral Report 30, 563p.

Boyd, R., Bowen, A.J., and Hall, R.K.
1983: Transgressive Coastal Sedimentation Along the Eastern Shore, Nova Scotia (abstract); Geological Society of America, Abstracts with Programs, Volume 15, p.194.

Brand, U., and Rust, B.R.
1977a: The Age and Upper Boundary of the Nepean Formation in its Type Section near Ottawa, Ontario; Canadian Journal of Earth Sciences, Volume 14, p.2002-2006.
1977b: The Age and Upper Boundary of the Nepean Formation in its Type Section near Ottawa, Ontario: Reply to Greggs and Bond; Canadian Journal of Earth Sciences, Volume 14, p.2671-2673.

Byers, C.W., and Dott, R.H., Jr.
1981: SEPM Research Conference on Modern Shelf and Ancient Cratonic Sedimentation - The Orthoquartzite-Carbonate Suite Revisited; Journal of Sedimentary Petrology, Volume 51, p.329-347.

Cant, D.J., and Walker, R.G.
1978: Fluvial Processes and Resulting Facies Sequences in the Sandy Braided South Saskatchewan River; Sedimentology, Volume 25, p.625-648.

Carson, D.M.
1982a: Paleozoic Geology of the Brockville-Mallorytown Area, Southern Ontario; Ontario Geological Survey, Preliminary Map P.2495, Geological Series, Scale 1:50 000.
1982b: Paleozoic Geology of the Gananoque-Wolfe Island Area, Southern Ontario; Ontario Geological Survey, Preliminary Map P.2496, Geological Series, Scale 1:50 000.

Clark, T.H.
1966: Chateauguay Area; Quebec Department of Natural Resources, Geological Report 122, 63p.

Cole, L.H.
1923: Silica in Canada, Its Occurrence, Exploitation and Uses; Canada Department of Mines, Number 555, Part 1, 126p.

Collings, R.K., and Andrews, P.R.A.
1983: Potsdam Sandstone of Ontario as Glass and Foundry Glass (Abstract); Canadian Institute of Mining and Metallurgy, Bulletin, Volume 76, p.72-73.

Collinson, J.D.
1970: Bedforms of the Tana River, Norway; Geographisca Annaler, Volume 52A, p.31-55.

Dalrymple, R.W.
1984: Morphology and Internal Structure of Sandwaves in the Bay of Fundy; Sedimentology, Volume 31, p.365-382.

Dorr, J.J.
1984: The Sedimentological Study of the Feldspathic Conglomerates and Sandstones of the Big Rideau Lake Area, Ontario; unpublished B.Sc. Thesis, Queen's University, Kingston, Ontario, 98p.

Emmons, E.
1838: Report of the Second Geological District of the State of New York; New York State Geological Survey, Second Annual Report, 214p.

Fisher, D.W.
1977: Correlation of the Hadrynian, Cambrian, and Ordovician Rocks of New York State; New York State Museum, Map and Chart Series, Number 25, 75p.

Globensky, Y.
1981: Region de Huntingdon; Ministere de L'Energie et des Ressources, Service des Leves Geologiques, Rapport Geologique 198, 53p.
1982a: Region de Lachute; Ministere de L'Energie et des Ressources, Service des Leves Geologiques, Rapport Geologique 200, 67p.
1982b: Region de Vaudreuil; Ministere de L'Energie et des Ressources, Service des Leves Geologiques, Rapport Geologique 199, 59p.

Greggs, R.G., and Bond, I.J.
1972: A Principal Reference Section Proposed for the Nepean Formation of Probable Tremadocian Age, near Ottawa, Ontario; Canadian Journal of Earth Sciences, Volume 9, p.933-941.
1977: The Age and Upper Boundary of the Nepean Formation in its Type Section near Ottawa, Ontario: Discussion of Brand and Rust; Canadian Journal of Earth Sciences, Volume 14, p.2669-2671.

Hunter, R.E.
1977a: Basic Types of Stratification in Small Eolian Dunes; Sedimentology, Volume 24, p.361-387.
1977b: Terminology of Cross-stratified Sedimentary Layers and Climbing-ripple Structures; Journal of Sedimentary Petrology, Volume 47, p.697-706.

Jansa, L.F.
1975: Tidal Deposits in the Monkman Quartzite (Lower Ordovician) Northeastern British Columbia, Canada; p.153-161, *in* Tidal Deposits: A Casebook of Recent Examples and Fossil Counterparts, edited by R.N. Ginsburg, Springer-Verlag, Berlin, 428p.

Keith, M.L.
1949: Sandstone as a Source of Silica Sands in Southeastern Ontario; Ontario Department of Mines, Annual Report for 1946, Volume 55, Part 5, 36p.

Kingston, P.W., and Papertzian, V.C.
1983: 1982 Report of the Eastern Region Resident Geologist; p.179-191, *in* Report of Activities, Regional and Resident Geologists, 1982, edited by C.R. Kustra, Ontario Geological Survey, Miscellaneous Paper 107, 211p.

Klugman, M.A., and Yen, W.T.
1980: Silica Sand Potential in Eastern Ontario, Preliminary Report 2 - Beneficiation; Ontario Geological Survey, Open File Report 5303, 39p.

Kocurek, G., and Fielder, G.
1982: Adhesion Structures: Journal of Sedimentary Petrology, Volume 52, p.1229-1241.

Liberty, B.A.
1972: Paleozoic Geology of Wolfe Island, Bath, Sydenham, and Gananoque Map Areas, Ontario; Geological Survey of Canada, Paper 70-35, 12p.

Logan, W.A.
1863: Geology of Canada; Geological Survey of Canada, Progress Report from its Commencement to 1863.

McKee, E.D.
1979: Ancient Sandstones Considered to be Aeolian; p.187-238 *in* A Study of Global Sand Seas, edited by E.D. McKee, United States Geological Survey, Professional Paper 1052, 423p.

Miall, A.D.
1977: A Review of Braided River Depositional Environments; Earth Science Reviews, Volume 13, p.1-62.
1978: Lithofacies Types and Vertical Profile Models in Braided River Deposits: a Summary; p.605-626 *in* Fluvial Sedimentology, edited by A.D. Miall, Canadian Society of Petroleum Geologists, Memoir 5, 859p.

Powell, R.D., and Klugman, M.A.
1979: Silica Sand Potential in Eastern Ontario, Preliminary Report 1; Ontario Geological Survey, Open File Report 5265, 100p.

Reineck, H.-E.
1972: Tidal Flats; p.146-159 *in* Recognition of Ancient Sedimentary Environments, edited by J.K. Rigby and W.K. Hamblin, Society of Economic Paleontologists and Mineralogists, Special Publication 17, 340p.

Reineck, H.-E., and Singh, I.B.
1980: Depositional Sedimentary Environments; 2nd Edition; Springer-Verlag, New York, 549p.

Rust, B.J.
1978: Depositional Models for Braided Alluvium; p.605-625 *in* Fluvial Sedimentology, edited by A.D. Miall, Canadian Society of Petroleum Geologists, Memoir 5, 859p.

Selleck, B.W.
1975: Paleoenvironments and Petrology of the Potsdam Sandstone, Theresa Formation, and Ogdensburg Dolomite (Upper Cambrian - Lower Ordovician) of the Southwestern St. Lawrence Valley, New York; Unpublished Ph.D. Thesis, University of Rochester, Rochester, New York, 210p.
1978: Syndepositional Brecciation in the Potsdam of Northern New York State; Journal of Sedimentary Petrology, Volume 48, p.1177-1184.

Steel, R.J., Maehle, S., Nilsen, H., Roe, S.L., and Spinnangr, A.
1977: Coarsening Upward Cycles in the Alluvium of Hornelen Basin (Devonian), Norway: Sedimentary Response to Tectonic Events; Geological Society of America, Bulletin, Volume 88, p.1124-1134.

Steel, R.J., and Aasheim, S.M.
1978: Alluvial Sand Deposition in a Rapidly Subsiding Basin (Devonian, Norway); p.385-412. *in* Fluvial Sedimentology, edited by A.D. Miall, Canadian Society of Petroleum Geologists, Memoir 5, 859p.

Thompson, R.W.
1968: Tidal Flat Sedimentation on the Colorado River Delta, Northwestern Gulf of California: Geological Society of America, Memoir 107, 133p.

Tsoar, H.
1982: Internal Structure and Surficial Geometry of Longitudinal (Seif) Dunes; Journal of Sedimentary Petrology, Volume 52, p.823-831.

Vos, M.A.
1981: Silica in Ontario, Industrial Minerals Supplement; Ontario Geological Survey Miscellaneous Paper 85, 36p.

Williams, D.A., and Wolf, R.R.
1982: Paleozoic Geology of the Northern Part of the Ottawa - St. Lawrence Lowland, Southern Ontario; p.132-134, *in* Summary of Field Work, 1982, by the Ontario Geological Survey, edited by John Wood, Owen L. White, R.B. Barlow, and A.C. Colvine, Ontario Geological Survey, Miscellaneous Paper 106, 235p.

Wilson, A.E.
1946: Geology of the Ottawa - St. Lawrence Lowland, Ontario and Quebec; Geological Survey of Canada, Memoir 241, 66p.

Wilson, M.E., and Dugas, J.
1961: Perth Map Area, Ontario; Geological Survey of Canada, Map 1089A, scale 1:63,360.

Wolf, R.R., and Dalrymple, R.W.
1984: Terrestrial and Shallow Marine Environments of the Potsdam Sandstone, Eastern Ontario (Abstract); Geological Association of Canada - Mineralogical Association of Canada, Annual Meeting, Program with Abstracts, Volume 9, p.117.

Wolf, R.R., and Williams, D.A.
1984a (in press): Paleozoic Geology of the Perth Area, Southern Ontario; Ontario Geological Survey Preliminary Map, Geological Series, scale 1:50 000.
1984b (in press): Paleozoic Geology of the Westport Area, Southern Ontario; Ontario Geological Survey Preliminary Map, Geological Series, scale 1:50 000.

Wright, J.F.
1923: Brockville-Mallorytown Map Area, Ontario; Geological Survey of Canada, Memoir 134, 63p.

Wynne-Edwards, H.R.
1967: Westport Map Area, Ontario, with Special Emphasis on the Precambrian Rocks; Geological Survey of Canada, Memoir 346, 142p.